THE UNIVERSITY
of EDINBURGH

The Role of microRNAs in Jaagsiekte Sheep Retrovirus Infection

Maria Contreras Garcia

This thesis is presented for the degree of Doctor of Philosophy

The University of Edinburgh

2019

Contents

Index of Figures

Index of tables

Declaration

I declare that the work presented in this thesis has been composed and completed by myself, unless otherwise stated. This work has not previously been submitted for any other degree or personal qualification.

Maria Contreras Garcia

Abstract

Ovine pulmonary adenocarcinoma (OPA) is a lung cancer that affects sheep, caused by jaagsiekte sheep retrovirus (JSRV). OPA is present in most sheep-rearing countries of the world, but, at present, there are no reliable early-stage tests to diagnose the disease, and OPA continues to pose an animal welfare threat and cause substantial economic losses. In addition, OPA is a valuable animal model to study early oncogenic events in human lung cancer. Specifically, OPA and some types of human lung cancer present similarities in activated signalling pathways (Ras-MEK-ERK1/2 and PI3K-AKT-mTOR) and their association with type II pneumocytes. Nevertheless, study of the molecular pathogenesis of OPA has been hindered due to the lack of a permissive cell line for JSRV replication. JSRV encodes an unusual envelope protein (Env) which is actively oncogenic and sufficient to drive transformation *in vivo* and *in vitro*. Despite the lack of a permissive cell line, early oncogenic events induced by JSRV can be studied by transfection of cell lines with plasmids encoding JSRV Env.

MicroRNAs (miRNAs) are short non-coding RNAs that regulate gene expression and essential cell processes such as cell proliferation and apoptosis. miRNAs are being extensively studied as biomarkers of several diseases, including cancer. The aims of this project were to investigate the role of miRNAs in the early oncogenic events induced by JSRV and to investigate their potential as OPA biomarkers.

miRNA expression levels were investigated using small RNA sequencing in lung tissue from cases of experimentally induced OPA. No evidence of JSRV-encoded miRNAs was found, but levels of 40 miRNAs were found differentially expressed between affected and control sheep. Of those, upregulation of nine microRNAs (miR-135b, miR-182, miR-183, miR-21, miR-200b, miR-205, miR-31, miR-503 and miR-96) was confirmed by RT-qPCR in experimental and natural cases of OPA, suggesting that increased levels of these miRNAs were characteristic of OPA affected lung tissue. To investigate miRNAs as potential biomarkers, miRNA expression was measured in serum and bronchoalveolar lavage fluid (BALF) macrophages of OPA affected sheep. small RNA sequencing revealed 74 microRNAs and 85 miRNAs differentially expressed in serum and BALF

macrophages, respectively. Interestingly, BALF macrophage microRNA expression was found to resemble more closely that of OPA affected sheep lungs. In addition, miRNA expression levels varied at different stages of the disease and no miRNAs were found to be consistently dysregulated in serum of OPA affected animals. Discordances in miRNA signatures in lung tissue and serum are not entirely unexpected. Lung tissue miRNAs might represent the tumour microenvironment and localised response to it, whereas miRNAs in serum may represent the global state of the animal, and tumour miRNAs might be released into circulation at low levels, making them difficult to detect.

Expression of the nine upregulated miRNAs was then investigated in *in vitro* models to study their involvement in transformation. Lentiviral vectors encoding green fluorescent protein (GFP) or a GFP-2A-Env fusion protein were produced and used to transduce cell lines. Transformation was verified by immunocytochemical detection of the transformation markers P-Akt and P-ERK1/2. Nevertheless, miRNA expression levels in culture did not resemble those observed in lung tissue of OPA-affected sheep. These differences might be due to species variation, upregulation of miRNAs late in the transformation process, or involvement of other cell types in tissue besides the transformed cells. To study these questions further, JSRV and the GFP-2A-Env encoding lentiviral vectors were used to infect lung slices in culture. Expression levels of miRNAs did not, in any of the cases, resemble lung tissue findings. Fewer than 5% of cells in lung slices were found to be infected, suggesting that changes in miRNA expression could be masked by the background of normal cells. Nevertheless, increasing JSRV21 concentration did not yield higher infection levels, indicating that those might be more dependent on the availability of JSRV's target cells, dividing type II pneumocytes, than viral concentration.

Taken together, this study has revealed new information on miRNA expression in OPA-affected sheep, including expression patterns in lung and serum. Future work should focus on developing a permissive replication system to allow the study of miRNAs in early JSRV-induced transformation events.

Lay Summary

Ovine pulmonary adenocarcinoma (OPA) is a lung cancer that affects sheep, caused by the jaagsiekte sheep retrovirus. OPA is present in most sheep-rearing countries of the world, but there are no diagnostic tests available for detection of the disease in its early stages. The disease is associated with significant economic losses for farmers and is a serious animal welfare issue. In addition, OPA has similarities to human lung cancer and can be used to study the human disease. However, advances in our understanding of OPA are slow because JSRV cannot be grown in laboratory settings. So far, our knowledge on the growth of tumours in OPA has derived from using a specific protein of JSRV that triggers the process of tumour formation.

In this thesis, I have investigated the relationship of a class of small molecules, called microRNAs (miRNAs), with OPA. miRNAs are present in all animals and regulate processes such as cell growth and cell death. In addition, they can be detected in tissues and body fluids, and the abundance of some miRNAs can be indicative of certain diseases. Improved understanding of how miRNAs change in sheep with OPA would provide a better understanding of the disease, and might allow us to use this class of molecules to detect the disease at an early stage.

When the abundance of miRNA was compared in lung tissue of OPA-affected sheep and unaffected sheep, the levels of 40 different miRNAs were discovered to be different in OPA-affected sheep. A panel of nine of those miRNAs was used to confirm in different groups of sheep that levels of those nine miRNAs appeared to be related to OPA disease. Also, the changes in the nine miRNAs could be observed in early stages and advanced stages of OPA.

Given that the nine miRNAs studied in lung seemed to distinguish between OPA-affected and unaffected sheep, their ability to diagnose OPA was assessed. Taking into consideration the potential use of a diagnostic test in the field, detection of the nine miRNAs was attempted in blood serum because it is more accessible than lung tissue. However, levels of the nine miRNAs in serum were not different between OPA-affected and unaffected sheep, indicating that they could not be used for diagnosis. Other miRNAs were detected in sheep serum,

but their levels were not clearly different between OPA-affected and unaffected sheep.

To discover the function of the nine miRNAs associated with OPA lung tissue, I performed experiments in cells grown in the laboratory. Cells in culture were exposed to the JSRV protein and tumour formation was observed. I then investigated if those cells in culture had similar abundance of the nine miRNAs compared to OPA lung tissue. However, levels of miRNAs in cultured cells were not a reflection of their levels in lung tissue. Because the cells grown and used in that experiment are different from the cells in sheep lung, the experiment was repeated in lung slices cultured in the laboratory. However, tumour formation was observed in a very small part of the lung slices, and quantities of the nine miRNAs were not similar to those in OPA lung tissue.

In summary, this study has provided new information on miRNAs and their relation to OPA, including their abundance in lung tissue and blood. Future work should focus on developing a system to grow JSRV in laboratory settings and study the function of miRNAs in JSRV infection and tumour formation.

Acknowledgements

Throughout this PhD project I have received a great deal of support and assistance.

I would first like to thank my supervisors, Dr. David Griffiths, Dr. Finn Grey and Dr. Karen Stevenson for all their guidance, supervision, encouragement and support. I would also like to thank Moredun Scientific for funding this project.

I am very grateful to several people at the Moredun Research Institute and Roslin Institute. To Ann Wood and Dr. Chris Cousens for their invaluable technical expertise, advice, support and encouragement over the past years. I am thankful to Dr. Mark Dagleish for his encouragement and help, to Val Forbes and Clare Underwood for processing the tissue samples, and to Helen Todd for her help with immunohistochemistry. Thanks must go to Dr Rebecca McLean, for her help and support. I am grateful to Deepali Vasoya, Professor Mick Watson and Siddhart Jayaraman for their help performing the bioinformatics analysis. Further thanks must go to Dr. Keith Ballingall and Dr. Mara Rocchi for their encouragement, especially during the last stages of this PhD. I am grateful to the members of the Grey lab for their support and help. A special thank you to Dr. Oliver Lin for his guidance and advice with northern blotting.

I am eternally grateful to Jeanie Finlayson (my PhD mom) for her invaluable technical advice with immunostaining techniques, for her support, advice and for all the baked goods.

A special thank you must go to Dr. Anna Karagianni: for her continued support in and out of the lab. Her technical help, support and guidance were invaluable at all stages of this PhD project.

I would also like to thank everyone in the PhD office, past and present members, for their support and encouragement in the good and bad days. I am forever grateful to Holly Hill and Katie Hildersley for striving to create an engaging and supportive environment for other PhD students. A special thank you must go to Ana Herrero, for being a continued source of enthusiasm, support and encouragement throughout this PhD.

On a more personal note, I would like to thank my friends for believing in me and for providing much-needed distractions. I am eternally grateful to my family: to my grandparents for believing in me and teaching me the value of hard work; to my Mom, Dad, and sister Laura for never doubting me, for encouraging me, and for listening to me talk (a lot) about science. Finally, a huge thank you to Marcos, this PhD wouldn't have been possible without his help, support, patience and encouragement.

List of abbreviations

Akt	Protein kinase B
AT2	Alveolar type II cells
CMV	Cytomegalovirus
CT	Cytoplasmic tail
CTE	Constitutive transport element
DMEM	Dulbecco's modified Eagle's medium
DMSO	Dimethyl sulfoxide
DNA	Deoxyribonucleic acid
EGFP	Enhanced green fluorescent protein
enJSRV	Endogenous jaagsiekte sheep retovirus
env	Envelope (gene)
ERK1/2	Extracellular signal-regulated protein kinases 1 and 2
FBS	Fetal bovine serum
gag	Group-specific antigen (gene)
GFP	Green fluorescent protein
HGF	Hepatocyte growth factor
HIV	Human immunodeficiency virus
IMDM	Iscove's modified Dulbecco's medium
JSRV	Jaagsiekte sheep retrovirus
KGF	Keratinocyte growth factor
LTR	Long terminal repeat
MAPK	Mitogen-activated protein kinase
MEME	Minimum essential medium Eagle

MMTV	Mouse mammary tumour virus
MOI	Multiplicity of infection
ORF	Open reading frame
PBS	Phosphate buffered saline
PI3K	Phosphoinositide-3-kinase
pol	Polymerase (gene)
pro	Protease (gene)
RNA	Ribonucleic acid
RT	Reverse transcriptase
RT-qPCR	Real-time quantitative polymerase chain reaction
sa	Splice acceptor
sd	Splice donor
SU	Surface unit
TM	Transmembrane
TU	Transducing units
UTR	Untranslated region
VMV	Visna/maedi virus

Chapter 1 Literature review

1.1 Ovine Pulmonary Adenocarcinoma

Ovine pulmonary adenocarcinoma (OPA) is a lung tumour caused by jaagsiekte sheep retrovirus (JSRV). The disease affects sheep and occasionally goats and mouflon, although they suffer from a less pathogenic form, cattle and other animals are not affected by it. OPA is an important issue for animal welfare and sheep production, due to the economic losses associated with it. In addition, OPA is an important model of human lung adenocarcinoma. Interestingly, JSRV is able to drive tumour formation due to an unusual Env protein, which is oncogenic and sufficient to drive transformation of cell lines *in vitro*, and tumour formation *in vivo*.

1.1.1 Clinical presentation

The presence of OPA in a flock is usually signalled by an increased number of adult sheep suffering from pneumonia that does not respond to antibiotic treatment (Griffiths et al, 2010). In individuals, signs of the illness include loss of weight, difficulty to breathe, cough and fluid discharge from the nostrils when the animal's head is lowered (De las Heras et al, 2003). This is known as the wheelbarrow test, and the presence of fluid discharge is a pathognomonic sign of OPA (Cousens et al, 2009; Sharp et al, 1983).

1.1.2 History and epidemiology of OPA

One of the first reports of OPA originated from South Africa in 1825, where it was described as "Jaagsiekte", an Afrikaans word that means chase-sickness, referring to the affected animals laboriously breathing, as if they had been chased (York & Querat, 2003). Similar descriptions were found a few years later in France and England (York & Querat, 2003). In 1888, a report detailed the pathology and clinical presentation of a disease outbreak causing extensive deaths in sheep flocks (Dykes & M'Fadyean, 1888). The disease description matched Jaagsiekte, but observation of parasite eggs led to the belief that *Strongylus* was the causative agent. Nevertheless, this was one of the first reports to suggest the contagious nature of Jaagsiekte and remark the unusual nature of the lung lesions observed. In 1891, further description of the disease and relation to an infectious agent was published (Hutcheon, 1891).

The disease continued to be described in several countries, and a number of terminologies were used to refer to it: sheep pulmonary adenomatosis, jaagsiekte, ovine pulmonary carcinoma (Palmarini & Fan, 2001; York & Querat, 2003). Until ovine pulmonary adenocarcinoma (OPA) was accepted as the term to describe the disease (Palmarini & Fan, 2001).

OPA has been reported in most sheep rearing countries of the world except for Australia and New Zealand (**Fig. 1.1**) (York & Querat, 2003). In 1952 it was successfully eradicated from Iceland after a strict slaughter policy (Pálsson, 1985). The prevalence of OPA varies between countries, and in endemic countries, such as South Africa and the UK, it is believed to account for up to 70% of sheep tumours, and imposes an animal health and economic burden (De las Heras et al, 2003; Griffiths et al, 2010).

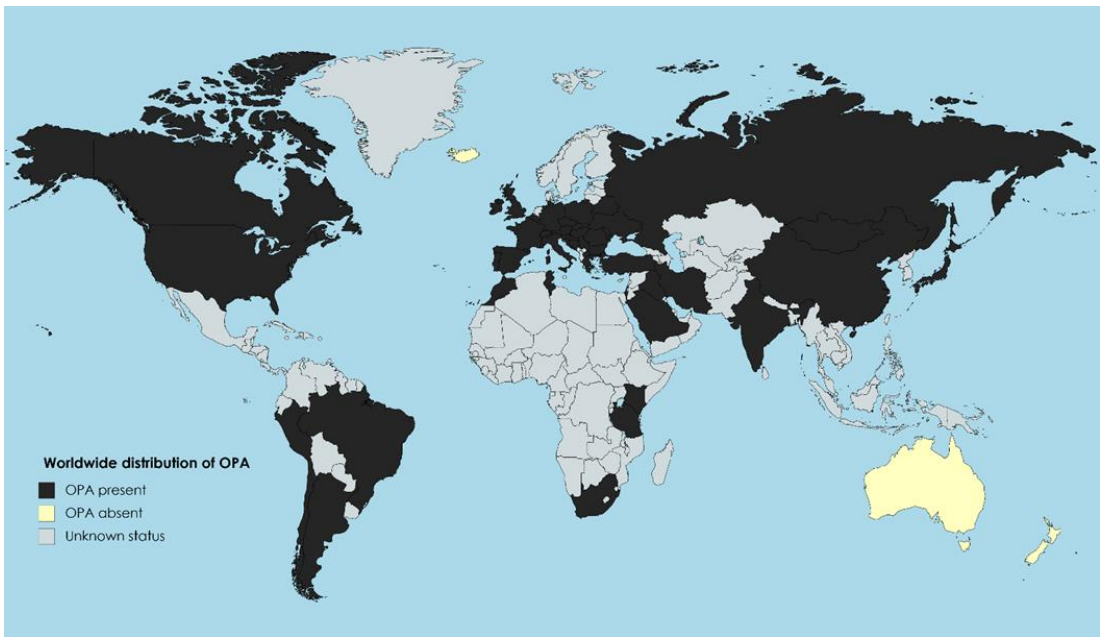

Figure 1.1. OPA distribution in the world. *Countries in which OPA cases have been reported are coloured in black. Countries free of OPA are coloured in yellow. Countries in which the OPA status is unknown are coloured in grey.*

Nonetheless, the true prevalence of JSRV and OPA is not known as not all JSRV-infected animals develop the disease, and many affected animals don't show clinical signs during their life span (Caporale et al, 2005; Salvatori et al, 2004). In addition, OPA is not a notifiable disease in most countries, with some exceptions:

for example, there is a requirement to notify OPA in Northern Ireland (Lee et al, 2017).

OPA mortality rates vary depending on how long the infection has been present in a flock. The epidemic in Iceland reported mortality between 30-50% in the first years after introduction of the disease, but once the disease became endemic mortality dropped to 1-5% (Dungal et al, 1938; Shirlaw, 1959; Tustin, 1969). Longitudinal studies of flocks where OPA is endemic, confirmed disease losses vary between 2-10%, and is estimated that only 30% of sheep in affected flocks develop OPA lesions (Sharp & DeMartini, 2003).

Sheep of all ages are susceptible to OPA, but most clinical OPA cases are seen in sheep 1-4 years old. Clinical disease is rarely seen in animals younger than 9 months (Dungal et al, 1938; González et al, 1993; Hunter & Munro, 1983; Tustin, 1969). In the majority of sheep, clinical signs of OPA are thought to start after a long incubation time, estimated to last between several months to years (Griffiths et al, 2010). OPA cases are observed throughout the year, with a peak incidence in winter (Hunter & Munro, 1983; Tustin, 1969). Although no breed or gender susceptibility to OPA has been demonstrated, it is possible that some breeds show greater or reduced susceptibility to developing the disease. Indeed, reports of affected flocks in Iceland, showed that up to 90% Gottorp breed sheep died but losses in the Aldalbol breed were only 10%, suggesting some inherent resistance to OPA (Dungal et al, 1938).

1.1.3 Pathology of ovine pulmonary adenocarcinoma

OPA tumours derive from proliferating type II pneumocytes, but, other cell types such as club cells, previously known as clara cells, and undifferentiated cells have also been detected in tumours (De las Heras et al, 2014; Martineau et al, 2011; Murgia et al, 2011). When tumours are small they have no clinical manifestations. Clinical signs of OPA start when the tumour is of considerable size and interferes with lung function. Sheep initially appear less active, have difficulty breathing and lose condition. As disease advances, sheep remain alert but respiration becomes deeper and more frequent and is associated with abdominal lift. Excess secretions build-up in the lungs, causing coughing and compromising respiration further (De las Heras et al, 2003). In some cases, lung fluid discharge from the nostrils can

be observed when the animal's head is lowered, and is a pathognomonic symptom of the disease (Cousens et al, 2009; Sharp et al, 1983). Importantly, lung fluid contains infectious JSRV particles that can spread the disease (Cousens et al, 2009; Martin et al, 1976; Sharp et al, 1983). Bacterial infections and visna-maedi virus (VMV), in countries where it is present, are often seen associated with OPA and exacerbate the pathology of OPA (Dungal et al, 1938; González et al, 1993; Markson et al, 1983). Death invariably occurs within a few weeks to months after the start of the clinical disease (Dungal et al, 1938).

Goats are believed to be less susceptible to OPA and suffer from a subclinical form of the disease. No clinical signs of OPA in goats have been described, natural cases of the disease are usually an incidental finding. In experimental infections of goats clinical signs were not observed, even though OPA lesions were apparent at necropsy (Sharp et al, 1983; Sharp et al, 1986; Tustin et al, 1988). OPA lesions in goats have an encapsulated appearance, suggesting cells were infected and transformed but that the virus did not spread within the lung. No metastases have been recorded in affected goats (Caporale et al, 2013).

1.1.3.1 Gross pathology

Pathological changes associated with OPA are usually restricted to the lungs, but thoracic lymph nodes are sometimes affected. Lung lesions vary from small discrete nodules to extensive tumours and are most frequently found in the cranioventral parts of all lung lobes, but any part of the lung can be affected. OPA tumours usually involve both lungs but not to the same extent. There are two histopathological forms of the disease: classical and atypical (De las Heras et al, 2003; Griffiths et al, 2010).

In classical OPA, lungs are enlarged and they do not collapse when the chest is opened at post-mortem. Lung weight is usually increased up to three times compared to normal lungs. Tumours are diffuse or nodular and light purple or light grey in colour, they do not protrude and have increased consistency (Cutlip & Young, 1982; Dungal et al, 1938; Tustin, 1969; Wandera, 1971). There is usually an emphysematous area surrounding the neoplastic lung, and pleurisy is a common finding. When the tumour is dissected, the cut surface exhibits multiple small nodules coalescing, and frothy fluid pours from bronchioles and bronchi

(Cutlip & Young, 1982; Dungal et al, 1938; Rosadio et al, 1988; Sharp & Angus, 1990; Wandera, 1971). In early cases, with no clinical presentation, solitary tumour nodules might be the only finding (Tustin, 1969). In more advanced cases, affected areas are fibrotic and appear white, solid and hard. It is common to find lesions of bacterial pneumonia, abscesses and maedi. Occasionally, small metastases can be seen in regional lymph nodes. In rare occasions, it has been observed in distant organs (Hunter & Munro, 1983; Mackay & Nisbet, 1966; Nobel et al, 1969). The existence of metastases in some animals provides evidence of the malignant nature of OPA.

Atypical OPA is a subclinical form of the disease found at necropsy, in which tumours appear more nodular in early and advanced cases(De las Heras et al, 2003; Garcia-Goti et al, 2000). Tumours are usually found in the diaphragmatic lobes, and are pearly white nodules of hard consistency. When the lung is sectioned, tumours appear very well demarcated and dry. In some cases multiple nodules 0.5-1 cm in diameter are found throughout the lung.

These two forms of OPA can coexist in a flock and in an individual sheep (Garcia-Goti et al, 2000). When analysed, no molecular differences were found between the JSRV associated with classical and atypical OPA. These two disease forms have been suggested to be extremes of disease spectrum rather than two separate forms (Garcia-Goti et al, 2000).

1.1.3.2 Histopathology

Histopathologically, OPA lesions present as epithelial cell neoplastic proliferation in alveolar and bronchiolar regions. These proliferations mostly have papillary appearance and can compress neighbouring alveoli and coalesce as they increase in size (De las Heras et al, 2003). Electron microscopy confirmed the majority of transformed cells constituting tumour tissue as type II pneumocytes, due to the presence of lamellar structures and microvilli in the apical surface of the cells (Cutlip & Young, 1982; Sharp & Angus, 1990). The cytoplasm of these transformed cells stains positively for glycogen deposits (Sharp & Angus, 1990; Wandera, 1971).

Another hystopathological feature are polypoid ingrowths in the terminal bronchioles arising from the bronchiolar epithelium (De las Heras et al, 2003). A moderate to severe inflammatory response, which includes lymphocytes, plasma cells and macrophages, can be seen surrounding affected bronchioles (De las Heras et al, 2003). A common finding is the presence of highly abundant macrophages surrounding neoplastic alveoli, whereas presence of neutrophils might indicate secondary bacterial infections (De las Heras et al, 2003; Sharp & Angus, 1990) . The stroma is generally thin except in advanced cases where it may be fibrotic (De las Heras et al, 2003; Sharp & Angus, 1990) .

The histopathological findings of atypical OPA are similar to those observed in the classical form of OPA. However, atypical OPA has a pattern more often acinar than papillary, and the stroma is more heavily infiltrated by lymphocytes, plasma cells and connective fibres (De las Heras et al, 1992; Garcia-Goti et al, 2000). Lymphoid proliferations can be observed in the neighbouring bronchioles, and fewer cells are positive for JSRV compared to classical OPA (Garcia-Goti et al, 2000). The histopathology of OPA in affected goats and mouflon closely resembles the described findings in sheep (Rajya & Singh, 1964; Sanna et al, 2001).

1.1.3.3 Similarities of OPA with human lepidic carcinoma

Human lepidic carcinoma, previously known as bronchioloalveolar carcinoma, shares several features in common with OPA.

Human lepidic carcinoma is described as an adenocarcinoma with pure bronchioloalveolar growth. It appears as multifocal nodules that evolve towards pneumonia with pulmonary shunting. Neoplastic cells are seen following alveolar septa, described as lepidic spread, and no invasion of stroma, vascular system or pleura is observed (Travis et al, 2015). Lepidic carcinoma is a rare form of lung cancer, and the survival rates for affected patients are better than in other forms of non-small cell lung cancer (NSCLC) (Mornex et al, 2003; Youssef et al, 2015). A more common occurrence is the presence of tumours containing areas of lepidic carcinoma and either papillary or acinar adenocarcinoma, these are known as mixed adenocarcinoma (Travis et al, 2015).

Following human lung cancer classification criteria, OPA would be described as a mixed adenocarcinoma, with a combination of lepidic carcinoma and papillary or acinar growth in advanced stages of the disease (Gray et al, 2019; Youssef et al, 2015)). In contrast, early cases of OPA would be described as minimally invasive carcinomas (Youssef et al, 2015).

In human and ovine malignancies tumours are generally well-differentiated, multifocal and found in the periphery (Palmarini & Fan, 2001; Youssef et al, 2015). Cells derived from tumours express markers of type II pneumocytes and club cells (Liu & Miller, 2007). Moreover, common signalling pathways can be seen activated in NSCLC and OPA: Ras-MEK-ERK1/2 and PI3K-AKT-mTOR (review by Youssef et al (2015)). Increased telomerase activity has also been detected in tumour cells of NSCLC and OPA (Suau et al, 2006).

Similarities between NSCLC and OPA raised the controversial question of whether JSRV or a related virus could be involved in human lung cancer (Linnerth-Petrik et al, 2014; Perk & Hod, 1982). The association of JSRV with the human disease was tested using antibodies raised against JSRV Gag in different human lung cancer types. Some authors reported 30-40% cases cross-reacting with antibodies against JSRV Gag, whereas other authors failed to detect JSRV in human tissue (De las Heras et al, 2000; De Las Heras et al, 2007; Hopwood et al, 2010; Linnerth-Petrik et al, 2014; Miller et al, 2017). The association of JSRV or a related retrovirus to human lung cancer was also tested using PCR and sequencing approaches but no retroviral genome was detected (Berthet et al, 2015; Yousem et al, 2001).

Although JSRV might not be associated with human lung cancer, OPA remains a good model for epithelial neoplasia in human malignancy (Gray et al, 2019; Youssef et al, 2015). In addition, OPA provides the opportunity to study early events of lung cancer, as human samples of early stages are rarely available. Furthermore, although there are murine models of human lung cancer, the use of sheep as model of NSCLC would have several advantages due to closer similarity in physiology and anatomy (Gray et al, 2019; Youssef et al, 2015). Sheep lungs are similar to human lungs in branching pattern, distribution of differentiated epithelial cells and size (**Fig. 1.2**) (reviewed by Gray et al (2019)). Moreover,

sheep are already used as models of human disease in asthma and cystic fibrosis (McLachlan et al, 2011).

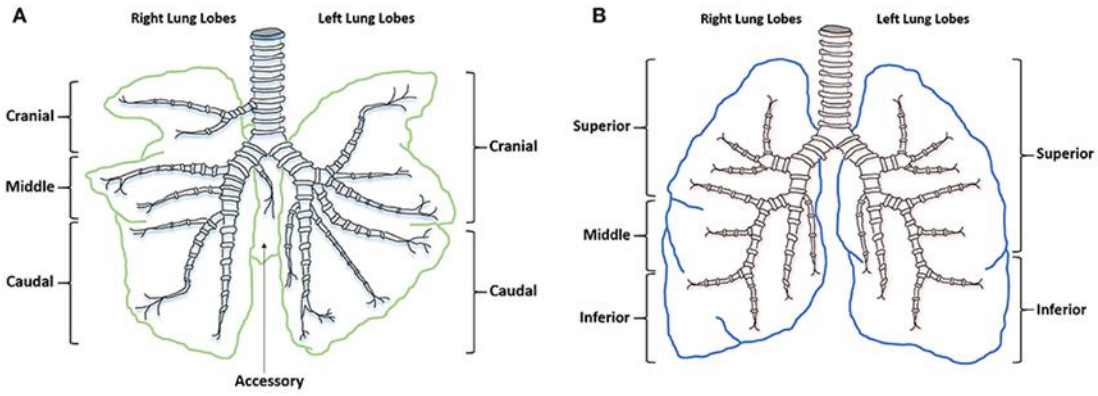

Figure 1.2. A. Anatomy of the ovine lower respiratory tract. B. Anatomy of the human lower respiratory tract. *Reproduced from Gray et al (2019).*

1.1.4 Aetiology of ovine pulmonary adenocarcinoma

The first sign that OPA was caused by a retrovirus was the observation of retroviral particles in the lungs of affected sheep using electron microscopy (Perk et al, 1974). Later on, reverse transcriptase activity and retroviral RNA were detected in tumour extracts. In 1976, particles with reverse transcriptase activity were successfully used to transmit OPA (Martin et al, 1976). Further investigation revealed an inverse relationship between the amount of reverse transcriptase and the time for appearance of clinical signs (Verwoerd 1981). Several years later, these findings were confirmed by the purification of JSRV from lung fluid of affected animals and their use to transmit the disease (DeMartini et al, 1987; Sharp et al, 1983).

JSRV cannot be grown in cell culture and early research focused on methods of isolation of the virus from tumour cells and lung fluid (Verwoerd et al, 1983). Optimal isolation was achieved from sucrose density gradient ultracentrifugation of lung fluid, and extracting the fraction with the peak of reverse transcriptase, which had a density of 1.186 g/ml in JSRV (reviewed by York & Querat (2003)).

The initial description of JSRV as the causative agent of OPA was complicated by frequent coinfection with the lentivirus maedi-visna virus (VMV). The finding that JSRV crossreacts with serum raised against the betaretroviruses mouse

mammary tumour virus (MMTV) and Mason-Pfizer monkey virus (MPMV) allowed distinction between the two (Sharp et al, 1983).

Further research had been hampered by the lack of a culture system for JSRV but, in 1992, the complete genome of JSRV was cloned and sequenced (York et al, 1992). An infectious molecular clone from an UK isolate ($JSRV_{21}$) was later used to produce virus *in vitro* and inoculate sheep to prove JSRV's involvement in OPA (Palmarini et al, 1999a). Production of JSRV particles *in vitro* was achieved by swapping the viral 5' U3 of $JSRV_{21}$ for the human cytomegalovirus (HCMV) immediate early promoter. This allowed for efficient expression of JSRV in 293T cells in culture and release of infectious particles, without the HCMV promoter, in the culture supernatant.

$JSRV_{21}$ particles were used to infect new-born lambs by intratracheal injection, and the experimental findings subsequently confirmed JSRV is sufficient and necessary to cause OPA (Palmarini et al, 1999b). Nevertheless, other agents such as lungworm, ovine herpesvirus and mycoplasma, consistently found associated with natural OPA, might enhance disease progression in the field (Dungal et al, 1938; Dykes & M'Fadyean, 1888; Krauss & Wandera, 1970; Tustin, 1969).

1.1.4.1 Transmission of JSRV

The natural route of JSRV transmission is mainly through the aerogenous route (Tustin, 1969; Wandera, 1971). Aerosols produced by infected animals are inhaled by uninfected animals, and it is believed that close quarters in sheep flocks facilitate this route of transmission. Lung fluid produced by affected animals contains high concentrations of JSRV particles and is considered the most efficient way of spreading the disease (Dungal, 1946).

An increasing number of studies have also reported transmission to newborn lambs via colostrum or milk from infected ewes (Borobia et al, 2016; Grego et al, 2008). Control strategies based on milk and colostrum management have proved effective in preventing virus spread from mother to lamb (Voigt et al, 2007b).

1.2 Retroviruses

JSRV, the causative agent of OPA, belongs to the *Retroviridae* family of viruses. Retroviruses are RNA viruses widespread in nature. They have been found to infect most vertebrate and many non-vertebrate species and are capable of inducing a wide range of diseases (Rosenberg & Jolicoeur, 1997). However, retrovirus which have best-adapted to their hosts do not cause clinical symptoms.

Members of the *Retroviridae* family present similarities in their virion structure, genomic organisation and replication cycle. Retrovirus virions are spherical with diameter between 100-150 nm, and are surrounded by an envelope with spikes composed of virus encoded glycoproteins (Rosenberg & Jolicoeur, 1997).

The internal viral core contains the viral genome and can either be spherical or rod-shaped, depending on the virus. The retroviral genome is between 7-10 kb in length, and composed of two copies of single stranded positive sense RNA (Rosenberg & Jolicoeur, 1997). The viral genomic RNA has similar features to mRNAs: a 5′ methylated cap and polyA tail at the 3′ end. Each of the genomic RNA copies is associated with a specific tRNA molecule at the primer binding site near the 5′ end of the RNA. These tRNA molecules are necessary to initiate the process of reverse transcription (Goff, 2013).

1.2.1 Retrovirus phylogeny and evolution

Retroviruses are classified into seven genera: alpharetroviruses, betaretroviruses, gammaretroviruses, deltaretroviruses, epsilonretroviruses, lentiviruses and spumaretroviruses (**Fig. 1.3**). This classification has recently been updated to categorise members of the spumaretrovirinae subfamily in five genera (Walker et al, 2019).

JSRV is classified as a betaretrovirus like MMTV and human endogenous retrovirus K (HERV-K). Historically, betaretroviruses have been separated into type B and type D virus. Differences between the two groups include core morphology, mode of RNA nuclear export, length of their long terminal repeats (LTRs) and presence of accessory genes. Phylogenetically, type B and type D retroviruses have evolved from an ancestor with the particular ability to assemble Gag particles in the cytoplasm, generating structures called A-type particles. The

ancestor of type D virus is believed to have acquired a new *env* gene, probably from primates. JSRV presents genetic similarity to B-type virus, in *env*, and D-type virus, in *gag* and *pol (York 1992).*

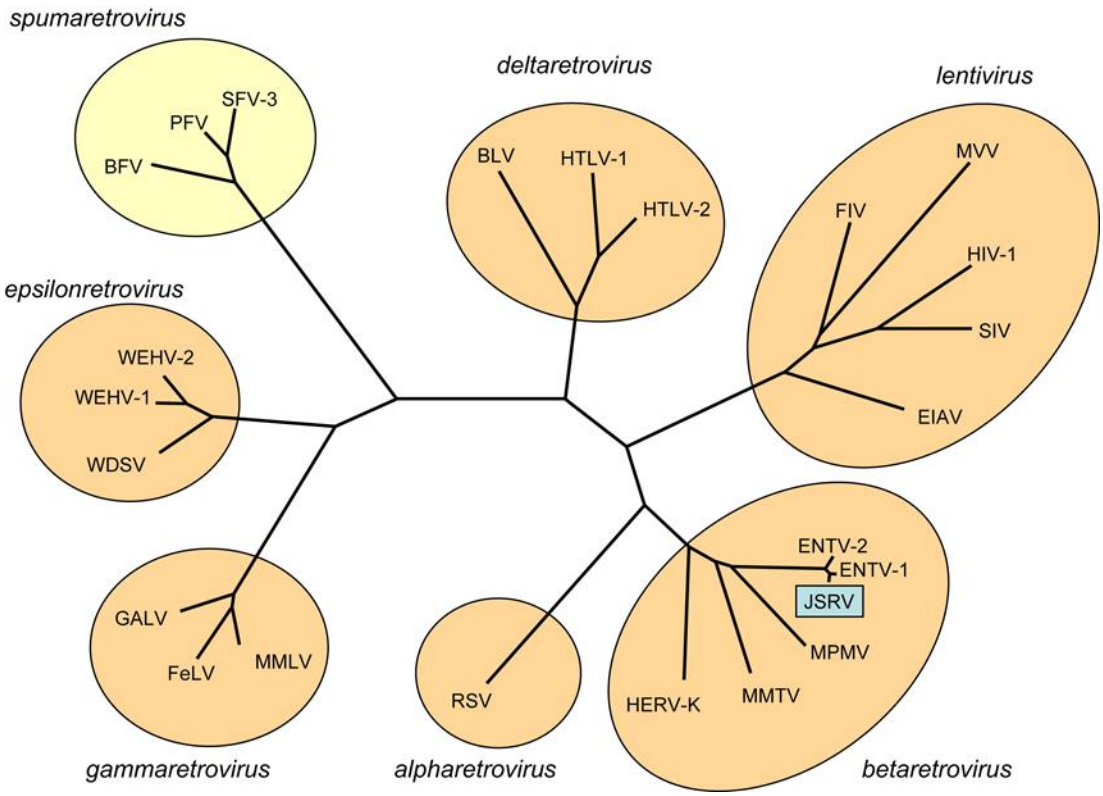

Figure 1.3. Phylogenetic tree of the Retroviridae family, representative members of each genera are shown. *BFV: bovine foamy virus, PFV: prototype foamy virus, SFV-3: simian foamy virus type 3, BLV: bovine leukemia virus, HTLV-1: human t-lymphotropic virus type 1, HTLV-2: human t-lymphotropic virus type 2, FIV: feline immunodeficiency virus, MVV: maedi-visna virus, HIV-1: human immunodeficiency virus type 1, SIV: simian immunodeficiency virus, EIAV: equine infectious anemia virus, ENTV-2: enzootic nasal tumour virus type 2, ENTV-1: enzootic nasal tumour virus type 2, JSRV: jaagsiekte sheep retrovirus, MPMV: Mason-Pfizer monkey virus, MMTV: mouse mammary tumour virus, HERV-K: human endogenous retrovirus K, RSV: Rous sarcoma virus, MMLV: Moloney murine leukemia virus, FELV: feline leukemia virus, GALV: gibbon ape leukemia virus, WDSV: walleye dermal sarcoma virus, WEHV-1: walleye epidermal hyperplasia virus type 1, WEHV-2: walleye epidermal hyperplasia virus type 2. Reproduced from Griffiths et al (2010).*

1.2.2 The retroviral genome

All retroviral genomes contain four main genes encoding proteins in the same order: *gag-pro-pol-env*. The *gag* gene encodes three proteins: the matrix protein (MA), the major capsid protein (CA) and the nucleocapsid protein (NC). The *pro* gene encodes a protease (PR). The *pol* gene encodes reverse transcriptase (RT) and integrase (IN). In some retroviruses there is no separate gene encoding the

protease, in alpharetroviruses PR is encoded by *gag*, and gammaretroviruses and lentiviruses encode PR in the pol gene. The *env* gene encodes the envelope glycoproteins surface (SU), and transmembrane (TM) (Rosenberg & Jolicoeur, 1997).

At the ends of the retroviral genome there are non-coding regions which are essential for their replication cycle. These regions are R, repeated at both ends, U5 present at 5′ and U3 present at 3′ end. The U3 region contains a basal RNA pol II promoter and enhancer sequences. The R-U5 region contains the polyadenylation and cleavage site (Rosenberg & Jolicoeur, 1997).

Retroviruses are considered simple if they encode only the genes described above. Complex retroviruses encode additional virion and non-virion proteins, which they use to regulate viral expression (see below, section 1.2.5).

1.2.2.1 Genetic structure of JSRV

Information on the genetic structure of JSRV comes from sequencing three strains of JSRV: $JSRV_{21}$ (Palmarini et al, 1999a), JSRV-SA (York 1991, York 1992), a South-African isolate, and JSRV-JS7, isolated from the JS7 cell line derived from an OPA tumour from the UK (DeMartini et al, 2001). Sequencing results indicated very low diversity between isolates. $JSRV_{21}$ and JSRV-JS7, strains isolated 10 years apart from the UK, have a 99.2% sequence similarity (DeMartini et al, 2001). Comparison of the UK isolates with JSRV-SA, an isolate from South Africa, revealed 93.3% identity to the South African sequence (DeMartini et al, 2001; Palmarini et al, 1999a).

The JSRV genome is approximately 7455 nt in length. It contains the classical retroviral gene arrangement (*gag-pro-pol-env*) with *pro* encoded in a different ORF than *pol*, and overlapping *gag* and *pol* (**Fig. 1.4**) (York et al, 1992). In addition to the protease, *pro* also encodes a dUTPase, an enzyme that catalyses the hydrolysis of deoxyuridine triphosphate into deoxyuridine monophosphate and prevents incorporation of uracil into viral DNA. The reverse transcriptase enzyme encoded by *pol* has an RNaseH domain which degrades viral RNA once it has been reverse transcribed into DNA (Palmarini & Fan, 2003).

Besides the classical retroviral genes, there is an ORF called *orf-x,* which overlaps with *gag*. *Orf-x* has a different codon usage than other protein coding regions in the JSRV genome and has no homologs in any other betaretrovirus. Nevertheless, *orf-x* is conserved across all JSRV isolates and, in the closely related enzootic nasal tumour virus (ENTV-1) *orf-x* is only interrupted by the presence of two stop codons (Cousens et al, 1999; Walsh et al, 2010). There are two splice acceptor sites close to *orf-x*, suggesting that the mRNA is expressed, but no protein has been detected. The predicted protein is very hydrophobic and contains 4 putative transmembrane domains and, although its function remains unknown, it has low sequence similarity to the adenosine 3A receptor (Auchampach et al, 1997).

Compared to other retroviruses, the envelope protein of JSRV is reported to be more resistant to degradation. In one study, a retroviral vector displaying the JSRV envelope was subjected to six freeze-thaw cycles or 30 minutes at room temperature with no reduction in infectious titre. In contrast, these same conditions decreased the titre of the retroviral vector displaying the murine leukemia virus (MuLV) envelope by 40% and 30% respectively. In addition, JSRV is resistant to lung surfactant, which is consistent with its role in lung colonisation (Coil et al, 2001).

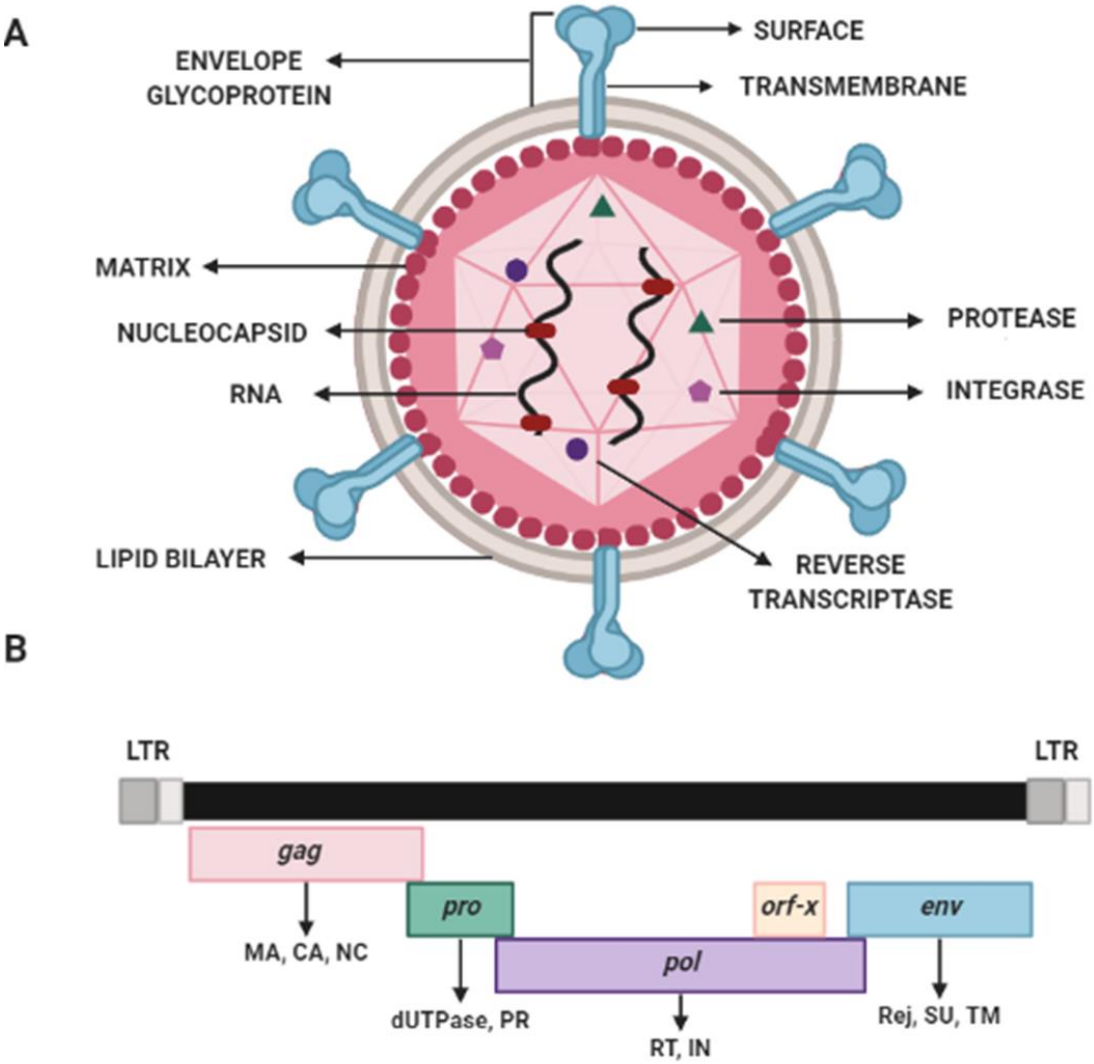

Figure 1.4. JSRV virion structure. *A. Representation of the JSRV virion structure, the main proteins are shown and colour-coded according to the gene they are encoded in. B. Structure of the JSRV genome, ORFs and encoded proteins are depicted. Adapted from Griffiths et al (2010). Produced with Biorender.*

1.2.3 Retroviral replication

Infection proceeds with a retrovirus particle binding one or more specific receptors on the surface of a cell. After binding, the envelope protein performs a conformational change that exposes a fusion domain. Exposure of the fusion domain triggers either fusion of the virion with the cell membrane, or internalisation of the virion by endocytosis and fusion with the endosomal membrane. In both cases, the virus core is released into the cytoplasm where the genome is uncoated (Goff, 2013). JSRV is internalised by endocytosis and requires low pH to trigger fusion (Cote et al, 2008).

After entry into the cell, the viral RNA genome is reverse-transcribed into DNA by the viral reverse transcriptase in the cytoplasm of the cell. During reverse transcription the viral DNA acquires the LTRs at either end, each LTR contains sequences of viral RNA U3-R-U5. LTRs are important for viral replication as they have sequences for initiation and termination of viral transcription and for viral integration (Rosenberg & Jolicoeur, 1997).

All retroviruses, except for lentiviruses, can only gain access to the cell nucleus efficiently during cellular division, when the nuclear membrane is disrupted. It is during division that the viral DNA is transferred to the nucleus and integrated in the cell genome by the integrase, forming a provirus. Once integrated, the provirus uses the host's cell machinery for transcription and translation of viral proteins. Transcription begins at the U3-R junction in the upstream LTR (Rosenberg & Jolicoeur, 1997). The replication cycle of a retroviruses is summarised in **Fig. 1.5.**

For most retroviruses, Env proteins are transcribed from a single spliced mRNA, while Gag and Pol are translated from unspliced viral RNA. Pol proteins are translated from read through of *pro* or *gag* genes by ribosomal shifting or amber suppression. Retroviral proteins are initially translated as polyproteins and cleaved during virion morphogenesis. Cleavage of polyproteins is performed by the viral protease in the case of Gag and Pol polyproteins whereas, a cellular protease carries out the cleavage of Env into SU and TM (Rosenberg & Jolicoeur, 1997).

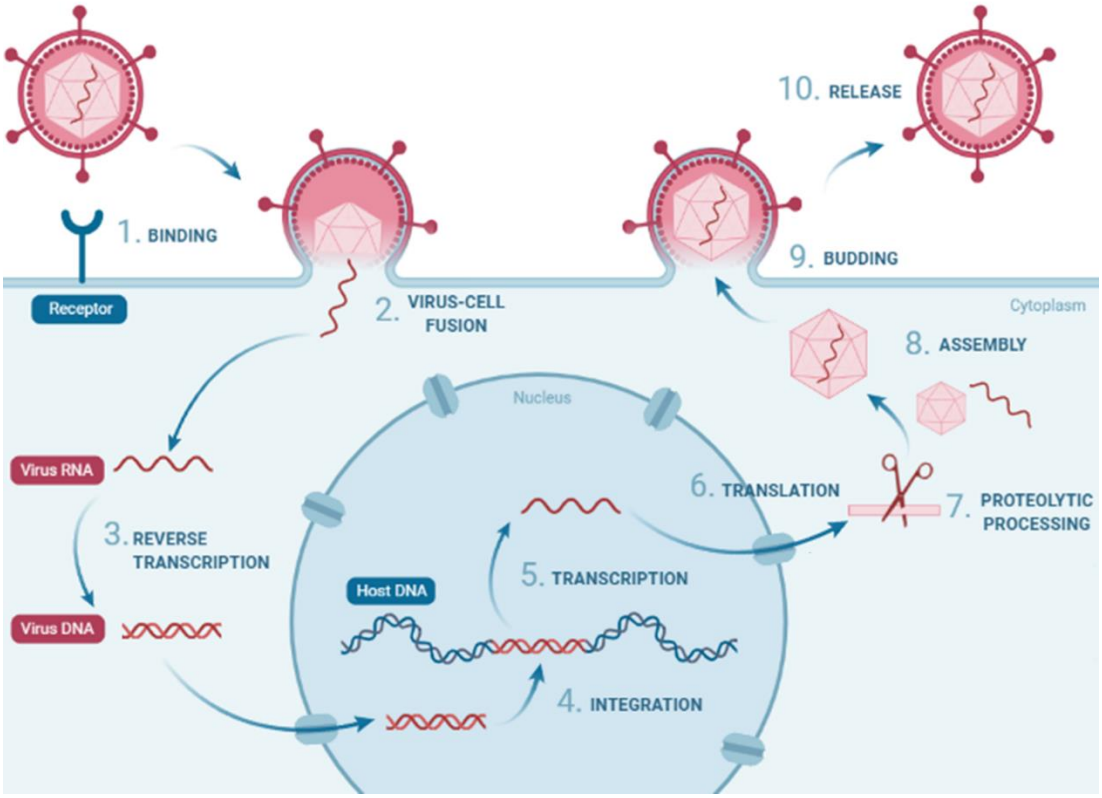

Figure 1.5. Retroviral replication cycle. *Retroviral particles bind to receptors on the cell surface. Binding to receptors triggers fusion of the retrovirus and host cell. In the cytoplasm, the viral RNA is reverse transcribed into DNA. DNA enters the cell nucleus and is inserted into the host cell genomic DNA by action of the integrase. Once integrated, the provirus uses the cell-machinery for transcription and translation of its proteins. After translation, the retroviral protease processes polyproteins, and assembly of virions takes place near the cell membrane. From the cell membrane retroviral particles bud and are released. Produced with Biorender.*

1.2.4 Retroviral receptors and tropism

Viral receptors are important determinants of host range and the type of disease induced. The cellular receptor for JSRV is hyaluronidase-2 (Hyal2), a glycosylphosphatidylinosityl anchored protein ubiquitously expressed on the surface of cells. Interaction with Hyal-2 occurs through Env SU. SU is anchored to the lipid bilayer of the envelope through the transmembrane domain of TM (Miller, 2008; Rai et al, 2001).

In humans, Hyal2, is encoded in a region of the chromosome 3 that is often deleted in cancer, suggesting it might be a tumour suppressor (Rai et al, 2001; Wistuba et al, 1997). In the context of OPA, the interaction of JSRV Env with Hyal-2 has been investigated (Danilkovitch-Miagkova et al, 2003) (section 1.2.6).

Despite the ubiquitous expression of Hyal2, JSRV can only efficiently replicate in secretory cells of the lungs (Palmarini et al, 2000a). In fact, JSRV RNA and DNA has been detected in lymphoid and myeloid cells, but high levels of expression occur only in type II pneumocytes and club cells (Holland et al, 1999). This specificity is due to the other determinant of cell tropism, the viral LTR. The upstream LTR of all retroviruses have a viral promoter and enhancer sequence, including a TATA sequence in U3. The LTR is able to bind cellular factors and RNA polymerase II to initiate transcription. In JSRV's case, only type II pneumocytes and club cells possess the transcription factors necessary to bind the LTR regions and activate them, allowing its efficient expression (McGee-Estrada & Fan, 2007; McGee-Estrada et al, 2002; Palmarini et al, 2000a).

1.2.5 Transcription

Retroviruses that use two mRNAs, full length for translation of *gag pro pol*, and single spliced for translation of *env*, are referred to as a simple retrovirus. Simple retroviruses regulate levels of their mRNAs by cis-acting elements located in the RNAs (Rosenberg & Jolicoeur, 1997). MPMV is an example of a simple retrovirus that contains a cis-acting element, called constitutive transport element (CTE), at the 3′ end. Unspliced RNA is usually not allowed to leave the nucleus. Many viruses, including retroviruses, need to export genomic RNA which is unspliced so various mechanisms have evolved for this. CTE ensures efficient export of unspliced viral transcripts from the nucleus by recruiting cellular factors (Bray et al, 1994). Complex retroviruses, on the other hand, encode additional spliced mRNAs that generate proteins that regulate transport and splicing of other retroviral mRNA species (Rosenberg & Jolicoeur, 1997). Complex retroviruses show a two stage expression pattern, in which regulatory proteins are expressed early, and the canonical genes *gag pol* and *env* are expressed later on (Rosenberg & Jolicoeur, 1997). Examples of regulatory proteins from complex retroviruses include Tat and Rev in HIV-1, and Rem in MMTV (Cullen, 2003; Indik et al, 2005).

Although JSRV was considered to be a simple retrovirus, a trans-acting factor named Rej or SP, encoded in the viral genome, was found to increase viral particle production (Caporale et al, 2009; Hofacre et al, 2009). Rej is located in the signal

peptide region of Env and its function depends on a responsive element located in the 3′ of *env* the viral genome (Caporale et al, 2009; Hofacre et al, 2009). Similarly to the MMTV encoded Rem factor, deletion of *rej* abolished production of Gag polyprotein (Hofacre et al, 2009). Rej was found to be involved in translation of unspliced RNA and transport, but these results were dependent on the cell line used for the study(Nitta et al, 2009).

Analysis of JSRV transcripts revealed a double spliced *env* mRNA from which Rej could be expressed (Hofacre et al, 2009). However, it is thought that Rej could also originate from cleavage of the Env polyprotein, specifically the signal peptide of JSRV Env (Caporale et al, 2009).

Alternative transcripts, apart from the two predicted mRNAs, have also been observed in JSRV infected cells and natural OPA tumours, suggesting their biological relevance. All spliced viral mRNAs derive from a 5′ splice donor site, and subgenomic mRNAs share 3′ and 5′ ends. These transcripts also revealed an alternative splice acceptor upstream of *orf-x,* and a spliced mRNA from which the putative Orf-x protein could potentially be expressed. JSRV transcripts experimentally detected are summarised in **Fig. 1.6** (Palmarini & Fan, 2003; Palmarini et al, 2002).

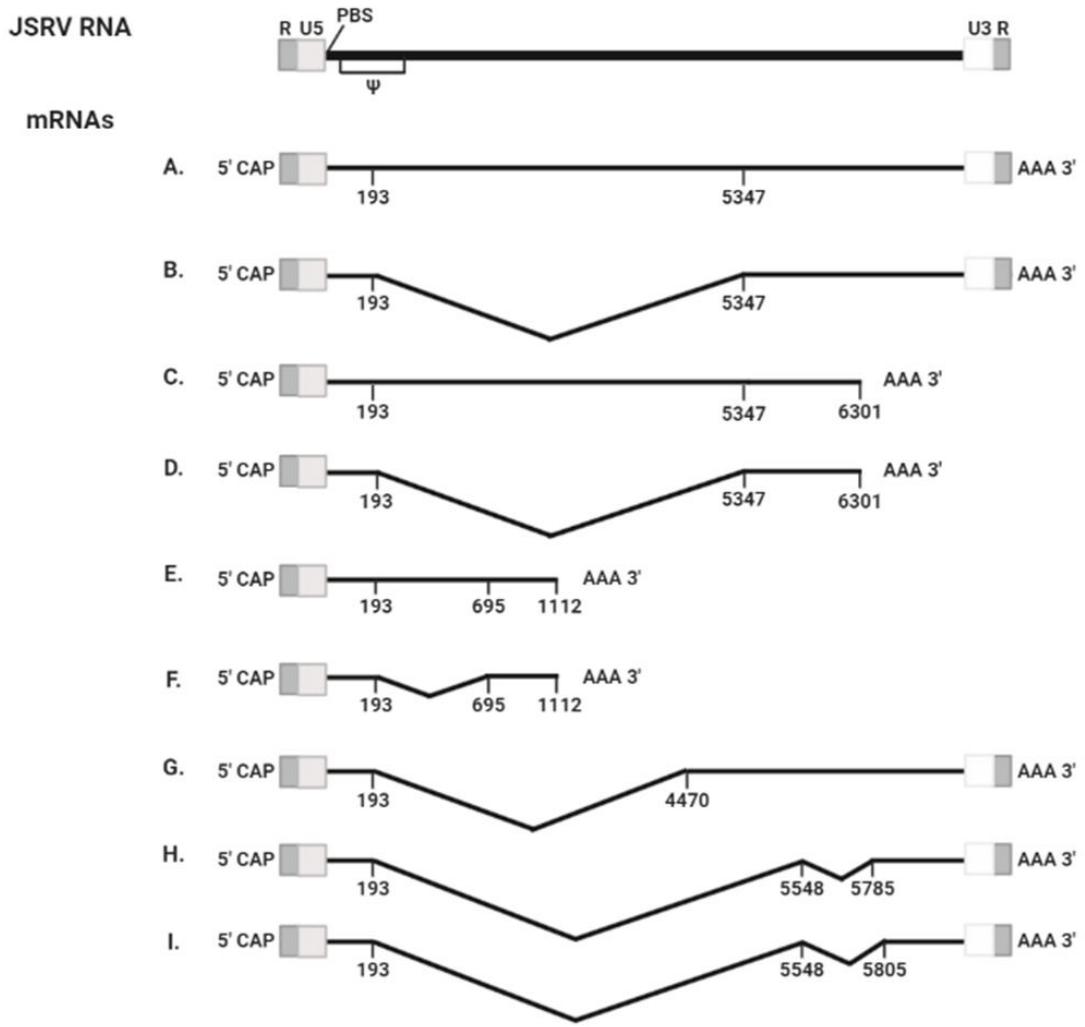

Figure 1.6. Structure of JSRV RNA and mRNA transcripts identified. *A. full-length JSRV mRNA, splice donor (193) and splice acceptor (5347) are indicated. PBS indicates primer binding site. B. Env-spliced transcript. C. full-length transcript prematurely polyadenylated. D. Env-spliced prematurely polyadenylated. E. Prematurely polyadenylated gag. F. Prematurely polyadenylated gag-spliced transcript. G. orf-x/env transcript, prematurely spliced, might be derived from internal promoter. H and I. double spliced mRNA species that might give origin to Rej protein from the signal peptide of env. Adapted from Palmarini & Fan (2003) and Hofacre et al (2009). Produced with Biorender.*

1.2.6 Retroviral transformation and oncogenesis

Many retroviruses are known for their capacity to induce transformation and oncogenic events in their hosts. Oncogenic retroviruses have historically been categorised depending on how fast they induce transformation. One group is the acute transforming retroviruses, which induce neoplasms rapidly. Usually, these viruses can induce tumours within a few weeks of infection and tumours are

generally polyclonal. Acute transforming retroviruses can also transform cells in culture. These properties are associated with the presence of viral oncogenes. Most retroviral oncogenes are derived from cellular genes (proto-oncogenes). Viral oncogenes have mutations compared to cellular proto-oncogenes that result in uncontrolled stimulation of cell growth (Rosenberg & Jolicoeur, 1997). These oncogenes are not required for viral replication, most acute transforming retrovirus are replication deficient and require co-infection with a replication competent retrovirus (Helper) (Rosenberg & Jolicoeur, 1997). This is the case with Abelson murine leukemia virus (A-MuLV), which encodes a modified version of the proto-oncogene c-*abl* (Gallo et al, 2012; Poirier et al, 1988).

Non-acute retroviruses are the second group of oncogenic retroviruses. They are replication competent and do not have oncogenes. They induce tumours slowly, taking months to years, and are not able to transform cells in vitro. They usually cause oncogenesis by insertional activation of proto-oncogenes. Insertion sites are usually random but there have been found to be preferred sites (Rosenberg & Jolicoeur, 1997). For instance, avian leukosis virus (ALV) causes lymphomas by integrating close to c-myc (Hayward et al, 1981). Activation of proto-oncogenes can be mediated by insertion close to a cellular proto-oncogene, putting the proto-oncogene under transcriptional control of the viral LTR (Hayward et al, 1981). Another activation mechanism is enhancer activation, in which the viral enhancer influences the cellular promoter of the proto-oncogene activating its expression, the insertion site can be distant from the gene (Payne et al, 1982). Non-acute retroviruses require longer time to cause tumourigenesis, because more rounds of infection and insertion are needed to end up activating a proto-oncogene. In addition, to successfully initiate tumourigenesis, activation of more than one proto-oncogene or inactivation of more than one tumour suppressor might be needed (Bear et al, 1989). The prototypic betaretrovirus MMTV is a non-acute transforming retrovirus (Ross et al, 1997).

Although JSRV requires a long incubation period to cause tumours in natural cases, it also has features that are more in line with those of acute transforming retrovirus. In experimental settings, JSRV is able to produce tumours in short periods of time, normally around 6 weeks but has been reported to produce

tumours in 10 days (Sharp et al, 1983; Verwoerd et al, 1983; Verwoerd et al, 1980). These differences in incubation period are associated with the sheep's age at infection and can be explained by the higher number of proliferating type II pneumocytes in young lambs (Martineau et al, 2011; Murgia et al, 2011; Salvatori et al, 2004). Moreover, OPA tumours are generally multifocal, a feature shared with acute transforming retroviruses.

However, at first sight, there were no obvious oncogenes encoded by JSRV's genome. Another important feature of acute transforming virus is their capacity to transform cells *in vitro*. The ability of JSRV to transform cells in culture was investigated by transfecting NIH 3T3 cells in culture with $pJSRV_{21}$, which resulted in transformation (Maeda et al, 2001). JSRV DNA could be detected in all transformants and similar results were achieved when the 208F cell line was used (Rai et al, 2001).

As *orf-x* had no known function, it was thought to be a good candidate as JSRV's oncogene. Nevertheless, mutations in *orf-x* did not affect transforming capacity *in vitro* or, as later shown, *in vivo* (Caporale et al, 2006; Cousens et al, 2007; Maeda et al, 2001; Wootton et al, 2005).

Identification of JSRV's oncogene was made by deleting *gag* and *pol* and mutating *orf-x*, leaving *env* intact. Transfection with this mutated clone was still sufficient to induce transformation, proving that *env* was the oncogene. JSRV's *env* transforming capacities were the first report of a functional retroviral *env* gene able to transform cells (Maeda et al, 2001). In subsequent experiments JSRV *env* was proven to form tumours when delivered by viral vectors into nude mice (Linnerth-Petrik et al, 2012; Wootton et al, 2005) and into sheep (Caporale et al, 2006; Cousens et al, 2007), and Env protein alone was later on found to be sufficient to cause tumours in mice (Wootton et al, 2005).

In summary, JSRV encodes an oncogene able to transform cells *in vitro*, a feature characteristic of acute transforming retrovirus. However, in animal disease, the course of the disease can be slow, more characteristic of non-acute transforming virus.

Since the demonstration that JSRV Env is oncogenic, several studies have investigated the domain involved in transformation, as well as the mechanism of transformation that JSRV uses. TM was found to be necessary for transformation, in particular the cytoplasmic tail of TM was found to be essential to drive cell transformation (Cousens et al, 2007; Liu & Miller, 2005; Palmarini et al, 2001). The cytoplasmic tail of TM possesses an YXXM domain, a putative binding site for phosphoinositide 3-kinase (PI3K/p85), activation of PI3K could lead to activation of transformation pathways in the cell. In this TM domain, mutation of Y590 to Y590F abolished transformation, but not infection, of sheep choroid plexus cells (Palmarini & Fan, 2003). Mutation of other tyrosine residues in TM did not affect transformation (Palmarini et al, 2001). However, in pull-down experiments the interaction between PI3K and Env TM has never been detected (Hsu et al, 2015; Liu et al, 2003; Liu & Miller, 2007). Y590 might be involved in trafficking Env to the cell surface and, thus, have an indirect role in transformation by ensuring its localisation at the appropriate site in the cell (Palmarini et al, 2001).

Despite TM being essential for transformation other domains within the Env protein might also participate in transformation. For example, some experiments suggest that SU could participate in transformation independently of TM (Hofacre & Fan, 2004), and some authors have suggested that SU might interact with toll like receptor 4 (TLR4) (cited as unpublished data in Hofacre & Fan (2004)). *In vivo*, both TM and SU have been shown to be necessary to induce oncogenesis in sheep. A report also suggested involvement of the Rej protein in transformation, after discovering that deletions in the signal peptide, which should not have affected the SU sequence, abolished transformation (Hofacre et al, 2009). However, co-transfection of N-terminal *env* mutants with *rej* did not result in transformation (Hofacre et al, 2009).

Env JSRV was found to be essential for viral replication, something not observed for other viral oncogenes. The infectious but transformation deficient Y590F mutant was not able to cause tumours *in vivo,* indicating both functions might be encoded by the same protein in JSRV (Cousens et al, 2007). It has been hypothesised that JSRV's oncogenic capacity might have developed as a mechanism to replicate efficiently.

The mechanisms by which JSRV Env causes cell transformation appears to differ depending on cell line and culture conditions used (Hofacre & Fan, 2010; Liu & Miller, 2007). For instance, it is believed that the cytoplasmic tail of TM interacts with an unidentified molecule and leads to activation of PI3K/Akt and MAPK signalling pathways. In a more recent study, it was reported that activation of the Akt signalling pathway was a result of binding between Env and RALBP1, an interaction found using the yeast two-hybrid system. Nevertheless, several other proteins were identified in the same screen but have not been characterised further (Monot et al, 2015). Interaction of JSRV Env with a nuclear-localised zinc finger protein (zfp111) has also been described, and reported to play a role in transformation of rodent fibroblasts (Hsu et al, 2015)

Activation of Akt and ERK has been shown in JSRV Env transformed cell lines as well as tissues obtained from natural cases of OPA and in OPA-derived cell lines (Cousens et al, 2015; De Las Heras et al, 2006; Maeda et al, 2005; Palmarini et al, 2001). However, relevance of each of these pathways appears to depend on the system used for study, reviewed in (Liu & Miller, 2007). Akt activation has been shown to be PI3K dependent in some cell lines, but was found to be independent of PI3K in NIH 3T3 cells (Maeda et al, 2003), suggesting that in those cells PI3K is not essential for transformation, and activation of Akt might be driven by another factor. In addition, in chicken fibroblasts (DF-1) mutation of Y590F in TM did not abolish transformation, suggesting again that other interactions might be responsible for initiation of the transformation process (Allen et al, 2002). Phosphorylation of ERK1/2 is detected in MDCK cells transformed by JSRV Env, but not when the 208F or NIH 3T3 cell lines are transformed by JSRV Env (Liu et al, 2003; Maeda et al, 2005). Nevertheless, in a study, use of inhibitors of the pathway abolished transformation of these cells, suggesting that the pathway is of importance for JSRV Env driven transformation in NIH 3T3 and 208F cells (Maeda et al, 2005)

In human bronchial epithelium cells (BEAS-2B) another mechanism was found to explain JSRV Env induction of oncogenesis. Hyal2 binds RON growth factor receptor, but binding of Env to the receptor Hyal2 releases RON, increasing its kinase activity and allowing it to activate signalling pathways such as the Akt and

MAPK pathways (Danilkovitch-Miagkova et al, 2003). However, RON is not expressed in alveolar cells of the lung (Danilkovitch-Miagkova et al, 2003), so the relevance of this mechanism in the natural JSRV infection of sheep lung is unclear.

Telomerase activation was reported in lung tissue of OPA affected sheep and epithelial cells isolated from OPA tumours (Suau et al, 2006). Telomerase might play a role in inhibiting cell senescence in JSRV Env transformed cells and, as Akt is an activator of telomerase, the authors suggested that Akt activation might drive telomerase activation in OPA tumours (Suau et al, 2006). After initial activation of signalling pathways by JSRV Env and induction of proliferation, more mutations or lesions might be required for OPA to develop, a scenario consistent with the long incubation period of OPA. Pathways such as the Wnt, EGFR and hippo pathways were reported to be upregulated in a sequencing study of experimental cases of OPA (Karagianni et al, 2019). Insertional mutagenesis might also potentiate the oncogenic effect of JSRV Env.

In summary, the pathways that have been reported to be activated in the cell lines transformed in vitro with JSRV Env are PI3K-Akt, Raf-MEK-MAPK and RON-Hyal2 (Hofacre & Fan, 2010; Liu & Miller, 2007). These pathways are summarised in **Fig. 1.7**. Development of an *in vitro* model that more closely resembles *in vivo* infection, for example using ovine type II pneumocytes, would provide valuable information on which of the signalling pathways and interactions are relevant for JSRV sheep infections and OPA.

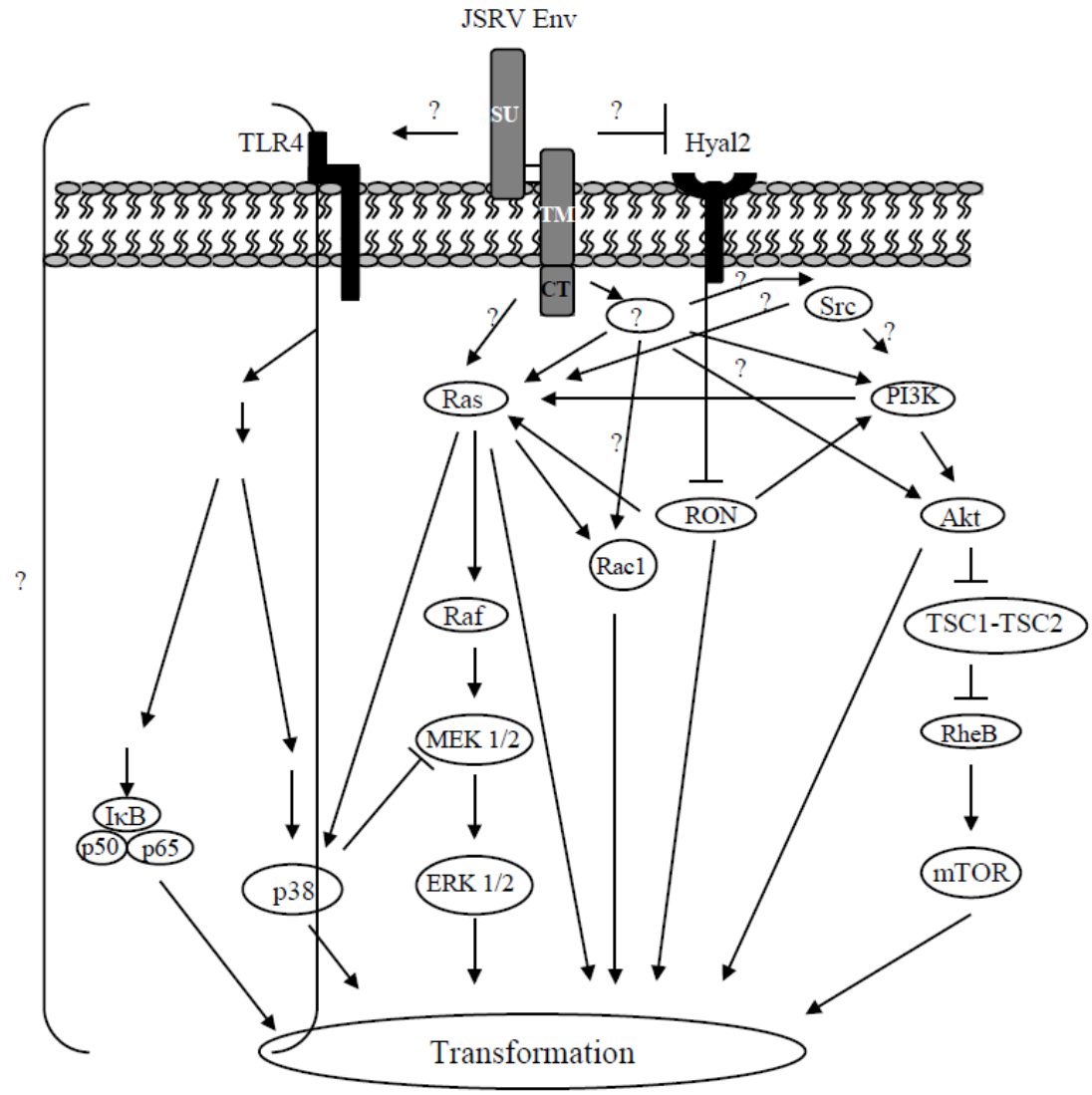

Figure 1.7. Signalling pathways activated by JSRV Env in various cell lines. *Reproduced from Hofacre & Fan (2010).*

1.2.7 Endogenous retrovirus in sheep

Endogenous retroviruses are a common finding in animal genomes. For example, 8 to 10 % of the mammalian genome derives from endogenous retroviruses (Mager & Stoye, 2015). Several families of endogenous retroviruses have been described in the sheep genome, including families related to exogenous gammaretroviruses and betaretroviruses. Some of these, are very closely related to JSRV, with over 90% nucleotide similarity with JSRV in most of their genome, these are called endogenous JSRV (enJSRV) (Palmarini et al, 2004). enJSRVs

are found in the genome of the *Ovis* and *Capra* genera. The sheep genome was initially thought to contain around 27 copies of enJSRV but, in a more recent analysis 462 enJSRV insertion sites were found in the genome of members of the *Ovis* genus (Arnaud et al, 2008); (Cumer et al, 2019).

Of the initial 27 sheep enJSRV, most have at least one of the genes interrupted by stop codons, but at least five enJSRV have intact ORFs for all genes, and encode viral particles (Black et al, 2010). Although the genome sequences of JSRV and enJSRV are highly similar, there are short regions of variability (VR), known as VR 1, 2 and 3 within the *gag* and *env* genes (Palmarini et al, 2000b). In addition, the U3 region of the LTR also differs between all enJSRV and JSRV, likely reflecting different cell type transcriptional specificity (Palmarini et al, 2000b).

enJSRVs are transcriptionally active, and their transcripts have been detected in sheep tissues. Expression of enJSRV is most abundantly detected in the female reproductive tract and fetal tissue, where the mRNA of *env* was found to be essential for trophectoderm elongation (Dunlap et al, 2006; Varela et al, 2009). enJSRV transcripts have also been detected in thymus, lungs, kidney, bone marrow, spleen and leukocytes (Palmarini et al, 1996b). Distinction between enJSRV and JSRV transcripts can be determined thanks to the presence of the SCaI restriction site in CA and the NdeI in SU present in JSRV but not in enJSRV, or by PCR of the U3 region (Bai et al, 1996; Palmarini et al, 1996a).

In general, endogenous retroviruses are thought to have no negative effects for the host, but in some cases they may have a role in some pathologies and they may reactivate or recombine with exogenous retroviruses. In the case of enJSRV, no evidence has been found to suggest a direct contribution to the pathogenesis of OPA. Nevertheless, the possibility that there is gene complementation between enJSRV and JSRV cannot be excluded (DeMartini et al, 2003).

In some species, endogenous retroviruses have been reported to have protective effects against some infections, for instance an ancient endogenous retrovirus found in the mouse genome interferes with MuLV infection (Yap et al, 2014). In enJSRV, alleles of enJSRV-20 and enJS56A1 have been found to interfere with Gag production and virus assembly (Arnaud et al, 2007; Mura et al, 2004; Murcia

et al, 2007). These two loci have alleles with a mutation in *gag* (arginine to tryptophan), which results in a Gag protein that interferes with the exogenous Gag protein during replication of JSRV (Arnaud et al, 2007; Murcia et al, 2007). Specifically, the enJS56A1 Gag protein is thought to be misfolded and form multimers with JSRV Gag (Arnaud et al, 2007). These multimers are proteosomally degraded, but their formation also prevented JSRV Gag from efficient trafficking to the cell surface and release of JSRV particles (Arnaud et al, 2007). The protective allele of enJSRV-20, but not enJS56A1, is found in sheep populations. In addition, due to the correlation observed between the number of enJSRV duplications and number of protective alleles, both alleles are thought to have a dose dependent effect (Armezzani et al, 2011; Cumer et al, 2019).

1.2.8 Immune response to JSRV

OPA is characterised by the absence of a strong humoral response against JSRV. Low titres of neutralising antibodies against JSRV Env have been found in some experimentally infected lambs (Caporale et al, 2013; Hudachek et al, 2010), and in naturally infected sheep (Griffiths unpublished). In addition, one study suggested that neutralising antibodies against JSRV Env could be transferred through colostrum (Hudachek et al, 2010).

Immunisation of sheep with JSRV CA or SU and an adjuvant led to production of antibodies, suggesting that sheep can mount an immune response to JSRV infection and are not intrinsically unresponsive (Sharp & DeMartini, 2003). The explanation for the general lack of antibodies against JSRV in infected sheep is suggested to be related to enJSRV encoded in the sheep genome. Expression of enJSRV early during development is believed to lead to elimination of JSRV specific T-cells during T-cell ontogeny. This hypothesis has not yet been experimentally validated, but enJSRV expression was detected in fetal thymus (Spencer et al, 2003).

Moreover, JSRV might interfere with the host immune responses. JSRV infects a wide range of myeloid and lymphoid cells, with the greatest proviral burden in macrophages, B cells, CD4 T lymphocytes and CD8 T lymphocytes. In natural cases of OPA, a marked peripheral neutrophilia and lymphopaenia affecting CD4 T lymphocytes can be observed, that may be attributed to coexisting bacterial

infections (Holland et al, 1999; Rosadio & Sharp, 1992; Summers et al, 2002). Alveolar macrophages in OPA affected sheep lungs have been found to produce interferon gamma, and tumour cells present downregulation of MHC-I factors. In addition, the overproduction of surfactant proteins by tumour cells might have immunomodulatory effects and contribute to the inefficient local immune response against JSRV (Summers et al, 2005).

A recent transcriptome analysis of OPA provided evidence of transcriptional changes relating to macrophage function, but relatively little evidence for lymphocyte related gene expression or for activation of type I interferon response. These results suggested that local events in the lung may also play a role (Karagianni et al, 2019).

1.3 Models of OPA

A number of i*n vivo* and *in vitro* models of OPA have been developed to facilitate the study of OPA and the oncogenic mechanisms used by JSRV. These models continue to provide valuable information on OPA and JSRV, and use of these models is especially important in the absence of a permissive cell line to grow JSRV *in vitro*.

1.3.1 Experimental models of OPA

An optimal procedure to induce OPA in experimental sheep was developed based on results of early studies. The procedure involves delivering JSRV particles to newborn lambs by intratracheal inoculation. Clinical signs of the disease are typically seen within several weeks to months. The incubation time until development of clinical signs is linked to both the lamb's age at inoculation and the JSRV dose used at infection (Salvatori et al, 2004).

The virus source used for infection are tumour extracts, virus isolated from lung fluid of OPA affected animals, or $JSRV_{21}$ produced *in vitro* by transfection of 293T cells with $pCMV2JSRV_{21}$ (Martin et al, 1976; Palmarini et al, 1999a; Tustin, 1969; Wandera, 1971). Pathological findings of experimentally infected animals closely resemble early cases of natural OPA cases and invariably have characteristics of the classical OPA form. In experimental OPA, multifocal discrete nodules, rather than large tumour masses commonly found in natural disease, are usually

observed. This is likely due to the fact that experimental cases are culled, for welfare reasons, before advanced lesions can develop, so they represent an earlier point in pathogenesis (Griffiths 2010). Pulmonary lesions consist of diffuse grey nodules with lung fluid being a histopathological finding rather than a clinical sign. The major difference between natural cases and experimental cases is the shortened incubation time. This is due to the increased number of proliferating type II pneumocytes present in newborn lambs compared to adults, meaning greater replication efficiency for JSRV (Caporale et al, 2005; Salvatori et al, 2004).

OPA has also been induced experimentally in goats. However, no clinical signs where observed in the case of goats, despite some having pulmonary lesions when examined post-mortem. Nevertheless, pulmonary lesions in JSRV-infected goats presented a slightly different histological pattern compared to sheep, suggestive of restricted viral spread in the goat lung (Caporale et al, 2013). Other animal species have been resistant to experimental JSRV infection and OPA induction (Sharp & DeMartini, 2003).

1.3.1.1 Small animal models of OPA

In mice, production of tumours lined by epithelial cells that resemble OPA tumours, was successfully achieved when tumour cells were transplanted in athymic nude mice (Verwoerd et al. 1977; Zimber et al. 1984).

Adeno-associated virus type 6 (AAV6) vectors encoding JSRV *env* were also used to infect immunodeficient mice and were found to drive long-term expression of Env, and lung tumour formation in 2-6 months. Lesions observed in mouse lung resembled those observed in OPA affected sheep and cells expressed SP-C, but the vectors used were also found to drive tumour formation in liver and endothelial cells (Wootton et al, 2005; Wootton et al, 2006). In subsequent studies, use of the AAV6 vector encoding JSRV *env* to infect immunocompetent mice also resulted in tumour formation (Linnerth-Petrik et al, 2012). The murine Hyal2 is not able to act as a receptor of JSRV, but the formation of lung tumours in mice infected with the vector encoding JSRV *env* suggested that interaction between JSRV Env and Hyal2 is not necessary to drive transformation, at least in mice (Wootton et al, 2005).

In vivo studies in mice have provided insight into the pathogenesis and molecular transformation driven by JSRV. Moreover, the use of small animal models has advantages associated with cost and time, added to the greater number of molecular biology reagents available to perform assays in mice compared to sheep. Nevertheless, biochemical and anatomical differences between the lungs of these two organisms, and the fact that JSRV is not able to infect mouse cells, could mean that findings in a mouse system might not represent natural cases of JSRV Infection (Youssef et al, 2015).

1.3.2 *In vitro* models of OPA

As previously stated, there is currently no permissive cell line that supports JSRV replication *in vitro*. Difficulties in establishing a culture system to grow JSRV are due to the nature of its main target cells, type II pneumocytes, which are difficult to isolate and readily dedifferentiate *in vitro,* losing their phenotype and capability to allow efficient JSRV replication (Dobbs, 1990; Gruenert et al, 1995; Johnson et al, 2011; Mason & Shannon, 1997). Nevertheless, several *in vitro* systems have been used and have provided valuable information on JSRV.

Initially, the possibility to establish an *in vitro* model was studied by infecting various sheep cell lines with $JSRV_{21}$. OAT-T3 cells (testes), CP cells (ovine choroid plexus), turbinate cells (FLT) and intestinal carcinoma cells (ST6) were infected with $JSRV_{21}$ (Palmarini et al, 1999a). Establishment of infection was observed: JSRV DNA was detected by PCR, levels of JSRV DNA increased with passages and infected cells released active RT (Palmarini et al, 1999a). Moreover, infection could be passed to other cells by co-cultivation. However, the amount of virus produced was very low and not a good source for new virus (Palmarini et al, 1999a).

Infection of sheep cell lines with JSRV, evidenced that the receptor was present in many cell types, but suggested that other specificity determinants were in place. The other determinant of cell specificity was then investigated: JSRV LTR activation was compared in several cell types and found to be highest in lung epithelial cell lines. In particular high LTR activity was observed in MLE-15 and MtCC1-2 (mouse cell lines derived from type II pneumocytes and Club cells) (Palmarini et al, 2000a). LTR activation was reduced in H441, H358, A549 (cell

lines derived from human lung adenocarcinoma) and JS7 (Palmarini et al, 2000a). LTR expression was found to correlate with SP-B expression (Palmarini et al, 2000a). However, lung epithelial cell lines readily dedifferentiate *in vitro,* losing surfactant production and their ability to trigger efficient LTR activation. On the other hand, the use of human lung cancer derived cell lines, might not be appropriate because they are already transformed: their signalling pathways are deregulated and might not respond to JSRV infection the way *in vivo* sheep cells would.

Because no permissive cell line for JSRV replication could be found, experiments focused on studying JSRV Env transformation. Various cell lines have been used as *in vitro* models of JSRV Env transformation: NIH 3T3 cells (mouse embryonic fibroblasts), 208F cells (rat embryonic fibroblasts), MDCK cells (dog epithelial kidney cells), DF-1 cells (chicken embryo fibroblasts) and BEAS-2B cells (human bronchial epithelium cells) (Allen et al, 2002; Danilkovitch-Miagkova et al, 2003; Liu et al, 2003; Liu & Miller, 2005; Palmarini et al, 2001). Use of these cell lines has provided information on activated pathways by JSRV Env transformation, as described in 1.2.6. Nevertheless, mechanisms of transformation vary between cell lines and might not reflect transformation events *in vivo.* In addition, use of the full-length virus would provide important information on the activation of the first signalling molecules after JSRV entry into the cell. For this reason, investigation on models that can better resemble JSRV infection and transformation *in vivo* is of serious importance.

1.3.2.1 OPA-derived cell lines

Primary cells derived from OPA tumours have been successfully cultured *in vitro* (Archer et al, 2007; DeMartini et al, 2001; Jassim et al, 1987; Suau et al, 2006). These cells expressed type II pneumocyte markers such as SP-C and alkaline phosphatase activity (Archer et al, 2007) and expressed JSRV. Nevertheless, maintenance of these cells in culture resulted in morphological changes, rapid loss of type II pneumocyte markers and inability to maintain JSRV expression (Archer et al, 2007; Johnson et al, 2011).

Interestingly, the OPA cell line JS7, which has an integrated copy of JSRV in the genome, exhibits different properties when grown in monolayer or 3D culture.

When grown in a monolayer, JS7 is not able to support JSRV expression of proteins from the LTR, and does not express markers of type II pneumocytes. However, growth of JS7 in 3D culture resulted in detection of SP-A and SP-C expression as well as JSRV RNA detection (Johnson et al, 2011). In 3D culture, JS7 cells were able to form spheres and establish cell to cell interactions (Johnson & Fan, 2011). These interactions are particularly important for epithelial cells and help maintain polarisation. In contrast, in 2D culture, tight junctions and polarisation were lost (Archer et al, 2007; Johnson et al, 2011). These results indicated that 3D growth of JS7 cells replicates characteristics of type II pneumocytes, and might represent events in sheep lung with more accuracy. However, viability of the JS7 cells in 3D culture decreased significantly after 15 days in culture, and SP-C expression was lower than in primary type II pneumocytes (Johnson & Fan, 2011). These findings indicate that optimisation of a method to culture lung epithelial cells is still needed.

1.3.3 *Ex vivo* models of OPA

An *ex vivo* system to model JSRV infection has been developed using precision cut lung slices from healthy sheep, which can be maintained in culture for at least three weeks (Cousens et al, 2015). JSRV has been shown to infect type II pneumocytes within the lung slices, successfully replicating to generate new viral particles and stimulate cell proliferation. Infected cells within the lung slices express activated ERK1/2 and Akt, similarly to infected cells *in vivo* (Cousens et al, 2015).

This model allows working with the natural host of JSRV and its main target cells, replicating many features observed *in vivo* and providing results that are more likely to reflect events of the *in vivo* infection. In addition, lung slices maintain tissue architecture and the diversity of cells seen in sheep lung, which might also play a role in disease development (Cousens et al, 2015). These features, as well as being able to study transformation caused by JSRV rather than just JSRV Env, might provide valuable information on early events that drive transformation.

1.4 Disease Control

To date, there are no treatment or effective methods for controlling the spread of OPA (Gray et al, 2019; Griffiths et al, 2010). During the incubation period of the

disease, varying from months to years, affected sheep appear normal but can transmit the disease.

Screening and culling strategies have been effective in controlling the spread of other diseases, but require a sensitive and specific diagnostic test that allows identification of infected animals (Synge & Ritchie, 2010). In OPA, such a test remains elusive. Due to lack of JSRV-specific antibodies no serological tests are available, and PCR tests are not reliable in early stages of the disease (De Las Heras et al, 2005; Ortin et al, 1998). Currently, the best strategy to avoid introducing OPA in an OPA-free flock is to quarantine new animals for several months (Griffiths et al, 2010). OPA affected animals can also be isolated, and contaminated areas disinfected to prevent the spread of OPA (Cousens et al, 2009). In high-value flocks, embryo transfer can be used to prevent transmission from infected ewes to lambs (Parker et al, 1998). However, these strategies are expensive and might not be practical for all farms (Griffiths et al, 2010).

1.4.1 Diagnosis of OPA

Even though there are no serological tests available to detect OPA, several diagnostic tests have been developed to diagnose OPA based on molecular or pathology techniques.

PCR tests to detect JSRV DNA in blood have proved to be highly specific and able to distinguish between enJSRV and exJSRV but have shown low sensitivity in the field setting, particularly in early stages of the disease when the virus load is low (Lewis et al, 2011). This high false-negative rate makes the test unreliable for use in individual animals, but it continues to be successfully used to gather epidemiological information and to identify infected flocks (Griffiths et al, 2010). Use of this PCR test in peripheral blood from sheep of OPA affected flocks revealed that 80% of sheep that were not affected by OPA, but in contact with affected sheep, were infected by JSRV (Garcia-Goti et al, 2000).

The PCR test to detect JSRV presence has improved performance when applied to bronchoalveolar lavage (BAL) samples instead of blood samples, due to the higher viral concentration in this sample type. However, obtaining BAL samples is

more laborious, is more invasive, and early cases can still be missed (Voigt et al, 2007a).

In the absence of laboratory tests, scanning methods are currently being investigated as a potential early screening test for OPA. Transthoracic ultrasound is a non-invasive test that allows the visualization of tumours in the lungs of sheep. Although it is specific, it has limitations on the tumour size it can accurately detect (1-2 cm), so its performance as a tool for early stage diagnosis is under investigation (Cousens & Scott, 2015; Scott et al, 2018).

Despite recent advances in OPA diagnosis, confirmation of the diagnosis still has to be done using pathological findings and histopathology post-mortem (Gray et al, 2019; Griffiths et al, 2010).

1.4.2 Vaccine efforts

An alternative to the screening and culling strategy would be the use of vaccination as means of disease control. However, due to the lack of JSRV-specific antibodies this is problematic. Although there have been several efforts to develop a vaccine for OPA, so far none has been successful. Immunisation with recombinant Gag protein and an adjuvant stimulated antibody responses, but challenge studies have not been performed (Summers et al, 2006). In addition, two important factors need to be considered: high similarity between JSRV and enJSRV could result in autoimmunity, and the existence of immune response could select for new strains of JSRV evolved by mutation (Overbaugh & Bangham, 2001).

1.5 microRNAs

microRNAs (miRNAs) are a class of short regulatory RNAs (~22 nt). In humans, they are estimated to represent around 2-3% of the coding genome (Landgraf et al, 2007). miRNAs and their associated proteins are one of the most abundant ribonucleoprotein complexes in the cell (Bartel, 2004).

The founding member of the miRNA class, lin-4, was first discovered in 1993 in the nematode *Caenorhabditis elegans* (*C. elegans*) (Lee et al, 1993). Although miRNAs were initially thought to be limited to nematodes, the later discovery of let-7 in *C. elegans,* and its homologues in the genomes of human, mouse and fly,

revealed that miRNAs were found in several, and distantly related species (Pasquinelli et al, 2000; Reinhart et al, 2000). Since then, miRNAs have been identified across the plant and animal kingdoms, and in some virus and protist species (Lagos-Quintana et al, 2001; Llave et al, 2002; Molnár et al, 2007; Pfeffer et al, 2004). miRNAs are notably well-conserved across species; over one third of *C.elegans* miRNAs have close homologs in humans (Lim et al, 2003). Nevertheless, miRNAs differ in their biogenesis, evolution and function depending on the kingdom to which the organism belongs (Bartel, 2018).

1.5.1 Biological relevance of miRNAs

miRNAs act post-transcriptionally, affecting the expression levels of their target mRNAs and their translation into proteins, and represent another layer of gene expression regulation (Bartel, 2004; Bushati & Cohen, 2007). miRNAs have a regulatory function in several processes such as cell proliferation and death, tissue differentiation, developmental timing in worms, haematopoiesis and many others (Brennecke et al, 2003; Chen et al, 2004; Kuhn et al, 2011; Xu et al, 2003). In an attempt to evaluate the extent of miRNA regulation, studies were performed in which independent knock-outs of diverse miRNA families were carried out in mouse embryos. These studies revealed that independent knock-out of 52 mammalian conserved miRNA families resulted in phenotypic alterations in mice. Of those, knock-out of 15 families had severe effects such as reduced viability, cancer, immune and neurological disorders, and infertility (reviewed in Bartel (2018)). These studies highlighted the biological relevance and the diversity of the processes regulated by miRNAs.

1.5.2 Biology and synthesis of metazoan miRNAs

Although there are other small RNA species involved in RNA silencing, such as siRNAs and piwiRNAs, miRNAs differ from other small RNAs in their biogenesis and precursor structure (Ambros et al, 2003).

miRNAs are primarily found in noncoding regions of the genome, processed from long-noncoding RNAs. However, some miRNAs have also been found in the introns of coding genes. Intron-residing miRNAs constitute up to 25% of miRNAs in humans, and are usually found in the same orientation as the pre-mRNA,

suggesting they are not transcribed independently from the mRNA (Chiang et al, 2010; Morlando et al, 2008).

In animals, biogenesis of a typical miRNA (**Fig. 1.8**) starts in the cell nucleus, where RNA polymerase II transcribes the miRNA gene to form the pri-miRNA (Bartel, 2018; Gebert & MacRae, 2019). This pri-miRNA contains a hairpin structure and UGU motif which are recognised by the microprocessor complex, formed by the RNase III enzyme Drosha and the Digeorge syndrome critical region 8 (DGCR8) protein (Bartel, 2018; Treiber et al, 2019). Drosha is responsible for pri-miRNA recognition and with DGCR8 cleaves the pri-miRNA giving origin to the pre-miRNA. Pre-miRNAs are usually hairpins of around 70 nucleotides with a 2-nucleotide overhang at the 3′ end, this overhang is recognised by Exportin 5 and actively exported to the cell cytoplasm (Gebert 2019). Once in the cytoplasm, the 5′ phosphate, loop structure and 3′ overhang of the pre-miRNA are recognised by another RNAse III enzyme (Dicer) (Gebert & MacRae, 2019). Dicer cleaves the pre-miRNA loop structure resulting in a 20 nt miRNA duplex with a 5′ phosphate and the 3′ overhang (Bartel, 2018). In vertebrates, Dicer action is modulated by an RNA binding protein called TAR (TARBP) and protein activator of the interferon- induced protein kinase (PACT) (Gebert & MacRae, 2019). One of the strands of the miRNA duplex is then loaded into the guide-strand channel of an Argonaute (AGO) protein, forming the Silencing complex also known as miRISC, the other strand is cleaved. The silencing complex can then target mRNAs for degradation or translational repression (Bartel, 2018; Gebert & MacRae, 2019; Treiber et al, 2019).

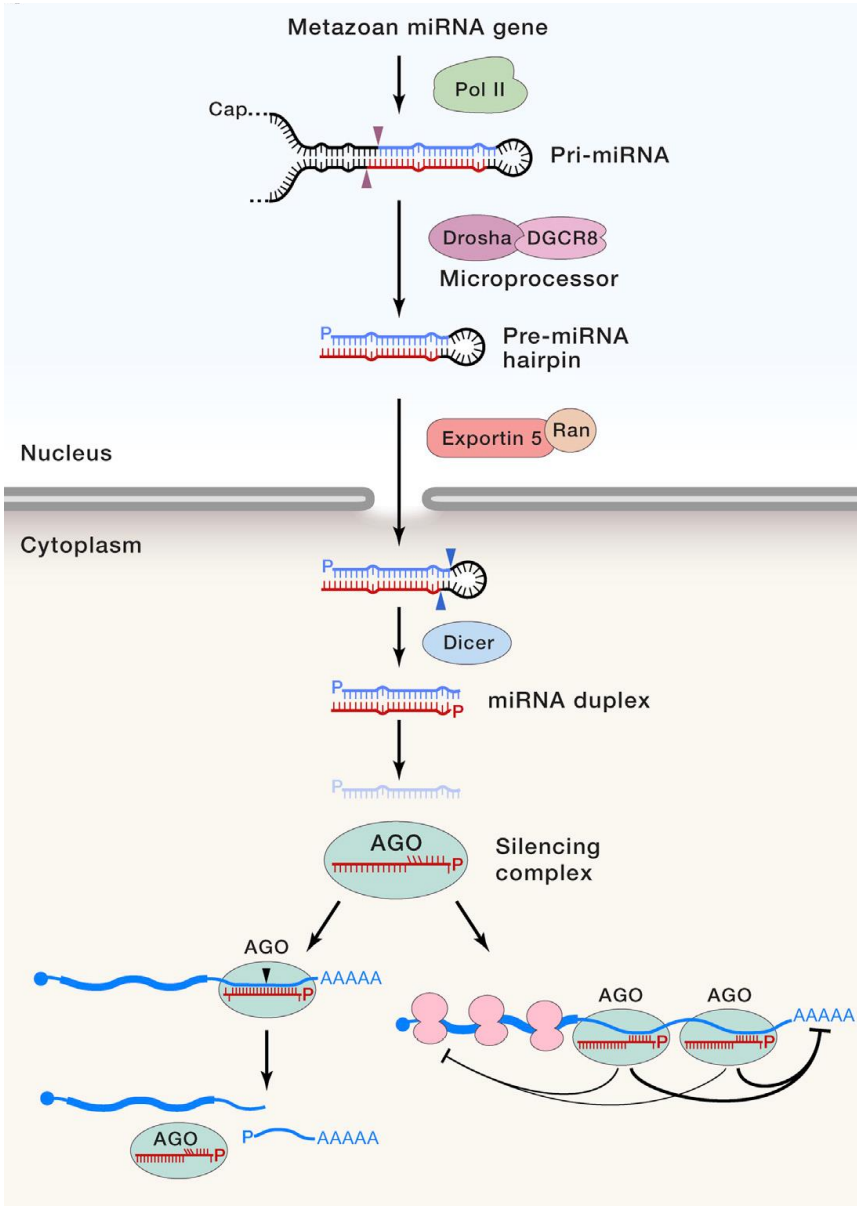

Figure 1.8. Metazoan canonical miRNA biogenesis. *miRNA genes are transcribed by pol II, generating a pri-miRNA hairpin, the pri-miRNA is then cleaved by the microprocessor generating a pre-miRNA. The pre-miRNA is exported to the cytoplasm by the action of exportin-5. In the cytoplasm the pre-miRNA is recognised by Dicer that cleaves the loop structure, generating a miRNA duplex. One of the duplex strands is then selected and loaded into AGO to form the silencing complex. The silencing complex targets mRNAs and depending on complementarity causes degradation or translational repression. Reproduced from Bartel (2018).*

Binding of the miRISC complex to the 3′UTR of an mRNA leads to silencing via translational inhibition or mRNA decay. Translation is inhibited at the initiation step: interaction of the miRISC with the eukaryotic initiation factor 4 A- I (eIF4A- I) and eIF4A-II promotes dissociation of the factors from mRNAs. Dissociation of eIF4A-I and eIF4A-II from mRNAs inhibits assembly of the eIF4 translation

initiation complex, thereby blocking mRNA translation (Fukao et al, 2014; Meijer et al, 2013). Nevertheless, the specific mechanism of miRISC translation inhibition is still not completely known. The better understood mechanism of mRNA decay involves the recruitment of GW182 (TNRC6 in humans) by AGO, which in turn interacts with PABPC, recruiting PAN2-PAN3 and CCR4-NOT, and promoting mRNA deadenylation. Deadenylation of mRNA triggers mRNA decapping by DCP1-DCP2, which renders the mRNA susceptible to degradation by XRN1 (reviewed in Gebert & MacRae (2019)). These two silencing mechanisms are thought to be linked, and mRNA decay has been found responsible for 66-90% of miRNA-mediated gene silencing (Eichhorn et al, 2014; Guo et al, 2010). Binding of the miRISC complex occasionally leads to mRNA cleavage when base complementarity between miRNA and target is extensive (Song et al, 2004; Yekta et al, 2004)

Pri-miRNAs can consist of a single miRNA or a cluster of related miRNAs. miRNAs that originate from the same pri-miRNA form a miRNA cluster and are transcribed as a multi-cistronic unit (Gebert & MacRae, 2019). In mammals there are four different AGO proteins. AGO2 is the one most commonly found forming the miRISC complex in humans, and the only one capable of directing mRNA cleavage (Diederichs & Haber, 2007; Liu et al, 2004).

1.5.2.1 Biogenesis of non-canonical miRNAs

Non-canonical miRNAs might enter the previously described biogenesis pathway at several stages. For instance, some intron contained miRNAs, called mirtrons, enter the pathway as pre-miRNAs after being processed by the spliceosome (Okamura et al, 2007; Ruby et al, 2007). Other mirtrons have a tail of RNA at 3′ or 5′ that is cleaved by nucleases before the pre-miRNA enters the miRNA biogenesis pathway (Babiarz et al, 2008; Ruby et al, 2007). Non-canonical miRNAs can also derive from endogenous short-hairpin RNAs (shRNAs), which are Dicer substrates that have a 5′ end determined by transcription and the 3′ end cleaved in a drosha-independent manner (Babiarz et al, 2008). Another class of non-canonical miRNAs are transcribed in tandem or are part of another small RNA, forming a chimeric hairpin that is processed by Dicer (Babiarz et al, 2008; Ender et al, 2008).

A special case of non-canonical miRNA is miR-451. This miRNA appears to be unique in that it requires Drosha but not Dicer during its biogenesis (Cheloufi et al, 2010; Yang et al, 2010a). Pre-miR-451 is too short for Dicer and instead is directly loaded into AGO2, the exonuclease PARN then performs further processing and generates a mature miR-451 (Cifuentes et al, 2010; Yoda et al, 2013). In general, non-canonical miRNAs of animals are not well conserved and are expressed at low levels (Bartel, 2018).

1.5.3 miRNA targets

Binding of miRNAs to mRNAs is generally determined by base complementarity of nucleotides 2-8 of the miRNA to the 3′UTR of mRNAs. Canonical target sites can vary in strength: the strongest ones have absolute complementarity in nucleotides 2-8 and also have an A at position 1 of the miRNA. Complementarity in positions 2-8 without an A at nucleotide 1 results in weaker targets. Following in strength are sites with complementarity in positions 2-7 and an A at nucleotide 1. The weakest of canonical sites constitute targets with complementarity to 2-7 or 3-8 and no A at position 1 (Agarwal et al, 2015). The increased affinity for a target conferred by the presence of an A at nucleotide 1 of the miRNA, is not directly linked to miRNA sequence, instead it is provided by a pocket in AGO that recognises and strongly binds A (Schirle et al, 2015; Schirle et al, 2014).

Non-canonical targets are target sites to which the miRNA seed does not show complementarity. These sites have been identified using crosslinking approaches and their biological function has been questioned (Agarwal et al, 2015; Helwak et al, 2013). A second miRNA region called supplemental (nucleotides 13-16) can affect target recognition and might be of particular importance in non-canonical sites (Agarwal et al, 2015; Grimson et al, 2007). In addition, the supplemental region is thought to enable miRNAs of the same family (with the same seed sequence) to target different mRNAs based on this second region of complementarity (Broughton et al, 2016). A single mRNA can also be targeted by many different miRNAs, and can have several binding sites, whereby occupancy of these binding sites by miRNAs can cause cooperative repression (Grimson et al, 2007; Saetrom et al, 2007; Selbach et al, 2008). Binding to non-canonical sites might be dependent on occupancy of canonical sites (Flamand et al, 2017).

Even though one miRNA has the potential to repress numerous target mRNAs, the level of repression they exercise in a particular target mRNA is generally modest (Selbach et al, 2008). Detectable repression requires high expression levels of miRNA. miRNAs enact effective regulation precisely by targeting several mRNAs in a network so that the effect of several modest interactions is additive. In addition, repression levels can be enhanced if miRNAs bind to several sites in a 3′ UTR (Grimson et al, 2007; Saetrom et al, 2007). Indirect effects of miRNA expression can also be detected, miRNAs can target transcription factors that will affect their downstream genes. The miR-200 family is an example of this in its role coordinating epithelial to mesenchymal transition (EMT), this miRNA family has multiple bindings sites in the 3′UTR zinc finger E-box binding homeobox 1 (ZEB1) exerting a strong repression (Bracken et al, 2016).

miRNA usually act as negative regulators of their targets, but some have reported that miRNAs could increase gene expression by binding complementary promoter sequences (Place et al, 2008). miRNA target sites have been reported in promoters; for example, miR-373 has a target site in the promoter of E-cadherin (Place et al, 2008).

Although several authors have highlighted the vast number of mRNAs regulated by miRNAs, thought to be up to 60% of mRNAs, a report stated that the biologically relevant targets of miRNAs have been overestimated (Pinzón et al, 2016). In this study, the authors analysed the effects of miR-223 in a pool of predicted targets and found that, for most targets inter-individual variability was higher than the effect of miR-223 repression. In addition, the authors reported that miRNA binding site conservation was higher in haplo-insufficient genes, which might suggest that the biological relevant targets are dose-dependent, and that some targets might not be functionally repressed (Pinzón et al, 2016). It was proposed that targets that are evolutionarily conserved but not dose-dependent, might act as titrators of miRNAs, and that in many cases phenotype effects might be driven by a few responsive targets (Pinzón et al, 2016). Although the study presented limitations, it highlighted the effect of inter-individual variation as well as the importance of confirming predicted targets and the effect of their repression experimentally.

1.5.3.1 Competitive endogenous RNA theory

The competitive endogenous RNA theory (ceRNA theory) proposes that repression of a certain target mRNA by a miRNA can be affected by the number of different miRNA targets, and the presence of miRNA sponges such as pseudogenes and long non coding RNAs, referred to as competitive endogenous RNAs (Poliseno et al, 2010; Salmena et al, 2011). According to the ceRNA theory the extent to which a miRNA efficiently represses a certain target depends on there being enough copies of the miRNA to bind all target mRNA copies (Salmena et al, 2011). The influence of ceRNA on miRNA function remains controversial and difficult to predict. However, in some cases, this theory might explain changes in miRNA function; for example, duplication of the MYCN gene, target of the miRNA let-7, results in more copies of MYCN mRNA and hampered let-7 function (Powers et al, 2016).

1.5.3.2 Target prediction

Several algorithms that aim to identify miRNA targets have been developed. These algorithms search for sequences complementary to the miRNA seed in the 3′UTR of mRNAs (Agarwal et al, 2015; Bartel, 2009). In order to refine the results some approaches include assessment of evolutionary conservation, evaluating the site position and additional sites within the 3′UTR, the potential for supplementary pairing and study of pairing stability (Baek et al, 2008; Bartel, 2009). Some of the best-performing predictive computer methods include TargetScan (Friedman et al, 2009), DIANA-microT (Maragkakis et al, 2009) and miRDB (Wong & Wang, 2015). DIANA-TarBase and miRTarBase (Chou et al, 2018; Karagkouni et al, 2018) are resources which include targets with some level of experimental validation.

In addition to predictive computational methods, experimental methods have also been developed to study targets of miRNAs. One of the approaches to investigate miRNA targets consists of altering a miRNA and measuring changes in the transcriptome using microarrays, miR-sequencing, and ribosome-profiling or luciferase assays (Boutz et al, 2011; Leivonen et al, 2009; Lim et al, 2005; Uhlmann et al, 2012). These high-throughput methods, with the exception of luciferase assays, which detects direct interaction between miRNA and target,

identify both direct and indirect targets of the miRNA (bracken 2016). Another experimental approach used to discover both canonical and non-canonical targets are immunoprecipitation or pull-down methods such as cross-linking, ligation and sequencing of hybrids (CLASH) (Helwak et al, 2013; Hendrickson et al, 2009; Karginov et al, 2007). During CLASH cross-linking of the miRISC complex is performed, followed by ligation of targets interacting with the miRNA of the miRISC complex, immunoprecipitation of AGO is then performed and RNA hybrids are sequenced (Helwak et al, 2013). Nonetheless, some of the observed interactions with these methods are not real and functional significance is not considered, so further validation is necessary (Bracken et al, 2016).

Genetic screening has been used to identify the biological relevance of miRNA-mRNA interactions (Ding & Grosshans, 2009; Hunter et al, 2013). These methods combine some of the previously discussed strategies, such as in mass methods, and performing mutations in miRNA genes *in vivo*. The disadvantages of these approaches are its difficulty to be applied in mammals and that it does not consider coordinated functions of genes (Bracken et al, 2016).

Although computer and lab-based methods for target prediction have improved their accuracy, false-positive and false-negative results are still observed with both approaches. Thus, caution needs to be exercised when interpreting results obtained from these methods.

1.5.4 miRNA nomenclature and classification

miRBase is the resource responsible for miRNA gene nomenclature. miRBase was first established in 2002 as a public repository for miRNA sequences and annotation; its current version (22.1) contains miRNA entries from 271 organisms and over 48000 mature miRNA sequences (Kozomara et al, 2019).

miRNA nomenclature was designed to convey information about the particular miRNA and in animals obeys the following set of rules: the three first letters of a miRNA are an abbreviation of the species name in which that particular miRNA is found (Ambros et al, 2003). Hsa- corresponds to *Homo sapiens* and oar- to *Ovis aries.* The species prefix is followed by either mir- or miR- denoting the pre-miRNA or mature miRNA form respectively. Numbers are given to miRNAs in sequential

order of discovery and miRNAs conserved through species (orthologues) usually have the same number. For example, hsa-miR-10 is a human mature miRNA. Paralog miRNAs within a species are denoted by a letter suffix such as hsa-miR-10a and hsa-miR-10b. Different hairpins which are processed into identical mature miRNAs are distinguished by a numerical suffix like the case of: hsa-mir-24-1 and hsa-mir-24-2 (Ambros et al, 2003).

In cases where mature miRNAs have been identified from both arms of the precursor hairpin the two sequences are differentiated using the -5p or -3p suffix: hsa-miR-10b-5p (Griffiths-Jones et al, 2006; Griffiths-Jones et al, 2008).

There are some exceptions to this nomenclature including lin-4 and the let-7 family of miRNAs, which were given names before the systematic nomenclature rules had been established (Griffiths-Jones et al, 2006).

miRNAs are also found grouped in families based on the similarity of their seed sequence (Griffiths-Jones et al, 2008; Kozomara et al, 2019). Members of the same seed family are usually, but not in all cases, evolutionary related, and their targets overlap (Bartel, 2009; 2018).

1.5.4.1 miRNA discovery

An increasing number of miRNAs are being discovered and described with the use of deep-sequencing approaches. Although these approaches give the opportunity to detect miRNAs expressed at low levels or expressed only in certain conditions, they have the potential to misidentify short RNA sequences of other origins as miRNAs (Bartel, 2018; Kozomara et al, 2019). Confidence in the existence of a new described miRNA is increased if there are reads mapping to both the 3′ and 5′ arms of the pre-miRNA, 3′ and 5′ mature miRNAs are expected to form a duplex with the characteristic 2 nt 3′ overhangs, and the 5′ terminus of the miRNAs is expected to be processed consistently (Kozomara et al, 2019).

1.5.4.2 miRNA isomers: Isomirs

Mature miRNAs, processed from the same hairpin, which differ in length or sequence are called isomirs (Neilsen et al, 2012). Isomirs can differ in their targets, stability and maturation steps. Isomir classification and formation are reviewed in **Fig.1.9**. Some miRNAs have no isomirs, whereas others have many,

for instance, miR-21-5p has several isomirs in humans (Telonis et al, 2015). Nevertheless, in cases in which a miRNA has several isomirs, it has been shown that only a few are expressed at high levels (Guo et al, 2015a). Predominant isomirs vary between tissues and are altered in cancer, which has attracted interest in their use as biomarkers (Guo et al, 2015a).

The presence of sequence variants, especially those at the 5′ terminus, may alter targets of the miRNAs due to the seed sequence being displaced (Bartel, 2018; Bracken et al, 2016).

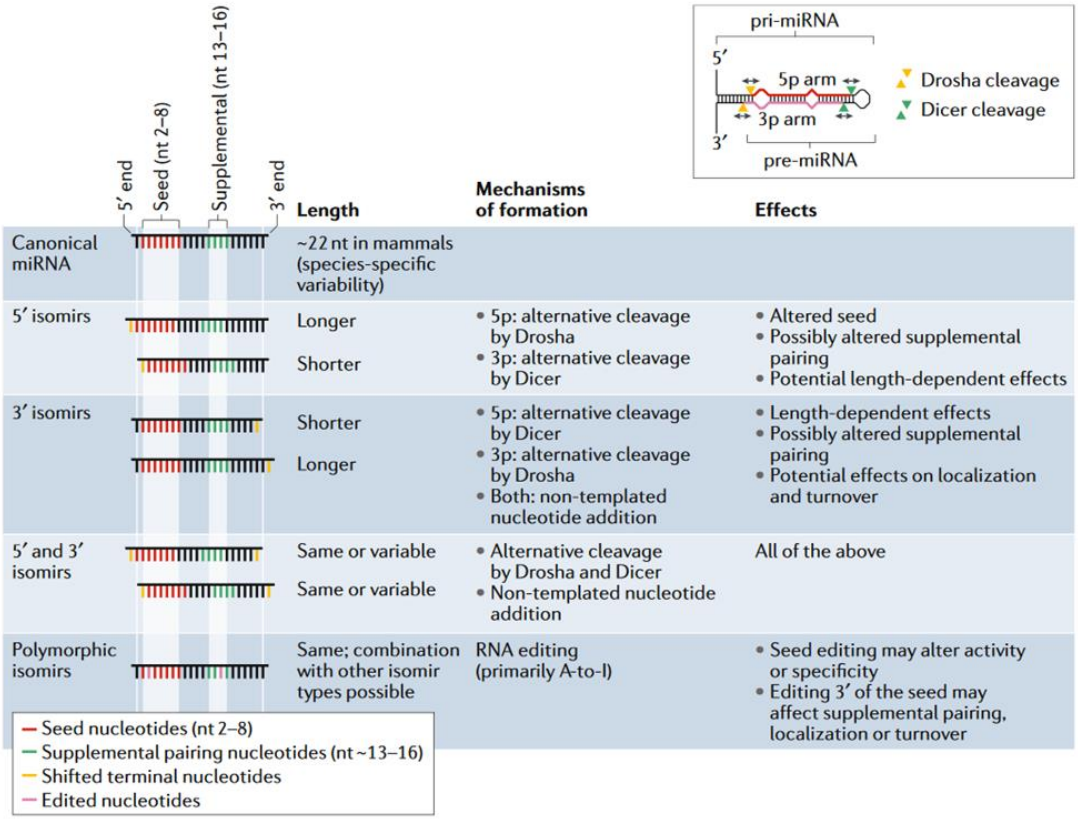

Figure 1.9. Isomir types and formation mechanisms. *Reproduced from Gebert & MacRae (2019).*

1.5.5 Regulation of miRNA expression

Most miRNAs are under RNA polymerase II transcriptional control and can be regulated at several steps of their biogenesis. After transcription, other mechanisms can regulate miRNA stability and processing, some examples are: positive-feedback loops, increase in Dicer or microprocessor availability, to which some miRNAs are more sensitive, and A to I editing of pri-miRNAs. RBPs can

also impact miRNA expression at all steps of miRNA biogenesis and can have positive or negative effects on expression (reviewed in Treiber et al (2019)).

miRNA turnover is regulated by several factors, and appears to be linked to sequence, for example: a 5′ G or C leads to faster turnover rates than a U in this position (Guo et al, 2015b). Turnover rates range from minutes to days and differ between miRNAs (Gebert & MacRae, 2019).

1.5.6 miRNA expression in tissue

miRNA expression has been found to vary depending on tissue type as well as developmental stage and disease state of the particular tissue of concern (Lagos-Quintana et al, 2002; Landgraf et al, 2007). Special interest has been placed in identifying miRNAs that are tissue specific due to their potential roles in tissue differentiation and disease, along with their appeal as markers. Housekeeping miRNAs, those expressed stably in all tissues, have also attracted attention as promising controls for miRNA transcriptomics studies and due to their potential association with housekeeping processes in cells. Nevertheless, tissue specific miRNAs have only been identified in a handful of tissue types: miR-1 and miR-133 are specifically expressed in heart and muscle (Kloosterman & Plasterk, 2006; Thum et al, 2008), miR-122 is only expressed at significant levels in liver (Chang et al, 2004; Lagos-Quintana et al, 2002), miR-9 and miR-124 are found in brain tissue (Landgraf et al, 2007; Ludwig et al, 2016), and miR-142-3p is specific of haematopoietic cells (Landgraf et al, 2007; Ludwig et al, 2016). Interestingly, it was found that the precursors of those miRNAs could be detected in several tissue types whereas the mature forms were only present at very low levels, an observation that could suggest that the processing to mature miRNA might be the determinant of tissue specificity (Li et al, 2013b; Ludwig et al, 2016).

Research on miRNA expression across 61 different human tissues found that over 80% of miRNAs detected did not fall into the definition of tissue-specific or housekeeping miRNAs. In addition, 143 miRNAs were found to be expressed in all tissue types assessed (Ludwig et al, 2016). Expression abundance of most miRNA pair members (-3p/-5p) was positively correlated in each specific tissue, as was abundance of cluster members, with the exception of miR-449. The study also compared miRNA expression between specific rat and human tissue types,

reporting that miRNAs highly abundant in specific human tissue types were similarly abundant in the same tissue type for rats (Ludwig et al, 2016). Notably, to date, no studies have found lung-specific miRNAs or miRNA families.

1.5.6.1 miRNA expression in lung tissue

Several studies have investigated lung miRNA expression in humans and rodents. This information can complement the limited information directly obtained from research in sheep lung, helping create a picture of miRNA expression in health and in association with lung disease.

In a mouse model of allergic asthma, miR-16, miR-21 and miR-126 were significantly upregulated in comparison to controls. Observation of this model system helped elucidate the function of miR-126 as a suppressor of the effector function of lung Th2 cells and regulator of antibody production- by targeting *OBF1* (Mattes et al, 2009).

Another study in a murine model of pulmonary fibrosis found a relationship between the expression level of miR-155 and the degree of pulmonary fibrosis observed. In addition, the authors observed that when bleomycin was delivered to induce fibrosis, miR-155 levels increased and subsequently keratinocyte growth factor (KGF) decreased, no longer exerting its effect protecting from pulmonary fibrosis (Jiang et al, 2010).

Small RNAs are known to play an essential role in the prenatal development of various organs. To study the small RNA effects in lung development, the effects of DICER mutations have been researched. Knock out of DICER in the lung resulted in death before gastrulation due to its involvement in cell survival, but when DICER was inactivated by conditional mutation in later stages of lung formation this resulted in smaller patterns of lung lobation and the formation of large epithelial pouches instead of the fine branching observed in normal lung. These findings suggest that DICER, and presumably miRNAs, are directly involved in lung epithelial morphogenesis (Harris et al, 2006).

1.5.7 Cell-free miRNAs

Stable levels of cell-free miRNAs in serum and plasma were first reported in 2008 (Mitchell et al, 2008). Since then, cell-free miRNAs have been identified in several

biological fluids including saliva, urine and milk (Schwarzenbach et al, 2014). Initial reports showed that miRNAs could be detected in blood fractions in an exceptionally stable form, despite high endogenous RNase concentration in blood expected to cause miRNA degradation (Mitchell et al, 2008). Mitchell et al. also showed that miRNA levels in plasma remained unaffected after being left at room temperature for 24h, and after eight cycles of freeze-thawing. On the other hand, addition of synthetic naked miRNAs to plasma resulted in degradation, suggesting that resistance to RNases was not an intrinsic property of miRNAs (Mitchell et al, 2008).

Subsequent experiments (Arroyo et al, 2011; Wang et al, 2010) identified two populations of cell-free miRNAs: vesicle enclosed miRNAs and protein-bound miRNAs. Association of miRNA species with either vesicles or proteins was found to be protective against RNAse degradation (Arroyo et al, 2011).

1.5.7.1 Vesicle miRNAs

Vesicles are cell-derived structures that enclose cargo in lipid bilayers. Vesicles are involved in physiological and pathological processes and are an important means of cell-to-cell communication. Their cargo includes proteins, lipids and nucleic acids (van Niel et al, 2018). Size fractionation of plasma showed that miRNAs could be found inside vesicles, specifically in microvesicles and exosomes (Arroyo et al, 2011). Microvesicles range from 50-1000 nm in diameter and derive from the plasma membrane. Exosomes, on the other hand, are generally smaller in size (50-150 nm) and derive from the endosome (van Niel et al, 2018) (**Fig. 1.10**). Although there is some variation in the size range of microvesicles and exosomes reported by some authors (van Niel et al, 2018; Wang et al, 2010); (Huang-Doran et al, 2017), studies agree that microvesicles are generally larger than exosomes.

Vesicles have attracted great interest in the cancer research field due to their involvement in intercellular communication, their role in establishing the tumour microenvironment, and their increased abundance in cancer patients (Cortez et al, 2011; Schwarzenbach et al, 2014). Thus, several reports have endeavoured to study components of cancer cell secreted vesicles. Importantly, the cargo of cancer cell derived vesicles was found to be enriched in miRNAs compared to

normal exosomes, and miRNAs were more abundant in metastatic cells compared to cancer cells (Melo et al, 2014).

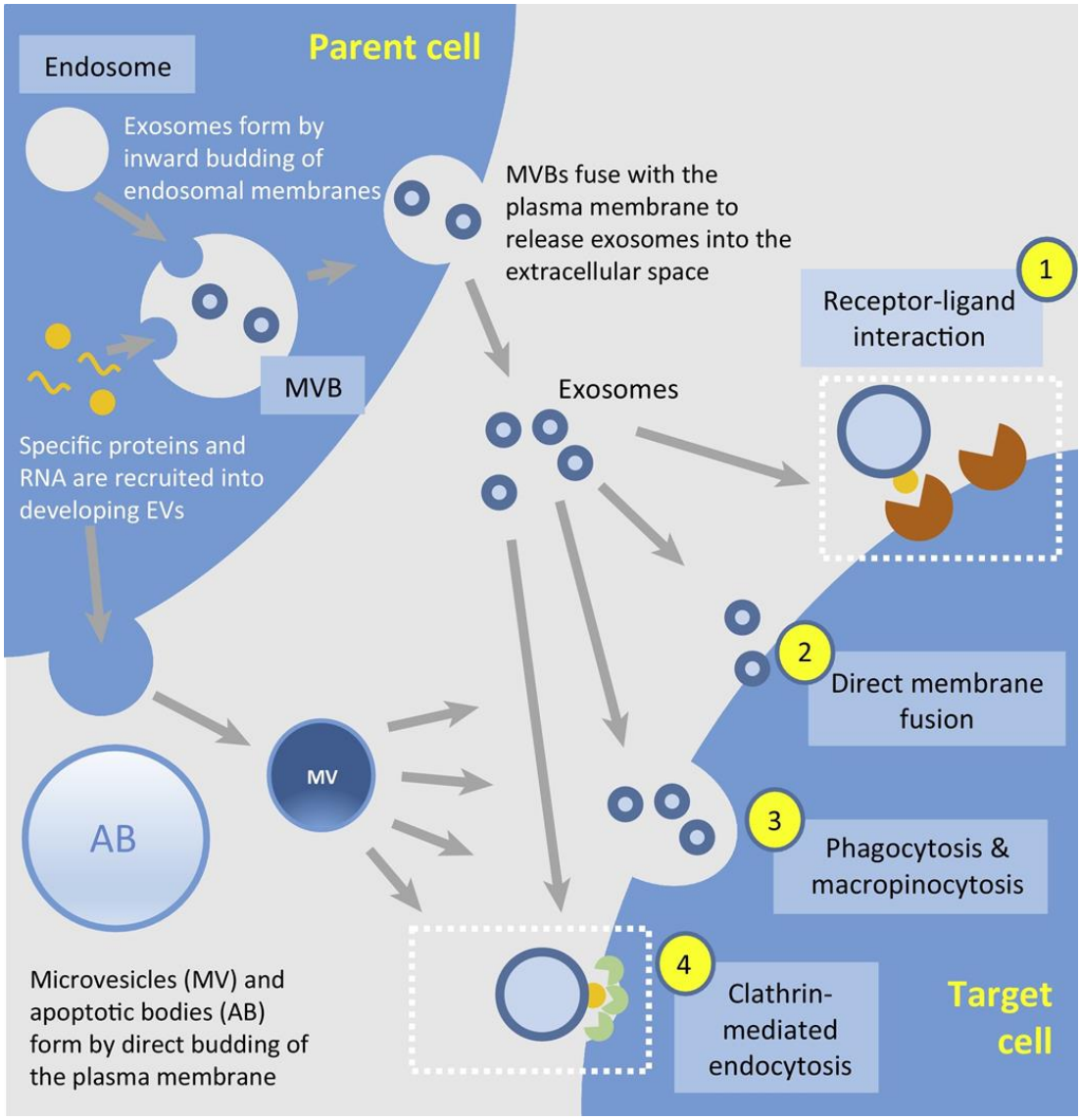

Figure 1.10. Formation and release of microvesicles, exosomes and apoptotic bodies. *EV; extracellular vesicles, MVB: multivesicular bodies. Reproduced from Huang-Doran et al (2017).*

Exosomes are secreted by stem cells, immune cells, epithelial cells, neurons and cancer cells (Théry, 2011). Cancer cell derived exosomes have also been found in the circulation. Exosome levels in serum from breast cancer patients was found to be greater than in controls (O'Brien et al, 2013). These exosomes were found to be derived from cancer cells and besides containing miRNAs they also contain Dicer, TRBP and AGO2, proteins involved in biogenesis of pre-miRNAs to mature

miRNAs and miRNA targeting (Melo et al, 2014). Maturation of exosomal miRNAs was reported to occur in exosomes. These cancer exosomes were able to alter the transcriptome of cancer cells in a Dicer-dependent manner. Impairing Dicer function in the exosome hindered tumour growth (Melo et al, 2014). The presence of Dicer in exosomes has been suggested as a marker of cancer (Melo et al, 2014).

Exosomes were also found to package mature miRNAs without the need for processing, for example mir-182-5p. However, for exosomal miRNAs to be able to alter the recipient cell's transcriptome, miRNAs have to be present in the exosome at an appropriately high abundance (Melo et al, 2014). Interestingly, some studies found that some secreted miRNAs were not represented inside the cell of origin, suggesting that they might be specifically expressed and secreted for cell-to-cell communication (Valadi et al, 2007).

Apoptotic bodies were also found to be able to transport miRNAs. Both exosomes and apoptotic bodies express phosphatidylserine on their surface which acts as a phagocytic signal. Interestingly, the receptor of phosphatidylserine, Tim4 (T-cell immunoglobulin- and mucin-domain-containing molecule) was found expressed in fibroblasts and was able to promote engulfment of both apoptotic bodies, and could also be involved in intercellular signalling mediated by exosomes (Kosaka et al, 2010).

1.5.7.2 Protein-bound miRNAs

Initially, the resistance of miRNAs to degradation in biological fluids was exclusively attributed to their presence inside vesicles. However, fractionation of plasma miRNAs identified a second population of miRNAs not associated with vesicles, and consistent with a miRNA-protein complex (Arroyo et al, 2011; Wang et al, 2010).

Treatment of those miRNA-protein complexes with protease K rendered miRNAs susceptible to the action of RNases, suggesting a protective effect when miRNAs are associated with certain proteins. Some of the proteins shown to associate with miRNAs in circulation, and protect them from degradation, are AGO2, one of the core members of the RISC complex, nucleophosmin 1 (NPM1) (Arroyo et al, 2011;

Wang et al, 2010) and high-density lipoproteins (HDL) (Vickers et al, 2011). Association of miRNAs with certain proteins has been suggested to be related to sequence preferences, but no mechanisms or evidence has been found yet.

The mechanism by which cells secrete miRNAs that are protein bound and are taken up by recipient cells remains unknown. To date, no evidence of cell surface receptors for protein bound miRNAs has been detected (Larrea et al, 2016).

Evidence that circulating miRNAs constituted two different populations, one vesicle enclosed and one protein associated, sparked examination on the functional relevance of each of the fractions. These were followed by studies on the preferential association of particular miRNAs in each of the populations. In one study, the majority of circulating miRNAs were found to cofractionate with proteins and not vesicles, specifically 66% of plasma miRNAs and 68% of serum miRNAs were not inside vesicles (Arroyo et al, 2011). This finding was confirmed by another report (Turchinovich et al, 2011). Particular miRNAs were also found to exhibit preference for their association in one of the fractions, such is the case of let-7a, preferentially associated with vesicles, and miR-122, preferentially bound to AGO2. Other miRNAs were present in both fractions and the authors suggested that differences in miRNA secretion and transport could be linked to the cell type of origin (Arroyo et al, 2011).

On the other hand, another study reported that most circulating miRNAs found in serum and other biological fluids, such as saliva, are found in vesicles (Gallo et al, 2012). In general, the sensitivity of miRNA detection was only marginally improved when exosomes were compared to whole serum (Gallo et al, 2012). Biomarker sensitivity might be improved by knowing the fraction in which a miRNA is present and concentrating miRNAs in that fraction.

1.5.7.3 Origin and function of circulating miRNAs

The presence of cell free miRNAs in biological fluids has raised questions on their origin, function and biological importance. Circulating miRNAs have heterogeneous origins, and the contribution of each of those origins to the cell-free miRNA population remains unclear. miRNAs are released to the circulation as a result of apoptosis and necrotic cell death. Some studies found a high

correlation between cell-free miRNAs in blood fractions and miRNAs in blood cells, reporting that most miRNAs originated from lysed blood cells (Chen et al, 2008; Pritchard et al, 2012), whereas another study reported significant differences between miRNAs in plasma and blood cells (Turchinovich et al, 2012). In general, damaged blood cells are accepted to contribute to the cell-free miRNA signature, and the influence of cell counts and haemolysis on the signature has been reported (Liang et al, 2014). Cell free miRNAs might also originate from endothelial cells or other organs exposed to high blood flow such as the liver, kidneys and lung, particularly when tissue damage has occurred (Machado et al, 2015; Turchinovich et al, 2011).

However, miRNAs have also been shown to be actively secreted by cells, and their function in cell-to-cell communication is being investigated (Larrea et al, 2016); (Turchinovich et al, 2011). The concept of miRNAs as message transmitters in intercellular communication implies that exported miRNAs are specifically selected in some way by the cell. Indeed, it has been shown that in the contents of vesicles contents are specifically selected and are not just a sample of cell contents. In such a mechanism, exporting cells would be able to identify and select miRNAs, package them suitably for extracellular transport and transport them to the extracellular space. This export is most likely energy dependent (Bhome et al, 2018; Guduric-Fuchs et al, 2012; Wang et al, 2011).

Circulating miRNAs have also been suggested to play a role in immunoregulation. Tumour-secreted miRNAs enclosed in exosomes can be transferred from cancer cells to surrounding macrophages (Fabbri et al, 2012). Normal cells surrounding a tumour might, on the other hand, be secreting tumour suppressor miRNAs (Kosaka et al, 2012).

1.5.8 miRNAs in serum

miRNA signatures in blood have been studied for a wide range of pathologies. miRNA signatures from serum, plasma and whole blood have not been reported to be significantly different (Gallo et al, 2012; Moldovan et al, 2014). However, it has been shown that the presence of blood cells in the sample has an effect on the results. Indeed, it has been reported that the effects of haemolysis in miRNA quantification in blood fractions has been underestimated (Moretti et al, 2017).

Both serum and plasma are regarded as acceptable sample types to study miRNA expression (Moretti et al, 2017). However, serum has less platelet contamination than plasma, which could decrease some bias in miRNA quantification (McDonald et al, 2011b). Blood cell count has been shown to have an effect on miRNA expression levels in plasma (McDonald et al, 2011b; Pritchard et al, 2012).

Importantly, it is difficult to directly compare studies in plasma and serum samples due to differences in sample preparation and measurements (McDonald et al, 2011b; Moretti et al, 2017). In general, comparisons between studies are also problematic due to differences in the normalisers of miRNA expression used. Many studies have used endogenous miR-16, but this miRNA has been found to be dysregulated in several cancers, including lung cancer (Moretti et al, 2017). U6, a small nuclear RNA, was another frequently used normaliser, but is known to fluctuate notably across samples, which could contribute to bias in miRNA expression levels reported (Xiang et al, 2014).

Besides blood, other biological fluids can provide information on the state and pathologies of organs associated with them (Larrea et al, 2016). For instance, miRNA signatures in urine have been investigated as markers of bladder and prostate cancer (Zhou et al, 2014). In the lung, miRNA expression in sputum and broncholoalveolar lavage fluid (BALF) have been investigated (Kim et al, 2015). These specimens have attracted interest due to their potential to reflect the pulmonary microenvironment.

1.5.9 miRNA expression in sheep

Although being one of the most agricultural important animals, few studies have investigated miRNA expression in sheep tissue. For example, miRBase v22.1 cites only 106 precursors and 153 mature miRNA sequences in domestic sheep (*O. aries*) (Kozomara et al, 2019). In comparison, the miRBase entry for the related ruminant species *Bos taurus* contains 1064 precursors and 1025 mature miRNA sequences, and the entry for humans (*H. sapiens*) boasts 1917 precursors and 2654 mature sequences. Given the fact that miRNA sequences are highly conserved across species, this suggests that the differences in miRNA numbers between these species are likely explained by the number of miRNA studies carried out in each of the species. An additional factor that has hindered miRNA

research in sheep is the poor annotation of the sheep genome compared to other domestic species, which makes target predictions and novel miRNA discovery a challenging task.

Most of the knowledge we presently have on miRNA expression and targets in sheep tissue derive from studies that focus on muscle and ovarian tissue (Donadeu et al, 2012; Hiard et al, 2010; McBride et al, 2012; Zhou et al, 2017). These studies have focused their efforts in investigating miRNA expression linked to muscle quantity, fat deposition and fertility, i.e., qualities important for production, but little attention has been placed on animal welfare and the study of miRNA association with sheep diseases.

Nevertheless, the published studies have provided a first insight to miRNA expression in sheep, and have provided meaningful information on the role of some miRNAs and their regulation.

In the context of sheep miRNAs and retroviral infections Esparza-Baquer et al (2015) characterised polymorphisms in the alleles of the restriction factor APOBEC3 and found that polymorphisms in the a3z1 gene might influence disease pathogenesis; a finding that might be conditioned by the frequency of some mutations. Strikingly, a low frequency allele for a3z1 was found to create target sites for miR-323 and miR-1287. However, the function of this target site, although hypothesised to silence APOBEC3, remains unknown.

To date, only three recently-published articles have examined miRNA expression in the sheep lung. Krauss et al. investigated miRNA expression in the context of early cardiopulmonary development in sheep and, despite the small sample size of the study, identified differential expression of miR-146a, miR-22, miR-335* and miR-210 between late gestation and neonatal lambs (Krauss et al, 2018). These findings highlighted the important role miRNAs play in early lung development. The observations in sheep were mostly in line with studies in mouse lung that had found miR-210 and miR-22 to be differentially expressed in response to oxygen levels (Chan et al, 2012); (Caruso et al, 2010). Nevertheless, in contrast to mouse studies, the miR-15 family was not found to be differentially expressed in sheep, a finding that could be due to sample size, but which also emphasises the possible

variations between species, cell type and other characteristics of the system studied (Krauss et al, 2018).

miRNA expression in the sheep lung has been studied in response to two viral infections: Visna/Maedi virus (MVV) and Peste-des-petits-ruminants virus (PPRV). MVV targets cells of the monocyte/macrophage lineage and the infection results in inflammatory lesions in several organs including the lung (Minguijón et al, 2015). In a study on lung tissue of MVV-naturally infected sheep (Bilbao-Arribas et al, 2019), differentially expressed miRNAs were found when seropositive animals and uninfected animals were compared, whereas comparison between seropositive carrier animals and seropositive animals with lesions showed no differential expression of miRNAs. Seropositive and seronegative animals showed differential expression of several miRNAs but validation of expression levels by RT-qPCR only confirmed the differential expression of miR-21 and miR-30c. The miRNA found to be more strongly upregulated in seropositive animals was miR-21, with a higher increase in animals with lesions (Bilbao-Arribas et al, 2019). Upregulation of miR-21 has been linked to viral infection and reported in viral infections caused by hepatitis C, Epstein Barr virus and influenza virus (Anastasiadou et al, 2015; Chen et al, 2013; Li et al, 2010). Some of the roles of miR-21 that might explain its upregulation in viral infections are regulation of proliferation and inflammation by targeting components of pathways such as PI3k-Akt, MAPK, erbB (Bilbao-Arribas et al, 2019; Chen et al, 2013; Pandey et al, 2017; Sheedy, 2015).

miRNA changes related to PPRV infection were studied in spleen and lung tissue of sheep and goats (Pandey et al, 2017). The study reported upregulation of miR-320a-1, miR-320a-2, miR-1246, miR-363, miR-760-3p and miR-21-3p, and downregulation of miR-34b and miR-150 in both infected sheep and goats. Nevertheless, these results need to be considered with caution due to the low number of specimens included in the study (n=2 each group), which limits the use of statistics and is likely to bias the results.

1.5.9.1 Cell-free miRNAs in sheep

Few studies have investigated cell-free miRNAs in sheep and, similarly to miRNA studies in tissue, most have focused on miRNA signatures in pregnancy. As in

humans, circulating miRNAs could be investigated as biomarkers for agricultural diseases, as they become easier and more cost-effective diagnostic tests.

In a study comparing miRNA expression of pregnant ewes at day 30 and day 90 of pregnancy, and of non-pregnant ewes, authors found that 25 miRNAs were differentially expressed. Some of the dysregulated miRNAs found by RT-qPCR included miR-183, miR-200b and miR-182. This study was performed in exosomes derived from blood and placentomes. When results were compared, only miR-379, out of 94 miRNAs dysregulated in placentomes, was found differentially expressed in serum exosomes and placentomes. (Cleys et al, 2014).

Interesting for the purpose of this thesis a study was carried out examining microvesicle formation in sheep uterus and delivery to the conceptus. The study found that those microvesicles contained 81 miRNAs as well as the enJSRV mRNAs *env* and *gag*. miRNAs contained in the microvesicles included well-studied miRNAs in reproduction such as the let-7 family, miR-18a, miR-19b, miR-21, miR-125a, miR-214, miR-223 and miR-423. The authors confirmed that the microvesicles could be taken up by cells in culture and that enJSRV RNAs could subsequently be detected in those cells (Burns et al, 2014). enJSRV *env* is essential for normal elongation of the conceptus (Dunlap et al, 2006) and the findings reported suggest that microvesicles might be the delivery method. Moreover, the findings of the study pose further questions on the interplay of the miRNAs contained in the microvesicle and the enJSRV genes. Looking at miRNA expression in gestation might shed light on possible miRNA interactions with the JSRV genome.

Circulating miRNAs have only been studied in the context of one infection in sheep, scrapie (Sanz Rubio et al, 2017). Levels of miRNAs previously shown to be overexpressed in brain tissue of scrapie affected sheep and other models of prion disease, were measured in the plasma of scrapie affected sheep. Of the investigated miRNAs, miR-21-5p and miR-342-5p were found to be overexpressed when compared to control unaffected sheep. miRNAs let-7b and let-7d also showed higher levels in affected sheep than controls, but quantification was not possible as they could not be detected in most control animals. The authors noted discrepancies between the results obtained in sheep and *in vitro* or

mice infected models, which they attributed to higher variability in natural disease compared to inoculated models. Elevated levels of miR-21-5p were also detected in the central nervous system (CNS) of scrapie sheep, and could suggest that the elevated levels in plasma have CNS origin. miR-21-5p was shown to mediate an anti-inflammatory response in prion-infected neuronal cells *in vitro* (Sanz Rubio et al, 2017).

1.5.10 miRNAs in cancer

miRNAs regulate complex networks, made more complex by the fact that some of their targets are transcription factors. They regulate cancer pathways at multiple levels, allowing them to achieve a stronger degree of regulation and fine-tuning. For example, miR-135b regulates EMT by targeting *LATS2, NDR2, MOB1* and *βTCRP*, all members of the Hippo pathway (Lin et al, 2013). This pathway is involved in the promotion of lung cancer metastasis (Pan, 2010) and is also important in type II pneumocyte differentiation (Chung et al, 2013). The role of miRNAs as regulators of biological functions such as cell proliferation and death, differentiation and metabolism, can affect tumour development (Bracken et al, 2016).

While mutations are rarely observed in miRNA genes, dysregulation in their expression levels is commonly observed in cancer (reviewed in Bracken et al (2016)). Some miRNAs have been classified as tumour suppressors or oncomirs due to their ability to suppress or promote tumourigenesis (Esquela-kerscher 2006). Overexpression of certain oncomirs in mouse models was sufficient to drive tumour formation in mouse (Lin Gregory 2015). Nonetheless, the effects of miRNAs on tumourigenesis appear to be context dependent: miRNAs can be oncomirs or oncosuppressors depending on cancer type. For example: miR-17-5p acts as an oncomir in hepatocellular carcinoma but is considered an oncosuppresor in cervical cancer; similarly, miR-200 can either promote or inhibit metastasis and invasion depending on cancer type (Bracken et al, 2016; Esquela-Kerscher & Slack, 2006).

The mechanisms of miRNA dysregulation in cancer are varied and can happen at various stages of miRNA biogenesis. Starting with transcription of pri-miRNAs there are several mechanisms that may alter this process. miRNAs genes are

frequently located in genome fragile sites or in sites subject to amplification, deletion or translocation (Calin et al, 2004; Esquela-Kerscher & Slack, 2006). Such events might affect transcription of the pri-miRNA and subsequently affect levels of mature miRNA. For instance, the loss of the locus which encodes miR-15a and miR-16-1 has been observed in chronic lymphocytic leukemia (Lerner et al, 2009). These two miRNAs usually target *BCL2* and control cell apoptosis (Calin et al, 2004). Other epigenetic silencing mechanisms directly related to pri-miRNA transcription are the hypermethylation of CpG islands found in promoters of miRNA genes, resulting in silencing of tumour suppressor miRNAs, or histone modifications (Bracken et al, 2016). Increased transcription of pri-miRNAs has also been observed related to their transcriptional activators, which in some cases are oncogenes or tumour suppressors themselves. The miR-34 family is transcriptionally activated by p53 (He et al, 2007). Members of the mir-34 family act as tumour suppressors by promoting apoptosis and avoiding uncontrolled cell proliferation (He et al, 2007). On the other hand, MYC promotes transcription of the oncomirs of the miR-17-92 cluster (Dews et al, 2006).

Mutations and expression changes in components of the miRNA biogenesis pathways are also common and well-reported mechanisms of miRNA dysregulation in cancer (reviewed in Lin & Gregory (2015) and Bracken et al (2016)). Disruption of components of the pathway accelerated tumour growth in a mouse model of lung cancer (Kumar et al, 2009). Levels of key components of the canonical miRNA biogenesis pathway like Drosha and Dicer are frequently suppressed in cancers such as lung cancer and ovarian cancer (Lin & Gregory, 2015). Knockdown of Drosha in lung adenocarcinoma was found to result in increased tumour proliferation *in vivo* and *in vitro* (Kumar et al, 2007). Limited expression of these proteins has an effect on all miRNAs that follow the canonical pathway, and is thought to be related to the reported global miRNA downregulation in cancer (Bushati & Cohen, 2007; Lin & Gregory, 2015). However, this global miRNA dysregulation observation remains controversial (Volinia et al, 2006). In fact, an upregulation of Drosha levels has been reported in multiple cancers and is observed in advanced stages of cervical cancer (Lin & Gregory, 2015; Muralidhar et al, 2011). These findings suggest that miRNA

dysregulation and the mechanisms by which it occurs are cancer type, and even stage, specific.

Inactivating mutations in exportin 5 (*XPO5*) are also related to miRNA processing defects and increased tumourigenesis in gastric, endometrial cancer and increased risk of developing breast cancer (Lin & Gregory, 2015; Melo et al, 2010).

DICER1 is considered a tumour suppressor, loss of a single copy increased tumourigenesis in a mouse model of lung cancer (Kumar et al, 2009). Common mutations in *DICER1* result in truncated proteins without the C-terminal catalytic domains or take place in metal-binding residues of the RNAse IIIb domain. This domain cleaves the 3′ end of the 5′ arm of the pre-miRNA, but when it is defective due to mutation, it blocks the maturation of 5p miRNAs but not 3p miRNAs (Anglesio et al, 2013). A particular example is that of the let-7 family, members of which are usually 5p derived (Anglesio et al, 2013). *DICER1* mutations are observed in hereditary types of cancer like Wilms tumour, cystic nephroma, pituitary blastoma and tumour predisposition syndrome (Lin & Gregory, 2015). TRBP mutations have also been linked to cancer (Garre et al, 2010).

In addition, DROSHA, DGCR8, DICER1 and TRBP, components of the biogenesis pathway, are all subject to post-translational regulation such as phosphorylation or acetylation. Nevertheless, the effects and significance of these post-translational modifications in miRNA dysregulation in cancer are unknown (reviewed in Ha & Kim (2014)).

Other factors associated to components of the pathway can cause alterations in miRNA processing. For instance, RNA binding proteins associated with microprocessor like DDX5 and DDX17 can disrupt its function (van Kouwenhove et al, 2011). Other RNA binding proteins like KSRP, SRSF1, FUS bind to regions of pri-miRNAs and facilitate drosha recruitment and processing (Lin & Gregory, 2015). Mediated by DDX5 and DDX17, p53 can also interact with the DROSHA complex and promote processing of tumour-suppressive pri-miRNAs (Lin & Gregory, 2015).

In special cases like miR-21, receptor SMADs associate with an element of the miR-21 stem loop and increase its processing by Drosha (Bracken et al, 2016).

During cancer triggered hypoxia, EGFR is activated, which promotes cell growth and oncogenesis. EGFR interacts with AGO2 and promotes its phosphorylation inhibiting interaction between DICER1 and AGO and blocking miRNA accumulation (Shen et al, 2013). Activation of LIN28A or LIN28B in cancer suppresses the tumour suppressor family let-7 and promotes proliferation and tumourigenesis. Binding of LIN28 promotes the addition of an oligouridine tail to pre-let7, preventing maturation and promoting its degradation. *In vitro* inactivation of these proteins was able to revert tumour growth (Lin & Gregory, 2015).

Nevertheless, in considering the effects of mutations on expression of Drosha, DICER and AGO proteins in cancer, it needs to be acknowledged that these proteins also have roles independent of miRNA biogenesis (Bracken et al, 2016).

miRNA dysregulation has also been observed in cases in which components of the biogenesis pathways showed no alteration in function, suggesting that other pathways, besides the miRNA biogenesis pathway, play a role in miRNA dysregulation (Lin & Gregory, 2015). The Hippo pathway is disrupted in many cancers, and YAP1 the downstream effector of hippo pathway is able to regulate miRNA biogenesis by targeting DDX17 and inhibiting drosha processing of pri-miRNAs (Mori et al, 2014).

Another mechanism to bypass miRNA regulation involves avoiding miRNA regulation instead of disrupting miRNA expression. It has been observed that some cancer cells produce mRNA isoforms with shorter 3′UTR, as a result of alternative cleavage or polyadenylation. As the 3′UTR contains miRNA binding sites, shortening of this region could mean lower level of miRNA repression (Mayr & Bartel, 2009). An example of this phenomenon is 3′ UTR shortening of PDL1, which is related to an increase in cell survival in a variety of cancers (Kataoka et al, 2016). This shortened version of PDL1 loses binding sites of miRNAs miR-200 and miR-34 (Bracken et al, 2016). Although negative selection usually prevents the occurrence of SNPs in the 3′UTR of mRNAs, compared to other regions of the mRNA, some cases of mutations that result in loss of miRNA-mRNA complementarity have been reported. One example is the mutation of the let-7 binding site in KRAS in non-small cell lung carcinoma (Chin et al, 2008).

Despite the insight in biological mechanism and interactions that observing several cancer types offers, miRNA dysregulation mechanisms as well as expression of particular miRNAs and their function seems to be vastly context dependent. It is therefore essential for the purpose of this project to build on these general cancer knowledge by specifically looking at lung cancer miRNA dysregulation and mechanisms.

1.5.11 miRNAs as biomarkers

Research on miRNAs and the discovery that they are deregulated in diseases such as cancer, viral infections, nervous system diseases, muscular and cardiovascular disorders and diabetes, has attracted great attention to their potential as biomarkers of disease (Cortez et al, 2011). In the specific case of cancer, research has shown that miRNAs are located in genomic regions often amplified or deleted in cancer (Calin et al, 2004). Their function as regulators of cellular processes important in cancer initiation, progress and metastasis, has led to some miRNAs being considered oncomirs or oncosuppressors: members of the let-7 family, for instance, are considered tumour suppressors due to their role targeting *Ras* genes (Esquela-Kerscher & Slack, 2006). In contrast, miR-21 is considered an oncomir that targets *PTEN* and *Spry2* and promotes invasion and migration (Ma et al, 2011). Some miRNA polymorphisms have also been associated with an increased cancer risk, and mutations in components involved in miRNA biogenesis, like *AGO2*, are a common finding in cancer (Lin & Gregory, 2015).

Besides their biological role in disease, miRNAs possess other qualities that make them good candidates as biomarkers. miRNAs are present in the circulation and body fluids such as urine, saliva and cerebrospinal fluid (Larrea et al, 2016). They have high stability in formalin-fixed paraffin embedded tissue samples, plasma and blood serum (Chen et al, 2008; Xi et al, 2007).

In cancer diagnosis, a common finding is an inverse relationship between levels of miRNAs in tissue and the circulation (Jarry et al, 2014). The mechanism by which this occurs is not known, but it might be a sign of dysregulated cancer pathways. Nevertheless, this has further complicated the interpretation and comparison of findings between studies.

In many cases, miRNAs initially identified to have great promise as biomarkers have subsequently shown poor specificity and reproducibility. The primary reason for this is that most initial studies do not consider other important factors such as age, gender and treatment (Armand-Labit & Pradines, 2017; Keller et al, 2017; Kosaka et al, 2010). Data reproducibility has also been a problem, standardisation of data processing, optimisation and methods is required to minimise variations, ensuring reliable results (Armand-Labit & Pradines, 2017; Keller et al, 2017; Witwer & Halushka, 2016); (Schwarzenbach et al, 2011). More understanding of miRNA biology is still needed for them to be used as specific and reliable markers in wide range of patients, and to develop simple detection methods.

1.5.12 Circulating miRNAs as biomarkers

Given the increased number of circulating miRNAs in pathologies such as cancer, and the increased abundance of specific miRNA species, circulating miRNAs have been considered as potential disease biomarkers. In addition, their detection in body fluids and use as biomarkers could constitute a minimally invasive test, would reduce testing costs, and if methods such as RT-qPCR were used, would give quick and easily analysed results (Bernardo et al, 2012; Gilad et al, 2008; Schwarzenbach et al, 2014). miRNAs are more stable than mRNAs and therefore less susceptible to changes that occur in sample processing (Chen et al, 2008). However, certain aspects of miRNA biology remain unknown and that information would be valuable in designing the best testing strategy and for interpreting results. For instance, the half-life of circulating miRNAs is still unknown and might vary between miRNAs (Schwarzenbach et al, 2014).

In cancer, miRNA signatures appear to be tissue specific, therefore detection of a particular miRNA signature in body fluids could potentially allow for distinction of cancer origin (Lu et al, 2005; Volinia et al, 2006). These miRNAs would ideally be expressed at high levels in affected individuals and low levels in healthy individuals, increasing possibilities of sensitive detection. Sensitivity and specificity might also be increased by using a panel of miRNAs instead of a single miRNA (Hu et al, 2010). The two most frequently investigated circulating miRNAs in cancer are miR-10b and miR-21, **Fig. 1.11** illustrates some of their roles in circulation (Larrea et al, 2016; Schwarzenbach et al, 2014).

One of the first studies to confirm miRNA secretion by tumour cells and their potential as biomarkers was by Mitchell et al (2008). In this study, the authors xenografted mice with human prostate cancer tumours to determine if cancer related miRNAs could be detected in the blood. They found that the presence of tumour did not result in a generalised increase of blood miRNAs, but they were able to detect the presence of two miRNAs with no murine homologs in the circulation. These miRNAs derived from the tumour cells, indicating that these cells secrete miRNAs and that they can be detected in body fluids (Mitchell et al, 2008). Differential expression of certain miRNAs in biological fluids has also been found to be indicative of other pathologies.

Although an increase in the abundance of a certain miRNA in the circulation might be indicative of cancer, it was shown that miRNA levels and tumour burden in patients only showed moderate correlation (Mitchell et al, 2008). In contrast, in pregnancy, correlation between miRNA levels and tissue was found to be high. Circulating miRNAs of placental origin were found to increase as pregnancy progressed, and declined within a day after delivery, suggesting miRNAs could be valuable biomarkers for pregnancy (Chim et al, 2008).

Due to high sensitivity and specificity, RT-qPCR is the gold-standard method for miRNA. miRNA-sequencing has also been used, but has potential limitations such as sequence-specific biases due to enzymatic ligation, higher cost and the need for trained bioinformaticians to analyse abundant data. Nevertheless, it has the advantage of not requiring prior knowledge of miRNAs present, making it a powerful exploratory tool (Bernardo et al, 2012; Schwarzenbach et al, 2014).

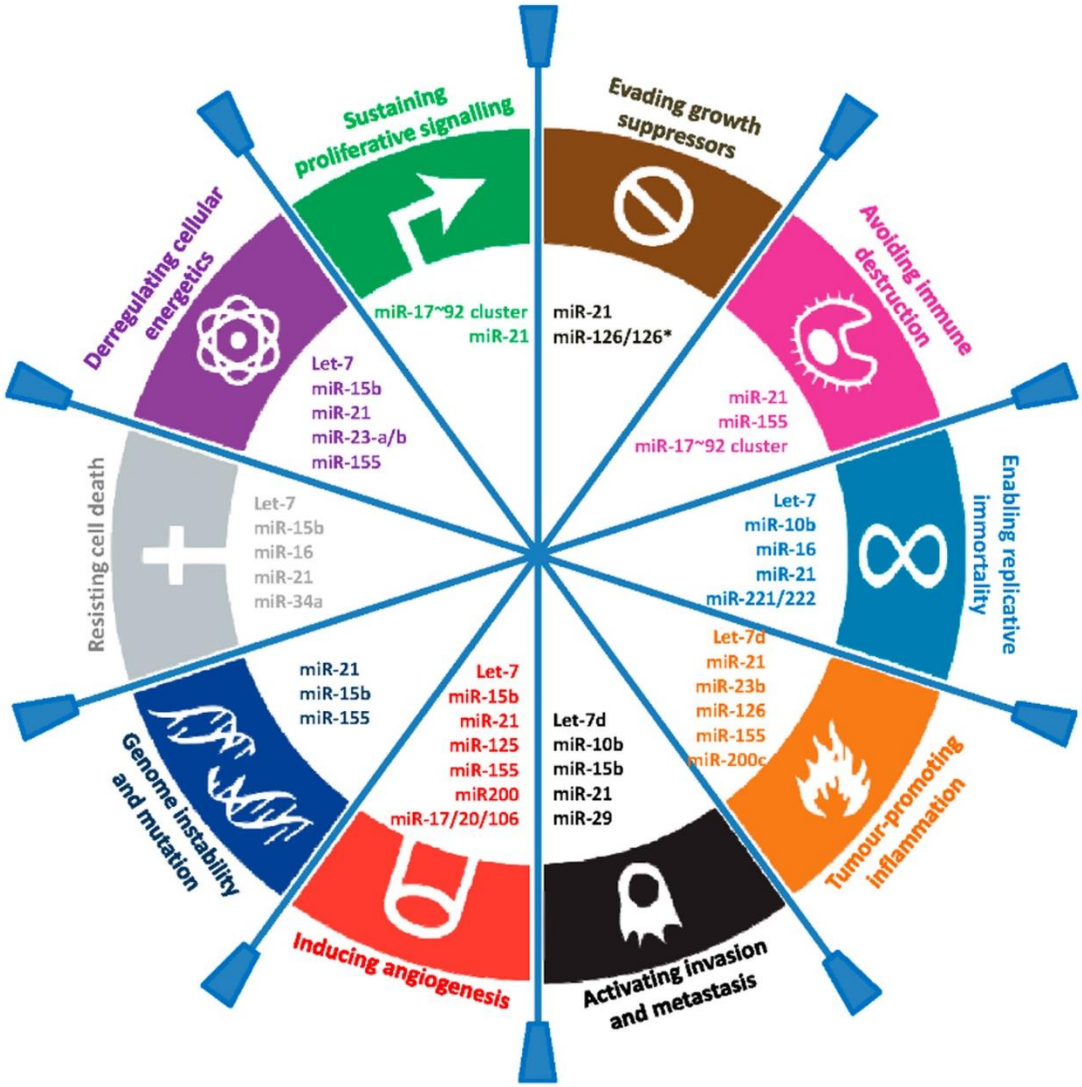

Figure 1.11. Known roles of some circulating miRNAs. *Reproduced from Larrea et al (2016).*

1.5.13 miRNA signatures in lung cancer

Most miRNA studies in lung have focused on discovering differences in miRNA expression in lung cancer and normal tissue with the aim of finding new diagnostic, prognostic and therapeutic approaches (reviewed in (Inamura, 2017; Yu et al, 2017)). Indeed, an early study found that miRNAs performed better than mRNAs as classifiers of cancer type and distinguished between normal and cancer tissue with greater precision (Lu et al, 2005). The findings of the aforementioned studies might be of special relevance for the present study due to the discussed similarities in histopathology, pathway activation and affected cell type between human lung adenocarcinoma and OPA.

Whereas several miRNAs are consistently found in lung adenocarcinoma studies, many others have been reported as highly expressed in only a small number (Guan et al, 2012). In fact, apart from the differences in detected miRNAs, comparison of different studies often shows disagreement in the expression trend, with some showing a clear upregulation and others downregulation. Most of these disagreements are likely caused by differences in tissue, cell type, disease stage or specific lung cancer type. However, sample number, experimental design and methods, also need to be considered as potential factors of the observed variance between studies. These differences in reported results emphasise the importance of consulting multiple sources and highlight the importance of a clear description of the sample material and methods followed in a study.

Some of the miRNAs that have been consistently linked to human lung adenocarcinoma are the let-7 family, miR-155, miR-16, the miR-17 cluster, the miR-183 family (miR-96, miR-182 and miR-183), miR-21, miR-31, miR-135b, the miR-200 family, miR-205, the miR-221 cluster and miR-503 (**Table 1.1**).

Nevertheless, due to the nature of miRNAs and similarities in activated pathways between cancers, several miRNAs dysregulated in lung cancer have also been found dysregulated in other cancer types and diseases (Bracken et al, 2016; Guan et al, 2012; Volinia et al, 2006). Hence, a single miRNA is not likely to predict a disease accurately. In trials, increased sensitivity and specificity has been reported when using not one but a combination of miRNAs as predictors or classifiers of disease state (Schwarzenbach et al, 2014). A particularly important aim is to find a miRNA signature able to distinguish between cancers or diseases of similar clinical or histopathological presentation to support the use of miRNAs as disease biomarkers (Shen et al, 2013).

Table 1.1. Summary of miRNAs frequently reported as dysregulated in human lung cancer.

miRNA	Cancer type[1]	Upregulated/downregulated	Known targets[2]	Genomic information[3]	Regulation[4]
Let-7 family	NSCLC	Downregulated in NSCLC (Takamizawa et al, 2004) downregulated in BAC (Inamura et al, 2007) Tumour suppressor (Wang et al, 2012b)	*RAS, HMGA2, MYC , BCL-2, CDC34, CYCLIN A2, CDK6 NSCLC* (Esquela-Kerscher et al, 2008; Johnson et al, 2007; Takamizawa et al, 2004)	Chromosome 3 Let-7g in 3p21 implicated in lung cancer (Johnson et al, 2007)	Transcription factors such as N-MYC, EGR1, also let-7 transcripts (Gaeta et al, 2017)
miR-130b	NSCLC	Upregulated, oncogene (Mitra et al, 2014; Tian et al, 2016)	*TGFBR2* (Mitra et al, 2014) *PPARγ , ZEB1* (Tian et al, 2016)	Chromosome 22 (Benson et al, 2013)	Not known in NSCLC
miR-132	NSCLC	Upregulated in some cancers like lung cancer (Yanaihara et al, 2006). Downregulated, tumour suppressor (You et al, 2014)	*ZEB2* (You et al, 2014) *ACVR2B, ACVR1, HB-EGF* (Jiang et al, 2015)	Chromosome 17, region lost in Cancer Cluster with miR-212.	Hypermethylation of promoter (You et al, 2014)
miR-135a	NSCLC	Downregulated, tumour suppressor, very low levels in lymph node metastasis (Shi et al, 2015). Predictor of treatment, related to paclitaxel and cisplatin resistance (Holleman et al, 2011; Zhou et al, 2013)	*HIF1AN* (Holleman et al, 2011) *KLF8*, E-cadherin and vimentin genes (Shi et al, 2015) *MCL1*(Zhou et al, 2013)	Encoded by two genes at chromosome 3 and 12 (Zhou et al, 2013)	DNA methylation of CpG islands (Zhou et al, 2013)
miR-135b	NSCLC, highly invasive	Oncogene in most reports. Upregulated (Lin et al, 2013). Downregulated in cisplatin resistance (Zhou et al, 2013)	Components of Hippo pathway *LATS2*, ß-*TrCP*, *NDR2*, *LZTS1* (Lin et al, 2013).	Intronic miRNA(Lin et al, 2013). Chromosome 1(Zhou et al, 2013) .	DNA demethylation and NFkb signalling (Lin et al, 2013).

[1] Type of lung cancer: NSCLC: non-small cell lung cancer, ADC: adenocarcinoma, SCC: squamous cell carcinoma, BAC: bronchioloalveolar carcinoma.
[2] Known targets lists only experimentally validated targets, targets predicted by bioinformatics have not been included.
[3] Genomic information includes clustering and family of miRNAs as well as genomic location in H. sapiens.
[4] Regulation refers to the mechanism by which the miRNA expression is activated or repressed.

Table 1.1. Summary of miRNAs frequently reported as dysregulated in human lung cancer.

miRNA	Cancer type[1]	Upregulated/downregulated	Known targets[2]	Genomic information[3]	Regulation[4]
miR-146b	NSCLC, SCC	Overexpression related to recurrence after surgery, poor prognostic marker (Patnaik et al, 2011) Overexpressed in serum, higher in stage 2 than others (Rani et al, 2013)	*HEF1* (Malleter et al, 2012)	Chromosome 10 (Patnaik et al, 2011)	Upregulated in response to lypopolisaccharide (Raponi et al, 2009)
miR-153	NSCLC	Downregulated, tumour suppressor, poor prognostic marker (Ren et al, 2019; Shan et al, 2015; Xu et al, 2013)	*SNAI1, ZEB2* (Xu et al, 2013) *ADAM19*, *AKT* (Shan et al, 2015)(Yuan et al, 2015)	Chromosome 2 (Benson et al, 2013)	No data found
miR-17/92 cluster	NSCLC, small-cell lung cancer	Overexpressed in lung tumours (Volinia et al, 2006) oncogene (Mogilyansky & Rigoutsos, 2013). Overexpressed in tumour and serum, but low levels detected in blood (Osada & Takahashi, 2011) Especially overexpressed in small-cell lung cancer (Hayashita et al, 2005)	*STAT3, MAPK14* (Carraro et al, 2009) *E2F1, HIF-1α, Tsp1, PTEN* (Osada & Takahashi, 2011),*CCND1, CDKN1* and *E2F1* (Shu et al, 2012)	Chromosome 13 (Hayashita et al, 2005)	Regulated by C-MYC (Mogilyansky & Rigoutsos, 2013; O'Donnell et al, 2005)
miR-182	NSCLC, SCC, ADC	Oncogene in most reports. Upregulated in primary lung tumours vs metastases (Del Vescovo & Denti, 2015; Vosa et al, 2013). Upregulation observed in tissue and sera (Zhu et al, 2011; Zhu et al, 2016). Enhances proliferation in NSCLC cell lines (Wang et al, 2018). Favourable prognostic marker (Stenvold et al, 2014) and showed tumour inhibiting properties. Stage classifier	*FBXW7, BRCAI, CADMI, FOXF2, MTSS-1* (Del Vescovo & Denti, 2015) *FOXO3* (W.-B. Yang et al. 2014), *HIF-1α* (Wang et al, 2018).	Chromosome 7 (cluster with 183, 96) (Benson et al, 2013)	Sp1 stimulates miR-182 expression (Yang et al, 2014)

Table 1.1. Summary of miRNAs frequently reported as dysregulated in human lung cancer.

miRNA	Cancer type[1]	Upregulated/downregulated	Known targets[2]	Genomic information[3]	Regulation[4]
miR-183	SCC, ADC. Higher in SCC. Lymph node metastasis (Zhu et al., 2011)	Oncogene in most reports. Upregulated (Dambal et al, 2015; Li et al, 2017a; Zhu et al, 2011; Zhu et al, 2016) . Upregulation observed in tissue and sera (Zhu et al, 2011; Zhu et al, 2016) Different results depending on cell line. Yang and Wang proved metastasis inhibitor activity (Wang et al, 2008; Yang et al, 2014)	*FOXO1, EGR1, PTEN* (Zhu et al, 2011) VIL2 activity (Wang et al, 2008; Wang et al, 2019a)	Chromosome 7 (cluster with 182, 96) (Benson et al, 2013)	No data found
miR-193b	NSCLC, ADC, SCC	Upregulated in tumours and serum (Nadal et al, 2015) (Nadal et al. 2015) downregulated, tumour suppressor (Hu et al, 2012)	*CCND1, uPA* (Hu et al, 2012)	Chromosome 16	No data found
miR-200	NSCLC, ADC, SCC	Downregulated in metastasis compared to primary tumours (Baffa et al, 2009; Chen et al, 2014a). Low levels part of signature that predict recurrence. Overexpressed in NSCLC (Pacurari et al, 2013). Promotes EMT (Gregory et al, 2008). Enhances radiosensitivity (Cortez et al, 2014). Low levels associated with poor survival (Pecot et al, 2013).	*E2F3, RND3* (Feng et al, 2012) *DLC1*, *HNRNPA3 and HFE, UBA6, UBE2I, ZEB1, ZEB2* (Pacurari et al, 2013) (Chen et al, 2014a; Gregory et al, 2008), *PRDX2*, *NRF2* (Cortez et al, 2014).	miR-200 family, chromosome 1 (Pacurari et al, 2013)	Regulated by p53 (Pacurari et al, 2013) Histone acetylation sp-1 dependent, PDL1 (Chen et al, 2014a)
miR-205	SCC, ADC, higher in SCC	Upregulated in most reports (Begum et al, 2015; Li et al, 2017a), higher in SCC (Cai et al, 2013; Vosa et al, 2013). Tumour suppressor and oncogene (Qin et al, 2013)	*PTEN* (Qin et al, 2013) *PHLPP* (Cai et al, 2013) *ZEB1, ZEB2* (Tellez et al, 2011)	Chromosome 1. Region amplified in cancer (Cai et al, 2013; Qin et al, 2013)	Promoter methylation (Tellez et al, 2011)

Table 1.1. Summary of miRNAs frequently reported as dysregulated in human lung cancer.

miRNA	Cancer type[1]	Upregulated/downregulated	Known targets[2]	Genomic information[3]	Regulation[4]
miR-21	NSCLC	Upregulated early in carcinogenesis (Seike et al, 2009) upregulated in lung cancer (Markou et al, 2008; Zhang et al, 2010b) (An et al, 2018; Bica-Pop et al, 2018)	*PTEN*, *PDCD4* (Xi et al, 2010) *SPRY1, SPRY2, BTG2, APAF1, FASLG, RHOB* (Hatley et al, 2010)	Inside FRAs/ amplified in lung cancer chromosome 17 (Yanaihara et al, 2006)	Activated by EGRF (Seike et al, 2009; Xi et al, 2010) activated by Ras (Hatley et al, 2010)
miR-212	NSCLC	Downregulated compared with normal lung, pro-apoptotic role (Incoronato et al, 2010; Incoronato et al, 2011). Tumour promoting, upregulated (Li et al, 2012).	*PED* (Incoronato et al, 2011) *PTCHI* (Li et al, 2012).	Chromosome 17, region lost in Cancer Cluster with miR-132	Histone modifications. CpG island found in promoter of miR-212 (Incoronato et al, 2011)
miR-31	NSCLC, ADC	Upregulated, oncogene (Li et al, 2017a; Liu et al, 2010; Vosa et al, 2013) Promotes metastasis (Chen et al, 2014b; Meng et al, 2013)	*LATS2*, *PPP2R2A* (Liu et al, 2010) *DKK*-1, *DACT3* (Xi et al, 2010)	Chromosome 9 (Meng et al, 2013)	C/EBP-β activated (Xi et al, 2010)Promoter methylation (Meng et al, 2013)
miR-34	NSCLC	Dowregulated in lung cancer (Okada et al, 2014) Tumour suppressor (Rupaimoole & Slack, 2017; Zhang et al, 2019)	*CDK4, CDK6, BCL-2, MET, MYC, PDL1* (Feng et al, 2019; Hermeking, 2010; Okada et al, 2014)	miR-34 family in chromosome 1	P53 during DNA damage response (Hermeking, 2007)
miR-503	NSCLC	Downregulated, tumor suppressor (Li et al., 2014; Yang et al., 2014). Regulates cisplatin resistance (Li et al., 2014)	*PI3K P85,IKK*-β (Yang et al., 2014) *FANCA, BCL-2* (Li et al., 2014)	Intragenic, chromosome X, belongs to miR-16 family (Yang et al., 2014)	Promoter methylation (Li et al., 2014)
miR-592	NSCLC	Downregulated (Hu et al, 2016). Down in primary lung ADC compared to colorectal mestastases in lung (Kim et al, 2014)	*CCND3* (Hu et al, 2016)	Chromosome 7 (Benson et al, 2013)	No data found

Table 1.1. Summary of miRNAs frequently reported as dysregulated in human lung cancer.

miRNA	Cancer type[1]	Upregulated/downregulated	Known targets[2]	Genomic information[3]	Regulation[4]
miR-96	SCC, ADC. Higher in SCC than ADC.	Oncogene in most reports (Fei et al, 2018; Li et al, 2017a). Upregulated in cancer vs. Normal (Zhu et al, 2011; Zhu et al, 2016). Upregulation found in tissue and sera, correlation in levels (Cai et al, 2017a; Zhu et al, 2011)	*FOXO3* (Zhu et al, 2011) *CHES1* (Zhang et al, 2013b)	Chromosome 7 (cluster with 182, 183) (Benson et al, 2013)	No data found

1.5.13.1 Circulating miRNAs as lung cancer biomarkers

Many studies have investigated circulating miRNAs in connection with lung cancer, and have tried to link miRNA signatures to prognosis, diagnosis, classification and response to therapy with mixed success. Some of the most relevant to the work described in this thesis are summarised in this section.

A review from 2016 looked at miRNA studies performed in biological fluids to diagnose lung cancer (Gyoba et al, 2016). Ten studies performed in serum from lung cancer patients reported miRNA signatures as specific and sensitive biomarkers, but no common miRNAs were found in these signatures. Similarly, in plasma, diagnostic signatures also varied greatly, but miR-21 appeared as part of a panel in five studies. miR-155, miR-210 and miR-486-5p were present in three studies. The review also included studies performed in sputum, but discussed the variability of sputum, including variability in cell numbers and types. Nevertheless, studies in sputum showed some consensus including the presence of miR-21, miR-31, miR-210 and miR-155 in various studies (Gyoba et al, 2016).

Another review was published in 2017 looking specifically at circulating miRNAs for diagnosis of stage I-II NSCLC (Moretti et al, 2017). Again, great variation was found between miRNAs reported to have diagnostic value in different studies. The authors of the article suggested screening based on their review findings of 20 quantitative studies. The suggested screening is a two-step process: first, use of four miRNAs reported to offer high sensitivity (miR-223, miR-20a, miR-448 and miR-145), followed by use of four miRNAs with high specificity (miR-628-3p, miR-29c, miR-210 and miR-1224). No reliable signature to distinguish between SCC and AC was found (Moretti et al, 2017).

A common finding reported by authors of both reviews was that the great majority of published studies used small sample sizes and did not follow general guidelines for biomarker research (Baker et al, 2002). In addition, smoking habits were not disclosed by some of the reviewed studies, and some circulating miRNAs have been found to be significantly dysregulated by smoking (Moretti et al, 2017).

Correspondence between miRNA levels in serum and tumours has been reported in some studies (Zhu et al, 2011; Zhu et al, 2016), including higher expression of

miR-21 and miR-155 in both tumor tissues and serum as predictors of recurrence and poor survival in NSCLC (Hou et al, 2016). However, other authors noted that several miRNAs dysregulated in lung tumour tissue compared to healthy individuals, including miR-20, miR-106a, miR-17-3p, miR-155, miR-145 miR-93, miR-137, miR-372 and miR-182-3p, were not detected in serum from the same patients (Hu et al, 2010). It has then been suggested that dysregulation of circulating miRNAs might have a predictive role independent of tissue, that could be related to other cells and immunity altered in cancer (Hu et al, 2010).

In lung cancer prognosis, a study found that poor survival of NSCLC patients correlated with high serum levels of miR-486, miR-30d and miR-125; and low levels of miR-1 and miR-499 (Chen et al, 2008). In an independent study, levels of miR-155-5p, miR-223-3p and miR-126-3p in adenocarcinoma patients correlated with higher risk of disease progression. This prognostic miRNA signature was found to be specific of adenocarcinoma; a different miRNA signature was found to be predictive of progression in plasma of SCC patients (Sanfiorenzo et al, 2013). Tumour-derived overexpressed miRNAs in plasma were significantly downregulated from 10 days to 14 days after surgical resection, giving an indication of circulating miRNA turnover, and indicating that at least some of the circulating miRNAs are of tumour origin (Le et al, 2012).

Aside from serum, cell-free miRNAs were studied in pleural effusions of lung cancer patients, and high levels of miR-100 and low levels of miR-93, miR-134, miR-151 and miR-345, were found to be useful prognostic markers of poor survival (Wang et al, 2012a).

In general, studies on circulating miRNAs as biomarkers of lung cancer present high variability on the miRNA signature suggested to have predictive value(Jarry et al, 2014). These differences, similarly to tissue, are most likely due to a combination of technical and biological variation.

1.5.14 Viral miRNAs

Viral infections have also been associated with miRNAs, which may be host-encoded and virus-encoded. Viruses have been found to use miRNAs in an effort to manipulate the host cell machinery for their benefit and have the advantage of

being small and non-antigenic (Cullen, 2010; Harwig et al, 2014). Host miRNAs, on the other hand, can target viral transcripts and impair essential functions (Bushati & Cohen, 2007).

The first viral miRNAs were identified in Epstein-Barr virus (EBV), member of the herpesvirus family (Pfeffer et al, 2004). Since then, a total of 530 miRNAs from 34 different viral species have been reported and are now listed in miRBase (miRBase v22.1). Most of the viral miRNAs described to date are encoded by members of the herpesvirus family, DNA viruses with a large genome. Herpesvirus are also more likely to contain a higher number of miRNAs in their genome, which might be related to the advantages miRNAs confer in their establishment of latent life-long infections in their hosts (Grey, 2015).

Besides herpesviruses, other nuclear DNA virus, e.g. polyomaviruses and papillomaviruses, encode miRNAs (Kincaid & Sullivan, 2012). However, cytoplasmic DNA viruses are thought not to encode miRNAs, as it is believed that they wouldn't have access to the cell machinery needed for miRNA biogenesis (Cullen, 2010). No viral encoded miRNAs have found in cytoplasmic DNA virus families.

RNA viruses were also initially believed not to encode miRNAs because processing of a miRNA from the viral genome by RNA polymerase II would induce cleavage and degradation of the genome. However, it has since been discovered that miRNAs can also be transcribed by RNApol III, indeed, RNApol III transcribes bovine foamy virus miRNAs (Cullen, 2006; Kincaid et al, 2012).

Viral miRNAs have been found to play a role in several steps of the viral infection. For instance, most herpesvirus miRNAs are found expressed in latent cells, and bovine herpes virus type 1 (BHV1) miRNAs bhv1-miR-B8 and bhv1-miR-B9, are reported to target viral transcripts and potentially limit viral replication (Cullen, 2006; Kanokudom et al, 2018). BK polyomavirus also encodes a miRNA: bkv-miR-B1 which auto-regulates early gene expression by cleaving their transcripts (Seo et al, 2008). Simian virus 40 (SV40) is reported to encode miRNAs able to downregulate expression of the T antigen, regulating the hosts cytokine release and, thus, the immune response to infection (Sullivan et al, 2005). Murine

gammaherpesvirus 68 (MHV68) encodes miRNAs that have been suggested to play important roles in infection and inhibition of the host response (Macrae et al, 2001). A mutant of MHV68, unable to express miRNAs, was attenuated *in vivo*: infection with the mutant virus resulted in lower levels of viral replication and pathogenesis, the inflammatory response to the mutant virus was greater, and the host was able to clear the infection faster (Macrae et al, 2001). Other examples of viral miRNAs that target host factors include miR-BART6-3p, encoded by EBV. miR-BART6-3p was reported to target the retinoic acid-inducible gene 1 (RIG-1), inhibiting interferon mediated immune responses (Lu et al, 2017).

Relevant to the present project, four retroviruses have been found to encode miRNAs. Bovine foamy virus (BFV) and simian foamy virus (SFV), members of the spumavirus genus, encode 4 and 13 mature miRNAs respectively. Human immunodeficiency virus 1 (HIV-1), encodes 4 mature miRNAs, and bovine leukemia virus (BLV), encodes 10 mature miRNAs. Retroviral miRNAs and their functions are summarised in **Table 1.2**.

The presence of HIV-1 encoded miRNAs has been a controversial topic. Some authors reported that no miRNAs were encoded by HIV-1 (Lin & Cullen, 2007; Pfeffer et al, 2005), whereas others reported that HIV-1 miRNAs could be experimentally detected (Bennasser et al, 2005; Omoto & Fujii, 2005; Omoto et al, 2004). It has been suggested that differences between these studies could be due to very low expression levels of the miRNAs or mutations in the HIV-1 genome that could alter miRNA expression (Kaul et al, 2009; Lamers et al, 2010). However, the presence of mutations would argue against a meaningful role of the miRNAs in HIV1 infection. It has also been suggested that HIV-1 miRNAs could potentially be expressed in a limited stage of the infection, or in a specific cell-type (Lamers et al, 2010). Of the potential HIV-1 encoded miRNAs, hiv1-miR-TAR appears to have good evidence supporting its existence, TAR was shown to be cleaved by Dicer and miRNAs processed from both arms of the precursor (Ouellet et al, 2008). In addition, in a later study hiv1-miR-TAR miRNAs were found to be loaded into Argonaute complexes, and reported to target host cell genes that promote apoptosis of infected cells (Ouellet et al, 2013). On the other hand, evidence of the authenticity of hiv1-miR-HN367 and hiv1-miR-H1 existence is weaker, these

potential miRNAs have been experimentally cloned and hiv1-miR-HN367 has been detected in northern blots but further characterisation of their biology or processing has not been performed (Balasubramaniam et al, 2018; Omoto & Fujii, 2005; Omoto et al, 2004).

The functions of HIV-1 miRNAs have been investigated: hiv1-miR-H1 was reported to target apoptosis antagonising transcription factor (*AATF*) and promote apoptosis of monocytes (Kaul et al, 2009). Hiv1-miR-N367 was reported to have a similar seed sequence to miR-192, and both were reported to target the poly-A binding protein 4 gene (*PAPBC4*), related to translational repression of infected cells (You et al, 2012).

BLV miRNAs were found in higher abundance than host miRNAs in infected cells, suggesting a biological role for them. This was confirmed when the BLV encoded blv-miR-B4 was found to have homology with a host miRNA (miR-29) associated with B-cell proliferation and oncogenesis (Kincaid et al, 2012). This finding indicated that viral miRNAs may play an important part in retroviral-mediated transformation (Kincaid et al, 2012). Some of the reported targets of blv-miR-B4-3p are granzyme A (*GZMA*), FBJ murine osteosarcoma viral oncogene homolog (*FOS*), and palmitoyl-protein thioesterase 1 (*PPT1*), which have roles in the immune response (Gillet et al, 2016). Interestingly, one study reported the presence of polymorphisms in BLV pre-miRNAs (pre-miR-B2, pre-miR-B3, pre-miR-B4 and pre-miR-B5) and found that some alleles were associated with increased white blood cell counts in infected hosts (Zyrianova & Koval'chuk, 2018). Similarly, Kaposi sarcoma associated herpesvirus (KSHV) and Marek's disease virus (MDV) encode a miRNA ortholog to the host miRNA miR-155, related to B-cell transformation (Gottwein et al, 2007; Zhao et al, 2011).

Table 1.2. Summary of retroviral-encoded miRNAs and their functions.

Virus	miRNAs	Genomic location	Function	References
BFV[1]	bfv-miR-BF1 bfv-miR-BF2	U3 region of the LTR. Transcribed by pol III to give a long pri-miRNA that is cleaved into two pre-miRNAs.	Unknown	(Cao et al, 2018; Whisnant et al, 2014)
BLV[2]	blv-miR-B1 blv-miR-B2 blv-miR-B3 blv-miR-B4 blv-miR-B5	Conserved cluster antisense of *rex-tax-env.* Transcribed by pol III and similar to tRNAs, drosha independent.	Blv-miR-B4, shares seed sequence with miR-29, can regulate same targets	(Burke et al, 2014; Kincaid et al, 2012; Rosewick et al, 2013; Zyrianova & Koval'chuk, 2018)
HIV-1[3]	hiv1-miR-H1 hiv1-miR-N367 hiv1-miR-TAR	Downstream of the NF-κB sites in the LTR, *nef* and *tat* genes, respectively	miR-H1 promotes apoptosis. miR-N367 is similar to miR-192 miR-TAR represses transcription by targeting the LTR	(Kaul et al, 2009) (Ouellet et al, 2008) (Klase et al, 2007; You et al, 2012)
SFV[4]	sfv-miR-S1 sfv-miR-S2 sfv-miR-S3 sfv-miR-S4 sfv-miR-S5 sfv-miR-S6 sfv-miR-S7	U3 region of the LTR. Transcribed by pol III, drosha dependent.	miR-S4-3p is similar to miR-155, which is lymphoproliferative and induces cell survival. miR-S6-3p is similar to miR-132, an innate immune suppressor.	(Kincaid et al, 2014)

[1] BFV: bovine foamy virus
[2] BLV: bovine leukemia virus
[3] HIV-1: human immunodeficiency virus 1
[4] SFV: simian foamy virus

Although there are some examples of virus which share miRNA homology, such as EBV and rhesus lymphocryptovirus, most miRNAs are not conserved in viral species and don't have host orthologs (Nair & Zavolan, 2006). Thus, making it difficult to predict if a certain virus encodes miRNAs. Many viruses have not been found yet to encode miRNAs, but have been reported to alter miRNA expression levels in their hosts during infection. These findings indicate that besides from the

expression of viral miRNAs, host miRNA expression might be indicative of the presence of infection.

Host miRNAs have been reported to play a role in controlling viral infections by inhibiting viral replication, and in some instances, viruses have been reported to downregulate these miRNAs to facilitate infection (Cullen, 2013b; Grassmann & Jeang, 2008). Nevertheless, it is now thought that most viruses might have evolved other mechanisms to avoid being controlled by host miRNAs, such as short 3'UTRs (reviewed in Cullen (2013a)). On the other hand, some viruses have been found to stimulate the expression of certain host miRNAs that target host mRNAs with antiviral potential or other host miRNAs that might benefit them (Cullen, 2013b; Grassmann & Jeang, 2008). Some well-known examples of dysregulated host miRNAs in viral infection are: EBV induced expression of miR-155 in infected B cells, miR-155 can promote oncogenic transformation in B cells, aiding infection spread (Cameron et al, 2008). A unique mechanism is the one used by HCV, miR-122 is known to bind to the 5′-UTR of the viral genome and enhance HCV replication (Jopling et al, 2005). In contrast, expression of host miRNAs miR-199a and miR-210 reduced replication of HBV by binding to viral proteins (Zhang et al, 2010a).

Some commonly deregulated miRNAs in oncogenic virus infections include miR-155, miR-21, miR-31, miR-130b, miR-93 (Bolisetty et al, 2009; Vojtechova & Tachezy, 2018; Yeung et al, 2008). Roles of these miRNAs include inhibition of apoptosis and promoting cell proliferation (Vojtechova & Tachezy, 2018).

To this date, no betaretroviruses have been reported to encode miRNAs. Analysis of MMTV revealed that it does not encode miRNAs, but host miRNA expression was found altered during infection. Infection with MMTV increased the expression of the oncogenic cluster miR-17-92 and miR-183 (Kincaid et al, 2018). miRNA expression has also been examined in ENTV-2 infection, no miRNAs have been reported to be encoded by the virus but miRNAs miR-34c, miR-143c, miR-190, miR-133a, miR-218, miR-490 and miR-10a were reported to be downregulated in nasal tumours of goats (Wang et al, 2016). Serine/threonine-protein kinase B-raf (*BRAF*) was a predicted target of miR-133a and novel identified miRNAs (Wang et al, 2016). Downregulation of miR-133a could thus, result in overexpression of

BRAF, which is a regulator upstream of the RAS-RAF-MEK-ERK pathway (Wang et al, 2016). Upregulation of this signalling pathway could lead to overproliferation. Similarities were found between miRNA expression in affected goats and studies of human nasopharyngeal carcinoma: miR-200 was found upregulated, and miR-9, miR-34 and miR-143 dowregulated in both samples from affected goats and humans (Wang et al, 2016). In addition, computational predictions have not identified miRNA candidates in any other member of the *Retroviridae* family (Burke et al, 2015; Kincaid et al, 2012; Kincaid et al, 2014). However, as previously mentioned, computational predictions might not be able to detect miRNAs that do not have a predicted morphology or the typical pol III promoter.

1.6 General aims

In the present study, it was hypothesised that miRNAs play a role in JSRV-infection and the oncogenic process. The hypothesis that expression of host encoded miRNAs is altered in JSRV-infection and, that JSRV encodes a miRNA were explored. In addition, it was hypothesised that differences in miRNA expression between JSRV-infected and uninfected animals could be exploited as biomarkers of OPA.

To explore these hypotheses the following aims were established:

- Detect miRNA expression in lung of JSRV-infected sheep and compare it to miRNA expression in uninfected sheep.
- Detect differences in miRNA expression in JSRV-infected and uninfected sheep in biofluids.
- Develop an *in vitro* system to study the role of miRNAs in the transformation process.

Chapter 2 Materials and Methods

2.1 Preparation of $JSRV_{21}$ viral particles

$JSRV_{21}$ viral particles were produced by *in vitro* transfection of the 293T cell line with the plasmid $pCMV2JS_{21}$, which encodes an infectious molecular clone (Palmarini et al, 1999b). Transfections were performed in T75 flasks with 10 µg total DNA per flask using Fugene HD according to the manufacturer's recommendations. Forty-eight hours post-transfection the supernatant from cell culture was collected and concentrated by ultracentrifugation onto a glycerol cushion. The concentrated supernatant was subsequently resuspended in PBS and by RT-qPCR it was determined to contain 2.5×10^9 RNA copies of $JSRV_{21}$ per ml. Mock inoculate was prepared in the same manner using supernatant from untransfected cells. Mutant $JSRV_{21}$ particles were produced in the same way with a JSRV-EnvM574A molecular clone, kindly gifted by Professor Hung Fan, University of California at Irvine. This molecular clone encodes an infectious but transformation deficient $JSRV_{21}$ mutant with a single amino acid change in the cytoplasmic tail region of Env (Hull & Fan, 2006).

2.2 Experimental infection of SPF lambs

Samples from two experimental infections that took place in 2007 and 2015 were used in this project. Animal experiments were approved by the Moredun Research Institute Animal Welfare and Ethical Review Board and performed in conformance with the Animal Scientific Procedures Act 1986.

In experimental infection 07, pregnant ewes were hysterectomised, and full-term Scottish blackface lambs still in the uterus were disinfected in tanks. Lambs were resuscitated, bottle fed and separated into two groups housed in different rooms under specific pathogen free (SPF) conditions. At six days of age lambs were inoculated intratracheally using an 18 gauge intravenous cannula to deliver the infectious inoculate and the mock inoculate to age-matched control lambs. Lambs were euthanised by intravenous injection of barbiturate at the first presentation of respiratory distress, and an age-matched control was euthanised at the same time.

Samples were collected post-mortem following a strict procedure that included taking lung tissue samples from 24 fixed sample sites, lymph nodes, kidney, liver and spleen to obtain a picture of the disease state of the lamb. Samples were preserved in 10% buffered formalin, and liquid nitrogen. **Fig. 2.1** shows a summary of the experimental design, the complete published study can be found at (Martineau et al, 2011).

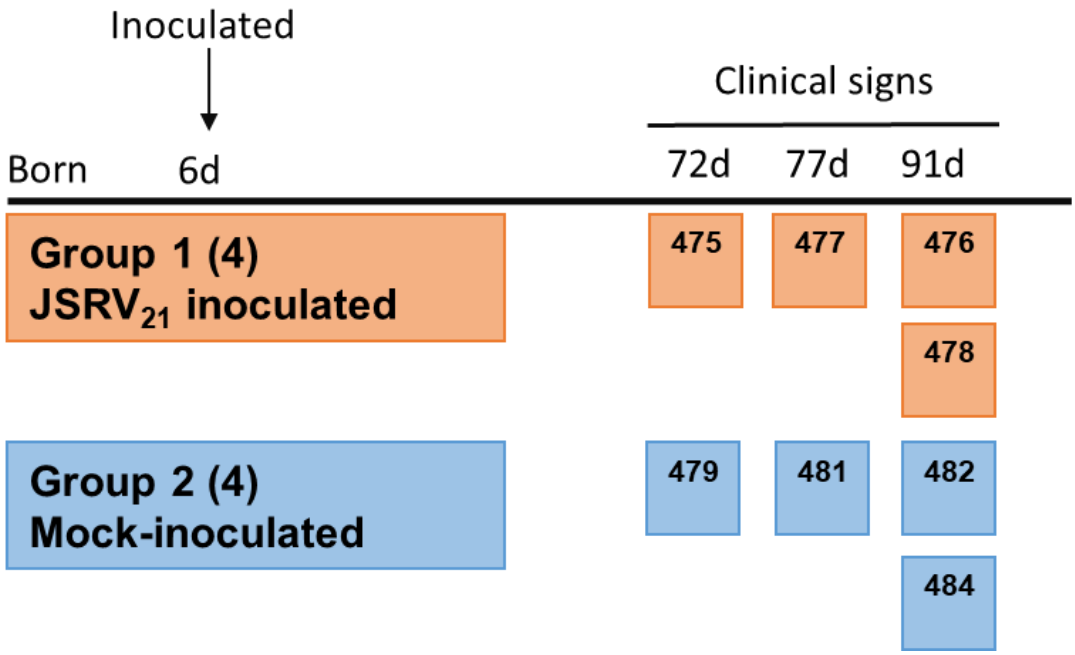

Figure 2.1. Summary representation of the samples used in this project from the experimental infection performed in 2007. *Numbers in brackets indicate the number of lambs per group. Each square represents an individual lamb with its ID number.*

In experimental infection 15, three groups, each containing 8 lambs, were studied. The first group was inoculated with wild-type JSRV, the second group was inoculated with the JSRV mutant ($JSRV_{mut}$) (JSRV-EnvM574A). The third group served as control and was mock-inoculated with 293T conditioned medium. The experimental infection procedure was carried out as described for infection 07. As in the previous experimental infection, animals showing signs of respiratory distress were euthanised with age-matched controls from the other two groups. **Fig. 2.2** shows a summary of the experimental design.

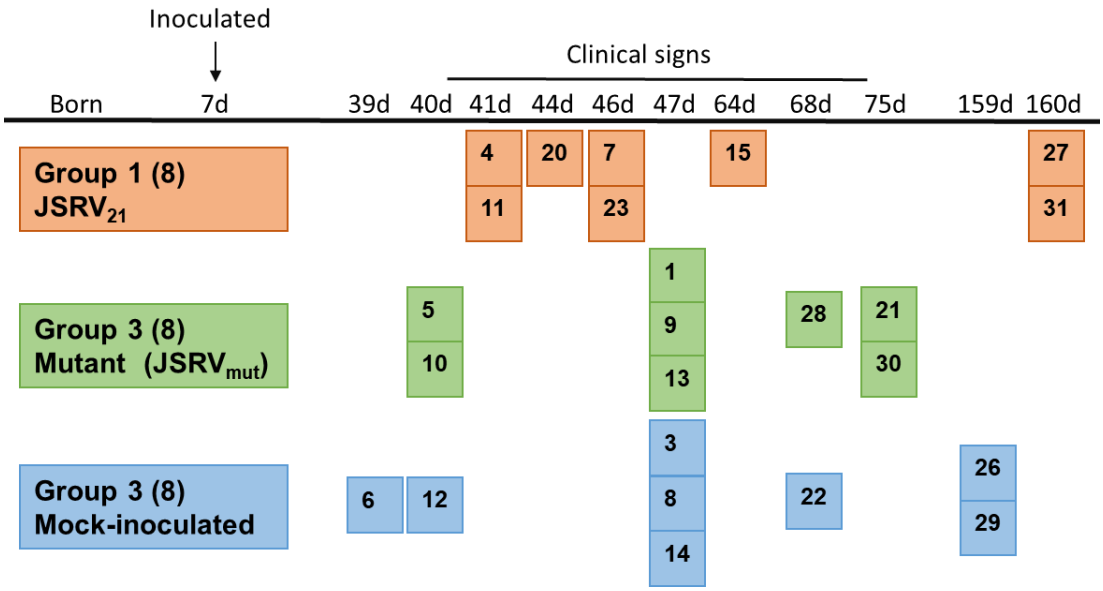

Figure 2.2. Summary representation of the experimental infection performed in 2015. Numbers in brackets indicate the number of lambs per group. *Each square represents an individual lamb with the reference SPF number inside.*

Table 2.1. Summary of lamb information for the 2007 experimental infection.

ID[1]	Group	Pathology findings	Gender	Date culled	Siblings
SPF475	$JSRV_{21}$ inoculated	Lung fluid[2], OPA lesions in both lungs	Male	66 dpi[3]	-
SPF476	$JSRV_{21}$ inoculated	Lung fluid	Female	85 dpi	SPF484
SPF477	$JSRV_{21}$ inoculated	Lung fluid, OPA lesions in one lung	Male	71 dpi	SPF481
SPF478	$JSRV_{21}$ inoculated	Lung fluid, OPA lesions and area of atelectasis	Male	85 dpi	SPF482
SPF479	Mock-inoculated	None	Male	66 dpi	-
SPF481	Mock-inoculated	None	Male	71 dpi	SPF477
SPF482	Mock-inoculated	None	Male	85 dpi	SPF478
SPF484	Mock-inoculated	None	Female	85 dpi	SPF476

[1] Only individuals used in RNA-sequencing are shown
[2] In all SPF cases described here, lung fluid was not a clinical finding but a pathological one. It was observed when lungs were cut post-mortem.
[3] Dpi: days post-infection.

Table 2.2. Summary of lamb information for the 2015 experimental infection.

ID[1]	Group	Pathology findings	Gender	Culled	Siblings
SPF4	$JSRV_{21}$	Lung lesions typical of OPA. Only lamb with lesion within bronchus. Allergic response.	Male	34 dpi[2]	SPF5, SPF6
SPF7	$JSRV_{21}$	Lung lesions typical of OPA	Female	39 dpi	SPF8, SPF9
SPF11	$JSRV_{21}$	Lung lesions typical of OPA	Female	34 dpi	SPF10, SPF12
SPF15	$JSRV_{21}$	Lung lesions typical of OPA. Allergic reaction.	Female	57 dpi	SPF13, SPF14
SPF20	$JSRV_{21}$	Lung lesions typical of OPA. Allergic reaction.	Male	37 dpi	SPF21
SPF23	$JSRV_{21}$	Lung lesions typical of OPA	Male	39 dpi	SPF22
SPF27	$JSRV_{21}$	Small OPA tumours	Female	153 dpi	-
SPF31	$JSRV_{21}$	OPA tumours	Male	153 dpi	SPF30, SPF29
SPF1	$JSRV_{mut}$	No OPA lesions. Higher number of macrophages than control.	Male	40 dpi	SPF3
SPF5	$JSRV_{mut}$	No OPA lesions. Allergic reaction.	Male	33 dpi	SPF4, SPF6
SPF9	$JSRV_{mut}$	No OPA lesions. Allergic reaction. More macrophages than control.	Female	40 dpi	SPF7, SPF8
SPF10	$JSRV_{mut}$	Mild suppurative bronchiolitis. Allergic reaction.	Female	33 dpi	SPF11, SPF12
SPF13	$JSRV_{mut}$	No OPA lesions. Higher number of macrophages than control.	Male	40 dpi	SPF14, SPF15
SPF3	Mock	No OPA lesions	Male	40 dpi	SPF1
SPF6	Mock	White muscle disease	Female	32 dpi	SPF4, SPF5
SPF8	Mock	No OPA lesions. Allergic reaction	Female	40 dpi	SPF7, SPF9
SPF12	Mock	No OPA lesions. Allergic reaction	Male	33 dpi	SPF10, SPF11
SPF14	Mock	None. Allergic reaction	Male	40 dpi	SPF13, SPF15
SPF22	Mock	Manipulation damage to lungs. No OPA lesions.	Female	61 dpi	SPF23
SPF26	Mock	No OPA lesions. Allergic reaction	Male	152 dpi	-
SPF29	Mock	None.	Female	152 dpi	SPF30, SPF31

[1] Only individuals used in miRNA RT-qPCR or small RNA sequencing are shown
[2] Dpi: days post-infection.

2.3 Natural cases of OPA

Twenty-three adult sheep were received at the post-mortem (PM) rooms of the Moredun Research Institute between the 1st of February 2016 and the 11th of February 2016 (**Table 2.3**). All animals were suspected cases of OPA from four different farms. Blood samples were extracted prior to euthanasia using 18 gauge needles (Greiner Bio-One) and red vacutainers with clot activator (BD 367895) (BD). Animals were euthanised by intravenous injection of pentobarbital and post-mortem, lungs were removed from the carcass. Lungs were visually examined for tumour presence and sectioned using a sharp blade; two tissue sections were collected in formal saline pots (Cellpath) and two were snap frozen in liquid nitrogen and stored at -80ºC for histopathology examination and further analysis.

In the study of serum, OPA negative sheep received at the post-mortem rooms were used as controls, and samples collected in the same manner as samples from OPA affected sheep. OPA negative status was confirmed by histological examination of several lung sites. As OPA negative animals received at PM rooms typically presented with poor condition and body score, four healthy adult sheep from the Moredun flock were also used as control blood donors.

In the study of natural OPA tissue, samples from ten adult sheep, received at the Moredun PM rooms, which had tested positive for OPA were used (**Table 2.4**). Six ewes were used as healthy controls, these ewes were the dams of lambs used in the experimental infection that took place of 2015 and had tested negative for OPA by histological examination of lung sections taken from six sites post-mortem.

In the study of miRNA expression from BALF macrophages, 11 adult sheep were received at the Moredun PM rooms from Scottish farms. Animals were classified in three groups: OPA-affected, Parasite-infected (where only lungworms were present) and healthy controls, if the lungs appeared healthy (**Table 2.5**).

BALF samples were obtained using established methods. Briefly, following euthanasia, the trachea was transected and occluded to prevent blood contamination of the lungs. The lungs, with trachea attached, were removed and transferred to a clean working area. The trachea was again transected at

approximately 14 cm from the carina. Approximately 1 L of sterile PBS (Sigma Aldrich) with 5% FBS (Sigma Aldrich) was instilled into the lungs using a cuffed endotracheal tube. Following gentle massage of the lungs, the BALF was retrieved by gravity. BALF was immediately placed on ice and processed within 30 minutes of collection.

Table 2.3. Animal information from healthy controls and natural OPA cases received at PM rooms for serum analysis.

Date	ID	Breed	Gender	Diagnosis	Lung fluid	Additional information
01-Feb-16	JA 811	Scottish Blackface	Male	Advanced OPA	Yes, >30 ml	It had an abscess in the lung too, tissue sample taken from other region
04-Feb-16	G21	Scottish Blackface	Female	Probably not OPA, or early OPA. Atelectasis	No	
04-Feb-16	G22	Scottish Blackface	Female	Early OPA	Yes, 30 ml	
04-Feb-16	G23	Scottish Blackface	Female	Not OPA	No	
08-Feb-16	A48	Scottish Blackface	Male	OPA	Yes, 4ml	
08-Feb-16	A49	Scottish Blackface	Female	Not OPA, massive bacterial abscess	No	
08-Feb-16	B14	Scottish Blackface	Female	Advanced OPA	Yes, 15 ml	
08-Feb-16	B16	Scottish Blackface	Female	OPA	No	
08-Feb-16	G14	Scottish Blackface	Female	OPA diffuse areas and large solid areas	Yes, 20ml	
08-Feb-16	G25	Scottish Blackface	Female	Advanced OPA	No	
08-Feb-16	G29	Scottish Blackface	Female	Not OPA	No	
08-Feb-16	G32	Scottish Blackface	Female	Advanced OPA	No	
10-Feb-16	A50	Scottish Blackface	Female	OPA	Yes, 20 ml	
10-Feb-16	A51	Scottish Blackface	Female	no visible OPA	No	

Table 2.3. Animal information from healthy controls and natural OPA cases received at PM rooms for serum analysis.

Date	ID	Breed	Gender	Diagnosis	Lung fluid	Additional information
10-Feb-16	A52	Scottish Blackface	Female	no visible OPA	No	
10-Feb-16	A53	Scottish Blackface	Female	OPA	Yes, 20ml	Little serum recovered, instead there was a white thick liquid. Could be related to high protein concentration.
10-Feb-16	A54	Scottish Blackface	Female	OPA and small abscess	No	
11-Feb-16	A55	Scottish Blackface	Female	not OPA	No	
11-Feb-16	A56	Scottish Blackface	Female	early OPA or atelectasis	No	
11-Feb-16	A57	Scottish Blackface	Female	Not OPA	No	
11-Feb-16	A58	Scottish Blackface	Female	OPA	Yes, 10ml	
11-Feb-16	A59	Scottish Blackface	Female	No visible OPA, could be early case	No	
11-Feb-16	JA812	Cheviot	Female	early OPA and chronic fibrous hepatitis	No	
24-May-16	6230	Texel x Scottish Greyface	Female	N/A	No	Healthy blood donor from Moredun flock.
27-May-16	6318	Texel x Scottish Greyface	Female	N/A	No	Healthy blood donor from Moredun flock.
27-May-16	6353	Texel x Scottish Greyface	Female	N/A	No	Healthy blood donor from Moredun flock.
27-May-16	6354	Texel x Scottish Greyface	Female	N/A	No	Healthy blood donor from Moredun flock.

Table 2.4. Animal information from healthy controls and natural OPA cases received at PM rooms for lung tissue analysis.

Date	ID	Breed	Gender	Diagnosis	Lung fluid	Additional information
4-May-17	JA874	Scottish Blackface	Female	Clinical OPA	Yes, 25 ml	Transthoracic ultrasound negative on Jan 17
4-May-17	JA875	Scottish Blackface	Female	Clinical OPA	Yes, 30 ml	Early OPA diagnosed on Jan 17 by transthoracic ultrasound
19-May-17	JA876	Scottish Greyface	Female	Clinical OPA	Yes	
10-Aug-17	JA894	Scottish Blackface	Female	Clinical OPA	Yes, 10 ml	Gut sample-inflammation
10-Aug-17	JA895	Scottish Blackface	Female	Clinical OPA smaller tumours	Yes, 5ml	
10-Aug-17	JA896	Scottish Blackface	Female	Clinical OPA	Yes, 30 ml	Very enlarged lungs due to tumour volume
10-Aug-17	JA897	Scottish Blackface	Female	Small OPA tumour	No	
10-Aug-17	JA898	Scottish Blackface	Female	OPA	Yes, > 30 ml	Abscess and worm lesions in other areas of the lung
11-Aug-17	JA899	Scottish Blackface	Female	OPA	Yes, > 30 ml	
11-Aug-17	JA901	Scottish Blackface	Female	OPA	Yes, > 30 ml	
11-Aug-17	JA902	Scottish Blackface	Female	OPA	Yes, > 30 ml	
5-Mar-15	MP15/ 170	Texel	Female	OPA- / Healthy	No	
5-Mar-15	MP15/ 171	Greyface	Female	OPA- / Healthy	No	
5-Mar-15	MP15/ 172	Greyface	Female	OPA- / Healthy	No	
5-Mar-15	MP15/ 173	Greyface	Female	OPA- / Healthy	No	
5-Mar-15	MP15/ 174	Greyface	Female	OPA- / Healthy	No	
5-Mar-15	MP15/ 175	Greyface	Female	OPA- / Healthy	No	

Table 2.5. Animal information from cases received for BALF macrophage isolation.

Date	ID	Breed	Gender	Diagnosis	Lung fluid	Additional information
26-Jan-17	OPA1	Scottish blackface	Female	Clinical OPA	No	
16-Feb-17	OPA2	Scottish blackface	Female	Clinical OPA	Yes	
20-Feb-17	OPA3	Scottish blackface	Female	Clinical OPA	Yes	
21-Feb-17	OPA4	Scottish blackface	Female	Clinical OPA	No	
1-Mar-17	OPA5	Scottish blackface	Female	Clinical OPA	No	Smaller tumours
3-Mar-17	CON1	Scottish blackface	Female	Healthy	No	
14-Mar-17	CON2	Scottish blackface	Female	Healthy	No	
21-Mar-17	CON3	Scottish blackface	Female	Healthy	No	
15-Mar-17	PARA1	Scottish blackface	Female	lungworms	No	
16-Mar-17	PARA2	Scottish blackface	Female	lungworms	No	
20-Mar-17	PARA3	Scottish blackface	Female	lungworms	No	

2.3.1 Histopathology examination

Examination of formalin fixed tissue sections was conducted by the Pathology Department at the Moredun Research Institute. Tissue staining with haematoxylin and eosin as well as immunohistochemistry for JSRV-Env (section 2.10) were performed. Test results were used to determine the presence or absence of OPA lesions in the tissue.

2.4 Processing of samples

2.4.1 Serum extraction from blood samples

Blood samples collected in vacutainers were left to clot at room temperature. After a maximum of 4 hours, blood samples were centrifuged at 1,912 × *g* for 10 minutes at 4°C. The supernatant, consisting of the serum fraction, was transferred to centrifuge tubes and spun at 17,000 × *g* for 10 minutes at 4°C to pellet any remainders from other blood fractions. Serum was preserved in 1 ml aliquots at -80ºC for future analysis.

Several reports have shown that haemolysis affects miRNA detection in serum and plasma samples (Kirschner et al, 2011; McDonald et al, 2011a; Pritchard et al, 2012). In this study, the extent of haemolysis was controlled by reducing the storage time of samples at room temperature to a maximum of 4 hours. Serum samples were also visually inspected, and aliquots with a detectable pink colour were discarded.

2.4.2 RNA extraction from serum samples

RNA extraction from sera was performed using TRIZOL LS (Thermo Fisher Scientific) and following the manufacturer's instructions with some modifications. Briefly, samples were first diluted 1:1 with distilled water, three volumes of Trizol LS were then added and mixed until homogenised. Chloroform (0.8 volumes) was then added and mixed vigorously to facilitate precipitation of DNA and proteins. After incubating for 10 minutes at room temperature, samples were spun at 17,000 × *g* for 10 minutes at 4°C in a table-top microcentrifuge. The aqueous phase, containing the RNA, was transferred to a new tube and two volumes of isopropanol and 1 µl of GlycoBlue (Invitrogen) were added and mixed. GlycoBlue consists of a blue dye linked to glycogen, it co-precipitates with nucleic acids and aids in pellet visualisation. After incubating for 10 minutes at room temperature, samples were centrifuged 17,000 × *g* for 30 minutes at 4°C, and the presence of blue pellets containing the precipitated RNA observed in the samples. Two washes were performed using two volumes of 70% ethanol. After the second wash, pellets were air-dried and resuspended in 15 µl of RNAse-free water. Extracted RNA samples were stored at -80°C.

2.4.3 Cryosectioning and homogenisation of lung tissue samples

Sections of lung tissue collected post-mortem were stored at -80°C until cryosections were to be cut. The FSE cryostat (Thermo Fisher Scientific) was set at -20°C chamber temperature, -55ºC cryobar temperature, -20ºC specimen temperature and 15 µm cut thickness. Three 15 µm sections from each specimen were added to Lysing matrix D 2 ml tubes (MP Biomedical) containing 350 µl of RLT plus buffer (Qiagen) with 5% β-mercaptoethanol (BDH). β-mercaptoethanol is a reducing agent that when present in the buffer inactivates the RNAses present in the sample helping to prevent RNA degradation.

For experimental cases, eight tissue sections, corresponding to eight distinct lung sites, were cryosectioned and extracted per animal. In contrast, for natural cases one section was used per animal. These differences in sample processing were made based on the nature of the tissue being used. As described in section 1.3.1, in early experimental OPA cases tumours tend to be small and diffuse with only a small percentage of tumour found per tissue section. Thus, processing eight sections from different locations in the lung ensures obtaining a global view of the events taking place in the lung. On the other hand, in advanced cases of OPA, tumours are larger and take up a higher proportion of the tissue sections obtained (in our case around 50%) meaning one section should give us a general representation of OPA affected lung.

Cryosectioned samples were kept on ice and homogenised using the Precellys 24 (Bertin Technologies). Two cycles of 30 s at 6,000 rpm, with a 2 minute interval on ice, were performed. After homogenisation samples were stored at -80°C for future RNA extraction.

2.4.4 Processing of BALF samples

BALF cells (section 2.3) were processed to isolate CD14-positive cells by Anna Karagianni, as previously described (Clark et al, 2017; Karagianni et al, 2017). Briefly, CD14 positive cells were isolated using human anti-CD14 magnetic microbeads (MACS, Miltenyi Biotec), according to the manufacturer's instructions.

Flow cytometry confirmed that over 95% of the purified CD14-positive cells also expressed the macrophage marker CD163 (Anna Karagianni, unpublished).

2.4.5 RNA extraction from lung tissue, BALF and cell culture samples

RNA extraction was performed using the RNeasy Plus micro kit (Qiagen) following the manufacturer instructions in Appendix D to obtain total RNA containing the small RNA fraction (<200 nt), where miRNAs are expected to be found. This kit uses gDNA binding columns to eliminate the small quantities of genomic DNA found in the sample, while RNA is eluted due to the high-salt buffer conditions. The eluate containing RNA is then mixed with ethanol to enable binding to the MinElute columns of the kit. After several washes to remove other contaminants, RNA is then eluted in RNAse-free water.

2.4.6 RNA extraction for high RNA yield

Some techniques performed in this project required high RNA concentrations and thus, higher quantities of starting material, not compatible with the previously reported methods for RNA extraction.

2.4.6.1 From cell culture samples

RNA extraction from cell culture samples was performed using the RNeasy plus mini kit (Qiagen) following the manufacturer's instructions in appendix D, which allow for extraction of total RNA containing small RNAs. Up to 1×10^7 cells were stored in 700 µl of RLT+ buffer, and homogenised centrifuging for 2 minutes at 20,000 × *g* in Qiashedder columns (Qiagen). Homogenised samples were loaded into gDNA eliminator columns and centrifuged at 20,000 × *g* for 30 s, the flow-through was saved. The flow-through, containing RNA, was mixed with 1.5 volumes of 100% ethanol and up to 700 µl loaded into an RNeasy spin column. The RNeasy spin columns were centrifuged for 30 s at 20,000 × *g* and the flow-through discarded, the process was repeated until all the sample had passed through. The column containing the adsorbed RNA was placed in a new collection tube and 500 µl RPE buffer added and centrifuged at 20,000 × *g* for 2 minutes. The flow-through was discarded, and the wash process repeated but centrifuging for 30 s. Once washed, the column was placed in a new collection tube and centrifuged for 1 minute at 20,000 × *g* to eliminate residual buffer. To elute the

RNA, the column was placed in a 1.5 ml tube and 30 µl RNase-free water added into the centre of the column. The column was left to stand for 2 minutes and RNA eluted by centrifuging 1 minute at 17,000 × *g*. RNA was kept at -80˚C.

2.4.6.2 From lung tissue

RNA extraction from lung tissue to obtain high RNA concentrations were performed using the Direct-zol RNA miniprep plus procedure (Zymo) and following the manufacturer's directions. All centrifugation steps were performed at 20,000 × *g*.

Up to 50 mg of lung tissue were placed in Lysing matrix D 2 ml tubes containing 600 µl of direct-zol reagent. Samples were homogenised in the Precellys 24 (four cycles of 30 s at 6000 rpm, with 2-minute intervals on ice). Homogenised samples were centrifuged to pellet remaining debris and the supernatant was transferred to a new tube, where it was mixed with an equal volume of 100% ethanol. Up to 700 µl of the sample was then loaded into the column and centrifuged for 30 s, the flow-through was discarded and process repeated until all the sample had passed through. The column was placed in a new collection tube and 400 µl of RNA wash buffer added, the column was centrifuged for 30 s and flow-through discarded. 5 µl of DNase were mixed with 75 µl of DNase buffer, loaded into the column and incubated for 15 minutes at room temperature to degrade DNA. After the incubation, two washes with 400 µl of direct-zol buffer were performed and flow-through discarded. 700 µl of RNA wash buffer were then added, centrifuged for 2 minutes and flow-through discarded. The column was placed in a 1.5 ml tube and 50 µl of RNase-free water added to the centre, left to stand for 1 minute and RNA eluted by centrifuging for 1 minute. RNA was stored at -80°C.

2.4.7 Concentration and purification of RNA samples

When highly concentrated RNA samples were required, RNA was concentrated by ethanol precipitation. 0.1 volumes of 3M sodium acetate (pH 5.0-5.2) (Sigma Aldrich) were added to RNA samples, followed by 2 volumes of ice-cold 100% ethanol, and 1 µl of 20 mg/ml glycogen (Roche) to aid pellet visualisation. Samples were incubated at -80°C for 1 hour. After incubation, samples were centrifuged at 20,000 × *g* for 15 minutes. The pellet was then washed with 75 % ethanol twice to remove residual phenol, after performing the washes the pellet was left to air-

dry until fully transparent. RNA was then resuspended in RNase-free water, to help RNA dissolve it was heated at 60 ◦C for 10 minutes.

2.4.8 Assessment of RNA concentration and quality

Assessing the RNA for integrity and purity is critical to ensure only high quality material is used in downstream analysis. It has been reported that low integrity and purity of RNA samples affects downstream applications and assays such as RT-qPCR, whereas high quality material produces reliable results (Becker 2010).

2.4.8.1 Spectrophotometric analysis of RNA

Nanodrop spectrophotometer ND-1000 and Nanodrop ONE (Thermo Scientific) were used to analyse the extracted RNA. The RNA measurement option was selected and the spectrophotometer blanked with RNase-free water except for serum samples, for which the blank contained the equivalent concentration of GlycoBlue of the samples to avoid the absorbance of the dye interfering with results. 1.1 µl from each sample were assayed. Nucleic acid concentration (measured at 260 nm), as well as 230 nm and 280 nm absorbance measures were obtained. Absorbance ratios were used to evaluate sample purity. The 260/280 ratio was used to determine the presence of proteins, which absorb at 280 nm, in the sample. For RNA, ratios of 2.0 are considered pure, and ratios above 1.8 are considered suitable for expression analysis (Becker et al, 2010). The 230/260 ratio indicates presence of contaminants such as phenols or other organic compounds. For pure RNA 230/260 ratios are between 2.0-2.2.

2.4.8.2 Electrophoresis analysis of RNA quality

Electrophoretic analysis of RNA was performed using the Agilent Bioanalyser 2100 (Agilent Technologies) and Agilent RNA 6000 Nano assay and RNA Nano chip (Agilent Technologies) to obtain concentration, integrity and size measurements. RNA samples were thawed on ice and all reagents were equilibrated at room temperature 30 minutes before use. The electrophoretic analysis was performed as instructed in the manufacturer's protocol. Electrode decontamination was performed using RNasezap (Invitrogen) and RNase-free water, before and after running the assay. Prior to the analysis samples were denatured at 70°C for 2 minutes. Once set up following manufacturer's

instructions the Nano chip was vortexed at 2400 rpm for 1 minute and processed in the Agilent 2100 analyser within 5 minutes of sample addition.

The Agilent Nanochip system provides measurements of RNA integrity which are expressed as RNA integrity numbers (RIN). RIN values are calculated based on the ratio of areas under the 18S and 28S peaks of the electropherogram, and can range from 1 to 10. A value of 1 indicates fragmentation and a value of 10 indicates intact RNA with little degradation.

Even though this assay was originally designed to measure RNA integrity and the RIN values obtained do not assay for small RNA species, such as miRNAs, studies have shown that high integrity values for total RNA are positively correlated with good integrity of miRNAs. RIN values above 5 have been reported to produce reliable results in RT-qPCR (Becker et al, 2010).

2.5 RNA sequencing

RNA samples were sent to Edinburgh Genomics to perform small RNA sequencing. Library preparation was done using the TruSeq Kit (Illumina) and checked by HS Qubit and Bioanalyser. Sequencing was performed using Ilumina Hiseq v4 HO 50-base single-end sequencing.

2.5.1 Bioinformatics analysis of RNA sequencing results

Bioinformatics analysis of small RNA sequencing data was performed by Edinburgh Genomics. In brief, raw data was analysed for quality and low quality reads and adapters trimmed using Cutadapt. Reads longer than 28 nt and shorter than 17 nt were filtered out. The remaining reads were then mapped to miRBase using novoalign (Novocraft Technologies) with parameters: -m, -s 1, -t 30, -h 60. Reads were mapped to ovine, bovine, human and caprine entries of mirBase v.22.1. Sequence distribution and length distribution plots were created using Rstudio.

Reads that mapped to miRNAs of different species (oar-, bta-, hsa-, chi-) with identical sequences were merged with the use of a custom-made R script. Bam files were then analysed and raw reads normalised in Matlab based on size factors. This normalisation approach consists in considering a size factor for each

library to compute the effective library size. The size factors are calculated by taking the median of the ratios of observed counts to those of a reference sample, whose counts are calculated by calculating the mean of each gene across all samples (Anders & Huber, 2010). By dividing the counts of each library by the corresponding size factors, all counts are in the same scale, making them comparable.

A threshold was then established to remove reads with low number of normalised counts from the differential expression analysis. An average of 50 normalised counts across samples was established as a cut-off, based on published literature and the present data (Koh et al, 2010; Motameny et al, 2010; Spornraft et al, 2014; Taxis et al, 2017).

Differential expression analysis and statistics were also performed in Matlab using the negative binomial model (nbintest) with the 'Constant' option. A threshold of FDR < 0.05 was established as statistically significant.

Data used for PCA plots consisted of normalised counts of all miRNAs above the established threshold of an average of 50 normalised counts. PCA plots were created using Rstudio, the pam {cluster} function of ggplot2 (ggfortify) was used. Default options of the pam function were used except for aesthetics, which were based on Group.

Data used for heatmaps consisted of the DE miRNAs. Heatmaps were created using Rstudio, the pheatmap function was used. Default options of the pheatmap function were used, with the following exceptions: scale was set to “row”, column clustering distance was "correlation", row clustering distance was “euclidean”, clustering method was “average” and the annotation_col argument was used to show samples assigned to groups in the plot.

Reads were also mapped to JSRV (AF105220.1) and enJSRV sequences (EF680301.1) to look for the presence of viral miRNAs. Reads were counted using a custom-made Perl Script that allowed only 1 mismatch. Alignments were visualised using IGV.

2.6 Reverse transcription quantitative polymerase chain reaction (RT-qPCR) for detection of miRNAs

The expression of miRNAs was assessed using reverse transcription quantitative PCR (RT-qPCR). The RT-qPCR approach chosen was the TaqMan™ Advanced miRNA cDNA Synthesis Kit (Applied Biosystems) in conjunction with Taqman Advanced miRNA assays (Applied Biosystems). The reasons for the selection of this approach were the high accuracy and reliability of Taqman probes and the ability of the method to detect low miRNA concentrations. All tissue RNA samples were diluted to a concentration of 5 ng/µl, and 2 µl used as starting material for the protocol, for serum samples 2 µl were used as starting material. All reactions were performed according to the manufacturer's protocol. In brief, the protocol included a poly-A tailing reaction and a ligation reaction to be performed before the reverse transcription reaction, allowing universal primers to be used in the reverse transcription reaction. A universal amplification reaction followed the reverse transcription, this reaction increased the starting cDNA input for qPCR. All these reactions were performed in the Biometra T-one thermocycler (Analytik Jena). Quantitative PCRs (qPCRs) were set up as instructed in the manufacturer's protocol using the Taqman universal PCR mastermix (Applied Biosystems) and each of the specific sample-target combinations were assayed in duplicate. qPCR reactions were set up in 96-well plates and run in the ABI 7500 Real time PCR system (Applied Biosystems) with the following cycling stages: 2 minutes at 50˚C, 10 minutes at 95˚C, and 40 cycles of 95˚C for 15 seconds followed by 1 minute at 60 ˚C.

Levels of nine miRNAs (miR-135b, miR-182, miR-183, miR-200b, miR-205, miR-21, miR-31, miR-503 and miR-96) and an endogenous control miRNA (miR-191) were investigated. miRNA sequences targeted by the assays and the sequences found in the small RNA sequencing data can be found in the **Appendix**. The assays selected could detect the miRNA sequences in sheep cells, human cells and dog cells.

2.6.1 Validation of RT-qPCR parameters

Efficiency was assessed by making six serial dilutions of the template in molecular grade water and performing the qPCR reaction in duplicate for each dilution.

Master mix preparation and cycling conditions were as stated in section 2.6. qPCR efficiency (E) was then calculated by plotting the Ct values of each reaction against the logarithm of the template concentration, and fitting a line through the points in the plot. The slope of the fitted line was used to calculate the efficiency percentage using the following equation: $E = (10^{(-1/slope)})-1$.

In ideal conditions the efficiency of the qPCR should be 100%, meaning that in each cycle of the logarithmic phase of the reaction the PCR product is doubling. Efficiencies that are too low might indicate poor primer or probe design, or need for reaction optimisation, whereas higher efficiencies might indicate presence of inhibitors in the mix (Bustin, 2004).

The calculated efficiency for miR-191 was 100.8%, while the efficiencies of miR-135b, miR-182, miR-183, miR-200b, miR-205, miR-21, miR-31 and miR-503 ranged from 92.35% to 107.71%. Although the efficiencies deviated from the ideal (100%) efficiency, the range of efficiencies achieved fell into what is considered acceptable for RT-qPCR studies (90-110%) (Bustin et al, 2009).

2.6.2 Analysis of RT-qPCR data

Data obtained from RT-qPCR of miRNAs was analysed following the ddCt method (Livak & Schmittgen, 2001). Given that the efficiency of each of the primer assays and the control miRNA assay (miR-191) differed by less than 10% (2.6.1), the ddCt method was suitable for the analysis of the RT-qPCR results. Because miR-191 had an efficiency of 100.8%, the base of the equation was not altered, reflecting the amplification rate of 2 (**Fig. 2.3**).

Briefly, dCts were calculated for each sample individually, averages for each group were then calculated and used to calculate ddCt and fold change as shown in **Fig. 2.3.**

$$dCt = (Ct_{\text{target miRNA}} - Ct_{\text{reference miRNA}})$$

$$ddCt = (dCt_{\text{treated group}} - dCt_{\text{reference group}})$$

$$\text{Fold change} = (2^{-ddCt})$$

Figure 2.3. Summary of equations used to calculate miRNA expression fold changes, based in the ddCt method.

Dot plots and bar charts of RT-qPCR data were created using Rstudio. Dot plots were used to plot individual dCt values. Dot plots were created using the ggplot (geom_point) function and the arguments stat_summary, fun.data, fun.args and geom= “crossbar” used to draw the mean ± standard deviation. Bar charts were created using ggplot (geom_col) and the argument geom_errorbar to depict standard deviations of the $\log_2$(fold change).

Correlation plots were created using Rstudio ggplot. The arguments geom_point, geom_smooth and geom_cor were used with default parameters. Confidence level was established at 0.95 and chosen method was “pearson”.

Statistical tests were performed on dCt values using Minitab 17. When pairwise comparisons were performed the two-sample t-test was used, when three groups were compared the one-way ANOVA test was used. In all cases, the threshold for statistical significance was established at $p< 0.05$.

2.7 Culture of cell lines

2.7.1 Heat inactivation of fetal bovine serum

Fetal bovine serum (FBS) was used in the culture of cell lines to supply growth factors needed for optimal *in vitro* culture. Heat inactivation of FBS was performed to inactivate complement factors as well as other factors that could inhibit cell growth.

FBS (Sigma Aldrich) was thawed at 37˚C. Once thawed, FBS was heat inactivated for 30 minutes at 56˚C swirling the FBS bottle every 10 minutes. Heat inactivated FBS (HI-FBS) was stored in 25 ml aliquots at -20°C.

2.7.2 Preparation of growth media

Preparation of growth media for culture of cell lines was done in class 2 microbiological safety cabinets (CAS) and maintaining sterility throughout the process. Various types of growth media were used and supplemented depending on the requirements of the cell lines to be grown. Complete media were kept at 4˚C for up to 1 month. A summary of the growth media and supplements needed to culture each cell line can be found in **Table 2.6.**

Table 2.6. Summary of growth media composition for each cell line used.

Cell line	Cell type	Growth medium	Supplements
208F (Topp, 1981)	Fischer rat fibroblast from embryo	Minimum Essential Media Eagle (MEME) (Sigma Aldrich)	2 mM glutamine (MRI in-house), 1% non-essential aminoacids (NEAA) (Sigma Aldrich), 10% HI-FBS
MDCK (Gaush et al, 1966)	Dog epithelial from kidney	Dulbecco's Modified Eagle Medium (DMEM) (Sigma Aldrich)	2 mM glutamine, 1% NEAA, 10% HI-FBS, 20 µg/ml gentamicin (Sigma Aldrich)
293T (DuBridge et al, 1987; Graham et al, 1977)	Human embryonic kidney adenovirus and SV40 transformed	Iscove's Modified Dulbecco's Medium (IMDM) (Sigma Aldrich)	4 mM glutamine, 1% NEAA, 10% HI-FBS, 20 µg/ml gentamicin (Sigma Aldrich)
CPT-Tert (Arnaud et al, 2010)	Sheep choroid plexus SV40 and hTERT transformed	IMDM	4 mM glutamine,10% HI-FBS
JA584 and JS-7 (Jassim et al, 1987)	Sheep OPA tumour	IMDM	4 mM glutamine, 10% HI-FBS, 20 µg/ml gentamicin, 1% Penicillin/Streptomycin (10,000 units penicillin/mL, 10,000 µg streptomycin/mL) (MRI in-house), 1.25 µg/ml Amphotericin B (Sigma Aldrich)
NIH 3T3 (Jainchill et al, 1969)	Fibroblast from NIH swiss mouse embryo	DMEM	2 mM glutamine, 1% NEAA, 10% HI-FBS, 20 µg/ml gentamicin
CRFK (Crandell et al, 1973)	Epithelial from cat kidney	DMEM	2 mM glutamine, 1% NEAA, 10% HI-FBS, 20 µg/ml gentamicin

2.7.3 Cell thawing

Cryovials of cells stored in liquid nitrogen were thawed in a 37˚C water bath. Thawed cells were then added to a T-75 cell culture flask (Corning) and 20 ml of growth medium added dropwise while gently swirling the flask to ensure an even mix and to aid the cells in the thawing process, decreasing dimethyl sulfoxide (DMSO) (Sigma Aldrich) concentration gradually.

2.7.4 Passage of cells in culture

Cell lines were passaged two-three times a week. Briefly, growth medium was removed, a phosphate buffered saline (PBS) (MRI in-house) wash was performed and a dissociation agent added and incubated at 37°C until cells had detached

from the culture vessel. An equal amount of growth medium was added to the cells suspended in the dissociation reagent to stop the reaction. The cell suspension was then split as required and cultured in new vessels. **Table 2.7** lists the dissociation reagents used for each cell line.

Table 2.7. Summary of dissociation reagents used for each cell line.

Cell line	Dissociation reagent	Incubation time
208F, CPT-Tert, JA584, JS-7, NIH 3T3	0.0125% Trypsin and Versene (3.2 mM EDTA) (MRI in-house)	5 minutes
MDCK, CRFK	TrypLE express (Gibco)	20 minutes
293T	0.00125% Trypsin and Versene (0.32 mM EDTA) in PBS	3 minutes

2.7.5 Cryopreservation of cells

Cells growing in T-75 flasks were harvested as described in section 2.7.4 and after the incubation time trypsin or TrypLE express were inactivated with 3 ml HI-FBS. The cell suspension was then transferred to a 50 ml Falcon tube and centrifuged for 10 minutes at 212 × *g* at room temperature. For each T-75 flask, three 1 ml aliquots were frozen (approximately 1 x 10^7 cells per vial). After centrifugation, the supernatant was discarded and cells resuspended in half the final freezing volume of medium containing 20% HI-FBS (e.g. 1.5 ml for each T-75 flask). Next, the same volume of medium containing 20% HI-FBS and 20% DMSO was added dropwise to facilitate cell adaptation to the DMSO concentration. The final medium composition was 20% HI-FBS and 10% DMSO. Cells were aliquoted in cryovials in volumes of 1 ml, placed in a freezing box containing isopropanol and stored at -80˚C overnight. The use of isopropanol in freezing boxes ensures a controlled freezing process, with an approximate temperature decrease of one degree Celsius per minute. The following day cells were transferred to liquid nitrogen storage.

2.7.6 Cell counts

The concentration of cells growing in culture was determined with the use of a 0.1 mm depth improved Neubauer chamber (Hawksley). Briefly, cells were harvested and diluted 1:1 in Trypan blue (Sigma Aldrich) to aid identification of dead cells. When using the dye, cells with intact membranes exclude it and appear

uncoloured, while dead cells present a dark blue colour when observed under the microscope. 100 ul of Trypan blue diluted cells were added to both chambers of the haemocytometer and the number of cells in the middle square of each of the chambers counted. If the difference in cell number between the two middle squares was less than 10% calculations were made from the average cell number. Otherwise, all squares were counted and averaged. Cell concentration was calculated as below:

$$cells/ml = \frac{average\ cell\ number \cdot dilution\ factor}{chamber\ volume\ (0.0001\ ml)}$$

2.8 Transfection of DNA plasmids

Introduction of DNA plasmids (**Table 2.8**) into cells in culture was performed by two different means of transfection depending on the ease of introducing DNA material in that particular cell line.

2.8.1 Lipid-based methods of transfection

Lipid based-transfection methods can be liposomal or non-liposomal. Liposomal methods contain lipids which encapsulate the DNA in a phospholipid bilayer, these liposomes have affinity for the cell membrane and are incorporated into the cell by endocytosis (Felgner et al, 1987; Jacobsen et al, 2004).

Non-liposomal methods of transfection are formed of a mix of lipids and polymers which do not form liposomes, but which also encapsulate the DNA in amphiphilic spheroid particles called micelles (Jacobsen et al, 2004).

Both these lipid-based methods result in transient transfection, meaning that unless there is a recombination event and chromosomal integration occurs-and is selected for, cells will only express the foreign nucleic acid for a short time period.

2.8.1.1 Non-liposomal transfection

The reagent selected to perform non-liposomal transfection was Fugene HD (Promega). The optimum ratio of Fugene HD and DNA was trialled by David

Griffiths prior to this study and found to be 3:1 (microliters of Fugene per micrograms of DNA).

Transfections were performed in cultures growing at 80% confluency which had been passaged two successive days before the transfection procedure was to be performed. Transfection complexes were prepared by mixing 150 µl Opti-MEM medium (Gibco) (or 1 ml for T-75 flasks) with Fugene HD, and then adding DNA at the desired ratio. The reagent mix was incubated at room temperature for 20 minutes to allow transfection complexes to form. In the meantime, medium from cells in culture was replaced with 1 ml of fresh medium per well of 6-well plates or 7 ml in the case of T-75 flasks.

Transfection complexes were added dropwise while lightly swirling the plate to ensure an even distribution. Transfections were left to proceed overnight at 37°C. The following day, cells were observed and media changed.

To select stably-transfected cells, when appropriate, cells transfected with a plasmid containing a neo resistance gene were selected by adding 0.5 mg/ml of the antibiotic Geneticin G418 (Sigma Aldrich) to growth media.

2.8.1.2 Liposomal transfection

The reagent selected to perform liposomal transfection was Lipofectamine 3000 (Invitrogen). Lipofectamine 3000 was used to transfect the NIH 3T3 and MDCK cell lines, in which the use of Fugene HD had resulted in low transfection efficiency.

P3000 reagent was mixed with DNA at a 2:1 ratio and 50 µl of Opti-MEM. Liposomes were prepared mixing Lipofectamine 3000 at 3:1 ratio (3 µl per µg of DNA) and 50 µl of Opti-MEM. The DNA mix was then mixed with the liposome mix and incubated for 15 minutes at room temperature. In the meantime, medium from cells in culture was replaced with 1 ml of fresh medium per well of 6-well plates. Transfection complexes were added dropwise while lightly swirling the plate to ensure an even distribution. Transfections were incubated overnight at 37 °C. The following day, cells were observed and medium was changed.

2.8.2 Nucleofection

The nucleofection method is based on the use of electroporation, a technique that uses electric pulses to create small pores in the cell membrane and deliver nucleic acids into the cell. However, contrary to traditional electroporation, nucleofection allows the nucleic acid to be delivered to the nucleus instead of the cell's cytoplasm (Maasho et al, 2004). Like lipid-based methods, nucleofection is a transient method of transfection unless stably transfected cells are selected for.

Nucleofection reagents (Lonza) and protocols are designed for each cell type, and compared to other transfection methods result in better transfection efficiencies for difficult to transfect cells (Maasho et al, 2004). For this reason, nucleofection was used to transfect MDCK and NIH 3T3 cells.

Briefly, the protocol used for nucleofection involved dissociating the cells from plates and using between 5×10^5 and 1×10^6 cells per reaction. Cells were pelleted at 212 × *g* for 10 minutes, supernatant removed and cells resuspended in 100 µl of pre-warmed Nucleofector solution, 2 µg of DNA were added and the mix transferred into a provided cuvette. The cuvette was inserted in the Nucleofector II (Amaxa) and the program used as recommended. Once nucleofection finished, 0.5 ml of media were added with the provided pipette, gently mixed with cells and transferred to a well of a 6-well plate containing 1.5 ml fresh media.

After several trials, Nucleofection kit L and kit R (Lonza) were used for MDCK and NIH 3T3 respectively, due to their higher observed efficiency. Program A-024 was used for MDCKs and U-030 for NIH 3T3.

2.8.3 Transformation assays

In some instances, cells transfected as described in sections 2.8.1 and 2.8.2 were maintained in culture to observe transformation events. In those cases, when cells reached confluency, the HI-FBS concentration was reduced to 4 % HI-FBS to slow the growth rate of non-transformed cells. Cells continued to be checked and split when necessary, and when foci of transformed cells were clearly visible these were subcultured into new culture plates.

Table 2.8. Summary of plasmids used for transfection of cell lines.

Plasmid name	Description	Reference
pCMV2JS21	Full-length $JSRV_{21}$ under the control of CMV promoter	Palmarini et al (1999b)
pJSRV21	Full-length molecular clone of $JSRV_{21}$.	Palmarini et al (1999b)
pCAG-Jsenv	JSRV *env* under the control of the CAG promoter	(Szafran, 2014)
pCMV3JS-dGPP	$JSRV_{21}$ under the control of CMV promoter, deletions of gag and pol	Maeda et al (2001)
pCMV2JSRV-GFP2A-Env	JSRV21 modified to insert a GFP coding region upstream and in-frame with env, separated by a 2A cleavage sequence	D. Griffiths, unpublished
pEGFP-flag	Encodes eGFP and FLAG epitope tag	Created by David Griffiths, derived from pEGFP-C1 (Clontech)
pmaxGFP	max GFP under the control of the CMV promoter	Lonza

2.9 Northern blot analysis for detection of miRNAs

The process of northern blot for detection of miRNAs and miRNA candidates was performed over the course of four days.

2.9.1 Electrophoresis of the denaturing acrylamide gel

Initially, a 15% acrylamide gel was made by combining 12 g of UREA (Sigma Aldrich), 12.5 ml of 30% bisacrylamide (29:1 solution) (Bio-Rad) and 2.5 ml of 5x TBE buffer (54 g Tris, 27.5 g boric acid, 2.92 g EDTA and water to 1 L) and 10 ml of water. The gel mix was incubated at 55 °C until components were dissolved and homogenous. 10 µl of TEMED (Sigma Aldrich) and 250 µl of 10% APS (Sigma Aldrich) were added to the gel mix, and it was immediately poured into Bio-Rad gel casts previously cleaned with RNase-Zap (Invitrogen). Gels were left to set for 1.5 h and then put in gel tanks with 1 L of 0.5x TBE buffer. Urea was cleaned off the gel wells by inserting 0.5x TBE buffer with a syringe and needle until no visible residue was left. RNA samples were prepared at a 1:1 ratio with NorthernMax-Gly loading dye (Invitrogen) and 26 µl added per well. This dye contains ethidium bromide, for nucleic acid visualisation, and bromophenol blue, which travels down

the gel and produces a band equivalent to ~10 nt in size that can be later used as a size indicator. DNA loading dye 6x (Thermo Scientific) containing xylene cyanol, was added to empty wells. This loading dye was included because xylene cyanol travels down the gel to produce a band equivalent to ~30 nt in size, which can also be used as a size marker. The gel was run at 300 V until the bromophenol blue band was ~ 1/3 of the way down.

2.9.2 Transfer of the acrylamide gel

Following electrophoresis, gels were removed from the cast and observed in a UV box to visualise tRNAs and assess sample degradation. The gels were transferred to Amersham hybond-N^+ membranes (GE healthcare) by putting the gel in contact with the membrane, and sandwiching the gel and membrane with filter paper and fibre pads. The sandwich was positioned inside a mini-protean gel cassette (Bio-rad) with the membrane facing the anode. The transfer was performed inside a cuvette filled with 1 L of 0.5x TBE for 45 minutes at 30V, followed by 15 minutes at 35 V and 15 minutes at 40 V, a stirrer bar was added to the cuvette to distribute the heat produced.

Once the transfer had been completed, the membranes were taken out of the cassettes. The marker bands corresponding to 70 nt (tRNAs observed due to ethidium bromide presence), 30 nt (band produced by xylene cyanol) and 10 nt (band produced by bromophenol blue) were marked with pencil in the membranes as size indicators.

Crosslinking of the RNA to the membranes was performed in the UV Stratalinker 1800 (Stratagene) at 1200 µJ/m^2. Membranes were left to dry overnight at RT.

2.9.3 Radioactive labelling of oligo probes

The procedure described in this section was performed in a designated space for the work with radioactive isotopes. Once dried, membranes were put inside scintillation vials (Biometra) and 8 ml of pre-warmed ExpressHyb buffer (Clontech) added. Membranes were incubated in buffer for 1 h at 55 °C.

Oligo probes were prepared for labelling by mixing 1 µl of 10 pmol oligo (**Table 2. 9**), 1 µl 4x T4 polynucleotide kinase (PNK) buffer (NEB), 6 µl of water, 1 µl T4

PNK (NEB), 1 µl ATP [γ-32P] 250 µCi (Perkin Elmer). The mix was incubated at 37 ˚C for 1h to allow P32 labelling of the probes.

Table 2.9. Oligonucleotide probes used for northern blot analysis of miRNAs.

Oligo ID	Target sequence	Sequence (from 5′ to 3′)	Manufacturer
JS-5p	Candidate JSRV miRNA (5p)	TCATACCAGGCTTCAGCTATT	Eurofins genomics
JS-3p	Candidate JSRV miRNA (3p)	AATAATTCTAAAGCAGTTTCA	IDT
miR-191	oar-miR-191 / hsa-miR-191	AGCTGCTTTTGGGATTCCGTTG	IDT

After incubation, the labelling mix was diluted in 40 µl of water. In order to separate P32-labelled oligonucleotides from free ATP [γ-32P], Illustra Microspin columns (GE healthcare) were used following the manufacturer's instructions.

2.9.4 Northern blot of miRNAs

Filtered, P32-labelled oligonucleotide probes were added to the pre-hybridised membranes in ExpressHyb buffer and incubated in a rolling incubator biometra OV5 (Analytik Jena) at 38.5˚C overnight.

The following day, membranes were washed with 40 ml pre-warmed washing buffer (2x SSC (20x SSC stock: 175.3 g of sodium chloride, 88.2 g of Sodium Citrate to 1 L with water), 0.1% SDS (Sigma Aldrich) in water). Four washes of 20 minutes were performed, incubations were performed at 38.5˚C in the rolling incubator.

Once membranes had been washed, they were put in contact with filter paper, prewetted with 2x SSC, and heat-sealed in seal-o-meal. Sealed membranes were positioned in contact with Biomax MR film (Carestream) and inside a Biomax MS screen (Carestream) to improve sensitivity. The intensifying screen, containing film and membranes, was put inside an exposure cassette and incubated a -80˚C overnight or for up to four days. The following day the film was developed with a SRX-101A film processor (Konica Minolta).

2.10 Immunostaining procedures

2.10.1 Dewaxing and rehydration of paraffin-embedded tissue

The process of dewaxing and rehydration is an essential step performed prior to immunostaining, it unmasks epitopes allowing antibodies to access them.

Dewaxing and rehydration were performed in the Varistain (Thermo Shandon). Slides were mounted in station 1 and the preset program 2 was used. Program 2 takes the slides through decreasing concentrations of xylene through to 100% ethanol, ethanol concentration is then gradually decreased while water concentration is increased reaching a final solution of 100% water.

2.10.2 Antigen retrieval

The fixation steps performed to preserve the tissue result in protein crosslinking and the formation of methylene bridges, which conceal antibody binding sites. The method of antigen retrieval exposes the antigenic sites for the primary antibody.

For JSRV-SU, antigen retrieval was performed by autoclaving the slides in citrate buffer. Briefly, 1 L of citrate buffer (2.1g of citric acid (Sigma Aldrich) in 1L ddH_2O at pH6.0 (buffered with 1 M NaOH (Fisher Scientific)) was prepared. Slides were placed in a metallic rack and inside a 3 L beaker containing 1 L of the citrate buffer. The slides were then autoclaved at 121ºC for 10 minutes. Once the slides had cooled down, they were washed twice in Tris buffered saline (TBS) (30 ml 5 M NaCl (Fisher Chemical), 10 ml Tris (Promega), 1 L water).

2.10.3 Blocking of endogenous peroxidase activity

Endogenous peroxidases found in the tissue sample can react with the substrate used to reveal immunostaining, resulting in unspecific background staining. To block endogenous peroxidase activity, slides were submerged in 0.03% H_2O_2 peroxidase solution (12 ml H_2O_2 (Sigma Aldrich) in 400 ml of methanol (VWR Chemicals) for 30 minutes at room temperature before washing with TBS.

2.10.4 Cytospin preparation

Fixation of cells to slides was performed using the cytospin technique. A cytofunnel (Thermo Scientific) was mounted to each slide and 200 µl of 5×10^5 cells/ml suspension added per slide. The cytospin 2 (Shandon) was used to spin

slides at 10000 rpm for 7 minutes. Slides were then fixed by immersion in methanol for 10 minutes and air-dried.

2.10.5 Growth of cells in chamber slides

An alternative to the cytospin technique is the use of chamber slides to perform immunocytochemistry (ICC) of cells in culture. The advantage of using chamber slides is that cells grow already attached to the slide that will be then used for ICC, meaning that they will retain their adherent morphology instead of presenting the rounded morphology of cells in suspension.

Cells growing in culture were counted, and up to 3×10^4 cells were transferred per well of an eight well Nunc lab-Tek II chamber slide (Thermo Scientific). Cells were grown overnight in the chambers and the following day the media was carefully removed and the chambers detached as per manufacturer's instructions. Slides were then submerged in methanol for 10 minutes in order to fix the cells.

2.10.6 Immunostaining

Slides were mounted in immunohistochemistry Sequenza chambers (Thermo Shandon), blocked with 100 µl of 25% normal goat serum (NGS) (Vector Laboratories) and incubated 30 minutes at room temperature. The primary antibody, or a matched isotype control antibody, was then applied and incubated at 4°C overnight. The following day slides were washed three times with either PBS/0.1% Tween 20 (PBS-T20), for immunocytochemistry or TBS, for immunohistochemistry. 100 µl of a horseradish peroxidase (HRP)-conjugated secondary antibody were then added to each of the slides and incubated 30 minutes at room temperature. Slides were then washed twice with PBST20 or TBS, and the substrate 3, 3'-Diaminobenzidine (DAB) (Dako) added and incubated for 8 minutes at room temperature. HRP catalyses the oxidation of the chromogenic substrate DAB in presence of H_2O_2, which results in a detectable colour change to dark brown. Slides were washed with distilled water and unloaded from Sequenza chambers. Counterstaining was performed using the Varistain in the preset program 3 that performs staining with haematoxylin-eosin, and dehydration with ethanol followed by xylene. Slides were mounted manually using Shandon Consul-Mount (Thermo Scientific). A summary of the antibodies used can be found in **Table 2.10**.

Table 2.10. Summary of antibodies and conditions used for immunostaining.

Primary antibody	Species	Dilution	Secondary antibody	Species	Dilution	Isotype control
Anti JSRV(SU) Wootton et al (2006)	Mouse monoclonal	1:100	Rabbit anti mouse (Dako)	Rabbit	1:1000	IgG1 mouse murine myeloma (Sigma Aldrich)
Anti-GFP (ab6556 abcam)	Rabbit monoclonal	1:10000	Goat anti rabbit (Dako)	Goat	1:1000	Rabbit IgG (Sigma Aldrich)
Anti-SP-C (Jeffrey Whitsett, Cincinnati Children's Hospital, Cincinnati, Ohio, USA)	Rabbit polyclonal serum	1:3000	Goat anti rabbit	Goat	1:1000	Normal rabbit serum
Anti-P-Akt (NEB)	Rabbit monoclonal	1:400	Goat anti rabbit	Goat	1:1000	Rabbit IgG
Anti-P-ERK1/2 (NEB)	Rabbit monoclonal	1:600	Goat anti rabbit	Goat	1:1000	Rabbit IgG

2.11 Isolation of type II pneumocytes

Isolation of sheep type II pneumocytes was carried out following a protocol established for isolation of human type II pneumocytes (Witherden & Tetley, 2001). The following variations were made to the published protocol: DCCM-1 (Geneflow) was used instead of LPHM and HI-FBS was used instead of newborn calf serum (NCS). Penicillin/Streptomycin, Hanks balanced salt solution (HBSS) and Glutamine were obtained from MRI in-house facility. Gentamicin and Amphotericin B were added to a final concentration of 20 µg/ml and 1.25 µg/ml respectively, to inhibit bacterial and fungal growth.

In preparation for the isolation process, cell culture plates (Corning) were coated with 1% dilution of PureCol collagen solution (Purecol). 300 µl and 75 µl of the 1 % solution were added to each well of 24 and 96-well plates, respectively, and left to air-dry overnight in a microbiological safety cabinet.

The isolation process took place over two days as suggested in the protocol. On the first day, lambs were euthanised by captive bolt at the Moredun PM rooms. Lungs were examined for visible signs of bacterial infection and other lesions that could compromise the viability of cells *in vitro*. Three sections of lung tissue were obtained from each lamb, and kept submerged in 0.15 M saline (MRI in-house) for up to 1 hour. Lung tissue sections were perfused with up to 100 ml of saline to wash off erythrocytes. Tissue was then stored overnight in the presence of DCCM-1 without HI-FBS. The following day, each tissue piece was instilled with 15 ml of 0.25 % trypsin (Sigma Chemical) until inflated and incubated at 37˚C for 15 minutes, this process was repeated three times to give a total trypsinisation time of 45 minutes. After trypsinisation, the tissue was chopped into 1 mm^3 with the use of scissors. In order to degrade DNA from ruptured cells 250 µg/ml DNaseI solution (Sigma Chemical) was added and the suspension shaken vigorously for 5 minutes. Tissue suspensions were then filtered through a large 300 µm mesh filter followed by 40 µm cell strainer (Falcon). The filtrate, containing released cells, was centrifuged at 290 × *g* for 10 minutes at 4˚C and the pellet resuspended in 30 ml 50% DCCM-1 and 50% HBSS with 100 µg/ml DNaseI. At this stage cell number was determined with the use of a haemocytometer. The cell suspension was plated in T-75 flasks and incubated at 37˚C for 1.5h for macrophages to adhere. After the incubation time, the supernatant from the flasks was removed, centrifuged again and the pellet was resuspended in 30 ml of complete DCCM-1 (with antibiotics and 10 % HI-FBS). Resuspended cells were plated in T-75 flasks and incubated for 1.5 h at 37˚C for fibroblasts to adhere. Finally, the supernatant was removed and centrifuged as previously, epithelial cells were counted and seeded at 1×10^6 cells/well of coated 24-well plates or 1×10^5 cells/well of coated 96-well plates. Cells were incubated at 37 ˚C and 5 % CO_2 overnight.

On day 3, the medium was changed in all seeded wells and substituted with fresh complete DCCM-1. The following day, a wash with PBS was performed to remove any remaining monocytes, and fresh media was added. Cells continued to be observed and medium changed every other day.

On one occasion, selective lysis of erythrocytes was performed by using RBC lysis buffer (Life Technologies). Briefly, cell suspensions were pelleted at 290 × *g*,

resuspended in 5 ml of RBC lysis buffer and incubated for 5 minutes at room temperature. The lysis reaction was then stopped by adding 20 ml of 1x PBS, cells were pelleted and resuspended in DCCM-1 to continue the isolation procedure.

2.12 Molecular cloning

2.12.1 Growth of bacterial cultures

Escherichia coli JM109 competent cells (Promega) were used for molecular cloning. Importantly, the strain is *end*A^{-} and *rec*A^{-}, containing a deletion of endonuclease A, which avoids DNA cleavage improving plasmid yield, and deletion of recA, which avoids recombination with the bacterial chromosome.

Cultures were grown on solid media as means to select specific bacterial colonies. Liquid media was used when a specific colony or culture was to be propagated. Solid cultures were grown at 37˚C and liquid cultures were grown at 37˚C in a shaking incubator at 200 rpm to allow aeration of the culture.

2.12.1.1 Preparation of growth media

Preparation of liquid and solid bacterial growth media was done under aseptic conditions. A Bunsen burner was used to create a sterility umbrella under which reagents were prepared.

Luria Bertani (LB) liquid medium was used to support the growth in suspension of *E. coli.* LB medium was obtained in-house. LB medium was supplemented with ampicillin, when required, at a final concentration of 100 µg/ ml.

LB agar (MRI in-house) was melted and ampicillin added when required. LB agar was poured in sterile petri dishes (Thermo Scientific) and left on the bench until solidified. LB agar plates were stored at 4˚C up to one month.

2.12.2 Bacterial transformation

Competent *E. coli* JM109 cells (NEB) were transformed with a variety of plasmids using the heat-shock procedure. Briefly, JM109 cells were grown overnight at 37 ◦C; the following day 30 µl of the JM109 cells were mixed with 1 µl of the desired plasmid and kept in ice for 45 minutes, flicking the tube regularly to mix cells. Cells were then incubated at 42 ◦C for 1 minute and put back in ice for 5 minutes. 200 µl SOC (NEB) medium was then added, and tubes were incubated at 37 ◦C at 200

rpm for 30 minutes. Transformed cells were then plated on LB agar plates with the appropriate antibiotics and incubated at 37 °C overnight. The following day colonies were picked and used to inoculate 5 ml flasks.

2.12.3 Plasmid isolation

Selected transformed bacterial colonies were grown overnight in either 5 ml liquid LB media, for minipreps, or 150 ml for maxipreps.

2.12.3.1 Small-scale plasmid isolation (miniprep)

Small-scale plasmid isolation was performed using the QIAprep Spin Miniprep Kit (Qiagen) and following the manufacturer instructions. Plasmid isolation is achieved through a series of steps: first, bacterial cells are subjected to alkaline lysis which disrupts the membrane and releases proteins and DNA. The lysis buffer is then neutralised and adjusted to high-salt, which results in genomic DNA and protein precipitation, while the smaller plasmid DNA is allowed to renature and binds to the silica membrane. The following steps wash remaining contaminants, and plasmid DNA is finally eluted in low salt concentration.

Elution was performed in molecular grade water instead of the provided TE buffer, which can interfere with enzymatic reactions such as DNA-sequencing.

2.12.3.2 Large-scale plasmid isolation (maxiprep)

Large-scale plasmid isolation was performed using the EndoFree Plasmid Maxi Kit (Qiagen), which removes endotoxins from the preparation, following manufacturer's instructions. Plasmid isolation begins with lysis steps similar to those used in miniprep isolation. However, the maxi kit uses anion-exchange based columns to ensure selective elution of plasmid DNA: plasmid DNA binds to the resin in low salt and low pH conditions, a wash in medium-salt conditions elutes proteins, RNA and other contaminants. Finally, plasmid DNA is eluted in high-salt conditions and salt removed with the use of isopropanol.

2.12.4 Enzyme restriction

Restriction reactions were set up depending on enzyme used and using buffers supplied by manufacturers as recommended **Table 2.11.** Reactions were incubated between 1-1.5 hours at 37°C.

Table 2.11. Summary of restriction enzymes and conditions used for DNA digests.

Enzyme	Provider	Target site	Restriction conditions
BglII	Roche	A▼GATCT TCTAG▲A	3 µg DNA, 1 µl enzyme, 7.5 µl buffer M, 20 µl water
AciI	NEB	C▼CGC GGC▲G	10 µg DNA, 3 µl enzyme, 5 µl cutsmart buffer, 30 µl water
HindIII	Roche	A▼AGCTT TTCGA▲A	2 µg DNA, 1 µl enzyme, 5 µl buffer B, water to 25 µl
NcoI	Promega	C▼CATGG GGTAC▲C	2 µg DNA, 1 µl enzyme, 4 µl buffer D, 0.4 µl BSA, water to 20 µl
SspI	Promega	AAT▼ATT TTA▲TAA	2 µg DNA, 1 µl enzyme, 4 µl buffer E, 0.4 µl BSA, water to 20 µl

2.12.5 Agarose gel electrophoresis

Agarose gels were prepared diluting agarose (Bioline) in Tris-acetate-EDTA (TAE) buffer to a 1% concentration with 1:10,000 Gel red (Biotium) nucleic acid dye. Electrophoresis was performed at 80 V for 1.5 hours, and bands were visualised with Alpha Imager 2200 (Alpha Innotech). Molecular weight markers were hyperladder 1Kb (Promega).

2.12.6 DNA sequencing

DNA sequencing of plasmids was performed by MWG Eurofins. The primers used for sequencing are shown in **Table 2.12** and **Fig. 2.4.** Sequencing analysis was perfomed with DNAStar software.

Table 2.12. Primer sequences and targets used in DNA-sequencing.

Primer	Sequence (from 5′ to 3′)	Target
5801R	GATATGATATGTCAGCTGATACCTG	pCSC-JSenv/ pCSC-GFP2AEnv
5680F	CCCGTATATGTTAATGATACGAGC	pCSC-JSenv/ pCSC-GFP2AEnv
7016F	CCCTGATTGGTGTAGGAATACTTG	pCSC-JSenv/ pCSC-GFP2AEnv
CSC-F1	TGGCTGTGGAAAGATACCTAAAGG	pCS-CG/ pCSC-JSenv/ pCSC-GFP2AEnv
6161F	TTACAGCCCAATATCAGTGGAAGC	pCSC-JSenv/ pCSC-GFP2AEnv
6569F	ATTCAAGCTGCGCACACGGTAGAC	pCSC-JSenv/ pCSC-GFP2AEnv
GFP2A-F	CGCATCAAATGCAACGCATGACG	pCSC-GFP2AEnv
pEGFPN1rev	GTCCAGCTCGACCAGGAT	pCSC-GFP2AEnv
pEGFPC1for	GATCACTCTCGGCATGGAC	pCSC-GFP2AEnv
pCR3.1-BGHrev	TAGAAGGCACAGTCGAG	pCSC-JSenv/ pCSC-GFP2AEnv

2.12.7 Preparation of glycerol stocks of bacterial cultures

Glycerol stocks were prepared by mixing an overnight bacterial culture with an equal volume of a sterile 40 % solution of glycerol in water. Aliquots were stored at -80 ◦C until required.

2.13 Preparation of lentiviral vectors

2.13.1 Plasmid design

For the production of lentiviral vectors a third generation lentiviral vector system was used, this system consists of four plasmids that when transfected into 293T cells produce a lentiviral vector encoding the gene of interest (Sakuma et al, 2012) **Table 2.13**.

The transfer vector encoding the gene of interest was created with the use of molecular cloning techniques by David Griffiths. Briefly, JSRV *env* or a construct of *gfp2Aenv,* previously designed and produced also by David Griffiths, were amplified by PCR and inserted into the NheI/XhoI sites of the transfer vector (pCS-CG; Addgene). Plasmids were amplified in JM109 (**2.12.2** and **2.12.3)**, sequences were verified by sequencing and plasmids maps created (**Fig 2.5** and **Fig 2.6**).

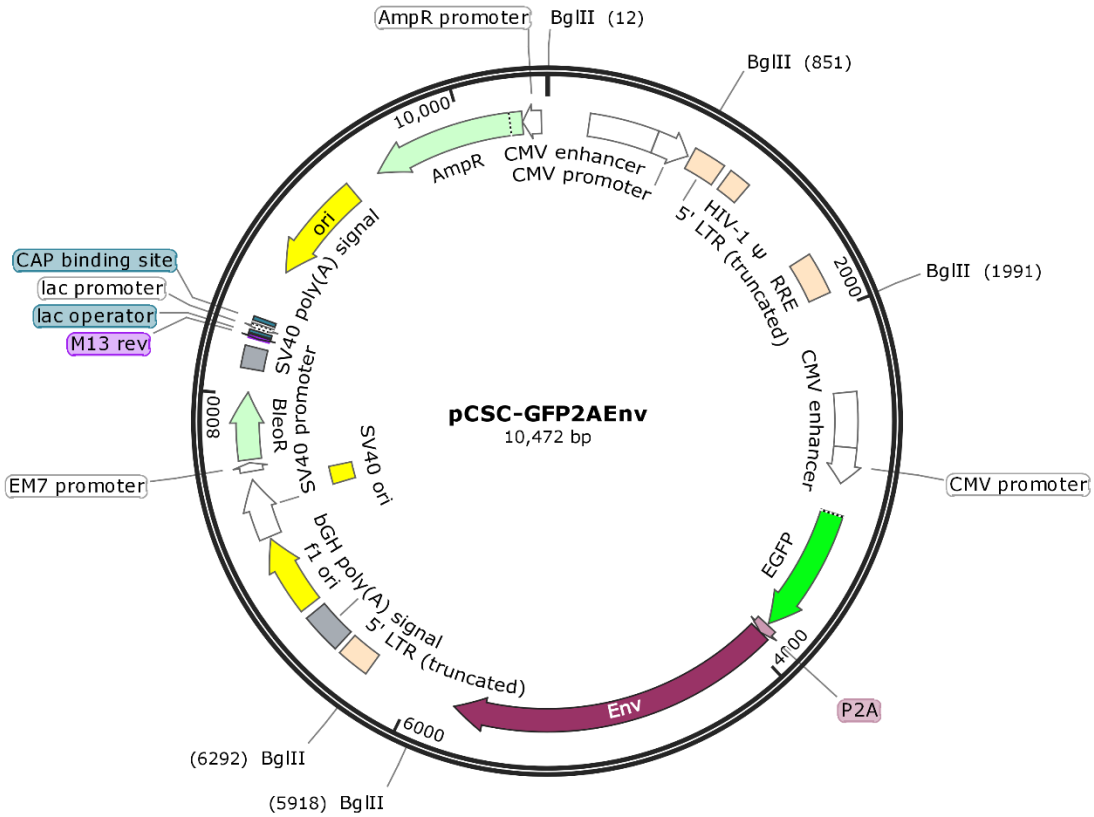

Figure 2.4. Plasmid map of pCSC-GFP2AEnv. *Restriction sites of enzyme BglII are shown and were used to verify the plasmid map by restriction digest.*

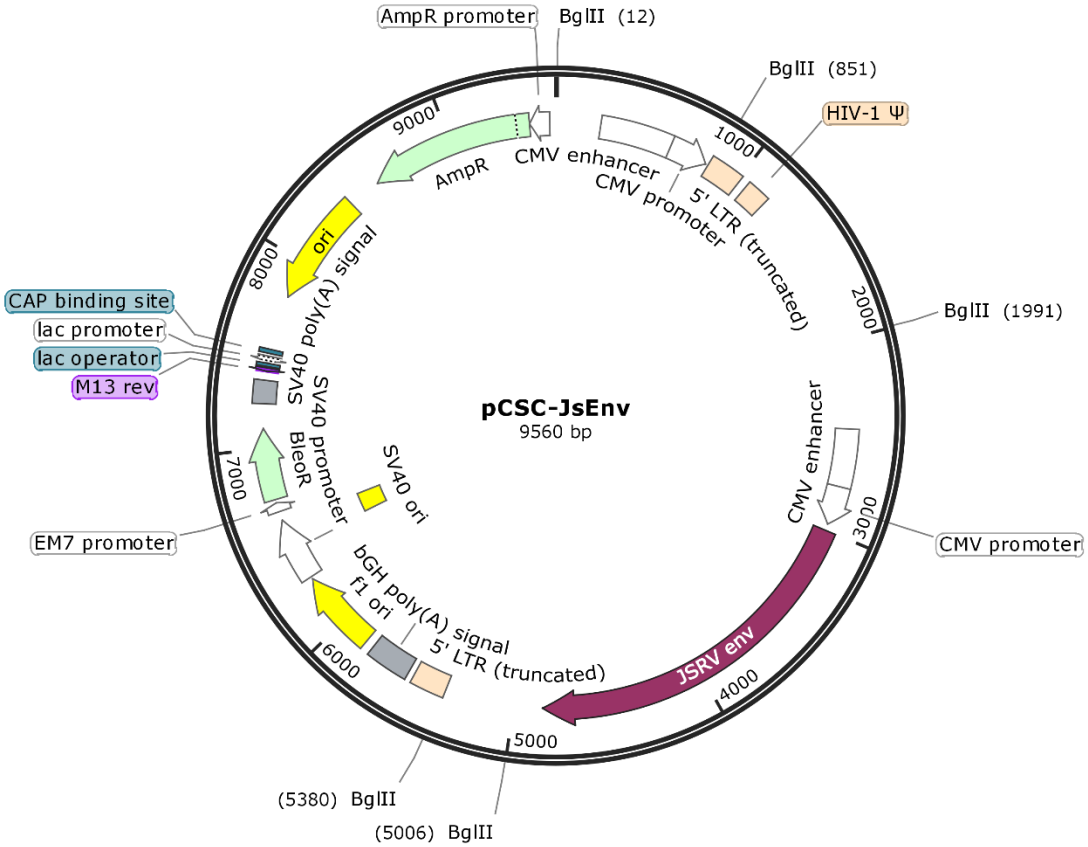

Figure 2.5. Plasmid map of pCSC-JsEnv. *Restriction sites of enzyme BglII are shown and were used to verify the plasmid map by restriction digest.*

2.13.2 Production of lentiviral vector particles

Work with lentiviral vectors was performed in an ACDP containment level 2 laboratory. Lentiviral vectors were prepared by transfection of 293T cells in T-75 flasks at 80% confluency using Fugene-HD (section 2.8.1). Each flask was transfected with 5.4 µg of vector plasmid (pCS-CG, pCSC-JSenv or pCSC-GFP2AEnv), 3.6 µg of gag-pol packaging plasmid (pMDLg/pRRE (Dull et al, 1998); obtained from Addgene), 1.2 µg of HIV Rev plasmid (pCNC-Rev (Ikeda et al, 2003); a kind gift from Dr Yasuhiro Takeuchi, University College London) and 1.8 µg of a plasmid encoding the vesicular stomatitis virus G protein (pMD2.G, Addgene).

The growth medium was replaced 16-20 hours following transfection and supplemented with 5 mM sodium butyrate (Sigma Aldrich). The supernatant (containing lentiviral vector particles) was harvested 48 hours post-transfection and centrifuged at 850 × *g* before being filtered through a 0.45 µm cellulose

acetate filter (Sartorius Stedim) to remove any cell debris present. Due to the low adherence of 293T cells, the supernatant was collected very carefully in order to avoid disturbing the cell layer. Fresh growth medium (10 ml, without sodium butyrate) was added to the flasks and cells were incubated for a further 24h, at which point a second harvest was performed in the same way. The filtered supernatants from the two harvests was combined and stored at -80°C.

2.14 Concentration of lentiviral vectors

Lentiviral vectors were concentrated by ultracentrifugation (Optima L-90K, SW32Ti rotor; Beckman Coulter. Filtered supernatants were thawed and centrifuged for 2 h at 38,080 × *g* to pellet the lentiviral vector particles. After centrifugation, the supernatant was removed and the pellet containing the lentiviral vectors was resuspended in appropriate medium (Opti-MEM, DMEM or Q286) by gentle pipetting and storage on ice for 30 minutes. The lentiviral vector suspension was then stored in cryovials in 250 µl aliquots and stored at -80°C until use.

2.15 Transduction of cell lines with lentiviral vectors

Transductions were performed under aseptic conditions. Briefly, cells passaged the day before transduction and seeded at 1 x 10^5 cells/well (of a 24-well plate) were used. Growth medium was removed and replaced with medium containing the desired lentiviral vector concentration and 8 µg/ml of polybrene (Sigma Aldrich). Polybrene has been shown to enhance the lentiviral transduction efficiency (Seitz et al, 1998). The final volume per well was 1 ml in 6-well plates, 500 µl in 12-well plates and 250 µl in 24-well plates. Transductions were incubated at 37°C for 4 hours and then cultures observed for cell death and medium replaced. Cultures continued to be checked for cell death and changes, and medium changed every other day.

2.15.1 Transformation assays

After transduction, when cells had reached confluency, serum concentration was reduced to 4% FBS to slow the growth rate of non-transformed cells. Cells continued to be checked and split when necessary, when transformed foci were clearly visible these were subcultured into new culture plates using pipette tips.

2.16 Flow cytometry

Flow cytometry was performed to examine transgene expression in transfected or transduced cells. Briefly, cell culture supernatant was collected and added to a tube containing 5 ml of PBS. Cells were washed with PBS, dissociated, resuspended in PBS and centrifuged at 850 × *g*. Cells were then resuspended in 200 µl of PBS containing 1 µl of Vioblue live/dead stain (Miltenyi Biotech) and incubated at room temperature for 30 minutes in the dark.

After incubation a wash with PBS was performed and pelleted cells then resuspended in 200 µl 1% paraformaldehyde (PFA) in order to fix the cells. Fixed cells were then analysed by flow cytometry measuring GFP+ and Vioblue stain in the MACSQuant (Miltenyi Biotech), 50000 events were counted. Analysis was performed in the MACSQuant software: GFP expression and Vioblue expression were analysed in the blue laser (488 nm) and violet laser (405 nm) respectively. Cell size, granularity and doublets were analysed using the forward scatter (FSC) and side scatter (SSC).

2.16.1 Titration of lentiviral vector particles

Titration of lentiviral vectors that encode GFP was performed by flow cytometry. Transductions of cell lines were performed as described in section 2.14, but serial dilutions of the lentiviral vectors performed to obtain a more accurate estimate of the concentrations.

Titrations were performed two to three days post-transduction at the peak of transgene expression. Preparation of cells and flow cytometry were performed as described in 2.16.

The percentage of live GFP expressing single cells was then used to calculate the lentiviral vector concentration using the following formulae:

$$TU/ml = \frac{target\ cell\ number\ \cdot \frac{\%\ GFP\ cells}{100}}{vector\ volume}$$

In which:

- TU= Transduction units or lentiviral vector particles able to transduce cells

- Target cell number = number of cells in culture when transduction was performed
- % GFP cells= percentage of cells expressing GFP as determined by flow cytometry. Wells where 10-20% cells were GFP positive were used to calculate titre.
- Vector volume = volume in ml of vector used in transduction.

2.17 Cell sorting

Sample preparation for cell sorting consisted in dissociating the cells and resuspending the cell pellet to a concentration of 5 × 10^6 cells/ml in serum free medium. 50 µl of serum free medium were added to each well of 96-well plates in preparation for sorting. Cell sorting was performed in the Bioimaging facility of the Roslin Institute, University of Edinburgh. The BD FACS Aria IIIu 4-laser was used and operated by Bob Fleming and Graeme Robertson. Separation of cells was based on the presence of GFP expression with the settings described in **Fig. 2.7** Single cells were sorted into four 96-well plates and a bulk population of GFP-expressing cells were obtained.

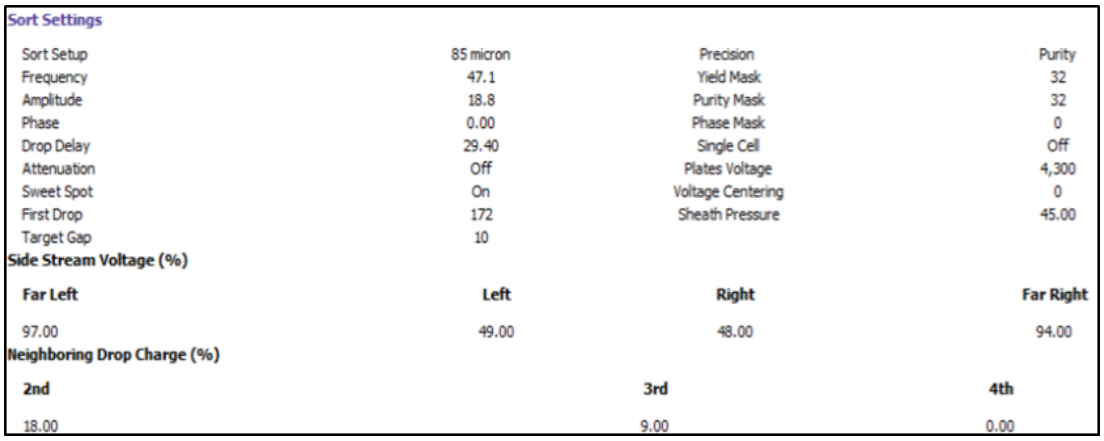

Sort Settings

Sort Setup	85 micron	Precision	Purity
Frequency	47.1	Yield Mask	32
Amplitude	18.8	Purity Mask	32
Phase	0.00	Phase Mask	0
Drop Delay	29.40	Single Cell	Off
Attenuation	Off	Plates Voltage	4,300
Sweet Spot	On	Voltage Centering	0
First Drop	172	Sheath Pressure	45.00
Target Gap	10		

Side Stream Voltage (%)

Far Left	Left	Right	Far Right
97.00	49.00	48.00	94.00

Neighboring Drop Charge (%)

2nd	3rd	4th
18.00	9.00	0.00

Figure 2.6. Settings used for FACS.

After cell sorting, 50 µl of conditioned medium, obtained from untransduced MDCK cells growing in culture and filtered through a 0.45 µm filter, were added to each well. 100 µl of medium containing 50% FBS was also added to each of the wells (final concentration 33% FBS). The bulk sorted population was seeded in a T-75 flask in 10% FBS containing medium.

2.18 Amplification of single cells in culture

Plates containing single sorted cells were examined microscopically daily for contamination and growth. After three days in culture, half of the growth medium was removed from all wells and replaced with fresh medium. Medium was then changed every three days and cells kept growing in the presence of 40% FBS concentration in the plates until they reached confluency. Cells were then sequentially passaged every time they reached confluency to 12-well plates, 6-well plates and FBS concentration lowered to 20%, T-25 flasks and finally, T-75 flasks when the FBS concentration was lowered to 10%.

2.19 Immunoblotting

Immunoblotting (western blot) was used to detect the presence of protein in samples of interest.

2.19.1 Preparation of protein extracts

Protein samples were obtained from cells cultured in 6 well-plates. Cells were washed in ice-cold PBS. Cells were scraped off from the culture plate and transferred to tubes. Cells were harvested by centrifugation at 2000 g for 2 minutes. The supernatant was then discarded and the cell pellet resuspended in ice cold RIPA buffer (150 mM NaCl, 1% NP40 (Sigma Aldrich), 0.5% sodium deoxycholate (Sigma Aldrich), 0.1% SDS, 50 mM Tris pH 8.0, diluted in dH_2O) containing 0.042 U/µl of Benzonase (Novagen). The cell suspension was then incubated in ice for 30 minutes and then stored at -80 ◦C.

2.19.2 Quantitation of total protein

Total protein concentration in extracts was calculated using the Pierce BCA protein assay kit (Thermo Scientific) as recommended. The enhanced test was used in all samples and both BSA standards and samples were assayed in duplicate. Standards and samples were set up in a 96- well plate and incubated for 30 minutes at 60 ◦C. The assay was read in a GloMax plate reader (Promega) using the BCA settings of the equipment. A standard curve was drawn from the results obtained for the standards and was used to determine the concentration of the samples

2.19.3 Preparation of buffers for immunoblotting

Buffers for immunoblotting were prepared and stored for up to one year at room temperature, except for the blocking solution which was prepared on the day of use (**Table 2.14**).

Table 2.13. Composition of buffers used for immunobloting.

Buffer	Composition
Stacking buffer	0.25 M Tris, 0.2% SDS in dH_2O (pH 6.8)
Resolving buffer	1.5 M Tris, 0.4% SDS, in dH_2O (pH 8.8)
Laemmli electrode buffer	25 mM Tris, 192 mM Glycine (Fisher Chemical), 0.1% SDS, in dH_2O
Transfer buffer	20 mM Tris, 0.15 M Glycine, 20% Methanol, in dH_2O
Blocking solution	5% dry milk powder (Marvel) diluted in 0.1% PBS T20
PBS-T20	0.1% Tween20 in PBS
4x Loading dye	120 mM Tris-HCl (pH 6.8), 2% SDS, 20% Sucrose (Thermo Fisher Scientific), 100 mM β-mercaptoethanol, bromophenol blue crystals, in dH_2O

2.19.4 SDS-PAGE electrophoresis

Gels for SDS-PAGE electrophoresis were prepared in single use Novex cassettes (Life Technologies). The stacking gel containing 3% acrylamide was made from 1 ml 30% acrylamide (Severn Biotech), 5 ml stacking buffer, 4 ml dH_2O, 10 µl TEMED (Sigma Aldrich) and 50 µl 10% APS (Sigma Aldrich). The resolving gel, containing 12% acrylamide, was made up from 5 ml 30% acrylamide, 3 ml resolving buffer, 4 ml dH_2O, 0.6 g sucrose, 10 µl TEMED and 90 µl 10% APS. 2ml of stacking gel were layered onto 6 ml of resolving gel.

Once the gel had set, it was introduced in Xcell Surelock cuvettes (Life Technologies) with Laemmli electrode buffer. Samples were boiled for 4 minutes to denature proteins and then, 5 µl of the Seablue ladder (Invitrogen) and 20 µl of the samples (with 1x loading dye) loaded in the wells. The gel was run at 140 V for 1.5 hours.

2.19.5 Protein transfer

The proteins contained in the SDS-PAGE gel were transferred to a 0.45 um Amersham Protran nitrocellulose membrane (GE Healthcare). Transfer was performed in the semidry transfer cell (Biorad) at 15 V for 48 minutes.

2.19.6 Antibody binding

Membranes were blocked by soaking in freshly-prepared blocking solution (Table 2.14) and incubating overnight at 4 ◦C. The following day the primary antibody was diluted in 10 ml of blocking solution and membranes soaked in the dilution for 1 hour at room temperature in a rocking platform. Three fifteen-minute washes were then performed with PBS/0.1%T20. The secondary antibody diluted in 10 ml of blocking solution was then applied in the same manner as the primary antibody and incubated for 1 hour at room temperature. Three fifteen-minute washes were performed with 0.1% PBS T20 and a final 3-minute wash performed with PBS. Blot was visualised with chemiluminescent substrate (Amersham ECL; GE Healthcare and exposed to photographic film (details). **Table 2.15** is a summary of antibodies and dilutions used in immunoblots.

Table 2.14. Antibodies used in immunoblotting.

Primary antibody	Species	Dilution	Secondary antibody	Species	Dilution
Anti-JSRV(SU)	Mouse	1:100	Rabbit anti mouse (Dako)	Rabbit	1:1000
Anti-GFP	Rabbit	1:10000	Goat anti rabbit (Dako)	Goat	1:1000

2.20 Culture of lung slices

2.20.1 Media and reagent preparation

DMEM was supplemented with 2mM glutamine, 1% penicillin/streptomycin, 1.25 µg/ml amphotericin B and 20 µg/ml gentamicin. Supplemented DMEM was kept at 4 ◦C for up to one month.

Quantum 286 (Q286) (PAA), designed to support epithelial cell growth, was used as growth medium for lung slices, as previously used by Archer et al. for OPA cell culture (Archer et al, 2007) Q286 was supplemented with 2mM glutamine, 1%

penicillin/streptomycin, 1.25 µg/ml amphotericin B and 20 µg/ml gentamicin. Growth factors were also added to support cell survival and maintenance of epithelial phenotype. Keratinocyte growth factor (KGF) (Sigma Aldrich) was added at a final concentration of 10 ng/ml to promote growth and division of epithelial cells (Rubin et al, 1989). Hepatocyte growth factor (HGF) (Sigma Aldrich) was added at a concentration of 5 ng/ml and is a pleiotropic factor with known functions as epithelial growth stimulator (Tsubari et al, 1999). Dexamethasone (Sigma Aldrich) was added at 100 nM final concentration to inhibit lung cell apoptosis (Wen et al, 1997)). 3-Isobutyl-1-methylxanthine (IBMX) (Sigma Aldrich) was added at 100 µM final concentration due to its role as phosphodiesterase inhibitor and raising cAMP levels (Parsons et al, 1988). 8-Bromoadenosine 3′,5′-cyclic monophosphate (8-Br-cAMP) (Sigma Aldrich) was added at 100 µM final concentration, 8-Br-cAMP is a cAMP analog that induces surfactant production (Ballard, 1989; Wade et al, 2006). Supplemented Q286 was prepared in 50 ml aliquots and kept at 4 ◦C for a maximum of one week before use.

Ultra-low gelling point agarose (LMP) (Sigma) was diluted in HBSS without calcium and magnesium (MRI in-house) to a concentration of 2.5%.

2.20.2 Preparation of lung slices

Lung slices were obtained from lambs between six and twelve months old following an established protocol (Cousens et al, 2015). Briefly, the whole lung was removed from the sheep and the right cranial lobe isolated with the use of clamps. Using a 50 ml syringe, 2.5% LMP solution at 37 ◦C was introduced into the selected lobe until it expanded. The expanded area was dissected from the rest of the lung, placed in ice-cold HBSS and stored on ice for 1 hour. The lung tissue section was then sliced transversely in approximately 0.75 cm sections, and cylindrical cores were prepared using the biopsy cutter (0.8 cm diameter). These cores were fed to the lung slicer (Krumdieck) in order to obtain the desired 300 µm slices. Slices were submerged in universal tubes (Thermo Scientific) containing 20 ml of HBSS. Approximately 30 sections were placed in each tube.

Slices contained in universal tubes were then washed twice with supplemented DMEM (**Table 2.6**) and placed on a rotating platform (1 rpm) at 39˚C and 5% CO_2. Slices were incubated for 30-45 minutes between washes.

Supplemented DMEM (500 µl) was then added to wells of 24-well plates and one lung slice transferred to each well. After one hour in rotation in the incubator, DMEM was removed and 300 µl of supplemented Q286 added per well. Slices were incubated overnight with rotation (1 rpm) at 39˚C and 5% CO_2.

The following day, lung slices were washed twice with supplemented DMEM to remove agarose, red blood cells and factors that could have been released by damaged cells. Cells were placed in 300 µl supplemented Q286 and returned to culture at 39°C with rotation. Cultures were checked every day for cilia activity and contamination and medium was replaced daily.

2.20.3 Transduction of lung slices with lentiviral vectors

Transduction of lung slices with lentiviral vectors was performed on the third day of culture. Briefly, the desired concentration of lentiviral vector was diluted in supplemented Q286 with 8 µg/ ml of polybrene and 150 µl of this transduction mix were added per well. Slices were incubated for 2 h at 39°C, before adding a further 150 µl of supplemented Q286 and incubating overnight. The following day, lung slices were washed once with supplemented DMEM for 30 minutes to remove any remaining vector particles, before adding 300 µl of fresh supplemented Q286. Lung slices were kept in culture, and observations and medium change performed every day.

2.20.4 Infection of lung slices with $JSRV_{21}$

Infections of lung slices with $JSRV_{21}$ were performed in the same way as transductions of lung slices with lentiviral vectors explained in section 2.20.3**.** The only difference between the protocols was that some infections were left to proceed for two days before medium was changed and then, three washes with supplemented DMEM were performed to remove remaining viral particles. In addition, incubation of lung slices after infection was performed with rotation (1 rpm).

2.20.5 Sample processing

At the desired time points, samples were collected for miRNA expression analysis, immunostaining and immunoblotting. Four lung slices were collected for each

method, time point and treatment. Supernatants were collected at the desired time points and stored at -80˚C for further analysis.

For analysis of miRNA expression, lung slices were directly added to lysing matrix D tubes containing 800 µl of RLT buffer plus with β-mercaptoethanol and shaken thoroughly. Tubes were stored at -80˚C until homogenisation and RNA extraction were to be performed. RNA extraction and analysis was performed as described in section 2.4.5.

Samples for immunostaining were collected in cellpath biopsy capsule and pad, and introduced in cassettes, submerged in formal saline pots and fixed overnight. The following day samples were submitted to the Moredun pathology unit for processing and serial cutting for slide preparation. Immunostaining was performed as described in section 2.10**.**

Samples for immunoblotting were collected in lysing matrix D tubes containing 400 µl of RIPA buffer with Benzonase and shaken thoroughly. Tubes were kept at -80 ◦C until homogenisation and immunoblotting were to be performed. Immunoblotting was performed as described in section 2.17.

2.20.5.1 RT-qPCR for the detection of JSRV in lung slices

Supernatants from lung slices were analysed for the presence of JSRV by RT-qPCR. RNA was extracted from supernatants following the method described in section 2.4.2 but no dilution of the sample was performed in the first step. RNA concentration was measured by Nanodrop as described in section 2.4.8. RT-qPCR was then performed in one step by mixing 20 µl of mastermix with 5 µl of RNA sample. The mastermix was prepared by mixing 12.5 µl of reaction mix (Thermo Scientific), 0.5 µl 40x RT/Taq (Thermo Scientific), 0.5 µM primers JSRV-P1 (5′-TGGGAGCTCTTTGGCAAAAGCC-3′) and JSRV-P6 (5′-TGATATTTCTGTGAAGCAGTGCC-3′) (Palmarini et al, 1996b), and 0.125 µM JSRV probe (5′-FAM-AGCAAACATCCGARCCTTAAGAGCTTTCAAAA-BHQ) (Cousens et al, 2009) and water to 20 µl.

RT-qPCR was performed with an ABI 7500 real time machine with cycling conditions: 30 minutes at 48 ◦C, 10 minutes at 95 ◦C followed by 40 cycles of 15

seconds at 95 °C and 1 minute at 60°C. The results were analysed using ABI 7500 software. Ct values were compared with the positive controls and Ct values under 30 considered as positive for JSRV presence.

2.20.5.2 Reverse Transcriptase-assay for JSRV quantification

$JSRV_{21}$ particles were quantified using a colorimetric Reverse Transcriptase (RT) assay (Roche) as recommended. The assay uses the ability of RT to synthesise DNA, and provides digoxigenin and biotin labelled nucleotides that are incorporated into the newly synthesised DNA. The newly synthesised labelled DNA is detected and quantified by sandwich ELISA. In the final step, cleavage of the substrate results in a coloured product that can be measured at 405 nm. JSRV was quantified by reference to the standard curve of known amounts of HIV1 RT provided with the kit.

Chapter 3 miRNA dysregulation in OPA lung tissue

3.1 Introduction

To date, no published studies have investigated miRNA expression in OPA. Nevertheless, the study of miRNA dysregulation in OPA would further knowledge and understanding of the disease in several dimensions. For example, studying miRNA expression in the ovine lung could potentially allow the differentiation of OPA-affected and unaffected sheep. Differences in miRNA expression could be exploited as disease biomarkers and, eventually, help tackle the issue of OPA diagnosis and disease control, reviewed in section 1.4.

Study of miRNA expression in OPA-affected sheep lung might also highlight miRNAs related to the transformation process driven by JSRV Env. The targets of dysregulated miRNAs could be investigated to understand better how JSRV Env activates signalling pathways PI3K-Akt and MAPK (section 1.2.6) *in vivo*, and to find interactions between pathways. Moreover, the study of miRNA expression in OPA could also unveil the presence of JSRV-encoded miRNAs. Similarly to other retroviral-encoded miRNAs (section 1.5.14), a JSRV-encoded miRNA could have significant repercussions on our study of JSRV infection and the Env driven transformation process.

In most infected animals, JSRV infection is known to elicit a poor and ineffective immune response (section 1.2.8), and histopathological lesions are normally confined to the lung (section 1.1.3). Studies on miRNA expression can be performed in other tissues or cell types to investigate molecular changes and response to JSRV beyond the infected cells. For instance, JSRV is reportedly spread via the aerogenous route to colonise the sheep lung (section 1.1.4). Therefore, the study of miRNA dysregulation in OPA in alveolar macrophages, the first line of defence in the lung, could reveal transcriptional changes that indicate their role in JSRV-infection.

Comparison of miRNA expression between OPA-affected and unaffected sheep, would, in turn, provide valuable information on the miRNA expression pattern of a healthy sheep lung. Given the low number of reports on sheep miRNAs, (section

1.5.9), such a study could help build a comprehensive database entry that would aid future studies on miRNA dysregulation in this important farm animal. In addition, further characterisation of OPA and the sheep lung could reveal more similarities to human lung cancer, and help to consolidate OPA as a large animal model of the human pathology (section 1.1.3).

In vivo study of miRNA dysregulation in the sheep lung is facilitated by the existence of an experimental animal model, reviewed in section 1.3.1. This animal model allows the study of early transformation events in neonatal lambs, where a small percentage of tissue (~10 %) exhibits a transformed phenotype (**Fig. 3.1**). In addition, use of this model in specified pathogen-free (SPF) animals allows the study of OPA alone, without the potentially confounding effects of bacterial infections that are commonly found associated with more advanced cases (section 1.1.3). Moreover, the availability of tissues from early and advanced cases of natural OPA permits a comparison of miRNA dysregulation across disease stages.

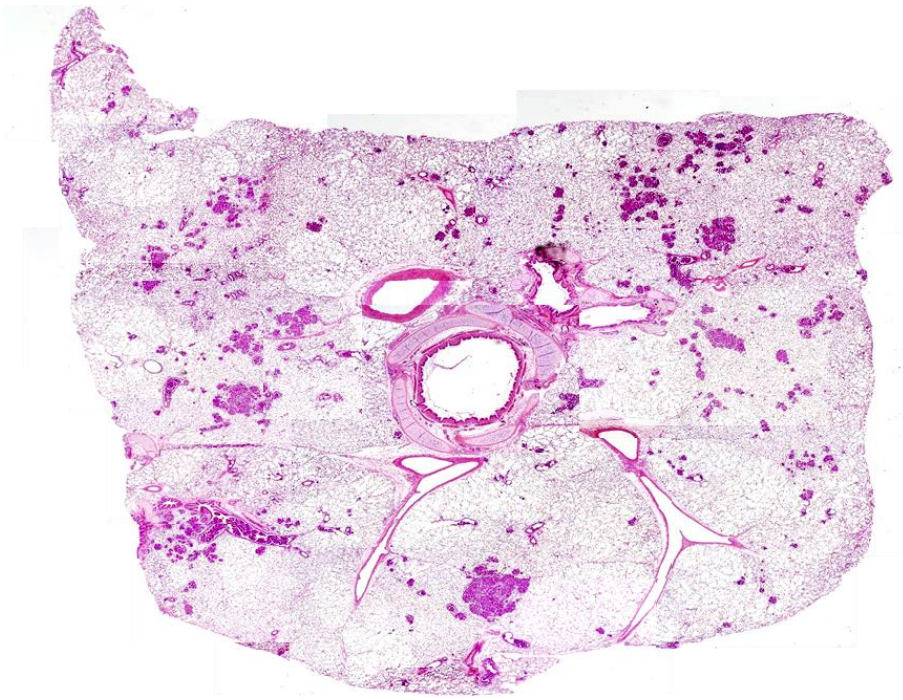

Figure 3.1. Haematoxylin and eosin staining of a lung section from a JSRV-infected lamb, 85 days post-infection. *Areas of increased cell density can be observed due to increased staining, these areas represent tumour foci. Reproduced from Martineau (2010).*

3.1.1 Hypothesis and aims

In this study, it was hypothesised that miRNAs can be detected in lung tissue from sheep, and that, when comparing JSRV-infected and uninfected sheep, a number of miRNAs would be differentially expressed between the two groups. In addition, it was also hypothesised that JSRV-encoded miRNAs could be detected in lung tissue of JSRV-infected sheep.

In order to explore these hypotheses the following aims were established:

- Detect miRNA expression in lung tissue of sheep
- Compare miRNA expression of infected and uninfected sheep lung
- Contrast findings from JSRV experimentally infected sheep and natural cases
- Detect miRNA expression in bronchoalveolar lavage macrophages
- Identify JSRV-encoded miRNAs or small RNAs in infected lung tissue

3.2 Results

3.2.1 miRNAs in OPA lung tissue identified by sequencing

In this section, the results for the initial miRNA screen performed in lung tissue are presented. The aim of this analysis was to identify viral and host miRNAs in lung tissue of $JSRV_{21}$-infected and mock-infected lambs. Besides the identification of miRNAs in the sheep lung we were interested in detecting which specific miRNAs, if any, were differentially expressed between the two groups analysed. Thus, this first screening would help determine candidates for further study as OPA biomarkers.

The tissues used in this study derived from an experimental infection which took place in 2007 (section 2.2). Tissue sections from eight distinct sites in the lung were obtained by cryodissection (section 2.4.3), RNA extraction was performed and samples from each lamb pooled. The lung tissue of $JSRV_{21}$-infected animals used for RNA extraction was of heterogeneous nature: consisting of mostly histologically normal tissue and up to 10% of tumour tissue (**Fig. 3.1**). Cryodissection and RNA extraction was performed by Jeannie Finlayson and Anna Karagianni prior to the start of this PhD project. The quality and integrity of RNA samples was measured (section 2.4.8) and only samples with RIN > 6, and 260/280 ratio > 1.9 were submitted for small-RNA sequencing (**Table 3.1**).

Table 3.1. RNA concentration of samples submitted for small RNA-sequencing of lung tissue.

Group	**JSRV-infected**			
Sample	SPF475	SPF476	SPF477	SPF478
RNA (ng/µl)	334	387	164	123
260/280 nm	2.02	1.99	2.05	2.05
RIN	7.2	7.9	8.4	8.1
Group	**Mock-infected**			
Sample	SPF479	SPF481	SPF482	SPF484
RNA (ng/µl)	222	220	288	323
260/280 nm	2.04	2.04	2.02	2.01
RIN	9	7.8	6.4	6.6

RNA samples were sequenced by Edinburgh Genomics (section 2.5). Bioinformatics analysis was performed by Siddharth Jayaraman and Deepali Vasoya, supervised by myself and with assistance from Mick Watson, David Griffiths and Finn Grey (section 2.5.1). Sequencing libraries were successfully constructed from all samples and miRNAs were detected in all samples. Total reads ranged from 19063580 reads to 29347531 reads, and presented more variability within the $JSRV_{21}$-infected samples (**Table 3.2**).

Table 3.2. Summary of reads for each sample of the lung tissue small RNA-sequencing study.

	Group	**JSRV-infected**			
	Sample	SPF475	SPF476	SPF477	SPF478
	Total reads	23042889	19063580	29347531	23400784
(%) total reads	**>28 nt**	6.51	6.82	8.44	9.93
	miRBase	68.77	72.68	64.66	64.86
	JSRV	0.00216	0.00119	0.00275	0.00156
	Group	**Mock-infected**			
	Sample	SPF479	SPF481	SPF482	SPF484
	Total reads	20380787	23674153	25491448	23304071
(%) total reads	**>28 nt**	5.69	9.29	9.60	4.03
	miRBase	69.18	68.43	69.58	79.10
	JSRV	0.00113	0.000765	0.000969	0.000755

The percentage of reads mapping to miRNAs on miRBase and other categories was consistent with slight variability between samples (**Table 3.2** and **Fig. 3.2**). No statistically significant differences were observed between groups (T-test $p<0.05$) (section 2.6.2). The presence of reads mapping to JSRV genome in mock-infected lambs might be due to the sequence similarity in regions of the JSRV and enJSRV genomes, some reads might map to both genomes. Sequence length distribution (**Fig. 3.3**) also revealed a similar pattern between $JSRV_{21}$-infected and mock-infected samples. These distribution results are comparable to previously published small RNA-sequencing studies, see (Chen et al, 2019; Li et al, 2013a; Peng et al, 2011).

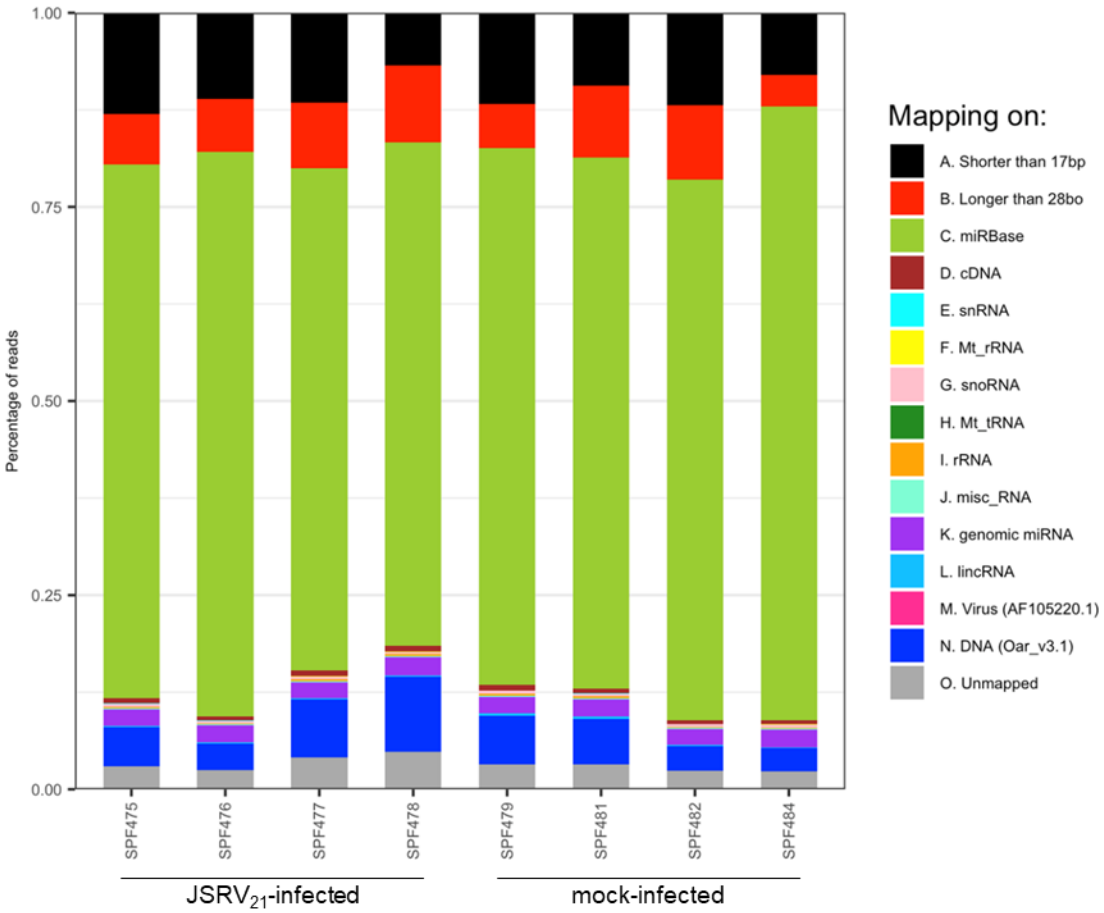

Figure 3.2. Sequence distribution in samples of lung tissue sequencing, presented as the percentage of total reads in each sample. *Each of the categories is represented by a colour shown in the legend. Small nuclear RNA(snRNA), mitochondrial ribosomal RNA (Mt_rRNA), small nucleolar RNA (snoRNA), mitochondrial transfer RNA (Mt_tRNA), ribosomal RNA (rRNA), miscellaneous RNA (misc_RNA), long non-coding RNA (lincRNA), JSRV viral genome (Virus), sheep genome (DNA), reads not mapping to any of the previous categories (Unmapped).*

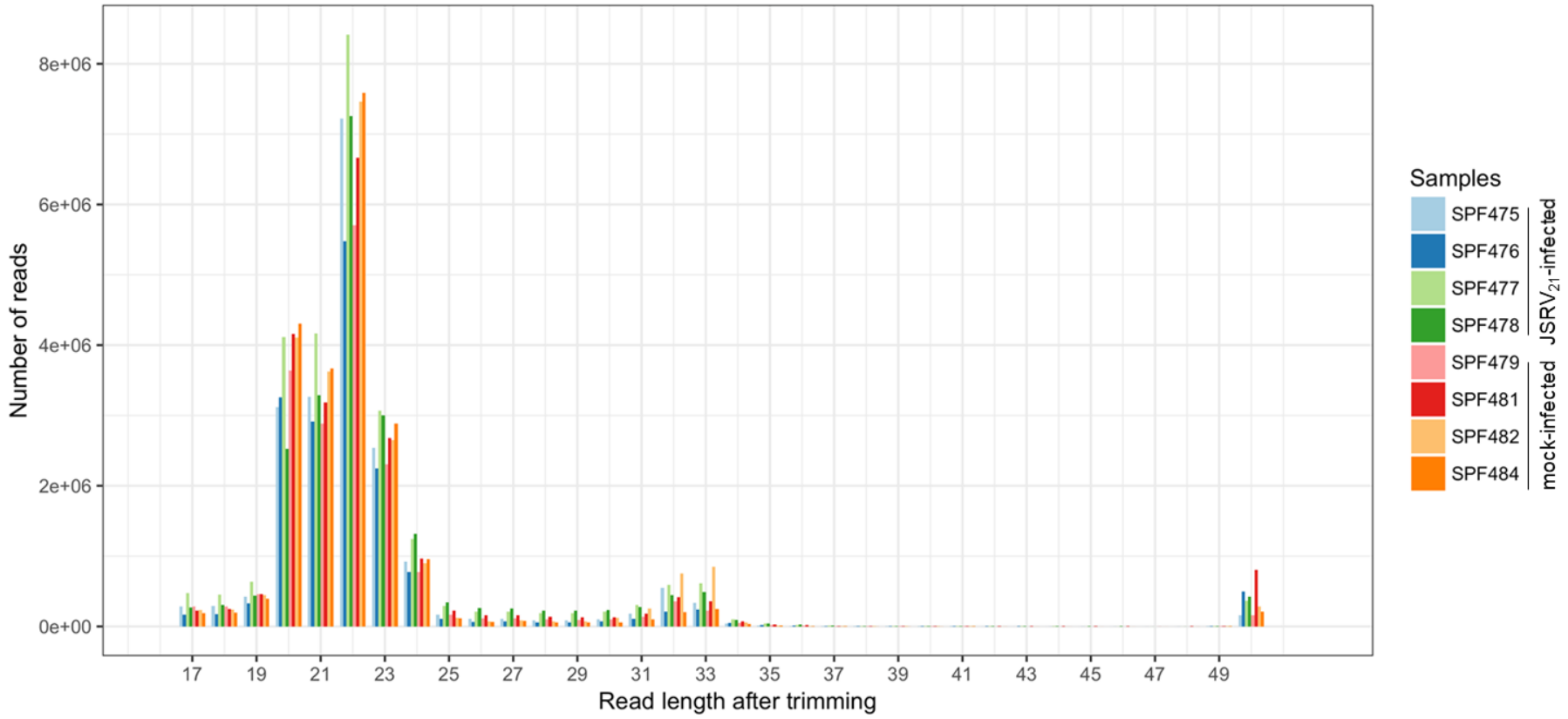

Figure 3.3. Length distribution of total sequencing reads after trimming was performed. *$JSRV_{21}$-infected samples (n=4, SPF475, SPF476, SPF477, SPF478); Mock-infected samples (n=4, SPF479, SPF481, SPF482, SPF484). The area with high read abundance observed corresponds to miRNA length (21-23nt). The length distribution appears similar between $JSRV_{21}$-infected samples and mock-infected samples.*

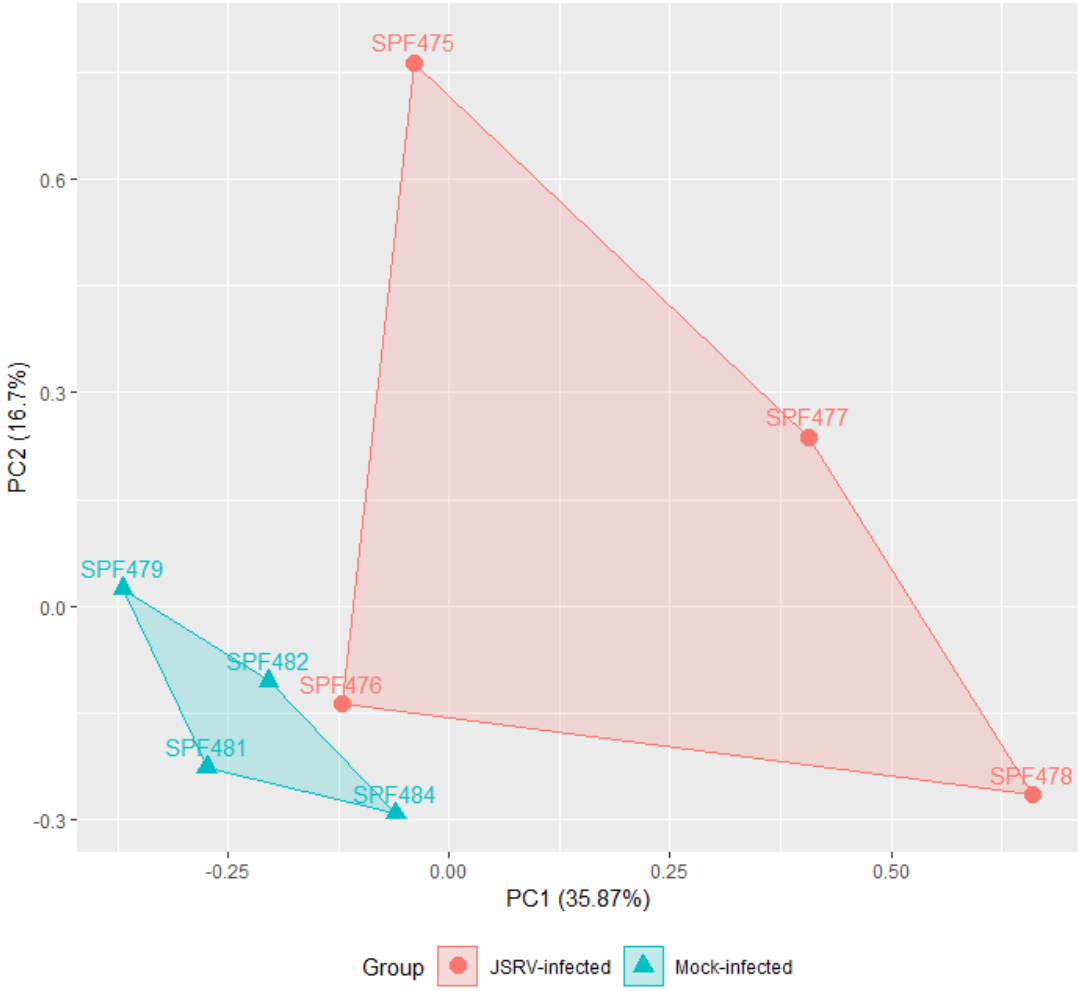

Figure 3.4. PCA plot of miRNA expression levels from lung tissue samples of JSRV$_{21}$-infected (n=4) and mock-infected controls (n=4). *Greater distance between samples in the plot indicates more expression differences between them. Control samples are seen clustering towards the left of the plot, whereas JSRV$_{21}$-infected samples can be seen occupying a larger part of the plot towards the right of the plot. Sample SPF476 of the JSRV$_{21}$-infected group is represented closer to the mock-infected group in both PC1 and PC2. The PCA plot indicates greater variability between JSRV$_{21}$-infected samples than among the control group and suggests global expression differences between the two groups.*

Comparison of miRNA expression from JSRV$_{21}$-infected and mock-infected lambs revealed 405 miRNAs detected in all analysed samples. Of those, 318 miRNAs were not listed in the miRBase entry for *O. aries*. This section will focus on host miRNAs, whereas reads mapping to the JSRV genome are analysed in section 3.2.6.

Expression levels of the 405 detected host miRNAs were represented in a principal component analysis (PCA) plot (**Fig. 3.4**). The PCA plot was used as an ordination analysis to observe variability among samples and evaluate the

clustering relations as a first indication of differences between groups. $JSRV_{21}$-infected and mock-infected lambs clustered separately in the PCA plot (**Fig. 3.4**) with higher variability within the JSRV-infected group. Nevertheless, one JSRV-infected sample, SPF476, was found to cluster closely with the mock-infected group, indicating that the global miRNA expression pattern of this sample was more similar to mock-infected lambs. This finding is in line with the PCA analysis performed in mRNA-sequencing of the same samples (Karagianni et al, 2019). The study found that clustering of samples in the PCA plot could largely be explained by the number of JSRV transcripts in each sample, samples clustering closer to the mock-infected group were found to have a lower viral-burden (Karagianni et al, 2019).

Given that the PCA plot suggested differences between the two groups, statistical analysis was performed (section 2.5.1) to identify the miRNAs that were differentially expressed between the groups. The fold change threshold was established at ≤ 0.75 for downregulated miRNAs and ≥ 1.5 for upregulated miRNAs. The decision to establish these fold changes as significant was made based on the low percentage of tumour tissue present in the samples to ensure potential differences were detected while acknowledging the potential for false positives. Of the 405 miRNAs present in all the samples, 32 miRNAs were found to be differentially expressed (FDR<0.05) between JSRV-infected and mock-infected lambs (**Fig. 3.5**). 26 miRNAs were found upregulated in JSRV-infected lambs (**Table 3.3**), whereas the remaining six miRNAs were downregulated (**Table 3.4**).

In the clustering analysis performed (**Fig. 3.5**), the RNA lung tissue sample from lamb SPF476 grouped with the mock-infected control group, instead of the JSRV-infected group, consistent with the PCA and again suggesting that the expression of DE miRNAs in this lamb resembled more that of control lambs.

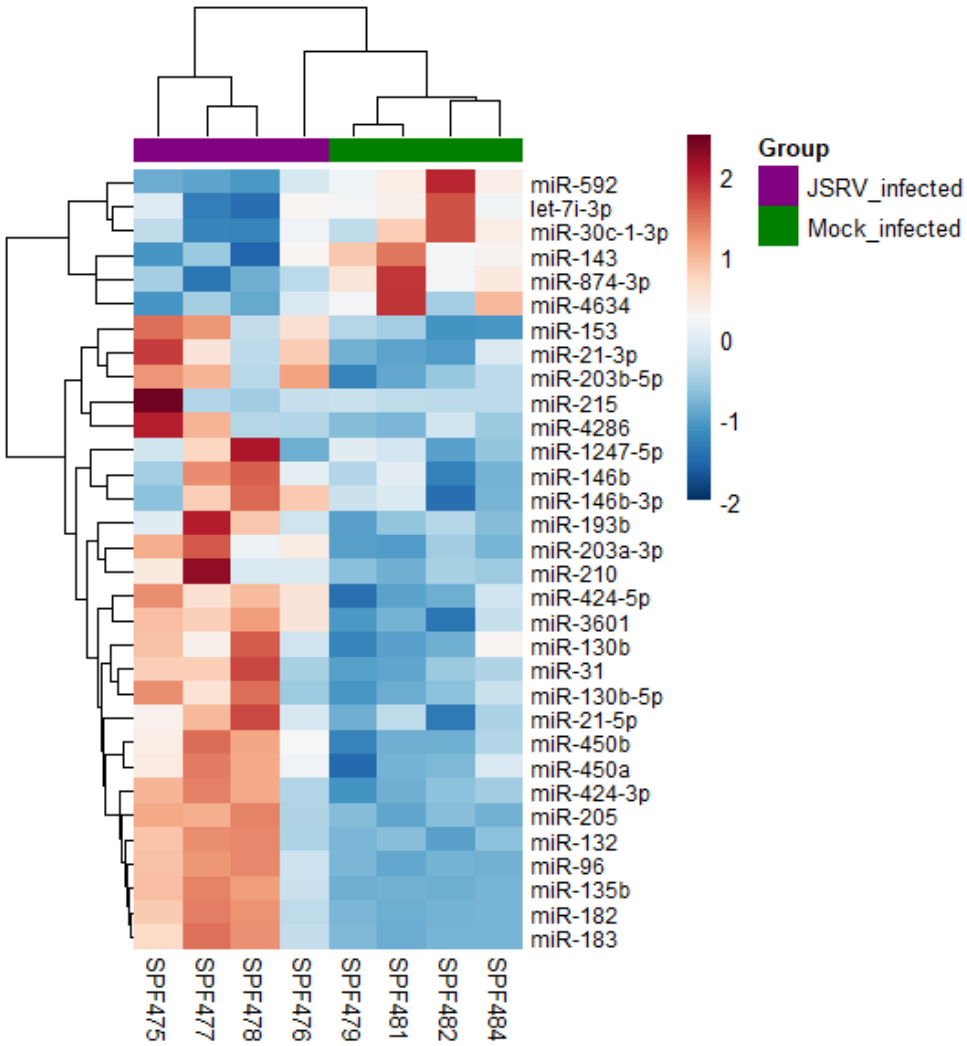

Figure 3.5. Heatmap of DE miRNAs (FDR<0.05, log_2(fold change) ≥ 0.58 or ≤ -0.42) between lung tissue of JSRV-infected and mock-infected lambs. *Dendrogram showing correlation clustering of individuals in groups. Legend represents values of log2 fold change.*

Table 3.3. Differentially upregulated miRNAs in lung tissue between JSRV-infected and mock-infected lambs.

miRNA	average counts[1]	log2(fold change)[2]	FDR[3]
miR-182	20880.16	3.20	0
miR-183	7512.52	3.03	4.28E-84
miR-96	343.43	3.15	5.94E-69
miR-135b	70.94	4.82	1.28E-61
miR-205	4802.59	1.29	1.01E-14
miR-132	118.12	1.40	2.09E-11
miR-450b	4841.10	1.04	1.25E-08
miR-424-3p	188.42	1.07	4.56E-07
miR-193b	1564.57	0.92	5.68E-07
miR-130b-5p	130.98	1.13	7.09E-07
miR-215	105.36	1.08	1.66E-06
miR-31	252.35	0.91	2.06E-05
miR-424-5p	1250.31	0.87	2.15E-05
miR-21-5p	28385.89	0.75	5.08E-05
miR-1247-5p	161.02	0.75	1.53E-04
miR-450a	1564.13	0.79	1.66E-04
miR-203b-5p	146.58	0.86	4.95E-04
miR-3601	141.28	0.82	6.74E-04
miR-210	547.69	0.70	8.33E-04
miR-146b	29159.79	0.61	8.61E-04
miR-21-3p	1407.30	0.69	1.22E-03
miR-153	94.21	0.74	2.95E-03
miR-130b	690.02	0.70	2.98E-03
miR-203a-3p	963.90	0.61	6.78E-03
miR-146b-3p	58.90	0.72	1.08E-02
miR-4286	90.54	0.61	4.02E-02

[1] Average normalised counts across all samples
[2] Threshold established at log2(fold change) ≥ 0.58
[3] FDR corrected by Benjamini-Hochberg, threshold FDR ≤ 0.05

Table 3.4. Differentially downregulated miRNAs in lung tissue between JSRV-infected and mock-infected lambs.

miRNA	average counts[1]	log2(fold change)[2]	FDR[3]
miR-143	3626500.56	-0.57	0
miR-592	119.44	-0.95	4.83E-05
miR-30c-1-3p	275.96	-0.53	3.06E-02
miR-874-3p	514.64	-0.57	3.13E-02
let-7i-3p	441.42	-0.51	3.72E-02
miR-4634	395.30	-0.56	3.80E-02

[1] Average normalised counts across all samples
[2] Threshold established at log2(fold change) ≤ -0.42
[3] FDR corrected by Benjamini-Hochberg, threshold FDR ≤ 0.05

3.2.2 Validation of OPA lung tissue miRNA expression by RT-qPCR

In order to investigate if the DE miRNAs observed by small RNA-sequencing could also be detected using another technique, RT-qPCR was used to analyse miRNA expression of the same RNA samples used in **3.2.1**.

The 40 miRNAs detected as differentially expressed from the results of small RNA-sequencing were examined for relative expression levels (normalised counts), variance of expression among samples of the same group, fold change of expression between groups, and involvement in human forms of lung cancer. Seven miRNAs were then selected for further validation using RT-qPCR. The criteria for selection was: fold change > 1.5, mean normalised counts >50, coefficient of variation within groups <50%, FDR<0.01 and a minimum of five independent studies reporting their dysregulation or involvement in human lung cancer (see **Table 1.1**).

The selected miRNAs were: miR-135b-5p, miR-182-5p, miR-183-5p, miR-miR-205-5p, miR-21-5p, miR-31-5p, and miR-96-5p.

In addition, miR-200b-5p and miR-503-5p were also added to the validation panel. Although they did not meet the criteria for selection (miR-200b-5p: fold change=

1.46, FDR= 0.016 and average counts= 274.65; miR-503-5p: fold change= 1.56, FDR= 0.0008 and average counts= 11.72), they were of interest due to their known involvement in lung cancer and validated targets (**Table 1.1**).

3.2.2.1 Selection of controls for RT-qPCR

The miRNAs miR-191 (hsa-miR-191-5p) and miR-103 (hsa-miR-103a-3p) were assessed as potential endogenous controls. The selection of those two miRNAs was made based on high expression level (mean normalised counts >150), low variance among all samples (coefficient of variance < 20%), no known involvement in lung cancer or viral infection, and was in line with literature and kit manufacturer recommendations.

A first RT-qPCR study to analyse the stability of miR-191-5p and miR-103a-3p was performed (section 2.6) with the results revealing 5.6% variance between samples and 11.2% variance between samples for miR-191-5p and miR-103a-3p respectively. On the basis of those results, miR-191-5p was chosen as the endogenous control for RT-qPCR.

3.2.2.2 RT-qPCR validation of DE miRNAs

Validation of the small RNA-sequencing results obtained was performed by RT-qPCR. Aliquots from the same RNA samples used for sequencing were reverse transcribed and assayed by qPCR (section 2.6).

RT-qPCR results were analysed following the ddCt method (section 2.6.2). The results showed higher expression levels of the nine selected miRNAs in the JSRV-infected group compared to the uninfected control group (**Fig. 3.6).** miR-183, detected in infected but not control samples, presented the greatest expression difference between groups. For representation and analysis purposes those miRNAs not detected by RT-qPCR were given a value of 40 Ct, the maximum number of cycles performed. The results of miRNA expression by RT-qPCR shown for each individual sample highlight the variability within groups, already observed in small RNA-sequencing results (**Fig. 3.6.A**).

Statistical analysis of the dCt values was performed (section 2.6.2). The nine assayed miRNAs presented p-values below the established threshold of 0.05,

allowing for rejection of the null hypothesis which considered that the means of the two groups were equivalent (**Table 3.5**). These findings indicated that dysregulation of miRNAs in OPA lung tissue could also be detected by RT-qPCR and validated the small RNA-sequencing results for the selected miRNAs.

In summary, the results of RT-qPCR confirmed the increased expression of the nine selected miRNAs in OPA-affected lung, when using the same RNA sample used for small RNA sequencing.

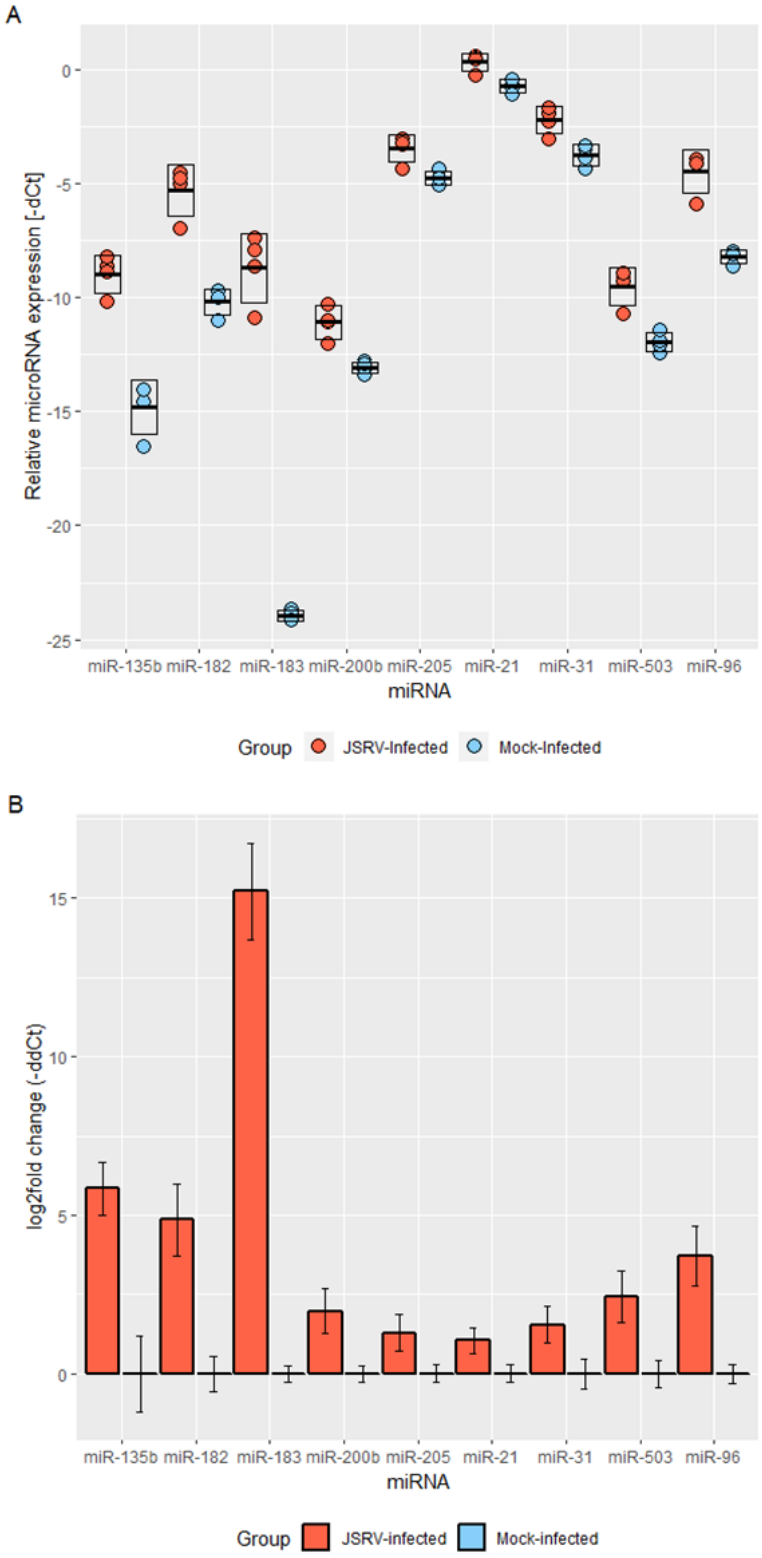

Figure 3.6. miRNA expression levels as detected by RT-qPCR in lung tissue of JSRV-infected (n=4) in red, and Mock-infected controls (n=4) in blue. *A. relative miRNA expression as -dCt (-Ct miR+Ct miR-191) of each individual sample per each miRNA assayed. Boxes show standard deviations of the mean, represented with a horizontal line. B. log_2fold change for each assayed miRNA between groups, calculated as (section 2.6.2). Error bars indicate standard deviation of miRNA expression within groups.*

Table 3.5. Statistics results of student's t-test performed on dCt values obtained by RT-qPCR.

miRNA	Group	Mean[1]	Stdev[2]	Estimated difference	DF[3]	p-value
miR-135b	JSRV-infected	8.967	0.837	-5.836	5	0
	Mock-infected	14.8	1.19			
miR-182	JSRV-infected	5.33	1.13	-7.72	4	0.02
	Mock-infected	10.187	0.562			
miR-183	JSRV-infected	8.72	1.52	-15.213	3	0
	Mock-infected	23.931	0.242			
miR-200b	JSRV-infected	11.087	0.722	-1.98	3	0.014
	Mock-infected	13.068	0.242			
miR-205	JSRV-infected	3.469	0.587	-1.295	4	0.016
	Mock-infected	4.765	0.282			
miR-21	JSRV-infected	-0.322	0.387	-1.043	5	0.007
	Mock-infected	0.721	0.278			
miR-31	JSRV-infected	2.229	0.583	-1.541	5	0.009
	Mock-infected	3.77	0.463			
miR-503	JSRV-infected	9.519	0.813	-2.44	4	0.006
	Mock-infected	11.959	0.427			
miR-96	JSRV-infected	4.485	0.939	-3.701	3	0.005
	Mock-infected	8.185	0.295			

[1] Null-hypothesis= no differences between the means of the two groups assessed, confidence level stablished at 95%.
[2] Stdev= standard deviation of the mean.
[3] DF= degrees of freedom.

3.2.3 Validation of miRNA expression in an independent experimental group by RT-qPCR

The elevated expression levels of miRNAs miR-135b, miR-182, miR-183, miR-21, miR-200b, miR-205, miR-31, miR-503 and miR-96 in JSRV-infected lambs were further investigated in an independent sample set. The samples were from animals experimentally infected in 2015 (section 2.2). In that experimental infection, lambs were infected with $JSRV_{21}$, mock-infected or infected with a JSRV mutant ($JSRV_{mut}$). The $JSRV_{mut}$ contains a point-mutation in Env: JSRV-Env-M574A. This $JSRV_{mut}$ originated from a panel created to study the role of JSRV

CT in transformation that aimed to create a transformation deficient, replication efficient form of JSRV (Hull and fan 2006). Single point mutants were analysed for infection and replication efficiency in ovine lung slices in our lab. Most mutants screened in lung slices did not infect lung slices efficiently. The $JSRV_{mut}$ used for infection of lambs was able to infect and replicate in ovine lung slices, but not as efficiently as $JSRV_{21}$, and it did not present Akt-P staining by IHC. Post-mortem examination of $JSRV_{mut}$-infected lung tissues did not reveal lesions consistent with OPA. In addition, Immunohistochemistry analysis of JSRV Env expression in 24 sites of each of the lambs revealed no positive staining. Overall, the results indicated that the $JSRV_{mut}$ was not able to infect and replicate efficiently in sheep lung. Nevertheless, gene expression in lung tissue samples from this experimental infection was investigated by mRNA-sequencing and changes in expression of some mRNAs noted (Karagianni, Griffiths, in preparation). Samples from $JSRV_{mut}$-infected lambs were also included in this study to investigate possible miRNA expression differences.

Lung tissue samples from $JSRV_{21}$-infected lambs (SPF4, SPF7, SPF11, SPF15, SPF20 and SPF23), mock-infected lambs (SPF6, SPF8, SPF12, SPF14) and $JSRV_{mut}$ infected lambs (SPF1, SPF9, SPF10, SPF13) were used in this study. Samples were cryosectioned (section 2.4.3) and RNA extraction performed (section 2.4.5). As in the 2007 experimental infection, eight tissue samples from each lamb were pooled.

miRNA expression levels of the selected miRNAs presented high levels of variability within groups and smaller fold changes between groups than in the original data set (**Fig. 3.7**). In addition, the expression of miR-183 could not be detected in any of the samples assayed, suggesting low copy numbers.

Statistical analysis on the dCt values obtained by RT-qPCR was performed (section 2.6.2). Three out of the eight assayed miRNAs presented p-values below the established threshold of 0.05 (**Table 3.6**). Interestingly, these miRNAs were the ones that presented higher fold-changes in the previous study (**3.2.1** and **3.2.2**). Based on the means and the distribution of the values in **Fig. 3.7** it can be predicted that the JSRV-infected group is statistically different to the other two groups. The results for the remaining five miRNAs did not allow for rejection of the

null hypothesis. This finding might be due to the high variability observed within groups, which might be due to age differences between lambs at PM and is further discussed in 3.3.

The variability within groups observed contrasts with the observations of the first experimental infection and can be related to some variables: several animals (**Table 2.2**) in all groups suffered from what was diagnosed as an allergic response, this has the potential to disrupt the miRNA expression and could explain the similarities between groups. Another variable is the length of infection, comparing the culling times between the experimental infections we could see notable differences: lambs of the 2007 experimental infection were culled between 72 and 91 days post-infection, whereas lambs of this infection were culled between 41 and 68 days post-infection. These differences could indicate different susceptibility of the lambs to the JSRV dose administered, or even an interaction with the allergy.

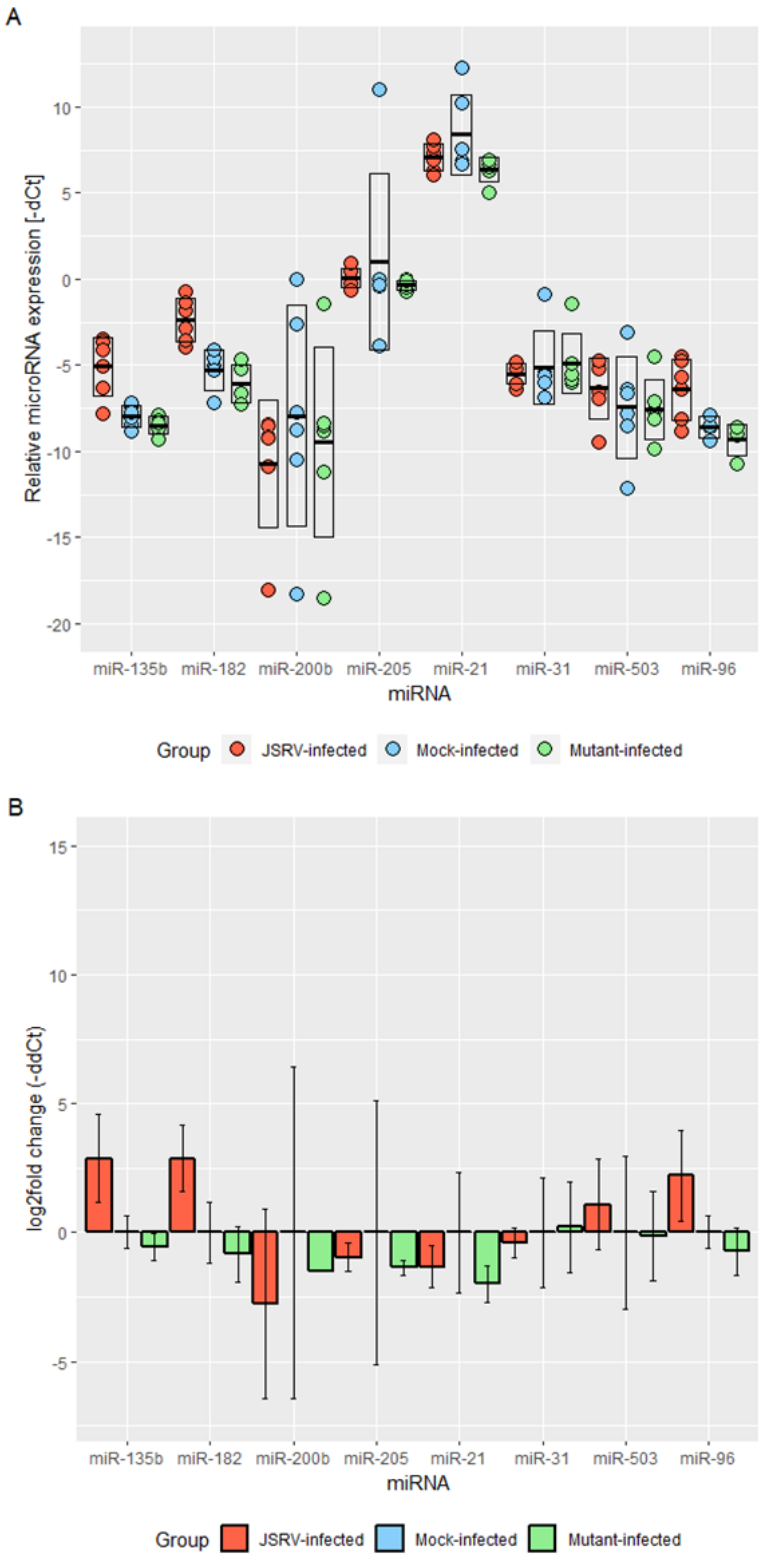

Figure 3.7. miRNA expression detected by RT-qPCR in lung tissue of $JSRV_{21}$-infected (n=6), mock-infected (n=4), and $JSRV_{mut}$-infected (n=4) lambs. *A. relative miRNA expression as -dCt (-Ct miR+Ct miR-191) of each sample per each miRNA assayed. Boxes show standard deviations of the mean, represented with a horizontal line. B. log_2fold change for each assayed miRNA between groups, calculated as pairwise comparisons $JSRV_{21}$-infected or $JSRV_{mut}$-infected vs. mock infected (section 2.6.2). Error bars indicate standard deviation of miRNA expression within groups.*

Table 3.6. Statistics results of the ANOVA test performed on dCt values obtained by RT-qPCR.

miRNA	Group	Mean[1]	Stdev[2]	DF[3]	p-value
miR-135b	JSRV-infected	5.065	1.696	6.25	0.011
	Mock-infected	7.955	0.517		
	mutant-infected	8.491	0.523		
miR-182	JSRV-infected	2.377	1.294	8.59	0.002
	Mock-infected	5.259	1.185		
	mutant-infected	6.091	1.084		
miR-200b	JSRV-infected	10.72	3.69	7.95	0.898
	Mock-infected	9.56	5.7		
	mutant-infected	11.08	4.3		
miR-205	JSRV-infected	-0.048	0.557	6.94	0.212
	Mock-infected	0.987	1.605		
	mutant-infected	0.424	0.245		
miR-21	JSRV-infected	7.06	0.808	6.7	0.336
	Mock-infected	7.594	1.517		
	mutant-infected	6.672	0.217		
miR-31	JSRV-infected	5.508	0.595	8.52	0.462
	Mock-infected	5.947	0.566		
	mutant-infected	5.584	0.435		
miR-503	JSRV-infected	6.338	1.768	7.866	0.165
	Mock-infected	8.29	2.3		
	mutant-infected	8.175	1.026		
miR-96	JSRV-infected	6.395	1.773	6.98	0.039
	Mock-infected	8.607	0.632		
	mutant-infected	9.343	0.936		

[1] Null-hypothesis= no differences between the means of the three groups assessed, alternative hypothesis= at least one of the group's means is different, confidence level stablished at 95%.
[2] Stdev= standard deviation of the mean.
[3] DF=degrees of freedom.

3.2.4 miRNA expression in lung tissue of natural cases of OPA by RT-qPCR

Given the nature of the experimental infection model, the samples assayed represented an early stage of OPA and all corresponded to lungs from young lambs (one to 3 months old). As mentioned in section 1.5.11, the miRNA signature has been shown to differ depending on disease stage and developmental stage, suggesting that the miRNA dysregulation signature observed in experimental samples might not equate to that of natural, more advanced, cases of the disease. In order to test this, the expression of the nine selected miRNAs (miR-135b, miR-182, miR-183, miR-21, miR-200b, miR-205, miR-31, miR-503 and miR-96) was analysed in samples from adult sheep affected by OPA. Ten lung tissue samples from OPA affected sheep (JA874, JA875, JA876, JA894, JA895, JA896, JA898, JA899, JA901 and JA902) and six healthy adult sheep (MP15/170, 171, 172, 173, 174 and 175) were collected and cryosectioned, RNA was extracted. RNA quality and integrity assessment was performed and all samples had a RIN >6 and 260/280 ratio >1.8. RT-qPCR was performed to compare miRNA expression levels of the selected miRNAs.

With the exception of miR-183, not detected in samples from the healthy control group, all tested miRNAs were detected in both groups. The same upregulation trend observed in samples from lambs' lung tissue was observed in samples from adult sheep (**Fig. 3.8**).

Statistical analysis on the dCt values obtained by RT-qPCR revealed that eight out of the nine assayed miRNAs presented p-values below the established threshold of 0.05. The exception was miR-31, which produced a p-value greater than the established threshold, indicating no difference between the groups (**Table. 3.7**). These findings indicate that most of the miRNAs significantly upregulated in experimental cases of OPA are also upregulated in natural cases of OPA, increasing confidence that they are involved in the pathogenesis of OPA, discussed in 3.3.

The variability observed within groups can be expected of natural cases of the disease, the sheep studied came from different farms, were different ages and

had suffered the disease for various lengths of time. Nevertheless, a cofounding factor should be considered when analysing the results of this particular study: all control animals were herd at the Moredun Group farms, whereas the OPA affected group were a more heterogeneous group coming from different farms. This could potentially bias the results observed and the differences between groups and similarities within groups, could in part be explained by the origin of the animals (**Table 2.4**).

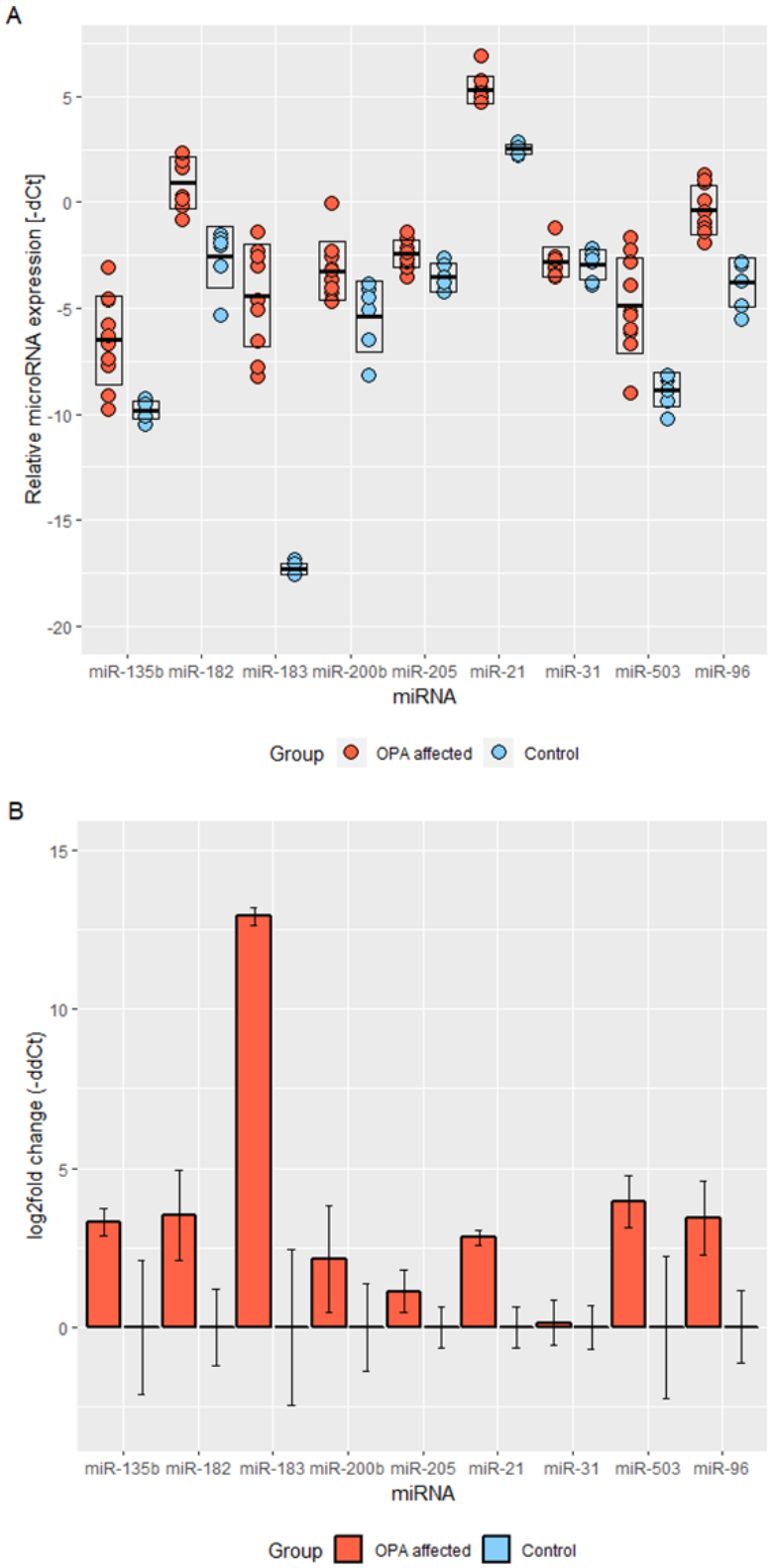

Figure 3.8. miRNA expression levels as detected by RT-qPCR in lung tissue of OPA-affected (n=10) and controls (n=6). *A. relative miRNA expression as -dCt (-Ct miR+Ct miR-191) of each individual sample per each miRNA assayed. Boxes show standard deviations of the mean, represented with a horizontal line. B. log_2fold change for each assayed miRNA between groups, calculated as (section 2.6.2). Error bars indicate standard deviation of miRNA expression within groups.*

Table 3.7. Statistics results of student's t-test on dCt values obtained by RT-qPCR.

miRNA	Group	Mean[1]	Stdev[2]	Estimated difference difference	DF[3]	p-value
miR-135b	OPA-affected	6.51	2.1	-3.295	10	0.001
	Unaffected control	9.805	0.442			
miR-182	OPA-affected	-0.93	1.2	-3.51	9	0.001
	Unaffected control	2.58	1.43			
miR-183	OPA-affected	4.39	2.43	-12.915	9	0
	Unaffected control	17.308	0.274			
miR-200b	OPA-affected	3.24	0.44	-2.124	9	0.028
	Unaffected control	5.36	0.68			
miR-205	OPA-affected	2.417	0.627	-1.122	10	0.008
	Unaffected control	3.539	0.665			
miR-21	OPA-affected	-5.337	0.641	-2.819	12	0
	Unaffected control	-2.517	0.24			
miR-31	OPA-affected	2.827	0.698	-0.127	10	0.735
	Unaffected control	2.954	0.71			
miR-503	OPA-affected	4.89	2.25	-3.969	12	0
	Unaffected control	8.854	0.816			

[1] Null-hypothesis= no differences between the means of the two groups assessed, confidence level stablished at 95%.
[2] Stdev= standard deviation of the mean.
[3] DF=degrees of freedom.

3.2.5 miRNA expression in OPA laser capture microdissected lung tissue

The previous analysis was done using samples from affected lung tissue that was not enriched for tumour. Therefore, presence of excess histologically normal tissue may reduce sensitivity to detect DE miRNAs in OPA. To address this, Laser capture microdissection (LCM) was used with the aim to enrich the samples for

tumour-affected tissue. The technique allows for microdissection of selected tumour tissue, and avoids the artefacts that a high percentage of normal tissue could pose on the analysis.

The LCM technique was performed in $JSRV_{21}$-infected (n=3), mock-infected control samples (n=3), $JSRV_{mut}$-infected samples (n=3), from the experimental infection that took place in 2015, also used in **3.2.3**. Anna Karagianni performed laser capture microdissection and RNA extraction from the LCM tissue. RNA samples were submitted to Liverpool genomics for sequencing (**Table 3.8**).

Table 3.8. RNA concentration of LCM lung tissue samples submitted for small RNA-sequencing.

Group	**JSRV-infected**		
Sample	SPF4	SPF7	SPF20
RNA (ng/µl)	60.77	68.98	80.64
260/280 nm	1.81	2.00	1.83
RIN	8.9	9.4	8.8
Group	**Mock-infected**		
Sample	SPF8	SPF12	SPF14
RNA (ng/µl)	83.63	62.05	65.42
260/280 nm	1.90	1.89	1.99
RIN	8.4	7.3	8.8
Group	**Mutant-infected**		
Sample	SPF1	SPF5	SPF9
RNA (ng/µl)	87.30	66.69	60.05
260/280 nm	2.03	1.86	1.8
RIN	8.8	7.8	7.5

Bioinformatics analysis was performed by Siddharth Jayaraman and Deepali Vasoya supervised by myself and with guidance from Mick Watson, Finn Grey and David Griffiths. Sequencing libraries were successfully constructed from all samples. Total reads ranged from 12270528 reads to 33069302 reads, and presented more variability within the $JSRV_{21}$-infected samples (**Table 3.9**). Statistically significant differences were found in the percentage of reads > 28 nt, as well as reads mapping to miRBase, between the $JSRV_{mut}$-infected samples and $JSRV_{21}$-infected or mock-infected samples ($p<0.05$). Furthermore, the

proportion of reads mapping to miRBase was lower than in the previously performed small RNA sequencing of lung tissue.

Table 3.9. Summary of reads for each sample of the LCM lung tissue small RNA-sequencing study.

	Group	**JSRV-infected**		
	Sample	SPF4	SPF7	SPF20
	Total reads	12270528	23697767	33069302
(%) total reads	**>28 nt**	25.55	20.44	24.87
	miRBase	14.08	37.61	41.47
	JSRV	0.00737	0.0194	0.000514
	Group	**Mock-infected**		
	Sample	SPF8	SPF12	SPF14
	Total reads	21363133	27847061	25887818
(%) total reads	**>28 nt**	20.90	20.87	21.80
	miRBase	41.23	46.06	42.90
	JSRV	0.00000562	0.0000898	0.0000425
	Group	**Mutant-infected**		
	Sample	SPF1	SPF5	SPF9
	Total reads	30771928	27375823	28314358
(%) total reads	**>28 nt**	18.42	14.76	13.01
	miRBase	49.14	54.84	61.59
	JSRV	0.0000520	0.0000694	0.0000706

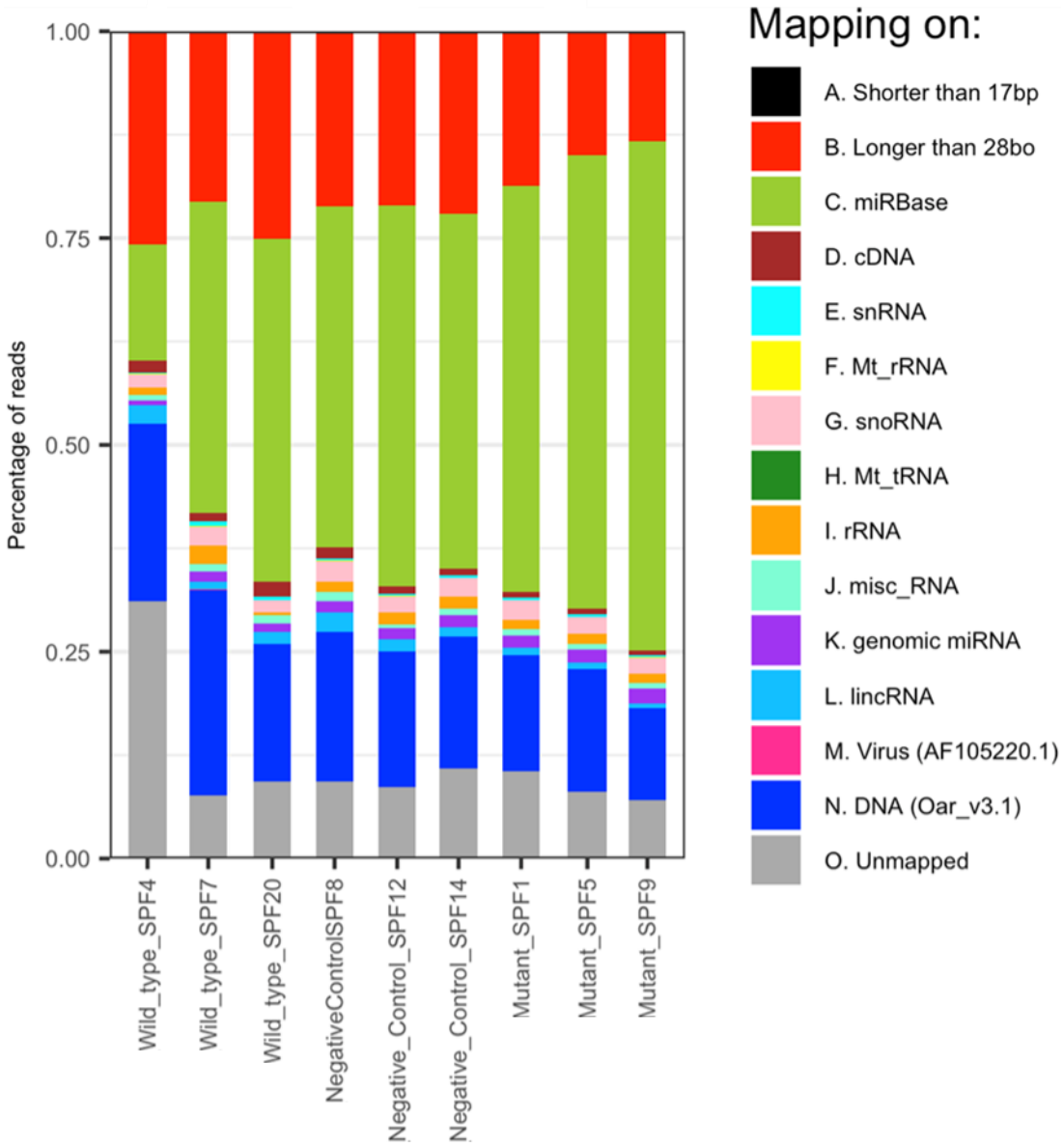

Figure 3.9. Sequence distribution in samples of LCM lung tissue sequencing, presented as percentage of total reads in each sample. *Each of the categories is represented by a colour shown in the legend. Small nuclear RNA(snRNA), mitochondrial ribosomal RNA (Mt_rRNA), small nucleolar RNA (snoRNA), mitochondrial transfer RNA (Mt_tRNA), ribosomal RNA (rRNA), miscellaneous RNA (misc_RNA), long non-coding RNA (lincRNA), JSRV viral genome (Virus), sheep genome (DNA), reads not mapping to any of the previous categories (Unmapped).*

The variability in reads mapping to different categories of RNA can also be appreciated in **Fig. 3.9**, but it does not appear to be related to total read number, RNA concentration or sample quality. Given the low number of samples in each group, the differences between groups might be an artifact and not representative. Nevertheless, the distinctive distribution pattern presented by SPF4 might be related to the lower number of total reads in the sample. Length distribution (**Fig.**

3.10) was found to be similar between groups, with the exception of SPF9, that presented a higher number of reads in the miRNA region.

Sequencing and analysis of the LCM samples detected 374 host miRNAs, a similar number to the 405 miRNAs detected in lung tissue in **3.2.1**. This section will focus on host miRNAs, reads mapping to the JSRV genome are discussed in **3.2.8**. Global miRNA expression between mock-infected controls and $JSRV_{mut}$-infected samples showed close clustering between the two groups. $JSRV_{21}$-infected samples presented higher within group variability of miRNA expression as well as levels of specific miRNAs compared to the other two groups (**Fig. 3.11**). Interestingly, SPF4, the sample that presents greater distance by PC1 to all other samples, had the lowest percentage of reads mapping to miRBase (**Table 3.9**). In addition, one of the $JSRV_{21}$-infected samples, SPF20, clustered closely with the mock-infected group.

Pairwise comparisons were then performed between groups to identify miRNAs differentially expressed between groups and to compare the findings with those of whole lung tissue.

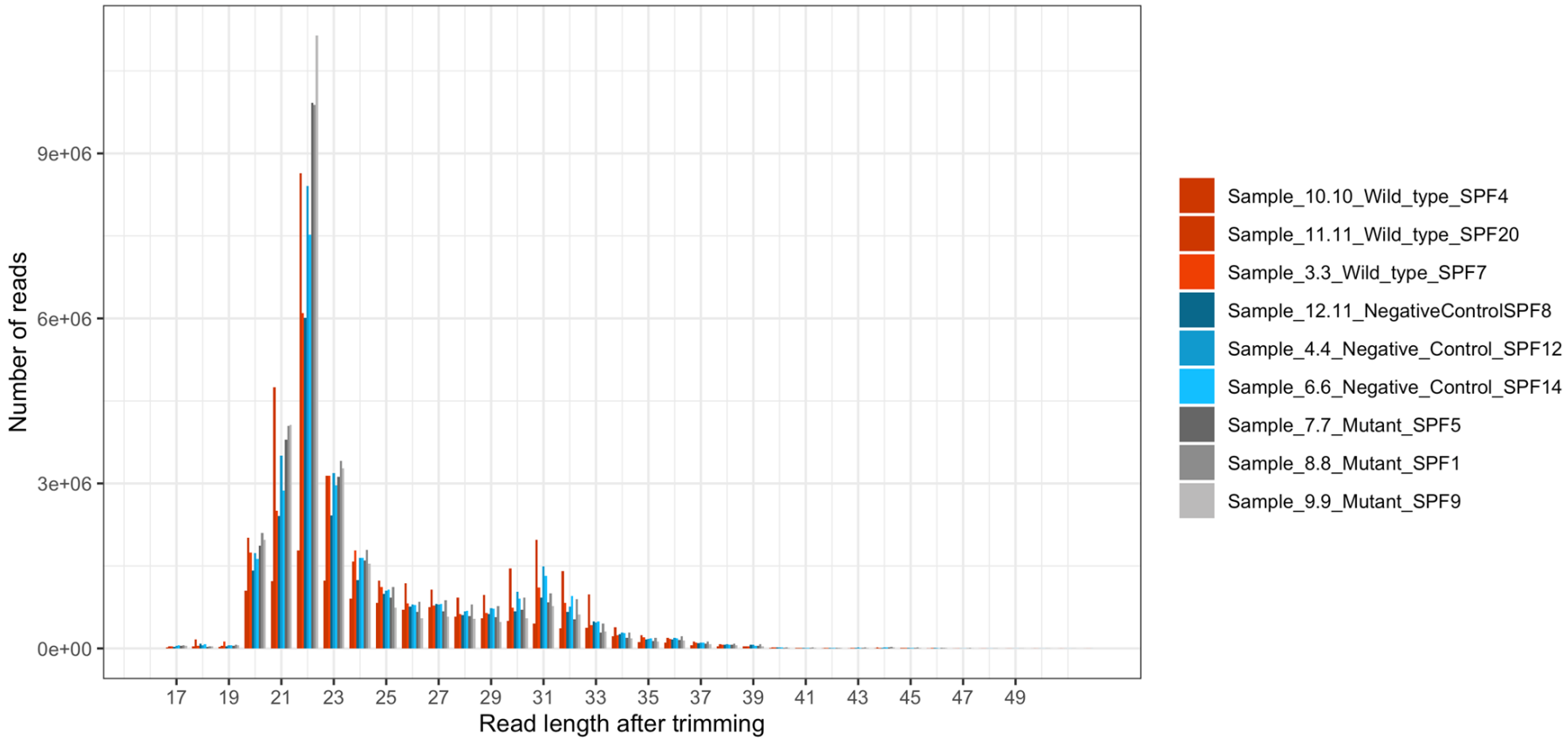

Figure 3.10. Length distribution of total sequencing reads after trimming was performed. *$JSRV_{21}$-infected samples (n=3, SPF4 SPF7, SPF20); Mock-infected control samples (n=3, SPF8, SPF12, SPF14); $JSRV_{mut}$-infected samples (n=3, SPF1, SPF5, SPF9). The area with high read abundance observed corresponds to miRNA length (21-23nt). Length distribution appears similar between groups, with SPF9 presenting a higher number of reads in the miRNA region.*

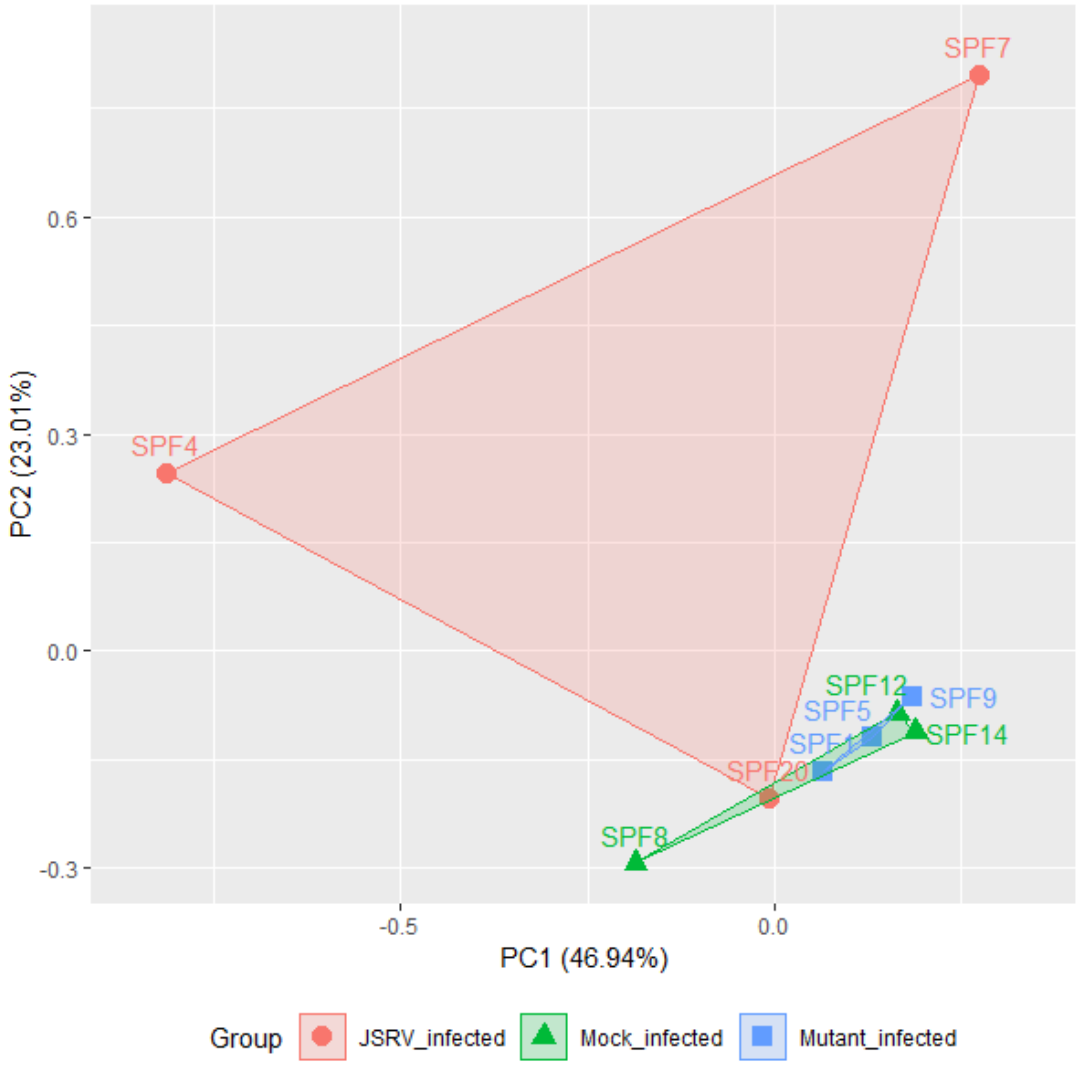

Figure 3.11. PCA plot of miRNA expression from LCM lung tissue samples of $JSRV_{21}$-infected (n=3), $JSRV_{mut}$-infected (n=3), and mock-infected lambs (n=3). *Control and $JSRV_{mut}$-infected samples cluster together towards the right of the plot, whereas $JSRV_{21}$-infected samples occupy a larger part of the plot. The PCA plot indicates greater variability between $JSRV_{21}$-infected samples in PC1 and PC2 than among the other groups. By PC1, SPF7 and SPF20 cluster closer to the control group than the $JSRV_{21}$-infected group. SPF20 also clusters closely to the control group by PC2. This plot suggests differences between $JSRV_{21}$-infected and the other groups as well as within the group.*

3.2.5.1 DE miRNAs between $JSRV_{21}$-infected and mock-infected LCM lung tissue

The DE threshold for the study of miRNA expression in LCM samples was established at fold change >2 or fold change < 0.5, and FDR <0.05. This threshold is more stringent than the one applied in lung tissue because LCM samples are enriched for tumour tissue. Therefore, levels of upregulation and downregulation

of miRNAs related to OPA were expected to be greater compared to lung tissue samples.

Comparison of DE miRNAs between the $JSRV_{21}$-infected and the mock-infected group revealed 67 miRNAs differentially expressed between the two groups. 60 miRNAs were upregulated and the remaining 7 were downregulated in the $JSRV_{21}$-infected group (**Table 3.10** and **Table 3.11**). Nevertheless, observing the heatmap of DE miRNAs (**Fig. 3.12**) DE of most miRNAs seems to be driven by the expression levels of one sample, either SPF4 or SPF7. In addition, clustering showed that SPF8, of the mock-infected group, clustered with $JSRV_{21}$-infected samples, while SPF7, of the $JSRV_{21}$-infected group clustered with mock-infected samples.

Potential reasons for the observed within group variability are discussed in 3.3.

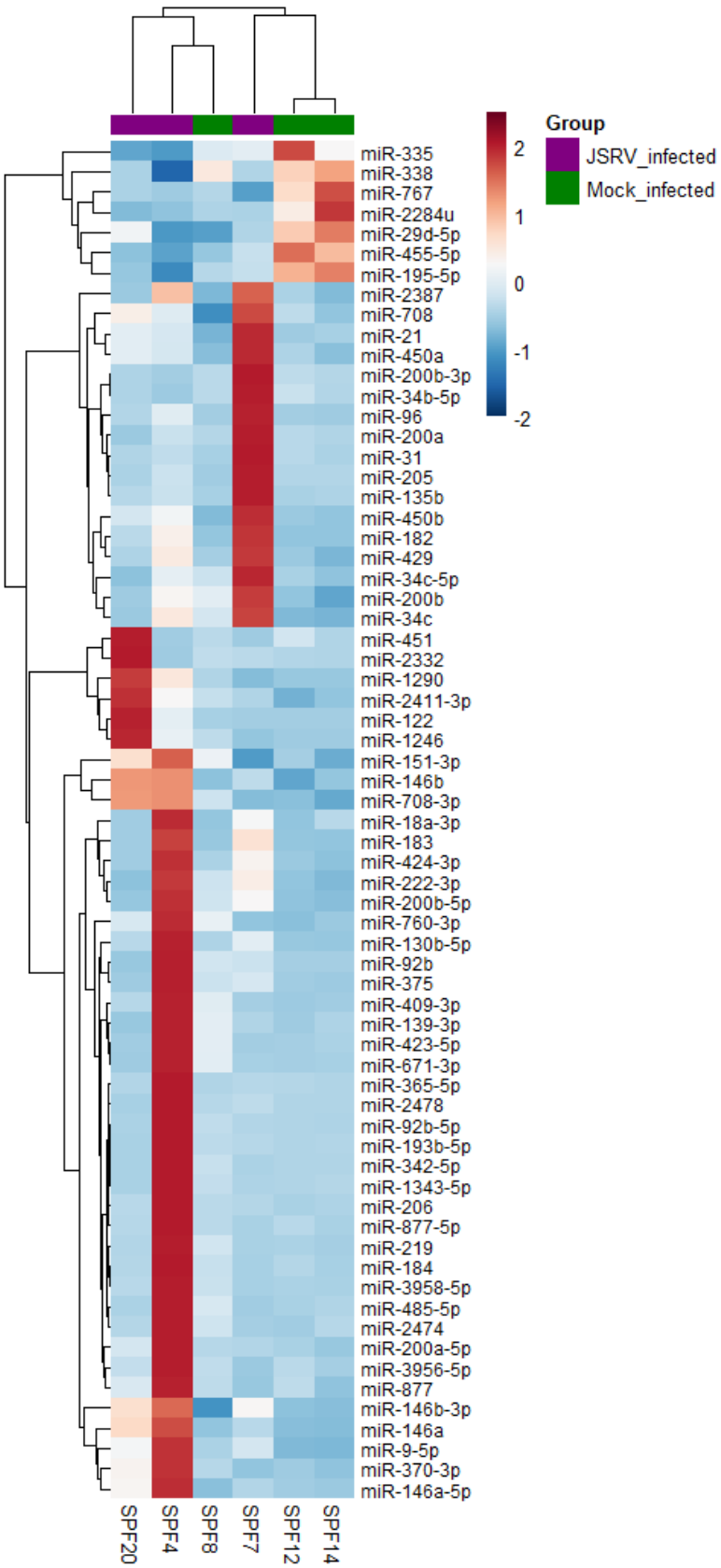

Figure 3.12. Heatmap of differentially expressed (FDR<0.05) miRNAs between JSRV$_{21}$-infected (n=3) and Mock-infected groups (n=3). *Dendrogram showing correlation clustering of individuals in groups. Legend represents values of log2 fold change.* ***Table 3.10.***

Differentially upregulated miRNAs between LCM tissue of JSRV21-infected lambs and mock-infected lambs.

miRNA	average counts[1]	log2(fold change)[2]	FDR[3]
miR-151-3p	144063.32	1.03	0
miR-21	236018.57	1.23	0
miR-423-5p	91283.28	1.62	0
miR-183	6386.05	5.40	4.12E-34
miR-182	7534.92	5.00	1.02E-30
miR-96	660.15	4.64	2.84E-26
miR-135b	276.31	4.76	4.96E-24
miR-122	139.89	3.88	4.05E-17
miR-365-5p	371.17	4.40	8.03E-13
miR-31	187.68	3.09	1.81E-11
miR-130b-5p	1329.29	2.83	5.35E-10
miR-92b-5p	556.75	3.68	5.42E-10
miR-1246	160.95	2.46	6.72E-09
miR-205	854.16	2.52	6.04E-08
miR-206	732.12	3.00	7.39E-08
miR-1290	99.74	2.43	1.6E-07
miR-200a-5p	4599.03	2.53	3.3E-07
miR-424-3p	3104.25	2.33	3.97E-07
miR-375	16309.86	2.38	5.7E-07
miR-2478	87.23	3.37	1.29E-06
miR-450b	2563.28	2.20	2.34E-06
miR-146a-5p	64.55	2.56	1.29E-05
miR-200b-5p	1956.40	1.91	1.46E-05
miR-2411-3p	802.53	1.80	1.57E-05
miR-370-3p	3685.74	1.98	5.15E-05
miR-184	307.68	2.54	6.96E-05
miR-193b-5p	143.39	2.72	7.77E-05
miR-1343-5p	146.03	3.01	1.05E-04
miR-146a	19478.62	1.84	1.49E-04
miR-708-3p	424.97	1.63	2.23E-04
miR-146b	8434.73	1.78	2.29E-04
miR-3958-5p	83.03	2.50	2.39E-04

[1] Average normalised counts across all samples
[2] Threshold established at log2(fold change) ≥ |1|
[3] FDR corrected by Benjamini-Hochberg, threshold FDR ≤ 0.05

miRNA	average counts[1]	log2(fold change)[2]	FDR[3]
miR-429	729.73	1.68	2.58E-04
miR-342-5p	2019.36	2.45	4.44E-04
miR-34c	5205.73	1.45	4.97E-04
miR-200b-3p	16237.08	1.63	5.63E-04
miR-146b-3p	134.48	1.92	7.14E-04
miR-92b	29506.68	2.01	7.88E-04
miR-219	72.79	2.21	1.24E-03
miR-3956-5p	300.72	2.17	1.46E-03
miR-34b-5p	169.87	1.57	1.83E-03
miR-409-3p	14252.99	1.69	1.94E-03
miR-200a	33209.16	1.48	2.33E-03
miR-2387	205.81	1.57	4.15E-03
miR-877-5p	100.91	2.09	4.45E-03
miR-450a	3249.99	1.48	4.84E-03
miR-708	242.75	1.66	6.08E-03
miR-451	13596.90	1.40	9.75E-03
miR-485-5p	3339.41	1.88	9.81E-03
miR-34c-5p	14451.31	1.22	9.82E-03
miR-2332	388.67	1.32	9.86E-03
miR-760-3p	102.32	1.39	1.15E-02
miR-222-3p	5379.06	1.22	2.11E-02

Table 3.11. Differentially downregulated miRNAs between LCM tissue of JSRV21-infected lambs and mock-infected lambs.

miRNA	average counts[1]	log2(fold change)[2]	FDR[3]
miR-2284u	59.51	-1.86	4.71E-03
miR-195-5p	60.52	-1.92	8.65E-03
miR-29d-5p	88.33	-1.27	2.75E-02
miR-335	585.20	-1.56	2.85E-02
miR-455-5p	1467.10	-1.26	4.04E-02
miR-767	223.37	-1.22	4.93E-02
miR-338	108.57	-1.69	4.96E-02

[1] Average normalised counts across all samples
[2] Threshold established at log2(fold change) ≥ |1|
[3] FDR corrected by Benjamini-Hochberg, threshold FDR ≤ 0.05

3.2.5.2 DE miRNAs between $JSRV_{21}$-infected and $JSRV_{mut}$-infected LCM lung tissue

The aim of this comparison was to observe which miRNAs were DE in the JSRV-driven transformation process, but not in JSRV viral infection. For this reason, miRNA expression in $JSRV_{21}$-infected samples was compared to that of a $JSRV_{mut}$ that was transformation deficient. Comparison of the DE miRNAs between the $JSRV_{21}$-infected and $JSRV_{mut}$-infected group also revealed differences. 121 miRNAs were found to be DE between the groups, 87 downregulated and 34 downregulated in the $JSRV_{21}$-infected group (**Table 3.12** and **Table 3.13**). Nevertheless, although miRNA dysregulation seemed consistent within groups for miRNAs represented in the top part of the heatmap, most miRNA DE appeared driven by expression in one sample of the $JSRV_{21}$-infected group (**Fig. 3.13**). Heatmap clustering classified members of each group separately, with $JSRV_{21}$-infected samples showing greater variability than $JSRV_{mut}$-infected ones.

Interestingly, comparison of $JSRV_{21}$-infected samples to $JSRV_{mut}$-infected samples resulted in a greater number of DE miRNAs than comparison to mock-infected samples. This result is likely due to the variability within groups, as the mock-infected group presented greater within group variability than the $JSRV_{mut}$-infected group, as observed in the PCA plot (**Fig. 3.11**).

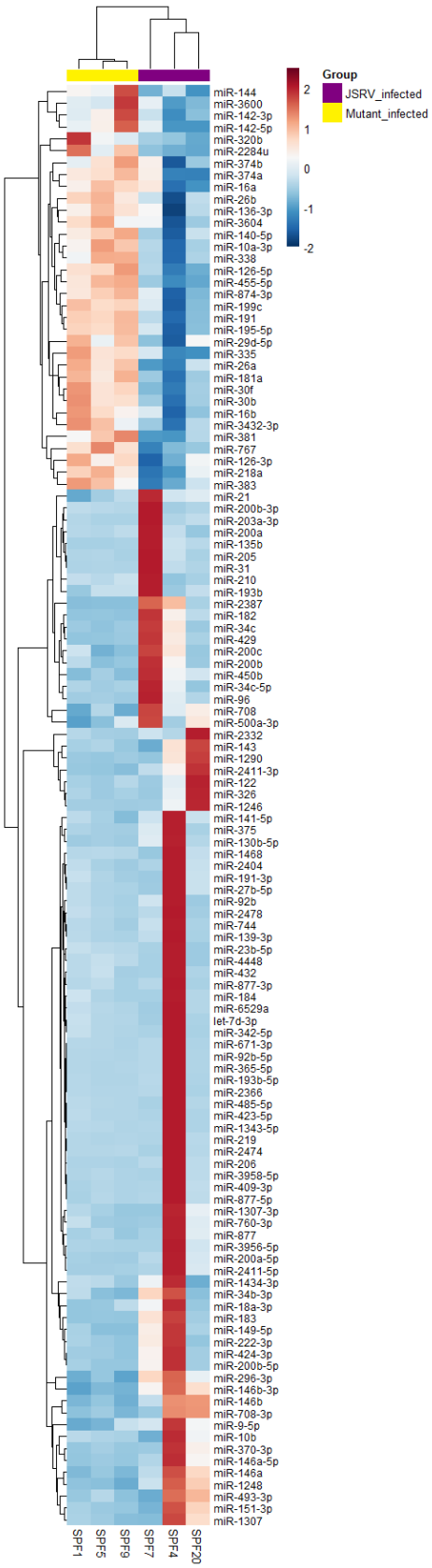

Figure 3.13. Heatmap of differentially expressed (FDR<0.05) miRNAs between $JSRV_{21}$-infected (n=3) and $JSRV_{mut}$-infected groups (n=3). *Dendrogram showing correlation clustering of individuals in groups. Legend represents values of log2 fold change.*

Table 3.12. Differentially upregulated miRNAs in LCM tissue between $JSRV_{21}$-infected lambs and $JSRV_{mut}$ infected lambs.

miRNA	Average counts[1]	log2(fold change)[2]	FDR[3]
miR-143	823954.95	1.05	0
miR-21	244120.67	1.07	0
miR-151-3p	123116.63	1.88	0
miR-92b	28535.09	2.28	0
miR-423-5p	80762.92	2.53	0
miR-375	14990.81	3.38	0
miR-182	7424.19	5.95	0
miR-183	6331.96	6.06	0
miR-135b	269.80	6.34	4.3E-148
miR-96	660.53	4.62	1.4E-137
miR-92b-5p	528.86	5.37	4.27E-93
miR-1246	142.86	4.37	1.59E-80
miR-3956-5p	257.80	4.39	1.09E-69
miR-200a-5p	4350.91	3.19	1.64E-68
miR-206	699.08	3.76	1.06E-67
miR-365-5p	372.92	4.26	2.17E-61
miR-31	188.61	3.03	1.24E-52
miR-2411-3p	723.87	2.64	1.99E-52
miR-200b-5p	1799.39	2.61	1.23E-50
miR-370-3p	3466.73	2.49	5.41E-45
miR-205	867.32	2.38	2.92E-44
miR-424-3p	3079.77	2.40	3.45E-44
miR-1290	92.60	3.31	4.29E-44
miR-122	148.38	2.92	1.25E-42
miR-130b-5p	1374.82	2.48	3.42E-42
miR-450b	2587.61	2.12	1.13E-36
miR-708-3p	387.94	2.27	1.45E-35
miR-2332	335.82	2.25	2.02E-35
miR-409-3p	12811.53	2.50	2.47E-35
miR-485-5p	3042.05	2.66	6.06E-33
miR-146a	19050.81	1.99	2.21E-31
miR-1343-5p	138.62	3.91	2.23E-31

[1] Average normalised counts across all samples
[2] Threshold established at log2(fold change) ≥ |1|
[3] FDR corrected by Benjamini-Hochberg, threshold FDR ≤ 0.05

Table 3.12. Differentially upregulated miRNAs in LCM tissue between $JSRV_{21}$-infected lambs and $JSRV_{mut}$ infected lambs.

miRNA	Average counts[1]	log2(fold change)[2]	FDR[3]
miR-139-3p	120.27	3.17	2.4E-29
miR-146b	8270.79	1.91	2.64E-29
miR-193b-5p	138.48	3.16	2.29E-28
miR-671-3p	566.09	2.43	2.4E-28
miR-326	240.28	2.04	1.88E-26
miR-342-5p	2011.62	2.49	3.24E-26
miR-1248	345.06	1.90	6.19E-25
miR-2387	193.28	1.97	8.11E-24
miR-200b-3p	16129.90	1.67	1.08E-23
miR-184	310.46	2.46	1.16E-23
miR-877-5p	92.91	2.86	3.66E-23
miR-146a-5p	64.63	2.55	5.96E-22
miR-146b-3p	132.38	2.04	6.85E-22
miR-3958-5p	79.00	3.06	9.26E-21
miR-2411-5p	82.48	2.42	4.11E-20
miR-708	240.96	1.70	1.71E-19
miR-1307	1080.54	1.59	3.65E-19
miR-744	2614.55	1.67	3.65E-19
miR-429	742.05	1.58	7.63E-19
miR-34c	5135.03	1.53	7.78E-19
miR-877	101.55	2.09	1.99E-18
miR-2478	91.10	2.78	2.43E-18
miR-219	68.37	2.81	3.01E-17
miR-6529a	4649.69	1.76	3.09E-17
miR-1307-3p	4355.63	1.50	6.59E-17
miR-2404	98.10	2.08	2.29E-16
miR-760-3p	92.48	2.01	3.21E-16
miR-34c-5p	14055.20	1.36	2.9E-15
miR-27b-5p	273.17	1.68	8.8E-15
miR-1468	19901.16	1.86	1.33E-14
miR-493-3p	6475.72	1.36	1.66E-14
miR-222-3p	5260.41	1.33	4.23E-14
miR-210	591.62	1.36	1.34E-13
miR-200a	34460.91	1.29	1.53E-13
miR-296-3p	708.17	1.28	1.86E-12

Table 3.12. Differentially upregulated miRNAs in LCM tissue between $JSRV_{21}$-infected lambs and $JSRV_{mut}$ infected lambs.

miRNA	Average counts[1]	log2(fold change)[2]	FDR[3]
miR-432	2107.14	1.41	1.9E-12
miR-34b-3p	5212.67	1.21	2.43E-12
miR-203a-3p	1692.35	1.22	7.66E-12
miR-1434-3p	184.09	1.45	7.66E-12
miR-193b	189.53	1.41	1E-11
let-7d-3p	10109.76	1.30	8.33E-11
miR-877-3p	97.85	1.67	1.9E-10
miR-200c	49514.06	1.08	2.87E-10
miR-141-5p	67.94	1.52	1.08E-09
miR-200b	16256.50	1.04	2.13E-09
miR-2474	56.44	1.95	3.72E-09
miR-10b	11689.82	1.08	9E-09
miR-4448	140.48	1.85	1.09E-08
miR-191-3p	359.99	1.16	1.17E-08
miR-9-5p	145.45	1.28	1.51E-08
miR-2366	51.64	1.78	4.78E-08
miR-23b-5p	290.37	1.26	8.37E-08
miR-149-5p	187.75	1.07	1.91E-07
miR-500a-3p	163.87	1.12	8.64E-07
miR-18a-3p	91.04	1.21	8.88E-07

Table 3.13. Differentially downregulated miRNAs in LCM tissue between $JSRV_{21}$-infected lambs and $JSRV_{mut}$-infected lambs.

miRNA	average counts[1]	log2(fold change)[2]	FDR[3]
miR-126-3p	985020.21	-1.15	0
miR-26a	1178136.69	-1.11	0
miR-455-5p	1850.26	-1.72	1.66E-11
miR-126-5p	8934.89	-1.63	4.6E-11
miR-335	651.69	-1.77	1.52E-10
miR-142-5p	648.82	-1.50	2.99E-10
miR-2284u	73.11	-2.23	4.09E-10

[1] Average normalised counts across all samples
[2] Threshold established at log2(fold change) ≥ |1|
[3] FDR corrected by Benjamini-Hochberg, threshold FDR ≤ 0.05

Table 3.13. Differentially downregulated miRNAs in LCM tissue between $JSRV_{21}$-infected lambs and $JSRV_{mut}$-infected lambs.

miRNA	average counts[1]	log2(fold change)[2]	FDR[3]
miR-10a-3p	472.05	-1.58	1.57E-09
miR-374a	3734.71	-1.45	3.52E-09
miR-30b	93.62	-1.90	1.37E-08
miR-30f	13493.42	-1.42	1.84E-08
miR-338	107.48	-1.67	2.06E-08
miR-140-5p	200.23	-1.40	1.74E-07
miR-383	192.94	-1.47	3.58E-07
miR-142-3p	1303.57	-1.12	3.81E-07
miR-144	148.13	-1.28	3.92E-07
miR-218a	11111.66	-1.24	4.83E-07
miR-191	76079.84	-1.18	5.4E-07
miR-3600	1010.05	-1.03	1.18E-06
miR-181a	70623.76	-1.11	1.73E-06
miR-26b	74352.92	-1.15	2.1E-06
miR-767	227.73	-1.26	2.37E-06
miR-374b	4622.67	-1.05	3.14E-06
miR-16b	42191.56	-1.16	5.18E-06
miR-195-5p	51.24	-1.61	6.29E-06
miR-874-3p	73.33	-1.36	1.61E-05
miR-29d-5p	89.68	-1.30	2.25E-05
miR-199c	382.29	-1.10	2.32E-05
miR-16a	198.14	-1.09	5.15E-05
miR-381	89.34	-1.11	9.24E-05
miR-3432-3p	50.55	-1.47	1.21E-04
miR-136-3p	232.33	-1.02	1.41E-04
miR-320b	538.30	-1.02	2.55E-04
miR-3604	59.99	-1.06	2.75E-03

3.2.5.3 DE miRNAs between $JSRV_{mut}$-infected and mock-infected LCM lung tissue

The main aim of this comparison was to investigate the effects of solely the JSRV infection in lung tissue, without considering the transformation that occurs with the wild-type version of $JSRV_{21}$. In order to investigate miRNA expression differences between $JSRV_{mut}$-infected lambs and mock-infected lambs a DE analysis was

performed. 14 miRNAs were found DE between groups, 5 were found to be upregulated and 9 downregulated (**Table 3.14** and **Table 3.15**). Heatmap clustering revealed the two groups clustering separately and SPF8 presenting the most distinct expression pattern (**Fig. 3.14**).

These results correlate with the group PCA plot in which the $JSRV_{mut}$-infected and the mock-infected group clustered together, so a low number of DE miRNAs was expected. These findings might indicate that $JSRV_{mut}$ infection modifies expression of a low set of miRNAs, suggesting that transformation is responsible for most miRNA changes observed. However, it should be noted that immunostaining analysis of the tissue samples of $JSRV_{mut}$-infected samples revealed no JSRV Env expression, which suggests that the low number of DE miRNAs between groups are due to low infection level. In addition, the lack of JSRV Env expression in $JSRV_{mut}$-infected samples raises the question of whether DE miRNAs between the analysed groups are genuine, or due to statistical noise. This is further discussed in 3.3**.**

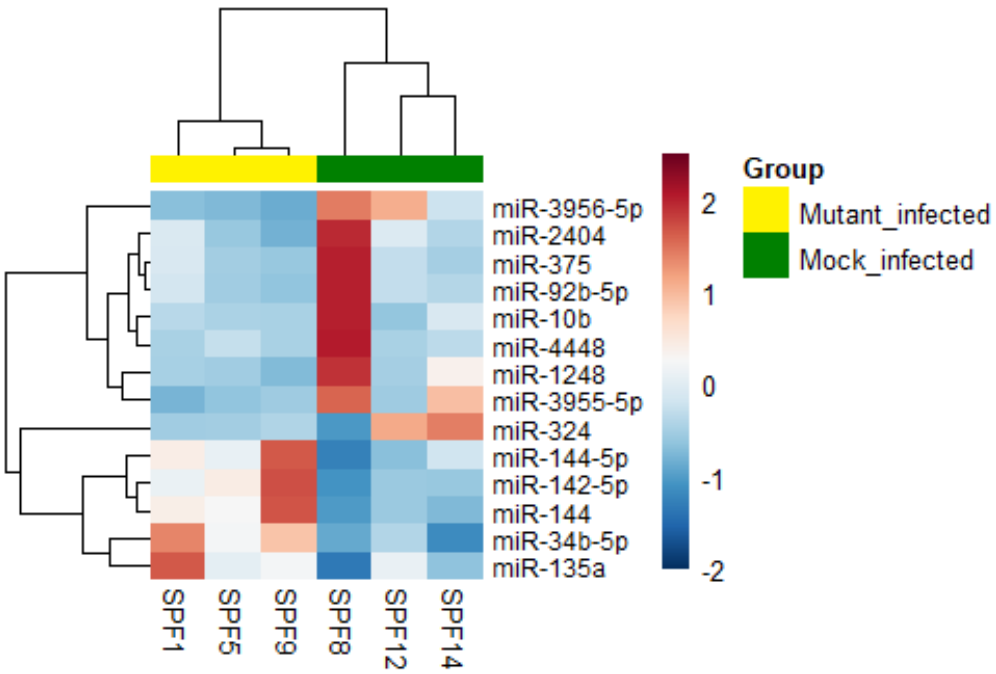

Figure 3.14. Heatmap of differentially expressed (FDR<0.05) miRNAs between $JSRV_{mut}$-infected (n=3) and mock-infected groups (n=3). *Dendrogram showing correlation clustering of individuals in groups. Legend represents values of log2 fold change.*

Table 3.14. Differentially upregulated miRNAs in LCM tissue between $JSRV_{mut}$- infected lambs and mock-infected lambs.

miRNA	average counts[1]	log2(fold change)[2]	FDR[3]
miR-142-5p	636.93	1.61	3.17E-11
miR-144	135.71	1.77	8.55E-11
miR-144-5p	85.98	1.13	9.37E-05
miR-34b-5p	128.83	1.01	5.22E-04
miR-135a	62.90	1.12	1.78E-03

[1] Average normalised counts across all samples
[2] Threshold established at log2(fold change) ≥ |1|
[3] FDR corrected by Benjamini-Hochberg, threshold FDR ≤ 0.05

Table 3.15. Differentially downregulated miRNAs in LCM tissue between $JSRV_{mut}$-infected lambs and mock-infected lambs.

miRNA	average counts[1]	log2(fold change)[2]	FDR[3]
miR-3955-5p	195.69	-2.24	1.57E-28
miR-3956-5p	66.45	-2.22	5.24E-20
miR-1248	288.63	-1.56	3.38E-16
miR-92b-5p	52.80	-1.70	1.6E-10
miR-10b	11987.95	-1.13	1.42E-09
miR-324	125.01	-1.24	1.89E-08
miR-375	3941.90	-1.00	6.93E-08
miR-4448	101.38	-1.22	8.37E-07
miR-2404	58.91	-1.09	3.84E-05

[1] Average normalised counts across all samples
[2] Threshold established at log2(fold change) ≥ |1|
[3] FDR corrected by Benjamini-Hochberg, threshold FDR ≤ 0.05

3.2.5.4 Comparison of DE miRNAs between all LCM samples

To investigate miRNAs DE expressed in samples with either wild-type $JSRV_{21}$ or $JSRV_{mut}$ compared to mock-infected samples, the pairwise comparisons were examined. Four miRNAs: miR-3956-5p, miR-92b-5p, miR-375 and miR-34b-5p were found DE in infected samples. Nevertheless, all but miR-34b-5p were upregulated in wild-type $JSRV_{21}$-infected samples and downregulated in $JSRV_{mut}$-infected samples. Although it could be speculated that miR-34b-5p upregulation

might be related to $JSRV_{21}$-infection, low levels of infection with the $JSRV_{mut}$ form, discussed in **3.2.4.3**, indicate further evidence is needed. Involvement of these miRNAs in JSRV-infection is further investigated in **3.2.7.**

3.2.6 DE miRNAs in bronchoalveolar lavage fluid (BALF) macrophages

Since lung tissue is composed of many cell types, we sought to focus on the miRNA expression of enriched cell types in the OPA lung. The use of the LCM technique allowed the study of samples enriched in tumour tissue. Nevertheless, it was not suitable for the enrichment of a known important cell type in cancer: macrophages. Alveolar macrophages are the first line of defence in the lung alveoli, and have been shown to increase in abundance in OPA. In addition, they may display phenotype variation in OPA (Karagianni et al, 2019).

In order to investigate if some of the miRNAs DE in lung tissue of OPA-affected animals were a result of a potential local immune response to JSRV presence, the miRNA expression of BALF macrophages was studied. If alveolar macrophages presented significant changes in miRNA expression between OPA-affected animals and controls, these could be further investigated as biomarkers of OPA.

BALF samples were collected from adult sheep received at the Moredun PM rooms by Chris Cousens and Anna Karagianni. The intention was to compare OPA and healthy animals, but during initial assessment it became clear that three of the healthy samples had actually had low levels of parasite infection in the lung. Therefore, the samples were divided into three groups: OPA-affected sheep, healthy control sheep and parasite-infected sheep. The cases selected had no obvious bacterial infection present. The parasite-infected group presented lungworms in the lung, and these samples were used to compare the $CD14^+$ macrophage response in lungworm infection and JSRV-infection. $CD14^+$ macrophages were isolated as described in (section 2.4.4) and RNA extracted (by Anna Karagianni). The concentration and quality of RNA samples was measured, and samples with 260/280 ratio > 1.8 and RIN number > 6 submitted for small RNA-sequencing (**Table 3.16**).

Table 3.16. RNA concentration of BALF CD14$^+$ macrophage samples submitted for small RNA-sequencing.

Group	**OPA-affected**				
Sample	OPA1	OPA2	OPA3	OPA4	OPA5
RNA (ng/µl)	421.20	241.83	547.04	376.24	573.02
260/280 nm	2.04	1.92	1.95	2.06	2.05
RIN	9.3	9.4	9.8	9.9	10
Group	**Healthy controls**				
Sample	CON1		CON2	CON3	
RNA (ng/µl)	215.40		320.11	478.80	
260/280 nm	2.02		2.06	2.06	
RIN	9.6		9.9	9.7	
Group	**Parasite-infected**				
Sample	PARA1		PARA2	PARA3	
RNA (ng/µl)	550.17		293.2	375.21	
260/280 nm	2		2.05	2	
RIN	9.6		9.8	9.8	

Small RNA-sequencing was performed by Edinburgh Genomics and bioinformatics analysis by Siddharth Jayaraman and Deepali Vasoya supervised by myself and with assistance from Mick Watson, David Griffiths and Finn Grey. Sequencing libraries were successfully constructed from all samples, and total reads ranged from 40079257 to 24631916 (**Table 3.17**). No statistically significant differences were found between groups in total reads or percentage of reads mapping to different categories (t-test $p<0.05$) (**Fig. 3.15**). In addition, the sequence length distribution (**Fig. 3.16**) also appeared similar between groups.

Table 3.17. Total reads of sequenced BALF CD14⁺ macrophage samples.

	Group	**OPA-affected**				
	Sample	OPA1	OPA2	OPA3	OPA4	OPA5
	Total reads	35193438	36042201	40079257	35148520	29244520
(%) total reads	**>28 nt**	10.30	2.57	6.19	4.88	9.68
	miRBase	55.17	81.19	73.55	77.58	67.56
	JSRV	0.00334	0.00289	0.00519	0.00387	0.00434
	Group	**Healthy controls**				
	Sample	CON1		CON2		CON3
	Total reads	24631916		35905431		32730088
(%) total reads	**>28 nt**	4.71		3.83		7.87
	miRBase	72.36		76.85		73.39
	JSRV	0.00591		0.00429		0.00412
	Group	**Parasite-infected**				
	Sample	PARA1		PARA2		PARA3
	Total reads	38491844		37247929		38616476
(%) total reads	**>28 nt**	9.64		6.23		5.97
	miRBase	72.50		73.42		76.64
	JSRV	0.00397		0.00472		0.00417

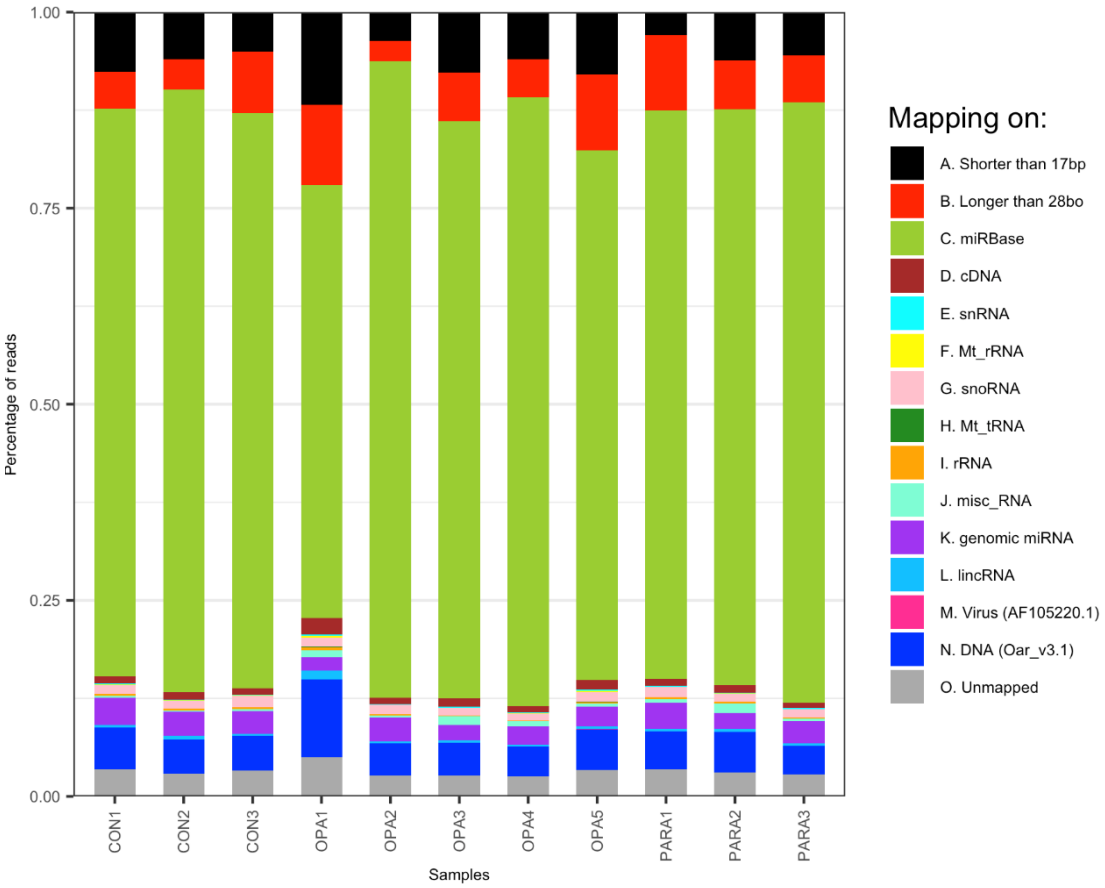

Figure 3.15. Sequence distribution in samples of BALF CD14⁺macrophages sequencing, presented as percentage of total reads in each sample. *Each of the categories is represented by a colour shown in the legend. Small nuclear RNA(snRNA), mitochondrial ribosomal RNA (Mt_rRNA), small nucleolar RNA (snoRNA), mitochondrial transfer RNA (Mt_tRNA), ribosomal RNA (rRNA), miscellaneous RNA (misc_RNA), long non-coding RNA (lincRNA), JSRV viral genome (Virus), sheep genome (DNA), reads not mapping to any of the previous categories (Unmapped).*

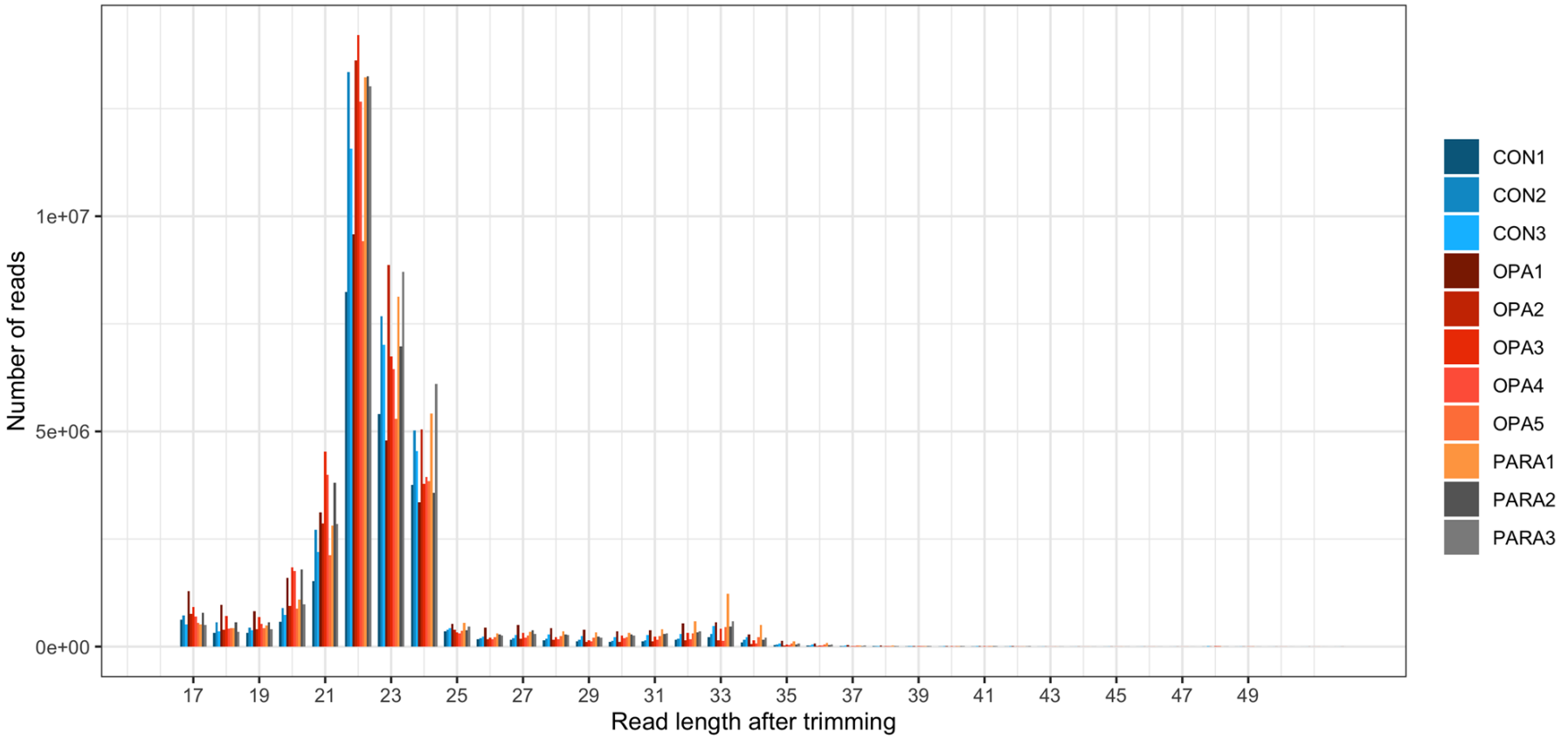

Figure 3.16. Length distribution of total sequencing reads after trimming was performed. *OPA-affected samples (n=5, OPA1, OPA2, OPA3, OPA4, OPA5); control samples (n=3, CON1, CON2, CON3); parasite-infected samples (n=3, PARA1, PARA2, PARA3). The area with high read abundance observed corresponds to miRNA length (21-23nt). Length distribution appears similar between groups.*

Bioinformatics analysis identified 356 miRNAs in all samples. Expression of these 356 miRNAs was represented in a PCA plot (**Fig. 3.17**). In the PCA plot, the three studied groups clustered separately, and the highest variability was observed within the OPA-affected group. This is likely due to individual-specific responses to JSRV, which might also be related to different viral-load between animals. Notably, OPA5 clustered closely with the parasite-infected group suggesting a pattern of miRNA expression more similar to them.

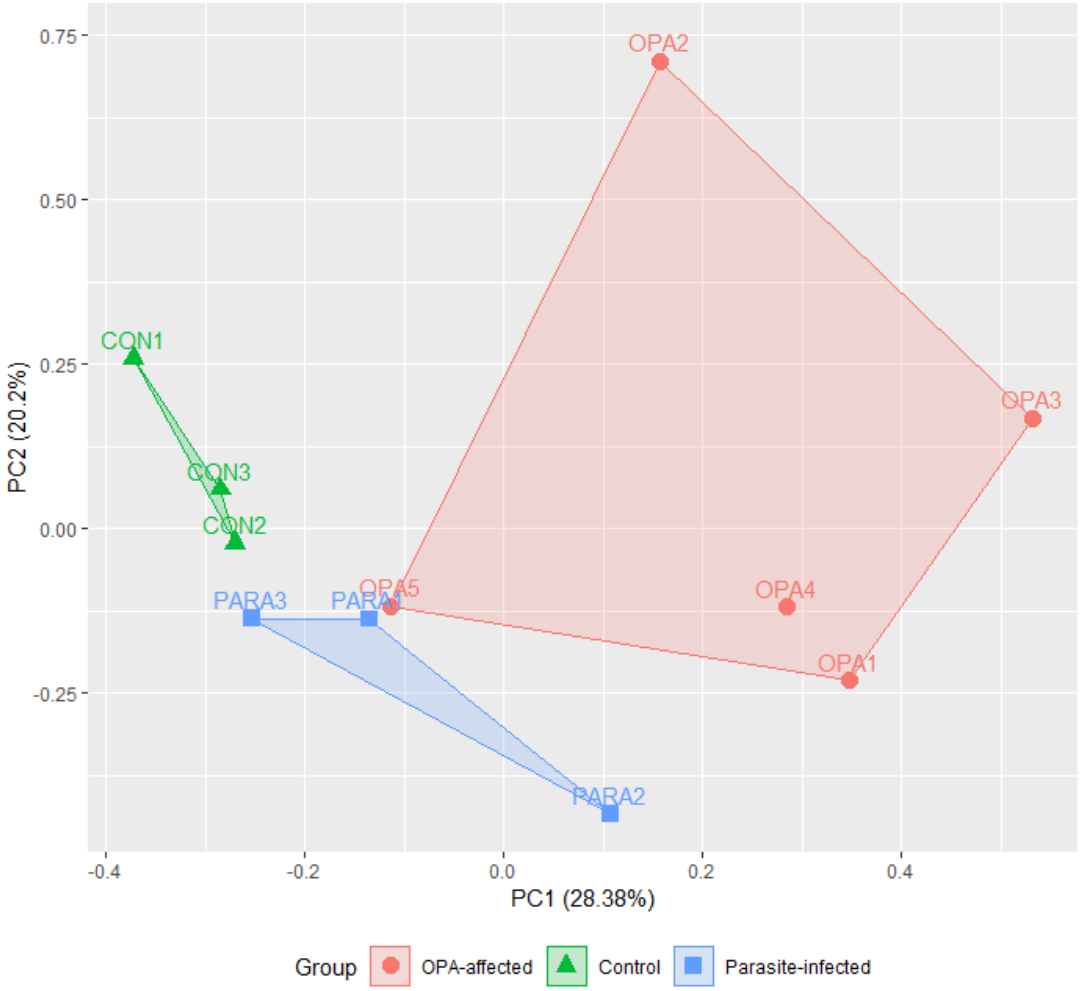

Figure 3.17. PCA plot of miRNA expression from BALF CD14⁺macrophage samples of OPA-affected (n=5), control (n=3), and parasite-infected samples (n=3). *The three groups can be seen clustering separately and, by PC1, a gradient can be observed with control samples towards the left of the plot, OPA-affected samples towards the right and parasite-infected samples between them. This gradient is not observed by PC2, as groups present more variability in this axis. Variability within the OPA-affected group is the greatest, and OPA5 clusters closely with the parasite-infected group. This plot suggests global miRNA expression differences between the three groups.*

3.2.6.1 DE miRNAs in BALF macrophages of OPA-affected and control samples

In order to investigate DE miRNAs between the groups pairwise comparisons were performed.

Comparison between BALF $CD14^+$ macrophages of OPA-affected sheep and healthy controls found 85 miRNAs DE between the two groups, 63 were upregulated and 22 were downregulated in OPA-affected sheep (**Table 3.18** and **Table 3.19**).

A heatmap representation of the DE miRNAs (**Fig. 3.18**) revealed that most DE miRNAs showed consistent expression within groups, suggesting that their expression might help to distinguish members of each group. Nevertheless, OPA5 was found to cluster with the control group instead of the OPA-affected group. Consistent with the PCA plot representation (**Fig. 3.17**). Nevertheless, no evident reason for the miRNA expression pattern observed was found.

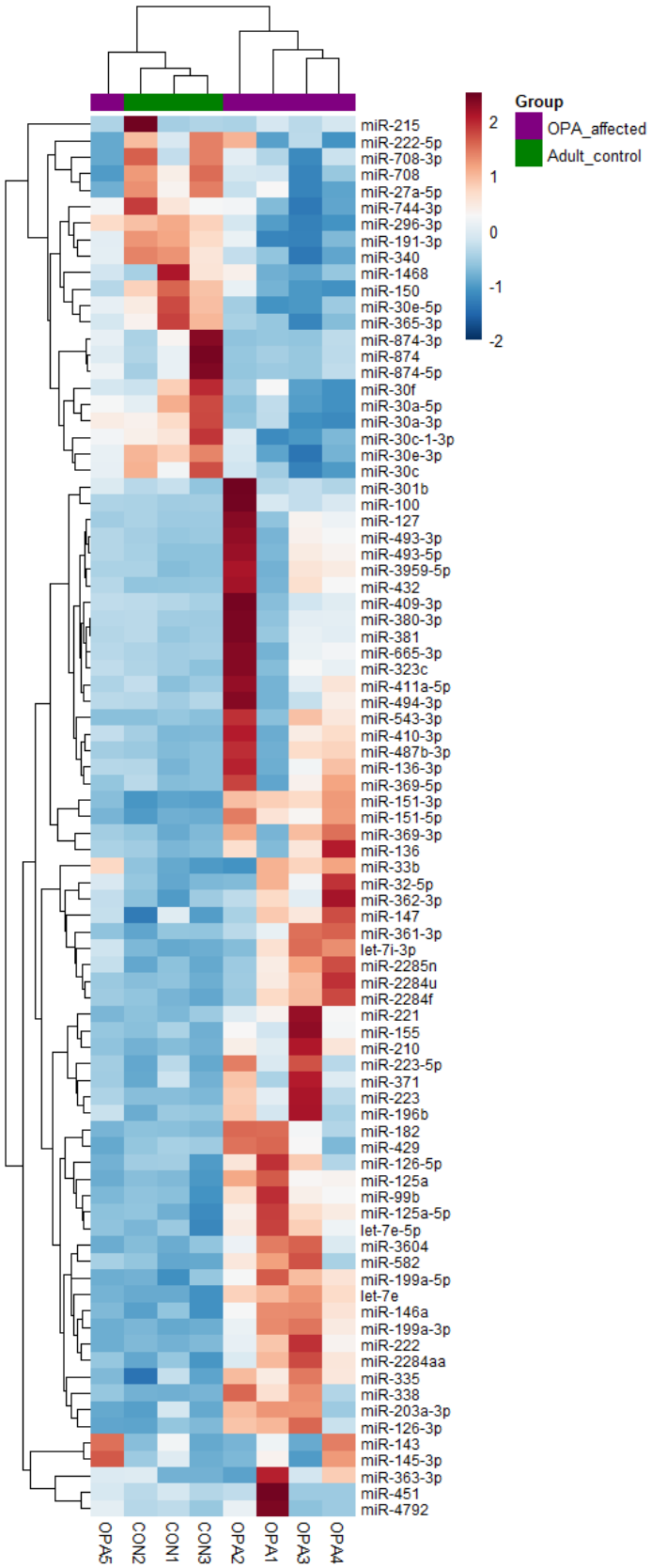

Figure 3.18. Heatmap of differentially expressed (FDR<0.05) miRNAs between OPA-affected (n=5) and control BALF CD14⁺macrophage samples (n=3). *Dendrogram showing correlation clustering of individuals in groups. Legend represents values of log2 fold change.*

Table 3.18. Differentially upregulated miRNAs between BALF CD14+ macrophages of OPA affected sheep and healthy controls.

miRNA	Average counts[1]	log2(fold change)[2]	FDR[3]
miR-143	203307.79	1.09	0
miR-100	91.77	4.17	6.45E-49
miR-199a-3p	1550.03	2.58	7.88E-47
miR-182	781.83	2.48	5.44E-42
miR-223	14922.90	2.23	9.86E-41
miR-146a	10025.11	2.13	1.19E-39
miR-338	61.73	3.80	1.26E-38
miR-127	13132.57	2.18	2.17E-36
miR-151-3p	5988.08	2.10	3.07E-35
miR-369-3p	229.45	2.51	1.87E-34
miR-222	438.58	2.20	2.21E-33
let-7e	390.07	2.17	5.24E-32
miR-210	1444.93	1.95	6.83E-32
miR-543-3p	53.11	2.96	2.3E-28
miR-151-5p	5795.73	1.82	8.51E-28
miR-493-3p	322.59	2.06	1.03E-27
miR-136	97.44	2.52	1.85E-26
miR-99b	827.70	1.89	2.51E-26
miR-199a-5p	303.12	2.10	2.89E-26
miR-487b-3p	195.38	2.12	2.97E-26
miR-125a-5p	1345.88	1.89	4.45E-26
miR-196b	271.26	1.84	6.48E-26
let-7e-5p	631.75	1.73	1.63E-23
miR-223-5p	856.30	1.55	3.58E-23
miR-155	2370.15	1.54	8.9E-23
miR-410-3p	403.24	1.83	1.58E-22
miR-493-5p	182.55	1.95	2.64E-22
miR-125a	1036.60	1.65	8.45E-21
miR-2284f	62.35	2.39	1.11E-20
miR-3959-5p	186.85	1.86	2.53E-20
miR-32-5p	2004.30	1.67	8.03E-20
miR-136-3p	424.13	1.74	1.08E-19

[1] Average normalised counts across all samples
[2] Threshold established at log2(fold change) ≥ |1|
[3] FDR corrected by Benjamini-Hochberg, threshold FDR ≤ 0.05

Table 3.18. Differentially upregulated miRNAs between BALF CD14+ macrophages of OPA affected sheep and healthy controls.

miRNA	Average counts[1]	log2(fold change)[2]	FDR[3]
miR-380-3p	455.51	1.68	1.16E-19
miR-361-3p	6593.80	1.41	6.03E-19
miR-432	69.03	2.04	2.55E-18
miR-33b	349.78	1.67	4.59E-18
miR-323c	77.54	2.00	8.03E-18
miR-3604	268.92	1.62	9.42E-18
miR-411a-5p	6756.54	1.53	2.07E-17
miR-221	10302.37	1.38	3.13E-17
miR-381	68.50	2.09	6.41E-17
let-7i-3p	185.79	1.61	2.97E-16
miR-371	195.38	1.32	1.93E-15
miR-409-3p	843.37	1.38	2.61E-15
miR-2285n	51.61	1.87	4.1E-14
miR-665-3p	115.39	1.52	3.7E-13
miR-451	484.16	1.35	7.02E-13
miR-301b	296.61	1.28	1.56E-12
miR-147	9087.84	1.00	1.2E-11
miR-429	111.00	1.32	2.36E-10
miR-2284aa	58.97	1.45	2.58E-10
miR-582	69.83	1.48	3.24E-10
miR-369-5p	51.84	1.55	1.64E-09
miR-126-5p	367.33	1.06	5.86E-09
miR-362-3p	132.98	1.21	5.37E-08
miR-335	67.79	1.11	6E-08
miR-203a-3p	95.32	1.04	6.36E-08
miR-2284u	117.30	1.10	9.63E-08
miR-145-3p	190.88	1.03	4.19E-07
miR-494-3p	92.89	1.13	4.24E-07
miR-4792	59.16	1.35	6.13E-07
miR-126-3p	53.22	1.09	2.73E-06
miR-363-3p	62.29	1.24	2.77E-05

Table 3.19. Differentially downregulated miRNAs between BALF CD14+ macrophages of OPA affected sheep and healthy controls.

miRNA	Average counts[1]	log2(fold change)[2]	FDR[3]
miR-30a-5p	100812.18	-1.23	0
miR-30e-5p	314695.85	-1.04	0
miR-874	170.71	-2.45	6.25E-45
miR-874-3p	185.01	-2.42	3.11E-44
miR-215	239.30	-1.65	2.85E-32
miR-874-5p	111.61	-2.16	3.27E-32
miR-150	32868.50	-1.53	3.58E-23
miR-1468	4215.35	-1.66	3.56E-21
miR-27a-5p	5254.89	-1.31	1.12E-20
miR-708-3p	31640.20	-1.24	9.1E-20
miR-30a-3p	695.41	-1.32	3.12E-19
miR-708	5738.72	-1.24	6.38E-18
miR-191-3p	2174.74	-1.23	9.37E-17
miR-30f	276.38	-1.33	3.3E-16
miR-30c-1-3p	342.99	-1.27	7.5E-16
miR-30c	7123.43	-1.02	1.84E-13
miR-365-3p	1651.36	-1.15	4.16E-13
miR-30e-3p	9456.56	-1.02	1.56E-12
miR-296-3p	877.33	-1.02	5.59E-12
miR-340	691.97	-1.00	2.72E-11
miR-744-3p	77.46	-1.07	1.42E-09
miR-222-5p	73.49	-1.08	6.57E-08

[1] Average normalised counts across all samples
[2] Threshold established at log2(fold change) ≥ |1|
[3] FDR corrected by Benjamini-Hochberg, threshold FDR ≤ 0.05

3.2.6.2 DE miRNAs between OPA-affected and parasite-infected BALF macrophages

In order to investigate if miRNA expression in BALF CD14^{+}macrophages was different depending on the pathogen (JSRV or lungworm) a DE analysis was performed. 59 miRNAs were found DE between OPA-affected and parasite-infected samples, 45 upregulated and 14 downregulated (**Table 3.20** and **Table**

3.21). The number of DE miRNAs was lower in this comparison than between OPA and healthy controls, which might suggest that there are common dysregulated miRNAs in JSRV infection and parasite infection. Expression levels of DE miRNAs also appeared more variable within groups (**Fig. 3.19**) with OPA2 presenting the most distinctive pattern. In addition, OPA5 clustered with the parasite infected group as in prior comparisons (**Fig. 3.17**). These findings might indicate that the ability to distinguish between OPA-affected sheep and parasite-infected sheep, based on miRNA expression in BALF $CD14^+$ macrophages, might be more difficult than distinction of OPA-affected samples and control samples. Although this result is to be expected, it has implications for the potential application of this methodology as source of biomarkers because lungworm infections are a common finding in farmed sheep (Panuska, 2006). This hypothesis is further investigated in **3.2.6.4**.

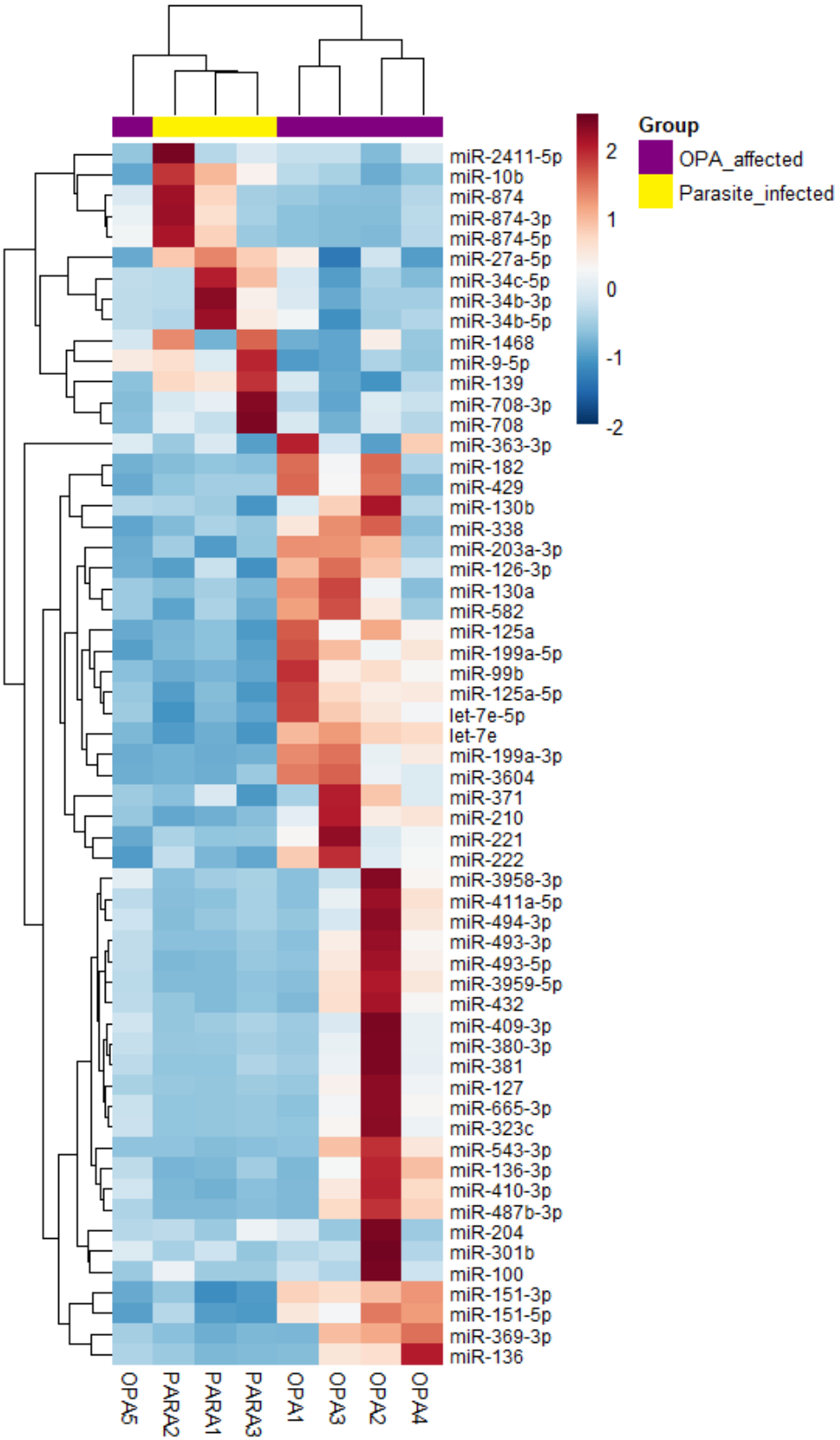

Figure 3.19. Heatmap of differentially expressed (FDR<0.05) miRNAs between OPA-affected (n=5) and parasite-infected BALF CD14⁺ macrophage samples (n=3). *Dendrogram showing correlation clustering of individuals in groups. Legend represents values of log2 fold change.*

Table 3.20. Differentially upregulated miRNAs between BALF CD14+ macrophages of OPA affected sheep and parasite infected sheep.

miRNA	Average counts[1]	log2(fold change)[2]	FDR[3]
miR-127	11882.88	3.25	2.67E-82
miR-493-3p	281.01	3.64	1.97E-74
miR-409-3p	692.56	2.88	1.28E-59
miR-410-3p	358.05	2.87	3.36E-55
miR-493-5p	160.71	3.22	2.84E-54
miR-487b-3p	177.00	3.13	1.12E-53
miR-411a-5p	5913.34	2.49	2.44E-52
miR-380-3p	399.36	2.74	4.31E-52
miR-3959-5p	163.88	3.07	3.04E-51
miR-199a-3p	1575.11	2.43	2.79E-48
miR-369-3p	224.08	2.76	2.79E-48
miR-210	1388.00	2.26	7.97E-44
miR-136-3p	390.09	2.36	2.64E-41
let-7e	378.87	2.42	3.9E-41
miR-99b	781.12	2.33	7.16E-41
miR-665-3p	96.31	3.00	1.15E-40
miR-125a-5p	1276.08	2.29	2.74E-40
miR-182	803.62	2.24	9.48E-39
let-7e-5p	584.78	2.29	1.06E-38
miR-381	60.97	3.33	1.48E-38
miR-323c	68.76	3.20	2.59E-38
miR-543-3p	51.21	3.50	6.43E-38
miR-136	95.43	2.74	3.21E-36
miR-3958-3p	261.68	2.32	3.96E-36
miR-432	65.13	2.53	7.59E-28
miR-494-3p	75.85	2.40	1.41E-26
miR-3604	266.38	1.68	2.49E-22
miR-125a	1042.52	1.61	1.24E-21
miR-151-3p	6574.61	1.50	4.96E-21
miR-199a-5p	327.59	1.59	1.38E-19
miR-222	496.06	1.41	3.52E-18
miR-151-5p	6379.96	1.28	1.32E-15

[1] Average normalised counts across all samples
[2] Threshold established at log2(fold change) ≥ |1|
[3] FDR corrected by Benjamini-Hochberg, threshold FDR ≤ 0.05

Table 3.20. Differentially upregulated miRNAs between BALF CD14+ macrophages of OPA affected sheep and parasite infected sheep.

miRNA	Average counts[1]	log2(fold change)[2]	FDR[3]
miR-301b	290.33	1.39	2.66E-14
miR-130a	190.30	1.34	8.26E-14
miR-204	460.86	1.09	8.29E-12
miR-221	11131.96	1.02	1.11E-11
miR-371	200.07	1.20	1.49E-11
miR-429	110.69	1.33	2.04E-11
miR-100	123.23	1.26	3.46E-11
miR-130b	2204.95	1.02	3.8E-10
miR-338	81.91	1.24	5.58E-10
miR-203a-3p	92.45	1.17	2.1E-09
miR-582	73.59	1.21	1.1E-08
miR-126-3p	51.78	1.22	1.97E-07
miR-363-3p	62.77	1.20	2.25E-06

Table 3.21. Differentially downregulated miRNAS between BALF CD14+ macrophages of OPA affected sheep and parasite infected sheep.

miRNA	Average counts[1]	log2(fold change)[2]	FDR[3]
miR-874	181.70	-2.56	2.5E-52
miR-874-3p	177.41	-2.34	8.41E-46
miR-874-5p	109.31	-2.13	2.91E-34
miR-34c-5p	3376.07	-1.67	1.88E-32
miR-10b	565.37	-1.89	5.34E-32
miR-1468	4095.24	-1.61	3.28E-25
miR-34b-3p	205.45	-1.56	1.36E-23
miR-708-3p	34004.57	-1.38	5.34E-19
miR-27a-5p	4942.85	-1.18	2.64E-16
miR-708	5703.37	-1.23	8.53E-15
miR-9-5p	3752.51	-1.16	1.53E-14
miR-34b-5p	212.61	-1.12	1.84E-13
miR-139	80.80	-1.35	4.8E-12
miR-2411-5p	112.62	-1.05	5.21E-08

[1] Average normalised counts across all samples
[2] Threshold established at log2(fold change) ≥ |1|
[3] FDR corrected by Benjamini-Hochberg, threshold FDR ≤ 0.05

3.2.6.3 DE miRNAs between parasite-infected and control BALF CD14^{+} macrophages

Lastly, a comparison of miRNA expression between parasite-infected and control samples was performed in order to investigate which miRNAs were related to infection. 34 miRNAs were found DE between parasite-infected and control samples, 19 upregulated and 15 downregulated (**Table 3.22** and **Table 3.23**). Heatmap representation (**Fig. 3.20**) revealed that the two groups clustered separately, and more consistency in expression level was found in the control group.

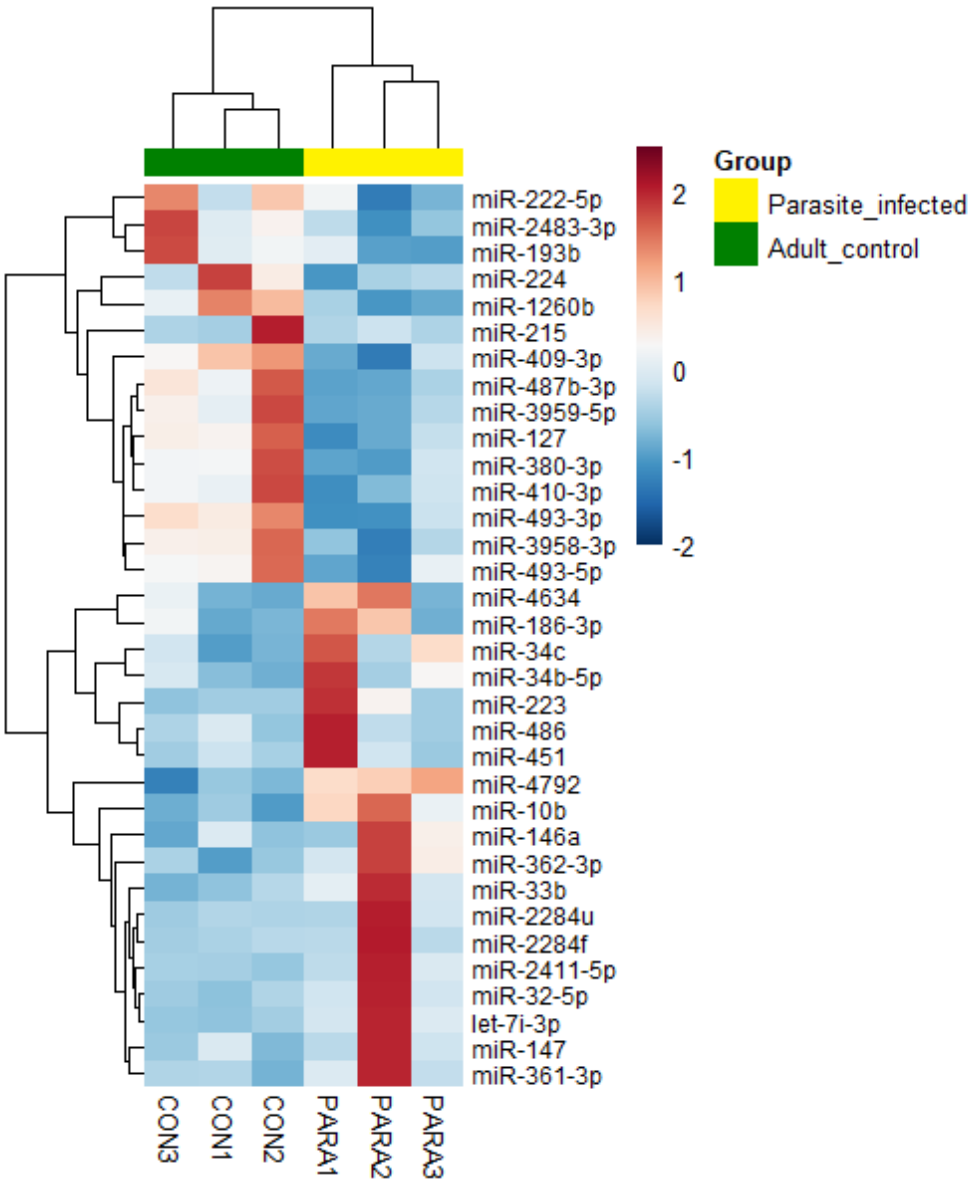

Figure 3.20. Heatmap of differentially expressed (FDR<0.05) miRNAs between parasite-infected (n=3) and control BALF CD14⁺ macrophage samples (n=3). *Dendrogram showing correlation clustering of individuals in groups. Legend represents values of log2 fold change.*

Table 3.22. Differentially upregulated miRNAs between BALF CD14+ macrophages of parasite infected sheep and healthy controls.

miRNA	Average counts[1]	log2(fold change)[2]	FDR[3]
miR-10b	566.82	1.88	2.83E-25
miR-451	565.08	1.65	1.21E-22
miR-2284f	69.50	2.57	6.06E-21

[1] Average normalised counts across all samples
[2] Threshold established at log2(fold change) ≥ |1|
[3] FDR corrected by Benjamini-Hochberg, threshold FDR ≤ 0.05

Table 3.22. Differentially upregulated miRNAs between BALF CD14+ macrophages of parasite infected sheep and healthy controls.

miRNA	Average counts[1]	log2(fold change)[2]	FDR[3]
miR-32-5p	2070.15	1.73	1.14E-19
miR-486	2820.43	1.36	5.19E-19
miR-4634	671.76	1.60	2.54E-18
miR-223	9778.13	1.45	1.73E-17
miR-147	10669.36	1.34	2.97E-16
miR-146a	6276.37	1.25	2.12E-13
miR-186-3p	222.79	1.44	6.05E-13
miR-33b	310.65	1.44	9.83E-13
miR-361-3p	5798.31	1.15	2.67E-11
let-7i-3p	170.11	1.43	2.85E-11
miR-2411-5p	102.91	1.50	7.14E-11
miR-34c	222.25	1.30	1.99E-10
miR-34b-5p	210.87	1.16	2.68E-09
miR-2284u	124.66	1.23	5.87E-08
miR-4792	59.88	1.38	1.16E-07
miR-362-3p	132.93	1.20	2.5E-07

Table 3.23. Differentially downregulated miRNAs between BALF CD14+ macrophages of parasite infected sheep and healthy controls.

miRNA	Average counts[1]	log2(fold change)[2]	FDR[3]
miR-215	235.37	-1.75	2.83E-25
miR-409-3p	316.70	-1.49	4.57E-16
miR-493-3p	83.33	-1.58	9.64E-13
miR-3958-3p	158.48	-1.40	1.49E-12
miR-127	3503.64	-1.08	3.92E-11
miR-224	2149.42	-1.17	1.9E-10
miR-380-3p	160.05	-1.06	5.29E-08
miR-410-3p	131.41	-1.03	1.57E-07
miR-193b	69.25	-1.32	1.94E-07
miR-493-5p	53.02	-1.26	3.06E-07
miR-3959-5p	57.79	-1.21	3.91E-07
miR-1260b	205.96	-1.06	4.59E-07

[1] Average normalised counts across all samples
[2] Threshold established at log2(fold change) ≥ |1|
[3] FDR corrected by Benjamini-Hochberg, threshold FDR ≤ 0.05

Table 3.23. Differentially downregulated miRNAs between BALF CD14+ macrophages of parasite infected sheep and healthy controls.

miRNA	Average counts[1]	log2(fold change)[2]	FDR[3]
miR-2483-3p	87.27	-1.11	1.97E-06
miR-222-5p	74.31	-1.03	2.23E-05
miR-487b-3p	54.67	-1.01	6.53E-05

3.2.6.4 Comparison of DE miRNAs between BALF samples

With the aim to identify specific miRNAs DE in infection and those DE only in JSRV-infection the results obtained from the pairwise analysis were compared. 22 miRNAs were found DE in OPA-affected or parasite-infected samples compared to controls, suggesting these miRNAs might be involved in transcriptional changes that occur in macrophages during response to infection. However, 8 of the 22 DE miRNAs in both infections presented dysregulation in different directions, which might indicate different responses depending on the pathogen. Interestingly, of the DE miRNAs, miR-215 and miR-33b, have consistently been reported as dysregulated in infections and both target XIAP, a major regulator of apopotosis (Nielsen et al, 2018). The remaining DE miRNAs in OPA-affected samples were not found to be DE in parasite-infected samples, suggesting this might be more specific of JSRV infection. To investigate if these miRNAs would be able to distinguish between OPA-affected and parasite-infected samples, expression of those miRNAs was studied in the pairwise comparison: 40 miRNAs were found DE in OPA-affected samples compared to either parasite-infected or control samples. All of these miRNAs presented similar dysregulation levels in OPA-affected samples compared to parasite-infected samples or control samples. These findings suggest that miRNAs specifically dysregulated in OPA-affected samples can be detected in BALF macrophages. These miRNAs could be further investigated and potentially exploited as biomarkers, this is further discussed in 3.3. In addition, the biological relevance of some of those miRNAs is further explored by comparing these findings to other datasets in 3.2.7.

3.2.7 Comparison of DE miRNAs between datasets

In order to gain a better understanding of the significance and origin of miRNA dysregulation in OPA, the results of DE miRNAs in JSRV-infected animals in the datasets presented in this chapter were compared.

Comparing lung tissue samples, LCM lung tissue samples and BALF $CD14^+$ macrophage samples, miR-182 was the only miRNA found to be consistently upregulated in JSRV-infected animals of all datasets. Suggesting the involvement of this miRNA in OPA. Confidence in the biological significance of miR-182 is increased due to results of RT-qPCR, which also found miR-182 significantly upregulated in lung tissue samples from independent experimental infections and natural OPA cases. In addition, upregulation of this miRNA might be able to distinguish JSRV-infected samples from lungworm-infected samples and $JSRV_{mut}$-infected samples. Potential roles of miR-182 in JSRV-infection and OPA are further discussed in 3.3.

Comparison of DE miRNAs in whole lung tissue and LCM lung tissue revealed 12 miRNAs DE in both datasets: miR-130b-5p, miR-135b, miR-146b, miR-146b-3p, miR-182, miR-183, miR-205, miR-31, miR-424-3p, miR-450a, miR-450b and miR-96. Interestingly, all these miRNAs were upregulated in both datasets. In addition, expression of 6 of those miRNAs was validated by RT-qPCR in lung tissue samples of experimentally infected and natural cases of OPA. It could thus, be hypothesised that these miRNAs are likely to be related to OPA tumour cells and transformation, this is further reviewed in 3.3. Differences in DE miRNAs between these datasets might be due to biological variation between samples that belong to each of the experimental infections but also to the nature of the sample: LCM samples are tumour-enriched. LCM lung tissue samples could reveal DE of miRNAs masked by the amount of normal tissue in the lung tissue samples of the first small RNA-sequencing study, this hypothesis is in line with the finding that all miRNAs DE in both datasets are upregulated. Also, the presence of lots of normal tissue is likely to mask downregulated miRNAs to a greater degree than upregulated miRNAs thus, it was expected that more DE downregulated miRNAs would be identified in LCM samples.

Five miRNAs were found DE in both JSRV-infected lung tissue and BALF CD14$^+$ macrophage datasets in the same direction: miR-182, miR-203a-3p, miR-210, miR-30c-1-3p and miR-874-3p. These findings could also indicate that miRNA expression detected in lung tissue also includes expression of immune cells infiltrating the tumour, discussed in 3.3.

3.2.8 JSRV genomic reads in lung tissue and BALF CD14$^+$ macrophages

Small RNA-sequencing reads from all datasets were mapped to the JSRV genome (AF105220.1) (section 2.5.1) in order to investigate the expression of potential miRNAs encoded by JSRV.

IGV was used to visualise the alignments of sequencing reads to the JSRV genome and to identify areas of the genome to which a dis-proportionately high number of reads aligned. Where these were consistent between samples, this would potentially indicate the presence of a miRNA. One such area was found around the nt 6400 of the JSRV genome (**Fig. 3.21**), this area contrasted with the rest of the genome for accumulating a considerably larger number of reads. Presence of reads in the same area was confirmed in LCM lung tissue samples and BALF macrophage samples (**Fig. 3.21** and **Fig. 3.22**). The accumulation of reads mapping to the 6400 nt of the JSRV genome was not detected in mock-infected lambs, $JSRV_{mut}$-infected lambs, adult controls or parasite-infected lambs, confirming that these reads were specific for JSRV-infected animals.

Given that the 6400 nt region of the JSRV genome is part of the *env* gene, which is known to structure some splice variants (Nitta et al, 2009), potential structural and sequence features that could explain the higher number of reads in this area were investigated (**Fig. 3.23**). However, no splice acceptors or other motifs were identified that could explain the results.

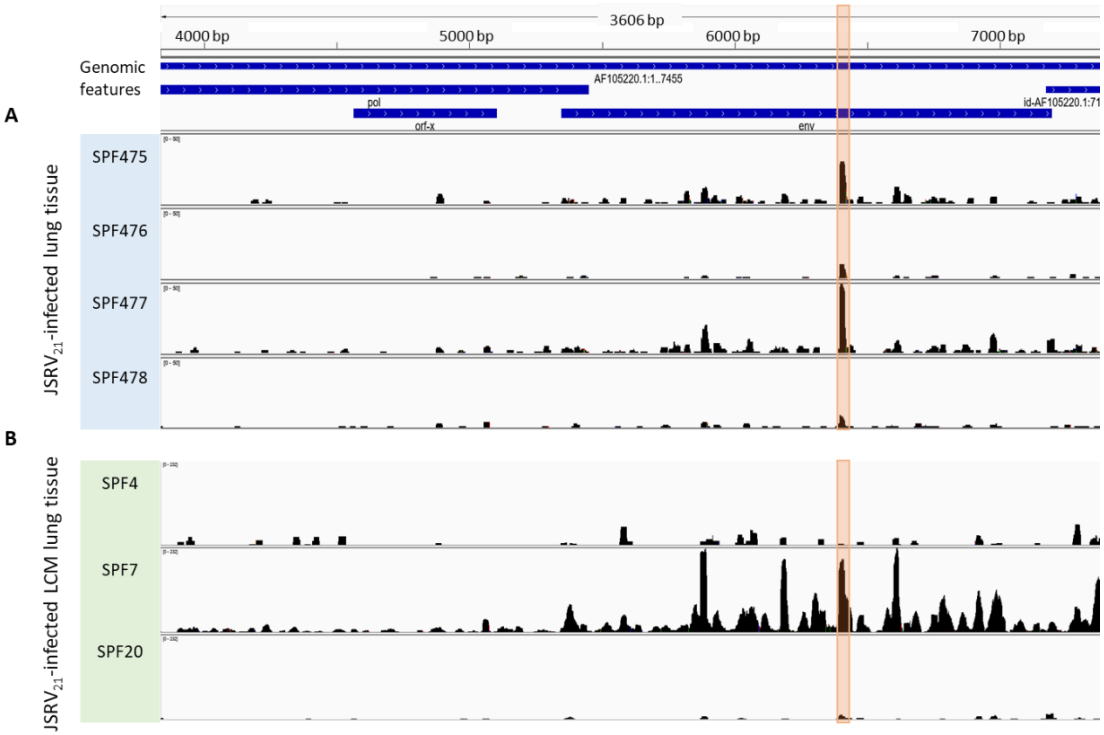

Figure 3.21. small RNA-sequencing reads of JSRV$_{21}$-infected lung tissue aligning to JSRV's genomic sequence, presented in the top panel. *A. Samples from whole lung tissue. B. Samples from LCM lung tissue. The genomic region highlighted in orange is where the highest number of reads where detected, only present in JSRV$_{21}$-infected lambs but not in mock-infected controls. Sequencing alignment was observed in IGV.*

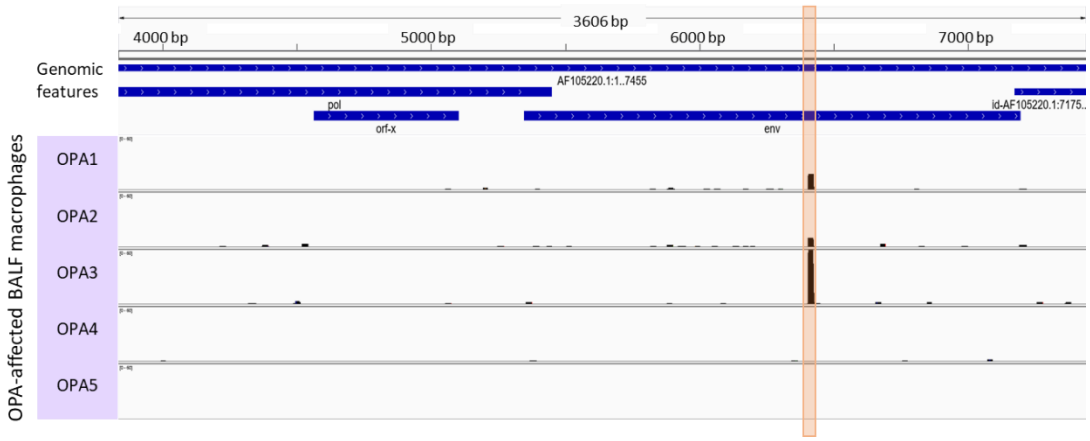

Figure 3.22. small RNA-sequencing reads of OPA-affected BALF CD14^{+} macrophage samples aligning to JSRV's genomic sequence, presented in the top panel. *The genomic region highlighted in orange is where the highest number of reads where detected, only present in OPA-affected sheep but not in controls. Sequencing alignment was observed in IGV.*

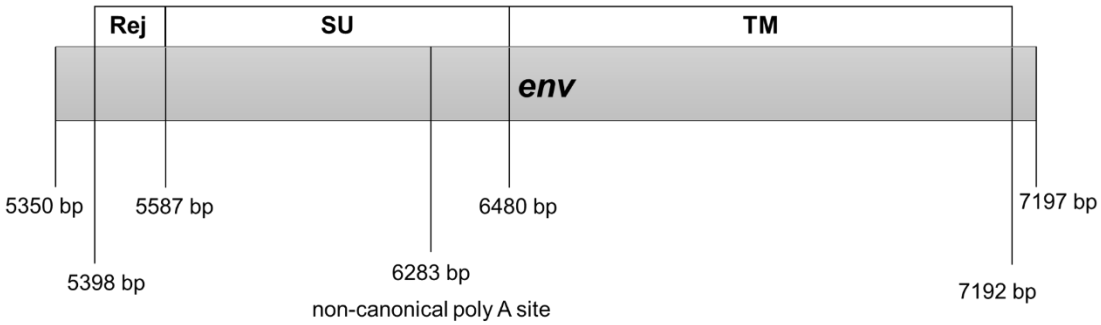

Figure 3.23. Diagram of the JSRV env gene. *Proteins encoded and polyA sites are represented. All positions are shown in relation to the JSRV sequence AF105220.1. (Hofacre et al, 2009; Palmarini & Fan, 2003; Palmarini et al, 1999b)*

Given that no explanation for the accumulation of reads had been found by examining the JSRV *env* gene, the JSRV genomic sequence surrounding 6400 bp was evaluated to find indications of a potential miRNA being encoded. RNA folding prediction programs were used to investigate the presence of a stem-loop that might encode a miRNA at 6400 bp. A stem-loop structure of 54 nt was found (**Fig. 3.24**). Although pre-miRNA stem-loops are usually longer (~ 70 nt), some retroviral miRNAs, such as the SFV miRNAs have stem-loops of a similar size to the one found in JSRV (Kincaid et al, 2014). Nevertheless, by examining the stem-loop it can be observed that the potential miRNA sequence (AATAGCTGAAGCCTGGTATGA) is not entirely encoded in the stem of the stem-loop structure, a requisite for DICER processing of miRNAs. This might be an indication that the reads found do not represent a JSRV miRNA. However, biogenesis of viral miRNAs is not entirely understood and biogenesis of some viral miRNAs, and some host miRNAs like miR-451, has been found to be DICER independent (section 1.5.2) (Cheloufi et al, 2010). In light of these findings, expression of this potential miRNA was experimentally evaluated using northern blotting.

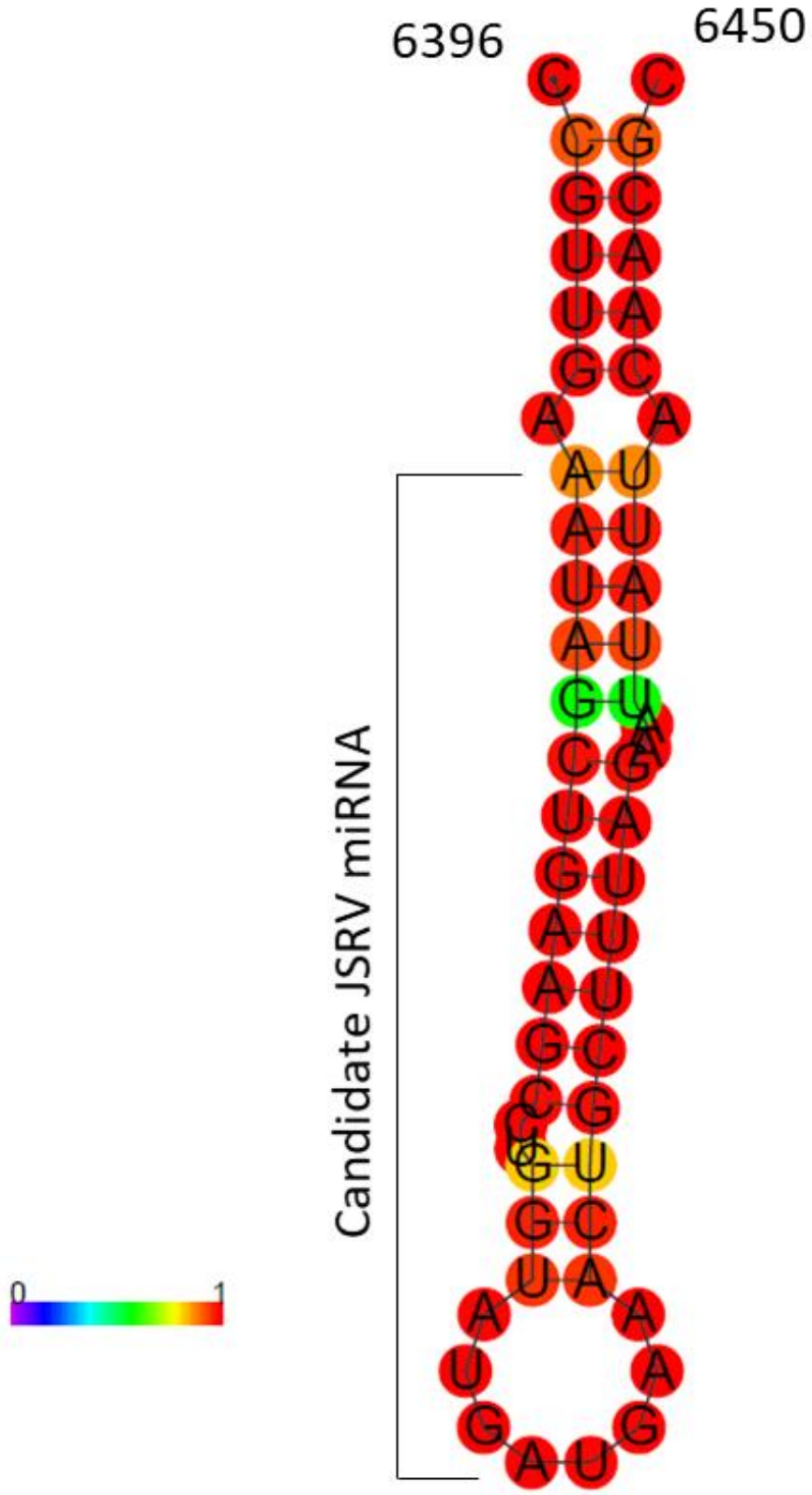

Figure 3.24. Secondary structure prediction of the JSRV nucleotide sequence (6396 – 6450 bp) surrounding the small RNA detected in small RNA sequencing. *Colour legend shows the base-pair probabilities. Created with RNAfold: (Langdon et al, 2018)*

3.2.8.1 Northern-blot for detection of putative JSRV small RNAs

In order to experimentally validate expression of the potential JSRV miRNA a northern blot was performed.

RNA was purified from lung tissue samples from OPA-affected sheep and healthy controls (section 2.4.6). In addition, 293T cells transfected with pEGFP-Flag and JSRV encoding plasmids ($pCMV2JS_{21}$ and $pJSRV_{21}$), were also harvested and RNA extracted (section 2.4.6). Cell culture samples were added to the study with two aims: investigate if the potential miRNA was also expressed *in vitro* and to differentiate enJSRV produced reads from JSRV produced reads.

RNA samples for northern blotting were concentrated to achieve concentrations greater than 800 ng/µl (section 2.4.7) (**Table 3.24**).

Table 3.24. RNA concentration of samples analysed by northern blot.

Group	**Healthy Control**		
Sample	172	173	
RNA (ng/µl)	838	785	
260/280 nm	1.89	1.91	
Group	**OPA-affected**		
Sample	JA875	JA876	JA898
RNA (ng/µl)	970	1588	1700
260/280 nm	1.95	2.00	2.01
Group	**Transfected 293T samples**		
Sample	pCMV2JS21	pJSRV21	pEGFP-Flag
RNA (ng/µl)	943	1115	1065
260/280 nm	2.04	2.03	2.05

The northern blot was performed as described in (section 2.9) loading 10 µg of each of the samples. Equivalent RNA loading of all samples was confirmed by staining the gel with ethidium bromide and observing the presence of tRNAs at the top of the gel. Hybridisation was performed with three labelled primers: two to detect the 5p and 3p versions of the potential miRNA, and one to detect miR-191, which was used as a positive control.

Analysis of the northern blot result (**Fig. 3.25**) revealed a band of ~ 20 nt in size, when RNA was hybridised with the labelled miR-191 primer. This result indicated that miR-191 could be detected in OPA-affected, control samples and 293T samples and that the northern blot technique had been successfully performed. In addition to the ~ 20 nt band, samples also presented a band of ~ 70 nt in size. This band was most clearly observed after the 4-day incubation and could represent the pre-miRNA mir-191. Size of the hybridisation products was determined by comparison to size markers, produced with loading dyes as described in sections 2.9.1 and 2.9.2.

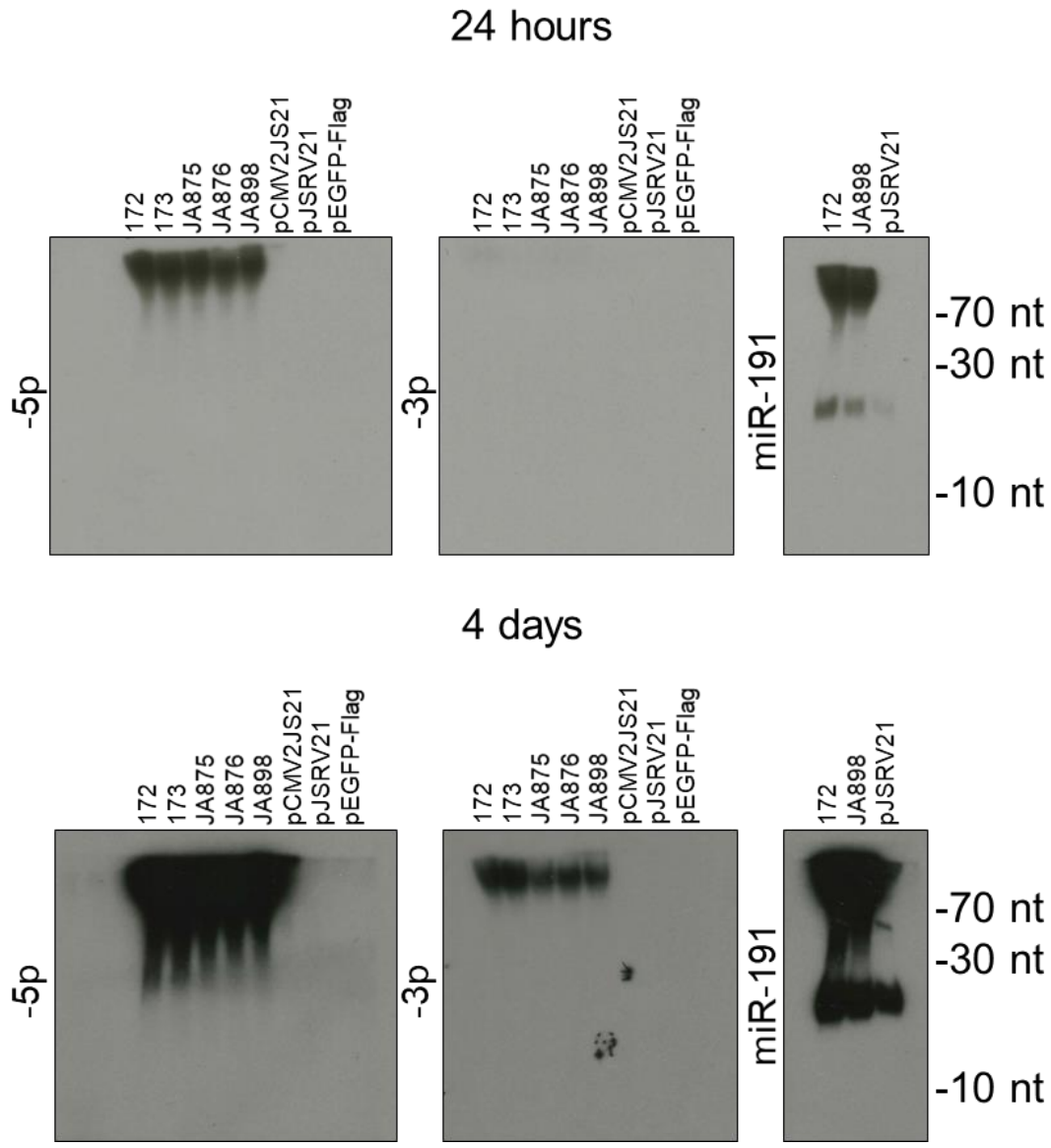

Figure 3.25. Northern blot analysis to identify the candidate JSRV miRNA. *Samples from lung tissue and in vitro culture were analysed and are indicated in each lane. Incubation was performed for 24 hours or 4 days. miR-191 was used as endogenous positive control.*

When RNA samples were hybridised with primers to detect -5p or -3p versions of the potential miRNA, no bands of the expected miRNA size (~ 21 nt) were observed (**Fig. 3.25**). Hybridisation was performed with both -5p and -3p primers because detection of both forms of a miRNA increases the confidence in presence of a miRNA (section 1.5.4). A band was detected at the top of some wells of both -5p and -3p primer hybridised gels. This band was detected in OPA-affected and control sheep samples, and in the 293T sample transfected with pCMV2JS$_{21}$, indicating that the primer was able to hybridise to a sequence present in the samples. However, the presence of this sequence in control sheep samples indicated that this sequence was not JSRV specific. Given that the band was not present in control 293T samples, it is possible that the primer could also be binding enJSRV sequences. Indeed, a BLAST search found 18/21 nt identity between the primer and some enJSRV forms encoded in the sheep genome, which would explain the presence of the band. The primer could, thus, anneal to JSRV sequences and enJSRV sequences and would have potentially been able to identify mature miRNA sequences produced by both enJSRV and JSRV.

Overall, the findings of the northern blot did not evidence that the reads found to align to the JSRV genome at 6400 nt were miRNAs. The potential origin of the sequencing reads detected is not known but may represent unknown genomic features of JSRV.

3.3 Discussion

The aim of this chapter was to investigate miRNA expression in the sheep lung, and detect expression changes that could be associated with OPA. miRNAs were successfully detected in lung tissue of both $JSRV_{21}$-infected and mock-infected sheep. In addition, differences in miRNA expression were detected between the two groups. An upregulation trend of nine miRNAs: miR-135b, miR-182, miR-183, miR-21, miR-200b, miR-205, miR-31, miR-503 and miR-96 was confirmed by RT-qPCR in samples from experimental and natural cases of OPA. These miRNAs were also found to be upregulated when enriched tumour samples were used, suggesting their upregulation originated from OPA lesions. Study of alveolar macrophages, highly abundant in OPA, revealed miRNA expression differences in OPA-affected sheep, suggesting phenotype alteration of immune cells in response to OPA. JSRV was not found to encode viral miRNAs.

The results presented in this chapter are the first description of miRNA expression in OPA cases and, suggest that upregulation of miR-135b, miR-182, miR-183, miR-21, miR-200b, miR-205, miR-31, miR-503 and miR-96 is associated with OPA. These findings are a first step towards understanding the role of miRNAs in OPA and could be potentially exploited as biomarkers of the disease or, as a tool to investigate the transformation process. In addition, they are a contribution towards further characterisation of OPA gene expression, which could aid the exploration of OPA as a human lung cancer model.

3.3.1 miRNA expression in whole lung tissue

The results obtained from small RNA-sequencing in lung tissue of experimentally infected lambs and controls revealed that miRNAs could be detected in lung tissue from sheep. 405 miRNAs were found to map to miRNAs in miRBase: most hits belonged to miRNAs of other species (cow, human and goat) and few to sheep. The reason for this mapping is likely to be that few miRNA studies have been performed in sheep, and there is a lack of annotated miRNAs in this species. Other studies (Bilbao-Arribas et al, 2019) have also used the approach of mapping sequencing reads to miRBase, and also found most miRNAs mapping to miRNAs of related species- emphasising the sequence conservation known of miRNAs. Apart from the reads that mapped to annotated miRNAs of the miRBase a

percentage of reads were unmapped. Some studies have taken the approach of mapping those novel miRNAs to the sheep genome, looking for predictors of miRNA stem-loops and other indicators that might suggest the sequence of interest is in fact a novel miRNA (Farrell et al, 2015). However, those studies also reported that the abundance of those novel miRNAs was very low (Farrell et al, 2015) and, in a study like the present the relevance of those novel miRNAs in the differential analysis is likely to be low and their detection in all samples difficult.

Differential analysis of lung tissue samples successfully detected 40 DE miRNAs in JSRV-infected lambs compared to mock-infected controls. Of those miRNAs only six were found downregulated with the vast majority presenting an upregulation in infected animals. These findings are in contrast with some reviews on miRNA dysregulation in cancer (section 1.5.10) which document that most miRNAs in cancer are downregulated. Nevertheless, the findings presented here might be explained by the nature of the sample used for the study: in lung tissue samples from $JSRV_{21}$-infected lambs small foci of tumoural cells can be observed, but the majority of the sample tissue, as much as 90%, is histologically normal. The high proportion of histologically normal tissue might therefore, be masking the downregulation of miRNAs and making it undetectable in our system. Such samples have greater sensitivity to detect upregulated miRNAs. The nature of the tissue used might also lead to the variability of $JSRV_{21}$-infected samples, as not all tissue will have the same proportion of tumour tissue. In addition to tumour cells, lung tissue has many cell types, each of which might change in relative abundance within the affected tissue, and each of which might change their expression phenotype in presence of JSRV-infected cells. The whole tissue approach provides a snapshot of global changes in the lung, but cell type specific changes require use of enriched or purified cell populations.

Clustering of samples based on miRNA expression showed that one of the $JSRV_{21}$-infected animals (SPF476) had an expression trend more similar to those of mock-infected controls. This unexpected grouping is likely to be related to the lower number of JSRV transcripts found in this lamb, as previously mentioned. Given that all lambs were administered equal amounts of the $JSRV_{21}$ preparation, this finding highlights that viral uptake by susceptible cells or clearance of the virus

is not equal in all lambs. Different levels of infection or tumour burden is a likely scenario in *in vivo* studies, and is likely to be a major factor in the biological variability observed.

Validation of the small RNA-sequencing results by RT-qPCR showed the same upregulation trend of the miRNAs of interest. Statistical analysis showed significant differences in the expression of all nine miRNAs between groups. Nevertheless, the magnitude of the upregulation (i.e. fold change) observed was not the same as that of small RNA-sequencing. Differences in miRNA detection sensitivity and specificity have previously been reported, and are linked to the way platforms identify miRNA isoforms or families, which have a very high sequence similarity (Mestdagh et al, 2014). In RT-qPCR, primers are designed to detect the canonical sequence of the miRNA but they are unlikely to detect all the isoform variants present in the sample. In the case of small RNA-sequencing, library construction and bioinformatics analysis performed can too affect the results (Giraldez et al, 2018). In addition, there are differences in how expression is calculated across platforms: in small RNA-sequencing the counts for a miRNA are expressed as relative to the total number detected, whereas in RT-qPCR they are calculated in relation to reference miRNAs.

The validation of miRNA expression in an independent experimental infection, discussed in section 3.2.3**,** showed the same miRNA upregulation trend observed in the previous study. However, differences between the $JSRV_{21}$-infected and control groups were not statistically significant for miRNAs miR-21, miR-31, miR-200b, miR-205 and miR-503. It can be observed how there is more variability within groups that may account for this lack of statistical significance. The $JSRV_{mut}$-infected group showed no significant differences in miRNA expression when compared to the mock-infected group. The explanation for this result could be due to low level of replication of $JSRV_{mut}$ in those animals, as also demonstrated by absence of positive IHC staining. If samples from the mock-infected group and $JSRV_{mut}$ infected group are grouped together, sensitivity to detect DE miRNAs in the $JSRV_{21}$-infected group might increase.

As several studies have commented on the disease stage dependent miRNA dysregulation (section 1.5.10) the expression of the selected miRNAs was also

studied in more advanced cases of OPA (natural cases). The same upregulation trend was observed for all miRNAs with the exception of miR-31. Differences in miR-31 expression could be related to the specific function and interactions with pathways that might be activated at this disease stage. Indeed, some of the validated targets of miR-31 in *Homo sapiens* include *RHOA*, *LATS2*, *PPP2R2A* and *FOXP3*, involved in transformation pathways, suggesting a shift in the expression of the miRNA could be related to a change in the activation in one of the transformation pathways (Begum et al, 2015; Liu et al, 2010; Vosa et al, 2013; Xi et al, 2010). Still, predictions on the reason for the observed shift are complex due to the multiple targets a miRNA has and the interactions of members of the affected pathway with other miRNAs which create an intricate regulatory network. Besides from a molecular reason for the change in miR-31 expression, reasons such as the age, breed and other health conditions the sheep might be suffering from, should be considered. Considering the differences in disease stage, breed and animals' age, the upregulation trend observed largely correlates with the results of experimental infections, and suggests an association of the selected miRNAs with OPA tumours.

Nevertheless, the complexity of the tumour and tumour microenvironment needs to be taken into account when interpreting the present results. Besides the transformed lung cells, other cell populations can be found infiltrating the tumour. These other cell populations could contribute to the miRNA signature detected in OPA affected lung tissue and the differences observed between JSRV-infected and uninfected tissue. In addition, miRNAs with altered expression in the tumour microenvironment could have targets and biological relevance not only in transformed lung cells but also in other infiltrating cells (Challagundla et al, 2014). OPA tumours have been previously shown to recruit immune cells, such as large numbers of macrophages, and recent studies have shown expression of T helper 1 (Th1) and T helper 2 (Th2) markers, indicating lymphocyte recruitment (Karagianni et al, 2019; Sharp & Angus, 1990). Although the presence of these cells does not affect the finding that the discussed miRNAs are associated with the presence of OPA tumours, it makes pinpointing the origin of the miRNA signature an intricate task. Whereas some of the dysregulated miRNAs might

originate from transformed lung cells, others might stem from other tumour infiltrating cells.

3.3.2 miRNA expression in enriched lung tumour samples

To study miRNA dysregulation in tumour tissue without normal surrounding tissue influencing the results the LCM technique was used in samples from the experimental infection of 2015. The PCA plot indicated a similar global miRNA expression pattern between mock-infected and $JSRV_{mut}$-infected lambs, potentially due to the $JSRV_{mut}$ not being able to replicate efficiently, and suggests that the global pattern of expression of $JSRV_{21}$-infected lambs, although highly variable, is different from the other groups. In fact, total reads varied between around twelve million and thirty-three million, with these two extremes belonging to samples of the $JSRV_{21}$-infected group, which might account for the high variability observed.

As expected, the number of DE miRNAs increased in LCM samples, but an increase in downregulated miRNAs was not observed. Once again, several factors need to be considered as plausible explanations for this observation. First, difficulties were encountered in obtaining high quality RNA. This is a recognised issue when performing LCM on lung tissue. Therefore, while RINs of samples used for library preparation were >7, the quality and amount of RNA may still have been an issue. Furthermore, as discussed before, the lambs suffered from allergic reactions that could also be contributing to the miRNA patterns observed. In addition, this comparison was performed with only three animals per group, which might make the data not representative.

Giraldez et al (2018) showed that results of sequencing can be affected by sequencing facility and sample type. This does not appear to have greatly affected data in this study, as all but one of the selected miRNAs (miR-503), were also found to be upregulated in these samples. Increasing confidence in the involvement of these miRNAs in OPA tumours. miR-503 might not appear as DE due to low number of counts, below the average of 50 normalised counts threshold established for DE analysis.

3.3.3 Targets of miRNAs upregulated in OPA lung tissue

Overall, there seems to be a trend observed across the analysed samples suggesting a consistent upregulation of miRNAs: miR-135b, miR-182, miR-183, miR-21, miR-200b, miR-205, miR-31, miR-503 and miR-96 in lung tissue samples of $JSRV_{21}$-infected sheep. The timing of the observed upregulation in JSRV infection is unknown, miRNAs appear upregulated in OPA tumours but with the present knowledge it can't be discerned if they are upregulated as a result of the viral infection per se or as a result of the cell transformation, or what their role in transformation is.

Targets of the nine selected miRNAs have not been investigated in sheep, but some potential targets have been identified in humans. Extrapolation between human and sheep studies is difficult due to differences in the genes present, differences in gene sequences and in regulatory networks. In addition, the poor annotation of the sheep genome makes target prediction of sheep miRNA targets with computer-based analysis challenging. Nevertheless, given the transcriptional similarities between OPA and human lung cancer (Karagianni et al, 2019), comparison to human cancer studies can give a first indication of the roles a miRNA might be involved in. Interestingly, the miRNAs consistently upregulated in these datasets have targets in pathways known to be activated in OPA: MAPK and pI3k-Akt (section 1.2.6). For instance, miR-96 targets KRAS in the MAPK pathway, and miR-21 targets *PTEN* in the PI3K-Akt pathway (Yu et al, 2010b; Zhang et al, 2010b). miR-183 targets *PPP2CB* in the PI3K-Akt pathway, PPP2CB decreases Akt activation (Ma et al, 2016). miR-205 targets *VEGFA*, *PTEN* in the Akt pathway (Cai et al, 2013; Li et al, 2017a; Wu & Mo, 2009). miR-31 targets *RASA1* and *SPRED1* in the MAPK pathway (Edmonds et al, 2016). None of the nine miRNAs were found to target components of the RON-HYAL2 pathway.

3.3.4 miRNA expression in alveolar macrophages

To further investigate the different cell types that could be involved in miRNA dysregulation in OPA, alveolar macrophages, were investigated. miRNA expression was detected in BALF macrophages and DE miRNAs identified between OPA-affected samples and control samples. DE miRNAs were also identified between OPA-affected samples and parasite-infected samples,

indicating differences in the immune response between the two organisms. The DE miRNA miR-33b has been reported dysregulated in macrophages and some of its targets are *BCL2*, involved in cell-death and apoptosis, and *PIM1* and *HMGA2* involved in inflammation (Jiménez-García et al, 2017). Some of the miRNAs DE in OPA-affected samples, might be related not only to JSRV-infection but also to tumour presence: during the bronchoalveolar lavage and isolation process tumour-associated macrophages might have also been isolated.

These differences in DE miRNAs are an encouraging step to better understand the role of alveolar macrophages in JSRV-infection. Moreover, these DE miRNAs could be further investigated as diagnostic biomarkers, discussed in 3.3.1. Indeed, cell-free miRNAs have been successfully detected in BALF and are being investigated as biomarkers (Lee et al, 2016; Li et al, 2017b).

miR-182, was the only miRNA found consistently and significantly upregulated in all datasets. This finding suggests biological relevance of miR-182 upregulation in OPA. Reviewing some of the targets of miR-182, it could be speculated that upregulation of miR-182 could result in downregulation of *FOXO1* and *FOXO3*, which are transcription factors that regulate proliferation, apoptosis and inflammation. Decreased levels of FOXO inhibit apoptosis and, interestingly P-Akt and P-ERK1/2 have also been found to inactivate FOXO transcription factors (Krishnan et al, 2013; Yang et al, 2010b). In addition, miR-182 targets *PTEN*, which decreases PiP3 that promotes Akt activation. Upregulation of miR-182, thus, could be expected to decrease levels of PiP3 and disrupt regulation of the Akt pathway, resulting in constitutive activation of Akt (Manning & Toker, 2017; Wang et al, 2019a; Yao et al, 2017). miR-182 also targets the tumour suppressor *PDCD4* (Chang et al, 2018).

3.3.5 Candidate JSRV miRNAs

A potential JSRV-encoded miRNA was detected in sequencing data alignments to the JSRV genome. However, the potential miRNA was not found in northern blot analysis of sheep tissue or cell culture samples, arguing against the sequencing reads representing a JSRV-encoded miRNA. This finding could be further confirmed by RT-qPCR analysis with a primer-probe designed to detect

the potential miRNA, a more sensitive method of detection. Nevertheless, lack of JSRV-encoded miRNAs is not a striking result as few RNA viruses have so far been discovered to encode viral miRNAs, reviewed in section 1.5.14. Only four retroviruses have so far been identified to encode miRNAs: BLV, HIV1, SFV and BFV (section 1.5.14). In addition, a closely related virus: ENTV, also member of the betaretrovirus, was recently found not to encode viral miRNAs but alter hosts miRNA expression levels (Wang et al, 2016). A finding similar to the one presented in this chapter.

3.3.6 Limitations of the study

The studies in this chapter are primarily built on findings from small RNA-sequencing of whole lung tissue. This sample type is likely to have reduced the sensitivity to detect DE miRNAs. To address this, the significance threshold was established at fold change ≥ 1.5 or ≤ 0.75, and FDR ≤ 0.05. These cut-offs are arbitrary and established to reduce false positives while maximising chances of discovering true changes in miRNA expression. In the sequencing studies of enriched cell types (tumour and macrophages), the cut-offs established were more stringent due to the sample offering more sensitivity to detect DE miRNAs.

The results obtained would have changed if different cut-offs had been established, indicating that caution should be exercised when interpreting the results. miRNAs presenting higher fold-changes and smaller FDR values in the comparison between groups are more likely to be validated, as confirmed in the results obtained by RT-qPCR in this chapter.

Overall, this chapter has revealed upregulation of miR-135b, miR-182, miR-183, miR-21, miR-200b, miR-205, miR-31, miR-503 and miR-96, associated with OPA. Nevertheless, the limited animal number used in these studies may have biased the results obtained. Further confirmation of the significance of these miRNAs in OPA could be confirmed by increasing the number of samples analysed, which would increase biological variability. In addition, mechanistic data on the role of this miRNAs would also increase confidence in their association with OPA.

3.3.7 Conclusions and future work

Dysregulated host miRNAs were detected in lung tissue of OPA affected animals. Nine of those miRNAs were found consistently upregulated in lung tissue of experimentally infected lambs and natural cases of OPA. Further studies should investigate the targets of these miRNAs in JSRV transformed cells and the mechanisms by which expression of those miRNAs is activated. This information would help understanding the role of miRNAs in JSRV Env transformation.

These results suggest that miRNA expression can be used to differentiate between OPA-affected animals and controls. Differences in miRNA expression could also be exploited as potential biomarkers of OPA. However, for miRNAs to be used as biomarkers it would be desirable that they could be detected in biological fluids for ease of sampling. OPA miRNA dysregulation was also detected in BALF macrophages, suggesting that miRNA expression changes due to OPA are not limited to lung tissue. In addition, DE miRNAs could distinguish between OPA-affected and lungworm infected samples. However, BALF macrophages might not be an appropriate sample for biomarker detection due to the long and complex isolation process. BALF or other biological fluids could be explored to investigate the potential of these miRNAs as biomarkers of OPA. In addition to miRNAs being able to differentiate between lungworm infected sheep and JSRV-infected sheep, it would be desirable to find miRNAs able to differentiate between bacterial pneumonias and OPA.

Chapter 4 Cell-free miRNAs in OPA

4.1 Introduction

In Chapter 3, some miRNAs were found to be consistently upregulated in OPA-affected lung tissue, suggesting that expression levels of these miRNAs could differentiate between OPA-affected and unaffected sheep. Those findings prompted the idea that the miRNAs upregulated in OPA tissue could be investigated as potential biomarkers of OPA. Specifically, they could be examined as diagnostic markers of OPA to aid early diagnosis and disease control.

Nevertheless, for those miRNAs to be used as diagnostic markers, it would be desirable to detect their expression levels in biological fluids, which are easier to sample than lung tissue. For instance, the expression of those miRNAs could be investigated in blood serum and detected by RT-qPCR. Obtaining serum samples is a relatively easy and minimally-invasive procedure for sheep. While RT-qPCR is a sensitive and specific detection technique and is being successfully optimised and applied in the field setting (Biava et al, 2018). Indeed, some studies have reported that miRNAs derived from tumour tissue could be detected in the circulation either inside exosomes or bound to proteins (section 1.5.7).

Another approach would be to investigate expression levels of the upregulated miRNAs in lung fluid or nasal secretions. Similarly to serum, nasal secretions could be easily sampled, and sampling would not be an invasive procedure for sheep. In addition, high concentrations of JSRV can be detected in lung fluid (section 1.1.3), reflecting infection in the lung, so lung fluid could potentially signal miRNA expression levels in the lung too.

If tumour miRNAs were not found to be dysregulated in biological fluids, as some have reported (section 1.5.12), miRNA expression in OPA could be investigated in biological fluids using sequencing approaches to identify new biomarker candidates. Studies have reported miRNA dysregulation in biological fluids originating from cells other than tumour cells and could reflect the host response to disease (sections 1.5.13 and 1.5.14).

Either way, the dysregulation of miRNAs in biological fluids of OPA-affected sheep would be an essential first step towards establishing them as diagnostic markers of OPA. Further studies would be necessary to determine if the same miRNAs could be used as diagnostic markers for different disease stages or if they would be limited to some stages. In addition, for miRNAs to be developed as diagnostic markers of OPA, it would be required to test large numbers of sheep and determine the sensitivity and specificity of the test. In this regard, it would be desirable for miRNAs used as diagnostic markers to be able to differentiate between OPA and other pathologies, particularly diseases of similar presentation, such as bacterial pneumonia (sections 1.1.1 and 1.1.3).

Besides the potential of miRNAs as diagnostic markers of OPA in biological fluids, studying miRNA dysregulation in biological fluids could unveil considerably more about OPA. For instance, it could be indicative of the host response to infection, or it could reveal signalling mechanisms used by tumour cells, such as exosomes. Furthermore, it could highlight the importance of certain miRNAs in OPA.

4.1.1 Hypothesis and aims

In this study, it was hypothesised that miRNAs can be detected in biological fluids of sheep, and that a number of miRNAs would be differentially expressed in OPA affected sheep when compared to controls. It was also hypothesised that miRNAs differentially expressed in lung tissue would also be differentially expressed in biological fluids.

In order to test the hypothesis the following aims were established for the present chapter:

- Detect miRNA expression in serum of sheep
- Detect miRNA expression in lung fluid
- Compare miRNA expression of infected and uninfected sheep
- Contrast findings from sheep experimentally infected with JSRV and natural cases
- Compare findings with data from JSRV-infected lung tissue.

4.2 Results

4.2.1 RT-qPCR of OPA tumour associated miRNAs in serum

Initially, a pilot analysis was performed to test if some of the miRNAs dysregulated in lung tissue could also be detected in serum samples, and to determine if those miRNAs were also differentially expressed between serum of OPA affected sheep and control animals, which could indicate their potential as biomarkers for the presence of OPA tumours.

In the first experiment, the expression of four miRNAs was measured in serum samples from natural cases of OPA and from sheep donated to Moredun, without OPA but with other pathologies (**Table 2.3**). Serum samples were prepared, RNA was extracted (sections 2.4.1 and 2.4.2) and RT-qPCR performed for miR-135b, miR-182, miR-183 and miR-96, as those had the highest fold-change in OPA affected lung tissue samples, and therefore might be predicted to show differential expression in the circulation. miR-191 was used as the endogenous control (**Fig. 4.1**). Because no previous data on sheep serum miRNAs was available, the choice of miR-191 as endogenous control was made based on previous data obtained in lung tissue (3.2.2.1). miR-191 expression levels obtained by RT-qPCR were compared across OPA-affected and control samples, to evaluate if miR-191 was an appropriate endogenous control in serum. The calculated coefficient of variance across the 8 samples was 2.88%, suggesting low variability in miR-191 expression and that miR-191 was an appropriate control.

Although all miRNAs tested by RT-qPCR were detected in sera from all 8 sheep, no statistically significant differences in expression (**Table 4.1**) were observed between the OPA-affected and control animals. The four miRNAs tested presented p-values above the established threshold of 0.05 thus, the null hypothesis, which considered that the means of the two groups were equivalent, could not be rejected. Taking into consideration the health status of the control animals used and the involvement of miRNAs in several diseases, the study of miRNA dysregulation in serum from OPA sheep would benefit from using healthy animals as controls to avoid miRNA dysregulation being masked in the initial stages of the study.

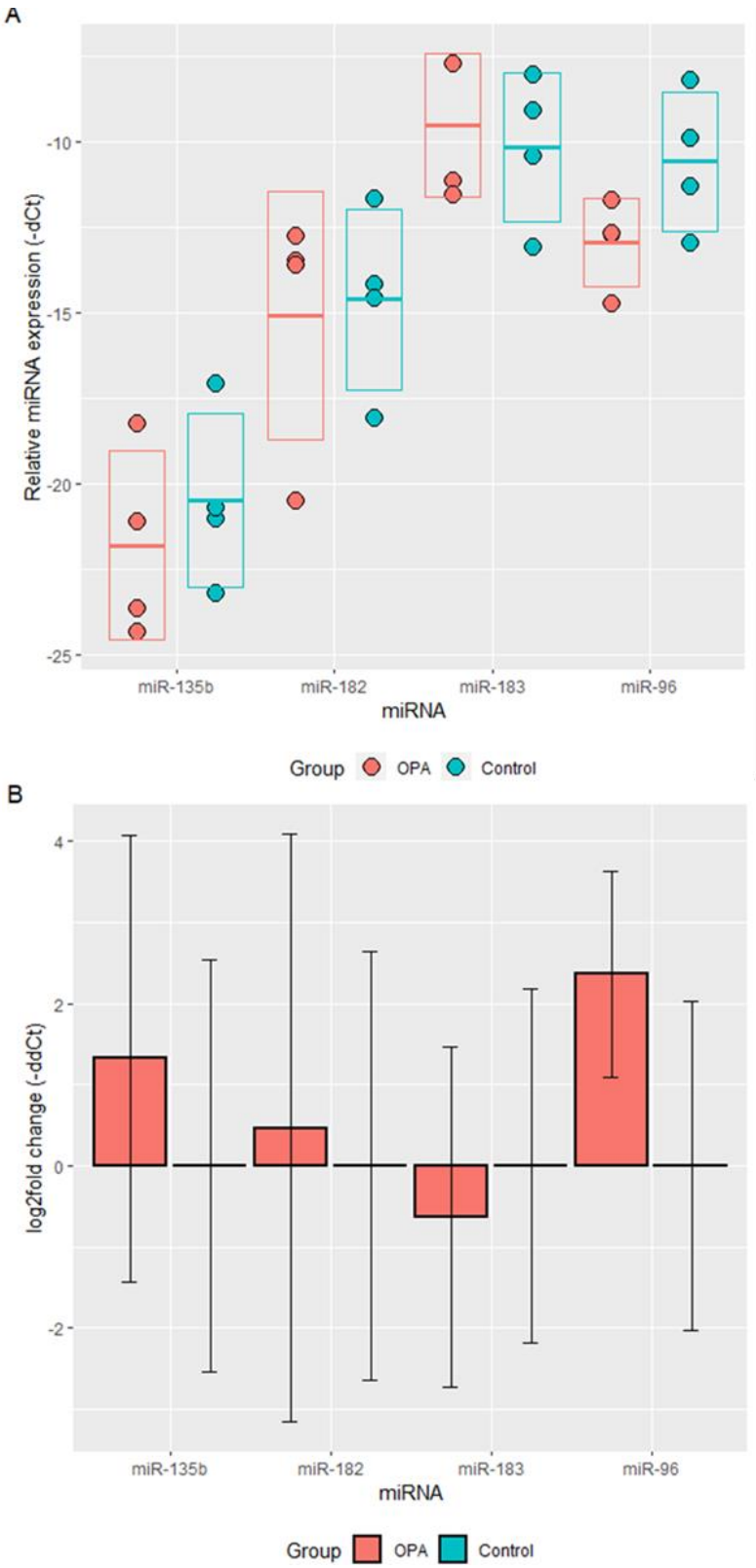

Figure 4.1. miRNA expression in serum samples of OPA-affected animals (n=4) compared to controls (n=4). *A. Relative miRNA expression (-dCt= -Ct miR+Ct miR-191) of*

each individual sample. Boxes show standard deviations of the mean, represented with a horizontal line. B. log2(fold change) expression between OPA-affected and control group (section 2.6.2). Error bars indicate standard deviation within groups.

Table 4.1. Statistical analysis (student's t-test) of dCt values obtained by RT-qPCR.

miRNA	Group	Mean[1]	Stdev[2]	Estimated difference	DF[3]	p-value
miR-135b	OPA-affected	21.81	2.76	1.32	5	0.512
	Control	20.49	2.54			
miR-182	OPA-affected	15.08	3.63	0.46	5	0.844
	Control	14.61	2.64			
miR-183	OPA-affected	9.54	2.1	-0.63	5	0.695
	Control	10.16	2.18			
miR-96	OPA-affected	12.96	1.28	2.36	5	0.105
	Control	10.59	2.02			

[1] Null-hypothesis= no differences between the means of the two groups assessed, confidence level stablished at 95%.
[2] Stdev= standard deviation of the mean.
[3] DF= degrees of freedom.

4.2.2 Serum miRNAs in OPA identified by miRNA sequencing (study 1)

Due to the limited number of miRNAs tested by RT-qPCR and the fact that miRNA dysregulation in serum might have an origin other than from the tumour (section 1.5.13), miRNA expression was subsequently studied using a sequencing approach to aid discovery of miRNA expression patterns related to OPA. Initially, three OPA-affected samples and three control samples were analysed as a proof of concept to evaluate if differences in miRNA expression in serum could be detected by sequencing. The decision to test a limited number of samples was made due to sequencing costs, and six samples were deemed sufficient to evaluate if sequencing was a viable option to detect miRNA patterns in serum related to JSRV-infection.

Samples for sequencing were prepared (section 2.5), the concentration of RNA extracted from serum samples was measured by Nanodrop (section 2.4.8) and was low due to the nature of the sample, which contains a high concentration of RNAses and lower concentration of RNAs compared to tissue samples. Low

260/280 nm were anticipated due to low RNA concentration, making 260/280 measurements unreliable (**Table 4.2**).

Table 4.2. RNA concentration of samples submitted for miRNA sequencing study 1.

	Control			OPA affected		
Sample	**S6230**	**S6318**	**S6354**	**B14**	**B16**	**G32**
RNA (ng/µl)	6.36	5.61	26.2	24.11	19.07	34.53
260/280 nm	1.44	1.31	1.63	1.45	1.4	1.51

Samples were submitted for sequencing and bioinformatics analysis to Edinburgh Genomics. Three OPA affected serum samples and three control serum samples were sequenced (**Table 2.3**). Bioinformatics analysis was performed to determine the abundance of each miRNA in each sample and to test for statistically significant differences between disease groups (section 2.5.1). Despite the low amount of RNA, sequencing libraries were successfully constructed from all samples. Total reads ranged from 37632783 reads to 50327639 reads, with greater variability within the OPA affected samples (**Table 4.3**). The percentage of reads mapping to miRNAs on miRBase and other categories also varied between samples, and the percentage of reads mapping to miRBase was notably higher in OPA affected samples (**Fig. 4.2** and **Fig. 4.3**).

Analysis of sequence length distribution (**Fig. 4.3**) also revealed that control samples contained more reads of length between 30-32 nt. Reads of this length do not fall into the miRNA category but could correspond to reads of another small RNA category called piwi-interacting RNAs (piRNA) (Cheng et al, 2011; Martinez et al, 2015; Umu et al, 2018), this possibility will be further reviewed in the discussion section 4.3.

Table 4.3. Summary of reads for each sample of the serum miRNA sequencing study 1.

		Control			OPA-affected		
	Sample	**S6230**	**S6318**	**S6354**	**B14**	**B16**	**G32**
	Total reads	44098605	43744988	46331994	41302403	50327639	37632783
(%) total reads	**>28 nt**	55.42	39.43	49.32	22.89	17.04	29.44
	miRBase	11.33	15.53	9.40	38.82	39.81	38.46
	JSRV	7.28E-04	1.62E-03	1.51E-03	6.39E-04	2.50E-04	3.11E-04

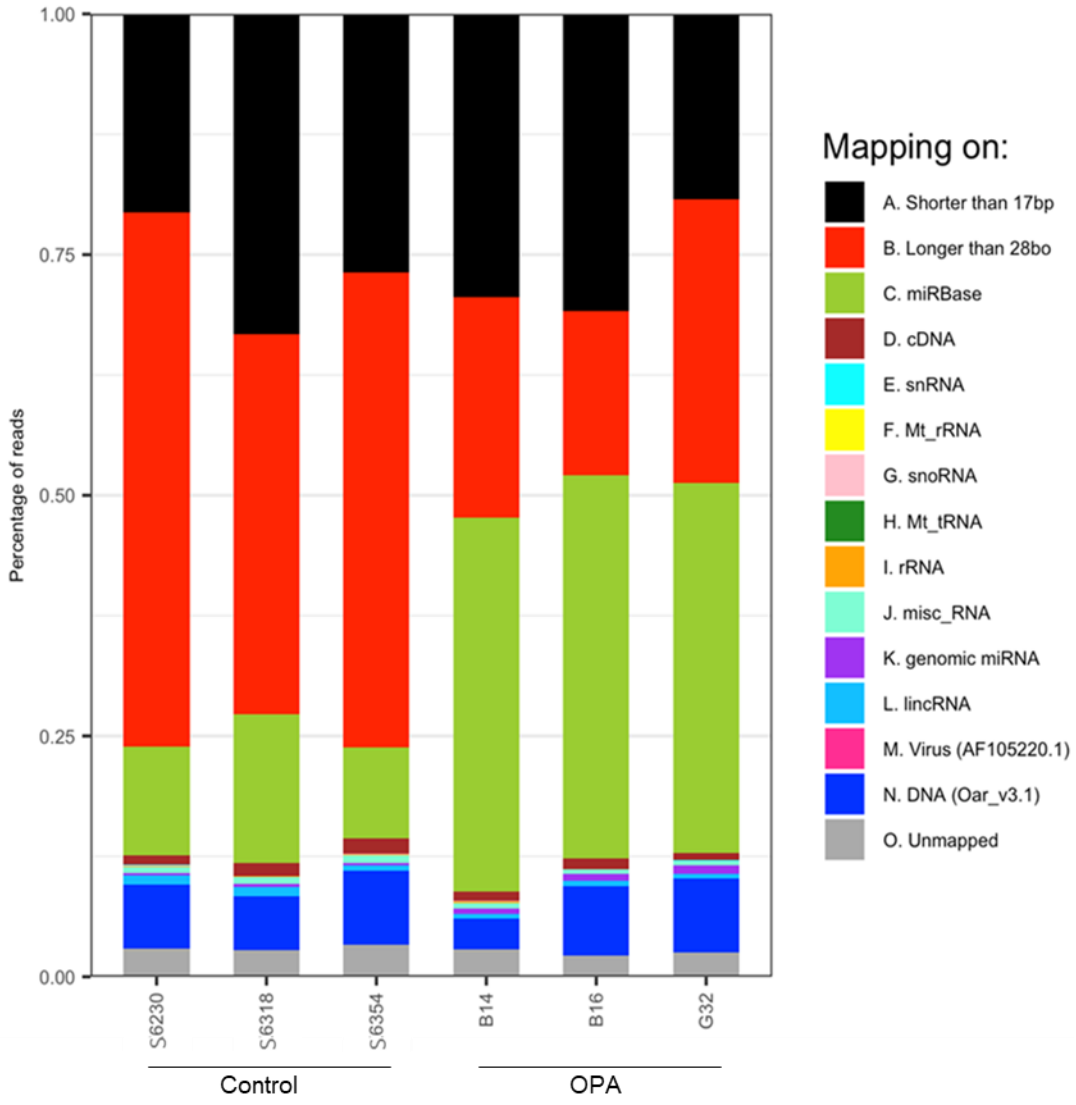

Figure 4.2. Sequence distribution in samples of sequencing study 1 presented as a percentage of total reads in each sample. *Each of the categories is represented by a colour shown in the legend. Small nuclear RNA(snRNA), mitochondrial ribosomal RNA (Mt_rRNA), small nucleolar RNA (snoRNA), mitochondrial transfer RNA (Mt_tRNA), ribosomal RNA (rRNA), miscellaneous RNA (misc_RNA), long non-coding RNA (lincRNA), JSRV viral genome (Virus), sheep genome (DNA), reads not mapping to any of the previous categories (Unmapped).*

In order to begin comparing miRNA expression between samples, a threshold of ≥ 50 average read counts was established as further explained in (section 2.5.1). Once miRNAs with read count below the threshold were removed, a total of 275 miRNAs were identified in serum of sheep. Expression levels of these 275 miRNAs were plotted with a principal component analysis to analyse global patterns of expression, and to investigate clustering of samples that might indicate expression differences between groups (**Fig. 4.4**). PC1 separates OPA and control samples in two distinct groups with no overlapping. Control samples,

compared to OPA samples, are plotted closer together implying lower within-group variability. OPA samples show greater divergence by PC2. Sample B14 appears distanced from all other samples, indicating a distinctive expression pattern. Higher variability within OPA samples than controls is not unexpected and could be due to different disease presentations or disease stage in individual cases.

Differential expression analysis was then performed to assess statistically significant differences in miRNA expression between OPA and control sheep. 74 miRNAs were found to be DE between groups (log_2(fold change) ≥ |1| and false discovery rate (FDR) ≤ 0.05) Of those, 43 miRNAs were upregulated and the remaining 31 downregulated in OPA affected sheep (**Fig. 4.5**, **Table 4.4 and Table 4.5**). The heatmap was generated using R studio pheatmap, and clustering performed using correlation (section 2.5.1) (**Fig. 4.5**). Of interest, miR-191, used as an endogenous control in the previous RT-qPCR analysis of serum (4.2.1), presented low variance among all samples (coefficient of variance 14.45%) confirming its suitability as an endogenous control for this study.

Observing the heatmap (**Fig. 4.5**), distinct expression patterns between groups can be seen, and clustering analysis of samples based on expression of DE miRNAs indicates two clusters corresponding to control samples and OPA samples. These results suggest that changes in miRNA expression can be detected in serum of OPA affected sheep. Nevertheless, due to the small sample size of this study and the variation in percentage of reads mapping to miRBase (**Fig. 4.2**), further characterisation of larger sample size groups was performed to confirm these results (**4.2.3**). In addition, it could have had an effect in the analysis of DE miRNAs, emphasising the need for further investigation.

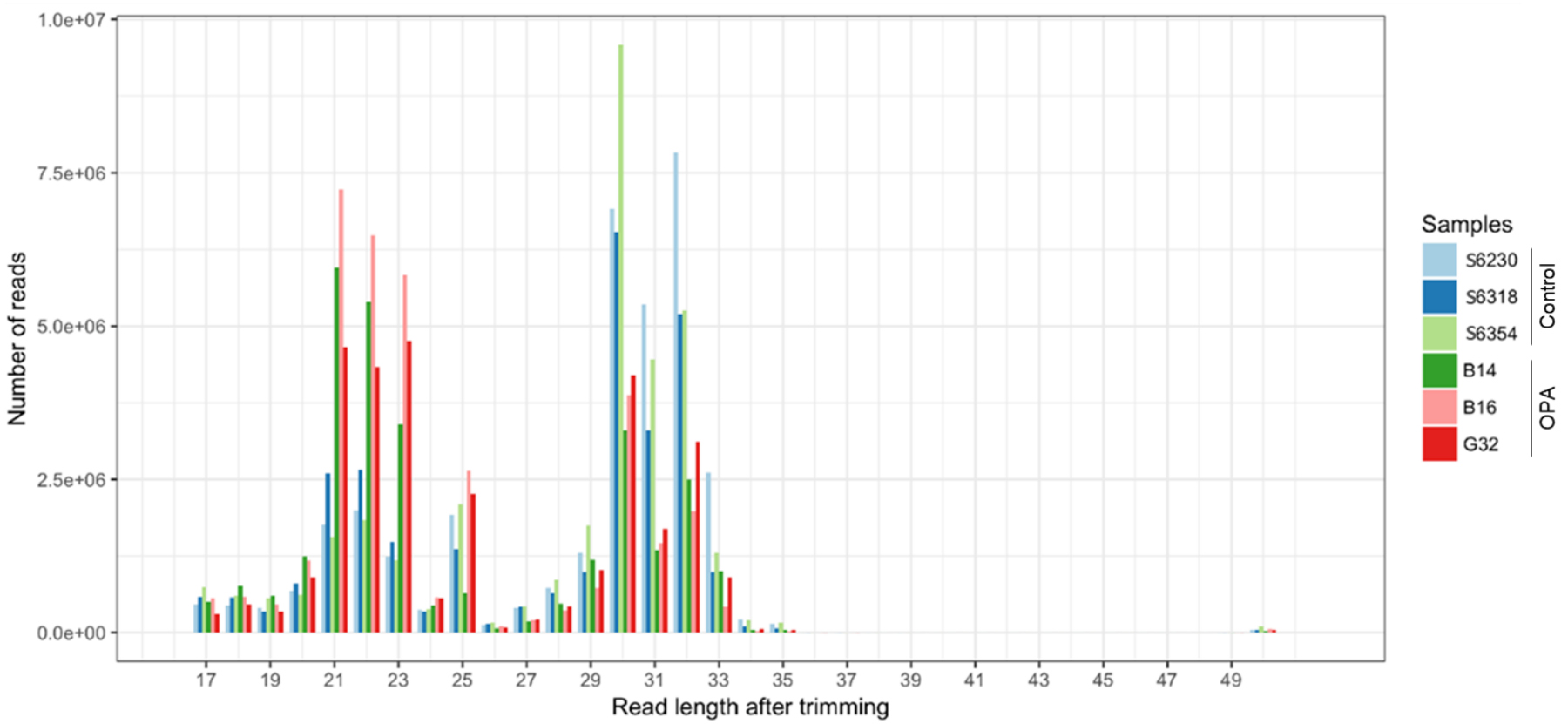

Figure 4.3. Length distribution of total sequencing reads from sheep sera (Study 1). *The figure shows the length distribution of reads in each serum after adapter trimming was performed. Control samples (n=3, S6230, S6318, S6354); OPA samples (n=3, B14, B16, G32). Two areas with high read abundance can be observed: corresponding to miRNA length (21-23nt) and longer length (30-32nt), which could correspond to piwi-RNAs. The presence reads with a length typical of miRNAs is higher in OPA affected samples, whereas control samples show a higher abundance of longer reads.*

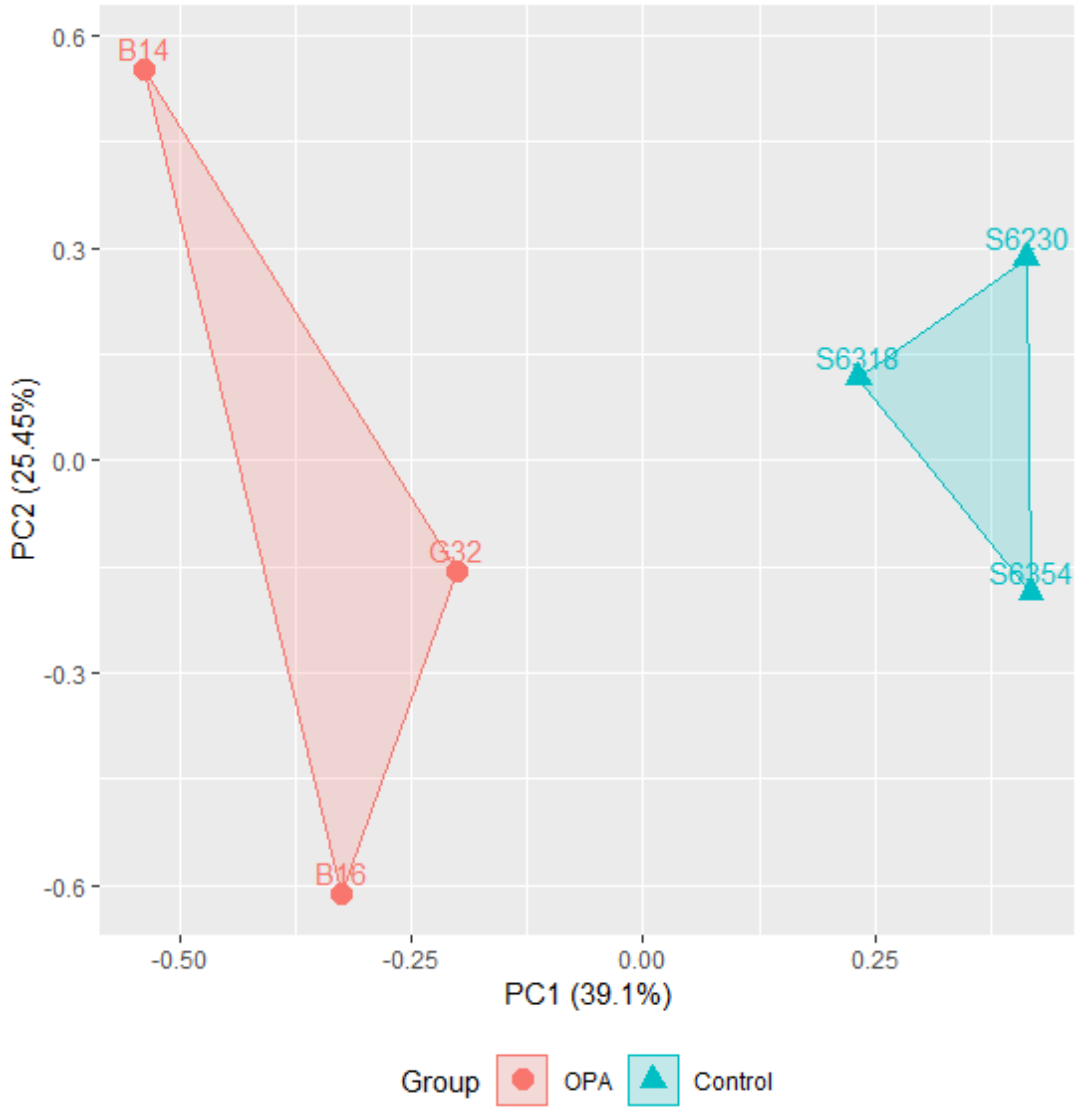

Figure 4.4. PCA plot of serum miRNA expression from sequencing study 1. *OPA affected sheep (n=3) and healthy controls (n=3). OPA-affected samples are represented as red circles and uninfected controls as turquoise triangles. Greater distance between samples in the plot indicates greater expression difference between samples. Control samples are seen clustering towards the right of the plot, whereas samples from OPA affected animals can be seen towards the left of the plot, occupying much of the vertical axis. The PCA plot suggests global expression differences between the two groups and more variability within the OPA affected group of animals.*

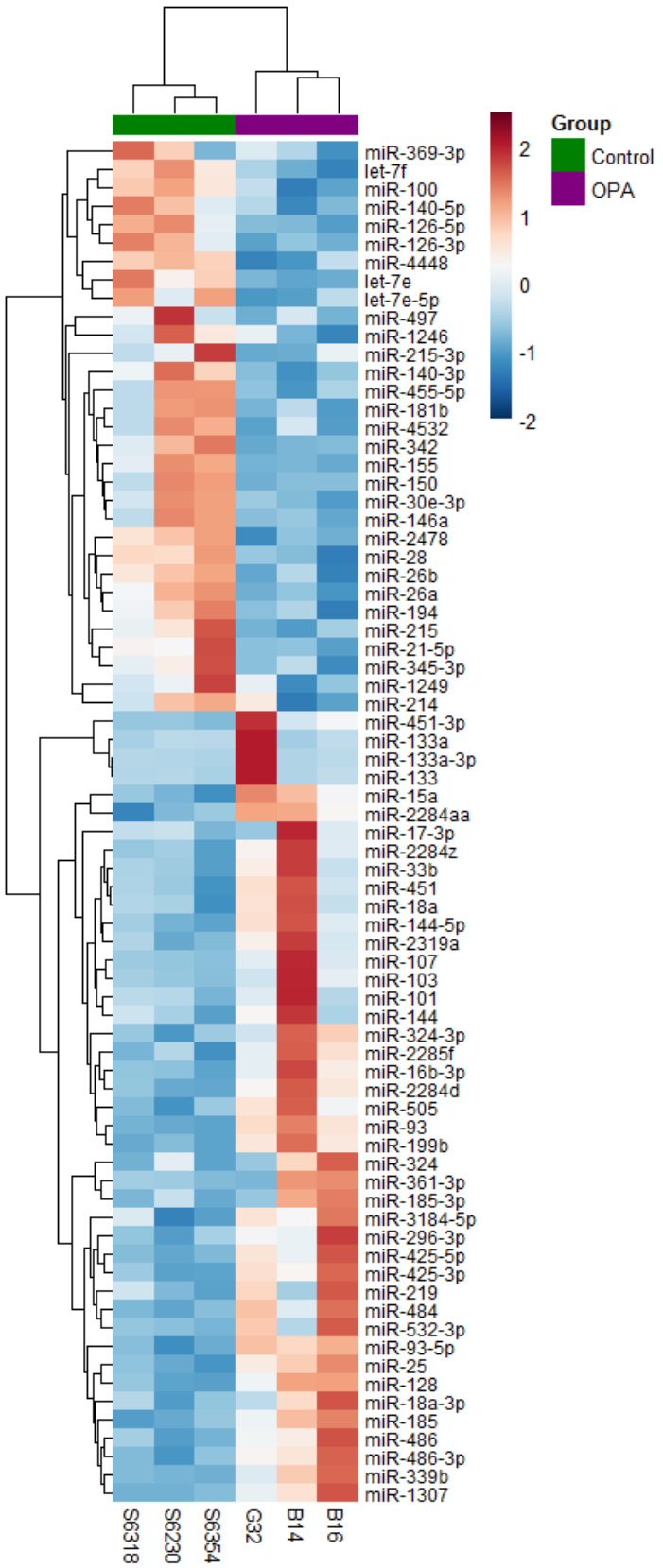

Figure 4.5. Heatmap of DE miRNAs (FDR ≤ 0.05, log_2(fold change) ≥ \|1\|) between OPA samples and controls of sequencing study 1. *Dendrogram showing correlation clustering of individuals in groups. Legend represents values of log2 fold change.*

Table 4.4. Differentially upregulated miRNAs between OPA-affected sheep and controls.

miRNA	average counts[1]	log2(fold change)[2]	FDR[3]
miR-25	197889.4	1.22	0
miR-451	172388.6	1.29	0
miR-486	4722656	1.46	0
miR-133a-3p	1871.92	4.76	1.46E-25
miR-133	1133.45	3.16	1.30E-12
miR-451-3p	274.67	3.1	2.02E-11
miR-133a	186.23	2.63	1.22E-08
miR-144-5p	864.63	2.14	3.77E-06
miR-16b-3p	299.26	2.11	7.10E-06
miR-199b	293.63	2.04	1.13E-05
miR-185	122.64	1.9	4.15E-05
miR-425-3p	50.92	2.16	5.36E-05
miR-103	33037.25	1.69	1.74E-04
miR-2284d	155.02	1.8	1.74E-04
miR-107	34393.82	1.65	2.39E-04
miR-2319a	83.91	1.77	2.65E-04
miR-93	18017.59	1.63	3.25E-04
miR-33b	326.42	1.71	3.49E-04
miR-486-3p	642.7	1.56	5.13E-04
miR-15a	12124.09	1.62	5.80E-04
miR-2284z	165.49	1.61	9.22E-04
miR-484	6487.74	1.49	1.03E-03
miR-296-3p	10239.01	1.38	2.04E-03
miR-2284aa	80.35	1.44	2.41E-03
miR-144	1609.13	1.4	3.77E-03
miR-219	50.95	1.6	4.64E-03
miR-128	14498.17	1.3	4.93E-03
miR-2285f	318.81	1.35	5.06E-03
miR-101	2917.92	1.28	6.07E-03
miR-18a-3p	879.88	1.25	6.74E-03
miR-18a	147.58	1.35	6.98E-03
miR-185-3p	75.26	1.38	7.03E-03

[1] Average normalised counts across all samples
[2] Threshold established at log2(fold change) ≥ |1|
[3] FDR corrected by Benjamini-Hochberg, threshold FDR ≤ 0.05

Table 4.4. Differentially upregulated miRNAs between OPA-affected sheep and controls.

miRNA	average counts[1]	log2(fold change)[2]	FDR[3]
miR-532-3p	137.15	1.34	7.35E-03
miR-425-5p	11523.1	1.22	8.18E-03
miR-324-3p	56.47	1.28	8.61E-03
miR-17-3p	308.95	1.23	1.09E-02
miR-339b	4904.6	1.14	1.35E-02
miR-3184-5p	68.94	1.28	1.38E-02
miR-505	171.91	1.05	2.29E-02
miR-1307	1419.68	1.03	2.73E-02
miR-361-3p	554.58	1.05	2.73E-02
miR-93-5p	5620.71	1.02	2.90E-02
miR-324	69.22	1.07	4.92E-02

Table 4.5. Differentially downregulated miRNAs between OPA-affected sheep and controls.

miRNA	average counts[1]	log2(fold change)[2]	FDR[3]
miR-150	28029.58	-2.58	0
miR-215	117063.1	-1.33	0
let-7e	198.07	-2.3	1.89E-06
miR-146a	125.02	-2.38	4.53E-06
miR-4532	55.25	-2.45	1.91E-05
miR-455-5p	50.77	-1.95	2.02E-04
miR-30e-3p	214.87	-1.84	2.42E-04
miR-155	246.08	-1.75	3.49E-04
miR-4448	373.79	-1.54	9.13E-04
miR-21-5p	858.87	-1.68	9.35E-04
miR-28	187.92	-1.63	1.03E-03
miR-140-5p	82.7	-1.49	1.15E-03
miR-215-3p	345.12	-1.58	2.21E-03
miR-2478	178.89	-1.5	2.40E-03
miR-1246	64.04	-1.48	3.03E-03
miR-26b	2696.43	-1.41	4.10E-03

[1]Average normalised counts across all samples
[2] Threshold established at log2(fold change) ≥ |1|
[3] FDR corrected by Benjamini-Hochberg, threshold FDR ≤ 0.05

Table 4.5. Differentially downregulated miRNAs between OPA-affected sheep and controls.

miRNA	average counts[1]	log2(fold change)[2]	FDR[3]
miR-126-3p	917.57	-1.27	4.69E-03
let-7e-5p	136.2	-1.34	5.98E-03
miR-181b	1090.97	-1.33	7.82E-03
let-7f	10253.2	-1.2	8.01E-03
miR-126-5p	12937.58	-1.17	8.01E-03
miR-26a	9949.14	-1.27	8.31E-03
miR-369-3p	89.47	-1.15	8.75E-03
miR-140-3p	14010.66	-1.17	9.71E-03
miR-342	3691.33	-1.21	1.23E-02
miR-497	139.83	-1.08	1.90E-02
miR-100	511.67	-1	2.66E-02
miR-214	58.93	-1.09	3.23E-02
miR-1249	97.49	-1.1	3.98E-02
miR-194	188.41	-1.04	4.40E-02
miR-345-3p	445.26	-1.04	4.90E-02

4.2.2.1 Comparison of differentially expressed miRNAs between tissue and serum

The results obtained of serum sequencing were compared to previous findings of miRNA dysregulation in lung tissue to find commonalities that could be, in the future, exploited as biomarkers of OPA. miR-215 and miR-21-5p were both found to be significantly upregulated in lung tissue of OPA affected sheep and significantly upregulated in this serum sequencing study 1.

Differences in DE miRNAs between lung tissue and serum could be due to low expression levels of certain miRNA in serum, or lung tissue miRNAs not released into circulation. To investigate this, expression levels of the nine miRNAs DE in lung tissue and validated (miR-135b, miR-18, miR-183, miR-200b, miR-205, miR-21, miR-31, miR-503 and miR-96) were inspected in serum. miR-182, miR-200b, miR-205 and miR-21 were identified in serum sequencing but not found DE between groups. miR-183, miR-31, miR-503 and miR-96 were detected below the count threshold established for DE analysis. miR-135b was not identified. Out of

the nine validated miRNAs, the ones not detected in serum had lower expression levels in lung tissue than the ones found in both datasets.

4.2.3 Serum miRNAs in OPA identified by miRNA sequencing (study 2)

To further study miRNA dysregulation in serum of OPA-affected sheep, a second miRNA-sequencing study was performed. In this study, the number of animals per group was increased and they were classified into groups depending on the disease stage. This classification was devised to allow examination of inter-individual variation in OPA-affected animals, while allowing comparison of the miRNA expression profile at different OPA disease stages.

Serum RNA samples were prepared for sequencing (section 2.4.1 and 2.4.2) and samples (**Table 2.2** and **Table 2.3**) were separated into disease-stage groups for comparison (**Table 4.6**). In cases in which sheep had presentations corresponding to both mid-stage OPA and advanced OPA, classification in a group was made based on presence or absence of lung fluid.

Two sets of controls were used to ensure that they were age-matched to OPA-affected samples. Age-matching controls and samples is crucial in miRNA expression experiments, as expression is widely recognised to vary in stages of development (Ameling et al, 2015). Thus, early stages of OPA, represented here by experimentally-infected lambs, and advanced cases of OPA, represented by natural cases of OPA in adult sheep, will present miRNA expression differences related to age, in addition to any changes due to disease.

In addition, samples from the previous sequencing run (study 1) were included in this miRNA-sequencing run to assess the repeatability of the method. Similarly to study 1, samples had low RNA concentration (**Table 4.7**), but sequencing libraries were successfully prepared.

Table 4.6. Criteria for classification of OPA affected sheep in disease-stage groups.

Group	Samples	Criteria for inclusion
Advanced OPA	A50, B14, G22, JA811, JA874, JA875	Presence of lung fluid. Body score condition lower than 2, both lungs affected and 40% or more of lung affected.
Mid-stage OPA	A20, A28, A29, B16, G32, JA794	No lung fluid, body condition score 2 or above. Less than 40% of lung tissue affected.
Adult control	S3882, S6230, S6318, S6353, S6354, JA856	Healthy adult sheep with no known pathologies and free of OPA.
Early stage OPA	SPF4, SPF7, SPF15, SPF23, SPF27, SPF31	Experimentally infected SPF lambs that were positive for OPA with tumours visible by histology.
Lamb control	SPF3, SPF8, SPF14, SPF22, SPF26, SPF29	Mock-infected lambs, negative for OPA.

Table 4.7. RNA concentration of samples submitted for serum sequencing study 2.

Group	**Advanced_OPA**					
Sample	A50	B14*	G22	JA811	JA874	JA875
RNA (ng/µl)	10.167	14.324	12.323	17.979	10.547	11.607
260/280 nm	1.35	1.31	1.32	1.33	1.15	1.30
Group	**Mid-stage OPA**					
Sample	A20	A28	A29	B16*	G32*	JA794
RNA (ng/µl)	10.529	6.352	6.779	5.459	10.527	6.318
260/280 nm	1.33	1.49	1.35	1.47	1.51	1.39
Group	**Adult_Control**					
Sample	S3882	S6230*	S6318*	S6353	S6354*	JA856
RNA (ng/µl)	8.025	8.753	5.223	8.568	5.223	11.636
260/280 nm	1.34	1.37	1.42	1.24	1.42	1.33
Group	**Early_OPA**					
Sample	SPF4	SPF7	SPF15	SPF23	SPF27	SPF31
RNA (ng/µl)	5.809	6.075	15.455	12.001	6.403	9.967
260/280 nm	1.28	1.58	1.28	1.37	1.14	1.58
Group	**Lamb_Control**					
Sample	SPF3	SPF8	SPF14	SPF22	SPF26	SPF29
RNA (ng/µl)	40.612	3.744	9.527	8.934	10.959	9.081
260/280 nm	1.355	1.099	1.315	1.406	1.289	1.305

* Indicates samples also sequenced in study 1

Library sizes ranged from 25433227 reads to 73183413 reads (**Table 4.8**). In general, there was a trend that advanced OPA samples had the highest numbers of total reads and early OPA samples had the lowest, greater variation in number of reads was also observed within these groups. The percentage of reads mapping to miRNAs on miRBase and other categories also varied between samples, and percentage of reads mapping to miRBase ranged from 1.8% (SPF4) to 44.6% (JA811) (**Fig. 4.6** and **Fig. 4.7**). The differences in the percentage of reads mapping to miRBase were significant between adult and lamb groups (t-test $p<0.05$) but not within age groups. As with study 1, analysis of sequence length distribution in serum small RNAs (**Fig. 4.8**) also revealed two distinct read populations, but no differences in read distribution were observed between the animal groups.

Table 4.8. Summary of reads for each sample of the serum sequencing study 2.

	Group	**Advanced_OPA**					
	Sample	A50	B14	G22	JA811	JA874	JA875
	Total reads	73183413	43261205	33810878	62028854	58549040	58727428
(%) total reads	**>28 nt**	47.24	42.37	30.17	36.34	51.08	42.45
	miRBase	31.13	33.29	22.58	44.59	7.69	27.22
	JSRV	2.61E-04	2.03E-04	4.08E-04	3.47E-04	3.14E-04	7.12E-04
	Group	**Mid-stage OPA**					
	Sample	A20	A28	A29	B16	G32	JA794
	Total reads	34742140	44620709	35559408	36239791	47319792	29321710
(%) total reads	**>28 nt**	10.31	29.33	10.67	20.22	23.43	8.22
	miRBase	8.54	14.96	27.75	42.72	34.77	11.15
	JSRV	2.91E-04	3.03E-04	3.32E-04	4.97E-04	1.07E-03	1.02E-03
	Group	**Adult_Control**					
	Sample	S3882	S6230	S6318	S6353	S6354	JA856
	Total reads	27387273	28532385	38220012	41842673	29562561	36944248
(%) total reads	**>28 nt**	27.73	34.86	36.12	33.71	51.42	18.51
	miRBase	6.20	22.99	35.79	37.38	6.03	20.49
	JSRV	7.30E-04	7.36E-05	3.92E-04	3.63E-04	1.22E-04	1.68E-03
	Group	**Early_OPA**					
	Sample	SPF4	SPF7	SPF15	SPF23	SPF27	SPF31
	Total reads	25433227	27643320	51647904	39896551	28135373	25540040
(%) total reads	**>28 nt**	60.35	41.77	32.96	33.84	6.09	8.47
	miRBase	1.78	2.62	4.98	5.95	8.72	9.62
	JSRV	4.88E-04	3.87E-04	1.17E-03	5.76E-04	3.66E-04	5.48E-04
	Group	**Lamb_Control**					
	Sample	SPF3	SPF8	SPF14	SPF22	SPF26	SPF29
	Total reads	54984608	40536216	36412973	34713360	59838575	53406224
(%) total reads	**>28 nt**	52.47	36.22	30.53	34.57	38.00	30.68
	miRBase	8.55	4.98	13.09	2.54	7.79	10.79
	JSRV	1.35E-03	1.35E-03	6.81E-04	1.67E-03	1.60E-03	1.27E-03

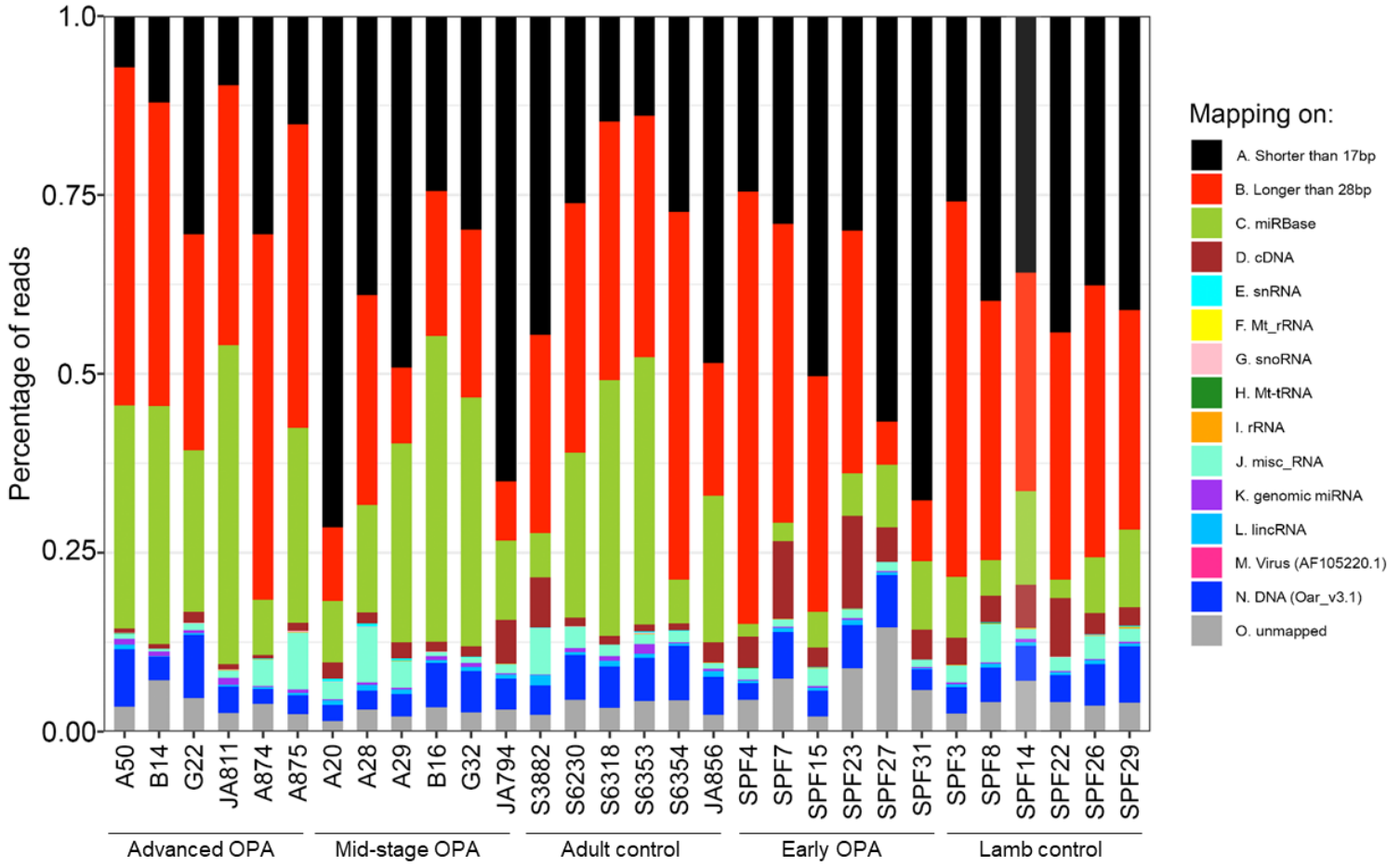

Figure 4.6 Sequence distribution in samples of sequencing study 2 presented as a percentage of total reads in each sample. *Each of the categories is represented by a colour shown in the legend. Small nuclear RNA(snRNA), mitochondrial ribosomal RNA (Mt_rRNA), small nucleolar RNA (snoRNA), mitochondrial transfer RNA (Mt_tRNA), ribosomal RNA (rRNA), miscellaneous RNA (misc_RNA), long non-coding RNA (lincRNA), JSRV viral genome (Virus), sheep genome (DNA), reads not mapping to any of the previous categories (Unmapped).*

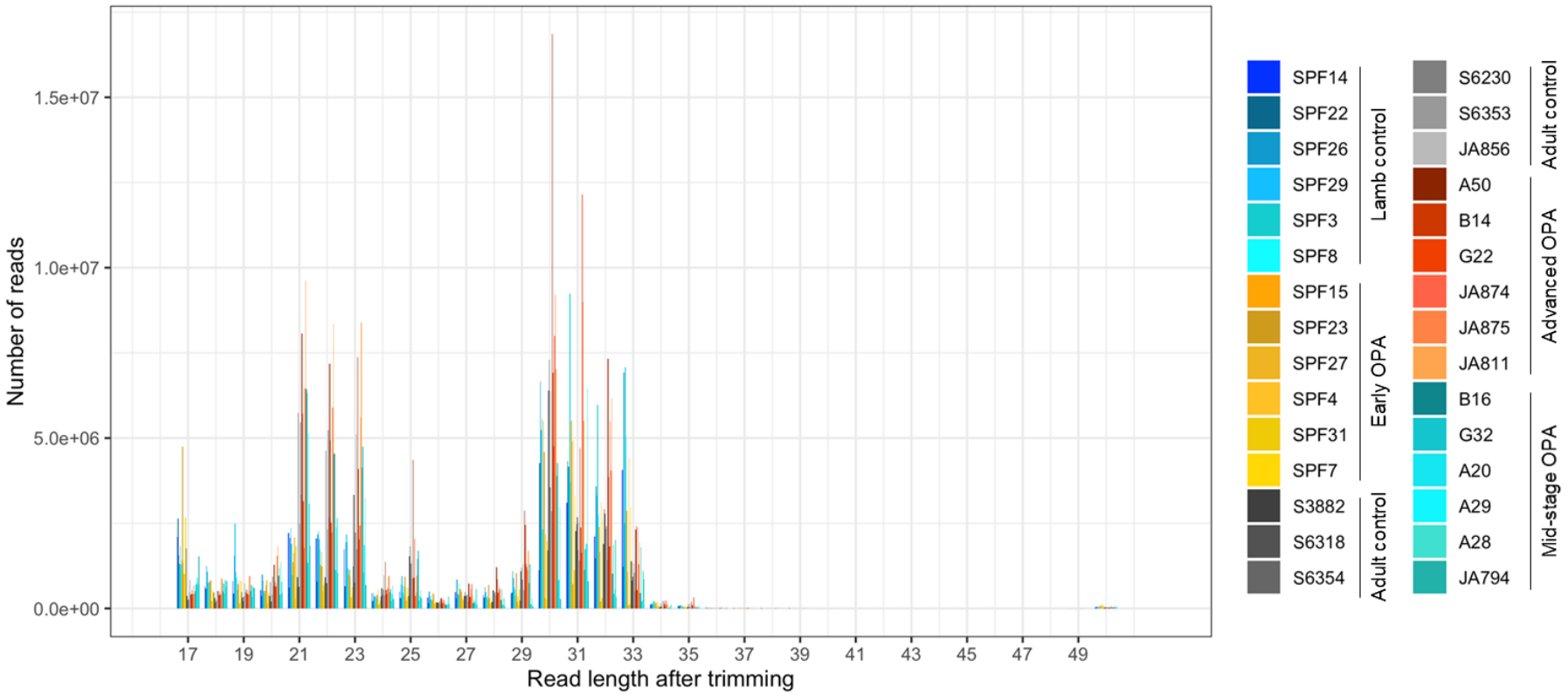

Figure 4.7. Length distribution of total sequencing reads after trimming was performed. *Two areas with high read abundance can be observed: corresponding to miRNA length (21-23nt) and longer length (30-32nt) which could correspond to piwi-RNAs. The abundance of reads in those two areas appears similar in all sample groups.*

4.2.3.1 Age effects on miRNA expression

Previous studies have reported age-dependent differences in miRNA expression in humans (Ameling et al, 2015) and mice (Victoria et al, 2015). To examine whether similar changes were evident in the samples of the present study, a comparison between control adult samples and control lamb samples was performed. Following removal of miRNAs of low abundance, 202 miRNAs were detected in the serum of healthy sheep. Expression changes were examined by PCA (**Fig. 4.8**).

Figure 4.8. PCA plot of miRNA expression levels of adult sheep and lambs in study 2. *Adult control (n=6) and lamb control (n=6). Adult samples are represented as red circles and lambs as turquoise triangles. Greater distance between samples in the plot indicates more expression differences between samples. Lamb samples are seen clustering towards the right of the plot, whereas adult sheep can be seen towards the left of the plot. The PCA plot suggests global expression differences between the two groups.*

The PCA plot (**Fig. 4.8**) suggested that adult and lamb samples cluster into two separate groups based on miRNA expression levels detected in serum. Differential expression analysis between adults and lambs revealed 78 miRNAs DE between the two tested age groups (log_2(fold change) ≥ |1| and FDR ≤ 0.05). Of those, 35 were upregulated and 43 downregulated in adults compared to lambs (**Fig. 4.9**, **Table 4.9 and Table 4.10**). Interestingly, miR-191 appeared DE between adult sheep and lambs, suggesting that expression of this miRNA is linked to age. Consequently, miR-191 would not be an adequate endogenous control in serum studies with samples from mixed age groups.

Distinct miRNA expression patterns can be seen between adults and lambs. Correlation clustering analysis of samples revealed two clusters corresponding to adult sheep samples and lamb samples (**Fig. 4.9**). However, sample S3882 clustered with the lamb samples instead of adult sheep samples. Consistent with this, sample S3882 also clustered closer to the lamb group in PC1 of the PCA plot (**Fig. 4.8**). These results suggest that changes in miRNA expression linked to age can be detected in serum of sheep, as previously shown in humans and mice. While the observations presented here are in line with previous published studies, it is possible that differences in library size and miRBase mapping could also have influenced the observed results. In addition, all lambs and adult sheep in this study (study 2) differed in the environment they had been subjected to: lambs were raised as SPF, whereas adult sheep lived on farm, therefore the two groups may have differed in a number of other ways, such as diet, infection exposure and environmental stressors. Consideration of these results indicated that it would be important to perform comparisons of OPA disease stages within age groups.

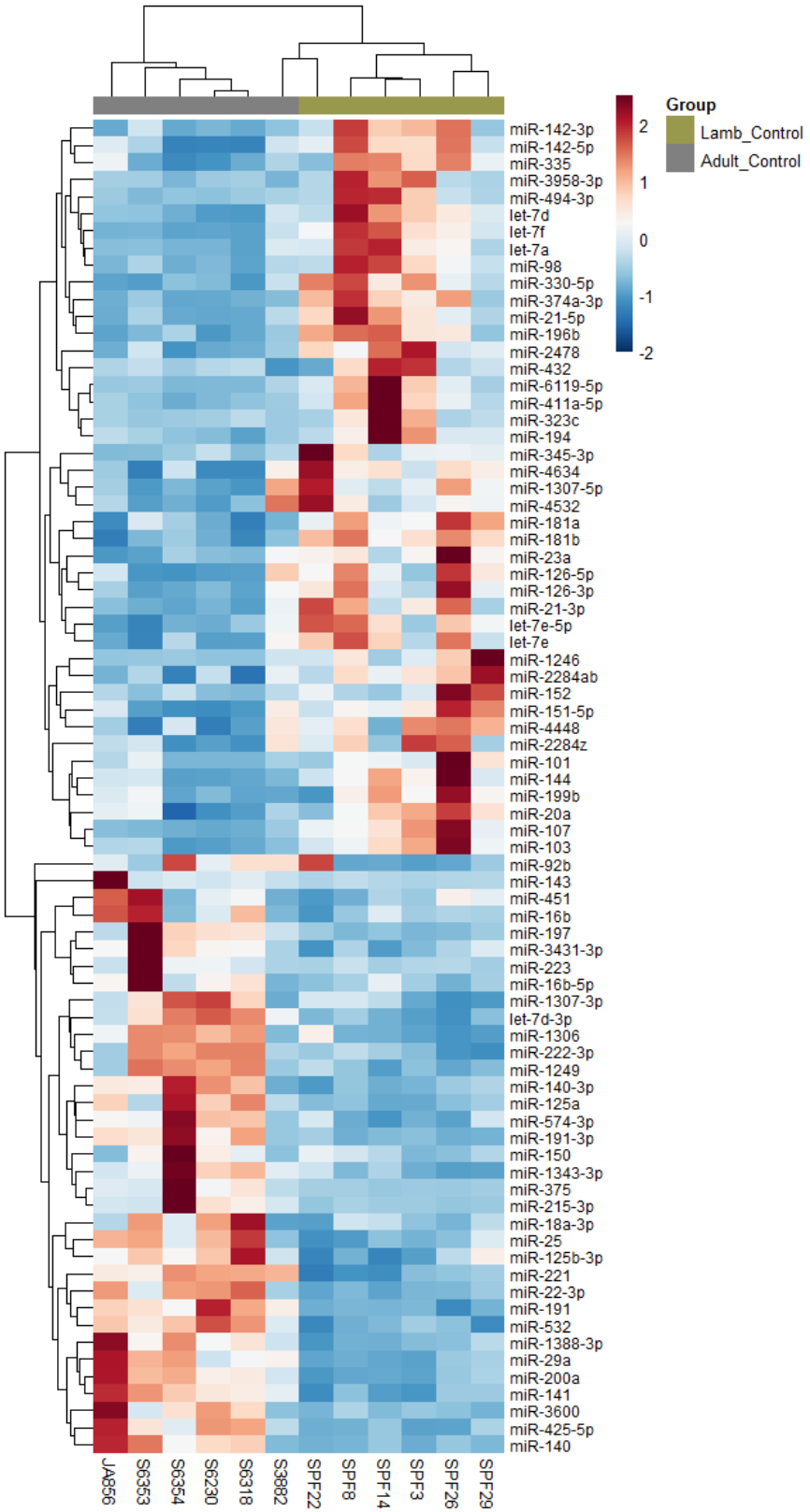

Figure 4.9. Heatmap of DE miRNAs (FDR ≤ 0.05, log_2(fold change) ≥ \|1\|) between control adults and control lambs of sequencing study 2. *Dendrogram showing correlation clustering of individuals in groups. Legend represents values of log2 fold change. Note that the animals cluster by age except for S3883, an adult sheep which clusters with the lambs.*

Table 4.9. Differentially upregulated miRNAs between adult sheep and lambs.

miRNA	average counts[1]	log2(fold change)[2]	FDR[3]
miR-451	29989.46	1.01	0
miR-25	30298.94	1.58	0
miR-215-3p	71	4.24	1.08E-10
miR-375	5822.53	3.29	8.78E-09
miR-143	3606.59	2.85	6.71E-07
miR-1249	60.83	2.53	1.30E-06
miR-223	964.39	2.59	2.62E-06
miR-197	682.82	2.39	7.49E-06
miR-200a	104.62	2.96	7.49E-06
miR-1306	138.77	1.87	1.34E-05
miR-191-3p	180.47	2.37	1.79E-05
miR-22-3p	8606.73	2.6	2.06E-05
miR-141	110.19	2.64	5.21E-05
miR-1343-3p	156.62	1.98	1.09E-04
miR-125a	372.51	2.34	1.20E-04
miR-1388-3p	324.67	2.53	1.28E-04
miR-29a	580.34	2.39	1.36E-04
miR-3600	28033.79	1.8	2.79E-04
miR-140	579.98	2.02	4.13E-04
miR-574-3p	897.9	1.66	2.44E-03
miR-140-3p	2437.84	1.96	2.91E-03
miR-1307-3p	310.47	1.39	3.48E-03
miR-3431-3p	96.44	1.9	4.72E-03
miR-425-5p	1754.73	1.59	5.82E-03
miR-92b	7069.65	1	6.43E-03
miR-221	2341.35	1.82	1.04E-02
miR-125b-3p	66.36	1.87	1.20E-02
miR-191	35549.07	1.37	1.28E-02
miR-222-3p	1106.94	1.32	1.37E-02
miR-16b-5p	574.09	1.17	2.17E-02
miR-150	18775.4	1.14	2.87E-02
miR-18a-3p	252.86	1.25	3.08E-02
miR-532	491.04	1.42	3.25E-02

[1] Average normalised counts across all samples
[2] Threshold established at log2(fold change) ≥ |1|
[3] FDR corrected by Benjamini-Hochberg, threshold FDR ≤ 0.05

Table 4.9. Differentially upregulated miRNAs between adult sheep and lambs.

miRNA	average counts[1]	log2(fold change)[2]	FDR[3]
miR-16b	858.46	1.27	3.73E-02
let-7d-3p	1836.91	1.24	3.90E-02

Table 4.10. Differentially downregulated miRNAs between adult sheep and lambs.

miRNA	average counts[1]	log2(fold change)[2]	FDR[3]
let-7f	21326.46	-2.86	0
miR-107	26198.08	-2.59	0
miR-1246	137.57	-2.67	1.37E-07
miR-6119-5p	1499.8	-3.4	1.97E-07
miR-374a-3p	51.39	-3.89	2.81E-07
miR-323c	254.67	-3.08	1.96E-06
miR-196b	53.11	-2.76	1.47E-05
miR-494-3p	80.84	-2.6	2.01E-05
miR-411a-5p	395.06	-2.65	6.36E-05
miR-21-5p	2083.75	-2.79	7.50E-05
miR-3958-3p	198.11	-2.62	1.80E-04
miR-330-5p	106.16	-2.05	4.62E-04
miR-144	417.17	-2.3	4.86E-04
miR-101	1078.57	-2.02	5.55E-04
miR-335	112.9	-1.98	5.85E-04
miR-98	575.55	-2.18	6.89E-04
miR-142-3p	156.79	-2.18	9.71E-04
miR-181b	1565.57	-1.83	1.93E-03
miR-21-3p	451.44	-1.79	2.20E-03
let-7a	6936.09	-1.8	2.51E-03
let-7d	1139.44	-1.72	3.48E-03
miR-103	14259.73	-1.71	3.66E-03
let-7e	99.64	-1.45	4.67E-03
miR-2284ab	52.83	-1.52	6.24E-03
miR-199b	116.08	-1.69	7.31E-03
miR-152	249.52	-1.26	7.31E-03
miR-4448	1271.28	-1.11	7.31E-03

[1] Average normalised counts across all samples
[2] Threshold established at log2(fold change) ≥ |1|
[3] FDR corrected by Benjamini-Hochberg, threshold FDR ≤ 0.05

miR-142-5p	2686.58	-1.64	8.70E-03
miR-345-3p	337.57	-1.97	9.31E-03
miR-194	65.24	-1.62	1.33E-02
let-7e-5p	115.83	-1.5	1.43E-02
miR-23a	3951.25	-1.13	1.64E-02
miR-2478	103.08	-1.76	2.03E-02
miR-151-5p	890.23	-1.1	2.32E-02
miR-126-5p	3471.37	-1.11	2.69E-02
miR-432	59.82	-1.5	3.34E-02
miR-1307-5p	1183.6	-1.12	3.61E-02
miR-126-3p	346.89	-1.12	3.79E-02
miR-181a	26473.75	-1.25	3.90E-02
miR-2284z	66.05	-1.11	4.03E-02
miR-20a	123.39	-1.29	4.17E-02
miR-4634	189.5	-1.19	4.39E-02
miR-4532	418.02	-1.13	4.57E-02

4.2.3.2 Comparison of miRNA expression in adult cases of OPA

The adult sheep samples of study 2 were classified into control, mid-stage OPA and advanced OPA cases, as per **Table 4.5**, to examine miRNA expression changes at different disease stages. Once miRNAs of low abundance had been filtered (section 2.5.1), a total of 200 miRNAs were detected in adult sheep sera. Differences in expression of these 200 miRNAs were explored by means of a PCA plot (**Fig. 4.10**), in which an overlap of samples of all three groups can be seen in the middle region of the plot. By PC1, mid-stage OPA samples were separated from control and advanced samples, which clustered closely towards the right of the plot, this separation was unexpected as a gradient corresponding to disease stage had been predicted. In contrast, by PC2, a gradient of control, mid-stage OPA and advanced OPA samples was observed. This representation suggests that although the disease stage of some animals could potentially be distinguished based on their global miRNA expression, in as much as 50% of the analysed samples, global miRNA expression is not an accurate classifier. Remarkably, the samples in the overlapping region were not the samples that could have been classified in either the mid-stage OPA or advanced OPA groups (i.e., B14, A29

and JA794) (Table 2.3). In the advanced OPA group, the distribution of samples in the PCA plot seemed to correlate with condition score, with lowest condition scores samples seen at the top of the plot (JA811, JA874, JA875) and higher condition scores (A50, G22, B14) seen towards the bottom of the distribution.

In order to further explore differences in miRNA expression, pairwise comparisons were then performed to detect DE miRNAs between groups.

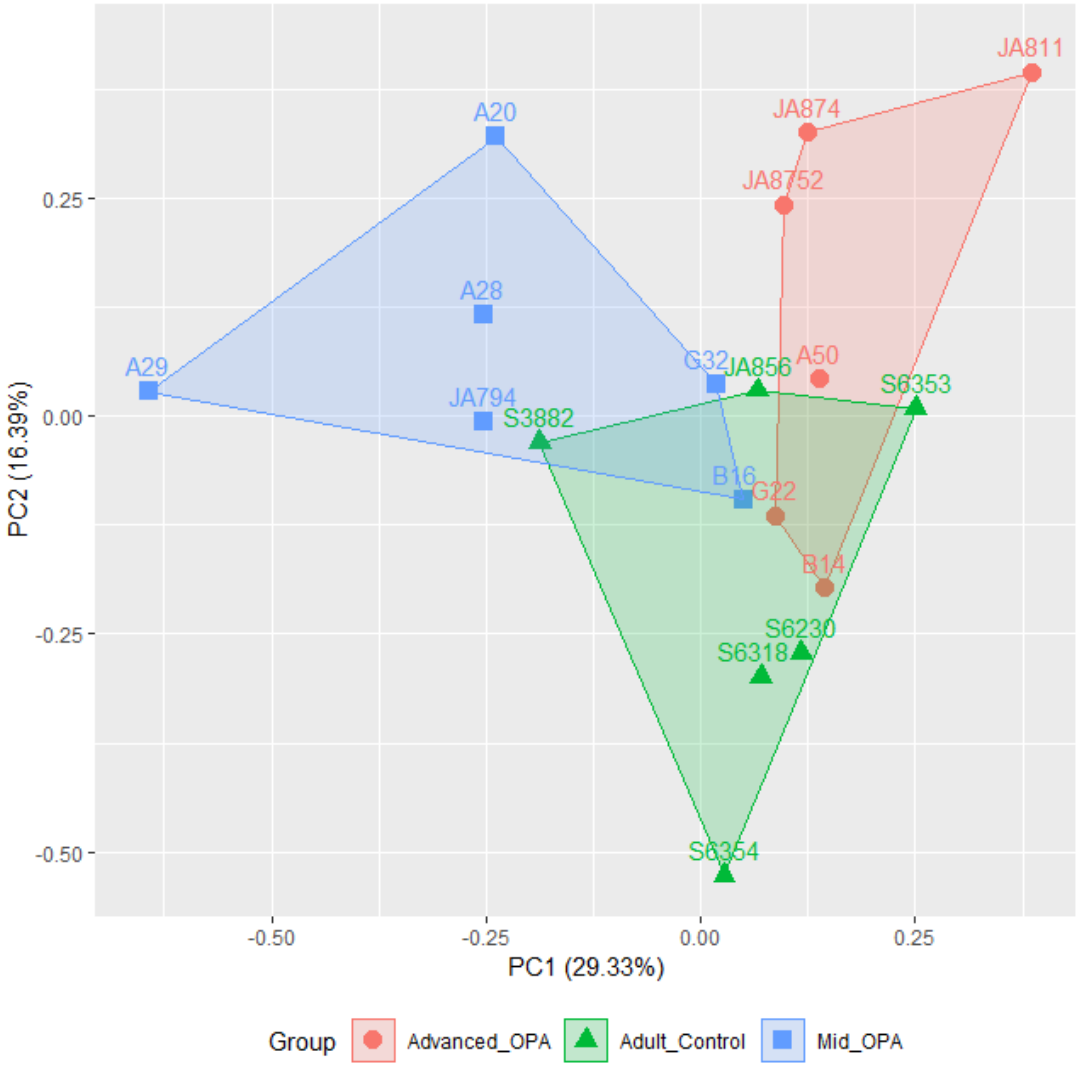

Figure 4.10 PCA plot of miRNA expression levels of adult serum samples in study 2. *Advanced OPA samples (n=6) are represented as red circles, Mid-stage OPA samples (n=6) as blue squares, and adult control samples (n=6) as green triangles. Greater distance between samples in the plot indicates greater expression differences between samples. Although a tendency to form separate clusters can be observed, samples from all three groups overlap in the middle region of the plot.*

1.6.1.1.1 Comparison 1: miRNA expression in advanced OPA cases and controls

Differential expression of miRNAs was assessed in advanced OPA cases and compared to adult controls. Three miRNAs were found to be differentially expressed between the two groups (FDR ≤ 0.05, $\log_2$(fold change) ≥ |1|) (**Fig. 4.11** and **Table 4.11**). However, in all three miRNAs, expression levels in a single sample were found to be substantially higher than in other samples within the same group. In addition, expression levels of these three miRNAs did not result in clustering of samples into two separate groups by disease stage.

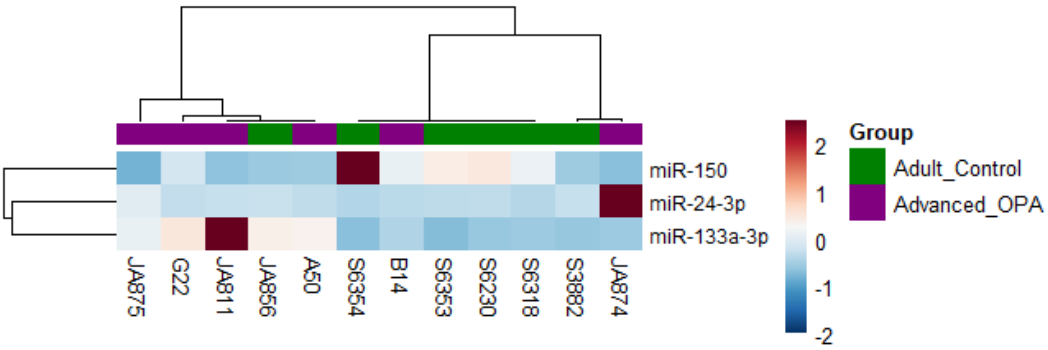

Figure 4.11. Heatmap of DE miRNAs (FDR ≤ 0.05, $\log_2$(fold change) ≥ |1|) between advanced OPA cases and control adults of sequencing study 2. *Dendogram showing correlation clustering of individuals in groups. Legend represents values of log2 fold change.*

Table 4.11. Differentially expressed miRNAs between advanced OPA cases and control adults.

miRNA	average counts[1]	log2(fold change)[2]	FDR[3]
miR-150	16900.70	-1.70	0
miR-133a-3p	247.99	2.12	3.44E-02
miR-24-3p	739.85	2.09	3.60E-02

[1] Average normalised counts across all samples
[2] Threshold established at log2(fold change) ≥ |1|
[3] FDR corrected by Benjamini-Hochberg, threshold FDR ≤ 0.05

1.6.1.1.2 Comparison 2: miRNA expression in mid-stage OPA cases and controls

Differential miRNA expression was then investigated in cases of mid-stage OPA compared to controls. 46 miRNAs were found to be differentially expressed between these two groups. 25 miRNAs were found upregulated and 21 downregulated in mid-stage cases compared to controls (**Fig. 4.12**, **Table 4.12 and Table 4.13**). Although separation of samples in the two clusters observed in the heatmap did not entirely correspond to the two groups, a pattern of miRNA expression in mid-stage OPA compared to controls was present in most of the analysed samples (**Fig. 4.12**). Causes of the unexpected observed clustering were investigated and were not found to be related to time of sample collection, gender or animal origin, and therefore are likely due to inter-individual variation.

Interestingly, these results indicate that there are more dysregulated miRNAs in mid-stage OPA than in advanced OPA when compared to controls. It had been predicted that advanced cases of OPA would present a more distinct miRNA signature when compared to controls, given that they presented overt signs of the disease and greater tumour burden which might be reflected in the circulation. However, the present findings appear to contradict that assumption, discussed further in section 4.3.

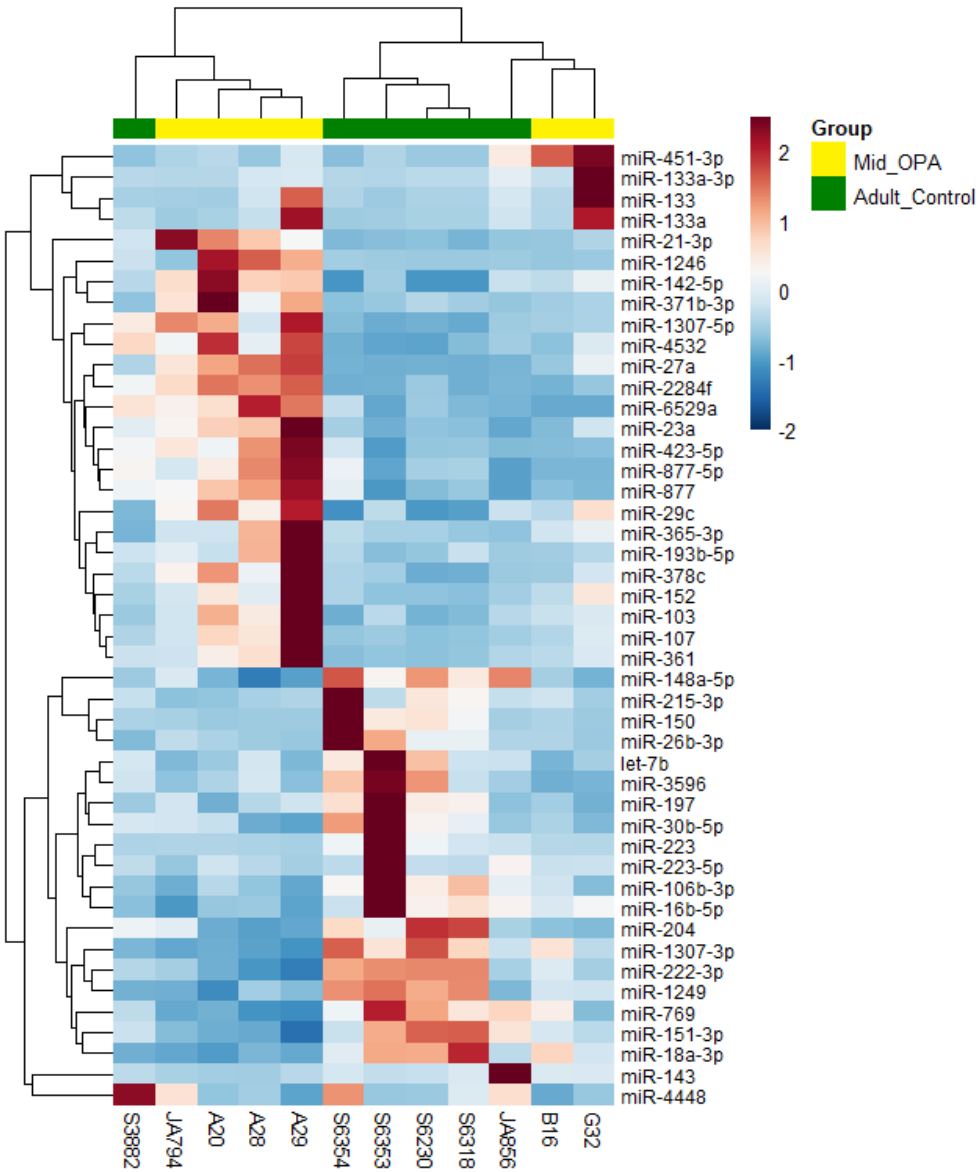

Figure 4.12. Heatmap of DE miRNAs (FDR ≤ 0.05, log_2(fold change) ≥ \|1\|) between mid-stage OPA cases and control adults of sequencing study 2. *Dendrogram showing correlation clustering of individuals in groups. Legend represents values of log2 fold change.*

Table 4.12. Differentially upregulated miRNAs between mid-stage OPA cases and control adults.

miRNA	average counts[1]	log2(fold change)[2]	FDR[3]
miR-423-5p	344864.7	1.04	0
miR-107	26453.58	2.6	0
miR-133a-3p	362.98	2.77	4.64E-10
miR-133a	55.53	2.9	6.70E-09
miR-133	462.55	2.58	2.69E-08
miR-2284f	65.51	2.66	5.12E-07
miR-371b-3p	197	3.75	1.04E-06
miR-1246	157.62	2.9	1.77E-06
miR-451-3p	119.69	1.98	1.19E-04
miR-152	382.3	2.07	3.97E-04
miR-21-3p	618.58	2.35	6.76E-04
miR-4532	566.61	1.73	9.07E-04
miR-27a	5148.23	1.92	2.37E-03
miR-193b-5p	101.28	1.77	3.49E-03
miR-142-5p	3346.18	2.04	7.26E-03
miR-1307-5p	1521.57	1.63	9.36E-03
miR-361	1176.62	1.66	1.05E-02
miR-6529a	18378.31	1.18	1.88E-02
miR-877	452.13	1.28	1.89E-02
miR-378c	360.53	1.69	1.89E-02
miR-103	15123.63	1.82	2.26E-02
miR-23a	4435.29	1.37	2.87E-02
miR-29c	140.62	1.75	2.98E-02
miR-877-5p	643.28	1.1	3.15E-02
miR-365-3p	127.44	1.42	3.45E-02

[1] Average normalised counts across all samples
[2] Threshold established at log2(fold change) ≥ |1|
[3] FDR corrected by Benjamini-Hochberg, threshold FDR ≤ 0.05

Table 4.13 Differentially downregulated miRNAs between mid-stage OPA cases and control adults.

miRNA	average counts[1]	log2(fold change)[2]	FDR[3]
miR-150	15476.01	-2.34	0
miR-223	955.59	-2.69	9.24E-10
miR-223-5p	54.41	-1.78	4.56E-05
miR-204	65.53	-1.95	1.00E-04
miR-106b-3p	871.39	-1.74	1.00E-04
miR-3596	161.25	-1.71	1.35E-04
miR-26b-3p	54.23	-1.88	2.60E-04
miR-215-3p	82.5	-2.16	3.58E-03
miR-143	4105.04	-1.76	8.43E-03
let-7b	717.74	-1.27	9.09E-03
miR-197	852.69	-1.04	9.80E-03
miR-30b-5p	452.84	-1.12	9.82E-03
miR-222-3p	1094.35	-1.38	1.27E-02
miR-16b-5p	549.89	-1.38	1.55E-02
miR-1249	70.51	-1.47	1.89E-02
miR-769	783.65	-1.22	1.89E-02
miR-1307-3p	302.01	-1.54	2.62E-02
miR-18a-3p	247.63	-1.36	2.93E-02
miR-151-3p	1581.25	-1.18	3.53E-02
miR-4448	564.14	-1.3	3.89E-02
miR-148a-5p	115.04	-1.11	4.10E-02

[1] Average normalised counts across all samples
[2] Threshold established at log2(fold change) ≥ |1|
[3] FDR corrected by Benjamini-Hochberg, threshold FDR ≤ 0.05

1.6.1.1.3 Comparison 3: miRNA expression in advanced OPA cases and mid-stage OPA cases

Differences in miRNA expression were also compared between advanced OPA cases and mid-stage cases. 19 miRNAs were found to be DE between groups, of those, ten were upregulated and nine downregulated in advanced cases compared to mid-stage ones (**Fig. 4.13**, **Table 4.14 and Table 4.15**). Surprisingly, two separate clusters corresponding to the disease stages were seen, although no separate clustering had been observed in advanced OPA cases and controls.

Nevertheless, high variability in miRNA expression levels was observed within groups (**Fig. 4.13**).

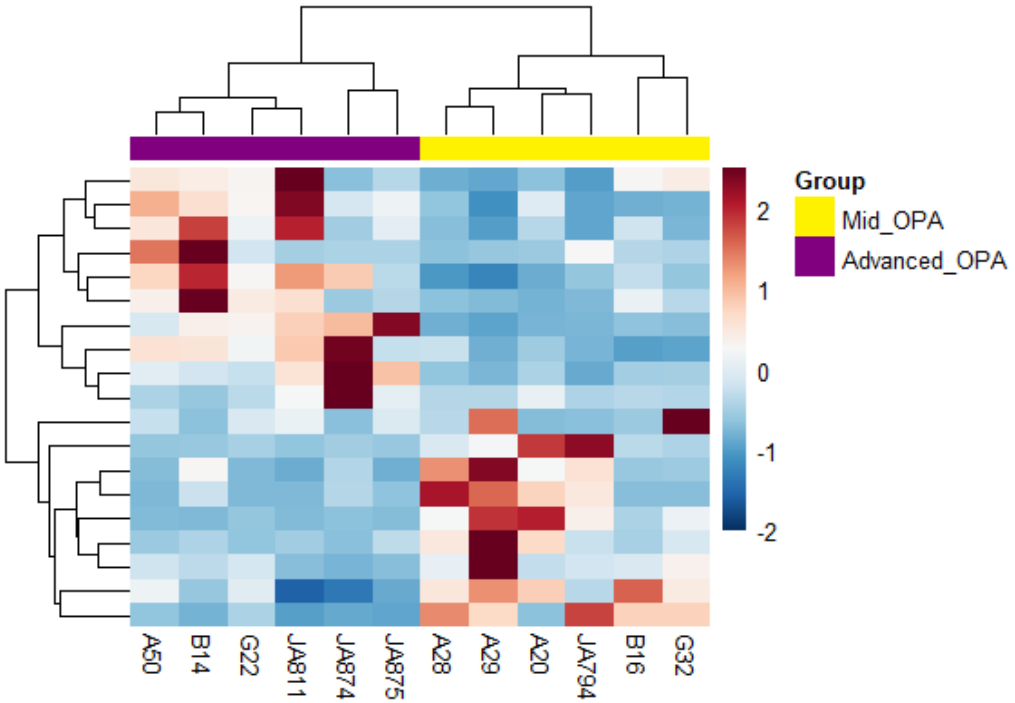

Figure 4.13. Heatmap of DE miRNAs (FDR ≤ 0.05, log_2(fold change) ≥ \|1\|) between advanced OPA cases and mid-stage OPA cases of sequencing study 2. *The dendogram shows correlation clustering of individuals in groups. Legend represents values of log2 fold change.*

Table 4.14. Differentially upregulated miRNAs between advanced OPA cases and mid-stage OPA cases.

miRNA	average counts[1]	log2(fold change)[2]	FDR[3]
miR-451	51056.13	1.27	0
miR-223	752.53	2.28	3.33E-04
miR-223-5p	76.07	2.38	6.25E-04
miR-3596	172.92	1.84	2.88E-03
miR-425-3p	107.08	1.56	1.18E-02
let-7g	1764.66	1.62	1.19E-02
miR-204	51.52	1.49	1.64E-02
miR-106b-3p	861.84	1.72	1.64E-02
miR-222-3p	1326.34	1.75	2.14E-02
miR-18a-3p	363.26	2.08	2.17E-02

[1] Average normalised counts across all samples
[2] Threshold established at log2(fold change) ≥ |1|
[3] FDR corrected by Benjamini-Hochberg, threshold FDR ≤ 0.05

Table 4.15. Differentially downregulated miRNAs between advanced OPA cases and mid-stage OPA cases.

miRNA	average counts[1]	log2(fold change)[2]	FDR[3]
miR-2904	2132.94	-3.99	0
miR-215	15159.64	-1.17	0
miR-6529a	16000.8	-1.97	0
miR-10b	27396.94	-1.25	0
miR-107	28481.7	-1.98	0
miR-423-5p	323008.2	-1.35	0
miR-133	581.84	-1.1	4.42E-03
miR-4532	454.47	-4.54	1.96E-02
miR-203b-5p	62.99	-2.45	3.76E-02

[1] Average normalised counts across all samples
[2] Threshold established at log2(fold change) ≥ |1|
[3] FDR corrected by Benjamini-Hochberg, threshold FDR ≤ 0.05

4.2.3.3 miRNA expression in lambs with experimentally-induced OPA

A total of 198 miRNAs were detected in the serum of lambs, once low abundance miRNAs had been removed. As before, PCA was performed and plotted to identify differences between groups (**Fig. 4.14**). Greater within-group variation than between-group variation was observed. However, a trend towards separate clusters could be observed in the PCA plot with overlapping between groups caused by the miRNA expression pattern of one individual of each group: SPF15 and SPF22. This apparent overlapping did not appear to be directly related to the number of viral counts, library size or pathological findings (**Table 2.2**).

Differential expression analysis was then performed and revealed four miRNAs DE between Early OPA samples and controls (**Fig. 4.15** and **Table 4.16**). Clustering of samples did not identify two separate groups corresponding to OPA affected lambs and controls.

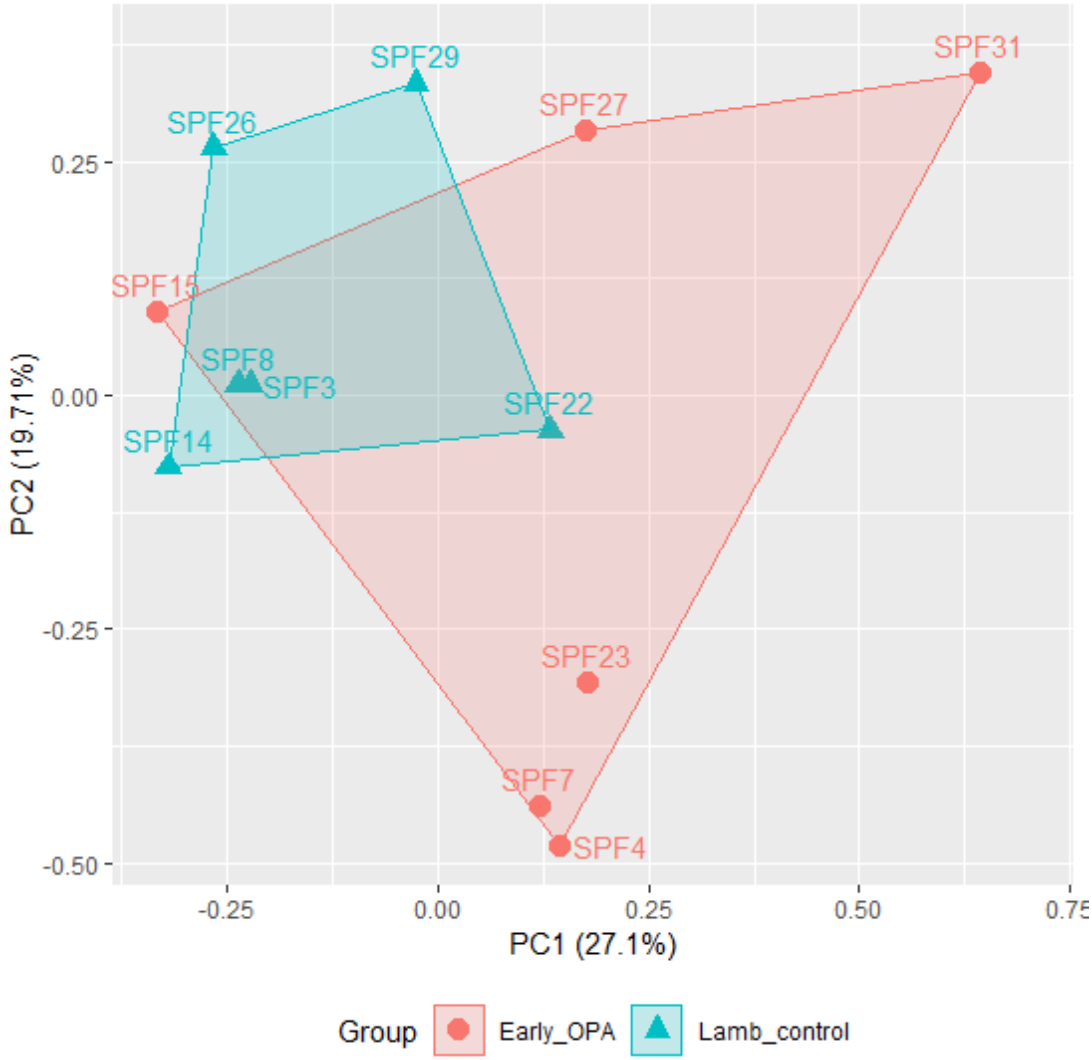

Figure 4.14. PCA plot of miRNA expression levels of early OPA and controls samples from sequencing study 2. *Early OPA samples (n=6) are represented as red circles and control lambs (n=6) as turquoise triangles. Greater distance between samples in the plot indicates more expression differences between samples. Early OPA samples are seen clustering towards the right of the plot, whereas controls can be seen towards the left of the plot. The PCA plot presents a slight overlapping between the two groups tested.*

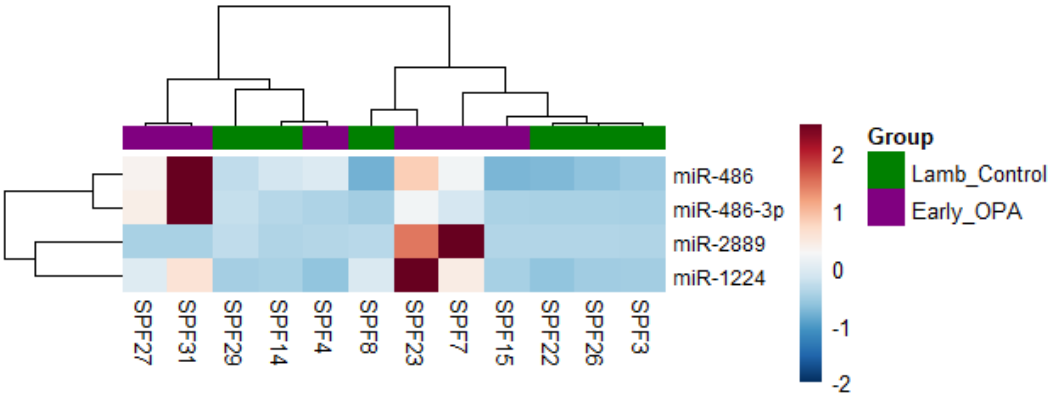

Figure 4.15. Heatmap of DE miRNAs (FDR ≤ 0.05, log2(fold change) ≥ |1|) between advanced OPA cases and mid-stage OPA cases of sequencing study 2. *Dendogram showing correlation clustering of individuals in groups. Legend represents values of log2 fold.*

Table 4.16 Differentially expressed miRNAs between early OPA cases and control lambs.

miRNA	average counts[1]	log2(fold change)[2]	FDR[3]
miR-486	4272554.10	1.54	0
miR-2889	1318.38	3.38	2.85E-03
miR-1224	53.67	2.61	2.74E-02
miR-486-3p	555.46	2.51	3.66E-02

[1] Average normalised counts across all samples
[2] Threshold established at log2(fold change) ≥ |1|
[3] FDR corrected by Benjamini-Hochberg, threshold FDR ≤ 0.05

4.2.3.4 Comparison of differentially expressed miRNAs between disease stages in serum

Having analysed changes in miRNA expression at each disease stage compared to control samples, common DE miRNAs in all disease stages were investigated by contrasting the results of the three comparisons. No miRNAs were found to be differentially expressed in all disease stages. Nevertheless, both advanced and mid-stage cases of OPA showed significantly increased levels of miR-133a-3p and reduced levels of miR-150 when compared to controls, although this was not reflected in all samples.

Interestingly, 20 miRNAs were found to be dysregulated both in mid-stage OPA cases compared to adult controls, and in adult controls compared to lambs. Of those, 19 miRNAs (miR-223, miR-150, miR-215-3p, miR-143, miR-197, miR-1307-3p, miR-1249, miR-16b-5p, miR-222-3p, miR-18a-3p, miR-1307-5p, miR-4532, miR-103, miR-107, miR-1246, miR-142-5p, miR-152, miR-21-3p, miR-23a) had increased expression levels in mid-stage OPA and lambs compared to adult controls. miR-150 showed increased expression in advanced OPA cases, mid-stage OPA cases and control lambs compared to adult sheep. These increased levels in lambs might contribute to the different pattern of miRNA dysregulation observed in Early OPA compared to other stages. Nevertheless, to investigate this effect further it would be necessary to source early cases of OPA in adult sheep, a challenging task due to the long asymptomatic period of OPA (section 1.1.2).

Comparison of DE miRNAs between the initial sequencing (study 1) and the present results (study 2) revealed common dysregulated miRNAs. Given that the three samples from sequencing study 1 belonged to 2 different OPA groups: mid-stage OPA (B16 and G32) and advanced stage OPA (B14), the results were compared to both mid-stage cases of OPA and to advanced cases of OPA from study 2. Thirteen miRNAs were commonly dysregulated between mid-stage OPA cases and adult controls in both sequencing runs. Of those, six miRNAs were upregulated (miR-107, miR-103, miR-133a, miR-451-3p, miR-133, miR-133a-3p), four miRNAs were downregulated (miR-215-3p, miR-4448, miR-150, miR-1249), and three miRNAs presented opposed levels of expression (miR-4532, miR-1246, miR-18a-3p). miR-150 and miR-133a-3p were also dysregulated in advanced cases of OPA. miR-486 and miR-486-3p were found upregulated both in study 1 and in early cases of OPA compared to lamb controls.

Since only ten miRNAs were found dysregulated and following the same expression pattern between both sequencing runs, the biological relevance of the present results was questioned. Factors such as technical repeatability and the effect of sample size and, thus, increased biological variation were considered and further explored (**4.2.4**).

4.2.4 Comparison of results between two sequencing runs

Considering that the six initial samples sequenced in study 1 were also included in study 2, the data statistics were compared for those six samples between both runs. The aim of the comparison was to investigate the effect of technical repeatability in the sequencing results.

Samples S6230, S6318, S6354, B14, B16 and G32 from both runs were compared. Initially, library sizes and percentage of reads mapping to miRBase and other categories were compared between sequencing study 1 and study 2 (**Table 4.17 and Table 4.18)**. No statistically significant differences were found between the two runs in library size, selected length, percentage of reads mapped to miRBase or reads mapped to viral genome (t-student test $p<0.05$).

Having found no significant differences in sequencing statistics between both runs, the normalised counts of the ten top differentially expressed miRNAs (five most upregulated and five most downregulated) between OPA cases and controls in study 1 were compared to their numbers in study 2 (**Table 4.19**). Generally, normalised counts were higher in sequencing study 1. No statistical differences were found in the normalised counts between sequencing runs in seven out of the ten miRNAs. However, three miRNAs (miR-146a, let-7e, and miR-455-5p) were found to have statistically different counts across samples between both sequencing runs. Interestingly, the average normalised counts of these miRNAs were the lowest of the selected miRNAs and in study 2 were filtered out due to low counts, suggesting that these DE signals could be an artefact of sequencing noise.

Considering the miRNA fold changes between groups in the two sequencing runs, it could be seen that only seven miRNAs followed the same trend, and of those four showed differences in fold change levels of greater than 50% in value. These findings imply that in addition to the increased biological variation introduced with having more samples in sequencing study 2, technical sequencing repeatability also contributed to the results observed. Nevertheless, six of the top ten dysregulated miRNAs were found to DE in mid-stage cases of OPA of study 2, and two in advanced cases, indicating that focusing on miRNAs with the highest

fold changes and higher numbers of counts might permit biologically relevant signals to be discriminated from background noise. The biological roles of these miRNAs will be further discussed in section 4.3.

Table 4.17. Comparison of read categories between sequencing study 1 and study 2. Average of six samples.

		average (study 1)	average (study 2)
	Total reads	43906402	37189291
Total reads (%)	**(17-28nt)**	37.68	42.81
	Too short	26.73	22.46
	Too long	35.59	34.74
Percentage of selected reads (%)	**miRBase**	62.76	64.18
	cDNA	3.54	2.92
	snRNA	0.07	0.04
	Mt_rRNA	0.01	0.00
	snoRNA	0.19	0.06
	Mt_tRNA	0.01	0.01
	rRNA	0.13	0.06
	misc_RNA	1.97	3.60
	miRNA	1.24	1.21
	lincRNA	2.13	1.12
	JSRV genome	0.00	0.00
	DNA	19.40	15.73
	Unmapped	8.55	11.07

Table 4.18. Comparison of read categories between samples of both sequencing runs.

	Sheep ID	6230[1]	6230[2]	6318[1]	6318[2]	6354[1]	6354[2]	B14[1]	B14[2]	B16[1]	B16[2]	G32[1]	G32[2]
	Total reads (x10^7)	4.41	2.85	4.37	3.82	4.63	2.96	4.13	4.33	5.03	3.62	3.76	4.73
(%) total	**(17-28nt)**	23.94	38.96	27.30	49.13	23.81	21.20	47.67	45.51	52.08	55.32	51.28	46.72
	Too short	20.64	26.18	33.27	14.75	26.87	27.39	29.44	12.11	30.89	24.46	19.29	29.86
	Too long	55.42	34.86	39.43	36.12	49.32	51.42	22.89	42.37	17.04	20.22	29.43	23.43
(%) selected reads	**miRBase**	47.32	59.01	56.88	72.86	39.48	28.43	81.44	73.15	76.45	77.23	75.00	74.42
	cDNA	4.11	3.20	4.76	2.32	6.85	4.88	2.05	1.32	2.06	2.56	1.41	3.25
	snRNA	0.13	0.05	0.07	0.03	0.10	0.08	0.03	0.02	0.03	0.02	0.03	0.04
	Mt_rRNA	0.01	0.00	0.01	0.00	0.02	0.00	0.02	0.01	0.01	0.01	0.01	0.01
	snoRNA	0.47	0.10	0.14	0.05	0.28	0.12	0.12	0.04	0.04	0.03	0.07	0.04
	Mt_tRNA	0.02	0.01	0.01	0.00	0.02	0.00	0.01	0.00	0.01	0.01	0.01	0.02
	rRNA	0.23	0.08	0.09	0.03	0.15	0.13	0.21	0.04	0.04	0.03	0.03	0.06
	misc_RNA	2.78	7.57	2.73	3.16	3.39	7.47	1.29	0.75	0.83	1.01	0.82	1.62
	miRNA	1.08	1.35	1.04	1.34	0.99	0.75	1.22	1.47	1.34	1.10	1.75	1.22
	lincRNA	3.72	1.23	3.60	1.68	2.46	1.71	0.85	0.26	1.14	0.68	0.99	1.14
	JSRV	0.00	0.00	0.01	0.00	0.01	0.00	0.00	0.00	0.00	0.00	0.00	0.00
	DNA	27.92	16.02	20.45	11.72	32.41	35.68	6.81	7.23	13.88	11.21	14.94	12.53
	Unmapped	12.19	11.37	10.21	6.81	13.85	20.74	5.95	15.72	4.19	6.12	4.93	5.66

[1] Samples of sequencing study 1
[2] Samples of sequencing study 2

Table 4.19. Normalised counts of the top ten DE miRNAs in sequencing study 1 and comparison to study 2.

	Study 1							Study 2						
	Log_2 (FC)	**S6230**	**S6318**	**S6354**	**B14**	**B16**	**G32**	**Log_2 (FC)[1]**	**S6230**	**S6318**	**S6354**	**B14**	**B16**	**G32**
miR-150	-2.58	64503.74	19284.44	60351.36	9250.64	9193.28	5594	-1.99	26541.11	19393.08	72187.65	18578.93	6657.51	4420.67
miR-4532	-2.45	128.96	36.53	114.79	48.66	0.00	2.55	1.32	28.68	163.08	98.31	11.88	183.89	530.75
miR-146a	-2.38	280.69	87.04	261.71	57.00	19.46	44.22	0.92	4.41	9.09	0.00	2.64	9.61	13.35
let-7e	-2.30	251.43	417.99	318.34	57.00	64.57	79.09	-0.43	33.83	34.43	74.98	59.42	26.99	19.59
miR-455-5p	-1.95	102.95	36.53	102.54	6.95	31.84	23.81	-2.04	22.06	6.22	11.66	0.00	6.86	2.84
miR-425-3p	2.16	13.00	29.01	13.77	62.56	112.33	74.84	-0.52	51.48	36.82	41.66	5.28	46.66	38.62
miR-133a	2.63	69.36	23.64	62.75	11.82	85.79	864.02	4.10	8.83	7.65	0.00	3.96	14.18	263.81
miR-451-3p	3.10	69.36	70.92	32.14	215.49	347.60	912.49	5.02	19.86	20.56	0.00	378.97	397.51	531.61
miR-133	3.16	286.11	250.36	146.93	221.05	472.31	5423.92	2.99	108.11	102.34	128.30	73.95	150.04	2464.64
miR-133a-3p	4.76	167.98	214.90	16.84	106.35	421.90	10303.57	1.41	48.54	57.87	19.99	104.32	119.39	3116.08

[1] Log_2 (fold change) calculated considering the six samples listed in the table.

4.2.5 Differentially expressed miRNAs in serum and lung tissue

Expression of miRNAs found to be DE in more than one of the serum datasets was compared to DE miRNAs in the tissue datasets discussed in Chapter 3. These miRNAs were: miR-107, miR-103, miR-133a, miR-451-3p, miR-133, miR-133a-3p, (upregulated in mid-stage or advanced OPA); miR-215-3p, miR-4448, miR-150, miR-1249 (downregulated in mid-stage or advanced OPA); miR-486 and miR-486-3p (upregulated in early OPA).

None of the aforementioned miRNAs were found to be DE in lung tissue of OPA-affected animals compared to controls nor in LCM tissue. However, miR-150 was found to be downregulated in BALF $CD14^{+}$ macrophages of OPA-affected sheep compared to controls. These results suggest that miRNA expression detected in the serum of OPA-affected sheep is not directly related to tumoural miRNAs. Indeed, having found miR-150 in common suggests that some of the DE miRNAs in serum might be related to other changes occurring in OPA affected sheep, such as immune responses. The roles of miR-150 are reviewed in section 4.3. Taking into consideration that miR-150 was also found upregulated in lamb's serum compared to adult's serum, the fact that no miRNAs are found DE both in serum and tissue could be, in part, related to age differences. On the other hand, given the number of comparisons performed in this study and the great number of miRNAs analysed, some miRNAs could be expected to appear DE in multiple datasets by chance.

Of the nine miRNAs further studied in tissue none were found DE in serum. miR-182, miR-205 and miR-21 were detected in serum sequencing data; miR-31, miR-183, miR-503 and miR-200b were detected but below the established threshold of abundance for DE analysis; miR-96 and miR-135b were not detected.

4.2.6 Sequencing reads in sheep serum mapping to the JSRV genome

Sequencing reads of length between 17-28 nt mapping to the genome of JSRV (AF105220.1) were analysed. In study 1, no differences were observed between

samples of the control and OPA groups. All reads from both groups mapped to the viral genome first 1000 nt, specifically between 128-178 nt and 620-645 nt, corresponding to the end of the LTR region and beginning of the *gag* gene. Nevertheless, these reads could have originated from enJSRV copies in the sheep genome. Indeed, the 128-178 nt region of JSRV is almost identical, with only one mismatch, to the 446-496 nt region of enJSRV (EF680301.1). The 620-645 nt region was not found to be identical to this enJSRV provirus. However, the fact that both infected and uninfected sheep had reads in this region suggests that the presence of those reads is not JSRV related; the origin of those reads might be other enJSRV copies in the sheep genome.

Similarly, in sequencing study 2, reads were found that map to the same regions of the JSRV genome mentioned above. A slight increase in reads mapping areas of the JSRV genome between 2000-7000 nt was observed in OPA-affected animals. However, differences are not likely to be meaningful due to the low number of reads, which in all cases did not add to 10 reads. JA874 showed an increase in reads mapping to the JSRV genome compared to other samples of the OPA-affected group. Nevertheless, the reads were scattered across the viral genome, and the number of reads in each region was lower than 5. Interestingly, JA874 did not show differences in number or percentage of RNA mapped to the viral genome compare to the other samples. This finding might be an indication of the sample being more degraded.

No reads in the 6400 nt region, investigated as a candidate miRNA in Chapter 3, were found in any of the samples. As expected, fewer reads were found to map to the JSRV genome compared to tissue samples discussed in Chapter 3.

4.3 Discussion

Previous studies in mice, humans and other species have investigated the potential exploitation of circulating miRNAs as diagnostic markers for disease (section 1.5.12). In this chapter, experiments were performed to profile circulating miRNAs in sheep and to identify miRNA species associated with OPA.

Two sequencing studies were performed. In the first, performed with two groups of three sheep, miRNAs were identified in sheep sera, and differences in expression detected between OPA-affected and control sheep. This provided the basis for a larger analysis performed by sequencing small RNA from the sera of 30 sheep, including animals of differing OPA disease states and from adults and lambs. Analysis of the data found interesting trends relating to the pattern of miRNA expression in the different groups, but did not identify miRNAs that are DE in all stages of OPA.

In order to assess miRNA expression changes at different stages of OPA, pairwise comparisons were performed. Initially, DE miRNAs were found between lambs and adult sheep, indicating that miRNA expression comparisons should be performed within age groups. Similarly to study 1, differentially expressed miRNAs were found between OPA and control cases, but no miRNA was found to be dysregulated at all stages of the disease. Similarities in DE miRNAs were found in advanced and mid-stage cases of OPA, relative to adult controls. Nevertheless, care should be taken when analysing the data due to relative low counts of some miRNAs, which might render their detection more influenced by background noise, and due to high within-group variability. Ten miRNAs were found differentially expressed in both study 1 and study 2.

At the outset of the present study, it was anticipated that advanced OPA cases would have more DE miRNAs than mid-stage disease, relative to controls. Indeed, this prediction was based on published studies that found that miRNA dysregulation varies depending on disease stage, for instance miR-21 has been found to be downregulated at initial stages and upregulated in more advanced cases of lung cancer (reviewed by Zheng et al (2018)), and expression of certain miRNAs has been used as prognostic marker. Nevertheless, the fact that no miRNAs were found to be consistently DE in all disease stages, and that only ten

miRNAs were DE in both study 1 and study 2, suggested that either biological variation and small sample size, or technical factors were contributing to the inconsistencies observed. The small sample size of the study might have reduced the power to detect DE miRNAs in samples with background noise and high biological variation.

Technical repeatability was assessed by comparing six samples sequenced in both studies, and given the variation observed in the top 10 DE miRNAs, found to influence the results. Indeed, several reports have argued that besides small sample size, technical factors contribute to the inconsistencies and variation observed in miRNA literature (sections 1.5.11 and 1.5.12). In addition, differentially expressed miRNAs with low fold changes between groups might be more difficult to validate and influenced by background noise to a greater degree, particularly in samples with low RNA concentration such as serum. In a study, six serum miRNAs with low fold change and p-adjusted value close to threshold failed to validate in the same samples using qPCR (Fernandez-Costa et al, 2016).

Indeed, low RNA concentration and background noise might have also influenced the read mapping to different small RNA categories, which was highly variable between samples.

To extend this study, and overcome some of the aforementioned limitations, it would be necessary to include a large number of animals per group. In many human studies around 100 samples have been used to identify miRNA signatures. Performing such a study in sheep would be expensive, but the cost could possibly be reduced by pooling samples for library preps. The pooling approach would involve losing some resolution of individual animals, but would allow obtaining higher RNA concentrations. In addition, if promising OPA-associated miRNAs had been identified, further validation could be performed by assaying expression of those miRNAs by RT-qPCR in archived serum samples. Shaughnessy et al. have previously reported stability of miRNA in frozen samples (Shaughnessy et al, 2015).

4.3.1 Comparison to human serum lung cancer studies

Data obtained in this chapter was compared to studies in human lung cancer to draw similarities between the two diseases. Taking into consideration the high variability observed in the results of this chapter, only miRNAs with the highest fold change values between OPA-affected and control sheep, DE in more than one of the analysed datasets, are reviewed here: upregulated miRNAs (miR-107, miR-103, miR-133a, miR-451, miR-133, miR-486) and downregulated miRNAs (miR-215, miR-4448, miR-150, miR-1249).

miRNAs miR-103 and miR-107 are paralogous members of the miR-15 family, which includes miR-503. A limited number of studies has investigated dysregulation of these miRNAs. In lung cancer, they have been reported to act as tumour suppressors (Takahashi et al, 2009). A report found that miR-107 was upregulated in plasma of NSCLC patients with EGFR mutations (Qu et al, 2017), whereas miR-103 was upregulated in serum of early stage adenocarcinoma patients (Lv et al, 2017).

miR-133 is considered a tumour suppressor in lung cancer, which targets include *IGF-1R*, *TGFBR1*, *EGFFR* (Wang et al, 2014a). A study reported that miR-133 was downregulated in serum and tumour tissue of NSCLC (Petriella et al, 2016). miR-133 was found to be the most common upregulated miRNA in airway epithelial cells (Chen et al, 2018).

miR-451 is highly expressed in erythrocytes and involved in erythrocyte differentiation and formation of epithelial cell basolateral polarity (Wang et al, 2011) (Pan et al, 2013). miR-451 is considered a tumour suppressor in lung cancer, and targets *RAB14*, member of the Ras family (Wang et al, 2014b; Wang et al, 2011; Yin et al, 2015). It has been found downregulated in NSCLC tissue, but in a study authors saw no changes in plasma expression levels (Markou et al, 2013). miR-451 targets *c-myc* and *MIF* which accelerates tumour growth by inducing MAPK, PI3K/Akt pathways (Goto et al, 2017).

Downregulation of miR-486 was observed in lung tumour tissue of stage I adenocarcinoma patients (Yu et al, 2010a). A meta-analysis that reviewed 20 studies on miRNA expression in serum of lung cancer patients found miR-486

downregulated as part of a 15-miRNA predictive signature (Vosa et al, 2013). This meta-analysis highlighted that studies performed in smaller number of patients tended to diverge more from the proposed signature (Vosa et al, 2013).

No studies have investigated the expression of miR-215 in circulation of lung cancer patients and just a few have addressed its expression in lung cancer tissue. miR-215 was found downregulated in NSCLC lung cancer tissue (Cai et al, 2017b; Hou et al, 2015). A study related its downregulation with metastasis of NSCLC (Yao et al, 2018). miR-215 is considered a tumour suppressor, induced by p53 (Hou et al, 2015) and some of its validated targets are *ZEB2*, and *MMP16* (Burke et al, 2015; Yao et al, 2018). No studies have investigated miR-4448 expression in serum or lung cancer.

miR-150 is considered an immunomodulatory miRNA (Kroesen et al, 2015) and has been investigated in the context of both lung cancer and viral infections. Most studies of miR-150 expression in lung cancer have focused on tissue expression and found that is commonly upregulated in lung cancer tissue compared to normal tissue (Cao et al, 2014; Li et al, 2016; Wang et al, 2013; Zhang et al, 2013a). Only one study found miR-150 downregulated in NSCLC (Sun et al, 2013). miR-150 targets the tumour suppressors *TP53*, *FOXO4* and *SRCIN1*, and activates Src/Ras/ERK pathways (Cao et al, 2014; Li et al, 2016; Zhang et al, 2013a). In a study in serum of NSCLC patients, miR-150 was found to be predictive of relapse as part of a 5 miRNA signature (Zhang et al, 2018), and enriched in extracellular vesicles produced by four NSCLC cell lines (Lawson et al, 2017). In the context of viral infection, it was found to be downregulated in HIV-1 patients (Moghoofei et al, 2018) (Chiang et al, 2012) and was predictive of disease progression in plasma (Munshi et al, 2014). Downregulation of miR-150 was suggested to occur after CD4+ T cell activation and facilitate HIV-1 infection (Chiang et al, 2012; Munshi et al, 2014). In contrast, downregulation of miR-150 was linked to better protection levels against acute viral infection by Lymphocytic choriomeningitis virus (LCMV) (Chen et al, 2017).

miR-1246 expression in lung cancer has been investigated in a limited number of studies. These studies found that miR-1246 is upregulated in NSCLC tissue and found that it was required for tumour initiation and metastasis (Kim et al, 2016;

Zhang et al, 2016). miR-1246 was also found upregulated in serum of stage I-III NSCLC compared to healthy controls (Zhang et al, 2016).

Although most literature on the differentially expressed miRNAs in human lung cancer seems to describe findings opposed to the ones found in this chapter, it has to be considered that most studies in lung cancer have examined lung cancer tissue samples and not circulating miRNAs. Studies that have examined both tissue samples and plasma or serum have sometimes reported dysregulation in opposite directions (Markou et al, 2013). In addition, some studies considered in this discussion have shown how type of mutation, stage, prognosis and other factors can be predicted in circulating miRNA signatures, suggesting that they might influence the circulating miRNAs detected. Moreover, the infectious nature of OPA needs to be taken into account when comparing findings to human lung cancer. miR-150, for instance showed different dysregulation in lung cancer than viral infections, and JSRV and the host response might play an important role in the dysregulated miRNAs observed. In addition, human studies are usually performed in large cohorts of patients which are not always available in animal studies, limiting the power and reproducibility of the studies.

4.3.2 Comparison with lung tissue results

Of the miRNAs DE in serum datasets of either study 1 or study 2, none were found DE in lung tissue of OPA-affected animals. One miRNA, miR-150 was found to be differentially downregulated in both BALF $CD14^{+}$ macrophages and natural cases of OPA.

Although it was initially expected to observe more DE miRNAs in advanced OPA cases than mid-stage cases, as well as similarities in DE miRNAs between serum and lung tissue of OPA-affected sheep, a number of factors could be related to the observed result. Unlike tissue samples, serum composition might be influenced by several aspects of the individual, causing them to be more complex to analyse and differentiate background noise from signals that reflect tumour presence. Circulating miRNAs remain poorly understood and its origin remains largely unknown. A study on the levels of circulating miRNAs found that 66% of them reflected tissue levels of expression, whereas levels of other miRNAs were

enriched in circulation and other miRNAs were retained in cells and not released to the circulation (Pan et al, 2013). In addition, factors that have an impact in circulating miRNA levels are yet to be studied. Other authors have also reported that miRNAs dysregulated in tissue were not found in serum (Petriella et al, 2016).

Enrichment of RNAs of 30-32 nt was observed in serum samples, which had not been observed in lung tissue sequencing, these could correspond to piwi-interacting RNAs (piRNA). piRNAs are small non-coding RNAs that have also been investigated as cancer biomarkers (Cheng et al, 2011; Martinez et al, 2015; Umu et al, 2018), but although these were present in greater abundance in control samples from study 1, in study 2 no differences were observed between groups. These findings might indicate that the enrichment of a 30-32 nt RNA population might be an artefact from sequencing. Upon reviewing the mapping of reads of 30-32 nt obtained from serum samples, only a small proportion of reads (0.08-4.4%) mapped to piRNAs, while most corresponded to long non-coding RNA or tRNA fragments. The higher abundance of these fragments in serum samples compared to tissue samples might be due to a higher level of RNA degradation in serum samples. These findings are in accordance with some reports, which have suggested that sequences of 30-32 nt have sometimes been wrongly catalogued as piRNAs and are likely to represent ubiquitous background from sequencing data (Genzor et al, 2019; Tosar et al, 2018).

4.3.3 Sequencing reads mapping to the JSRV genome

Sequencing reads that mapped to JSRV were low amongst all samples, and no differences were observed between OPA-affected sheep and controls. The enrichment of reads mapping to the 6400 nt region of the JSRV genome seen in lung tissue and $CD14^+$ samples was not observed in the serum datasets. The reason for these findings might be the expected lower concentration of JSRV in serum compared to lung tissue.

4.3.4 Cell-free miRNAs in lung fluid

In a pilot study, examination of OPA-related miRNA signatures was performed in lung fluid, to investigate other potential sources of biomarker detection. miRNA expression was detected in lung fluid of seven natural OPA cases. However,

expression levels of the four tested miRNAs were low and they did not correlate with miRNA expression in matched lung tissues (data not shown).

Other miRNAs could be tested to investigate significant correlations to lung tissue expression. Nevertheless, sheep that produce lung fluid are already presenting a pathognomonic sign of OPA thus, testing miRNA expression in lung fluid is not likely to render a biomarker with potential to be used as diagnostic. Nasal swabs could be investigated as minimally invasive tests for OPA biomarker miRNAs. In order to explore this possibility, miRNA patterns of expression and stability would first have to be investigated in nasal swabs from OPA-affected sheep and controls.

4.3.5 Conclusions

This first look at miRNA expression in OPA sheep sera has provided valuable information on the diversity of miRNA expression in sheep sera. Throughout this chapter, miRNA expression has been detected in serum of OPA affected and control sheep, and a trend towards group separation based on miRNA expression has been observed. However, extracting a miRNA signature related to OPA from the data presented here was challenging: DE miRNAs in OPA-affected sheep were identified but found to be inconsistent across datasets. In addition, they did not correlate with miRNA lung tissue expression. These findings are largely due to the nature of the sample analysed, in which low RNA concentration is liable to be affected by background signals. Background noise increases the challenge of differentiating biologically relevant signals from artefacts of the method.

Some studies have examined miRNA signatures in the circulation of other ruminant species. Those studies, also had small sample sizes and reported within-group variability in small-RNA composition (Farrell et al, 2015; Shaughnessy et al, 2015; Zheng et al, 2014).

Considering the large number of research studies examining miRNAs as circulating biomarkers, and their sometimes contradictive findings, it seems that the background noise and limitations of the present study are common. The great promise of miRNAs as biomarkers might need to be reassessed to be applied in clinical or field settings. A remarkable effort in understanding circulating miRNAs

as clinical markers has been performed in recent years by members of the Extracellular RNA Communication Consortium (ERCC). The ERCC was established to investigate extracellular vesicles and extracellular RNAs, and their potential role in intercellular communication and possible clinical applications (Das 2019). One of the aims of the ERCC is to establish a catalogue of extracellular RNAs present in biofluids of healthy humans, which could be used as a reference in studies of clinical biomarkers (Das et al, 2019). The miRNA profiles from healthy sheep sequenced in this chapter could in the future serve a similar purpose and, help populate a database of circulating miRNA signatures in sheep.

4.3.6 Further research

Besides increasing the animal number in future studies of miRNA dysregulation in serum, an additional approach to obtain a cleaner miRNA dysregulation signal would be to concentrate and examine miRNA expression in serum exosomes. However, the value of this approach, as discussed in section 1.5.7, is controversial.

In addition, another step towards understanding miRNA dysregulation in OPA would be to study the role of differentially expressed miRNAs in tissue and *in vitro* models of OPA. These studies could potentially help distinguish noise signals from biologically relevant ones.

Chapter 5 miRNA dysregulation in *in vitro* and *ex vivo* OPA models

5.1 Introduction

The finding of a set of miRNAs consistently upregulated in OPA lung tissue motivated the study of their role and importance in the oncogenic process. JSRV *env* is the active oncogene of JSRV and is sufficient to cause transformation of cells *in vitro* and drive tumour formation in *in vivo* models. Due to the lack of a permissive cell line for JSRV, studies of JSRV transformation have been classically performed in cell lines transfected with JSRV Env-encoding plasmids. These studies have contributed valuable information on the signalling pathways activated by JSRV Env and, comparison with findings in sheep lung has revealed that activation of the MAPK and Akt signalling pathways is associated with JSRV-driven transformation.

Although activation of several protein kinases and signalling pathways is known to occur in OPA lung tissue, the mechanism by which JSRV Env initiates the signalling cascade that leads to cell transformation remains unknown. In addition, the importance and sequential activation of signalling pathways in OPA is not entirely understood. miRNAs are known to promote oncogenesis in several malignancies, reviewed in section 1.5.10, and have been reported to target members of signalling pathways important for transformation (section 1.5.10). Therefore, it is possible that miRNAs might play a role in JSRV Env-driven transformation and may help unveil the missing pieces of information.

The set of miRNAs upregulated in OPA lung tissue (miR-135b, miR-182, miR-183, miR-200b, miR-205, miR-21, miR-31, miR-503 and miR-96) has been related to human forms of lung cancer. Moreover, targets of these miRNAs in humans include members of the Akt and MAPK pathways. For instance, miR-21 targets *PTEN* in the MAPK pathway, and miR-31 targets *RASA1* (Edmonds et al, 2016; Zhang et al, 2010b). Nevertheless, targets of these miRNAs might be different in sheep lung.

Several *in vitro* systems were selected and evaluated to study the role of miRNAs in JSRV Env transformation. *In vitro* systems permit the use of knock-down and

overexpression experiments to alter the expression of the miRNA of interest, whereas techniques such as reporter assays can help identify targets of the miRNAs. Differences in JSRV Env activation of signalling pathways have been noted depending on species (sections 1.2.6 and 1.3.3), suggesting that some in vitro findings might not translate to events occurring in sheep lung tissue. In order to identify the role of miRNAs in JSRV Env driven transformation in the sheep lung, an *in vitro* model that would closely resemble miRNA expression changes in the OPA sheep lung was sought. It could be anticipated that a model that mimics miRNA expression levels of the OPA sheep lung would be more likely to mimic the role of miRNA in transformation *in vivo*.

With that aim in mind, in this chapter, miRNA expression was investigated in transfected cell lines, in sheep-derived primary cells and in an *ex vivo* culture of sheep tissue.

5.1.1 Hypothesis and aims

Following the findings from Chapter 3 that suggested that some miRNAs upregulated in OPA lung tissue are related to JSRV Env driven transformation, in this chapter, the hypothesis that these miRNAs are also upregulated *in vitro,* in models of JSRV transformation was explored. If found to be true, this would provide a tractable *in vitro* system for studying the role of these miRNAs and their function in transformation. To examine the working hypothesis, several *in vitro* experimental systems were studied, including cell lines and lung slice models.

In order to test these hypotheses, the following aims were established for the present chapter:

- Induce JSRV Env driven transformation in cell lines
- Examine miRNA expression in JSRV Env transformed cell lines
- Develop an *in vitro* model derived from sheep type II pneumocytes that resembles JSRV Env transformation in sheep lung
- Detect miRNA expression after JSRV infection in ovine lung slices
- Compare miRNA expression results of *in vitro* models to miRNA expression in OPA *in vivo*

5.2 Results

5.2.1 Transfection of cell lines with JSRV Env-encoding plasmids

In order to study miRNA expression in *in vitro* models of OPA, the initial approach taken was to induce JSRV Env driven transformation in cell lines. miRNA expression in transformed cells could then be compared to miRNA expression in non-transformed control cells. Cell lines previously used to study the molecular mechanisms of JSRV transformation, as described in section 1.3.2, were used, including a rat fibroblast line, 208F (Hofacre & Fan, 2004; Hull & Fan, 2006), a mouse fibroblast line, NIH 3T3 (Maeda et al, 2001), and a dog epithelial line, MDCK (Liu & Miller, 2005).

Nevertheless, transfection of these cell lines with JSRV Env-encoding plasmids, and culture of the transfected cells for three weeks, did not result in morphological changes or an increased growth rate, which would have been suggestive of transformation, in any of the experiments performed. Immunocytochemical analysis for detection of JSRV Env in transfected cell lines, and comparison to primary cultured OPA tumour cells JA548 (**Fig. 5.1**), revealed that JSRV Env expression was low. As previous studies in our laboratory had demonstrated that plasmids pCAG-JSenv and pCMV3JS-ΔGPP are able to drive expression of JSRV Env in 208F cells (D. Griffiths, personal communication), this suggested that low transfection efficiency was the cause of the poor expression in this experiment.

In an effort to establish a stably transformed cell line that could be compared to the parent cells, plasmid linearization and antibiotic selection were used. Plasmid pCAG-JSenv encodes a Geneticin resistance gene, Geneticin was added to select transfected cells and indirectly encourage permanent expression of JSRV Env. Nevertheless, neither of these approaches resulted in an improved transfection efficiency nor did they enhance the level of JSRV Env expression, and no transformation was observed.

The transfection efficiency of three different methods was then tested 48 h post-transfection by flow cytometry (2.16) to determine the optimal method (**Table 5.1**). Nucleofection (section 2.8.2) of MDCK and NIH 3T3 cells with the pmaxGFP plasmid showed high transfection efficiency. However, when nucleofection was

performed with the plasmid pCMV2JSRV-GFP2A-Env, encoding EGFP and JSRV Env, the transfection efficiency was again markedly reduced. The reason for this is unclear although might potentially be due to differences in the plasmid transfected, including size and preparation, which can affect transfection efficiency. Nonetheless, these results indicated that a more efficient means to deliver JSRV *env* into cell lines were needed to achieve JSRV Env driven transformation and explore miRNA expression *in vitro*.

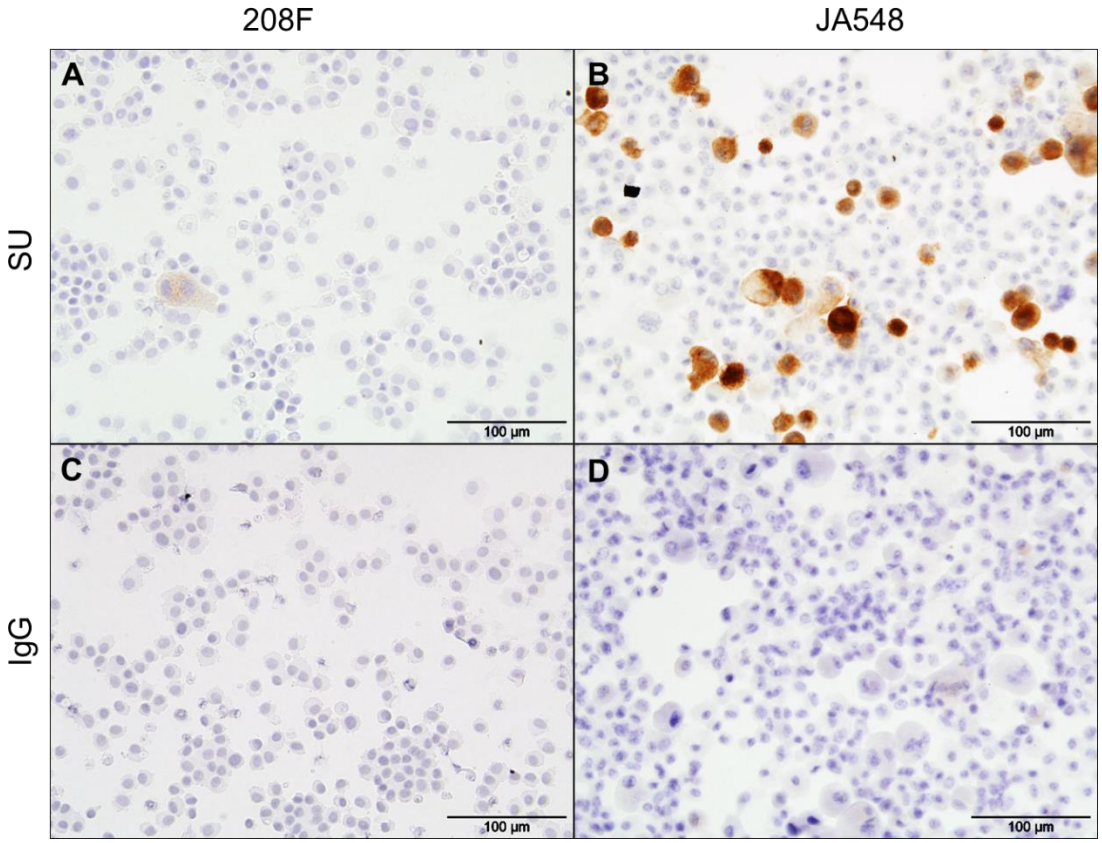

Figure 5.1. **Immunocytochemical detection of JSRV SU protein in cultured cells.** A. 208F cells transfected with the JSRV Env-expressing pCAG-JSenv. B. JA548 cells. A and B were stained with an antibody to JSRV SU. C and D. Isotype control (IgG) stained 208F cells and JA548 cells respectively. Brown staining indicates positive staining of JSRV Env. JA548 cells are a mixed primary culture of cells obtained from bronchioloalveolar lavage of an OPA-affected sheep.

Table 5.1. Summary of efficiency and viability obtained by each transfection method in MDCK and NIH 3T3 cells.

MDCK transfection			
Method	**Fugene HD**	**Lipofectamine 3000**	**Nucleofection**
Cell count	1.18×10^6 cells/ml	1×10^6 cells/ml	2.31×10^6 cells/ml
Viability	84.31%	80.06%	79.39%
GFP expression	0.22%	2.05%	85.27%
NIH 3T3 transfection			
Method	**Fugene HD**	**Lipofectamine 3000**	**Nucleofection**
Cell count	1.18×10^5 cells/ml	1.64×10^5 cells/ml	2.02×10^5 cells/ml
Viability	71.62%	78.76%	87.93%
GFP expression	6.88%	6.04%	61.07%

5.2.2 Transduction of cell lines with JSRV-*env* encoding lentiviral vectors

The experiments described in 5.2.1 indicated that JSRV Env expression in transfected MDCK and NIH3T3 cells was low, seemingly due to the method used to deliver the transgene into cell lines. To achieve better delivery of JSRV Env into cell lines and efficient expression of the transgene, a transduction strategy using HIV-based lentiviral vectors was devised. In addition, this method would integrate the transgene into the genome, allowing for longer-lasting expression of JSRV Env.

5.2.2.1 Construction of a lentiviral vector for JSRV Env expression

The lentiviral vector system chosen to deliver JSRV Env was a third generation self-inactivating HIV system. This system consists of four plasmids that contain all the elements needed to create a lentiviral vector that is replication deficient and able to transduce cells at high efficiency. In this study, vectors were used that encode GFP (Miyoshi et al, 1998), JSRV Env (D. Griffiths unpublished) and a GFP-2A-Env fusion protein (D. Griffiths, unpublished) (see section 2.13 for details).

5.2.2.2 Assessment of transfer plasmids

As a first step to determine if the transfer plasmids created were able to drive expression of JSRV Env or GFP2AEnv in cell lines, these plasmids were

transfected into the easily transfected cell line 293T (section 2.8.1). In addition, other JSRV *env* or *gfp* encoding plasmids were transfected into cells to be used as positive controls (**Table 5.2**).

Forty-eight hours after transfection, cells were harvested to perform cytospins (section 2.10.4) and protein extracts (section 2.19.1) to assess expression of JSRV Env and GFP by immunostaining and immunoblotting techniques (sections 2.10 and 2.19).

Table 5.2. Summary of plasmids transfected into 293T cells.

Plasmid	*gfp* encoded	GFP detected	JSRV *env* encoded	Env detected
pCMV2JS21	No	No	Yes	Yes
pCMV3-JSΔGPP	No	No	Yes	Yes
pCMV2JSRV-GFP2A-Env	Yes	Yes	Yes	Yes
pCSC-GFP2AEnv	Yes	Yes	Yes	Yes
pCSC-JSenv	No	No	Yes	No
pEGFP-Flag	Yes	Yes	No	No
pCSC-G	Yes	Yes	No	No
Non- transfected	No	No	No	No

Anti-JSRV SU immunostained 293T cells exhibited brown staining, indicative of JSRV Env expression, when transfected with plasmids pCMV2JS$_{21}$ (not shown), pCMV3-JSΔGPP, pCMV2JSRV-GFP2A-Env and pCSC-JSenv (**Fig. 5.2**), albeit different levels of expression were observed, being the lowest in pCSC-JSenv transfected cells.

When immunostained with anti-GFP antibody, 293T cells transfected with 2JSRV-GFP2A-Env, pCSC-GFP2AEnv, pCSC-JSenv and pCSC-G (not shown) presented brown staining indicative of GFP expression (**Fig. 5.2**). These results were interpreted as specific because staining was not observed when cells transfected with any of the plasmids were incubated with an isotype control for anti-JSRV SU (mouse IgG) or anti-GFP (rabbit IgG).

JSRV Env and GFP expression in 293T cells was further analysed by western blotting (**Fig. 5.3**). Western blot for JSRV SU expression detected a band consistent with the expected size for JSRV SU (~ 49 kDa) in 293T cells transfected with JSRV *env* encoding plasmids: pCMV2JS$_{21}$, pCMV3-JSdGPP, pCMV2JSRV-GFP2A-Env, but not in pCSC-JSenv transfected 293T cells. These findings were consistent with the results of immunocytochemistry, which showed lower Env expression levels in pCSC-JSenv transfected 293T cells. A band of similar, but slightly smaller, size was detected in all samples, including the non-transfected negative control. A number of other bands were also detected in all samples analysed, indicating a high background staining level that is likely due to antibody cross-reactivity, further discussed in 5.3.

Western blotting for detection of GFP expression in transfected 293T cells, revealed a band in protein extracts from 293T cells transfected with pCMV2JSRV-GFP2A-Env, pCSC-GFP2AEnv, pEGFP-Flag and pCSC-G. The slightly different band sizes between samples are likely due to the form of GFP encoded by each of the plasmids: pCMV2JSRV-GFP2A-Env and pCSC-GFP2AEnv have an expected molecular GFP weight of ~35kDa, pEGFP-Flag of ~33kDa, and pCSC-G of ~ 27kDa. Additional bands of lower molecular weight were detected in some samples. As these were only present in lanes containing samples expected to have GFP, they are likely to be cleavage products or truncated forms of GFP.

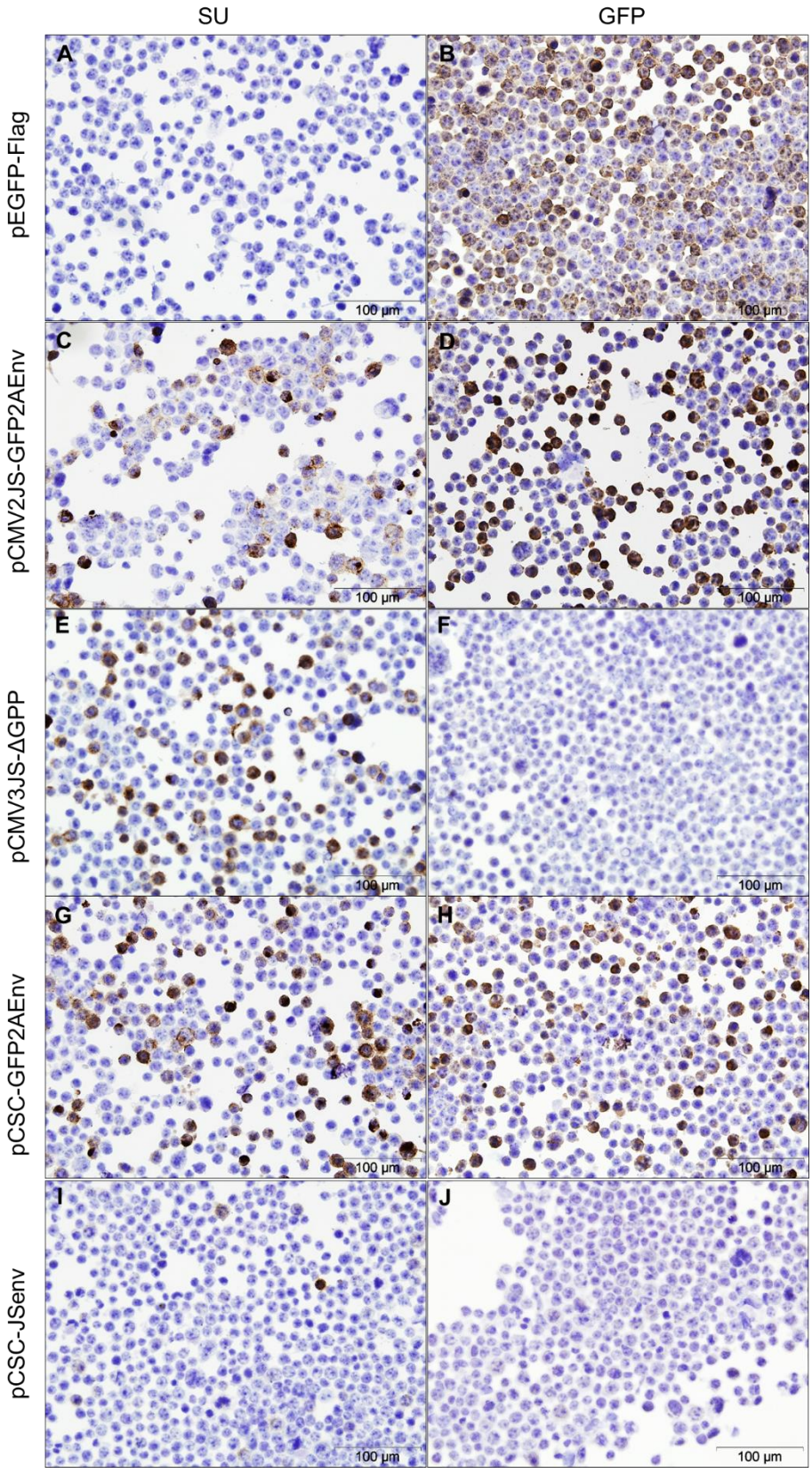

Figure 5.2. Immunostaining of transfected 293T cells with antibodies to GFP and JSRV SU. *Top labels indicate the protein detected, labels to the left of the plot indicate the plasmid transfected into the cells. The presence of brown pigment indicates positive staining.*

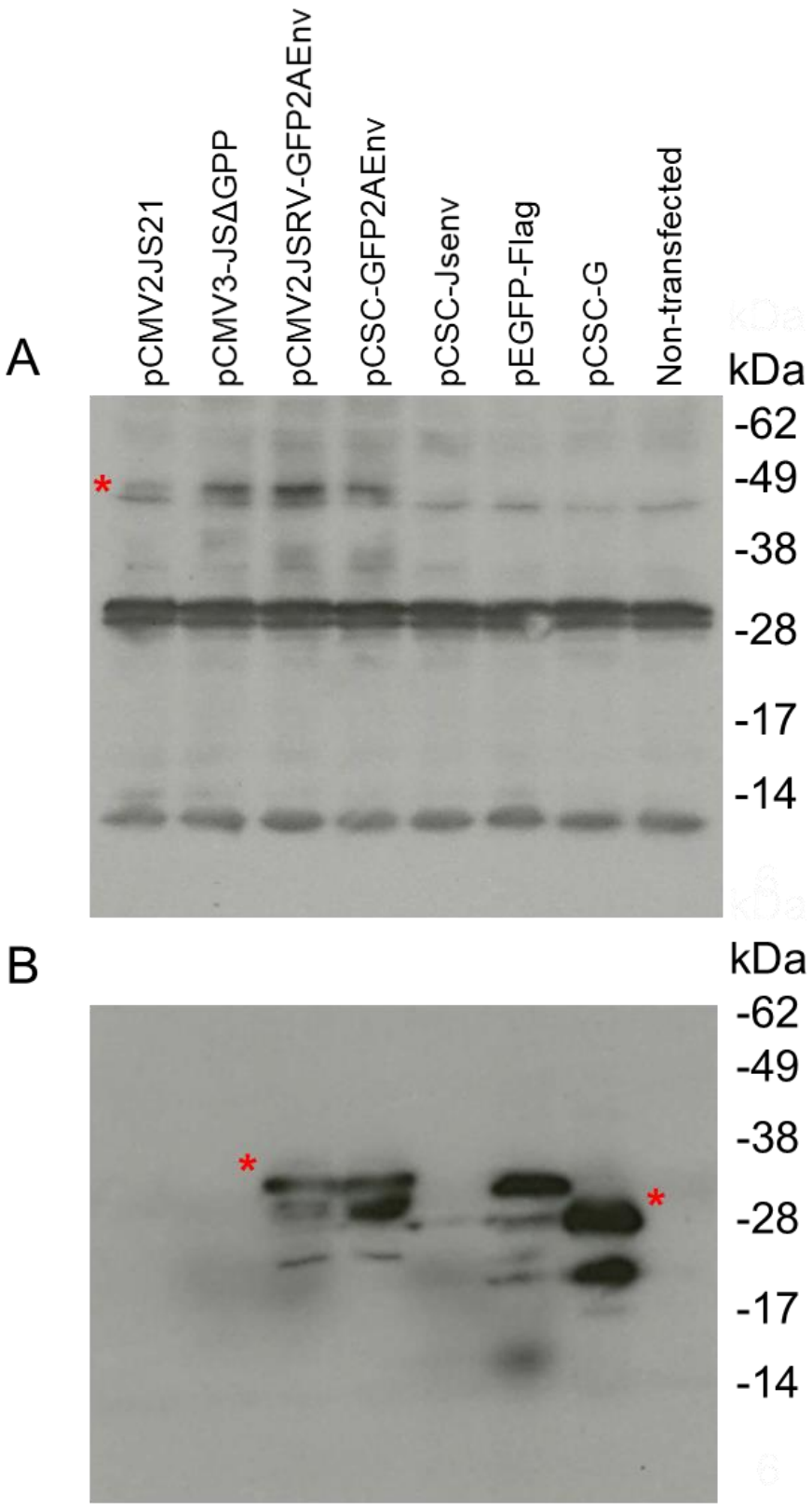

Figure 5.3. Western blot of extracts from 293T cells transfected with the indicated plasmids. *A. Analysis of SU protein expression in transfected 293T cells. B. Analysis of GFP protein expression in transfected 293T cells. The red asterisks indicate the bands corresponding to the expected size of SU in panel A, and GFP in panel B.*

Overall, these findings revealed that pCSC-GFP2AEnv was able to successfully drive expression of GFP and JSRV Env in 293T cells. On the other hand, pCSC-JSenv was, unexpectedly, only able to drive low levels of JSRV Env expression in 293T cells.

In order to investigate if the inability of pCSC-JSenv to drive efficient expression of JSRV Env was due to sequence mutations or errors introduced during the cloning process, DNA sequencing of pCSC-G, pCSC-JSenv and pCSC-GFP2AEnv was performed (section 2.12.6). A mutation that disrupted a BglII restriction site in the backbone of the plasmid was found, indicating that the sequence for pCSC-G cited in the Addgene website contains inaccuracies; however, no mutations that could affect *env* transgene expression were detected.

During the cloning process, other pCSC-JSenv plasmid preparations had been isolated from transformed *E. coli* clones (section 2.12), these were tested to investigate if any could drive JSRV Env expression in 293T cells more efficiently. The results of immunocytochemistry (**Fig. 5.4**) revealed similar and low JSRV Env expression efficiencies in all six plasmid preparations when transfected into 293T cells, confirming the results of (**Fig. 5.2** and **Fig. 5.3**). Possible causes of inefficient JSRV Env expression from pCSC-JSenv are further discussed in 5.3.

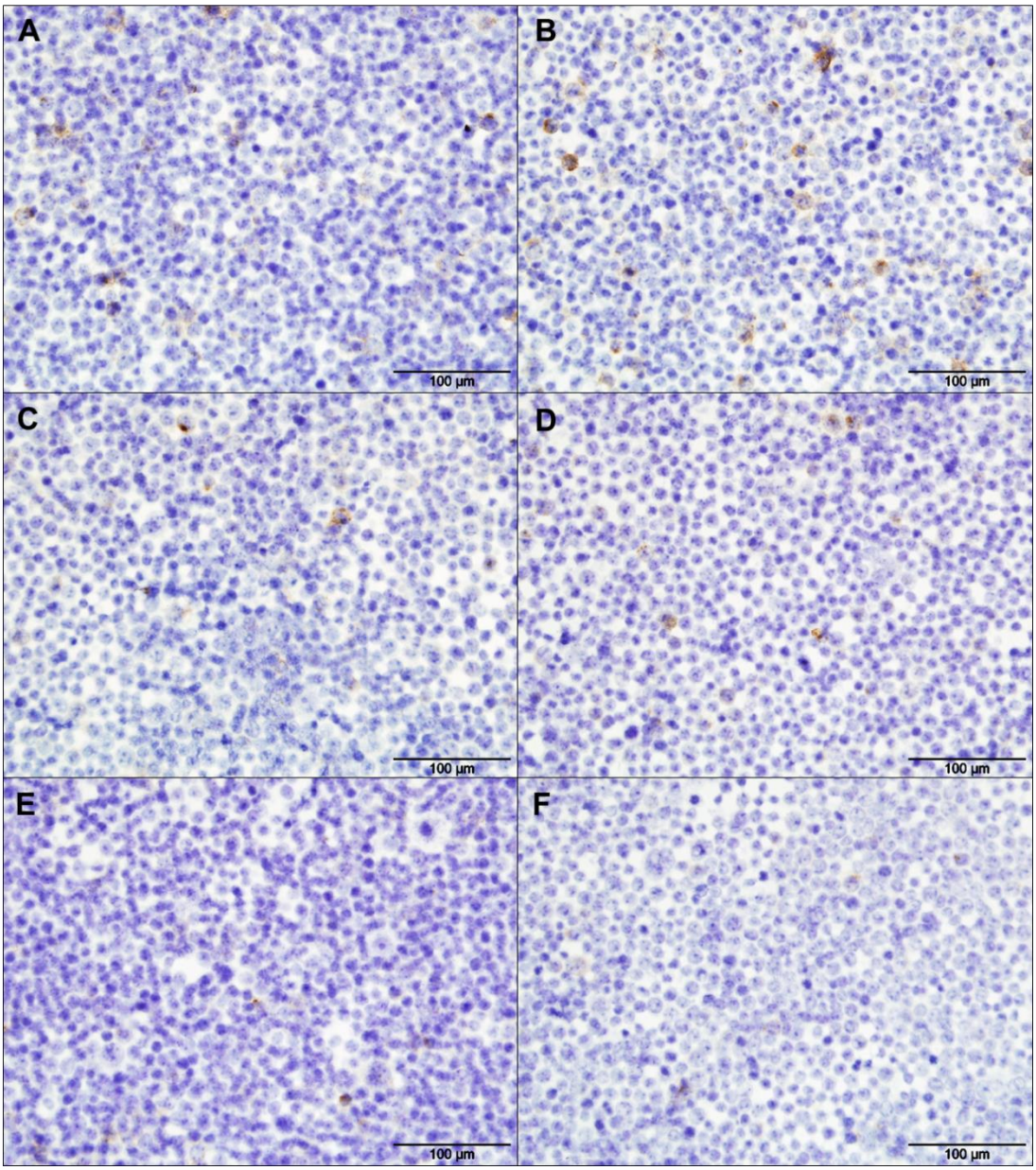

Figure 5.4. Anti JSRV-SU staining of 293T cells transfected with six different plasmid preparations of pCSC-JSenv. *A. p2953. B. p2954. C. p2955. D. p2956. E. p2957. F. p2958. The presence of brown prigment indicates positive staining.*

5.2.2.3 Transduction of cell lines with lentiviral vectors encoding JSRV Env

Having confirmed that the transfer plasmid pCSC-GFP2AEnv was able to efficiently drive JSRV Env expression, and that pCSC-JSenv was also able to drive JSRV Env expression, albeit at low levels, production of lentiviral vectors was started. Lentiviral vectors were prepared using the four plasmid, 3rd generation system (section 2.13.2). The vectors produced encoded GFP, GFP2AEnv, or Env alone.

Lentiviral vectors CSC-G, CSC-JSenv and CSC-GFP2AEnv, named after the transfer plasmid used for production, were used to transduce 208F cells and MDCK cells in culture (section 2.15). Using fluorescent microscopy, GFP fluorescence was observed in both cell lines transduced with CSC-G and CSC-GFP2AEnv, as expected, suggesting that cells had been successfully transduced.

Immunocytochemistry was performed to evaluate JSRV Env expression in transduced cell lines (**Fig. 5.5**) five days after transduction. 208F and MDCK cells transduced with GFP2AEnv expressed JSRV Env, as indicated by the presence of brown staining. CSC-G transduced cells did not express JSRV Env, as expected. However, Env staining was also absent in cells transduced with CSC-JSEnv. The reason for this is unclear but is consistent with the results of pCSC-JSenv transfection in 293T cells (section 5.2.1). As CSC-JSenv did not drive expression of JSRV Env efficiently, it was excluded from further experiments.

Importantly, CSC-GFP2AEnv was shown to transduce and drive efficient expression of GFP and JSRV Env in 208F and MDCK cells. GFP could, therefore, be used as transduction marker for this lentiviral vector. In addition, the present results suggested that the lentiviral vector system created was efficient at delivering and driving JSRV Env expression.

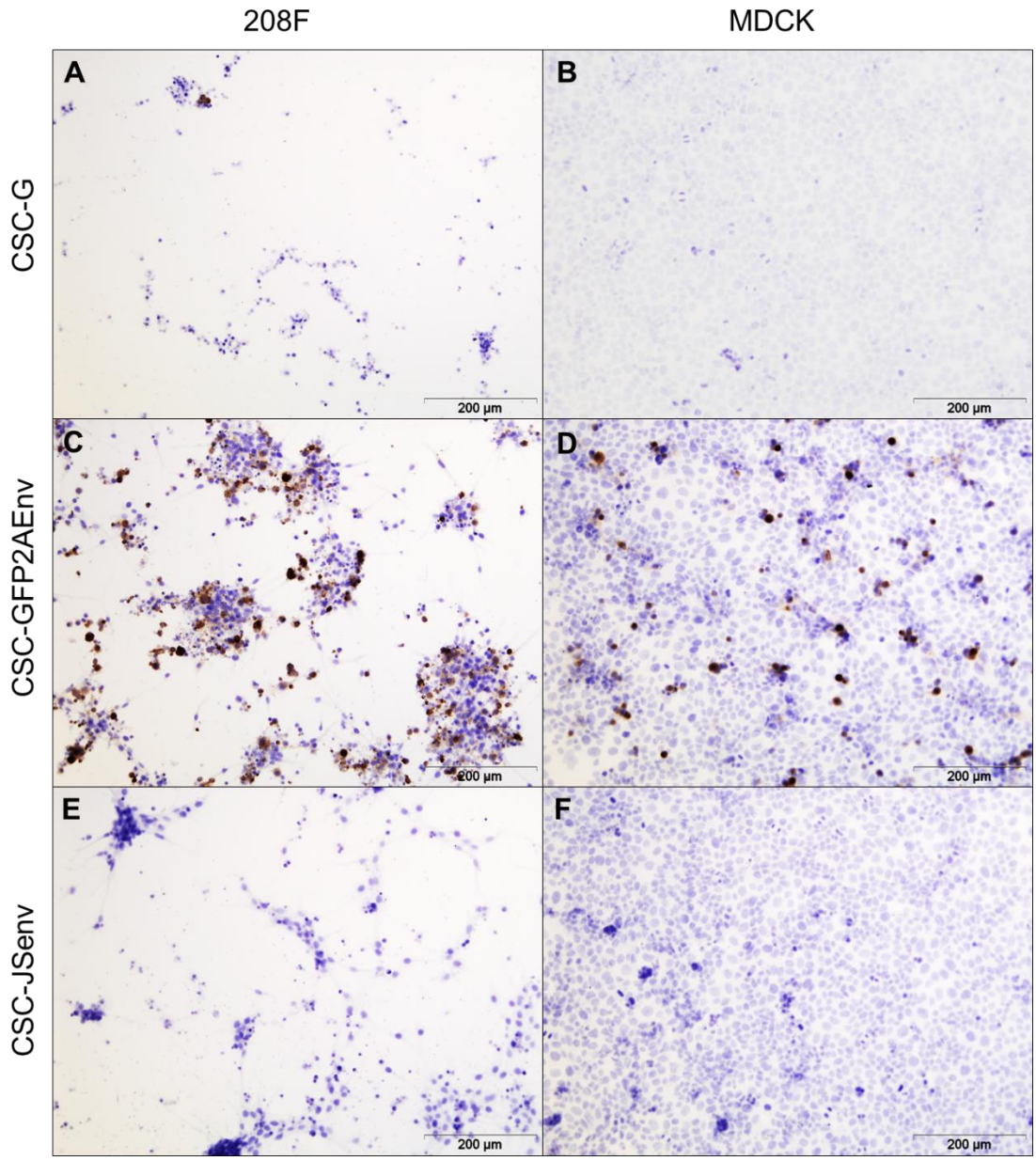

Figure 5.5. Immunostaining of transduced cell lines with an antibody anti-JSRV SU. *The top labels indicate the cell line transduced, labels to the left indicate the lentiviral vector used for transduction. Brown pigment indicates positive staining.*

Titration of lentiviral vectors

Titration of lentiviral vectors was performed by transducing 208F and MDCK cells and measuring GFP fluorescence by flow cytometry (section 2.16.1). Vector titre was greater for CSC-G than CSC-GFP2AEnv, and in 208F cells than MDCK cells (**Table 5.4**). These results reflect differences in lentiviral vector concentration as well as differences in susceptibility of each cell line to transduction.

Table 5.3. Titre of lentiviral vectors in 208F cells and MDCK cells measured by flow cytometry.

	Lentiviral vector	
Cell line	**CSC-G**	**CSC-GFP2AEnv**
208F	2.32×10^6 TU/ml	1.58×10^6 TU/ml
MDCK	1.22×10^6 TU/ml	4.98×10^5 TU/ml

5.2.3 Transformation of transduced cell lines

Having found an efficient system to drive JSRV Env expression in cell lines, I sought to investigate the transformation process. In order to investigate if transduction of 208F and MDCK cells with lentiviral vectors encoding JSRV Env was able to stimulate cellular transformation, 208F and MDCK cells were transduced with CSC-GFP and CSC-GFP2AEnv as above (**5.2.2**) at an MOI ~0.3, in 208F cells, and ~0.5 in MDCK cells, and maintained in culture with reduced serum media. The MOIs selected were the highest that could be used without inducing significant cytotoxicity. Cell morphology and GFP fluorescence were evaluated every three days by microscopy and any changes noted. GFP fluorescence observed in 208F (not shown) and MDCK cells transduced with CSC-G and CSC-GFP2AEnv, indicated cells had been successfully transduced (**Fig. 5.6**).

In 208F cells, which were more sensitive to high MOIs, more dead cells were observed and fewer green cells. The percentage of cells expressing GFP was assessed by flow cytometry 3 days post-transduction and found to be ~ 40% in MDCK cells and ~25% in 208F cells transduced with CSC-G. When transduced with CSC-GFP2AEnv GFP-positive cells represented a ~35% in MDCK cells and ~16% in 208F cells.

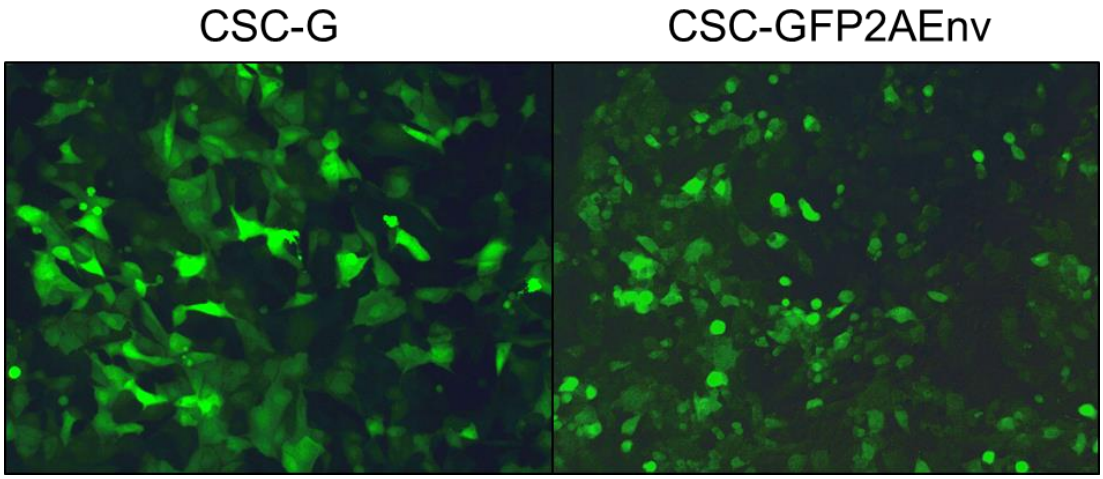

Figure 5.6. EGFP expression in transduced MDCKs 48 h after transduction. *The labels above the panels indicate the lentiviral vector used for transduction. Differences in morphology can be observed: CSC-GFP2AEnv transduced MDCK cells appear more rounded than CSC-G transduced cells. Images captured at 40x magnification.*

Seventeen days after transduction, morphological changes were observed in 208F cells. The morphological changes observed consisted of focus formation, i.e., areas of increased cell density that protruded above the cell monolayer. Notably, these foci also exhibited GFP fluorescence. The changes observed were suggestive of transformation driven by JSRV Env, given that they were observed in CSC-GFP2AEnv transduced cells. A maximum of 5 foci per well, of a 24-well plate, were observed in CSC-GFP2AEnv transduced cells. No foci formation was observed in non-transduced cells or cells transduced with CSC-G.

In order to isolate 208F transformed cells and create a pure culture of transformed 208F cells, in which miRNA expression could be compared to non-transformed cells, individual foci were isolated and cultured with added conditioned media (section 2.15.1). Fluorescence and growth rate were monitored by microscopy. Three 208F foci were isolated and expanded in culture but new cells radiating from the original foci did not exhibit GFP fluorescence. In addition, immunostaining of the foci and cells growing from them (**Fig. 5.7**) revealed that these apparently transformed 208F foci did not express JSRV Env. Four weeks after transduction, foci detached from the culture plate and GFP fluorescence became fainter, foci did not keep on dividing. The three 208F isolated foci failed to keep dividing in culture and did not establish a pure culture of transformed 208F cells. Culture conditions might have had an effect on 208F foci growth, foci were small when

isolated and the medium used might have not fulfilled their growth requirements. In addition, it is possible that the isolated foci were a mix of transduced and non-transduced cells, and non-transduced cells might have outgrown transduced cells. However, lack or loss of JSRV Env expression, the oncogene that supports increased growth, might also be the cause of their inability to keep expanding. These points will be further discussed in 5.3.

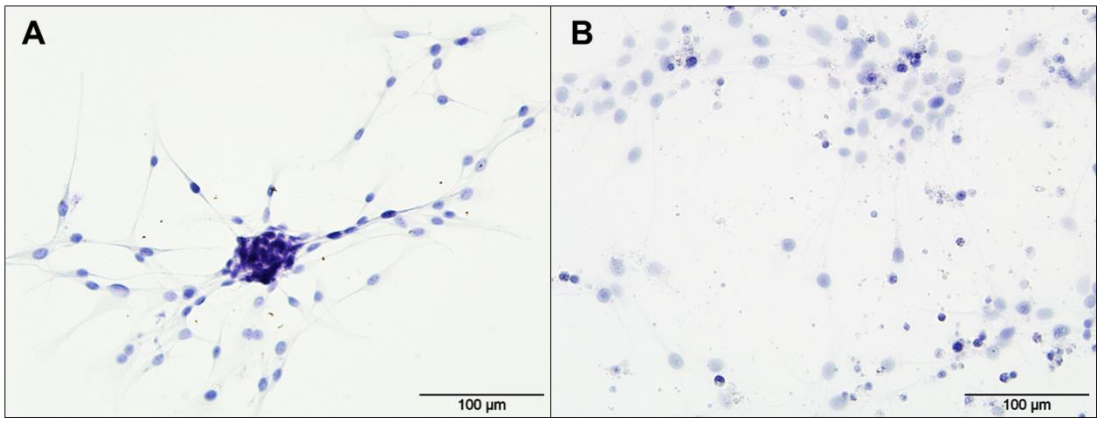

Figure 5.7. Staining of transduced 208F cells with an anti-JSRV SU antibody. *A. 208F focus isolated from culture and grow in a chamber slide, 16 days after isolation. B. 208F cells non-transduced. No brown pigment, indicative of positive staining was observed.*

Morphological changes were observed in MDCK cells 23 days after transduction with CSC-GFP2AEnv. In contrast, no morphological changes were observed in non-transduced MDCK cells. MDCK cells presented more subtle morphological changes, protuberant cells were observed as strings of cells across the culture plate, not organised in foci. These protuberant cells were invariably positive for GFP fluorescence, confirming they had been transduced by CSC-GFP2AEnv and suggesting they had also been transformed by JSRV Env. Immunostaining was performed in transformed cells and revealed the presence of JSRV Env.

5.2.3.1 Cell sorting of transformed MDCK cells

Transformed MDCK cells could not be easily isolated because they did not grow as discrete foci as did 208F cells. Therefore, cell sorting was performed in order to isolate transformed MDCK cells from the mixed population in culture. As transformed MDCK cells expressed GFP, this attribute was used to differentiate transformed cells from non-transformed cells by fluorescence activated cell sorting (FACS).

MDCK cells transduced with CSC-GFP2AEnv were maintained in culture with reduced serum media (section 2.15.1) until day 52 post-transduction. The cells were then harvested and prepared for FACS (section 2.17). FACS was performed by Graeme Robertson and Robert Fleming (Roslin Institute). Non-transduced MDCK cells were used to determine gating parameters and a threshold to distinguish GFP-positive cells from GFP-negative cells was established (**Fig. 5.8**). Single GFP-positive cells were sorted directly into wells of four 96-well plates, with a single cell per well. GFP positive cells were also collected as a bulk population of sorted cells. The purpose of single cell isolation was to obtain clones with JSRV Env integrated in the same genetic location and therefore with less variability in expression.

Single GFP-positive cells were expanded in culture (section 2.18) and their growth monitored by microscopy. The remaining bulk population of GFP-positive cells was seeded in two T-75 flasks.

The bulk population of GFP-positive cells was assessed for JSRV Env expression by immunocytochemistry and western blotting (**Fig. 5.9 and Fig. 5.10**). Immunocytochemistry identified a small number of positively-staining cells, indicative of JSRV presence, close to the edge of the slide (**Fig. 5.9**) but not in cells observed in other areas of the slide.

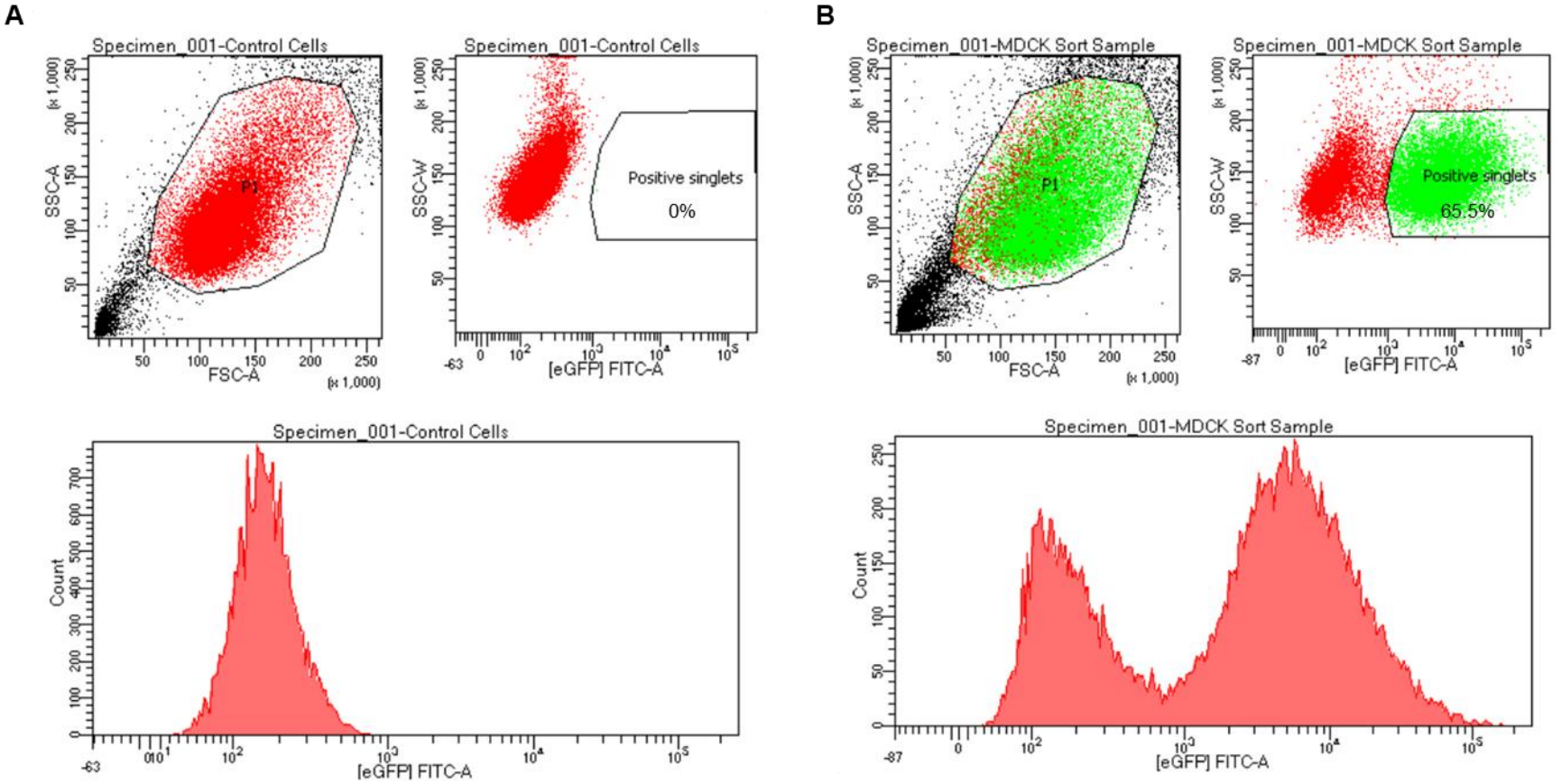

Figure 5.8. Fluorescence activated cell sorting of MDCK cells. *A. Gating of control MDCK cells. Cells were selected based on expected size (SSC vs. FSC) and fluorescence signal emitted detected in (SSC vs. FITC). Background MDCK fluorescence was established as threshold. B. Sorting of CSC-GFP2AEnv transduced MDCK cells. Cells were selected based on expected size. From the selected population two subpopulations can be seen, coloured in red and green, these cell populations differed in GFP expression levels, acquired as FITC-A. The two populations can also be seen in the lower panel as two peaks corresponding to two levels of fluorescent signal acquired as FITC-A.*

Western blot analysis indicated that 293T cells transfected with plasmids encoding JSRV Env yielded a band corresponding to the expected size of SU (~49 kDa). However, the intensity of the band was faint in some of the samples, indicating poor expression in those samples. A band representing Env was not detected in either MDCK parental cells or the bulk population of cells, consistent with the low expression identified by immunocytochemistry. Interestingly, at the time JSRV Env expression tests were performed, the cells continued to express GFP, although GFP expression was lost weeks later. These results are further discussed in 5.3.

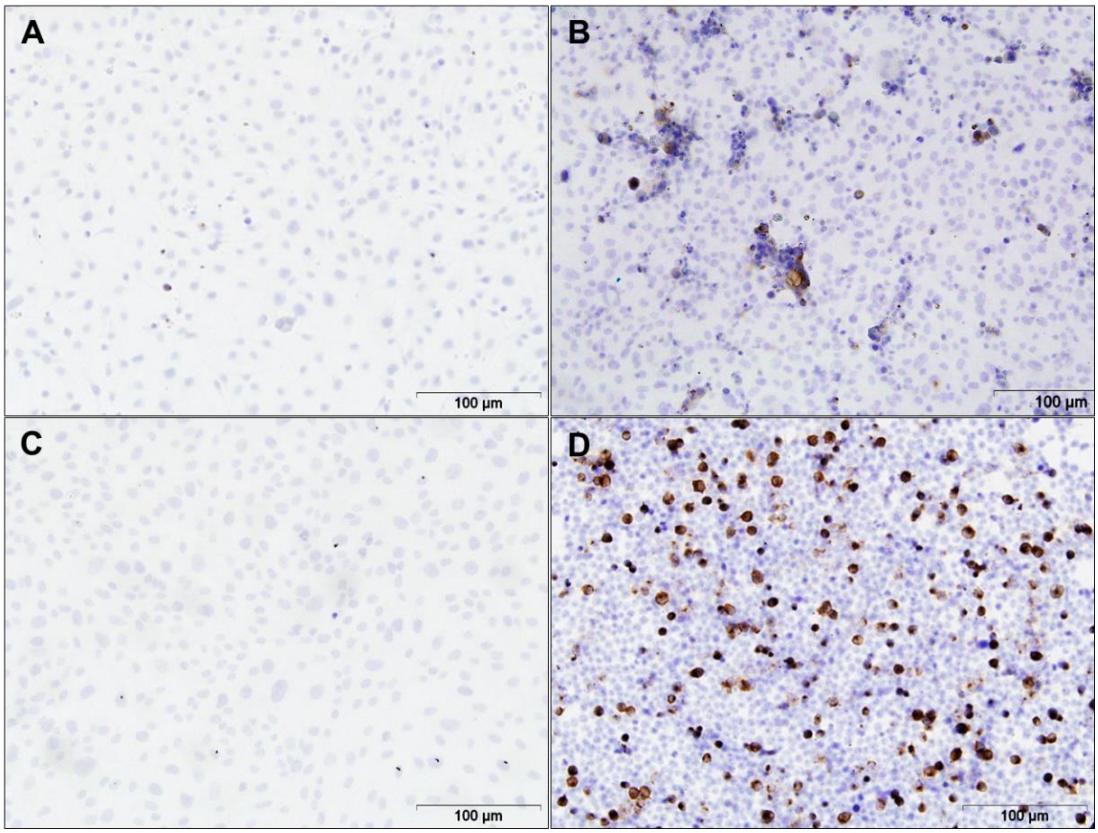

Figure 5.9. Staining of MDCK cells with anti-JSRV SU antibody. *A and B. Bulk population of GFP-positive cells sorted by FACS. C. Non-transduced MDCK cells used as negative control. D. 293T cells transfected with pCSC-GFP2AEnv used as positive control. Brown pigment indicates positive staining.*

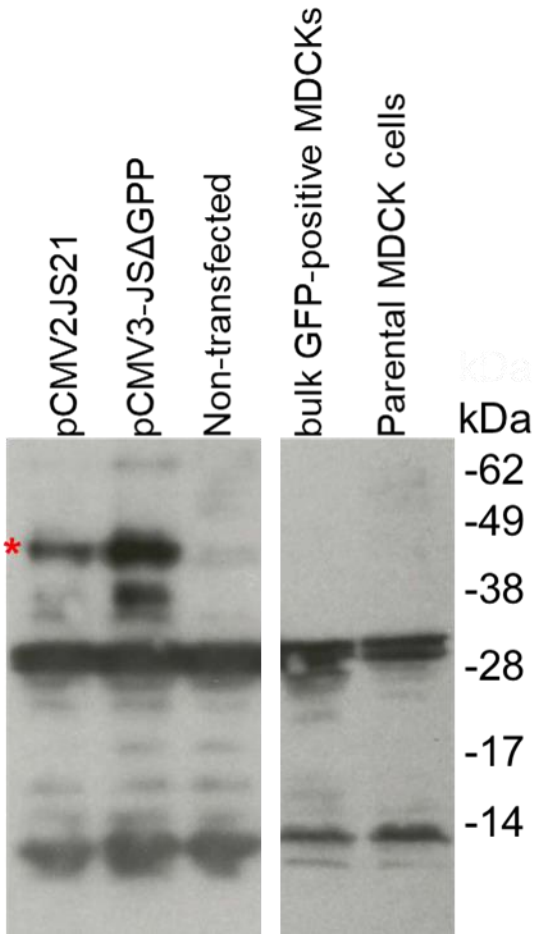

Figure 5.10. Western blot of JSRV Env expression in transformed sorted GFP-positive MDCK cells and controls, using anti-JSRV SU antibody. *Top labels indicate the plasmids used for 293T transfection or MDCK sample phenotype. The asterisk marks the region were a band corresponding to JSRV SU is expected to be detected. The two panels correspond to the same western blot, lanes not-relevant for this study were removed.*

In the four 96-well plates seeded with GFP-positive single cells, clones started expanding at different rates. Ten days after FACS, 12 wells had successfully expanded from single cells, and 28 days after FACS, a total of 72 clones had expanded from single cells. All these clones presented GFP fluorescence and were sequentially transferred to 12-well plates, 6-well plates, T-25 flasks and T-75 flasks to keep on expanding their population. In order to assess JSRV Env expression in these clones, cells were harvested and seeded in chamber slides (section 2.10.5) and immunocytochemistry was performed one month after sorting.

Of the 72 screened clones, nine stained positively for JSRV Env by immunocytochemistry (**Fig. 5.11**). The nine Env positive clones were kept in

culture and tested again for JSRV Env expression one week and two weeks later, in order to examine the stability of JSRV Env expression. Clones 1E5, 2E3 and 3C9 were found to exhibit high levels of JSRV Env expression at all tested time points, whereas JSRV Env expression in the remaining six clones, including 1C9, was markedly reduced over this time period (**Fig. 5.12**).

Interestingly, and contrary to what was expected, two of the clones with a high level of JSRV Env expression by immunocytochemistry: 2E3 and 3C9, exhibited a slower growth rate than other transformed clones and untransformed MDCK cells. The reason for this is unclear as all clones were grown under the same conditions, and other clones expressing JSRV Env seemed to grow at faster rates. In addition, the fact that some of the clones expressing GFP fluorescence did not express JSRV Env was intriguing. These findings are further discussed in 5.3.

JSRV Env expression in clone 1E5 was reduced after 31 days in culture and being frozen and thawed once. JSRV Env expression in clones 2E3 and 3C9 was reduced after 51 days in culture and being frozen and thawed once. These findings indicated that JSRV Env expression could be observed in some MDCK clones over a month after cell-sorting, and almost 3 months after transduction, leaving an ample time window to perform *in vitro* experiments.

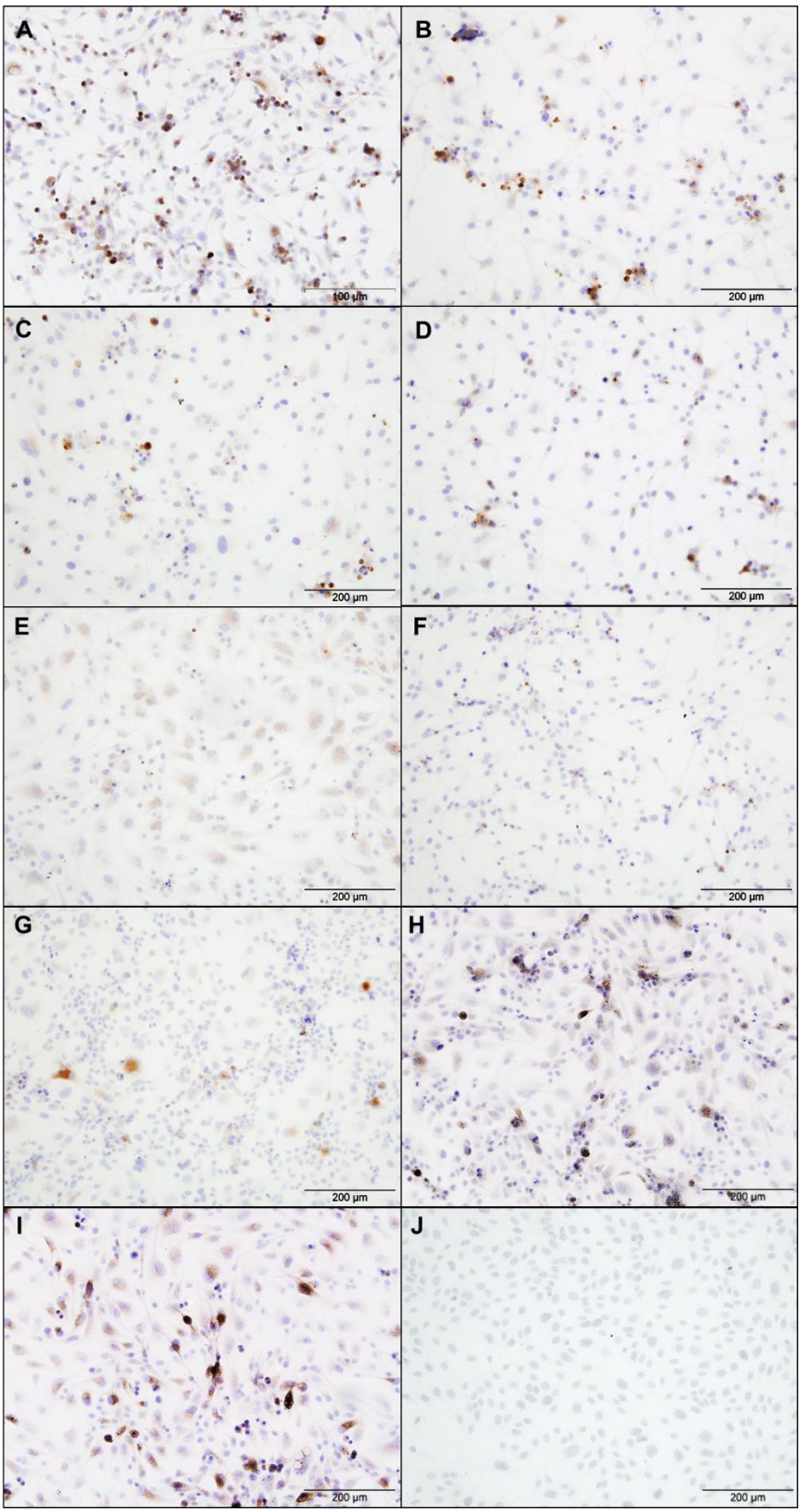

Figure 5.11. Staining of GFP-positive clones with anti-JSRV SU antibody. *A to I. Nine clones found to express JSRV-Env. J. Control MDCK cells. Brown pigment indicates positive staining.*

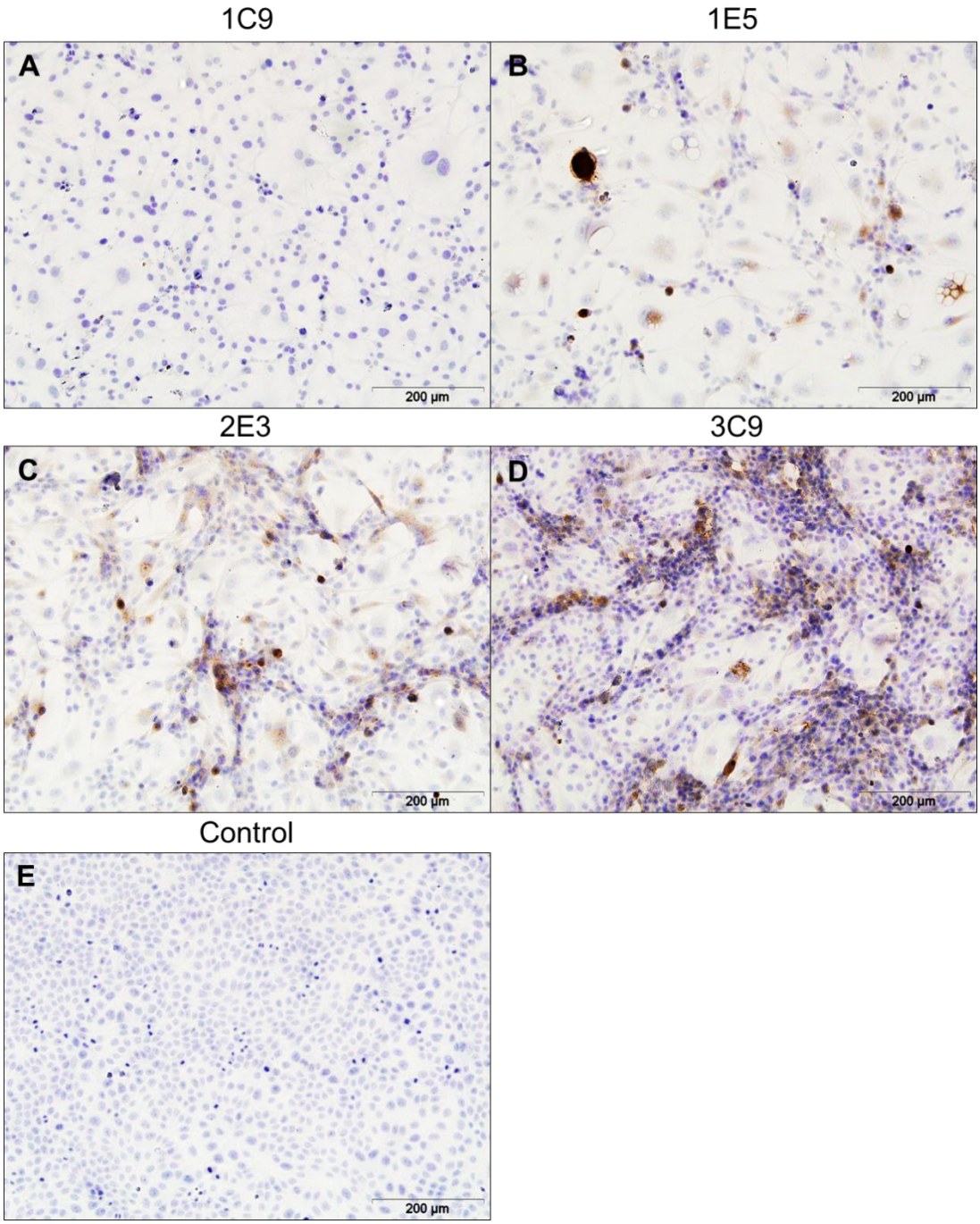

Figure 5.12. Staining of GFP-positive clones with anti JSRV-SU antibody after two weeks. *A. Clone 1C9. B. Clone 1E5. C. Clone 2E3. D. Clone 3C9. E. Control non-transduced MDCK cells. Brown pigment indicates positive staining. Note that IC9 had no detectable JSRV SU expression, although still appeared faint GFP positive.*

5.2.3.2 Characterisation of transformed MDCK clones

Morphological changes were the first suggestion of transformation observed in MDCK cells in culture. The morphology of isolated clones was assessed and compared to non-transduced MDCK cells that had been grown in culture for the same length of time.

Differences in shape and growth were observed when clones expressing JSRV-Env were compared to MDCK cells. Regarding shape, cells appeared more irregular in shape compared to control cells, their growth was accelerated in some cases, and growing patterns became more irregular and protruding from the culture surface, illustrated in **Fig. 5.13**. In contrast, clone 1C9, which was found not to express JSRV Env, had a morphology closer to that of control MDCK cells but still retained some features in common to transformed clones. Clones 1E5, 2E3 and 3C9, which did express Env, became more loosely attached to the surface of culture flasks. For example, during passaging the incubation time required for their detachment was ~10 minutes, whereas control MDCK cells and clones that did not express JSRV Env, such as 1C9, required ~20 minutes of incubation to be successfully detached. Moreover, transformed clones did not form a confluent monolayer but instead started overgrowing, indicating loss of contact-inhibition, another hallmark of transformation.

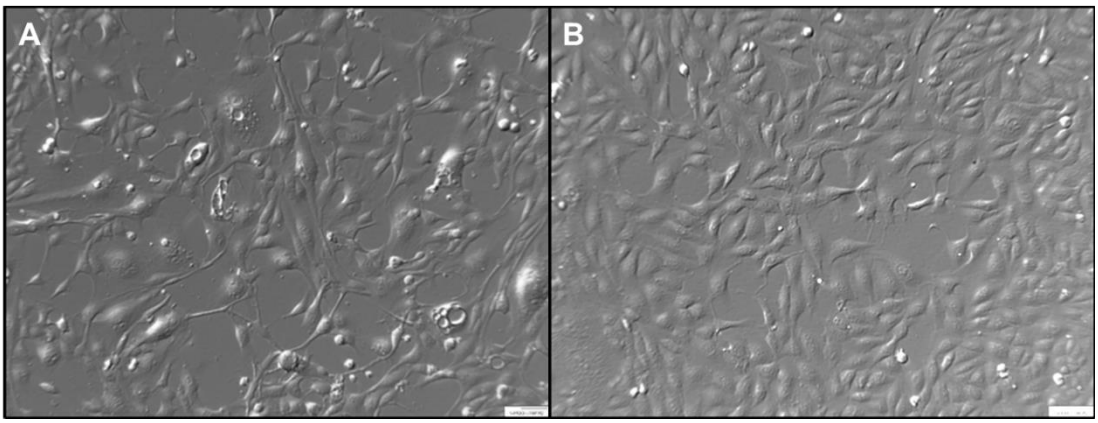

Figure 5.13. Microscopy images of MDCK cells in culture. *A. JSRV-Env expressing clone 1E5, cell morphology appears more irregular and protruding areas are observed. B. Control MDCK cells, growth pattern is organised and morphology is similar in all of the cells in culture.*

Transformation markers

Morphological changes observed in clones were indicative of transformation. But, in order to investigate this further, markers associated with JSRV Env transformation were analysed in the clones.

Phosphorylation of Akt and ERK1/2 proteins are known markers of JSRV Env transformation that have been detected in several JSRV Env transformed cell lines, including MDCK cells (sections 1.2.6 and 1.3.2). The presence of phosphorylated Akt and ERK1/2 in JSRV-Env expressing clones (1E5, 2E3 and 3C9), a non-JSRV-Env expressing clone 1C9, and untransformed MDCKs was examined by immunocytochemistry. As the presence of FBS in culture medium is known to activate these transformation markers and potentially interfere with results, the clones and parent cells were FBS starved for 24 h before immunocytochemistry. Cells growing in the presence of FBS were used as positive controls for detection of phosphorylated Akt and ERK1/2 expression.

Clones 1E5, 2E3 and 3C9 were found to stain positively for Akt-P and ERK1/2-P (**Fig. 5.14**) although the expression levels of these two markers were consistently different in all three clones. While expression of ERK1/2-P was detected in all cells, Akt-P expression seemed limited to a subpopulation of cells.

Control MDCK cells and clone 1C9 did not exhibit activated forms of Akt, but low levels of phosphorylated ERK1/2 were observed, indicating background levels of this protein are present in these cells, further discussed in 5.3. These results indicated differences in transformation marker expression between JSRV-Env expressing clones and control cells, suggesting that JSRV Env expression had driven transformation of these cells and confirming their transformed state.

Interestingly, the transformation markers were detected in cells even when JSRV Env expression was later markedly reduced. Suggesting that although Env may have initiated transformation in these clones, it is not required to maintain the transformed phenotype. Nevertheless, it is possible that expression of the transformation markers might be reduced and, eventually lost, at later time points, similarly to the observations of clone 1C9.

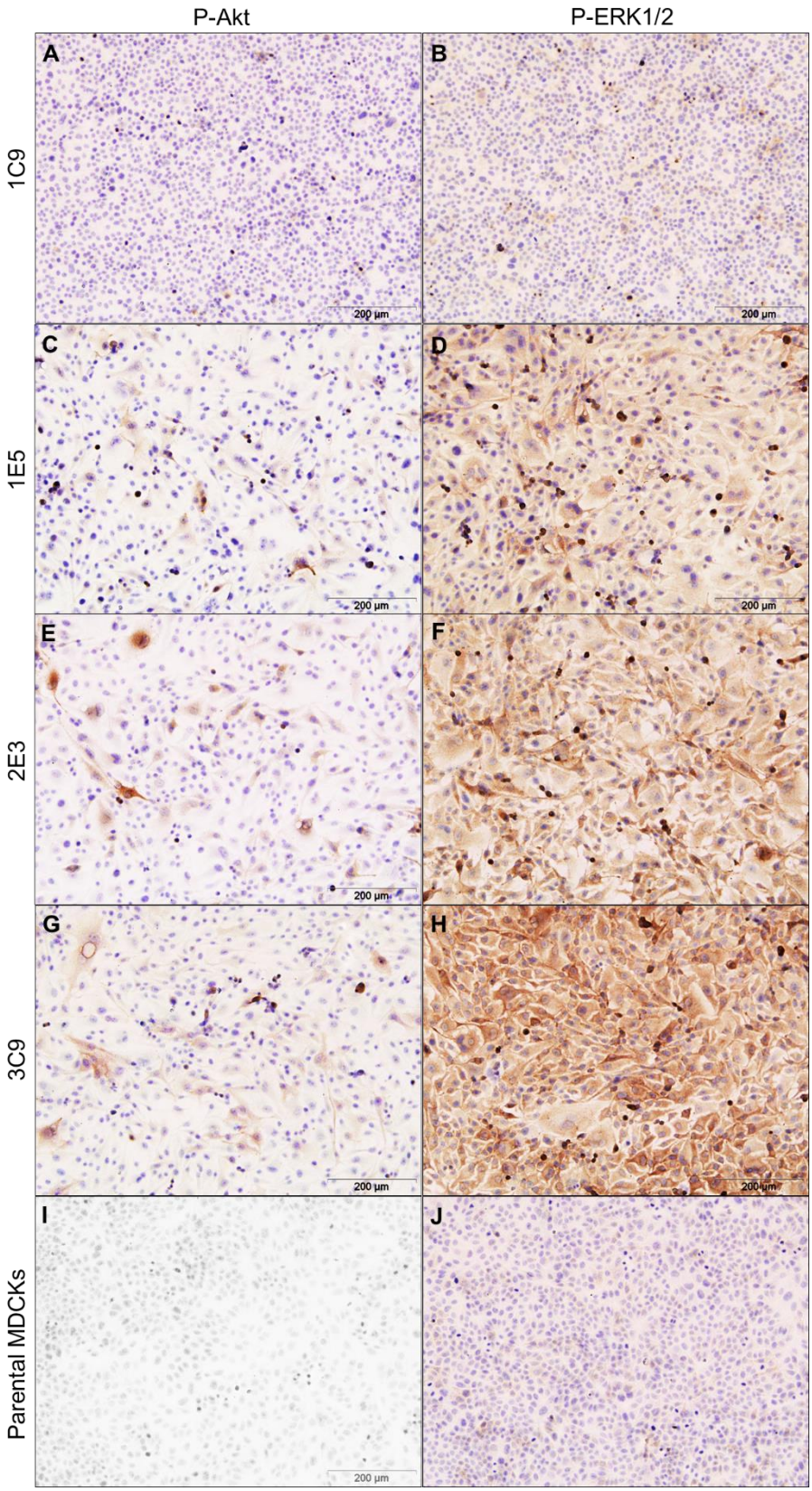

Figure 5.14. Immunocytochemical analysis of Akt-P and ERK1/2-P expression in MDCK clones. *Top labels indicate the protein detected, labels to the left indicate clone names. Brown pigment indicates positive staining.*

5.2.3.3 miRNA expression in transformed clones

The analysis of transduced MDCK cell clones suggested that come of them had retained Env expression and exhibited features expected of transformed cells (i.e., morphological changes and phosphorylation of Akt and ERK1/2). Next, expression of miRNAs in these clones was studied. To investigate if expression levels of miR-135b, miR-182, miR-183, miR-200b, miR-205, miR-21, miR-31, miR-503 and miR-96 were upregulated in JSRV Env transformed cells, RT-qPCR was performed on RNA from the high expressing JSRV Env clones (1E5, 2E3, 3C9) to compare miRNA expression levels of these clones to control non-transformed MDCK cells (section 2.6) (**Fig. 5.15**).

The results of RT-qPCR indicated that transformed MDCK clones expressing JSRV Env presented a different pattern of miRNA expression compared to control MDCKs. Expression levels of miR-135b, miR-205, miR-21 and miR-31 were found to be increased in JSRV Env expressing clones, following the pattern observed in OPA lung tissue. However, miRNAs miR-182, miR-183, miR-200b and miR-503 showed differential expression in the opposite direction to that observed in OPA lung tissue. No differential expression was detected for miR-96. These results suggest that expression of the tested miRNAs is altered in JSRV Env induced transformed MDCK cells. However, expression of some of the miRNAs does not follow the trend observed in lung tissue. These results may be related to multiple factors, and, in particular, the changes observed in tissue might reflect the complexity of the tissue made up from several different types of cells as opposed to the clonal epithelial cell lines used here. In addition, they may reflect species-specific differences between the canine cell line and the ovine lung tumour. Differing results from *in vitro* and *in vivo* studies have been reported in the literature (discussed further in section 5.3).

The experiments described above showed that although cell lines can be used to study Env transformation and miRNA expression, this approach is complicated by poor transfection efficiency and the instability of transformed clones. Potential reasons for this are discussed in section 5.3. However, as the aim of this study is to identify an *in vitro* system that closely models the role of miRNAs in JSRV Env-induced transformation, it is required to find an *in vitro* model that can reflect as

closely as possible *in vivo* early events of transformation. However, alternative approaches to establish an *in vitro* model for transformation were explored, including primary AT2 culture (**5.2.4**) and ovine lung slice culture (**5.2.5**).

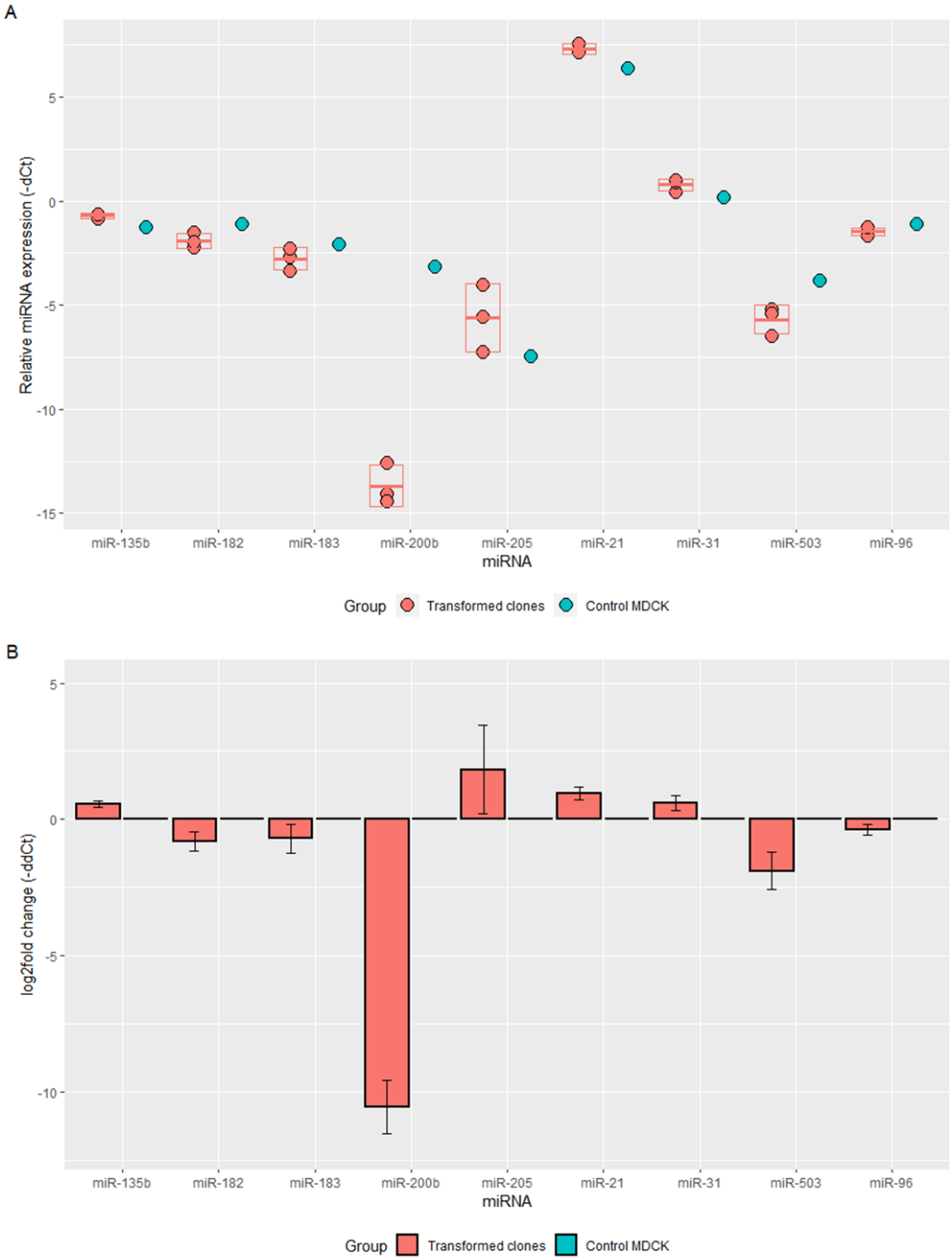

Figure 5.15. miRNA expression in JSRV Env transformed clones (n=3) compared to control MDCK cells (n=1) measured by RT-qPCR*. A. Relative miRNA expression (-dCt= -Ct miR+Ct miR-191) of each individual sample. Boxes show standard deviations of the mean, represented with a horizontal line. B. log2(fold change) expression between transformed clones and control MDCKs calculated (section 2.6.2). Error bars indicate standard deviation within groups.*

5.2.4 Isolation of type II pneumocytes

As a second approach to develop an *in vitro* model that would resemble *in vivo* miRNA expression in the sheep lung, the culture of cells derived from sheep was explored.

However, there are few established sheep cell lines currently available and those there are represent tissues other than the lung. Therefore, it was decided to attempt to establish primary sheep cell cultures from isolated type II pneumocytes (AT2), the target of JSRV in the sheep lung. If successful, such cultures would conceivably result in an *in vitro* model close to the *in vivo* situation. In addition, it could potentially allow for culture and replication of JSRV, a break-through that would facilitate further studies of infection and transformation not only using JSRV Env, but the whole virus. This would allow more detailed study of virus:host cell interactions during JSRV infection.

Isolation and culture of AT2 cells is notoriously challenging due to their sensitivity to the isolation procedures and due to their propensity to lose differentiation state (Witherden & Tetley, 2001). In addition, protocols that have been successfully developed in one species may not transfer successfully to other species (Lee et al, 2018). In the present study, isolation of AT2 cells was performed from lambs with no known lung pathologies. From each lamb three lung tissue pieces of ~12 cm^3 were collected, submerged in ice-cold HBSS and transferred to the lab. In the lab, tissue pieces were cut into ~5 cm^3 pieces. Isolation and culture of AT2 cells was performed a total of four times with cells from six animals, following an isolation protocol previously used for human lung AT2 cells (Witherden & Tetley, 2001) (section 2.11).

In the first isolation trial, cells from two lambs were used. At day 5, patches of cells of epithelial morphology became apparent in some wells (**Fig. 5.16**) suggesting that cells had been successfully isolated. Nevertheless, bacterial contamination was present in most wells, Gentamicin was added to the cultures (section 2.11) in an effort to stop bacterial growth. In successive isolations gentamicin was added to culture medium and solutions at all steps of the isolation and culture process. Another variation between AT2 isolation attempts were the selective attachment incubations, which varied between 40 minutes and 1:30 hours. Nevertheless, no

significant differences in cell yield were observed by increasing the incubation time.

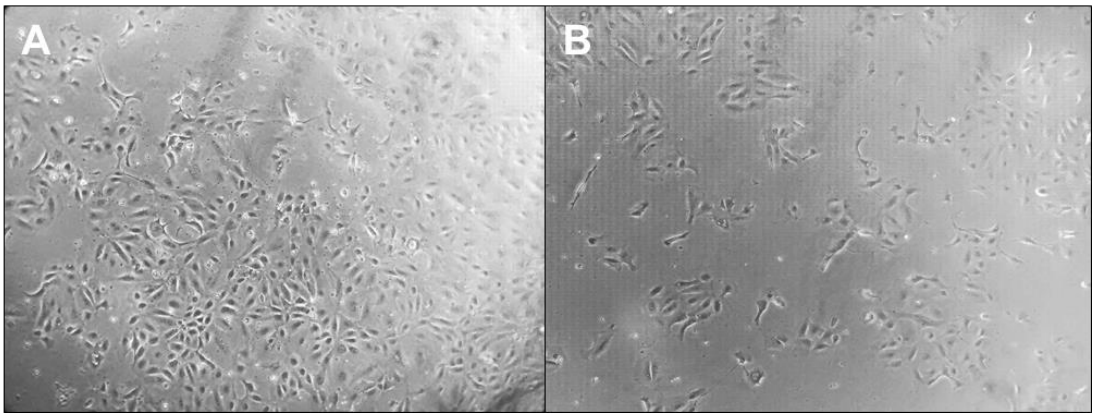

Figure 5.16. Microscopy images of cells isolated following an AT2 protocol at day 5. *A and B cells isolated and seeded at high and low density respectively.*

5.2.4.1 Characterisation of isolated cells

In order to investigate if the isolated cells were AT2 cells, they were tested for the presence of SP-C, a specific marker present only in AT2 cells. Cells were harvested 6 days post-isolation and cytospin preparations performed for immunocytochemistry (sections 2.10.4 and 2.10.6).

The presence of brown staining indicated that a high proportion of the isolated cells presented SP-C (**Fig. 5.17**), suggesting that they were AT2 cells. The isotype control presented no brown staining, indicating that staining was specific. Variability in size and morphology could be observed in SP-C positive cells.

The presence of SP-C in purified AT2 cell preparations indicated that the isolation and culture procedure had been successful. Cells obtained following the isolation procedure were counted before seeding and ranged between $4 \times 10^7 – 1 \times 10^8$ cells/ lamb. However, an issue encountered in all isolations performed occurred during the initial steps performed to wash off monocytes, erythrocytes and alveolar macrophages of sheep tissue. Installation of saline as described in the protocol did not render a pale section of tissue, and the erythrocyte count remained high. High erythrocyte concentration was observed throughout the isolation process and this interfered with the cell counts performed to determine the AT2 cells seeding concentration. These erythrocytes remained in culture until day four post-

isolation, when a PBS wash was performed in the cell culture plates and most were washed off.

In addition, the presence of erythrocytes interfered with results of immunostaining (**Fig. 5.18**). Brown staining indicating the presence of SP-C was observed in two different cell types: AT2 cells and anucleated cells of smaller size. In the isotype control, brown staining was observed only in the anucleated cells. Presence of these smaller cells is consistent with observations of erythrocytes in culture, and the brown staining observed is not specific, but a false positive result produced by the presence of endogenous peroxidases in erythrocytes.

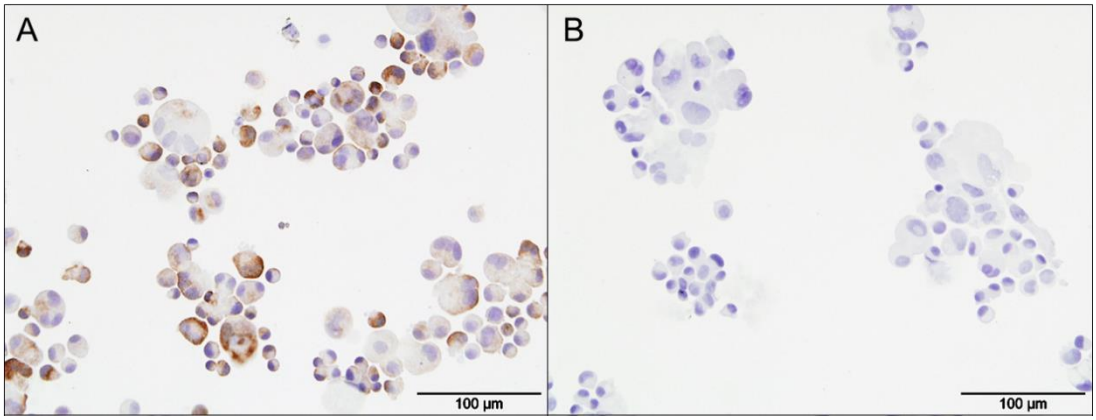

Figure 5.17. Immunostaining for AT2 cell markers in purified cells from sheep lung at day 6 post-isolation. *A. anti-SP-C staining of purified cells. B. Isotype control. Brown pigment indicates positive staining.*

In order to mitigate the effect of erythrocytes in the isolation, a method to selectively lyse them was tested (section 2.11) after removal of macrophages by incubating cells without FBS. Although erythrocyte lysis was successful and fewer numbers were observed in culture, the population of AT2 cells also appeared reduced, and many cells appeared dead. These findings might indicate that the lysis solution had a detrimental effect on the isolation process by also affecting AT2 cells. Nevertheless, as this process was only tested in one occasion, other factors such as the tissue status could have caused the low number of cells observed.

To further confirm that the isolated cells were AT2 cells other markers could be used. For example, AT2 cells also produce alkaline phosphatase which can be tested *in vitro*, but expression is lost when they start differentiating.

Interestingly, although AT2 isolation was attempted with lung tissue from 6 lambs, cells were obtained from only four lambs in all the isolation attempts performed. Given that the same isolation protocol had been performed in all cases, these differences might be an indication of biological variability in AT2 cell numbers or their accessibility in the tissue. In addition, as may be seen comparing **Fig. 5.17** and **Fig. 5.18**, variability in SP-C staining of AT2 cells was observed. Cells from **Fig. 5.17** appeared to present higher expression of SP-C even though they were tested at a later time point.

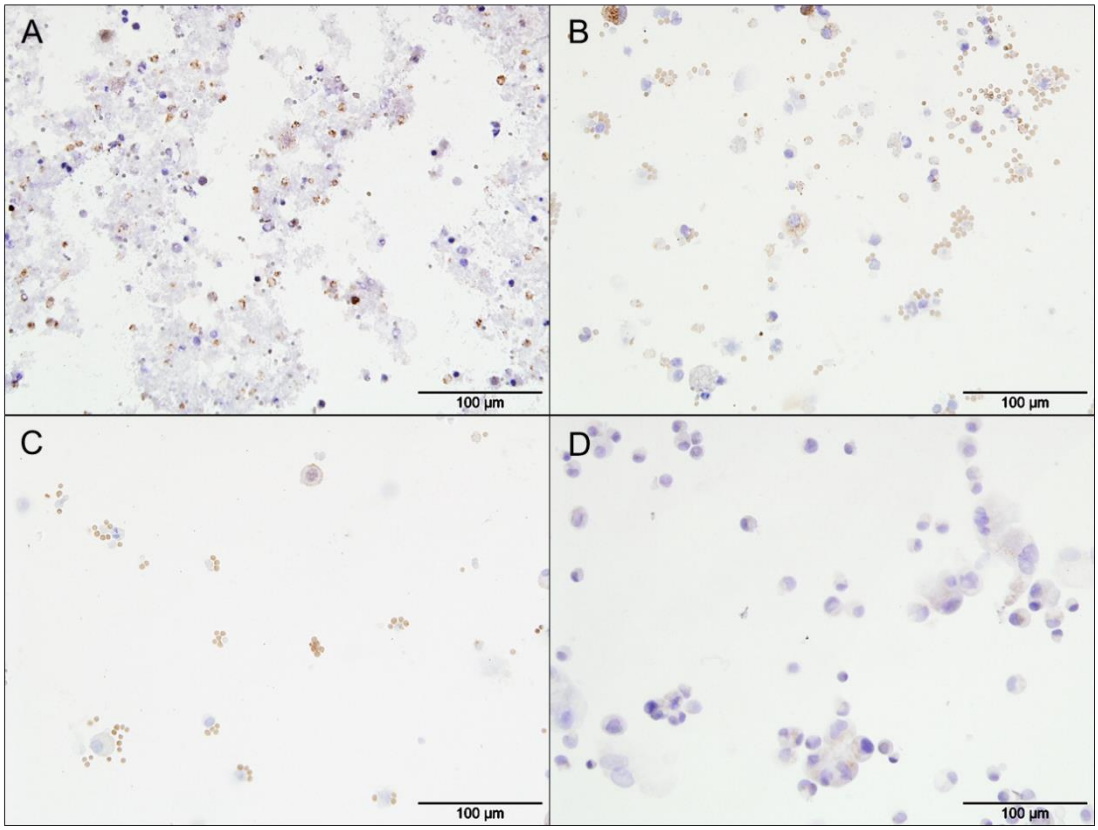

Figure 5.18. Staining of sheep lung cells at four different points during type AT2 cell isolation with an antibody anti-SP-C. *A. anti-SP-C staining of the cell suspension after filtration (40 µm) and centrifugation. B. anti-SP-C staining of the cell suspension after selective removal of macrophages. C. anti-SP-C staining of the cell suspension after selective removal of fibroblasts. D. anti-SP-C staining of isolated cells 4 days after isolation.*

5.2.4.2 Infection of type II pneumocytes with JSRV

In general, a low number of cells were present in the initial days after isolation but the cell population increased over time in culture, reaching 80% confluency by day 6. However, by day 7 morphological changes were evident: cell morphology became less regular, some cells became flattened and enlarged. Morphological

changes became more obvious in successive days and were suggestive of AT2 cell dedifferentiation. In addition, immunocytochemical analysis revealed that by day 8 SP-C expression could not be detected in cells (**Fig. 5.19**). The time window in which the cell population had increased sufficiently but no dedifferentiation changes were observed was, therefore only 2 to 3 days. These circumstances made it difficult to perform infections in cells to determine if JSRV was able to infect and replicate, and if JSRV Env induced transformation could be achieved.

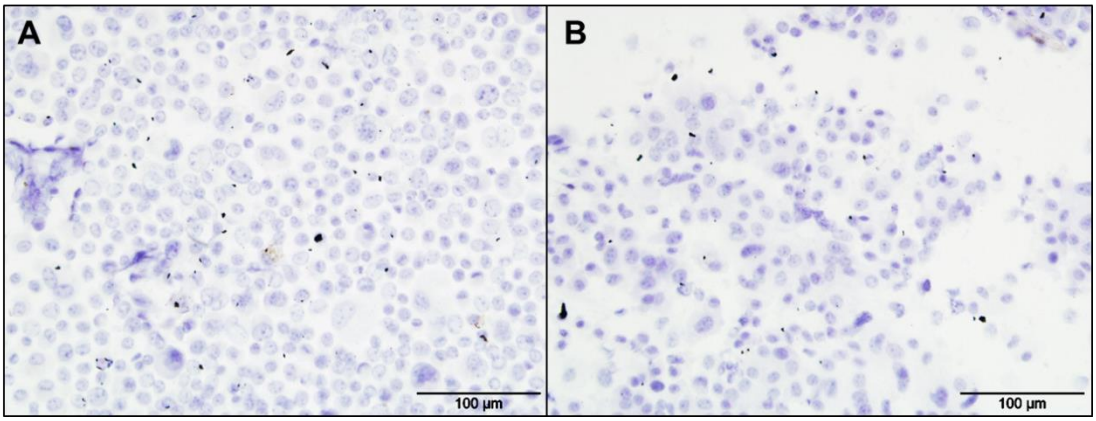

Figure 5.19. Immunostaining for AT2 cell markers in purified cells from sheep lung at day 8 post-isolation. *A. anti-SP-C staining of purified cells. B. Isotype control. Brown pigment indicates positive staining.*

Nevertheless, JSRV infection of AT2 cells was attempted on two occasions. Infections were performed on day 6 with $JSRV_{21}$ (*i.e.*, replication-competent virus) and a replication-deficient JSRV reporter virus (JSRV-GFP) (Szafran, 2014). This vector encodes EGFP under the control of a HCMV promoter and allows an assessment of the ability of JSRV to complete early steps in JSRV replication by quantifying GFP-positive cells. Three days post infection, fluorescence was detected in cells in all infected wells and controls, for both $JSRV_{21}$ and JSRV-GFP, indicating that the signal was due to autofluorescence in the AT2 cells. The fluorescent signal appeared greater in some cells in wells infected with JSRV-GFP but the limited number of cells available precluded the possibility of quantifying this by flow cytometry. Further analysis of $JSRV_{21}$-infected cells was also not performed due to the limited number of cells. Autofluorescence increased over subsequent days and cells died in all wells at day 10, indicating that the autofluorescence observed might have been a marker of cytotoxicity.

Although the infection experiments did not provide useful data, this work did demonstrate that the AT2 sheep cell isolation can be performed successfully following a protocol used for human lung, and this is a valuable starting point for future studies. Nevertheless, the low cell yields obtained complicated the JSRV studies. In order to improve the yield of viable cells, further optimisation and adaptation of the protocol to the ovine lung would be needed, discussed in section **5.3.** Although this system has potential to be an ideal *in vitro* model of JSRV infection, technical limitations and limited time to complete this project led to a decision to explore other systems in which miRNA expression could be studied. For this reason, further experiments were performed using ovine lung slices.

5.2.5 Lung slices as OPA model

As a further approach to develop a model that could recapitulate changes in miRNA expression in OPA-affected lung tissue, the use of ex vivo cultured lung slices was explored. Precision cut lung slices are an *ex-vivo* model of sheep lung that has the advantages of incorporating signals not only from infected AT2 cells but also surrounding cells. In addition, the system had already been successfully established in our laboratory and JSRV had been shown to be able to replicate in this system (Cousens et al, 2015) (section 1.3.3).

Lung tissue was obtained from lambs and lung slices prepared and grown in culture (section 2.20). The condition of the lung slices was assessed under the microscope and cilia movement in airways considered a sign of cell viability. Lung slices in culture were either transduced with lentiviral vectors or infected with JSRV.

5.2.5.1 Transduction of lung slices with lentiviral vectors

Lentiviral vectors were produced, concentrated and titrated in MDCK cells by flow cytometry (section 2.16.1). The titre of CSC-G was 1.6×10^5 TU/ml and for 4.5×10^4 TU/ml for CSC-GFP2AEnv. Nevertheless, due to time constraints the titration of vectors was performed after the transductions had been performed.

Because the titres of the lentiviral vectors were initially unknown, lung slices were transduced with equal volumes of CSC-G, CSC-GFP2AEnv or mock-transduced with concentrated supernatant of 293T cells (2.20.3). Lung slices transduced with

CSC-G were transduced at two different concentrations: either 4.8×10^3 CSC-G TU or 9.6×10^3 CSC-G per lung slice. Lung slices transduced with CSC-GFP2AENV were transduced with either 1.35×10^3 CSC-GFP2AEnv TU or 2.7×10^3 CSC-GFP2AEnv TU per lung slice. These two concentrations were used to assess whether JSRV Env expression in lung slices was correlated with vector concentration. CSC-G vectors and 293T supernatants were used as negative controls to differentiate miRNA expression changes induced by time in culture or response to the lentiviral vector, to those changes due to JSRV Env expression.

Lung slices exposed to either CSC-G or CSC-GFP2AEnv had foci of green fluorescent cells when observed under the microscope, suggesting that transgene expression and transduction had occurred successfully. The size of some green foci increased with time in culture indicating that the cells were dividing.

Lung slices were harvested at day 0, before transduction, and at day 8 and day 18 after transduction (section 2.20.5). Four lung slices were harvested and pooled together as samples for immunohistochemistry (section 2.10). The process was repeated to obtain four lung slices as samples for western blot (section 2.19), and four lung slices for RNA extraction (section 2.4.5).

Green foci were counted 12 days after transduction (**Table 5.4**) and the number of green foci counted used to assess differences in transduction between the two concentrations used. Lung slices that had been exposed to either CSC-G or CSC-JSenv had a greater number of green foci when transduced with a higher concentration of vector. In both cases, doubling the lentiviral vector input resulted in a 33% increase in the number of transduced foci. These differences suggested that the number of transduced cells could be increased further by increasing the amount of lentiviral vector particles used. However, the lowest concentrations of both vectors appeared to have the most favourable yield of transduced foci, as measured by the number of foci per TU. This unexpected result might be due to saturation of accessible and susceptible cells, or due to cytotoxicity of the vector at higher concentrations.

The difference in total number of foci between CSC-G and CSC-GFP2AEnv transduced lung slices was found to be statistically significant (T-test $p < 0.05$).

However, this may also be due to the different concentration of lentiviral vectors used.

Table 5.4. Number of green foci in lung slices 12 days after transduction.

	CSC-G (4.8×10^3 TU)	**CSC-G (9.6×10^3 TU)**	**CSC-GFP2AEnv (1.35×10^3 TU)**	**CSC-GFP2AEnv (2.7×10^3 TU)**
GFP-positive foci per lung slice	6	12	5	5
	5	13	3	6
	5	11	5	4
	10	8	4	5
	16	9	3	3
	9	7	1	4
	12	8	3	3
	5	19	2	5
	4	15	5	3
	8	7	4	6
	7	8	3	6
	10	13	5	8
	Average number of foci			
	8.1	10.8	3.6	4.8
	Total number of foci			
	97	130	43	58
	Number of foci per 10^3 TU of vector			
	20.21	13.54	31.85	21.48

JSRV Env expression in transduced lung slices

In order to assess JSRV Env expression in transduced lung slices, immunohistochemistry was performed with samples harvested at day 8 and day 18 (section 2.10). JSRV Env expression was not detected in any CSC-GFP2AEnv transduced slice at day 8, while at day 18, JSRV Env was detected in one of the transduced four lung slices (**Fig. 5.20**). As expected, JSRV Env was not detected in any CSC-G or mock-transduced lung slice. Isotype controls showed no brown pigment, indicating specificity of brown staining for JSRV Env presence.

Because the lentiviral vectors used are able to drive JSRV Env expression in several cell types efficiently, a higher percentage of JSRV Env expressing cells

was expected than was observed. The results presented here might be due to the low concentration of the lentiviral vectors used. As seen in the number of green foci detected, increasing the vector concentration results in an increase of transduced foci. Nevertheless, the present system is at best semi-quantitative, so the effects of lentiviral concentration on JSRV Env expression should be further investigated.

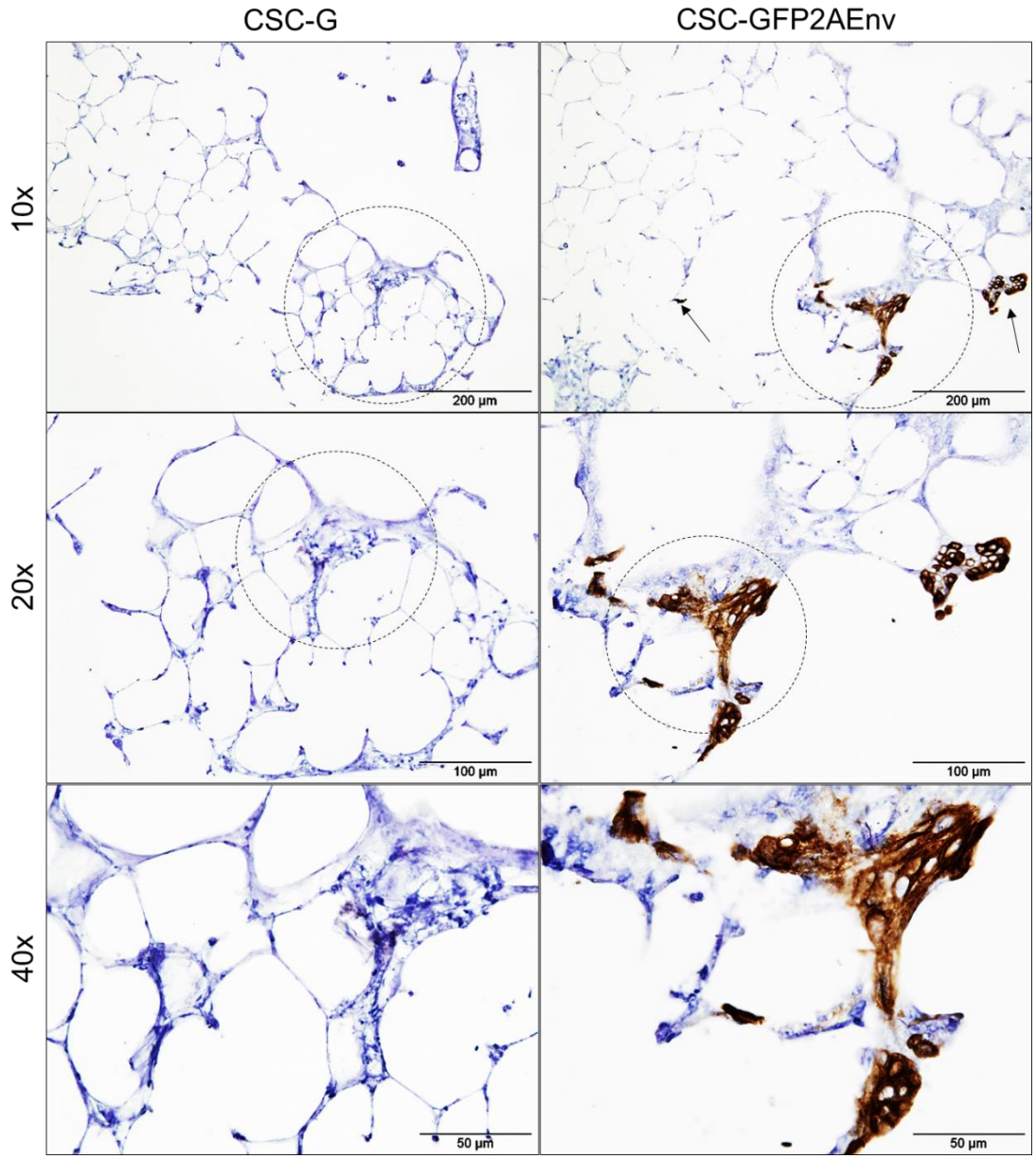

Figure 5.20. Staining of transduced lung slices at day 18 with anti-JSRV SU antibody. *Top labels indicate the vectors used for transduction, labels on the left indicate the magnification used. Brown pigment indicates positive staining. Arrows indicate foci with positive staining.*

miRNA expression in transduced lung slices

Despite the low number of positively transduced foci per slice, miRNA expression was evaluated from samples at day 8 and day 18 post-transduction to compare between CSC-C, CSC-GFP2AEnv and mock-transduced lung slices. This comparison aimed to identify miRNA expression changes due to JSRV Env expression.

Expression levels of miR-135b, miR-182, miR-183, miR-200b, miR-205, miR-21, miR-31, miR-503 and miR-96 were assessed by RT-qPCR. Levels of miRNA expression of CSC-G transduced lung slices and CSC-GFP2AEnv transduced lung slices were compared to miRNA expression in mock-transduced lung slices.

At day 8, differences in miRNA expression were observed between lung slices transduced at high and low concentrations of CSC-G and CSC-GFP2AEnv (**Fig. 5.21)**. However, expression levels of all the miRNAs tested, with the exception of miR-135b, were similar between CSC-G and CSC-GFP2AEnv transduced lung slices. miR-135b appeared downregulated in CSC-GFP2AENV transduced lung slices in comparison to mock-transduced (not represented) and CSC-G transduced lung slices at high concentration.

At day 18, similar miRNA expression patterns were observed in lung slices transduced with low and high concentration of the vectors, but fold change differences were higher in lung slices exposed to the higher concentration (**Fig. 5.22**). No differences in miRNA expression were observed between CSC-G and CSC-GFP2AEnv transduced lung slices, with the exception of miR-135b and miR-200b. Comparing findings at day 8 and day 18, most miRNAs followed the same expression trend, with the exception of miR-135b.

These findings indicated that there were differences in miRNA expression levels in lentiviral vector transduced lung slices compared to mock-transduced lung slices. However, in most cases, no differences in expression were observed between those transduced with CSC-G and CSC-GFP2AEnv, suggesting that the observed miRNA expression changes is caused by the lentiviral transduction and not by JSRV Env expression. Notably, the miRNA expression pattern in transduced lung slices did not mirror than of infected lung tissue. This difference

in miRNA expression between transduced lung slices and lung tissue could be due to a number of factors: miRNAs might become upregulated later on the transformation process or other proteins of JSRV might also play a role in their upregulation. In addition, these results seemed to indicate that expression of miR-135b was the most variable under the present transduction and culture conditions.

In order to further investigate if the changes in miR-135b observed were related to JSRV Env expression, and to address the role of other JSRV proteins in miRNA expression changes, further experiments were performed with $JSRV_{21}$.

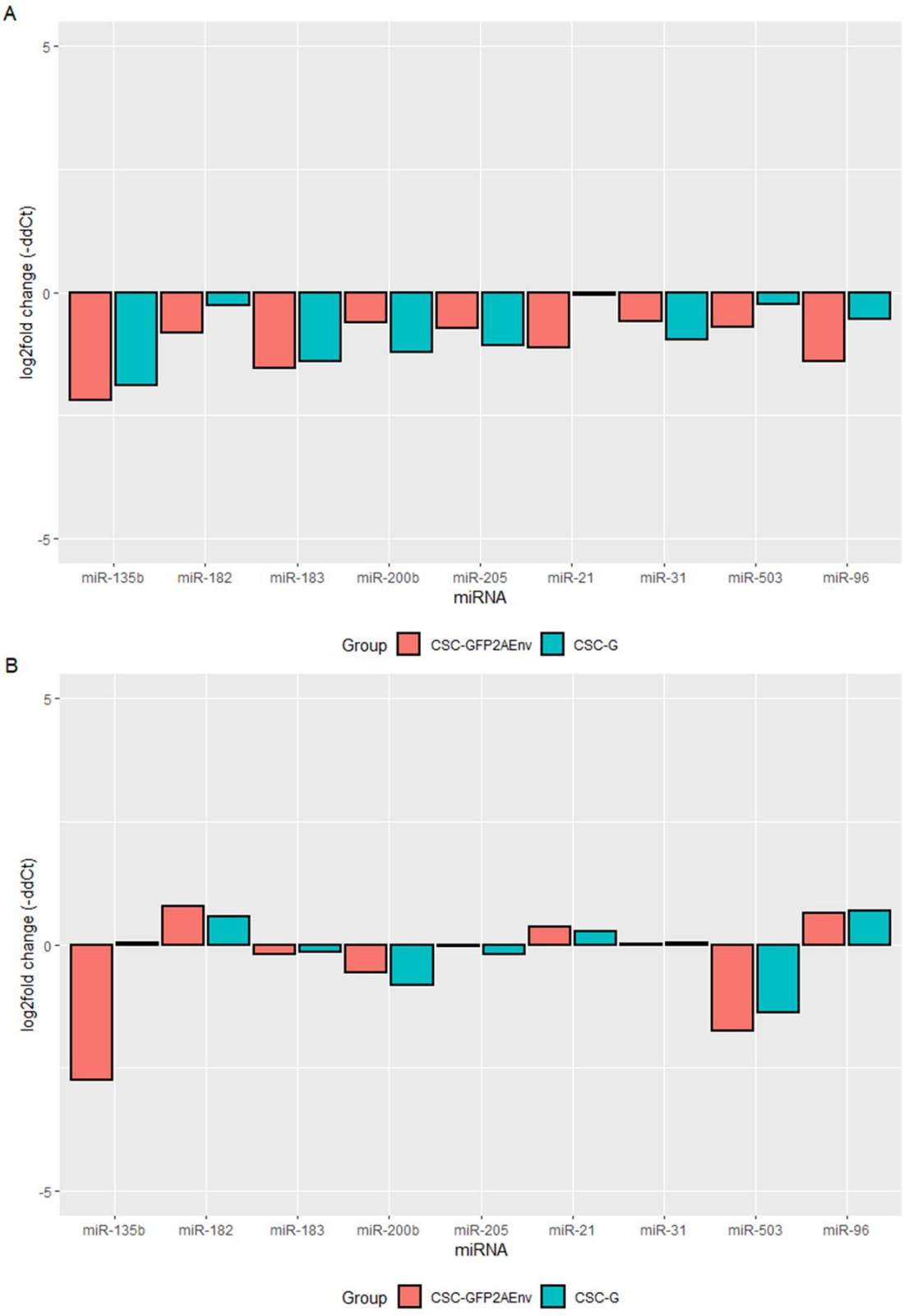

Figure 5.21. miRNA expression at day 8 in transduced lung slices with CSC-GFP2AEnv and CSC-G. *The figure shows miRNA expression relative to mock-transduced lung slices (not represented) measured by RT-qPCR. A and B. log2(fold change) expression of transduced lung slices with low (A) and high (B) concentrations of lentiviral vectors.*

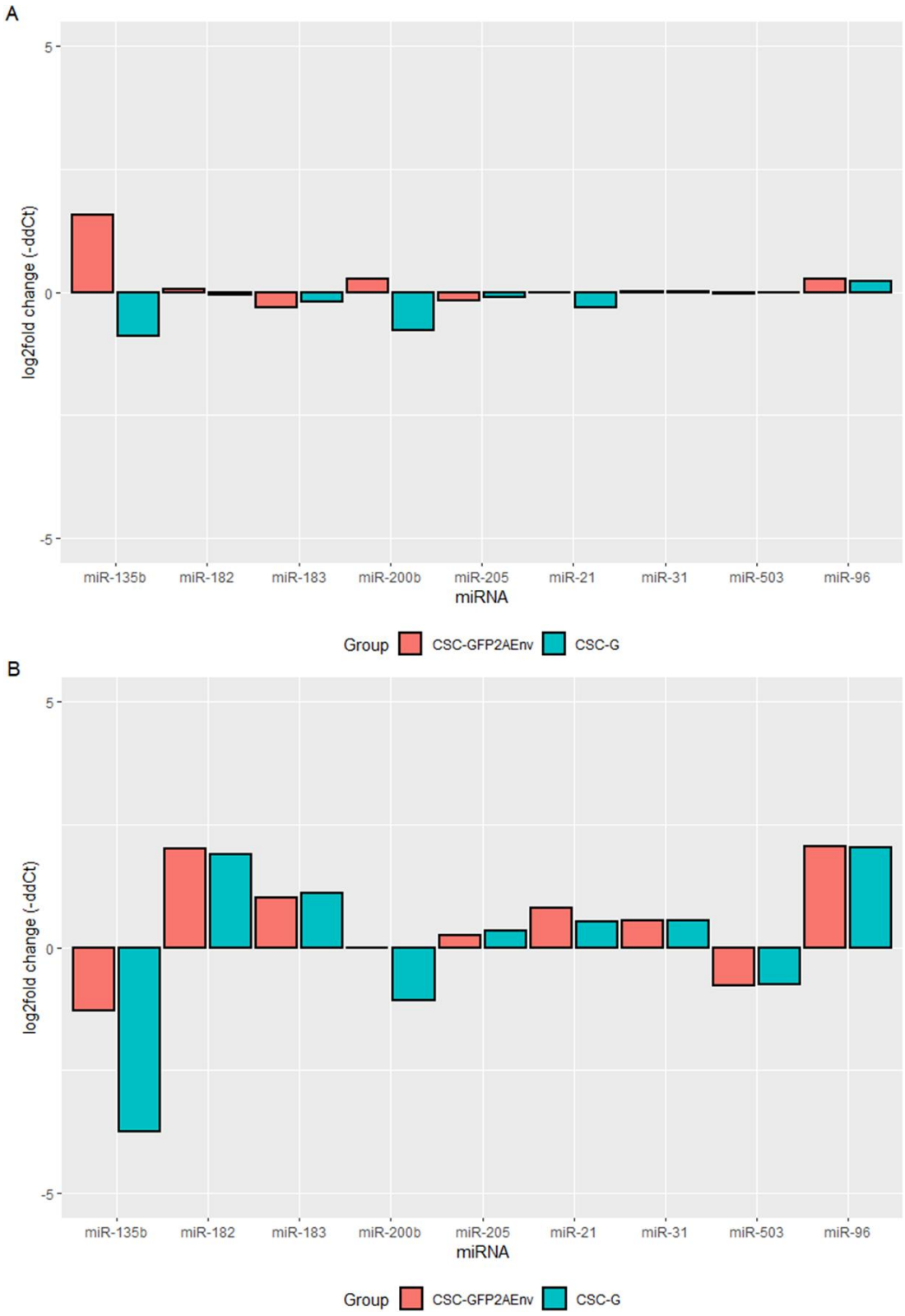

Figure 5.22. miRNA expression at day 18 in transduced lung slices with CSC-GFP2AEnv and CSC-G. *The figure shows miRNA expression relative to mock-transduced lung slices (not represented) measured by RT-qPCR. A and B. log2(fold change) expression of transduced lung slices with low (A) and high (B) concentrations of lentiviral vectors.*

5.2.5.2 Infection of lung slices with JSRV21

In order to address the possibility that miRNA changes had not been observed due to other JSRV proteins playing a role in upregulation of the tested miRNAs, infections with JSRV were performed. In addition, lung slices from two lambs were used to assess the effect of biological variation and perform statistical tests.

$JSRV_{21}$ was produced *in vitro* by transient transfection of 293T cells, and concentrated by ultracentrifugation. As there is no permissive cell line for JSRV replication, it is not possible to determine the infectious titre. Therefore, the virus was quantified by assaying for reverse transcriptase activity (section 2.20.5). As a negative control, lung slices were mock-infected with concentrated 293T supernatant, the cells used to produce the virus.

JSRV (10.5 ng RT/slice) was used to infect lung slices in culture (section 2.20.4). The viability of lung slices post-infection was assessed by microscopy: cilia mobility was considered a sign of good viability, whereas detachment of cells from the lung slices and media acidification were considered signs of a poor lung slice status. Infected and mock-infected lung slices presented good viability.

Lung slices were harvested at day 0, before infection and day 10 after infection (section 2.20.5). At each time point, four lung slices were collected for immunohistochemistry, and four lung slices collected for RNA extraction. Supernatant from lung slices was also collected to measure JSRV presence by RT-qPCR (section 2.20.5.1).

JSRV Env expression in infected lung slices

To assess JSRV Env expression in infected lung slices, immunohistochemistry was performed (section 2.10) with samples harvested at day 10 after infection.

In lung slices infected with JSRV a small number of foci of cells expressing JSRV Env was found (**Fig. 5.23**). The brown staining observed was only observed on cells on the periphery of the slices and not on cells in the interior of the slice. No brown staining indicative of JSRV Env expression was detected in mock-infected lung slices or in cells treated with the isotype control antibody.

Similar to lentiviral vector transduced lung slices, the number of foci staining positive for JSRV Env represented a low percentage of the tissue. Lentiviral vectors are able to infect and potentially drive protein expression in several cell types of the lung slices due to JSRV *env* expression being driven by a CMV promoter, which was expected to result in a higher number of cells expressing JSRV Env. In contrast, JSRV can only efficiently express its proteins in AT2 cells but is able to replicate, meaning that re-infection is possible.

In order to investigate if JSRV expression could be detected in lung slices and if replication had occurred, RT-qPCR was performed to detect JSRV expression (section 2.20.5.1) in the supernatants of lung slices and controls.

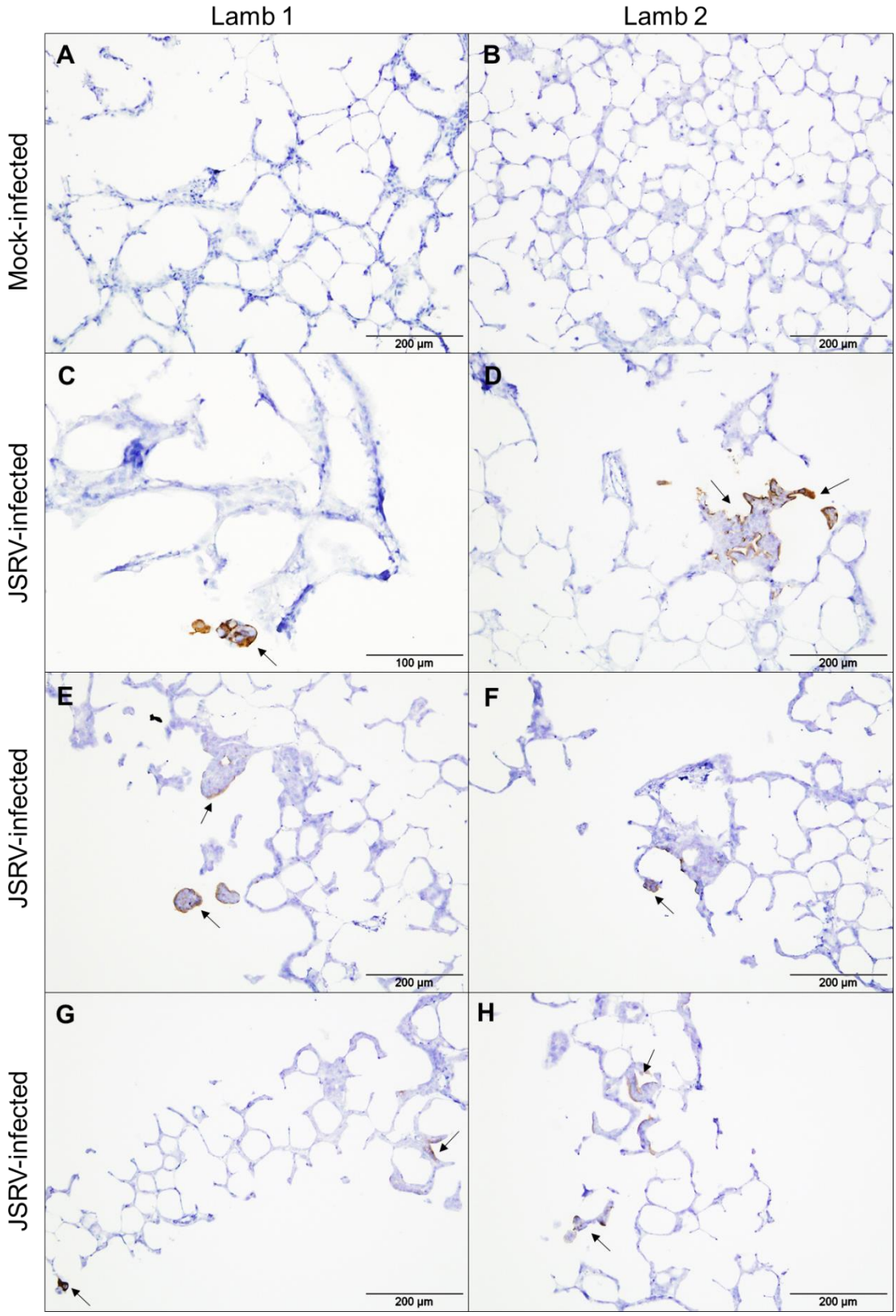

Figure 5.23. Staining of lung slices at day 10 post-infection with anti-JSRV SU antibody. *Top labels indicate the lamb from which lung slices were derived, labels on the left indicate the virus used for infection. Arrows identify areas in which brown pigment was observed. Brown pigment indicates positive staining.*

The results of RT-qPCR (**Table. 5.5**) indicated that JSRV was present in the supernatant of lung slices of both lambs at day 10. Compared to the positive controls used, higher Ct values were obtained, indicating a lower concentration of JSRV. Nevertheless, when comparing these results, it needs to be considered that the input virus is a concentrated stock produced from 293T cells, where more than 50% of the cells in culture are producing virus. In lung slices, only a small number of cells produce virus. JSRV was not observed in the supernatant of lung slices before infection or in mock-infected lung slices. These results suggested that JSRV had successfully replicated in the lung slices and had been released to the medium. It could be argued that presence of JSRV in supernatants might be residual from the initial inoculate. However, supernatants had been collected 10 days after infections and medium changes performed every day since infection, making the JSRV expression observed unlikely to originate from the inoculate. In addition, previous work (Cousens et al, 2015) suggested that all input virus was undetectable at day 4 post-infection.

Table 5.5. Ct values of JSRV expression in supernatants of lung slices and controls by RT-qPCR.

	Sample	Ct
	$JSRV_{21}$ virus preparation	14.01
	Lung fluid	16.38
	Water (negative control)	40
Lamb 1	Supernatant before infection	40
	Supernatant day 10- $JSRV_{21}$ infected	23.85
	Supernatant day 10- Mock infected	40
Lamb 2	Supernatant before infection	40
	Supernatant day 10- $JSRV_{21}$ infected	22.87
	Supernatant day 10- Mock infected	40

miRNA expression in transduced lung slices

Having successfully detected the presence and replication of JSRV in lung slices, albeit with only a small number of positive foci, RT-qPCR was performed to study miRNA expression. In order to compare miRNA expression in infected lung slices, RNA was prepared and expression levels assessed by RT-qPCR (method). miRNA expression in lung slices infected with JSRV or mock-infected were

compared to miRNA expression in lung slices before infection. The use of mock-infected lung slices controlled for miRNA changes occurring due to lung slices aging in culture.

Levels of miRNA expression in lung slices of Lamb 1 and Lamb 2 (**Fig. 5.24**) presented in some cases differences, most notable in expression levels of miR-135 and miR-503. Levels of all tested miRNAs changed compared to miRNA levels before infection (**Fig. 5.24**). However, levels of miRNA expression were similar in mock-infected and JSRV-infected lung slices. These findings indicated that miRNA expression changed with time in culture, maybe due to lung slices aging.

In addition, the results indicated that the infection conditions used did not alter miRNA expression by day 10. Lack of miRNA expression changes in infected lung slices might be due to several factors: because few cells were seen to express JSRV Env it could be that miRNA expression changes due to aging in culture might have masked miRNA expression changes due to JSRV infection. It might also indicate that miRNA changes do not occur shortly after infection but later on, after other molecular events.

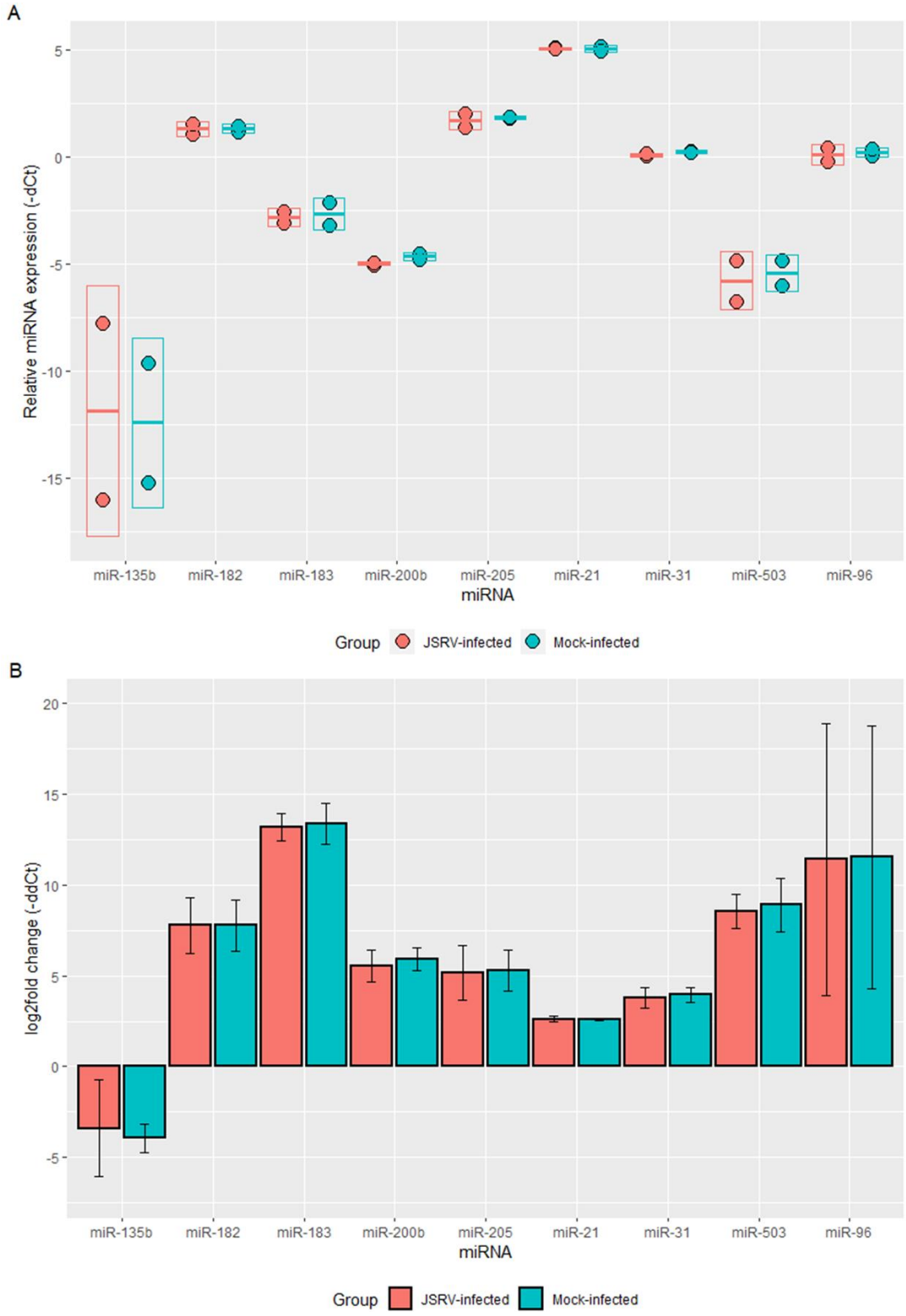

Figure 5.24. miRNA expression in lung slices at day 10 post-infection, compared to miRNA expression at day 0 (not represented) measured by RT-qPCR. *A. Relative miRNA expression (-dCt= -Ct miR+Ct miR-191) of lung slices infected with JSRV (n=2) and mock-infected (n=2). Boxes show standard deviations of the mean, represented with a horizontal line. B. log2(fold change) expression between JSRV and mock-infected lung slices at day 10 compared to day 0, calculated as explained in section 2.6.2.*

5.2.5.3 Infection of lung slices with $JSRV_{21}$- study 2

In order to investigate if the lack of miRNA changes in JSRV infection were due to the low number of JSRV Env expressing cells or due to the time window selected to analyse miRNA expression, another experiment was performed.

To address whether low levels of infection were responsible for the results obtained, JSRV concentration in lung slices was increased, expecting it would have an effect in the number of infected cells. To address whether 10 days were insufficient to observe miRNA expression changes in JSRV infection, sample points were increased.

Lung slices from three lambs were used and infected with 143.52 ngRT, 13.7-fold more JSRV than used in the previous study, as measured by RT-assay (section 2.20.5.2). In addition, the initial infection time was increased from 24 h to 48 h and medium changes were performed every two days instead of every day to increase chances of re-infection. As before, a parallel series of lung slices was treated with 293T supernatant to provide a mock-infected control. Samples for immunohistochemistry, RNA extraction and western blotting were collected before infection and at day 7, day 14 and day 28 post-infection.

Lung slices were observed under the microscope every day to assess their viability. From day 10 after infection, the viability appeared to decrease both in JSRV infected and mock-infected lung slices, cells detached from the tissue slice at an increased rate and the culture medium became a yellowish colour, indicating acidification. These changes had not been observed in published studies until day 21 in culture (Cousens et al, 2015) (section 1.3.3), suggesting that the culture conditions had accelerated aging and degradation of the lung slices. Because the main change performed was the frequency of medium changes, exhaustion and acidification of the culture medium might have been responsible for the degradation observed. From day 14 after infection, the culture medium volume was doubled to avoid exhaustion. However, progressive degradation was observed and the experiment was ended at day 28, but no immunocytochemistry samples could be collected at this point due to extensive degradation.

JSRV Env expression in infected lung slices

In order to determine if increasing JSRV concentration in infection had caused an increase in cells expressing JSRV Env, immunocytochemistry was performed with samples taken before infection, and at day 7 and day 14 after infection.

The results of immunohistochemistry revealed that brown staining indicative of JSRV Env was present at day 7 and day 14 after JSRV infection of lung slices from lambs 3, 4 and 5. In contrast JSRV Env was detected in lung slices from lambs 2 and 3 infected with JSRV only at day 7 after infection. Therefore, the increase in virus inoculum did not result in the expected increase in JSRV-positive cells compared to the previous experiment. In fact, in lambs 2 and 3, infection was lower than in previous studies. **Fig. 5.25** is a sample of the immunohistochemistry results obtained, and shows the foci with the greatest positive staining at each time point. Mock-infected lung slices of all lambs were negative for JSRV Env presence as expected, as were isotype controls, indicating specificity. Positive controls of JSRV Env presence (**Fig. 5.25**) presented brown staining as expected.

These findings indicated that increasing JSRV concentration during infection did not result in an increased number of cells expressing JSRV Env. These results added to differences in cells expressing JSRV Env between lambs, suggested that the frequency of JSRV Env expressing cells was not directly correlated to JSRV concentration, but could be related to biological variability in susceptible cells. This and alternatives to increase JSRV Env expression will be further discussed in 5.3.

miRNA expression in these samples was not measured due to the low number of cells expressing JSRV Env and the lung slice degradation observed, which could have masked changes in miRNA expression by the low number of JSRV Env expressing cells.

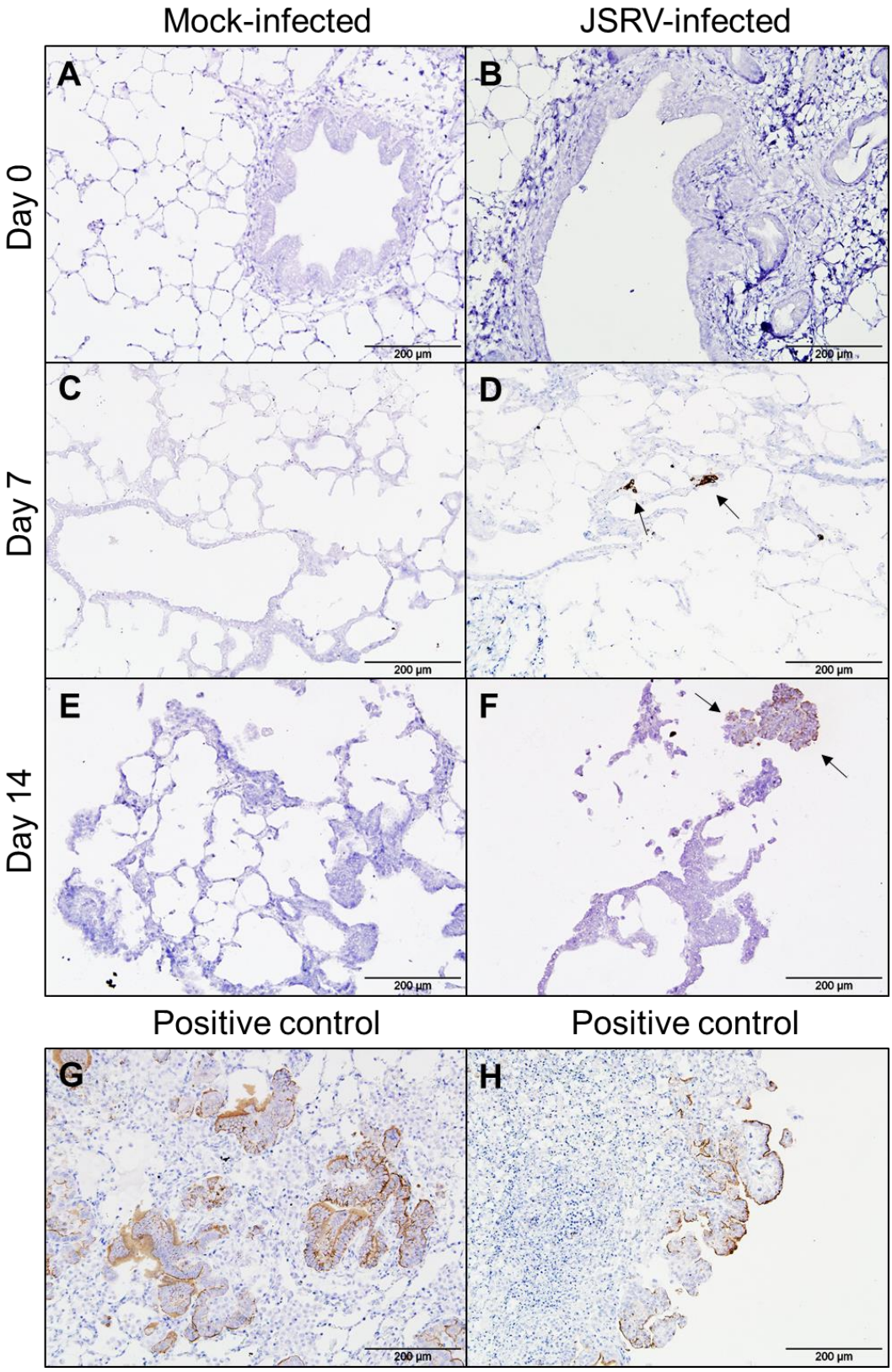

Figure 5.25. Staining of lung slices and controls with anti-JSRV SU antibody. *Top labels indicate the virus used to infect lung slices, the labels to the left indicate sampling time points post-infection. G. lung tissue from a natural OPA case. H. Lung slice from a previous infection. Arrows indicate areas with brown pigment. Brown pigment indicates positive staining.*

5.3 Discussion

The ultimate aim of this chapter was to explore the role of miRNAs that are upregulated in OPA lung tissue, in JSRV Env mediated transformation. Nevertheless, to achieve this, an *in vitro* model that would allow the study of miRNAs had to be established. Initially, previously established JSRV Env transformation models were explored. However, cell lines were not efficiently transfected, which ruled out analysis of miRNA changes mediated by JSRV Env. The use of lentiviral vectors proved to be an efficient delivery system of JSRV Env, but transformed cells were unstable and did not reflect miRNA expression changes observed in lung tissue. To obtain an *in vitro* model that would more closely reflect changes in the OPA lung, sheep AT2 cells were isolated from sheep lung and cultured. The isolation process was successful, but due to low yield and cell dedifferentiation the system could not be used to study JSRV infection. Ovine lung slices were then explored as an *ex vivo* model of JSRV infection. Infection of lung slices was successful but, it appears that due to the small number of foci expressing JSRV Env, miRNA changes due to JSRV Env expression were not observed. Increasing JSRV concentration did not result in an increase in JSRV Env expression, indicating that availability and susceptibility of AT2 cells might be the limiting factor. Overall, this chapter has applied new and established approaches to study JSRV Env transformation to the study of miRNA expression. However, further work is required to establish a model in which miRNA changes associated to JSRV can be studied.

5.3.1 JSRV Env transformation of cell lines

Transformation of *in vitro* cultured cell lines with oncogene-carrying retrovirus is a long-standing technique used in the study of these virus. In the JSRV field, this approach has been used to establish the role of Env and determine some activated pathways. However, when transfection was used to deliver plasmids encoding JSRV Env into cell lines no transfection was achieved. Cell lines transfected with JSRV *env* encoding plasmids expressed JSRV Env in only a low percentage of cells, suggesting the transfection efficiency was suboptimal. The efficiency of three transfection methods was assessed in MDCK and NIH 3T3 cells, and nucleofection was found to be the method with the highest efficiency.

Nevertheless, transfection efficiency was markedly reduced when plasmids encoding JSRV Env, rather than pGFPmax, were used to transfect cells.

Subsequently, Induction of transformation by JSRV Env was successfully achieved using lentiviral vectors to deliver JSRV *env* into MDCK and 208F cells. Lentiviral vectors encoding g*fp2Aenv* or *env* were produced, and their ability to drive GFP and Env expression assessed in 293T cells by immunostaining and immunoblotting. Whereas immunostaining of JSRV Env with an anti-JSRV SU antibody appeared specific, the use of the same antibody to validate findings by western blot resulted in background unspecific staining of JSRV Env. Because in immunostaining the proteins are in their native state and in immunoblotting the proteins assessed are denatured proteins, these findings might indicate that the anti-JSRV SU antibody used recognises a specific protein conformation or part of a sequence that is close in space, but not in the primary protein sequence.

Whereas pCSC-gfp2Aenv was found to efficiently express GFP and Env in transfected 293T cells, pCSC-JSenv only elicited expression of JSRV Env in a low proportion of cells in culture. Because transfections were performed simultaneously with pCSC-GFP2AEnv, which resulted in high expression of JSRV Env, the transfection process was not likely to be the cause of it. A possibility is that insertion of the *env* ORF into the CSC backbone allowed for unanticipated splicing that prevented expression of the full-length *env* transcript. This hypothesis could be tested by performing an RT-qPCR or northern blot and looking for expression of transcripts of different length. However, if that is the explanation it is unclear why it did not affect expression in GFP2AEnv.

CSC-GFP2AEnv was used to transduce MDCK and 208F cells and morphological changes consistent with transformation events observed between 2-3 weeks after transduction. Transformed 208F cells presented foci formation and GFP expression, these foci were expanded in culture but cells growing from them were not GFP or JSRV Env positive, indicating that they had lost expression of the transgenes.

Transformed MDCK cells were sorted based on their expression of GFP. Sorted clones were successfully expanded in culture from single cells expressing GFP,

and their JSRV Env expression assessed by immunocytochemistry. Nine clones were found to express both JSRV and GFP and of those, three expressed JSRV Env in most of the cells tested. Interestingly, two of the clones presented a slower growth rate than other clones or parental MDCKs. These findings could be due to differences in the site of insertion of the transgene, or due to heterogeneity of MDCK cells (Arthur, 2000). Interestingly, the loss of JSRV Env expression was also observed in some of the clones. Because the construct G*FP2AEnv* is under control of the same promoter (CMV) and expressed as a single mRNA, GFP expression was expected to be indicative of JSRV Env expression. It has been reported that use of the self-cleaving peptide P2A does not result in 100% efficient cleaving, which might result in protein forms that are not functional (Cai et al, 2017b), and the first protein in the transcript being expressed more efficiently than the second one (Liu et al, 2017). These might explain differences in expression levels between GFP and JSRV Env. However, this would appear to be unlikely to explain the total lack of JSRV Env expression. Another possibility is that splicing variants might exist for the produced mRNA, resulting in functional and non-functional versions of JSRV Env, and these splicing variants might be expressed in MDCK cells. Expression of JSRV Env might represent a burden to the cells and cells expressing it might have been negatively selected. The presence of splicing variants of the *gfp2Aenv* in transduced MDCK cells could be tested for by RT-qPCR or northern blot.

Another possibility is the accumulation of point mutations in the JSRV *env* gene inserted in MDCKs, which could result in a non-functional version of the protein while not affecting GFP expression. If JSRV Env is cytotoxic to MDCK cells these mutations could confer a selective advantage. This hypothesis could be tested by performing DNA extraction from the clones and performing a PCR to amplify the JSRV *env* gene, the amplified gene could then be sequenced and mutations identified.

The three clones were assessed for presence of transformation markers and were found to present Akt-P and ERK1/2-P, markers of JSRV Env driven transformation. These results indicated that MDCK cells had successfully been transformed with JSRV Env. The expression pattern of ERK1/2-P and Akt-P was

found to be different in the transformed clones, since ERK1/2-P was expressed by all cells and Akt-P only by a subpopulation. These findings are in contrast with studies of transformation in JSRV-infected lung slices and OPA lung tissue, in which Akt-P is detected in more cells and more intensely than ERK1/2-P (Cousens et al, 2015). These differences might indicate that the importance of these signalling pathways in JSRV Env transformation is species dependent. Another explanation is that activation, transduction and transformation with JSRV Env might present signalling differences compared to infection and transformation with the whole JSRV virus; other viral proteins might play a role in signalling in sheep.

5.3.2 miRNA expression in transformed MDCK clones

Expression of upregulated miRNAs in OPA lung tissue was measured in transformed clones and compared to miRNA expression in parental MDCKs. Differences in expression were found between transformed clones and parental MDCKs, these differences are likely to reflect the effects of JSRV Env transformation in MDCKs. Nevertheless, expression of some tested miRNAs did not follow the same upregulation pattern observed in OPA lung tissue. Although further testing would be needed to achieve better representation of miRNA expression in MDCKs, there are several factors that could explain the difference in miRNA expression between transformed MDCKs and OPA lung tissue. MDCK cells are a cell line derived from dog cells, but sheep are the natural host of JSRV, so there might be species differences in miRNA response to JSRV Env expression. This explanation is consistent with the observation that JSRV Env activates different signalling pathways depending on cell type (Hofacre & Fan, 2010; Liu & Miller, 2007). Another potential reason for differences in miRNA expression is that MDCK cells represent only one cell type, whereas lung tissue is a complex tissue made up from diverse cell types, which includes not only infected and transformed cells but also cells responding to transformation such as macrophages. Differences between miRNA expression in tissue and cell lines have been reported (Dambal et al, 2015; Patnaik et al, 2012). In addition, culture conditions have the potential to alter the expression levels of certain miRNAs, and a study found that the use of FBS could interfere with miRNA detection in extracellular vesicles (Ikari et al, 2015; Kuosmanen et al, 2017; Wei et al, 2016).

Expression of miR-200b was markedly different between transformed MDCK cells and OPA tissue. miR-200b is a miRNA involved in EMT. MDCK cells have been widely used to study EMT, and it has been shown that activation of the MAPK pathway in these cells causes autocrine production of TGF-β (Lehmann et al, 2000). Synergistic action between TGF-β and ERK MAPK promotes phenotypic changes in the cell, from epithelial to mesenchymal (Nicolas et al, 2003). Therefore, it might be possible that miR-200b is different between transformed MDCK cells and OPA lung tissue due to differences in EMT activation. Transformed MDCK cells might be undergoing EMT, whereas OPA tumours in lung tissue are not usually highly invasive or undifferentiated, suggesting that they might not be undergoing EMT.

In summary, MDCK cells did not replicate miRNA expression seen in sheep lung, but they may be a useful model for investigating miRNAs with similar expression levels to sheep lung. In that case, levels of specific miRNAs could be knockdown or overexpressed to study their effect in JSRV Env transformation. In addition, targets of specific miRNAs could be investigated by performing reporter assays or approaches such as CLASH-seq (section 1.5.3).

5.3.3 Isolation and culture of AT2 cells

An alternative approach to develop an *in vitro* system for studying miRNAs in Env-mediated transformation, the isolation and culture of ovine AT2 cells was attempted. Such a system might resemble the events of natural infection more closely than MDCK and other cell lines, and help address the issue of species specificity. Isolation of AT2 cells is known to be challenging, and methods that work in one species such as mice, might not work in sheep. Here a method previously used for human lung was selected. Isolation of AT2 cells was successful as confirmed by the presence of SP-C in isolated cells. However, the number of cells obtained during the isolation process was low and this was an impediment to performing infections with JSRV in the short time window before dedifferentiation of the cells. One issue was the presence of erythrocytes that were not successfully removed from culture, which interfered with cell counts and identification. In addition, the low yield of AT2 cells might also be due to the isolation process performed. The protocol performed was optimised for the use of

human AT2 cells and there might be differences in tissue structure between sheep and human that make the protocol used not optimal for the release and isolation of sheep AT2 cells. Isolation of AT2 cells from normal and tumour tissue of sheep lung has been reported in a study (Archer et al, 2007). However, the study was centred on isolation of tumour AT2 cells and reported that AT2 cells from normal lung tissue could be maintained in culture for less than 10 days. In addition, SP-C expression was tested only 4-7 days after isolation. Review of the isolation protocol in that study revealed no selective adherence steps, which could result in isolation of other cell types. The study found that JSRV could be detected in AT2 tumour-derived cells in culture, but expression of JSRV was lost after ~5 passages. The authors reported that JSRV expression in AT2 cells was extended when cells were cultured in 3-D, consistent with previous findings (Johnson & Fan, 2011).

A recently published study reported a protocol for the isolation of bovine AT2 cells (Lee & Chambers, 2019; Lee et al, 2018). This protocol for AT2 cell isolation might be better adapted for sheep than the human lung isolation protocol, due to expected similarities between lung tissue of ruminant species. The article also reported dedifferentiation of AT2 cells, but culture in matrigel resulted in formation of structures similar to alveoli.

Future work would be important to compare the protocols of Lee et al (2018)with that used in the present study (Witherden & Tetley, 2001). In addition, isolation of AT2 cells could be optimised to improve cell yields and perform infections with JSRV. However, the effect that JSRV infection would have on these cells in *in vitro* culture remains unknown. Improved cell yields would also permit the use of 3D culture systems in matrigel or prefabricated scaffolds (reviewed in Duval et al (2017)). 3D culture has been previously used to culture both cell lines and primary cells (Elia & Lippincott-Schwartz, 2009; Gkatzis et al, 2018; Johnson & Fan, 2011) and has been able to maintain cell polarity and adhesion for extended periods of time (Baker & Chen, 2012). Nevertheless, the culture of cells in 3-D remains low-throughput and standardisation more troublesome (Duval et al, 2017).

5.3.4 miRNA expression in lung slices transduced with JSRV Env encoding vectors

As previous work had confirmed that JSRV can infect and transform cells in lung slices, dysregulation of miRNAs in response to JSRV Env was investigated in lung slices in culture. Lentiviral vectors encoding *gfp* or *gfp2Aenv* were used to transduce lung slices in culture. Immunostaining revealed that the vector CSC-GFP2AEnv was able to drive expression of JSRV Env, but only in a low number of cells within each lung slice. miRNA expression in CSC-GFP2AEnv transduced lung slices was compared to expression in control mock-transduced and CSC-G transduced, lung slices at two different time points. Differences in miRNA expression were found between mock-transduced and lentiviral vector transduced lung slices, indicating miRNA expression changed in response to lentiviral vectors. However, no significant differences in expression were found between the miRNAs assessed in the two groups at the two different time points. Low lentiviral vector titres and JSRV Env expression might be the reason why no changes were observed between them. Nevertheless, miRNA expression changes triggered by a lentiviral vector encoding JSRV Env might differ from those triggered by the whole length virus.

5.3.5 miRNA expression in JSRV-infected lung slices

In order to evaluate if infection of lung slices with JSRV induced the miRNA expression pattern observed in OPA lung tissue, infections with JSRV and JSRVGFP were performed. Immunostaining revealed that JSRV infection had been successful at driving JSRV Env expression in cells. However, as with lentiviral transduction, only a very small number of cells expressed JSRV Env. miRNA expression in infected and mock-infected lung slices at day 10 post-infection was compared to miRNA expression before infection to identify changes. Expression levels of the tested miRNAs at day 10 were found to be altered in comparison to levels before infection. However, miRNA expression levels were not found to be different between JSRV infected and mock-infected lung slices, indicating that the changes were likely a result of lung slices aging in culture. These findings might suggest that the expression levels of the miRNAs tested does not change in early events of transformation in infected cells, miRNA expression changes in OPA lung tissue might occur later on in transformation or

might originate from other cells responding to infection and transformation. In addition, it could be that the miRNA signal of the low number of cells expressing JSRV Env is masked by the aging process taking place in all the lung slice. In order to investigate these hypotheses, another study of JSRV infection of lung slices was performed extending the sampling time and points, and increasing viral concentration.

A 14-fold increase in JSRV concentration did not produce an increase in cells expressing JSRV Env within the lung slices. These findings suggest that infection of cells in lung slices might be more dependent on the availability of target cells than on the viral concentration used. JSRV, unlike lentiviral vectors, preferentially infects and replicates in actively dividing cells, and, in particular, AT2 cells. It is then anticipated that above a certain JSRV concentration threshold, the increase of viral particles would not result in more infected cells. Nevertheless, using tissue from younger lambs could potentially result in higher numbers of JSRV infected cells in lung slices, and help address if the lack of miRNA changes observed in this study is due to the miRNA expression being masked. Age effects in lung slices have been previously described (Cousens et al, 2015) and are consistent with observations of natural cases of OPA and experimental infections. Dividing AT2 cells are found at higher frequency in early stages of development and, in lambs compared to adult sheep (Murgia et al, 2011). Murgia et al (2011) showed that lung damage in adult sheep promotes proliferation of AT2 cells and permits JSRV infection and tumourigenesis. This suggests that in natural disease, lung damage by infection might increase AT2 cell proliferation in a similar way and promote infection by JSRV (Murgia et al, 2011).

It should be noted that the finding of low infection levels is consistent with previous work in our lab (Cousens et al, 2015). However, these results contrast with a study of JSRV infection in lung slices of 6-month old lambs, in which high levels of JSRV infection and Env expression were reported (Rosales Gerpe et al, 2018). Nevertheless, caution should be taken when interpreting the results of that study due to background staining observed in uninfected lung slices, and due to the detection of JSRV Env in cells other than AT2 cells, which are not expected in a

JSRV infection. It is likely that the immunostaining conditions used for JSRV Env detection made the technique not entirely specific.

Reduced survival of lung slices in the last experiment performed is likely to be due to decrease in cell culture changes that resulted in media acidification damaging cells (Ian Freshney, 2005). In the future these could be easily resolved by changing media more frequently, increasing medium volume or adding a buffering reagent to prevent media acidification.

5.3.6 Conclusions and future work

Lack of an *in vitro* model of JSRV infection and transformation continues to hinder research into the molecular pathology and transformation events caused by the virus. Although models of JSRV transformation are available, these do not accurately reflect miRNA changes in OPA lung tissue. In order to study miRNA expression in JSRV Env transformation and the involvement of miRNAs in pathogenicity, development of a model that permits JSRV infection and replication is needed.

Currently, the model more likely to resemble events in natural infection is the use of lung slices for JSRV infection. However, the use of lung slices has limitations on the length of study and the tests that can be performed to study miRNA involvement in JSRV infection and transformation. In addition, it is not a quantitative system.

In summary, despite taking several approaches the work described in this chapter did not result in an *in vitro* model suitable for replicating miRNA expression in OPA. Nevertheless, the results of MDCK transformation and AT2 cell isolation provide important information for future studies in this area.

Chapter 6 Summary, conclusions and future work

Ovine pulmonary adenocarcinoma is an important disease that causes significant economic losses for farmers. To date, no reliable early-stage diagnostic tests are available for OPA, making disease control problematic. Moreover, OPA is a valuable model for human lung adenocarcinoma and a fascinating disease in which to investigate the interplay of viral infection, oncogenesis, immunity and tolerance. Nevertheless, study of the molecular pathogenesis of OPA and Env-driven transformation has been hindered due to the lack of a permissive cell line for JSRV replication. A better understanding of the disease is needed to stimulate the creation of new control strategies, and to increase our knowledge of the similarities and differences with human lung adenocarcinoma. miRNAs are regulators of gene expression, and study of their prevalence in OPA could advance the current knowledge on the molecular pathogenesis of OPA and improve disease control strategies. miRNAs are involved in many cell processes and are being extensively studied as biomarkers of several diseases, including cancer. In this thesis, miRNA expression in OPA was examined with two overarching aims: to study their role in the early oncogenic events in OPA and to explore their potential as disease biomarkers.

In the first experimental chapter, global miRNA expression was studied in sheep lung and 40 miRNAs DE in OPA-affected sheep were identified. RT-qPCR confirmed DE of nine of these miRNAs in experimental cases and natural cases of the disease, representing early and advanced forms of the disease. However, due to the limited sensitivity of analysing whole specimens of lung tissue, miRNA expression was subsequently examined in samples enriched for specific cell types. Isolation of tumour cells by LCM was complex and technically challenging. Nevertheless, sequencing of enriched tumour samples largely confirmed the upregulation of the nine selected miRNAs, indicating that they might be associated with OPA tumours. Sequencing of $CD14^+$ macrophages purified from sheep lung also revealed DE miRNAs in OPA-affected sheep. These results suggest that immune cells might change their phenotype as a response to the presence of JSRV in the lung.

In addition to studying host miRNA expression, the potential for JSRV to encode miRNAs was investigated. Small RNA sequencing revealed a region of the JSRV genome that was overrepresented in the sequencing data, and that was not present in uninfected samples. RNA folding indicated the presence of a stem-loop enclosing the area with high read abundance. However, the existence of this putative JSRV-encoded miRNA could not be confirmed experimentally. Although these results appear to indicate that it is unlikely that JSRV encodes miRNAs, it is difficult to completely rule this out due to the sensitivity of the method used.

In the second experimental chapter, the presence of miRNAs in sheep serum was explored to investigate their potential as biomarkers. The nine miRNAs upregulated in lung tissue were found not to be DE in serum. Small RNA sequencing was then performed on ovine sera and successfully identified 74 DE miRNAs in the serum of OPA-affected sheep. However, additional sequencing of a larger number of samples revealed that no miRNAs were consistently DE at all stages of the disease. The disagreement between the two studies was discovered to be partly due to low repeatability between experiments. Lung fluid was then investigated as a source of miRNAs, but low miRNA expression levels were detected, and no correlation with tissue levels was found. The findings of the second experimental chapter suggested that it would be difficult to exploit circulating miRNAs as diagnostic markers for OPA in serum or lung fluid.

In parallel with studying miRNA expression *in vivo*, in the third experimental chapter, I sought to establish a model in which the role of DE miRNAs could be studied. Such a model could help to elucidate the mechanism by which JSRV Env activates signalling pathways in the host cell, and support the association of the selected miRNAs with OPA. Initially, established cell lines were used, but low transfection efficiency and Env expression prevented the study of the transformation process. JSRV Env expression in cell lines was improved by using lentiviral vectors encoding GFP-2A-Env. MDCK and 208F cells were successfully transformed by JSRV Env. Three transformed MDCK clones were found to express JSRV Env and associated transformation markers P-Akt and P-ERK1/2 for approximately three months after transduction. However, the differences found

in miRNA expression between transformed MDCK clones and non-transformed MDCK cells did not resemble the changes seen in OPA-affected lung tissue.

Sheep-derived cells and tissue were then explored as model systems to study miRNA expression in OPA. Isolation and culture of AT2 cells was successful, as indicated by the presence of the AT2-specific marker SP-C. However, variability in cell yield and SP-C expression was observed between cells derived from different lambs. The low yield of AT2 cells retrieved per animal, together with their rapid dedifferentiation restricted the time window in which infections with JSRV could be performed. Overall, this experiment was a valuable first step towards developing a future *in vitro* system that could potentially support JSRV replication. However, further development of the current protocol is needed to maximise recovery of AT2 cells from sheep lung and to optimise conditions for their *in vitro* culture.

miRNA expression was also investigated in ovine lung slices exposed to lentiviral vectors encoding GFP2AEnv or $JSRV_{21}$. In both cases, immunohistochemistry revealed expression of JSRV Env in only a small proportion of cells and no miRNA changes that could be related to Env expression were detected. The proportion of infected cells was not increased by adding larger amounts of virus. This finding suggested that the availability of target cells rather than viral concentration might be the bottleneck to achieving high levels of JSRV Env expression. Overall, the *results from* experiments performed in cell lines and sheep cells emphasise the need for improved *in vitro* models of OPA, and in particular, systems that are more quantitative and not subject to the high degree of technical variability observed here.

This is the first study to explore miRNA expression in OPA, and the first to identify the association of some miRNAs with OPA. The upregulation of miR-135b, miR-182, miR-183, miR-200b, miR-205, miR-21, miR-31, miR-503 and miR-96 observed in lung tissue of OPA-affected sheep, correlates with findings in human lung cancer studies. Nevertheless, in human lung cancer, some studies have reported contradictory findings, which might be related to the heterogeneous nature of the disease or to demographic differences in the groups studied. In OPA, a trend towards upregulation of the selected miRNAs was observed in all tissue

samples analysed. However, the number of samples analysed here is limited compared to human lung cancer studies. Further investigation on miRNA expression in larger animal cohorts would be needed to ensure that the miRNA upregulation observed is a consistent feature of OPA-affected animals. On the other hand, inconsistent results in human lung cancer studies might also stem from classifying different forms of the disease, with different histopathology an oncogene activation, under the umbrella term of lung cancer. OPA might, thus, be expected to exhibit a more uniform miRNA expression pattern across samples due to the similarities in lesions and transformation markers observed across cases.

Given the limitations of assessing gene expression in whole tissue samples or pooled cell populations, in the future, single-cell sequencing could be used to dissect specific patterns in miRNA expression and to correlate these patterns with specific cell types. This approach would facilitate the study of miRNA expression in specific cell types, for example normal and Env transformed AT2 cells. One of the most popular approaches for single-cell sequencing is to use droplet-based technologies for high-throughput sequencing (Zhang et al, 2019). Of the droplet-based technologies, Chromium 10x is reported to be the most sensitive and to have lower levels of technical noise (Zhang et al, 2019). However, Chromium 10x offers shallow sequencing depth, which might not detect low abundance transcripts or miRNAs (Baran-Gale et al, 2018; Zhang et al, 2019). Approaches to obtain higher read-depth are also available; for example Smart-seq 2 (Baran-Gale et al, 2018). Nevertheless, this approach might, in the case of OPA, require some prior purification of AT2 cells or tumour cells to ensure a representative amount of the cells of interest are sequenced. Another current major obstacle is the absence of commercially available kits for small RNA single-cell sequencing. It is expected that such reagents will become available in the near future, and some protocols have recently been developed to allow single-cell sequencing of small RNAs (Faridani et al, 2016; Hagemann-Jensen et al, 2018). In addition, single-cell sequencing has been successfully applied to co-sequence mRNA and miRNA from single cells, allowing the study of the correlation between them (Wang et al, 2019b; Xiao et al, 2018).

In this thesis, the serum analysis did not identify any miRNAs as potential diagnostic markers for OPA. This finding echoes the current status of miRNA biomarker development in human diseases. Although the number of miRNA studies continues to increase, reaching ~11000 studies in 2018 (Bonneau et al, 2019), no FDA or EMA approved diagnostic tests are currently available (www.fda.gov, www.ema.europa.eu). Nevertheless, diagnostic tests to classify cancers of unknown origin, and osteoporosis-linked risk of fractures are commercially available in the US (Heilmeier et al, 2016; Kocijan et al, 2016) (osteomiR^{TM}, TAmiRNA GmbH, Austria). These tests use panels of more than ten miRNAs to increase sensitivity and specificity, and might be useful in conjunction with other diagnostic tests. In addition, another commercially available test seeks to improve the diagnostic accuracy for thyroid cancer by using a combination of a miRNA panel and an oncogene panel (Labourier et al, 2015) (ThyraMIR®, Interpace Diagnostics, LLC, NJ USA). Overall, the work in this thesis, and review of the literature highlight the potential of miRNAs as biomarkers but, emphasise that further research and development is needed in order for them to be used in a clinical or field setting.

Another approach towards increasing the sensitivity of miRNAs as diagnostic markers would be the use of new detection methods. For example, DestiNA Genomics, an Edinburgh based company, has developed a highly-sensitive detection system that does not require prior RNA extraction or PCR, with applications in field and clinical settings (Detassis et al, 2019; Marín-Romero et al, 2018; Rissin et al, 2017). Besides the use of miRNAs as biomarkers of OPA, other molecules could be considered as part of integrative approaches such as multi-omics (Hasin et al, 2017). However, although hugely informative, multi-omics approaches remain time-consuming and expensive, requiring further development for their clinical application (Hasin et al, 2017).

In case miRNA detection is not suitable for the diagnosis of OPA, other recently developed methods and approaches could be investigated for this purpose. Considering the viral origin of OPA, detection of the pathogen's genome in sheep offers a route to early diagnosis and effective disease control. In the past, detection of JSRV in the blood using PCR has not proved to be a sensitive

approach due to the low number of viral copies present in circulation (Lewis et al, 2011). Nevertheless, highly sensitive methods for pathogen detection continue to be developed, which could make sensitive JSRV detection in the blood a reality in the future. One example is SHERLOCK2, a method based on isothermal amplification and Cas13, able to detect viral RNA at low concentrations (2 attomolar) (Gootenberg et al, 2018). In addition, to its sensitivity SHERLOCK2 produces quantitative detection data, which could provide information on viral load and relation to pathological findings.

At present, miRNAs might not offer diagnostic accuracy for OPA but, studying their role in OPA has the potential to reveal information on the early events of JSRV Env-mediated transformation. The studies performed in *in vitro* models in this thesis sought to explore the role of miRNAs in OPA. Nevertheless, problems with their agreement with the *in vivo* findings, and variability in primary cultures were encountered. These issues highlight that better models are needed to continue the study of JSRV infection and oncogenesis. In addition, better *in vitro* models of OPA would result in a reduced need for experimental animals, driving research in a more ethical and less costly direction.

Ideally, a model of OPA would be able to support replication of JSRV. The problem in developing such model has been the challenge of maintaining AT2 cells *in vitro*. However, culture systems such as 3D systems allow for extended culture of AT2 cells expressing their features (Nandkumar et al, 2015; Sucre et al, 2018), which could result in efficient replication of JSRV. New advances have also made possible the culture of lung organoids from stem-cells and their co-culture with endothelial or mesenchymal cells (Gkatzis et al, 2018). In addition, a revolutionary system: Lung-on-chip, based on the use of microfluidics, has made possible to reproduce interactions between cells and critical functions of the lung (Benam et al, 2016; Huh et al, 2010). A combination of organoids and the lung on-chip approach has also been suggested to overcome limitations of the methods (Takebe et al, 2017). Although these models would suppose an exciting new platform for studying lung diseases such as OPA, they are currently not quantitative.

In conclusion, this study has provided new knowledge on the expression of miRNAs in OPA and provides a foundation for future work examining the role of these molecules in the pathogenesis of this interesting disease.

References

Agarwal, V., Bell, G. W., Nam, J. W. & Bartel, D. P. (2015) Predicting effective microRNA target sites in mammalian mRNAs. *Elife*, 4.

Allen, T. E., Sherrill, K. J., Crispell, S. M., Perrott, M. R., Carlson, J. O. & DeMartini, J. C. (2002) The jaagsiekte sheep retrovirus envelope gene induces transformation of the avian fibroblast cell line DF-1 but does not require a conserved SH2 binding domain. *Journal of General Virology*, 83(11), 2733-2742.

Ambros, V., Bartel, B., Bartel, D. P., Burge, C. B., Carrington, J. C., Chen, X., Dreyfuss, G., Eddy, S. R., Griffiths-Jones, S., Marshall, M., Matzke, M., Ruvkun, G. & Tuschl, T. (2003) A uniform system for microRNA annotation. *RNA*, 9(3), 277-9.

Ameling, S., Kacprowski, T., Chilukoti, R. K., Malsch, C., Liebscher, V., Suhre, K., Pietzner, M., Friedrich, N., Homuth, G. & Hammer, E. (2015) Associations of circulating plasma microRNAs with age, body mass index and sex in a population-based study. *BMC medical genomics*, 8(1), 61.

An, Y., Zhang, Q., Li, X., Wang, Z., Li, Y. & Tang, X. (2018) Upregulated microRNA miR-21 promotes the progression of lung adenocarcinoma through inhibition of KIBRA and the Hippo signaling pathway. *Biomed Pharmacother*, 108, 1845-1855.

Anastasiadou, E., Garg, N., Bigi, R., Yadav, S., Campese, A. F., Lapenta, C., Spada, M., Cuomo, L., Botta, A., Belardelli, F., Frati, L., Ferretti, E., Faggioni, A. & Trivedi, P. (2015) Epstein-Barr virus infection induces miR-21 in terminally differentiated malignant B cells. *Int J Cancer*, 137(6), 1491-7.

Anders, S. & Huber, W. (2010) Differential expression analysis for sequence count data. *Genome Biology*, 11(10), R106.

Anglesio, M. S., Wang, Y., Yang, W., Senz, J., Wan, A., Heravi-Moussavi, A., Salamanca, C., Maines-Bandiera, S., Huntsman, D. G. & Morin, G. B. (2013) Cancer-associated somatic DICER1 hotspot mutations cause defective miRNA processing and reverse-strand expression bias to predominantly mature 3p strands through loss of 5p strand cleavage. *J Pathol*, 229(3), 400-9.

Archer, F., Jacquier, E., Lyon, M., Chastang, J., Cottin, V., Mornex, J. F. & Leroux, C. (2007) Alveolar type II cells isolated from pulmonary adenocarcinoma: a model for JSRV expression in vitro. *Am J Respir Cell Mol Biol*, 36(5), 534-40.

Armand-Labit, V. & Pradines, A. (2017) Circulating cell-free microRNAs as clinical cancer biomarkers. *Biomol Concepts*, 8(2), 61-81.

Armezzani, A., Arnaud, F., Caporale, M., di Meo, G., Iannuzzi, L., Murgia, C. & Palmarini, M. (2011) The signal peptide of a recently integrated endogenous sheep betaretrovirus envelope plays a major role in eluding gag-mediated late restriction. *J Virol*, 85(14), 7118-28.

Arnaud, F., Black, S. G., Murphy, L., Griffiths, D. J., Neil, S. J., Spencer, T. E. & Palmarini, M. (2010) Interplay between ovine bone marrow stromal cell antigen 2/tetherin and endogenous retroviruses. *Journal of virology*, 84(9), 4415-4425.

Arnaud, F., Murcia, P. R. & Palmarini, M. (2007) Mechanisms of late restriction induced by an endogenous retrovirus. *Journal of virology*, 81(20), 11441-11451.

Arnaud, F., Varela, M., Spencer, T. E. & Palmarini, M. (2008) Coevolution of endogenous betaretroviruses of sheep and their host. *Cell Mol Life Sci*, 65(21), 3422-32.

Arroyo, J. D., Chevillet, J. R., Kroh, E. M., Ruf, I. K., Pritchard, C. C., Gibson, D. F., Mitchell, P. S., Bennett, C. F., Pogosova-Agadjanyan, E. L., Stirewalt, D. L., Tait, J. F. & Tewari, M. (2011) Argonaute2 complexes carry a population of circulating microRNAs independent of vesicles in human plasma. *Proc Natl Acad Sci U S A*, 108(12), 5003-8.

Arthur, J. (2000) The MDCK cell line is made up of populations of cells with diverse resistive and transport properties. *Tissue and Cell*, 32(5), 446-450.

Auchampach, J. A., Jin, X., Wan, T. C., Caughey, G. H. & Linden, J. (1997) Canine mast cell adenosine receptors: cloning and expression of the A3 receptor and evidence that degranulation is mediated by the A2B receptor. *Molecular pharmacology*, 52(5), 846-860.

Babiarz, J. E., Ruby, J. G., Wang, Y., Bartel, D. P. & Blelloch, R. (2008) Mouse ES cells express endogenous shRNAs, siRNAs, and other microprocessor-independent, dicer-dependent small RNAs. *Genes and Development*, 22(20), 2773-2785.

Baek, D., Villén, J., Shin, C., Camargo, F. D., Gygi, S. P. & Bartel, D. P. (2008) The impact of microRNAs on protein output. *Nature*, 455(7209), 64-71.

Baffa, R., Fassan, M., Volinia, S., O'Hara, B., Liu, C. G., Palazzo, J. P., Gardiman, M., Rugge, M., Gomella, L. G. & Croce, C. M. (2009) MicroRNA expression profiling of human metastatic cancers identifies cancer gene targets. *The Journal of Pathology: A Journal of the Pathological Society of Great Britain and Ireland*, 219(2), 214-221.

Bai, J., Zhu, R., Stedman, K., Cousens, C., Carlson, J., Sharp, J. & DeMartini, J. (1996) Unique long terminal repeat U3 sequences distinguish exogenous jaagsiekte sheep retroviruses associated with ovine pulmonary carcinoma from endogenous loci in the sheep genome. *Journal of virology*, 70(5), 3159-3168.

Baker, B. M. & Chen, C. S. (2012) Deconstructing the third dimension–how 3D culture microenvironments alter cellular cues. *J Cell Sci*, 125(13), 3015-3024.

Baker, S. G., Kramer, B. S. & Srivastava, S. (2002) Markers for early detection of cancer: statistical guidelines for nested case-control studies. *BMC Med Res Methodol*, 2, 4.

Balasubramaniam, M., Pandhare, J. & Dash, C. (2018) Are microRNAs Important Players in HIV-1 Infection? An Update. *Viruses*, 10(3), 110.

Ballard, P. L. (1989) Hormonal regulation of pulmonary surfactant. *Endocrine Reviews*, 10(2), 165-181.

Baran-Gale, J., Chandra, T. & Kirschner, K. (2018) Experimental design for single-cell RNA sequencing. *Briefings in Functional Genomics*, 17(4), 233-239.

Bartel, D. P. (2004) MicroRNAs: genomics, biogenesis, mechanism, and function. *cell*, 116(2), 281-297.

Bartel, D. P. (2009) MicroRNAs: target recognition and regulatory functions. *Cell*, 136(2), 215-33.

Bartel, D. P. (2018) Metazoan MicroRNAs. *Cell*, 173(1), 20-51.

Bear, S. E., Bellacosa, A., Lazo, P. A., Jenkins, N. A., Copeland, N. G., Hanson, C., Levan, G. & Tsichlis, P. N. (1989) Provirus insertion in Tpl-1, an Ets-1-related oncogene, is

associated with tumor progression in Moloney murine leukemia virus-induced rat thymic lymphomas. *Proceedings of the National Academy of Sciences*, 86(19), 7495-7499.

Becker, C., Hammerle-Fickinger, A., Riedmaier, I. & Pfaffl, M. W. (2010) mRNA and microRNA quality control for RT-qPCR analysis. *Methods*, 50(4), 237-43.

Begum, S., Hayashi, M., Ogawa, T., Jabboure, F. J., Brait, M., Izumchenko, E., Tabak, S., Ahrendt, S. A., Westra, W. H., Koch, W., Sidransky, D. & Hoque, M. O. (2015) An integrated genome-wide approach to discover deregulated microRNAs in non-small cell lung cancer: Clinical significance of miR-23b-3p deregulation. *Sci Rep*, 5, 13236.

Benam, K. H., Villenave, R., Lucchesi, C., Varone, A., Hubeau, C., Lee, H.-H., Alves, S. E., Salmon, M., Ferrante, T. C. & Weaver, J. C. (2016) Small airway-on-a-chip enables analysis of human lung inflammation and drug responses in vitro. *Nature methods*, 13(2), 151.

Bennasser, Y., Le, S. Y., Benkirane, M. & Jeang, K. T. (2005) Evidence that HIV-1 encodes an siRNA and a suppressor of RNA silencing. *Immunity*, 22(5), 607-19.

Benson, D. A., Cavanaugh, M., Clark, K., Karsch-Mizrachi, I., Lipman, D. J., Ostell, J. & Sayers, E. W. (2013) GenBank. *Nucleic Acids Res*, 41(Database issue), D36-42.

Bernardo, B. C., Charchar, F. J., Lin, R. C. Y. & McMullen, J. R. (2012) A MicroRNA Guide for Clinicians and Basic Scientists: Background and Experimental Techniques. *Heart, Lung and Circulation*, 21(3), 131-142.

Berthet, N., Frangeul, L., Olaussen, K. A., Brambilla, E., Dorvault, N., Girard, P., Validire, P., Fadel, E., Bouchier, C. & Gessain, A. (2015) No evidence for viral sequences in five lepidic adenocarcinomas (former “BAC”) by a high-throughput sequencing approach. *BMC research notes*, 8(1), 782.

Bhome, R., Del Vecchio, F., Lee, G.-H., Bullock, M. D., Primrose, J. N., Sayan, A. E. & Mirnezami, A. H. (2018) Exosomal microRNAs (exomiRs): Small molecules with a big role in cancer. *Cancer Letters*, 420, 228-235.

Biava, M., Colavita, F., Marzorati, A., Russo, D., Pirola, D., Cocci, A., Petrocelli, A., Guanti, M. D., Cataldi, G. & Kamara, T. (2018) Evaluation of a rapid and sensitive RT-qPCR assay for the detection of Ebola Virus. *Journal of virological methods*, 252, 70-74.

Bica-Pop, C., Cojocneanu-Petric, R., Magdo, L., Raduly, L., Gulei, D. & Berindan-Neagoe, I. (2018) Overview upon miR-21 in lung cancer: focus on NSCLC. *Cell Mol Life Sci*, 75(19), 3539-3551.

Bilbao-Arribas, M., Abendaño, N., Varela-Martínez, E., Reina, R., de Andrés, D. & Jugo, B. M. (2019) Expression analysis of lung miRNAs responding to ovine VM virus infection by RNA-seq. *BMC genomics*, 20(1), 62-62.

Black, S. G., Arnaud, F., Burghardt, R. C., Satterfield, M. C., Fleming, J. A., Long, C. R., Hanna, C., Murphy, L., Biek, R., Palmarini, M. & Spencer, T. E. (2010) Viral particles of endogenous betaretroviruses are released in the sheep uterus and infect the conceptus trophectoderm in a transspecies embryo transfer model. *J Virol*, 84(18), 9078-85.

Bolisetty, M. T., Dy, G., Tam, W. & Beemon, K. L. (2009) Reticuloendotheliosis virus strain T induces miR-155, which targets JARID2 and promotes cell survival. *J Virol*, 83(23), 12009-17.

Bonneau, E., Neveu, B., Kostantin, E., Tsongalis, G. J. & De Guire, V. (2019) How close are miRNAs from clinical practice? A perspective on the diagnostic and therapeutic market. *Electronic Journal of the International Federation of Clinical Chemistry and Laboratory Medicine*, 30(2), 114-127.

Borobia, M., De Las Heras, M., Ramos, J. J., Ferrer, L. M., Lacasta, D., De Martino, A., Fernandez, A., Loste, A., Marteles, D. & Ortin, A. (2016) Jaagsiekte Sheep Retrovirus Can Reach Peyer's Patches and Mesenteric Lymph Nodes of Lambs Nursed by Infected Mothers. *Vet Pathol*, 53(6), 1172-1179.

Boutz, D. R., Collins, P. J., Suresh, U., Lu, M., Ramirez, C. M., Fernandez-Hernando, C., Huang, Y., Abreu Rde, S., Le, S. Y., Shapiro, B. A., Liu, A. M., Luk, J. M., Aldred, S. F., Trinklein, N. D., Marcotte, E. M. & Penalva, L. O. (2011) Two-tiered approach identifies a network of cancer and liver disease-related genes regulated by miR-122. *J Biol Chem*, 286(20), 18066-78.

Bracken, C. P., Scott, H. S. & Goodall, G. J. (2016) A network-biology perspective of microRNA function and dysfunction in cancer. *Nat Rev Genet*, 17(12), 719-732.

Bray, M., Prasad, S., Dubay, J. W., Hunter, E., Jeang, K.-T., Rekosh, D. & Hammarskjöld, M. L. (1994) A small element from the Mason-Pfizer monkey virus genome makes human immunodeficiency virus type 1 expression and replication Rev-independent. *Proceedings of the National Academy of Sciences*, 91(4), 1256-1260.

Brennecke, J., Hipfner, D. R., Stark, A., Russell, R. B. & Cohen, S. M. (2003) bantam encodes a developmentally regulated microRNA that controls cell proliferation and regulates the proapoptotic gene hid in Drosophila. *Cell*, 113(1), 25-36.

Broughton, J. P., Lovci, M. T., Huang, J. L., Yeo, G. W. & Pasquinelli, A. E. (2016) Pairing beyond the Seed Supports MicroRNA Targeting Specificity. *Mol Cell*, 64(2), 320-333.

Burke, J. M., Bass, C. R., Kincaid, R. P. & Sullivan, C. S. (2014) Identification of tri-phosphatase activity in the biogenesis of retroviral microRNAs and RNAP III-generated shRNAs. *Nucleic Acids Research*, 42(22), 13949-13962.

Burke, J. M., Kuny, C. V., Kincaid, R. P. & Sullivan, C. S. (2015) Identification, validation, and characterization of noncanonical miRNAs. *Methods*, 91, 57-68.

Burns, G., Brooks, K., Wildung, M., Navakanitworakul, R., Christenson, L. K. & Spencer, T. E. (2014) Extracellular vesicles in luminal fluid of the ovine uterus. *PLoS One*, 9(3), e90913.

Bushati, N. & Cohen, S. M. (2007) microRNA functions. *Annu Rev Cell Dev Biol*, 23, 175-205.

Bustin, S. A. (2004) *AZ of quantitative PCR*International University Line La Jolla, CA.

Bustin, S. A., Benes, V., Garson, J. A., Hellemans, J., Huggett, J., Kubista, M., Mueller, R., Nolan, T., Pfaffl, M. W., Shipley, G. L., Vandesompele, J. & Wittwer, C. T. (2009) The MIQE guidelines: minimum information for publication of quantitative real-time PCR experiments. *Clin Chem*, 55(4), 611-22.

Cai, J., Fang, L., Huang, Y., Li, R., Yuan, J., Yang, Y., Zhu, X., Chen, B., Wu, J. & Li, M. (2013) miR-205 targets PTEN and PHLPP2 to augment AKT signaling and drive malignant phenotypes in non-small cell lung cancer. *Cancer Res*, 73(17), 5402-15.

Cai, T., Long, J., Wang, H., Liu, W. & Zhang, Y. (2017a) Identification and characterization of miR-96, a potential biomarker of NSCLC, through bioinformatic analysis. *Oncol Rep*, 38(2), 1213-1223.

Cai, X., Peng, D., Wei, H., Yang, X., Huang, Q., Lin, Z., Xu, W., Qian, M., Yang, C., Liu, T., Yan, W. & Zhao, J. (2017b) miR-215 suppresses proliferation and migration of non-small cell lung cancer cells. *Oncol Lett*, 13(4), 2349-2353.

Calin, G. A., Sevignani, C., Dumitru, C. D., Hyslop, T., Noch, E., Yendamuri, S., Shimizu, M., Rattan, S., Bullrich, F., Negrini, M. & Croce, C. M. (2004) Human microRNA genes are frequently located at fragile sites and genomic regions involved in cancers. *Proc Natl Acad Sci U S A*, 101(9), 2999-3004.

Cameron, J. E., Fewell, C., Yin, Q., McBride, J., Wang, X., Lin, Z. & Flemington, E. K. (2008) Epstein-Barr virus growth/latency III program alters cellular microRNA expression. *Virology*, 382(2), 257-66.

Cao, M., Hou, D., Liang, H., Gong, F., Wang, Y., Yan, X., Jiang, X., Wang, C., Zhang, J., Zen, K., Zhang, C. Y. & Chen, X. (2014) miR-150 promotes the proliferation and migration of lung cancer cells by targeting SRC kinase signalling inhibitor 1. *Eur J Cancer*, 50(5), 1013-24.

Cao, W., Heit, A., Hotz-Wagenblatt, A. & Lochelt, M. (2018) Functional characterization of the bovine foamy virus miRNA expression cassette and its dumbbell-shaped pri-miRNA. *Virus Genes*, 54(4), 550-560.

Caporale, M., Arnaud, F., Mura, M., Golder, M., Murgia, C. & Palmarini, M. (2009) The signal peptide of a simple retrovirus envelope functions as a posttranscriptional regulator of viral gene expression. *J Virol*, 83(9), 4591-604.

Caporale, M., Centorame, P., Giovannini, A., Sacchini, F., Di Ventura, M., De las Heras, M. & Palmarini, M. (2005) Infection of lung epithelial cells and induction of pulmonary adenocarcinoma is not the most common outcome of naturally occurring JSRV infection during the commercial lifespan of sheep. *Virology*, 338(1), 144-153.

Caporale, M., Cousens, C., Centorame, P., Pinoni, C., De las Heras, M. & Palmarini, M. (2006) Expression of the jaagsiekte sheep retrovirus envelope glycoprotein is sufficient to induce lung tumors in sheep. *J Virol*, 80(16), 8030-7.

Caporale, M., Martineau, H., De las Heras, M., Murgia, C., Huang, R., Centorame, P., Di Francesco, G., Di Gialleonardo, L., Spencer, T. E., Griffiths, D. J. & Palmarini, M. (2013) Host species barriers to Jaagsiekte sheep retrovirus replication and carcinogenesis. *J Virol*, 87(19), 10752-62.

Carraro, G., El-Hashash, A., Guidolin, D., Tiozzo, C., Turcatel, G., Young, B. M., De Langhe, S. P., Bellusci, S., Shi, W., Parnigotto, P. P. & Warburton, D. (2009) miR-17 family of microRNAs controls FGF10-mediated embryonic lung epithelial branching morphogenesis through MAPK14 and STAT3 regulation of E-Cadherin distribution. *Dev Biol*, 333(2), 238-50.

Caruso, P., MacLean, M. R., Khanin, R., McClure, J., Soon, E., Southgate, M., MacDonald, R. A., Greig, J. A., Robertson, K. E., Masson, R., Denby, L., Dempsie, Y., Long, L., Morrell, N. W. & Baker, A. H. (2010) Dynamic changes in lung microRNA profiles during the development of pulmonary hypertension due to chronic hypoxia and monocrotaline. *Arterioscler Thromb Vasc Biol*, 30(4), 716-23.

Challagundla, K. B., Fanini, F., Vannini, I., Wise, P., Murtadha, M., Malinconico, L., Cimmino, A. & Fabbri, M. (2014) microRNAs in the tumor microenvironment: solving the riddle for a better diagnostics. *Expert Review of Molecular Diagnostics*, 14(5), 565-574.

Chan, Y. C., Banerjee, J., Choi, S. Y. & Sen, C. K. (2012) miR-210: the master hypoxamir. *Microcirculation*, 19(3), 215-23.

Chang, H., Liu, Y.-H., Wang, L.-L., Wang, J., Zhao, Z.-H., Qu, J.-F. & Wang, S.-F. (2018) MiR-182 promotes cell proliferation by suppressing FBXW7 and FBXW11 in non-small cell lung cancer. *American journal of translational research*, 10(4), 1131-1142.

Chang, J., Nicolas, E., Marks, D., Sander, C., Lerro, A., Buendia, M. A., Xu, C., Mason, W. S., Moloshok, T., Bort, R., Zaret, K. S. & Taylor, J. M. (2004) miR-122, a mammalian liver-specific microRNA, is processed from hcr mRNA and may downregulate the high affinity cationic amino acid transporter CAT-1. *RNA Biol*, 1(2), 106-13.

Cheloufi, S., Dos Santos, C. O., Chong, M. M. & Hannon, G. J. (2010) A dicer-independent miRNA biogenesis pathway that requires Ago catalysis. *Nature*, 465(7298), 584.

Chen, C. Z., Li, L., Lodish, H. F. & Bartel, D. P. (2004) MicroRNAs modulate hematopoietic lineage differentiation. *Science*, 303(5654), 83-6.

Chen, D.-Q., Pan, B.-Z., Huang, J.-Y., Zhang, K., Cui, S.-Y., De, W., Wang, R. & Chen, L.-B. (2014a) HDAC 1/4-mediated silencing of microRNA-200b promotes chemoresistance in human lung adenocarcinoma cells. *Oncotarget*, 5(10), 3333.

Chen, F., Xu, X. Y., Zhang, M., Chen, C., Shao, H. T. & Shi, Y. (2019) Deep sequencing profiles MicroRNAs related to Aspergillus fumigatus infection in lung tissues of mice. *Journal of Microbiology, Immunology and Infection*, 52(1), 90-99.

Chen, L., He, X., Xie, Y., Huang, Y., Wolff, D. W., Abel, P. W. & Tu, Y. (2018) Up-regulated miR-133a orchestrates epithelial-mesenchymal transition of airway epithelial cells. *Scientific Reports*, 8(1).

Chen, T., Yao, L. Q., Shi, Q., Ren, Z., Ye, L. C., Xu, J. M., Zhou, P. H. & Zhong, Y. S. (2014b) MicroRNA-31 contributes to colorectal cancer development by targeting factor inhibiting HIF-1alpha (FIH-1). *Cancer Biol Ther*, 15(5), 516-23.

Chen, X., Ba, Y., Ma, L., Cai, X., Yin, Y., Wang, K., Guo, J., Zhang, Y., Chen, J., Guo, X., Li, Q., Li, X., Wang, W., Zhang, Y., Wang, J., Jiang, X., Xiang, Y., Xu, C., Zheng, P., Zhang, J., Li, R., Zhang, H., Shang, X., Gong, T., Ning, G., Wang, J., Zen, K., Zhang, J. & Zhang, C. Y. (2008) Characterization of microRNAs in serum: a novel class of biomarkers for diagnosis of cancer and other diseases. *Cell Res*, 18(10), 997-1006.

Chen, Y., Chen, J., Wang, H., Shi, J., Wu, K., Liu, S., Liu, Y. & Wu, J. (2013) HCV-induced miR-21 contributes to evasion of host immune system by targeting MyD88 and IRAK1. *PLoS Pathog*, 9(4), e1003248.

Chen, Z., Stelekati, E., Kurachi, M., Yu, S., Cai, Z., Manne, S., Khan, O., Yang, X. & Wherry, E. J. (2017) miR-150 Regulates Memory CD8 T Cell Differentiation via c-Myb. *Cell Rep*, 20(11), 2584-2597.

Cheng, J., Guo, J.-M., Xiao, B.-X., Miao, Y., Jiang, Z., Zhou, H. & Li, Q.-N. (2011) piRNA, the new non-coding RNA, is aberrantly expressed in human cancer cells. *Clinica chimica acta*, 412(17-18), 1621-1625.

Chiang, H. R., Schoenfeld, L. W., Ruby, J. G., Auyeung, V. C., Spies, N., Baek, D., Johnston, W. K., Russ, C., Luo, S., Babiarz, J. E., Blelloch, R., Schroth, G. P., Nusbaum, C. & Bartel, D. P. (2010) Mammalian microRNAs: Experimental evaluation of novel and previously annotated genes. *Genes and Development*, 24(10), 992-1009.

Chiang, K., Sung, T. L. & Rice, A. P. (2012) Regulation of cyclin T1 and HIV-1 Replication by microRNAs in resting CD4+ T lymphocytes. *J Virol*, 86(6), 3244-52.

Chim, S. S., Shing, T. K., Hung, E. C., Leung, T. Y., Lau, T. K., Chiu, R. W. & Lo, Y. M. (2008) Detection and characterization of placental microRNAs in maternal plasma. *Clin Chem*, 54(3), 482-90.

Chin, L. J., Ratner, E., Leng, S., Zhai, R., Nallur, S., Babar, I., Muller, R. U., Straka, E., Su, L., Burki, E. A., Crowell, R. E., Patel, R., Kulkarni, T., Homer, R., Zelterman, D., Kidd, K. K., Zhu, Y., Christiani, D. C., Belinsky, S. A., Slack, F. J. & Weidhaas, J. B. (2008) A SNP in a let-7 microRNA complementary site in the KRAS 3' untranslated region increases non-small cell lung cancer risk. *Cancer Res*, 68(20), 8535-40.

Chou, C. H., Shrestha, S., Yang, C. D., Chang, N. W., Lin, Y. L., Liao, K. W., Huang, W. C., Sun, T. H., Tu, S. J., Lee, W. H., Chiew, M. Y., Tai, C. S., Wei, T. Y., Tsai, T. R., Huang, H. T., Wang, C. Y., Wu, H. Y., Ho, S. Y., Chen, P. R., Chuang, C. H., Hsieh, P. J., Wu, Y. S., Chen, W. L., Li, M. J., Wu, Y. C., Huang, X. Y., Ng, F. L., Buddhakosai, W., Huang, P. C., Lan, K. C., Huang, C. Y., Weng, S. L., Cheng, Y. N., Liang, C., Hsu, W. L. & Huang, H. D. (2018) miRTarBase update 2018: a resource for experimentally validated microRNA-target interactions. *Nucleic Acids Res*, 46(D1), D296-d302.

Chung, C., Kim, T., Kim, M., Kim, M., Song, H., Kim, T.-S., Seo, E., Lee, S.-H., Kim, H., Kim, S. K., Yoo, G., Lee, D.-H., Hwang, D.-S., Kinashi, T., Kim, J.-M. & Lim, D.-S. (2013) Hippo-Foxa2 signaling pathway plays a role in peripheral lung maturation and surfactant homeostasis. *Proceedings of the National Academy of Sciences*, 110(19), 7732-7737.

Cifuentes, D., Xue, H., Taylor, D. W., Patnode, H., Mishima, Y., Cheloufi, S., Ma, E., Mane, S., Hannon, G. J., Lawson, N. D., Wolfe, S. A. & Giraldez, A. J. (2010) A novel miRNA processing pathway independent of dicer requires argonaute2 catalytic activity. *Science*, 328(5986), 1694-1698.

Clark, E. L., Bush, S. J., McCulloch, M. E. B., Farquhar, I. L., Young, R., Lefevre, L., Pridans, C., Tsang, H. G., Wu, C., Afrasiabi, C., Watson, M., Whitelaw, C. B., Freeman, T. C., Summers, K. M., Archibald, A. L. & Hume, D. A. (2017) A high resolution atlas of gene expression in the domestic sheep (Ovis aries). *PLoS Genet*, 13(9), e1006997.

Cleys, E. R., Halleran, J. L., McWhorter, E., Hergenreder, J., Enriquez, V. A., da Silveira, J. C., Bruemmer, J. E., Winger, Q. A. & Bouma, G. J. (2014) Identification of microRNAs in exosomes isolated from serum and umbilical cord blood, as well as placentomes of gestational day 90 pregnant sheep. *Mol Reprod Dev*, 81(11), 983-93.

Coil, D. A., Strickler, J. H., Rai, S. K. & Miller, A. D. (2001) Jaagsiekte sheep retrovirus Env protein stabilizes retrovirus vectors against inactivation by lung surfactant, centrifugation, and freeze-thaw cycling. *J Virol*, 75(18), 8864-7.

Cortez, M. A., Bueso-Ramos, C., Ferdin, J., Lopez-Berestein, G., Sood, A. K. & Calin, G. A. (2011) MicroRNAs in body fluids--the mix of hormones and biomarkers. *Nature reviews. Clinical oncology*, 8(8), 467-477.

Cortez, M. A., Valdecanas, D., Zhang, X., Zhan, Y., Bhardwaj, V., Calin, G. A., Komaki, R., Giri, D. K., Quini, C. C. & Wolfe, T. (2014) Therapeutic delivery of miR-200c enhances radiosensitivity in lung cancer. *Molecular Therapy*, 22(8), 1494-1503.

Cote, M., Zheng, Y. M., Albritton, L. M. & Liu, S. L. (2008) Fusogenicity of Jaagsiekte sheep retrovirus envelope protein is dependent on low pH and is enhanced by cytoplasmic tail truncations. *J Virol*, 82(5), 2543-54.

Cousens, C., Alleaume, C., Bijsmans, E., Martineau, H. M., Finlayson, J., Dagleish, M. P. & Griffiths, D. J. (2015) Jaagsiekte sheep retrovirus infection of lung slice cultures. *Retrovirology*, 12, 31.

Cousens, C., Maeda, N., Murgia, C., Dagleish, M. P., Palmarini, M. & Fan, H. (2007) In vivo tumorigenesis by Jaagsiekte sheep retrovirus (JSRV) requires Y590 in Env TM, but not full-length orfX open reading frame. *Virology*, 367(2), 413-21.

Cousens, C., Minguijon, E., Dalziel, R. G., Ortin, A., Garcia, M., Park, J., Gonzalez, L., Sharp, J. M. & de las Heras, M. (1999) Complete sequence of enzootic nasal tumor virus, a retrovirus associated with transmissible intranasal tumors of sheep. *Journal of virology*, 73(5), 3986-3993.

Cousens, C. & Scott, P. (2015) Assessment of transthoracic ultrasound diagnosis of ovine pulmonary adenocarcinoma in adult sheep. *Veterinary Record*, 177(14), 366-366.

Cousens, C., Thonur, L., Imlach, S., Crawford, J., Sales, J. & Griffiths, D. J. (2009) Jaagsiekte sheep retrovirus is present at high concentration in lung fluid produced by ovine pulmonary adenocarcinoma-affected sheep and can survive for several weeks at ambient temperatures. *Res Vet Sci*, 87(1), 154-6.

Crandell, R. A., Fabricant, C. G. & Nelson-Rees, W. A. (1973) Development, characterization, and viral susceptibility of a feline (Felis catus) renal cell line (CRFK). *In Vitro*, 9(3), 176-85.

Cullen, B. R. (2003) Nuclear mRNA export: insights from virology. *Trends in Biochemical Sciences*, 28(8), 419-424.

Cullen, B. R. (2006) Viruses and microRNAs. *Nat Genet*, 38 Suppl, S25-30.

Cullen, B. R. (2010) Five questions about viruses and microRNAs. *PLoS Pathog*, 6(2), e1000787.

Cullen, B. R. (2013a) How Do Viruses Avoid Inhibition by Endogenous Cellular MicroRNAs? *PLOS Pathogens*, 9(11), e1003694.

Cullen, B. R. (2013b) MicroRNAs as mediators of viral evasion of the immune system. *Nature Immunology*, 14(3), 205-210.

Cumer, T., Pompanon, F. & Boyer, F. (2019) Old origin of a protective endogenous retrovirus (enJSRV) in the Ovis genus. *Heredity (Edinb)*, 122(2), 187-194.

Cutlip, R. & Young, S. (1982) Sheep pulmonary adenomatosis (jaagsiekte) in the United States. *American journal of veterinary research*, 43(12), 2108-2113.

Dambal, S., Shah, M., Mihelich, B. & Nonn, L. (2015) The microRNA-183 cluster: the family that plays together stays together. *Nucleic Acids Res*, 43(15), 7173-88.

Danilkovitch-Miagkova, A., Duh, F.-M., Kuzmin, I., Angeloni, D., Liu, S.-L., Miller, A. D. & Lerman, M. I. (2003) Hyaluronidase 2 negatively regulates RON receptor tyrosine kinase and mediates transformation of epithelial cells by jaagsiekte sheep retrovirus. *Proceedings of the National Academy of Sciences*, 100(8), 4580-4585.

Das, S., Extracellular, R. N. A. C. C., Ansel, K. M., Bitzer, M., Breakefield, X. O., Charest, A., Galas, D. J., Gerstein, M. B., Gupta, M., Milosavljevic, A., McManus, M. T., Patel, T., Raffai, R. L., Rozowsky, J., Roth, M. E., Saugstad, J. A., Van Keuren-Jensen, K., Weaver, A. M. & Laurent, L. C. (2019) The Extracellular RNA Communication Consortium: Establishing

Foundational Knowledge and Technologies for Extracellular RNA Research. *Cell*, 177(2), 231-242.

De las Heras, M., Barsky, S., Hasleton, P., Wagner, M., Larson, E., Egan, J., Ortin, A., Gimenez-Mas, J., Palmarini, M. & Sharp, J. (2000) Evidence for a protein related immunologically to the jaagsiekte sheep retrovirus in some human lung tumours. *European Respiratory Journal*, 16(2), 330-332.

De las Heras, M., Calafat, J., Jaime, J., Garcia de Jalon, J., Ferrer, L., García-Goti, M. & Minguijon, E. (1992) Sheep pulmonary adenomatosis (jaagsiekte) in slaughtered sheep: variation in pathological characteristics. *Medicina Veterinaria*, 9, 52-53.

De las Heras, M., de Martino, A., Borobia, M., Ortin, A., Alvarez, R., Borderias, L. & Gimenez-Más, J. (2014) Solitary tumours associated with Jaagsiekte retrovirus in sheep are heterogeneous and contain cells expressing markers identifying progenitor cells in lung repair. *Journal of comparative pathology*, 150(2-3), 138-147.

De las Heras, M., Gonzalez, L. & Sharp, J. M. (2003) Pathology of ovine pulmonary adenocarcinoma, *Jaagsiekte Sheep Retrovirus and Lung Cancer*Springer-Verlag, 25-54.

De Las Heras, M., Murcia, P., Ortin, A., Azua, J., Borderias, L., Alvarez, R., Jimenez-Mas, J. A., Marchetti, A. & Palmarini, M. (2007) Jaagsiekte sheep retrovirus is not detected in human lung adenocarcinomas expressing antigens related to the Gag polyprotein of betaretroviruses. *Cancer Lett*, 258(1), 22-30.

De Las Heras, M., Ortin, A., Benito, A., Summers, C., Ferrer, L. M. & Sharp, J. M. (2006) In-situ demonstration of mitogen-activated protein kinase Erk 1/2 signalling pathway in contagious respiratory tumours of sheep and goats. *J Comp Pathol*, 135(1), 1-10.

De Las Heras, M., Ortin, A., Salvatori, D., Perez de Villareal, M., Cousens, C., Miguel Ferrer, L., Miguel Cebrian, L., Garcia de Jalon, J. A., Gonzalez, L. & Michael Sharp, J. (2005) A PCR technique for the detection of Jaagsiekte sheep retrovirus in the blood suitable for the screening of ovine pulmonary adenocarcinoma in field conditions. *Res Vet Sci*, 79(3), 259-64.

Del Vescovo, V. & Denti, M. A. (2015) microRNA and Lung Cancer. *Adv Exp Med Biol*, 889, 153-77.

DeMartini, J., Carlson, J. O., Leroux, C., Spencer, T. E. & Palmarini, M. (2003) Endogenous Retroviruses Related to Jaagsiekte Sheep Retrovirus, in Fan, H. (ed), *Jaagsiekete Sheep Retrovirus and Lung Cancer* Springer-Verlag, 118-137.

DeMartini, J. C., Bishop, J. V., Allen, T. E., Jassim, F. A., Sharp, J. M., De las Heras, M., Voelker, D. R. & Carlson, J. O. (2001) Jaagsiekte sheep retrovirus proviral clone JSRV JS7, derived from the JS7 lung tumor cell line, induces ovine pulmonary carcinoma and is integrated into the surfactant protein a gene. *Journal of Virology*, 75(9), 4239-4246.

DeMartini, J. C., Rosadio, R. H., Sharp, J. M., Russell, H. I. & Lairmore, M. D. (1987) Experimental coinduction of type D retrovirus-associated pulmonary carcinoma and lentivirus-associated lymphoid interstitial pneumonia in lambs. *Journal of the National Cancer Institute*, 79(1), 167-177.

Detassis, S., Grasso, M., Tabraue-Chávez, M., Marín-Romero, A., López Longarela, B., Ilyine, H., Ress, C., Ceriani, S., Erspan, M. & Maglione, A. (2019) A new platform for the direct profiling of microRNAs in biofluids. *Analytical chemistry*.

Dews, M., Homayouni, A., Yu, D., Murphy, D., Sevignani, C., Wentzel, E., Furth, E. E., Lee, W. M., Enders, G. H., Mendell, J. T. & Thomas-Tikhonenko, A. (2006) Augmentation of tumor angiogenesis by a Myc-activated microRNA cluster. *Nat Genet*, 38(9), 1060-5.

Diederichs, S. & Haber, D. A. (2007) Dual role for argonautes in microRNA processing and posttranscriptional regulation of microRNA expression. *Cell*, 131(6), 1097-108.

Ding, X. C. & Grosshans, H. (2009) Repression of C. elegans microRNA targets at the initiation level of translation requires GW182 proteins. *Embo j*, 28(3), 213-22.

Dobbs, L. G. (1990) Isolation and culture of alveolar type II cells. *American Journal of Physiology-Lung Cellular and Molecular Physiology*, 258(4), L134-L147.

Donadeu, F. X., Schauer, S. N. & Sontakke, S. D. (2012) Involvement of miRNAs in ovarian follicular and luteal development. *J Endocrinol*, 215(3), 323-34.

DuBridge, R. B., Tang, P., Hsia, H. C., Leong, P.-M., Miller, J. & Calos, M. (1987) Analysis of mutation in human cells by using an Epstein-Barr virus shuttle system. *Molecular and cellular biology*, 7(1), 379-387.

Dull, T., Zufferey, R., Kelly, M., Mandel, R. J., Nguyen, M., Trono, D. & Naldini, L. (1998) A third-generation lentivirus vector with a conditional packaging system. *Journal of virology*, 72(11), 8463-8471.

Dungal, N. (1946) Experiments with jaagsiekte. *The American journal of pathology*, 22, 737-759.

Dungal, N., Gislason, G. & Taylor, E. (1938) Epizootic adenomatosis in the lungs of sheep—comparisons with jaagsiekte, verminous pneumonia and progressive pneumonia. *Journal of Comparative Pathology and Therapeutics*, 51, 46-68.

Dunlap, K. A., Palmarini, M., Varela, M., Burghardt, R. C., Hayashi, K., Farmer, J. L. & Spencer, T. E. (2006) Endogenous retroviruses regulate periimplantation placental growth and differentiation. *Proceedings of the National Academy of Sciences*, 103(39), 14390-14395.

Duval, K., Grover, H., Han, L. H., Mou, Y., Pegoraro, A. F., Fredberg, J. & Chen, Z. (2017) Modeling Physiological Events in 2D vs. 3D Cell Culture. *Physiology (Bethesda)*, 32(4), 266-277.

Dykes, J. R. & M'Fadyean, J. (1888) Lung disease in sheep, caused by the Strongylus rufescens. *Journal of Comparative Pathology and Therapeutics*, 1, 139-146.

Edmonds, M. D., Boyd, K. L., Moyo, T., Mitra, R., Duszynski, R., Arrate, M. P., Chen, X., Zhao, Z., Blackwell, T. S., Andl, T. & Eischen, C. M. (2016) MicroRNA-31 initiates lung tumorigenesis and promotes mutant KRAS-driven lung cancer. *Journal of Clinical Investigation*, 126(1), 349-364.

Eichhorn, S. W., Guo, H., McGeary, S. E., Rodriguez-Mias, R. A., Shin, C., Baek, D., Hsu, S. H., Ghoshal, K., Villen, J. & Bartel, D. P. (2014) mRNA destabilization is the dominant effect of mammalian microRNAs by the time substantial repression ensues. *Mol Cell*, 56(1), 104-15.

Elia, N. & Lippincott-Schwartz, J. (2009) Culturing MDCK cells in three dimensions for analyzing intracellular dynamics. *Curr Protoc Cell Biol*, Chapter 4, Unit 4 22.

Ender, C., Krek, A., Friedländer, M. R., Beitzinger, M., Weinmann, L., Chen, W., Pfeffer, S., Rajewsky, N. & Meister, G. (2008) A Human snoRNA with MicroRNA-Like Functions. *Molecular Cell*, 32(4), 519-528.

Esparza-Baquer, A., Larruskain, A., Mateo-Abad, M., Minguijon, E., Juste, R. A., Benavides, J., Perez, V. & Jugo, B. M. (2015) SNPs in APOBEC3 cytosine deaminases and their association with Visna/Maedi disease progression. *Vet Immunol Immunopathol*, 163(3-4), 125-33.

Esquela-Kerscher, A. & Slack, F. J. (2006) Oncomirs - microRNAs with a role in cancer. *Nat Rev Cancer*, 6(4), 259-69.

Esquela-Kerscher, A., Trang, P., Wiggins, J. F., Patrawala, L., Cheng, A., Ford, L., Weidhaas, J. B., Brown, D., Bader, A. G. & Slack, F. J. (2008) The let-7 microRNA reduces tumor growth in mouse models of lung cancer. *Cell cycle*, 7(6), 759-764.

Fabbri, M., Paone, A., Calore, F., Galli, R., Gaudio, E., Santhanam, R., Lovat, F., Fadda, P., Mao, C., Nuovo, G. J., Zanesi, N., Crawford, M., Ozer, G. H., Wernicke, D., Alder, H., Caligiuri, M. A., Nana-Sinkam, P., Perrotti, D. & Croce, C. M. (2012) MicroRNAs bind to Toll-like receptors to induce prometastatic inflammatory response. *Proc Natl Acad Sci U S A*, 109(31), E2110-6.

Fan, H. (2003) *Jaagsiekte Sheep Retrovirus and Lung Cancer*Springer-Verlag.

Faridani, O. R., Abdullayev, I., Hagemann-Jensen, M., Schell, J. P., Lanner, F. & Sandberg, R. (2016) Single-cell sequencing of the small-RNA transcriptome. *Nature biotechnology*, 34(12), 1264.

Farrell, D., Shaughnessy, R. G., Britton, L., MacHugh, D. E., Markey, B. & Gordon, S. V. (2015) The Identification of Circulating MiRNA in Bovine Serum and Their Potential as Novel Biomarkers of Early Mycobacterium avium subsp paratuberculosis Infection. *PLoS One*, 10(7), e0134310.

Fei, X., Zhang, J., Zhao, Y., Sun, M., Zhao, H. & Li, S. (2018) miR-96 promotes invasion and metastasis by targeting GPC3 in non-small cell lung cancer cells. *Oncol Lett*, 15(6), 9081-9086.

Felgner, P. L., Gadek, T. R., Holm, M., Roman, R., Chan, H. W., Wenz, M., Northrop, J. P., Ringold, G. M. & Danielsen, M. (1987) Lipofection: a highly efficient, lipid-mediated DNA-transfection procedure. *Proc Natl Acad Sci U S A*, 84(21), 7413-7.

Feng, B., Wang, R., Song, H. Z. & Chen, L. B. (2012) MicroRNA-200b reverses chemoresistance of docetaxel-resistant human lung adenocarcinoma cells by targeting E2F3. *Cancer*, 118(13), 3365-76.

Feng, H., Ge, F., Du, L., Zhang, Z. & Liu, D. (2019) MiR-34b-3p represses cell proliferation, cell cycle progression and cell apoptosis in non-small-cell lung cancer (NSCLC) by targeting CDK4. *J Cell Mol Med*, 23(8), 5282-5291.

Fernandez-Costa, J. M., Llamusi, B., Bargiela, A., Zulaica, M., Alvarez-Abril, M. C., Perez-Alonso, M., de Munain, A. L., Lopez-Castel, A. & Artero, R. (2016) Six Serum miRNAs Fail to Validate as Myotonic Dystrophy Type 1 Biomarkers. *PloS one*, 11(2), e0150501.

Flamand, M. N., Gan, H. H., Mayya, V. K., Gunsalus, K. C. & Duchaine, T. F. (2017) A non-canonical site reveals the cooperative mechanisms of microRNA-mediated silencing. *Nucleic Acids Res*, 45(12), 7212-7225.

Friedman, R. C., Farh, K. K.-H., Burge, C. B. & Bartel, D. P. (2009) Most mammalian mRNAs are conserved targets of microRNAs. *Genome research*, 19(1), 92-105.

Fukao, A., Mishima, Y., Takizawa, N., Oka, S., Imataka, H., Pelletier, J., Sonenberg, N., Thoma, C. & Fujiwara, T. (2014) MicroRNAs trigger dissociation of eIF4AI and eIF4AII from target mRNAs in humans. *Mol Cell*, 56(1), 79-89.

Gaeta, X., Le, L., Lin, Y., Xie, Y. & Lowry, W. E. (2017) Defining transcriptional regulatory mechanisms for primary let-7 miRNAs. *PloS one*, 12(1), e0169237.

Gallo, A., Tandon, M., Alevizos, I. & Illei, G. G. (2012) The majority of microRNAs detectable in serum and saliva is concentrated in exosomes. *PLoS One*, 7(3), e30679.

Garcia-Goti, M., Gonzalez, L., Cousens, C., Cortabarria, N., Extramiana, A., Minguijon, E., Ortin, A., De las Heras, M. & Sharp, J. (2000) Sheep pulmonary adenomatosis: characterization of two pathological forms associated with jaagsiekte retrovirus. *Journal of Comparative Pathology*, 122(1), 55-65.

Garre, P., Perez-Segura, P., Diaz-Rubio, E., Caldes, T. & de la Hoya, M. (2010) Reassessing the TARBP2 mutation rate in hereditary nonpolyposis colorectal cancer. *Nat Genet*, 42(10), 817-8; author reply 818.

Gaush, C. R., Hard, W. L. & Smith, T. F. (1966) Characterization of an established line of canine kidney cells (MDCK). *Proc Soc Exp Biol Med*, 122(3), 931-5.

Gebert, L. F. R. & MacRae, I. J. (2019) Regulation of microRNA function in animals. *Nat Rev Mol Cell Biol*, 20(1), 21-37.

Genzor, P., Cordts, S. C., Bokil, N. V. & Haase, A. D. (2019) Aberrant expression of select piRNA-pathway genes does not reactivate piRNA silencing in cancer cells. *Proceedings of the National Academy of Sciences*, 116(23), 11111-11112.

Gilad, S., Meiri, E., Yogev, Y., Benjamin, S., Lebanony, D., Yerushalmi, N., Benjamin, H., Kushnir, M., Cholakh, H., Melamed, N., Bentwich, Z., Hod, M., Goren, Y. & Chajut, A. (2008) Serum MicroRNAs Are Promising Novel Biomarkers. *PLOS ONE*, 3(9), e3148.

Gillet, N. A., Hamaidia, M., de Brogniez, A., Gutiérrez, G., Renotte, N., Reichert, M., Trono, K. & Willems, L. (2016) Bovine Leukemia Virus Small Noncoding RNAs Are Functional Elements That Regulate Replication and Contribute to Oncogenesis In Vivo. *PLOS Pathogens*, 12(4), e1005588.

Giraldez, M. D., Spengler, R. M., Etheridge, A., Godoy, P. M., Barczak, A. J., Srinivasan, S., De Hoff, P. L., Tanriverdi, K., Courtright, A., Lu, S., Khoory, J., Rubio, R., Baxter, D., Driedonks, T. A. P., Buermans, H. P. J., Nolte-'t Hoen, E. N. M., Jiang, H., Wang, K., Ghiran, I., Wang, Y. E., Van Keuren-Jensen, K., Freedman, J. E., Woodruff, P. G., Laurent, L. C., Erle, D. J., Galas, D. J. & Tewari, M. (2018) Comprehensive multi-center assessment of small RNA-seq methods for quantitative miRNA profiling. *Nat Biotechnol*, 36(8), 746-757.

Gkatzis, K., Taghizadeh, S., Huh, D., Stainier, D. Y. & Bellusci, S. (2018) Use of three-dimensional organoids and lung-on-a-chip methods to study lung development, regeneration and disease. *European Respiratory Journal*, 52(5), 1800876.

Goff, S. P. (2013) Retroviridae, in Knipe, D. M. & Howley, P. (eds), *Fields Virology*Wolters Kluwer Health, 1424-1473.

González, L., Juste, R., Cuervo, L., Idigoras, I. & De Ocariz, C. S. (1993) Pathological and epidemiological aspects of the coexistence of maedi-visna and sheep pulmonary adenomatosis. *Research in veterinary science*, 54(2), 140-146.

Gootenberg, J. S., Abudayyeh, O. O., Kellner, M. J., Joung, J., Collins, J. J. & Zhang, F. (2018) Multiplexed and portable nucleic acid detection platform with Cas13, Cas12a, and Csm6. *Science*, 360(6387), 439-444.

Goto, A., Tanaka, M., Yoshida, M., Umakoshi, M., Nanjo, H., Shiraishi, K., Saito, M., Kohno, T., Kuriyama, S., Konno, H., Imai, K., Saito, H., Minamiya, Y. & Maeda, D. (2017) The low expression of MIR-451 predicts a worse prognosis in non-small cell lung cancer cases. *PLoS ONE*, 12(7).

Gottwein, E., Mukherjee, N., Sachse, C., Frenzel, C., Majoros, W. H., Chi, J. T., Braich, R., Manoharan, M., Soutschek, J., Ohler, U. & Cullen, B. R. (2007) A viral microRNA functions as an orthologue of cellular miR-155. *Nature*, 450(7172), 1096-9.

Graham, F. L., Smiley, J., Russell, W. C. & Nairn, R. (1977) Characteristics of a human cell line transformed by DNA from human adenovirus type 5. *J Gen Virol*, 36(1), 59-74.

Grassmann, R. & Jeang, K.-T. (2008) The roles of microRNAs in mammalian virus infection. *Biochimica et Biophysica Acta (BBA) - Gene Regulatory Mechanisms*, 1779(11), 706-711.

Gray, M. E., Meehan, J., Sullivan, P., Marland, J. R. K., Greenhalgh, S. N., Gregson, R., Clutton, R. E., Ward, C., Cousens, C., Griffiths, D. J., Murray, A. & Argyle, D. (2019) Ovine Pulmonary Adenocarcinoma: A Unique Model to Improve Lung Cancer Research. *Front Oncol*, 9, 335.

Grego, E., De Meneghi, D., Alvarez, V., Benito, A. A., Minguijon, E., Ortin, A., Mattoni, M., Moreno, B., Perez de Villarreal, M., Alberti, A., Capucchio, M. T., Caporale, M., Juste, R., Rosati, S. & De las Heras, M. (2008) Colostrum and milk can transmit jaagsiekte retrovirus to lambs. *Vet Microbiol*, 130(3-4), 247-57.

Gregory, P. A., Bert, A. G., Paterson, E. L., Barry, S. C., Tsykin, A., Farshid, G., Vadas, M. A., Khew-Goodall, Y. & Goodall, G. J. (2008) The miR-200 family and miR-205 regulate epithelial to mesenchymal transition by targeting ZEB1 and SIP1. *Nature cell biology*, 10(5), 593.

Grey, F. (2015) Role of microRNAs in herpesvirus latency and persistence. *J Gen Virol*, 96(Pt 4), 739-51.

Griffiths-Jones, S., Grocock, R. J., van Dongen, S., Bateman, A. & Enright, A. J. (2006) miRBase: microRNA sequences, targets and gene nomenclature. *Nucleic Acids Res*, 34(Database issue), D140-4.

Griffiths-Jones, S., Saini, H. K., van Dongen, S. & Enright, A. J. (2008) miRBase: tools for microRNA genomics. *Nucleic Acids Res*, 36(Database issue), D154-8.

Griffiths, D. J., Martineau, H. M. & Cousens, C. (2010) Pathology and pathogenesis of ovine pulmonary adenocarcinoma. *J Comp Pathol*, 142(4), 260-83.

Grimson, A., Farh, K. K., Johnston, W. K., Garrett-Engele, P., Lim, L. P. & Bartel, D. P. (2007) MicroRNA targeting specificity in mammals: determinants beyond seed pairing. *Mol Cell*, 27(1), 91-105.

Gruenert, D. C., Finkbeiner, W. E. & Widdicombe, J. H. (1995) Culture and transformation of human airway epithelial cells. *American Journal of Physiology-Lung Cellular and Molecular Physiology*, 268(3), L347-L360.

Guan, P., Yin, Z., Li, X., Wu, W. & Zhou, B. (2012) Meta-analysis of human lung cancer microRNA expression profiling studies comparing cancer tissues with normal tissues. *Journal of Experimental & Clinical Cancer Research*, 31(1), 54.

Guduric-Fuchs, J., O'Connor, A., Camp, B., O'Neill, C. L., Medina, R. J. & Simpson, D. A. (2012) Selective extracellular vesicle-mediated export of an overlapping set of microRNAs from multiple cell types. *BMC Genomics*, 13(1), 357.

Guo, H., Ingolia, N. T., Weissman, J. S. & Bartel, D. P. (2010) Mammalian microRNAs predominantly act to decrease target mRNA levels. *Nature*, 466(7308), 835-40.

Guo, L., Yu, J., Yu, H., Zhao, Y., Chen, S., Xu, C. & Chen, F. (2015a) Evolutionary and expression analysis of miR-#-5p and miR-#-3p at the miRNAs/isomiRs levels. *Biomed Res Int*, 2015, 168358.

Guo, Y., Liu, J., Elfenbein, S. J., Ma, Y., Zhong, M., Qiu, C., Ding, Y. & Lu, J. (2015b) Characterization of the mammalian miRNA turnover landscape. *Nucleic Acids Res*, 43(4), 2326-41.

Gyoba, J., Shan, S., Roa, W. & Bedard, E. L. (2016) Diagnosing Lung Cancers through Examination of Micro-RNA Biomarkers in Blood, Plasma, Serum and Sputum: A Review and Summary of Current Literature. *Int J Mol Sci*, 17(4), 494.

Ha, M. & Kim, V. N. (2014) Regulation of microRNA biogenesis. *Nat Rev Mol Cell Biol*, 15(8), 509-24.

Hagemann-Jensen, M., Abdullayev, I., Sandberg, R. & Faridani, O. R. (2018) Small-seq for single-cell small-RNA sequencing. *Nature protocols*, 13(10), 2407.

Harris, K. S., Zhang, Z., McManus, M. T., Harfe, B. D. & Sun, X. (2006) Dicer function is essential for lung epithelium morphogenesis. *Proceedings of the National Academy of Sciences*, 103(7), 2208-2213.

Harwig, A., Das, A. T. & Berkhout, B. (2014) Retroviral microRNAs. *Curr Opin Virol*, 7, 47-54.

Hasin, Y., Seldin, M. & Lusis, A. (2017) Multi-omics approaches to disease. *Genome biology*, 18(1), 83.

Hatley, M. E., Patrick, D. M., Garcia, M. R., Richardson, J. A., Bassel-Duby, R., van Rooij, E. & Olson, E. N. (2010) Modulation of K-Ras-dependent lung tumorigenesis by MicroRNA-21. *Cancer Cell*, 18(3), 282-93.

Hayashita, Y., Osada, H., Tatematsu, Y., Yamada, H., Yanagisawa, K., Tomida, S., Yatabe, Y., Kawahara, K., Sekido, Y. & Takahashi, T. (2005) A polycistronic microRNA cluster, miR-17-92, is overexpressed in human lung cancers and enhances cell proliferation. *Cancer Res*, 65(21), 9628-32.

Hayward, W. S., Neel, B. G. & Astrin, S. M. (1981) Activation of a cellular onc gene by promoter insertion in ALV-induced lymphoid leukosis. *Nature*, 290(5806), 475.

He, L., He, X., Lim, L. P., de Stanchina, E., Xuan, Z., Liang, Y., Xue, W., Zender, L., Magnus, J., Ridzon, D., Jackson, A. L., Linsley, P. S., Chen, C., Lowe, S. W., Cleary, M. A. &

Hannon, G. J. (2007) A microRNA component of the p53 tumour suppressor network. *Nature*, 447(7148), 1130-4.

Heilmeier, U., Hackl, M., Skalicky, S., Weilner, S., Schroeder, F., Vierlinger, K., Patsch, J. M., Baum, T., Oberbauer, E., Lobach, I., Burghardt, A. J., Schwartz, A. V., Grillari, J. & Link, T. M. (2016) Serum miRNA Signatures Are Indicative of Skeletal Fractures in Postmenopausal Women With and Without Type 2 Diabetes and Influence Osteogenic and Adipogenic Differentiation of Adipose Tissue-Derived Mesenchymal Stem Cells In Vitro. *J Bone Miner Res*, 31(12), 2173-2192.

Helwak, A., Kudla, G., Dudnakova, T. & Tollervey, D. (2013) Mapping the human miRNA interactome by CLASH reveals frequent noncanonical binding. *Cell*, 153(3), 654-65.

Hendrickson, D. G., Hogan, D. J., McCullough, H. L., Myers, J. W., Herschlag, D., Ferrell, J. E. & Brown, P. O. (2009) Concordant Regulation of Translation and mRNA Abundance for Hundreds of Targets of a Human microRNA. *PLOS Biology*, 7(11), e1000238.

Hermeking, H. (2007) p53 enters the microRNA world. *Cancer Cell*, 12(5), 414-8.

Hermeking, H. (2010) The miR-34 family in cancer and apoptosis. *Cell Death Differ*, 17(2), 193-9.

Hiard, S., Charlier, C., Coppieters, W., Georges, M. & Baurain, D. (2010) Patrocles: a database of polymorphic miRNA-mediated gene regulation in vertebrates. *Nucleic Acids Res*, 38(Database issue), D640-51.

Hofacre, A. & Fan, H. (2004) Multiple domains of the Jaagsiekte sheep retrovirus envelope protein are required for transformation of rodent fibroblasts. *J Virol*, 78(19), 10479-89.

Hofacre, A. & Fan, H. (2010) Jaagsiekte sheep retrovirus biology and oncogenesis. *Viruses*, 2(12), 2618-48.

Hofacre, A., Nitta, T. & Fan, H. (2009) Jaagsiekte sheep retrovirus encodes a regulatory factor, Rej, required for synthesis of Gag protein. *Journal of Virology*, 83(23), 12483-12498.

Holland, M. J., Palmarini, M., Garcia-Goti, M., Gonzalez, L., McKendrick, I., de las Heras, M. & Sharp, J. M. (1999) Jaagsiekte retrovirus is widely distributed both in T and B lymphocytes and in mononuclear phagocytes of sheep with naturally and experimentally acquired pulmonary adenomatosis. *Journal of Virology*, 73(5), 4004-4008.

Holleman, A., Chung, I., Olsen, R. R., Kwak, B., Mizokami, A., Saijo, N., Parissenti, A., Duan, Z., Voest, E. E. & Zetter, B. R. (2011) miR-135a contributes to paclitaxel resistance in tumor cells both in vitro and in vivo. *Oncogene*, 30(43), 4386-98.

Hopwood, P., Wallace, W. A., Cousens, C., Dewar, P., Muldoon, M., Norval, M. & Griffiths, D. J. (2010) Absence of markers of betaretrovirus infection in human pulmonary adenocarcinoma. *Hum Pathol*, 41(11), 1631-40.

Hou, J., Meng, F., Chan, L. W., Cho, W. C. & Wong, S. C. (2016) Circulating Plasma MicroRNAs As Diagnostic Markers for NSCLC. *Front Genet*, 7, 193.

Hou, Y., Zhen, J., Xu, X., Zhen, K., Zhu, B., Pan, R. & Zhao, C. (2015) miR-215 functions as a tumor suppressor and directly targets ZEB2 in human non-small cell lung cancer. *Oncol Lett*, 10(4), 1985-1992.

Hsu, T., Phung, A., Choe, K., Kim, J. W. & Fan, H. (2015) Role for a Zinc Finger Protein (Zfp111) in Transformation of 208F Rat Fibroblasts by Jaagsiekte Sheep Retrovirus Envelope Protein. *J Virol*, 89(20), 10453-66.

Hu, H., Li, S., Liu, J. & Ni, B. (2012) MicroRNA-193b modulates proliferation, migration, and invasion of non-small cell lung cancer cells. *Acta Biochim Biophys Sin*, 44(5), 424-430.

Hu, L., Ai, J., Long, H., Liu, W., Wang, X., Zuo, Y., Li, Y., Wu, Q. & Deng, Y. (2016) Integrative microRNA and gene profiling data analysis reveals novel biomarkers and mechanisms for lung cancer. *Oncotarget*, 7(8), 8441.

Hu, Z., Chen, X., Zhao, Y., Tian, T., Jin, G., Shu, Y., Chen, Y., Xu, L., Zen, K., Zhang, C. & Shen, H. (2010) Serum microRNA signatures identified in a genome-wide serum microRNA expression profiling predict survival of non-small-cell lung cancer. *J Clin Oncol*, 28(10), 1721-6.

Huang-Doran, I., Zhang, C. Y. & Vidal-Puig, A. (2017) Extracellular Vesicles: Novel Mediators of Cell Communication In Metabolic Disease. *Trends Endocrinol Metab*, 28(1), 3-18.

Hudachek, S. F., Kraft, S. L., Thamm, D. H., Bielefeldt-Ohmann, H., DeMartini, J. C., Miller, A. D. & Dernell, W. S. (2010) Lung tumor development and spontaneous regression in lambs coinfected with Jaagsiekte sheep retrovirus and ovine lentivirus. *Vet Pathol*, 47(1), 148-62.

Huh, D., Matthews, B. D., Mammoto, A., Montoya-Zavala, M., Hsin, H. Y. & Ingber, D. E. (2010) Reconstituting organ-level lung functions on a chip. *Science*, 328(5986), 1662-1668.

Hull, S. & Fan, H. (2006) Mutational analysis of the cytoplasmic tail of jaagsiekte sheep retrovirus envelope protein. *J Virol*, 80(16), 8069-80.

Hunter, A. & Munro, R. (1983) The diagnosis, occurrence and distribution of sheep pulmonary adenomatosis in Scotland 1975 to 1981. *British Veterinary Journal*, 139(2), 153-164.

Hunter, S. E., Finnegan, E. F., Zisoulis, D. G., Lovci, M. T., Melnik-Martinez, K. V., Yeo, G. W. & Pasquinelli, A. E. (2013) Functional genomic analysis of the let-7 regulatory network in Caenorhabditis elegans. *PLoS Genet*, 9(3), e1003353.

Hutcheon, D. (1891) Reply to query no. 191 about jaagsiekte or chronic catarrhal pneumonia. *Agric J Cape of Good Hope*, 4, 87-89.

Ian Freshney, R. (2005) Culture of animal cells: a manual of basic technique. *USA: John Wiley & Sons.–2005.–642 p*.

Ikari, J., Smith, L. M., Nelson, A. J., Iwasawa, S., Gunji, Y., Farid, M., Wang, X., Basma, H., Feghali-Bostwick, C. & Liu, X. (2015) Effect of culture conditions on microRNA expression in primary adult control and COPD lung fibroblasts in vitro. *In Vitro Cellular & Developmental Biology-Animal*, 51(4), 390-399.

Ikeda, Y., Takeuchi, Y., Martin, F., Cosset, F. L., Mitrophanous, K. & Collins, M. (2003) Continuous high-titer HIV-1 vector production. *Nat Biotechnol*, 21(5), 569-72.

Inamura, K. (2017) Diagnostic and Therapeutic Potential of MicroRNAs in Lung Cancer. *Cancers*, 9(5), 49.

Inamura, K., Togashi, Y., Nomura, K., Ninomiya, H., Hiramatsu, M., Satoh, Y., Okumura, S., Nakagawa, K. & Ishikawa, Y. (2007) let-7 microRNA expression is reduced in bronchioloalveolar carcinoma, a non-invasive carcinoma, and is not correlated with prognosis. *Lung Cancer*, 58(3), 392-6.

Incoronato, M., Garofalo, M., Urso, L., Romano, G., Quintavalle, C., Zanca, C., Iaboni, M., Nuovo, G., Croce, C. M. & Condorelli, G. (2010) miR-212 increases tumor necrosis factor-related apoptosis-inducing ligand sensitivity in non-small cell lung cancer by targeting the antiapoptotic protein PED. *Cancer Res*, 70(9), 3638-46.

Incoronato, M., Urso, L., Portela, A., Laukkanen, M. O., Soini, Y., Quintavalle, C., Keller, S., Esteller, M. & Condorelli, G. (2011) Epigenetic regulation of miR-212 expression in lung cancer. *PLoS One*, 6(11), e27722.

Indik, S., Gunzburg, W. H., Salmons, B. & Rouault, F. (2005) A novel, mouse mammary tumor virus encoded protein with Rev-like properties. *Virology*, 337(1), 1-6.

Jacobsen, L. B., Calvin, S. A., Colvin, K. E. & Wright, M. (2004) FuGENE 6 Transfection Reagent: the gentle power. *Methods*, 33(2), 104-112.

Jainchill, J. L., Aaronson, S. A. & Todaro, G. J. (1969) Murine sarcoma and leukemia viruses: assay using clonal lines of contact-inhibited mouse cells. *Journal of virology*, 4(5), 549-553.

Jarry, J., Schadendorf, D., Greenwood, C., Spatz, A. & van Kempen, L. C. (2014) The validity of circulating microRNAs in oncology: Five years of challenges and contradictions. *Molecular Oncology*, 8(4), 819-829.

Jassim, F., Sharp, J. & Marinello, P. (1987) Three-step procedure for isolation of epithelial cells from the lungs of sheep with jaagsiekte. *Research in veterinary science*, 43(3), 407-409.

Jiang, X., Chen, X., Chen, L., Ma, Y., Zhou, L., Qi, Q., Liu, Y., Zhang, S., Luo, J. & Zhou, X. (2015) Upregulation of the miR-212/132 cluster suppresses proliferation of human lung cancer cells. *Oncol Rep*, 33(2), 705-12.

Jiang, X., Tsitsiou, E., Herrick, S. E. & Lindsay, M. A. (2010) MicroRNAs and the regulation of fibrosis. *The FEBS Journal*, 277(9), 2015-2021.

Jiménez-García, M. P., Lucena-Cacace, A., Robles-Frías, M., Ferrer, I., Narlik-Grassow, M., Blanco-Aparicio, C. & Carnero, A. (2017) Inflammation and stem markers association to PIM1/PIM2 kinase-induced tumors in breast and uterus. *Oncotarget*, 8(35), 58872-58886.

Johnson, C. & Fan, H. (2011) Three-dimensional culture of an ovine pulmonary adenocarcinoma-derived cell line results in re-expression of surfactant proteins and Jaagsiekte sheep retrovirus. *Virology*, 414(1), 91-6.

Johnson, C., Jahid, S., Voelker, D. R. & Fan, H. (2011) Enhanced proliferation of primary rat type II pneumocytes by Jaagsiekte sheep retrovirus envelope protein. *Virology*, 412(2), 349-56.

Johnson, C. D., Esquela-Kerscher, A., Stefani, G., Byrom, M., Kelnar, K., Ovcharenko, D., Wilson, M., Wang, X., Shelton, J. & Shingara, J. (2007) The let-7 microRNA represses cell proliferation pathways in human cells. *Cancer research*, 67(16), 7713-7722.

Jopling, C. L., Yi, M., Lancaster, A. M., Lemon, S. M. & Sarnow, P. (2005) Modulation of hepatitis C virus RNA abundance by a liver-specific MicroRNA. *Science*, 309(5740), 1577-81.

Kanokudom, S., Mahony, T. J., Smith, D. R. & Assavalapsakul, W. (2018) Modulation of bovine herpesvirus 1 infection by virally encoded microRNAs. *Virus Res*, 257, 1-6.

Karagianni, A., Kapetanovic, R., Summers, K., McGorum, B., Hume, D. & Pirie, R. (2017) Comparative transcriptome analysis of equine alveolar macrophages. *Equine veterinary journal*, 49(3), 375-382.

Karagianni, A. E., Vasoya, D., Finlayson, J., Martineau, H. M., Wood, A. R., Cousens, C., Dagleish, M. P., Watson, M. & Griffiths, D. J. (2019) Transcriptional response of ovine lung to infection with jaagsiekte sheep retrovirus. *Journal of virology*, 93(21), e00876-19.

Karagkouni, D., Paraskevopoulou, M. D., Chatzopoulos, S., Vlachos, I. S., Tastsoglou, S., Kanellos, I., Papadimitriou, D., Kavakiotis, I., Maniou, S., Skoufos, G., Vergoulis, T., Dalamagas, T. & Hatzigeorgiou, A. G. (2018) DIANA-TarBase v8: a decade-long collection of experimentally supported miRNA-gene interactions. *Nucleic Acids Res*, 46(D1), D239-d245.

Karginov, F. V., Conaco, C., Xuan, Z., Schmidt, B. H., Parker, J. S., Mandel, G. & Hannon, G. J. (2007) A biochemical approach to identifying microRNA targets. *Proceedings of the National Academy of Sciences*, 104(49), 19291-19296.

Kataoka, K., Shiraishi, Y., Takeda, Y., Sakata, S., Matsumoto, M., Nagano, S., Maeda, T., Nagata, Y., Kitanaka, A., Mizuno, S., Tanaka, H., Chiba, K., Ito, S., Watatani, Y., Kakiuchi, N., Suzuki, H., Yoshizato, T., Yoshida, K., Sanada, M., Itonaga, H., Imaizumi, Y., Totoki, Y., Munakata, W., Nakamura, H., Hama, N., Shide, K., Kubuki, Y., Hidaka, T., Kameda, T., Masuda, K., Minato, N., Kashiwase, K., Izutsu, K., Takaori-Kondo, A., Miyazaki, Y., Takahashi, S., Shibata, T., Kawamoto, H., Akatsuka, Y., Shimoda, K., Takeuchi, K., Seya, T., Miyano, S. & Ogawa, S. (2016) Aberrant PD-L1 expression through 3′-UTR disruption in multiple cancers. *Nature*, 534, 402.

Kaul, D., Ahlawat, A. & Gupta, S. D. (2009) HIV-1 genome-encoded hiv1-mir-H1 impairs cellular responses to infection. *Mol Cell Biochem*, 323(1-2), 143-8.

Keller, A., Rounge, T., Backes, C., Ludwig, N., Gislefoss, R., Leidinger, P., Langseth, H. & Meese, E. (2017) Sources to variability in circulating human miRNA signatures. *RNA biology*, 14(12), 1791-1798.

Kim, G., An, H. J., Lee, M. J., Song, J. Y., Jeong, J. Y., Lee, J. H. & Jeong, H. C. (2016) Hsa-miR-1246 and hsa-miR-1290 are associated with stemness and invasiveness of non-small cell lung cancer. *Lung Cancer*, 91, 15-22.

Kim, J., Lim, N. J., Jang, S. G., Kim, H. K. & Lee, G. K. (2014) miR-592 and miR-552 can distinguish between primary lung adenocarcinoma and colorectal cancer metastases in the lung. *Anticancer Res*, 34(5), 2297-302.

Kim, J. O., Gazala, S., Razzak, R., Guo, L., Ghosh, S., Roa, W. H. & Bedard, E. L. (2015) Non-small cell lung cancer detection using microRNA expression profiling of bronchoalveolar lavage fluid and sputum. *Anticancer Res*, 35(4), 1873-80.

Kincaid, R. P., Burke, J. M. & Sullivan, C. S. (2012) RNA virus microRNA that mimics a B-cell oncomiR. *Proc Natl Acad Sci U S A*, 109(8), 3077-82.

Kincaid, R. P., Chen, Y., Cox, J. E., Rethwilm, A. & Sullivan, C. S. (2014) Noncanonical microRNA (miRNA) biogenesis gives rise to retroviral mimics of lymphoproliferative and immunosuppressive host miRNAs. *MBio*, 5(2), e00074-14.

Kincaid, R. P., Panicker, N. G., Lozano, M. M., Sullivan, C. S., Dudley, J. P. & Mustafa, F. (2018) MMTV does not encode viral microRNAs but alters the levels of cancer-associated host microRNAs. *Virology*, 513, 180-187.

Kincaid, R. P. & Sullivan, C. S. (2012) Virus-Encoded microRNAs: An Overview and a Look to the Future. *PLOS Pathogens*, 8(12), e1003018.

Kirschner, M. B., Kao, S. C., Edelman, J. J., Armstrong, N. J., Vallely, M. P., van Zandwijk, N. & Reid, G. (2011) Haemolysis during sample preparation alters microRNA content of plasma. *PloS one*, 6(9), e24145-e24145.

Klase, Z., Kale, P., Winograd, R., Gupta, M. V., Heydarian, M., Berro, R., McCaffrey, T. & Kashanchi, F. (2007) HIV-1 TAR element is processed by Dicer to yield a viral micro-RNA involved in chromatin remodeling of the viral LTR. *BMC Mol Biol*, 8, 63.

Kloosterman, W. P. & Plasterk, R. H. A. (2006) The Diverse Functions of MicroRNAs in Animal Development and Disease. *Developmental Cell*, 11(4), 441-450.

Kocijan, R., Muschitz, C., Geiger, E., Skalicky, S., Baierl, A., Dormann, R., Plachel, F., Feichtinger, X., Heimel, P. & Fahrleitner-Pammer, A. (2016) Circulating microRNA signatures in patients with idiopathic and postmenopausal osteoporosis and fragility fractures. *The Journal of Clinical Endocrinology & Metabolism*, 101(11), 4125-4134.

Koh, W., Sheng, C. T., Tan, B., Lee, Q. Y., Kuznetsov, V., Kiang, L. S. & Tanavde, V. (2010) Analysis of deep sequencing microRNA expression profile from human embryonic stem cells derived mesenchymal stem cells reveals possible role of let-7 microRNA family in downstream targeting of hepatic nuclear factor 4 alpha. *BMC genomics*, 11(1), S6.

Kosaka, N., Iguchi, H. & Ochiya, T. (2010) Circulating microRNA in body fluid: a new potential biomarker for cancer diagnosis and prognosis. *Cancer Sci*, 101(10), 2087-92.

Kosaka, N., Iguchi, H., Yoshioka, Y., Hagiwara, K., Takeshita, F. & Ochiya, T. (2012) Competitive interactions of cancer cells and normal cells via secretory microRNAs. *J Biol Chem*, 287(2), 1397-405.

Kozomara, A., Birgaoanu, M. & Griffiths-Jones, S. (2019) miRBase: from microRNA sequences to function. *Nucleic Acids Res*, 47(D1), D155-D162.

Krauss, H. & Wandera, J. (1970) Isolation and properties of Mycoplasma from the respiratory tract of sheep with jaagsiekte in Kenya. *Journal of comparative pathology*, 80(3), 389-397.

Krauss, R. H., Phipson, B., Oshlack, A., Prasad-Gupta, N., Cheung, M. M., Smolich, J. J. & Pepe, S. (2018) Shifts in ovine cardiopulmonary microRNA expression in late gestation and the perinatal period. *PLoS One*, 13(9), e0204038.

Krishnan, K., Steptoe, A. L., Martin, H. C., Wani, S., Nones, K., Waddell, N., Mariasegaram, M., Simpson, P. T., Lakhani, S. R., Gabrielli, B., Vlassov, A., Cloonan, N. & Grimmond, S. M. (2013) MicroRNA-182-5p targets a network of genes involved in DNA repair. *RNA*, 19(2), 230-242.

Kroesen, B. J., Teteloshvili, N., Smigielska-Czepiel, K., Brouwer, E., Boots, A. M. H., van den Berg, A. & Kluiver, J. (2015) Immuno-miRs: critical regulators of T-cell development, function and ageing. *Immunology*, 144(1), 1-10.

Kuhn, S., Johnson, S. L., Furness, D. N., Chen, J., Ingham, N., Hilton, J. M., Steffes, G., Lewis, M. A., Zampini, V., Hackney, C. M., Masetto, S., Holley, M. C., Steel, K. P. & Marcotti, W. (2011) miR-96 regulates the progression of differentiation in mammalian cochlear inner and outer hair cells. *Proceedings of the National Academy of Sciences of the United States of America*, 108(6), 2355-2360.

Kumar, M. S., Lu, J., Mercer, K. L., Golub, T. R. & Jacks, T. (2007) Impaired microRNA processing enhances cellular transformation and tumorigenesis. *Nature Genetics*, 39(5), 673-677.

Kumar, M. S., Pester, R. E., Chen, C. Y., Lane, K., Chin, C., Lu, J., Kirsch, D. G., Golub, T. R. & Jacks, T. (2009) Dicer1 functions as a haploinsufficient tumor suppressor. *Genes Dev*, 23(23), 2700-4.

Kuosmanen, S. M., Kansanen, E., Sihvola, V. & Levonen, A. L. (2017) MicroRNA Profiling Reveals Distinct Profiles for Tissue-Derived and Cultured Endothelial Cells. *Sci Rep*, 7(1), 10943.

Labourier, E., Shifrin, A., Busseniers, A. E., Lupo, M. A., Manganelli, M. L., Andruss, B., Wylie, D. & Beaudenon-Huibregtse, S. (2015) Molecular testing for miRNA, mRNA, and DNA on fine-needle aspiration improves the preoperative diagnosis of thyroid nodules with indeterminate cytology. *The Journal of Clinical Endocrinology & Metabolism*, 100(7), 2743-2750.

Lagos-Quintana, M., Rauhut, R., Lendeckel, W. & Tuschl, T. (2001) Identification of Novel Genes Coding for Small Expressed RNAs. *Science*, 294(5543), 853-858.

Lagos-Quintana, M., Rauhut, R., Yalcin, A., Meyer, J., Lendeckel, W. & Tuschl, T. (2002) Identification of Tissue-Specific MicroRNAs from Mouse. *Current Biology*, 12(9), 735-739.

Lamers, S. L., Fogel, G. B. & McGrath, M. S. (2010) HIV-miR-H1 evolvability during HIV pathogenesis. *Biosystems*, 101(2), 88-96.

Landgraf, P., Rusu, M., Sheridan, R., Sewer, A., Iovino, N., Aravin, A., Pfeffer, S., Rice, A., Kamphorst, A. O., Landthaler, M., Lin, C., Socci, N. D., Hermida, L., Fulci, V., Chiaretti, S., Foa, R., Schliwka, J., Fuchs, U., Novosel, A., Muller, R. U., Schermer, B., Bissels, U., Inman, J., Phan, Q., Chien, M., Weir, D. B., Choksi, R., De Vita, G., Frezzetti, D., Trompeter, H. I., Hornung, V., Teng, G., Hartmann, G., Palkovits, M., Di Lauro, R., Wernet, P., Macino, G., Rogler, C. E., Nagle, J. W., Ju, J., Papavasiliou, F. N., Benzing, T., Lichter, P., Tam, W., Brownstein, M. J., Bosio, A., Borkhardt, A., Russo, J. J., Sander, C., Zavolan, M. & Tuschl, T. (2007) A mammalian microRNA expression atlas based on small RNA library sequencing. *Cell*, 129(7), 1401-14.

Langdon, W. B., Petke, J. & Lorenz, R. (2018) *Evolving better RNAfold structure prediction.* 2018.

Larrea, E., Sole, C., Manterola, L., Goicoechea, I., Armesto, M., Arestin, M., Caffarel, M. M., Araujo, A. M., Araiz, M., Fernandez-Mercado, M. & Lawrie, C. H. (2016) New Concepts in Cancer Biomarkers: Circulating miRNAs in Liquid Biopsies. *Int J Mol Sci*, 17(5).

Lawson, J., Dickman, C., MacLellan, S., Towle, R., Jabalee, J., Lam, S. & Garnis, C. (2017) Selective secretion of microRNAs from lung cancer cells via extracellular vesicles promotes CAMK1D-mediated tube formation in endothelial cells. *Oncotarget*, 8(48), 83913-83924.

Le, H. B., Zhu, W. Y., Chen, D. D., He, J. Y., Huang, Y. Y., Liu, X. G. & Zhang, Y. K. (2012) Evaluation of dynamic change of serum miR-21 and miR-24 in pre- and post-operative lung carcinoma patients. *Med Oncol*, 29(5), 3190-7.

Lee, A. M., Wolfe, A., Cassidy, J. P., Mc, V. M. L. L., Moriarty, J. P., O'Neill, R., Fahy, C., Connaghan, E., Cousens, C., Dagleish, M. P. & McElroy, M. C. (2017) First confirmation by PCR of Jaagsiekte sheep retrovirus in Ireland and prevalence of ovine pulmonary adenocarcinoma in adult sheep at slaughter. *Ir Vet J*, 70, 33.

Lee, D. F. & Chambers, M. A. (2019) Isolation of Alveolar Type II Cells from Adult Bovine Lung. *Curr Protoc Toxicol*, 80(1), e71.

Lee, D. F., Salguero, F. J., Grainger, D., Francis, R. J., MacLellan-Gibson, K. & Chambers, M. A. (2018) Isolation and characterisation of alveolar type II pneumocytes from adult bovine lung. *Scientific Reports*, 8(1), 11927.

Lee, H., Zhang, D., Zhu, Z., Dela Cruz, C. S. & Jin, Y. (2016) Epithelial cell-derived microvesicles activate macrophages and promote inflammation via microvesicle-containing microRNAs. *Sci Rep*, 6, 35250.

Lee, R. C., Feinbaum, R. L. & Ambros, V. (1993) The C. elegans heterochronic gene lin-4 encodes small RNAs with antisense complementarity to lin-14. *cell*, 75(5), 843-854.

Lehmann, K., Janda, E., Pierreux, C. E., Rytomaa, M., Schulze, A., McMahon, M., Hill, C. S., Beug, H. & Downward, J. (2000) Raf induces TGFbeta production while blocking its apoptotic but not invasive responses: a mechanism leading to increased malignancy in epithelial cells. *Genes Dev*, 14(20), 2610-22.

Leivonen, S. K., Makela, R., Ostling, P., Kohonen, P., Haapa-Paananen, S., Kleivi, K., Enerly, E., Aakula, A., Hellstrom, K., Sahlberg, N., Kristensen, V. N., Borresen-Dale, A. L., Saviranta, P., Perala, M. & Kallioniemi, O. (2009) Protein lysate microarray analysis to identify microRNAs regulating estrogen receptor signaling in breast cancer cell lines. *Oncogene*, 28(44), 3926-36.

Lerner, M., Harada, M., Loven, J., Castro, J., Davis, Z., Oscier, D., Henriksson, M., Sangfelt, O., Grander, D. & Corcoran, M. M. (2009) DLEU2, frequently deleted in malignancy, functions as a critical host gene of the cell cycle inhibitory microRNAs miR-15a and miR-16-1. *Exp Cell Res*, 315(17), 2941-52.

Lewis, F., Brülisauer, F., Cousens, C., McKendrick, I. & Gunn, G. (2011) Diagnostic accuracy of PCR for Jaagsiekte sheep retrovirus using field data from 125 Scottish sheep flocks. *The Veterinary Journal*, 187(1), 104-108.

Li, C., Yin, Y., Liu, X., Xi, X., Xue, W. & Qu, Y. (2017a) Non-small cell lung cancer associated microRNA expression signature: integrated bioinformatics analysis, validation and clinical significance. *Oncotarget*, 8(15), 24564-24578.

Li, H., Jiang, Z., Leng, Q., Bai, F., Wang, J., Ding, X., Li, Y., Zhang, X., Fang, H., Yfantis, H. G., Xing, L. & Jiang, F. (2017b) A prediction model for distinguishing lung squamous cell carcinoma from adenocarcinoma. *Oncotarget*, 8(31), 50704-50714.

Li, H., Ouyang, R., Wang, Z., Zhou, W., Chen, H., Jiang, Y., Zhang, Y., Li, H., Liao, M., Wang, W., Ye, M., Ding, Z., Feng, X., Liu, J. & Zhang, B. (2016) MiR-150 promotes cellular metastasis in non-small cell lung cancer by targeting FOXO4. *Sci Rep*, 6, 39001.

Li, N., You, X., Chen, T., Mackowiak, S. D., Friedländer, M. R., Weigt, M., Du, H., Gogol-Döring, A., Chang, Z., Dieterich, C., Hu, Y. & Chen, W. (2013a) Global profiling of miRNAs and the hairpin precursors: Insights into miRNA processing and novel miRNA discovery. *Nucleic Acids Research*, 41(6), 3619-3634.

Li, P., Hua, X., Zhang, Z., Li, J. & Wang, J. (2013b) Characterization of regulatory features of housekeeping and tissue-specific regulators within tissue regulatory networks. *BMC systems biology*, 7(1), 112.

Li, Y., Chan, E. Y., Li, J., Ni, C., Peng, X., Rosenzweig, E., Tumpey, T. M. & Katze, M. G. (2010) MicroRNA Expression and Virulence in Pandemic Influenza Virus-Infected Mice. *Journal of Virology*, 84(6), 3023-3032.

Li, Y., Zhang, D., Chen, C., Ruan, Z., Li, Y. & Huang, Y. (2012) MicroRNA-212 displays tumor-promoting properties in non-small cell lung cancer cells and targets the hedgehog pathway receptor PTCH1. *Mol Biol Cell*, 23(8), 1423-34.

Liang, H., Gong, F., Zhang, S., Zhang, C.-Y., Zen, K. & Chen, X. (2014) The origin, function, and diagnostic potential of extracellular microRNAs in human body fluids. *WIREs RNA*, 5(2), 285-300.

Lim, L. P., Lau, N. C., Garrett-Engele, P., Grimson, A., Schelter, J. M., Castle, J., Bartel, D. P., Linsley, P. S. & Johnson, J. M. (2005) Microarray analysis shows that some microRNAs downregulate large numbers of target mRNAs. *Nature*, 433(7027), 769.

Lim, L. P., Lau, N. C., Weinstein, E. G., Abdelhakim, A., Yekta, S., Rhoades, M. W., Burge, C. B. & Bartel, D. P. (2003) The microRNAs of Caenorhabditis elegans. *Genes & development*, 17(8), 991-1008.

Lin, C. W., Chang, Y. L., Chang, Y. C., Lin, J. C., Chen, C. C., Pan, S. H., Wu, C. T., Chen, H. Y., Yang, S. C., Hong, T. M. & Yang, P. C. (2013) MicroRNA-135b promotes lung cancer metastasis by regulating multiple targets in the Hippo pathway and LZTS1. *Nat Commun*, 4, 1877.

Lin, J. & Cullen, B. R. (2007) Analysis of the interaction of primate retroviruses with the human RNA interference machinery. *J Virol*, 81(22), 12218-26.

Lin, S. & Gregory, R. I. (2015) MicroRNA biogenesis pathways in cancer. *Nat Rev Cancer*, 15(6), 321-33.

Linnerth-Petrik, N. M., Santry, L. A., Yu, D. L. & Wootton, S. K. (2012) Adeno-associated virus vector mediated expression of an oncogenic retroviral envelope protein induces lung adenocarcinomas in immunocompetent mice. *PLoS One*, 7(12), e51400.

Linnerth-Petrik, N. M., Walsh, S. R., Bogner, P. N., Morrison, C. & Wootton, S. K. (2014) Jaagsiekte sheep retrovirus detected in human lung cancer tissue arrays. *BMC research notes*, 7(1), 160.

Liu, J., Carmell, M. A., Rivas, F. V., Marsden, C. G., Thomson, J. M., Song, J. J., Hammond, S. M., Joshua-Tor, L. & Hannon, G. J. (2004) Argonaute2 is the catalytic engine of mammalian RNAi. *Science*, 305(5689), 1437-41.

Liu, S. L., Lerman, M. I. & Miller, A. D. (2003) Putative phosphatidylinositol 3-kinase (PI3K) binding motifs in ovine betaretrovirus Env proteins are not essential for rodent fibroblast transformation and PI3K/Akt activation. *J Virol*, 77(14), 7924-35.

Liu, S. L. & Miller, A. D. (2005) Transformation of madin-darby canine kidney epithelial cells by sheep retrovirus envelope proteins. *J Virol*, 79(2), 927-33.

Liu, S. L. & Miller, A. D. (2007) Oncogenic transformation by the jaagsiekte sheep retrovirus envelope protein. *Oncogene*, 26(6), 789-801.

Liu, X., Sempere, L. F., Ouyang, H., Memoli, V. A., Andrew, A. S., Luo, Y., Demidenko, E., Korc, M., Shi, W., Preis, M., Dragnev, K. H., Li, H., Direnzo, J., Bak, M., Freemantle, S. J., Kauppinen, S. & Dmitrovsky, E. (2010) MicroRNA-31 functions as an oncogenic microRNA

in mouse and human lung cancer cells by repressing specific tumor suppressors. *J Clin Invest*, 120(4), 1298-309.

Liu, Z., Chen, O., Wall, J. B. J., Zheng, M., Zhou, Y., Wang, L., Ruth Vaseghi, H., Qian, L. & Liu, J. (2017) Systematic comparison of 2A peptides for cloning multi-genes in a polycistronic vector. *Scientific Reports*, 7(1), 2193.

Livak, K. J. & Schmittgen, T. D. (2001) Analysis of relative gene expression data using real-time quantitative PCR and the 2(-Delta Delta C(T)) Method. *Methods*, 25(4), 402-8.

Llave, C., Kasschau, K. D., Rector, M. A. & Carrington, J. C. (2002) Endogenous and silencing-associated small RNAs in plants. *The Plant Cell*, 14(7), 1605-1619.

Lu, J., Getz, G., Miska, E. A., Alvarez-Saavedra, E., Lamb, J., Peck, D., Sweet-Cordero, A., Ebert, B. L., Mak, R. H., Ferrando, A. A., Downing, J. R., Jacks, T., Horvitz, H. R. & Golub, T. R. (2005) MicroRNA expression profiles classify human cancers. *Nature*, 435(7043), 834-8.

Lu, Y., Qin, Z., Wang, J., Zheng, X., Lu, J., Zhang, X., Wei, L., Peng, Q., Zheng, Y., Ou, C., Ye, Q., Xiong, W., Li, G., Fu, Y., Yan, Q. & Ma, J. (2017) Epstein-Barr Virus miR-BART6-3p Inhibits the RIG-I Pathway. *J Innate Immun*, 9(6), 574-586.

Ludwig, N., Leidinger, P., Becker, K., Backes, C., Fehlmann, T., Pallasch, C., Rheinheimer, S., Meder, B., Stähler, C., Meese, E. & Keller, A. (2016) Distribution of miRNA expression across human tissues. *Nucleic Acids Research*, 44(8), 3865-3877.

Lv, S., Xue, J., Wu, C., Wang, L., Wu, J., Xu, S., Liang, X. & Lou, J. (2017) Identification of a panel of serum microRNAs as biomarkers for early detection of lung adenocarcinoma. *Journal of Cancer*, 8(1), 48.

Ma, X., Kumar, M., Choudhury, S. N., Becker Buscaglia, L. E., Barker, J. R., Kanakamedala, K., Liu, M.-F. & Li, Y. (2011) Loss of the miR-21 allele elevates the expression of its target genes and reduces tumorigenesis. *Proceedings of the National Academy of Sciences*, 108(25), 10144-10149.

Ma, Y., Liang, A. J., Fan, Y.-P., Huang, Y.-R., Zhao, X.-M., Sun, Y. & Chen, X.-F. (2016) Dysregulation and functional roles of miR-183-96-182 cluster in cancer cell proliferation, invasion and metastasis. *Oncotarget*, 7(27), 42805-42825.

Maasho, K., Marusina, A., Reynolds, N. M., Coligan, J. E. & Borrego, F. (2004) Efficient gene transfer into the human natural killer cell line, NKL, using the Amaxa nucleofection system. *J Immunol Methods*, 284(1-2), 133-40.

Machado, M. T., Navega, S., Dias, F., de Sousa, M. J. C., Teixeira, A. L. & Medeiros, R. (2015) microRNAs for peripheral blood fraction identification: Origin, pathways and forensic relevance. *Life Sciences*, 143, 98-104.

Mackay, J. & Nisbet, D. (1966) Jaagsiekte--a hazard of intensified sheep husbandry. *Veterinary Record*, 78(1), 18-24.

Macrae, A. I., Dutia, B. M., Milligan, S., Brownstein, D. G., Allen, D. J., Mistrikova, J., Davison, A. J., Nash, A. A. & Stewart, J. P. (2001) Analysis of a Novel Strain of Murine Gammaherpesvirus Reveals a Genomic Locus Important for Acute Pathogenesis. *Journal of Virology*, 75(11), 5315-5327.

Maeda, N., Fu, W., Ortin, A., de las Heras, M. & Fan, H. (2005) Roles of the Ras-MEK-mitogen-activated protein kinase and phosphatidylinositol 3-kinase-Akt-mTOR pathways in

Jaagsiekte sheep retrovirus-induced transformation of rodent fibroblast and epithelial cell lines. *J Virol*, 79(7), 4440-50.

Maeda, N., Inoshima, Y., Fruman, D. A., Brachmann, S. M. & Fan, H. (2003) Transformation of mouse fibroblasts by Jaagsiekte sheep retrovirus envelope does not require phosphatidylinositol 3-kinase. *J Virol*, 77(18), 9951-9.

Maeda, N., Palmarini, M., Murgia, C. & Fan, H. (2001) Direct transformation of rodent fibroblasts by jaagsiekte sheep retrovirus DNA. *Proceedings of the National Academy of Sciences of the United States of America*, 98(8), 4449-4454.

Mager, D. L. & Stoye, J. P. (2015) Mammalian Endogenous Retroviruses. *Microbiol Spectr*, 3(1), MDNA3-0009-2014.

Malleter, M., Jacquot, C., Rousseau, B., Tomasoni, C., Juge, M., Pineau, A., Sakanian, V. & Roussakis, C. (2012) miRNAs, a potential target in the treatment of Non-Small-Cell Lung Carcinomas. *Gene*, 506(2), 355-9.

Manning, B. D. & Toker, A. (2017) AKT/PKB Signaling: Navigating the Network. *Cell*, 169(3), 381-405.

Maragkakis, M., Reczko, M., Simossis, V. A., Alexiou, P., Papadopoulos, G. L., Dalamagas, T., Giannopoulos, G., Goumas, G., Koukis, E., Kourtis, K., Vergoulis, T., Koziris, N., Sellis, T., Tsanakas, P. & Hatzigeorgiou, A. G. (2009) DIANA-microT web server: elucidating microRNA functions through target prediction. *Nucleic Acids Res*, 37(Web Server issue), W273-6.

Marín-Romero, A., Robles-Remacho, A., Tabraue-Chávez, M., López-Longarela, B., Sánchez-Martín, R. M., Guardia-Monteagudo, J. J., Fara, M. A., López-Delgado, F. J., Pernagallo, S. & Díaz-Mochón, J. J. (2018) A PCR-free technology to detect and quantify microRNAs directly from human plasma. *Analyst*, 143(23), 5676-5682.

Markou, A., Sourvinou, I., Vorkas, P. A., Yousef, G. M. & Lianidou, E. (2013) Clinical evaluation of microRNA expression profiling in non small cell lung cancer. *Lung Cancer*, 81(3), 388-396.

Markou, A., Tsaroucha, E. G., Kaklamanis, L., Fotinou, M., Georgoulias, V. & Lianidou, E. S. (2008) Prognostic value of mature microRNA-21 and microRNA-205 overexpression in non-small cell lung cancer by quantitative real-time RT-PCR. *Clin Chem*, 54(10), 1696-704.

Markson, L., Spence, J. & Dawson, M. (1983) Investigations of a flock heavily infected with maedi-visna virus. *The Veterinary record*, 112(12), 267-271.

Martin, W. B., Scott, F. M., Sharp, J. M., Angus, K. W. & NORVAL, M. (1976) Experimental production of sheep pulmonary adenomatosis (Jaagsiekte). *Nature*, 264(5582), 183.

Martineau, H. (2010) *Early events of Jaagsiekte sheep retrovirus infection in the ovine lung*. PhD University of Glasgow.

Martineau, H. M., Cousens, C., Imlach, S., Dagleish, M. P. & Griffiths, D. J. (2011) Jaagsiekte sheep retrovirus infects multiple cell types in the ovine lung. *J Virol*, 85(7), 3341-55.

Martinez, V. D., Vucic, E. A., Thu, K. L., Hubaux, R., Enfield, K. S., Pikor, L. A., Becker-Santos, D. D., Brown, C. J., Lam, S. & Lam, W. L. (2015) Unique somatic and malignant expression patterns implicate PIWI-interacting RNAs in cancer-type specific biology. *Scientific reports*, 5, 10423.

Mason, R. & Shannon, J. (1997) Alveolar type II cells. The Lung: Scientific Foundations. *Crystal RG, West JB, Weibel ER, Barnes PJ*.

Mattes, J., Collison, A., Plank, M., Phipps, S. & Foster, P. S. (2009) Antagonism of microRNA-126 suppresses the effector function of TH2 cells and the development of allergic airways disease. *Proceedings of the National Academy of Sciences*, pnas.0905063106.

Mayr, C. & Bartel, D. P. (2009) Widespread shortening of 3'UTRs by alternative cleavage and polyadenylation activates oncogenes in cancer cells. *Cell*, 138(4), 673-84.

McBride, D., Carre, W., Sontakke, S. D., Hogg, C. O., Law, A., Donadeu, F. X. & Clinton, M. (2012) Identification of miRNAs associated with the follicular-luteal transition in the ruminant ovary. *Reproduction*, 144(2), 221-33.

McDonald, J. S., Milosevic, D., Reddi, H. V., Grebe, S. K. & Algeciras-Schimnich, A. (2011a) Analysis of Circulating MicroRNA: Preanalytical and Analytical Challenges. *Clinical Chemistry*, 57(6), 833-840.

McDonald, J. S., Milosevic, D., Reddi, H. V., Grebe, S. K. & Algeciras-Schimnich, A. (2011b) Analysis of circulating microRNA: preanalytical and analytical challenges. *Clin Chem*, 57(6), 833-40.

McGee-Estrada, K. & Fan, H. (2007) Comparison of LTR enhancer elements in sheep beta retroviruses: insights into the basis for tissue-specific expression. *Virus Genes*, 35(2), 303-12.

McGee-Estrada, K., Palmarini, M. & Fan, H. (2002) HNF-3beta is a critical factor for the expression of the Jaagsiekte sheep retrovirus long terminal repeat in type II pneumocytes but not in Clara cells. *Virology*, 292(1), 87-97.

McLachlan, G., Davidson, H., Holder, E., Davies, L. A., Pringle, I. A., Sumner-Jones, S. G., Baker, A., Tennant, P., Gordon, C., Vrettou, C., Blundell, R., Hyndman, L., Stevenson, B., Wilson, A., Doherty, A., Shaw, D. J., Coles, R. L., Painter, H., Cheng, S. H., Scheule, R. K., Davies, J. C., Innes, J. A., Hyde, S. C., Griesenbach, U., Alton, E. W., Boyd, A. C., Porteous, D. J., Gill, D. R. & Collie, D. D. (2011) Pre-clinical evaluation of three non-viral gene transfer agents for cystic fibrosis after aerosol delivery to the ovine lung. *Gene Ther*, 18(10), 996-1005.

Meijer, H. A., Kong, Y. W., Lu, W. T., Wilczynska, A., Spriggs, R. V., Robinson, S. W., Godfrey, J. D., Willis, A. E. & Bushell, M. (2013) Translational repression and eIF4A2 activity are critical for microRNA-mediated gene regulation. *Science*, 340(6128), 82-5.

Melo, S. A., Moutinho, C., Ropero, S., Calin, G. A., Rossi, S., Spizzo, R., Fernandez, A. F., Davalos, V., Villanueva, A., Montoya, G., Yamamoto, H., Schwartz, S., Jr. & Esteller, M. (2010) A genetic defect in exportin-5 traps precursor microRNAs in the nucleus of cancer cells. *Cancer Cell*, 18(4), 303-15.

Melo, S. A., Sugimoto, H., O'Connell, J. T., Kato, N., Villanueva, A., Vidal, A., Qiu, L., Vitkin, E., Perelman, L. T., Melo, C. A., Lucci, A., Ivan, C., Calin, G. A. & Kalluri, R. (2014) Cancer exosomes perform cell-independent microRNA biogenesis and promote tumorigenesis. *Cancer Cell*, 26(5), 707-21.

Meng, W., Ye, Z., Cui, R., Perry, J., Dedousi-Huebner, V., Huebner, A., Wang, Y., Li, B., Volinia, S., Nakanishi, H., Kim, T., Suh, S. S., Ayers, L. W., Ross, P., Croce, C. M., Chakravarti, A., Jin, V. X. & Lautenschlaeger, T. (2013) MicroRNA-31 predicts the presence of lymph node metastases and survival in patients with lung adenocarcinoma. *Clin Cancer Res*, 19(19), 5423-33.

Mestdagh, P., Hartmann, N., Baeriswyl, L., Andreasen, D., Bernard, N., Chen, C., Cheo, D., D'Andrade, P., DeMayo, M., Dennis, L., Derveaux, S., Feng, Y., Fulmer-Smentek, S., Gerstmayer, B., Gouffon, J., Grimley, C., Lader, E., Lee, K. Y., Luo, S., Mouritzen, P., Narayanan, A., Patel, S., Peiffer, S., Ruberg, S., Schroth, G., Schuster, D., Shaffer, J. M., Shelton, E. J., Silveria, S., Ulmanella, U., Veeramachaneni, V., Staedtler, F., Peters, T., Guettouche, T., Wong, L. & Vandesompele, J. (2014) Evaluation of quantitative miRNA expression platforms in the microRNA quality control (miRQC) study. *Nat Methods*, 11(8), 809-15.

Miller, A. D. (2008) Hyaluronidase 2 and its intriguing role as a cell-entry receptor for oncogenic sheep retroviruses. *Semin Cancer Biol*, 18(4), 296-301.

Miller, A. D., De Las Heras, M., Yu, J., Zhang, F., Liu, S. L., Vaughan, A. E., Vaughan, T. L., Rosadio, R., Rocca, S., Palmieri, G., Goedert, J. J., Fujimoto, J. & Wistuba, II (2017) Evidence against a role for jaagsiekte sheep retrovirus in human lung cancer. *Retrovirology*, 14(1), 3.

Minguijón, E., Reina, R., Pérez, M., Polledo, L., Villoria, M., Ramírez, H., Leginagoikoa, I., Badiola, J. J., García-Marín, J. F., de Andrés, D., Luján, L., Amorena, B. & Juste, R. A. (2015) Small ruminant lentivirus infections and diseases. *Veterinary Microbiology*, 181(1), 75-89.

Mitchell, P. S., Parkin, R. K., Kroh, E. M., Fritz, B. R., Wyman, S. K., Pogosova-Agadjanyan, E. L., Peterson, A., Noteboom, J., O'Briant, K. C. & Allen, A. (2008) Circulating microRNAs as stable blood-based markers for cancer detection. *Proceedings of the National Academy of Sciences*, 105(30), 10513-10518.

Mitra, R., Edmonds, M. D., Sun, J., Zhao, M., Yu, H., Eischen, C. M. & Zhao, Z. (2014) Reproducible combinatorial regulatory networks elucidate novel oncogenic microRNAs in non-small cell lung cancer. *RNA*, 20(9), 1356-68.

Miyoshi, H., Blomer, U., Takahashi, M., Gage, F. H. & Verma, I. M. (1998) Development of a self-inactivating lentivirus vector. *J Virol*, 72(10), 8150-7.

Moghoofei, M., Bokharaei-Salim, F., Esghaei, M., Keyvani, H., Honardoost, M., Mostafaei, S., Ghasemi, A., Tavakoli, A., Javanmard, D., Babaei, F., Garshasbi, S. & Monavari, S. H. (2018) MicroRNAs 29, 150, 155, 223 level and their relation to viral and immunological markers in HIV-1 infected naive patients. *Future Virology*, 13(9), 637-645.

Mogilyansky, E. & Rigoutsos, I. (2013) The miR-17/92 cluster: a comprehensive update on its genomics, genetics, functions and increasingly important and numerous roles in health and disease. *Cell Death Differ*, 20(12), 1603-14.

Moldovan, L., Batte, K. E., Trgovcich, J., Wisler, J., Marsh, C. B. & Piper, M. (2014) Methodological challenges in utilizing miRNAs as circulating biomarkers. *Journal of Cellular and Molecular Medicine*, 18(3), 371-390.

Molnár, A., Schwach, F., Studholme, D. J., Thuenemann, E. C. & Baulcombe, D. C. (2007) miRNAs control gene expression in the single-cell alga Chlamydomonas reinhardtii. *Nature*, 447(7148), 1126.

Monot, M., Erny, A., Gineys, B., Desloire, S., Dolmazon, C., Aublin-Gex, A., Lotteau, V., Archer, F. & Leroux, C. (2015) Early Steps of Jaagsiekte Sheep Retrovirus-Mediated Cell Transformation Involve the Interaction between Env and the RALBP1 Cellular Protein. *J Virol*, 89(16), 8462-73.

Moretti, F., D'Antona, P., Finardi, E., Barbetta, M., Dominioni, L., Poli, A., Gini, E., Noonan, D. M., Imperatori, A. & Rotolo, N. (2017) Systematic review and critique of circulating miRNAs as biomarkers of stage I-II non-small cell lung cancer. *Oncotarget*, 8(55), 94980.

Mori, M., Triboulet, R., Mohseni, M., Schlegelmilch, K., Shrestha, K., Camargo, F. D. & Gregory, R. I. (2014) Hippo signaling regulates microprocessor and links cell-density-dependent miRNA biogenesis to cancer. *Cell*, 156(5), 893-906.

Morlando, M., Ballarino, M., Gromak, N., Pagano, F., Bozzoni, I. & Proudfoot, N. J. (2008) Primary microRNA transcripts are processed co-transcriptionally. *Nat Struct Mol Biol*, 15(9), 902-9.

Mornex, J. F., Thivolet, F., De las Heras, M. & Leroux, C. (2003) Pathology of Human Bronchioloalveolar Carcinoma and its Relationship to the Ovine Disease, in Fan, H. (ed), *Jaagsiekte Sheep Retrovirus and Lung Cancer*Springer-Verlag, 226-248.

Motameny, S., Wolters, S., Nürnberg, P. & Schumacher, B. (2010) Next generation sequencing of miRNAs–strategies, resources and methods. *Genes*, 1(1), 70-84.

Munshi, S. U., Panda, H., Holla, P., Rewari, B. B. & Jameel, S. (2014) MicroRNA-150 is a potential biomarker of HIV/AIDS disease progression and therapy. *PLoS One*, 9(5), e95920.

Mura, M., Murcia, P., Caporale, M., Spencer, T. E., Nagashima, K., Rein, A. & Palmarini, M. (2004) Late viral interference induced by transdominant Gag of an endogenous retrovirus. *Proceedings of the National Academy of Sciences of the United States of America*, 101(30), 11117.

Muralidhar, B., Winder, D., Murray, M., Palmer, R., Barbosa-Morais, N., Saini, H., Roberts, I., Pett, M. & Coleman, N. (2011) Functional evidence that Drosha overexpression in cervical squamous cell carcinoma affects cell phenotype and microRNA profiles. *The Journal of Pathology*, 224(4), 496-507.

Murcia, P. R., Arnaud, F. & Palmarini, M. (2007) The transdominant endogenous retrovirus enJS56A1 associates with and blocks intracellular trafficking of Jaagsiekte sheep retrovirus Gag. *J Virol*, 81(4), 1762-72.

Murgia, C., Caporale, M., Ceesay, O., Di Francesco, G., Ferri, N., Varasano, V., de las Heras, M. & Palmarini, M. (2011) Lung adenocarcinoma originates from retrovirus infection of proliferating type 2 pneumocytes during pulmonary post-natal development or tissue repair. *PLoS Pathog*, 7(3), e1002014.

Nadal, E., Truini, A., Nakata, A., Lin, J., Reddy, R. M., Chang, A. C., Ramnath, N., Gotoh, N., Beer, D. G. & Chen, G. (2015) A Novel Serum 4-microRNA Signature for Lung Cancer Detection. *Sci Rep*, 5, 12464.

Nair, V. & Zavolan, M. (2006) Virus-encoded microRNAs: novel regulators of gene expression. *Trends in Microbiology*, 14(4), 169-175.

Nandkumar, M. A., Ashna, U., Thomas, L. V. & Nair, P. D. (2015) Pulmonary surfactant expression analysis--role of cell-cell interactions and 3-D tissue-like architecture. *Cell Biol Int*, 39(3), 272-82.

Neilsen, C. T., Goodall, G. J. & Bracken, C. P. (2012) IsomiRs--the overlooked repertoire in the dynamic microRNAome. *Trends Genet*, 28(11), 544-9.

Nicolas, F. J., Lehmann, K., Warne, P. H., Hill, C. S. & Downward, J. (2003) Epithelial to mesenchymal transition in Madin-Darby canine kidney cells is accompanied by down-regulation of Smad3 expression, leading to resistance to transforming growth factor-beta-induced growth arrest. *J Biol Chem*, 278(5), 3251-6.

Nielsen, K. O., Jacobsen, K. S., Mirza, A. H., Winther, T. N., Størling, J., Glebe, D., Pociot, F. & Hogh, B. (2018) Hepatitis B virus upregulates host microRNAs that target apoptosis-regulatory genes in an in vitro cell model. *Experimental Cell Research*, 371(1), 92-103.

Nitta, T., Hofacre, A., Hull, S. & Fan, H. (2009) Identification and mutational analysis of a Rej response element in Jaagsiekte sheep retrovirus RNA. *J Virol*, 83(23), 12499-511.

Nobel, T., Neumann, F. & Klopfer, U. (1969) Histological patterns of the metastases in pulmonary adenomatosis of sheep (jaagsiekte). *Journal of comparative pathology*, 79(4), 537-IN20.

O'Brien, K., Rani, S., Corcoran, C., Wallace, R., Hughes, L., Friel, A. M., McDonnell, S., Crown, J., Radomski, M. W. & O'Driscoll, L. (2013) Exosomes from triple-negative breast cancer cells can transfer phenotypic traits representing their cells of origin to secondary cells. *European Journal of Cancer*, 49(8), 1845-1859.

O'Donnell, K. A., Wentzel, E. A., Zeller, K. I., Dang, C. V. & Mendell, J. T. (2005) c-Myc-regulated microRNAs modulate E2F1 expression. *Nature*, 435(7043), 839-43.

Okada, N., Lin, C. P., Ribeiro, M. C., Biton, A., Lai, G., He, X., Bu, P., Vogel, H., Jablons, D. M., Keller, A. C., Wilkinson, J. E., He, B., Speed, T. P. & He, L. (2014) A positive feedback between p53 and miR-34 miRNAs mediates tumor suppression. *Genes Dev*, 28(5), 438-50.

Okamura, K., Hagen, J. W., Duan, H., Tyler, D. M. & Lai, E. C. (2007) The Mirtron Pathway Generates microRNA-Class Regulatory RNAs in Drosophila. *Cell*, 130(1), 89-100.

Omoto, S. & Fujii, Y. R. (2005) Regulation of human immunodeficiency virus 1 transcription by nef microRNA. *J Gen Virol*, 86(Pt 3), 751-5.

Omoto, S., Ito, M., Tsutsumi, Y., Ichikawa, Y., Okuyama, H., Brisibe, E. A., Saksena, N. K. & Fujii, Y. R. (2004) HIV-1 nef suppression by virally encoded microRNA. *Retrovirology*, 1, 44-44.

Ortin, A., Minguijon, E., Dewar, P., Garcia, M., Ferrer, L. M., Palmarini, M., Gonzalez, L., Sharp, J. M. & De las Heras, M. (1998) Lack of a specific immune response against a recombinant capsid protein of Jaagsiekte sheep retrovirus in sheep and goats naturally affected by enzootic nasal tumour or sheep pulmonary adenomatosis. *Vet Immunol Immunopathol*, 61(2-4), 229-37.

Osada, H. & Takahashi, T. (2011) let-7 and miR-17-92: small-sized major players in lung cancer development. *Cancer Sci*, 102(1), 9-17.

Ouellet, D. L., Plante, I., Landry, P., Barat, C., Janelle, M. E., Flamand, L., Tremblay, M. J. & Provost, P. (2008) Identification of functional microRNAs released through asymmetrical processing of HIV-1 TAR element. *Nucleic Acids Res*, 36(7), 2353-65.

Ouellet, D. L., Vigneault-Edwards, J., Létourneau, K., Gobeil, L.-A., Plante, I., Burnett, J. C., Rossi, J. J. & Provost, P. (2013) Regulation of host gene expression by HIV-1 TAR microRNAs. *Retrovirology*, 10, 86-86.

Overbaugh, J. & Bangham, C. R. (2001) Selection forces and constraints on retroviral sequence variation. *Science*, 292(5519), 1106-1109.

Pacurari, M., Addison, J. B., Bondalapati, N., Wan, Y. W., Luo, D., Qian, Y., Castranova, V., Ivanov, A. V. & Guo, N. L. (2013) The microRNA-200 family targets multiple non-small cell lung cancer prognostic markers in H1299 cells and BEAS-2B cells. *Int J Oncol*, 43(2), 548-60.

Palmarini, M., Cousens, C., Dalziel, R. G., Bai, J., Stedman, K., DeMartini, J. C. & Sharp, J. M. (1996a) The exogenous form of jaagsiekte retrovirus is specifically associated with a contagious lung cancer of sheep. *Journal of Virology*, 70(3), 1618-1623.

Palmarini, M., Datta, S., Omid, R., Murgia, C. & Fan, H. (2000a) The long terminal repeat of Jaagsiekte sheep retrovirus is preferentially active in differentiated epithelial cells of the lungs. *Journal of virology*, 74(13), 5776-5787.

Palmarini, M. & Fan, H. (2001) Retrovirus-induced ovine pulmonary adenocarcinoma, an animal model for lung cancer. *Journal of the National Cancer Institute*, 93(21), 1603-1614.

Palmarini, M. & Fan, H. (2003) Molecular Biology of Jaagsiekte Sheep Retrovirus, in Fan, H. (ed), *Jaagsiekte Sheep Retrovirus and Lung Cancer*Springer-Verlag, 82-115.

Palmarini, M., Hallwirth, C., York, D., Murgia, C., De Oliveira, T., Spencer, T. & Fan, H. (2000b) Molecular cloning and functional analysis of three type D endogenous retroviruses of sheep reveal a different cell tropism from that of the highly related exogenous jaagsiekte sheep retrovirus. *Journal of virology*, 74(17), 8065-8076.

Palmarini, M., Holland, M. J., Cousens, C., Dalziel, R. G. & Sharp, J. M. (1996b) Jaagsiekte retrovirus establishes a disseminated infection of the lymphoid tissues of sheep affected by pulmonary adenomatosis. *Journal of General Virology*, 77(12), 2991-2998.

Palmarini, M., Maeda, N., Murgia, C., De-Fraja, C., Hofacre, A. & Fan, H. (2001) A phosphatidylinositol 3-kinase docking site in the cytoplasmic tail of the Jaagsiekte sheep retrovirus transmembrane protein is essential for envelope-induced transformation of NIH 3T3 cells. *J Virol*, 75(22), 11002-9.

Palmarini, M., Mura, M. & Spencer, T. E. (2004) Endogenous betaretroviruses of sheep: teaching new lessons in retroviral interference and adaptation. *J Gen Virol*, 85(Pt 1), 1-13.

Palmarini, M., Murgia, C. & Fan, H. (2002) Spliced and prematurely polyadenylated Jaagsiekte sheep retrovirus-specific RNAs from infected or transfected cells. *Virology*, 294(1), 180-8.

Palmarini, M., Sharp, J. M., Lee, C. & Fan, H. (1999a) In vitro infection of ovine cell lines by jaagsiekte sheep retrovirus. *Journal of Virology*, 73(12), 10070-10078.

Palmarini, M., Sharp, M., De Las Heras, M. & Fan, H. (1999b) Jaagsiekte sheep retrovirus is necessary and sufficient to induce a contagious lung cancer in sheep. *Journal of Virology*, 73(8), 6964-6972.

Pálsson, P. (1985) Maedi/visna of sheep in Iceland. Introduction of the disease to Iceland, clinical features, control measures and eradication, *Slow viruses in sheep, goats and cattle: in particular maedi visna, jaagsiekte, and in caprines, arthritis, encephalitis and pneumonitis: proceedings of two workshops/edited by JM Sharp and R. Hoff-Jorgensen*. Luxembourg: Commission of the European Communities, 1985.

Pan, D. (2010) The hippo signaling pathway in development and cancer. *Dev Cell*, 19(4), 491-505.

Pan, X., Wang, R. & Wang, Z. X. (2013) The potential role of miR-451 in cancer diagnosis, prognosis, and therapy. *Molecular Cancer Therapeutics*, 12(7), 1153-1162.

Pandey, A., Sahu, A. R., Wani, S. A., Saxena, S., Kanchan, S., Sah, V., Rajak, K. K., Khanduri, A., Sahoo, A. P., Tiwari, A. K., Mishra, B., Muthuchelvan, D., Mishra, B. P., Singh, R. K. & Gandham, R. K. (2017) Modulation of Host miRNAs Transcriptome in Lung and Spleen of Peste des Petits Ruminants Virus Infected Sheep and Goats. *Front Microbiol*, 8, 1146.

Panuska, C. (2006) Lungworms of ruminants. *Veterinary Clinics: Food Animal Practice*, 22(3), 583-593.

Parker, B. N., Wrathall, A. E., Saunders, R. W., Dawson, M., Done, S. H., Francis, P. G., Dexter, I. & Bradley, R. (1998) Prevention of transmission of sheep pulmonary adenomatosis by embryo transfer. *Vet Rec*, 142(25), 687-9.

Parsons, W. J., Ramkumar, V. & Stiles, G. L. (1988) Isobutylmethylxanthine stimulates adenylate cyclase by blocking the inhibitory regulatory protein, Gi. *Molecular pharmacology*, 34(1), 37-41.

Pasquinelli, A. E., Reinhart, B. J., Slack, F., Martindale, M. Q., Kuroda, M. I., Maller, B., Hayward, D. C., Ball, E. E., Degnan, B. & Müller, P. (2000) Conservation of the sequence and temporal expression of let-7 heterochronic regulatory RNA. *Nature*, 408(6808), 86.

Patnaik, S. K., Dahlgaard, J., Mazin, W., Kannisto, E., Jensen, T., Knudsen, S. & Yendamuri, S. (2012) Expression of microRNAs in the NCI-60 cancer cell-lines. *PLoS One*, 7(11), e49918.

Patnaik, S. K., Kannisto, E., Mallick, R. & Yendamuri, S. (2011) Overexpression of the lung cancer-prognostic miR-146b microRNAs has a minimal and negative effect on the malignant phenotype of A549 lung cancer cells. *PLoS One*, 6(7), e22379.

Payne, G. S., Bishop, J. M. & Varmus, H. E. (1982) Multiple arrangements of viral DNA and an activated host oncogene in bursal lymphomas. *Nature*, 295(5846), 209.

Pecot, C. V., Rupaimoole, R., Yang, D., Akbani, R., Ivan, C., Lu, C., Wu, S., Han, H.-D., Shah, M. Y. & Rodriguez-Aguayo, C. (2013) Tumour angiogenesis regulation by the miR-200 family. *Nature communications*, 4, 2427.

Peng, X., Gralinski, L., Ferris, M. T., Frieman, M. B., Thomas, M. J., Proll, S., Korth, M. J., Tisoncik, J. R., Heise, M. & Luo, S. (2011) Integrative deep sequencing of the mouse lung transcriptome reveals differential expression of diverse classes of small RNAs in response to respiratory virus infection. *MBio*, 2(6), e00198-11.

Perk, K. & Hod, I. (1982) Sheep lung carcinoma: an endemic analogue of a sporadic human neoplasm. Oxford University Press.

Perk, K., Michalides, R., Spiegelman, S. & Schlom, J. (1974) Biochemical and morphologic evidence for the presence of an RNA tumor virus in pulmonary carcinoma of sheep (Jaagsiekte). *Journal of the National Cancer Institute*, 53(1), 131-135.

Petriella, D., De Summa, S., Lacalamita, R., Galetta, D., Catino, A., Logroscino, A. F., Palumbo, O., Carella, M., Zito, F. A., Simone, G. & Tommasi, S. (2016) miRNA profiling in serum and tissue samples to assess noninvasive biomarkers for NSCLC clinical outcome. *Tumor Biology*, 37(4), 5503-5513.

Pfeffer, S., Sewer, A., Lagos-Quintana, M., Sheridan, R., Sander, C., Grasser, F. A., van Dyk, L. F., Ho, C. K., Shuman, S., Chien, M., Russo, J. J., Ju, J., Randall, G., Lindenbach, B.

D., Rice, C. M., Simon, V., Ho, D. D., Zavolan, M. & Tuschl, T. (2005) Identification of microRNAs of the herpesvirus family. *Nat Methods*, 2(4), 269-76.

Pfeffer, S., Zavolan, M., Grässer, F. A., Chien, M., Russo, J. J., Ju, J., John, B., Enright, A. J., Marks, D. & Sander, C. (2004) Identification of virus-encoded microRNAs. *Science*, 304(5671), 734-736.

Pinzón, N., Li, B., Martinez, L., Sergeeva, A., Presumey, J., Apparailly, F. & Seitz, H. (2016) The number of biologically relevant microRNA targets has been largely overestimated. *Genome Research*.

Place, R. F., Li, L.-C., Pookot, D., Noonan, E. J. & Dahiya, R. (2008) MicroRNA-373 induces expression of genes with complementary promoter sequences. *Proceedings of the National Academy of Sciences*, 105(5), 1608-1613.

Poirier, Y., Kozak, C. & Jolicoeur, P. (1988) Identification of a common helper provirus integration site in Abelson murine leukemia virus-induced lymphoma DNA. *Journal of virology*, 62(11), 3985-3992.

Poliseno, L., Salmena, L., Zhang, J., Carver, B., Haveman, W. J. & Pandolfi, P. P. (2010) A coding-independent function of gene and pseudogene mRNAs regulates tumour biology. *Nature*, 465(7301), 1033-1038.

Powers, J. T., Tsanov, K. M., Pearson, D. S., Roels, F., Spina, C. S., Ebright, R., Seligson, M., de Soysa, Y., Cahan, P., Theißen, J., Tu, H.-C., Han, A., Kurek, K. C., LaPier, G. S., Osborne, J. K., Ross, S. J., Cesana, M., Collins, J. J., Berthold, F. & Daley, G. Q. (2016) Multiple mechanisms disrupt the let-7 microRNA family in neuroblastoma. *Nature*, 535(7611), 246-251.

Pritchard, C. C., Kroh, E., Wood, B., Arroyo, J. D., Dougherty, K. J., Miyaji, M. M., Tait, J. F. & Tewari, M. (2012) Blood cell origin of circulating microRNAs: a cautionary note for cancer biomarker studies. *Cancer Prev Res (Phila)*, 5(3), 492-497.

Qin, A. Y., Zhang, X. W., Liu, L., Yu, J. P., Li, H., Wang, S. Z., Ren, X. B. & Cao, S. (2013) MiR-205 in cancer: an angel or a devil? *Eur J Cell Biol*, 92(2), 54-60.

Qu, L., Li, L., Zheng, X., Fu, H., Tang, C., Qin, H., Li, X., Wang, H., Li, J. & Wang, W. (2017) Circulating plasma microRNAs as potential markers to identify EGFR mutation status and to monitor epidermal growth factor receptor-tyrosine kinase inhibitor treatment in patients with advanced non-small cell lung cancer. *Oncotarget*, 8(28), 45807.

Rai, S. K., Duh, F.-M., Vigdorovich, V., Danilkovitch-Miagkova, A., Lerman, M. I. & Miller, A. D. (2001) Candidate tumor suppressor HYAL2 is a glycosylphosphatidylinositol (GPI)-anchored cell-surface receptor for jaagsiekte sheep retrovirus, the envelope protein of which mediates oncogenic transformation. *Proceedings of the National Academy of Sciences*, 98(8), 4443-4448.

Rajya, B. & Singh, C. (1964) The pathology of pneumonia and associated respiratory disease of sheep and goats. I. Occurrence of jagziekte and maedi in sheep and goats in India. *American journal of veterinary research*, 25, 61-67.

Rani, S., Gately, K., Crown, J., O'Byrne, K. & O'Driscoll, L. (2013) Global analysis of serum microRNAs as potential biomarkers for lung adenocarcinoma. *Cancer Biol Ther*, 14(12), 1104-12.

Raponi, M., Dossey, L., Jatkoe, T., Wu, X., Chen, G., Fan, H. & Beer, D. G. (2009) MicroRNA classifiers for predicting prognosis of squamous cell lung cancer. *Cancer Res*, 69(14), 5776-83.

Reinhart, B. J., Slack, F. J., Basson, M., Pasquinelli, A. E., Bettinger, J. C., Rougvie, A. E., Horvitz, H. R. & Ruvkun, G. (2000) The 21-nucleotide let-7 RNA regulates developmental timing in Caenorhabditis elegans. *nature*, 403(6772), 901.

Ren, Z. P., Hou, X. B., Tian, X. D., Guo, J. T., Zhang, L. B., Xue, Z. Q., Deng, J. Q., Zhang, S. W., Pan, J. Y. & Chu, X. Y. (2019) Identification of nine microRNAs as potential biomarkers for lung adenocarcinoma. *FEBS Open Bio*, 9(2), 315-327.

Rissin, D. M., López-Longarela, B., Pernagallo, S., Ilyine, H., Vliegenthart, A. B., Dear, J. W., Díaz-Mochón, J. J. & Duffy, D. C. (2017) Polymerase-free measurement of microRNA-122 with single base specificity using single molecule arrays: Detection of drug-induced liver injury. *PloS one*, 12(7), e0179669.

Rosadio, R. & Sharp, J. (1992) Leukocyte frequency alterations in sheep with naturally and experimentally induced lung cancer. *Veterinary Medicine*, 49-51.

Rosadio, R. H., Lairmore, M. D., Russell, H. I. & DeMartini, J. C. (1988) Retrovirus-associated ovine pulmonary carcinoma (sheep pulmonary adenomatosis) and lymphoid interstitial pneumonia. I. Lesion development and age susceptibility. *Vet Pathol*, 25(6), 475-83.

Rosales Gerpe, M. C., van Vloten, J. P., Santry, L. A., de Jong, J., Mould, R. C., Pelin, A., Bell, J. C., Bridle, B. W. & Wootton, S. K. (2018) Use of Precision-Cut Lung Slices as an Ex Vivo Tool for Evaluating Viruses and Viral Vectors for Gene and Oncolytic Therapy. *Mol Ther Methods Clin Dev*, 10, 245-256.

Rosenberg, N. & Jolicoeur, P. (1997) Retroviral Pathogenesis, in Coffin, J. M., Hughes, S. H. & Varmus, H. E. (eds), *Retroviruses*Cold Spring Harbor Laboratory Press.

Rosewick, N., Momont, M., Durkin, K., Takeda, H., Caiment, F., Cleuter, Y., Vernin, C., Mortreux, F., Wattel, E., Burny, A., Georges, M. & Van den Broeke, A. (2013) Deep sequencing reveals abundant noncanonical retroviral microRNAs in B-cell leukemia/lymphoma. *Proceedings of the National Academy of Sciences*, 110(6), 2306-2311.

Ross, S. R., Dzuris, J. L., Golovkina, T. V., Clemmons, W. C. & van den Hoogen, B. (1997) Mouse mammary tumor virus (MMTV), a retrovirus that exploits the immune system. *Medicina (Buenos Aires)*, 57, 34-42.

Rubin, J. S., Osada, H., Finch, P. W., Taylor, W. G., Rudikoff, S. & Aaronson, S. A. (1989) Purification and characterization of a newly identified growth factor specific for epithelial cells. *Proceedings of the National Academy of Sciences*, 86(3), 802-806.

Ruby, J. G., Jan, C. H. & Bartel, D. P. (2007) Intronic microRNA precursors that bypass Drosha processing. *Nature*, 448(7149), 83-86.

Rupaimoole, R. & Slack, F. (2017) Identification of miR-34 Synergistic Small Molecule Inhibitor for Therapy Against NSCLC. *Journal of Thoracic Oncology*, 12(8, Supplement), S1542.

Saetrom, P., Heale, B. S., Snove, O., Jr., Aagaard, L., Alluin, J. & Rossi, J. J. (2007) Distance constraints between microRNA target sites dictate efficacy and cooperativity. *Nucleic Acids Res*, 35(7), 2333-42.

Sakuma, T., Barry, M. A. & Ikeda, Y. (2012) Lentiviral vectors: basic to translational. *Biochem J*, 443(3), 603-18.

Salmena, L., Poliseno, L., Tay, Y., Kats, L. & Pandolfi, Pier P. (2011) A ceRNA Hypothesis: The Rosetta Stone of a Hidden RNA Language? *Cell*, 146(3), 353-358.

Salvatori, D., Gonzalez, L., Dewar, P., Cousens, C., de las Heras, M., Dalziel, R. G. & Sharp, J. M. (2004) Successful induction of ovine pulmonary adenocarcinoma in lambs of different ages and detection of viraemia during the preclinical period. *J Gen Virol*, 85(Pt 11), 3319-24.

Sanfiorenzo, C., Ilie, M. I., Belaid, A., Barlesi, F., Mouroux, J., Marquette, C. H., Brest, P. & Hofman, P. (2013) Two panels of plasma microRNAs as non-invasive biomarkers for prediction of recurrence in resectable NSCLC. *PLoS One*, 8(1), e54596.

Sanna, M. P., Sanna, E., De Las Heras, M., Leoni, A., Nieddu, A. M., Pirino, S., Sharp, J. M. & Palmarini, M. (2001) Association of jaagsiekte sheep retrovirus with pulmonary carcinoma in Sardinian moufflon (Ovis musimon). *J Comp Pathol*, 125(2-3), 145-52.

Sanz Rubio, D., Lopez-Perez, O., de Andres Pablo, A., Bolea, R., Osta, R., Badiola, J. J., Zaragoza, P., Martin-Burriel, I. & Toivonen, J. M. (2017) Increased circulating microRNAs miR-342-3p and miR-21-5p in natural sheep prion disease. *J Gen Virol*, 98(2), 305-310.

Schirle, N. T., Sheu-Gruttadauria, J., Chandradoss, S. D., Joo, C. & MacRae, I. J. (2015) Water-mediated recognition of t1-adenosine anchors Argonaute2 to microRNA targets. *Elife*, 4.

Schirle, N. T., Sheu-Gruttadauria, J. & MacRae, I. J. (2014) Structural basis for microRNA targeting. *Science*, 346(6209), 608-13.

Schwarzenbach, H., Hoon, D. S. B. & Pantel, K. (2011) Cell-free nucleic acids as biomarkers in cancer patients. *Nature Reviews Cancer*, 11(6), 426-437.

Schwarzenbach, H., Nishida, N., Calin, G. A. & Pantel, K. (2014) Clinical relevance of circulating cell-free microRNAs in cancer. *Nat Rev Clin Oncol*, 11(3), 145-56.

Scott, P. R., Dagleish, M. P. & Cousens, C. (2018) Development of superficial lung lesions monitored on farm by serial ultrasonographic examination in sheep with lesions confirmed as ovine pulmonary adenocarcinoma at necropsy. *Ir Vet J*, 71, 23.

Seike, M., Goto, A., Okano, T., Bowman, E. D., Schetter, A. J., Horikawa, I., Mathe, E. A., Jen, J., Yang, P. & Sugimura, H. (2009) MiR-21 is an EGFR-regulated anti-apoptotic factor in lung cancer in never-smokers. *Proceedings of the National Academy of Sciences*, 106(29), 12085-12090.

Seitz, B., Baktanian, E., Gordon, E. M., Anderson, W. F., LaBree, L. & McDonnell, P. J. (1998) Retroviral vector-mediated gene transfer into keratocytes: in vitro effects of polybrene and protamine sulfate. *Graefes Arch Clin Exp Ophthalmol*, 236(8), 602-12.

Selbach, M., Schwanhäusser, B., Thierfelder, N., Fang, Z., Khanin, R. & Rajewsky, N. (2008) Widespread changes in protein synthesis induced by microRNAs. *Nature*, 455(7209), 58-63.

Seo, G. J., Fink, L. H. L., O'Hara, B., Atwood, W. J. & Sullivan, C. S. (2008) Evolutionarily conserved function of a viral microRNA. *Journal of Virology*, 82(20), 9823-9828.

Shan, N., Shen, L., Wang, J., He, D. & Duan, C. (2015) MiR-153 inhibits migration and invasion of human non-small-cell lung cancer by targeting ADAM19. *Biochem Biophys Res Commun*, 456(1), 385-91.

Sharp, J. & Angus, K. (1990) Sheep pulmonary adenomatosis: clinical, pathological and epidemiological aspects, *Maedi-Visna and related diseases*Springer, 157-175.

Sharp, J., Angus, K., Gray, E. & Scott, F. (1983) Rapid transmission of sheep pulmonary adenomatosis (jaagsiekte) in young lambs. *Archives of virology*, 78(1-2), 89-95.

Sharp, J., Angus, K., Jassim, F. & Scott, F. (1986) Experimental transmission of sheep pulmonary adenomatosis to a goat. *Veterinary Record*, 119(10), 245-245.

Sharp, J. M. & DeMartini, J. (2003) Natural History of JSRV in Sheep, in Fan, H. (ed), *Jaagsiekte Sheep Retrovirus and Lung Cancer*Springer-Verlag, 55-80.

Shaughnessy, R. G., Farrell, D., Riepema, K., Bakker, D. & Gordon, S. V. (2015) Analysis of biobanked serum from a Mycobacterium avium subsp paratuberculosis bovine infection model confirms the remarkable stability of circulating miRNA profiles and defines a bovine serum miRNA repertoire. *PLoS One*, 10(12), e0145089.

Sheedy, F. J. (2015) Turning 21: Induction of miR-21 as a Key Switch in the Inflammatory Response. *Front Immunol*, 6, 19.

Shen, J., Xia, W., Khotskaya, Y. B., Huo, L., Nakanishi, K., Lim, S. O., Du, Y., Wang, Y., Chang, W. C., Chen, C. H., Hsu, J. L., Wu, Y., Lam, Y. C., James, B. P., Liu, X., Liu, C. G., Patel, D. J. & Hung, M. C. (2013) EGFR modulates microRNA maturation in response to hypoxia through phosphorylation of AGO2. *Nature*, 497(7449), 383-7.

Shi, H., Ji, Y., Zhang, D., Liu, Y. & Fang, P. (2015) MiR-135a inhibits migration and invasion and regulates EMT-related marker genes by targeting KLF8 in lung cancer cells. *Biochem Biophys Res Commun*, 465(1), 125-30.

Shirlaw, J. (1959) Studies on jaagsiekte in Kenya. *Bull Epizoot Dis Afr*, 7, 287-302.

Shu, J., Xia, Z., Li, L., Liang, E. T., Slipek, N., Shen, D., Foo, J., Subramanian, S. & Steer, C. J. (2012) Dose-dependent differential mRNA target selection and regulation by let-7a-7f and miR-17-92 cluster microRNAs. *RNA Biol*, 9(10), 1275-87.

Song, J. J., Smith, S. K., Hannon, G. J. & Joshua-Tor, L. (2004) Crystal structure of Argonaute and its implications for RISC slicer activity. *Science*, 305(5689), 1434-7.

Spencer, T. E., Mura, M., Gray, C. A., Griebel, P. J. & Palmarini, M. (2003) Receptor usage and fetal expression of ovine endogenous betaretroviruses: implications for coevolution of endogenous and exogenous retroviruses. *J Virol*, 77(1), 749-53.

Spornraft, M., Kirchner, B., Haase, B., Benes, V., Pfaffl, M. W. & Riedmaier, I. (2014) Optimization of extraction of circulating RNAs from plasma–enabling small RNA sequencing. *PLoS One*, 9(9), e107259.

Stenvold, H., Donnem, T., Andersen, S., Al-Saad, S., Busund, L.-T. & Bremnes, R. M. (2014) Stage and tissue-specific prognostic impact of miR-182 in NSCLC. *BMC cancer*, 14(1), 138.

Suau, F., Cottin, V., Archer, F., Croze, S., Chastang, J., Cordier, G., Thivolet-Bejui, F., Mornex, J. F. & Leroux, C. (2006) Telomerase activation in a model of lung adenocarcinoma. *Eur Respir J*, 27(6), 1175-82.

Sucre, J. M. S., Jetter, C. S., Loomans, H., Williams, J., Plosa, E. J., Benjamin, J. T., Young, L. R., Kropski, J. A., Calvi, C. L., Kook, S., Wang, P., Gleaves, L., Eskaros, A., Goetzl, L., Blackwell, T. S., Guttentag, S. H. & Zijlstra, A. (2018) Successful Establishment of Primary Type II Alveolar Epithelium with 3D Organotypic Coculture. *Am J Respir Cell Mol Biol*, 59(2), 158-166.

Sullivan, C. S., Grundhoff, A. T., Tevethia, S., Pipas, J. M. & Ganem, D. (2005) SV40-encoded microRNAs regulate viral gene expression and reduce susceptibility to cytotoxic T cells. *Nature*, 435(7042), 682-6.

Summers, C., Dewar, P., van der Molen, R., Cousens, C., Salvatori, D., Sharp, J. M., Griffiths, D. J. & Norval, M. (2006) Jaagsiekte sheep retrovirus-specific immune responses induced by vaccination: a comparison of immunisation strategies. *Vaccine*, 24(11), 1821-9.

Summers, C., Neill, W., Dewar, P., Gonzalez, L., van der Molen, R., Norval, M. & Sharp, J. M. (2002) Systemic immune responses following infection with Jaagsiekte sheep retrovirus and in the terminal stages of ovine pulmonary adenocarcinoma. *Journal of general virology*, 83(7), 1753-1757.

Summers, C., Norval, M., De Las Heras, M., Gonzalez, L., Sharp, J. M. & Woods, G. M. (2005) An influx of macrophages is the predominant local immune response in ovine pulmonary adenocarcinoma. *Vet Immunol Immunopathol*, 106(3-4), 285-94.

Sun, Y., Su, B., Zhang, P., Xie, H., Zheng, H., Xu, Y., Du, Q., Zeng, H., Zhou, X., Chen, C. & Gao, W. (2013) Expression of miR-150 and miR-3940-5p is reduced in non-small cell lung carcinoma and correlates with clinicopathological features. *Oncol Rep*, 29(2), 704-12.

Synge, B. A. & Ritchie, C. M. (2010) Elimination of small ruminant lentivirus infection from sheep flocks and goat herds aided by health schemes in Great Britain. *Vet Rec*, 167(19), 739-43.

Szafran, B. (2014) *Virus-host interactions in an ovine model of lung cancer*. PhD University of Glasgow.

Takahashi, Y., Forrest, A. R., Maeno, E., Hashimoto, T., Daub, C. O. & Yasuda, J. (2009) MiR-107 and MiR-185 can induce cell cycle arrest in human non small cell lung cancer cell lines. *PloS one*, 4(8), e6677.

Takamizawa, J., Konishi, H., Yanagisawa, K., Tomida, S., Osada, H., Endoh, H., Harano, T., Yatabe, Y., Nagino, M. & Nimura, Y. (2004) Reduced expression of the let-7 microRNAs in human lung cancers in association with shortened postoperative survival. *Cancer research*, 64(11), 3753-3756.

Takebe, T., Zhang, B. & Radisic, M. (2017) Synergistic engineering: organoids meet organs-on-a-chip. *Cell Stem Cell*, 21(3), 297-300.

Taxis, T. M., Bauermann, F. V., Ridpath, J. F. & Casas, E. (2017) Circulating microRNAs in serum from cattle challenged with bovine viral diarrhea virus. *Frontiers in genetics*, 8, 91.

Tellez, C. S., Juri, D. E., Do, K., Bernauer, A. M., Thomas, C. L., Damiani, L. A., Tessema, M., Leng, S. & Belinsky, S. A. (2011) EMT and stem cell-like properties associated with miR-205 and miR-200 epigenetic silencing are early manifestations during carcinogen-induced transformation of human lung epithelial cells. *Cancer Res*, 71(8), 3087-97.

Telonis, A. G., Loher, P., Jing, Y., Londin, E. & Rigoutsos, I. (2015) Beyond the one-locus-one-miRNA paradigm: microRNA isoforms enable deeper insights into breast cancer heterogeneity. *Nucleic Acids Res*, 43(19), 9158-75.

Théry, C. (2011) Exosomes: secreted vesicles and intercellular communications. *F1000 biology reports*, 3, 15-15.

Thum, T., Catalucci, D. & Bauersachs, J. (2008) MicroRNAs: novel regulators in cardiac development and disease. *Cardiovascular Research*, 79(4), 562-570.

Tian, J., Hu, L., Li, X., Geng, J., Dai, M. & Bai, X. (2016) MicroRNA-130b promotes lung cancer progression via PPARgamma/VEGF-A/BCL-2-mediated suppression of apoptosis. *J Exp Clin Cancer Res*, 35(1), 105.

Topp, W. C. (1981) Normal rat cell lines deficient in nuclear thymidine kinase. *Virology*, 113(1), 408-411.

Tosar, J. P., Rovira, C. & Cayota, A. (2018) Non-coding RNA fragments account for the majority of annotated piRNAs expressed in somatic non-gonadal tissues. *Communications biology*, 1(1), 2.

Travis, W. D., Brambilla, E., Nicholson, A. G., Yatabe, Y., Austin, J. H. M., Beasley, M. B., Chirieac, L. R., Dacic, S., Duhig, E., Flieder, D. B., Geisinger, K., Hirsch, F. R., Ishikawa, Y., Kerr, K. M., Noguchi, M., Pelosi, G., Powell, C. A., Tsao, M. S., Wistuba, I. & Panel, W. H. O. (2015) The 2015 World Health Organization Classification of Lung Tumors: Impact of Genetic, Clinical and Radiologic Advances Since the 2004 Classification. *J Thorac Oncol*, 10(9), 1243-1260.

Treiber, T., Treiber, N. & Meister, G. (2019) Regulation of microRNA biogenesis and its crosstalk with other cellular pathways. *Nat Rev Mol Cell Biol*, 20(1), 5-20.

Tsubari, M., Taipale, J., Tiihonen, E., Keski-Oja, J. & Laiho, M. (1999) Hepatocyte growth factor releases mink epithelial cells from transforming growth factor β1-induced growth arrest by restoring Cdk6 expression and cyclin E-associated Cdk2 activity. *Molecular and cellular biology*, 19(5), 3654-3663.

Turchinovich, A., Weiz, L. & Burwinkel, B. (2012) Extracellular miRNAs: the mystery of their origin and function. *Trends in Biochemical Sciences*, 37(11), 460-465.

Turchinovich, A., Weiz, L., Langheinz, A. & Burwinkel, B. (2011) Characterization of extracellular circulating microRNA. *Nucleic Acids Res*, 39(16), 7223-33.

Tustin, R. (1969) Ovine jaagsiekte. *Journal of the South African Veterinary Medical Association*, 40, 3-23.

Tustin, R., York, D., Williamson, A.-L. & Verwoerd, D. W. (1988) Experimental transmission of jaagsiekte (ovine pulmonary adenomatosis) to goats.

Uhlmann, S., Mannsperger, H., Zhang, J. D., Horvat, E. A., Schmidt, C., Kublbeck, M., Henjes, F., Ward, A., Tschulena, U., Zweig, K., Korf, U., Wiemann, S. & Sahin, O. (2012) Global microRNA level regulation of EGFR-driven cell-cycle protein network in breast cancer. *Mol Syst Biol*, 8, 570.

Umu, S. U., Langseth, H., Bucher-Johannessen, C., Fromm, B., Keller, A., Meese, E., Lauritzen, M., Leithaug, M., Lyle, R. & Rounge, T. B. (2018) A comprehensive profile of circulating RNAs in human serum. *RNA biology*, 15(2), 242-250.

Valadi, H., Ekstrom, K., Bossios, A., Sjostrand, M., Lee, J. J. & Lotvall, J. O. (2007) Exosome-mediated transfer of mRNAs and microRNAs is a novel mechanism of genetic exchange between cells. *Nat Cell Biol*, 9(6), 654-9.

van Kouwenhove, M., Kedde, M. & Agami, R. (2011) MicroRNA regulation by RNA-binding proteins and its implications for cancer. *Nat Rev Cancer*, 11(9), 644-56.

van Niel, G., D'Angelo, G. & Raposo, G. (2018) Shedding light on the cell biology of extracellular vesicles. *Nat Rev Mol Cell Biol*, 19(4), 213-228.

Varela, M., Spencer, T. E., Palmarini, M. & Arnaud, F. (2009) Friendly viruses: the special relationship between endogenous retroviruses and their host. *Ann N Y Acad Sci*, 1178, 157-72.

Verwoerd, D. W., Payne, A.-L., York, D. & Myer, M. (1983) Isolation and preliminary characterization of the jaagsiekte retrovirus (JSRV). *The Onderstepoort journal of veterinary research*, 50(4), 309-316.

Verwoerd, D. W., Williamson, A. L. & De Villiers, E. M. (1980) Aetiology of jaagsiekte: transmission by means of subcellular fractions and evidence for the involvement of a retrovirus. *Onderstepoort J Vet Res*, 47(4), 275-80.

Vickers, K. C., Palmisano, B. T., Shoucri, B. M., Shamburek, R. D. & Remaley, A. T. (2011) MicroRNAs are transported in plasma and delivered to recipient cells by high-density lipoproteins. *Nat Cell Biol*, 13(4), 423-33.

Victoria, B., Dhahbi, J. M., Nunez Lopez, Y. O., Spinel, L., Atamna, H., Spindler, S. R. & Masternak, M. M. (2015) Circulating microRNA signature of genotype-by-age interactions in the long-lived Ames dwarf mouse. *Aging Cell*, 14(6), 1055-66.

Voigt, K., Brugmann, M., Huber, K., Dewar, P., Cousens, C., Hall, M., Sharp, J. M. & Ganter, M. (2007a) PCR examination of bronchoalveolar lavage samples is a useful tool in pre-clinical diagnosis of ovine pulmonary adenocarcinoma (Jaagsiekte). *Res Vet Sci*, 83(3), 419-27.

Voigt, K., Krämer, U., Brügmann, M., Dewar, P., Sharp, J. & Ganter, M. (2007b) Eradication of ovine pulmonary adenocarcinoma by motherless rearing of lambs. *Veterinary record*, 161(4), 129-132.

Vojtechova, Z. & Tachezy, R. (2018) The Role of miRNAs in Virus-Mediated Oncogenesis. *International journal of molecular sciences*, 19(4), 1217.

Volinia, S., Calin, G. A., Liu, C.-G., Ambs, S., Cimmino, A., Petrocca, F., Visone, R., Iorio, M., Roldo, C., Ferracin, M., Prueitt, R. L., Yanaihara, N., Lanza, G., Scarpa, A., Vecchione, A., Negrini, M., Harris, C. C. & Croce, C. M. (2006) A microRNA expression signature of human solid tumors defines cancer gene targets. *Proceedings of the National Academy of Sciences*, 103(7), 2257-2261.

Vosa, U., Vooder, T., Kolde, R., Vilo, J., Metspalu, A. & Annilo, T. (2013) Meta-analysis of microRNA expression in lung cancer. *Int J Cancer*, 132(12), 2884-93.

Wade, K. C., Guttentag, S. H., Gonzales, L. W., Maschhoff, K. L., Gonzales, J., Kolla, V., Singhal, S. & Ballard, P. L. (2006) Gene induction during differentiation of human pulmonary type II cells in vitro. *American journal of respiratory cell and molecular biology*, 34(6), 727-737.

Walker, P. J., Siddell, S. G., Lefkowitz, E. J., Mushegian, A. R., Dempsey, D. M., Dutilh, B. E., Harrach, B., Harrison, R. L., Hendrickson, R. C., Junglen, S., Knowles, N. J., Kropinski, A. M., Krupovic, M., Kuhn, J. H., Nibert, M., Rubino, L., Sabanadzovic, S., Simmonds, P., Varsani, A., Zerbini, F. M. & Davison, A. J. (2019) Changes to virus taxonomy and the

International Code of Virus Classification and Nomenclature ratified by the International Committee on Taxonomy of Viruses (2019). *Archives of Virology*, 164(9), 2417-2429.

Walsh, S. R., Linnerth-Petrik, N. M., Laporte, A. N., Menzies, P. I., Foster, R. A. & Wootton, S. K. (2010) Full-length genome sequence analysis of enzootic nasal tumor virus reveals an unusually high degree of genetic stability. *Virus Res*, 151(1), 74-87.

Wandera, J. (1971) Sheep pulmonary adenomatosis (Jaagsiekte). *Advances in veterinary science and comparative medicine*, 15, 251.

Wang, B., Ye, N., Cao, S. J., Wen, X. T., Huang, Y. & Yan, Q. G. (2016) Identification of novel and differentially expressed MicroRNAs in goat enzootic nasal adenocarcinoma. *BMC Genomics*, 17(1), 896.

Wang, D., Lu, G., Shao, Y. & Xu, D. (2018) MiR-182 promotes prostate cancer progression through activating Wnt/β-catenin signal pathway. *Biomedicine & Pharmacotherapy*, 99, 334-339.

Wang, D. T., Ma, Z. L., Li, Y. L., Wang, Y. Q., Zhao, B. T., Wei, J. L., Qi, X., Zhao, X. T. & Jin, Y. X. (2013) miR-150, p53 protein and relevant miRNAs consist of a regulatory network in NSCLC tumorigenesis. *Oncol Rep*, 30(1), 492-8.

Wang, G., Mao, W. & Zheng, S. (2008) MicroRNA-183 regulates Ezrin expression in lung cancer cells. *FEBS Lett*, 582(25-26), 3663-8.

Wang, H., Ma, Z., Liu, X., Zhang, C., Hu, Y., Ding, L., Qi, P., Wang, J., Lu, S. & Li, Y. (2019a) MiR-183-5p is required for non-small cell lung cancer progression by repressing PTEN. *Biomedicine & Pharmacotherapy*, 111, 1103-1111.

Wang, K., Zhang, S., Weber, J., Baxter, D. & Galas, D. J. (2010) Export of microRNAs and microRNA-protective protein by mammalian cells. *Nucleic Acids Res*, 38(20), 7248-59.

Wang, L. K., Hsiao, T. H., Hong, T. M., Chen, H. Y., Kao, S. H., Wang, W. L., Yu, S. L., Lin, C. W. & Yang, P. C. (2014a) MicroRNA-133a suppresses multiple oncogenic membrane receptors and cell invasion in non-small cell lung carcinoma. *PLoS ONE*, 9(5).

Wang, N., Zheng, J., Chen, Z., Liu, Y., Dura, B., Kwak, M., Xavier-Ferrucio, J., Lu, Y. C., Zhang, M., Roden, C., Cheng, J., Krause, D. S., Ding, Y., Fan, R. & Lu, J. (2019b) Single-cell microRNA-mRNA co-sequencing reveals non-genetic heterogeneity and mechanisms of microRNA regulation. *Nature Communications*, 10(1).

Wang, R., Chen, D. Q., Huang, J. Y., Zhang, K., Feng, B., Pan, B. Z., Chen, J., De, W. & Chen, L. B. (2014b) Acquisition of radioresistance in docetaxel-resistant human lung adenocarcinoma cells is linked with dysregulation of miR- 451/c-Myc-survivin/rad-51 signaling. *Oncotarget*, 5(15), 6113-6129.

Wang, R., Wang, Z. X., Yang, J. S., Pan, X., De, W. & Chen, L. B. (2011) MicroRNA-451 functions as a tumor suppressor in human non-small cell lung cancer by targeting ras-related protein 14 (RAB14). *Oncogene*, 30(23), 2644-2658.

Wang, T., Lv, M., Shen, S., Zhou, S., Wang, P., Chen, Y., Liu, B., Yu, L. & Hou, Y. (2012a) Cell-free microRNA expression profiles in malignant effusion associated with patient survival in non-small cell lung cancer. *PLoS One*, 7(8), e43268.

Wang, X., Cao, L., Wang, Y., Wang, X., Liu, N. & You, Y. (2012b) Regulation of let-7 and its target oncogenes. *Oncology letters*, 3(5), 955-960.

Wei, Z., Batagov, A. O., Carter, D. R. & Krichevsky, A. M. (2016) Fetal Bovine Serum RNA Interferes with the Cell Culture derived Extracellular RNA. *Sci Rep*, 6, 31175.

Wen, L. P., Madani, K., Fahrni, J. A., Duncan, S. R. & Rosen, G. D. (1997) Dexamethasone inhibits lung epithelial cell apoptosis induced by IFN-gamma and Fas. *Am J Physiol*, 273(5), L921-9.

Whisnant, A. W., Kehl, T., Bao, Q., Materniak, M., Kuzmak, J., Lochelt, M. & Cullen, B. R. (2014) Identification of novel, highly expressed retroviral microRNAs in cells infected by bovine foamy virus. *J Virol*, 88(9), 4679-86.

Wistuba, I. I., Montellano, F. D., Milchgrub, S., Virmani, A. K., Behrens, C., Chen, H., Ahmadian, M., Nowak, J. A., Muller, C. & Minna, J. D. (1997) Deletions of chromosome 3p are frequent and early events in the pathogenesis of uterine cervical carcinoma. *Cancer research*, 57(15), 3154-3158.

Witherden, I. R. & Tetley, T. D. (2001) Isolation and Culture of Human Alveolar Type II Pneumocytes. *Methods Mol Med*, 56, 137-46.

Witwer, K. W. & Halushka, M. K. (2016) Toward the promise of microRNAs – Enhancing reproducibility and rigor in microRNA research. *RNA Biology*, 13(11), 1103-1116.

Wong, N. & Wang, X. (2015) miRDB: an online resource for microRNA target prediction and functional annotations. *Nucleic Acids Res*, 43(Database issue), D146-52.

Wootton, S. K., Halbert, C. L. & Miller, A. D. (2005) Sheep retrovirus structural protein induces lung tumours. *Nature*, 434(7035), 904.

Wootton, S. K., Metzger, M. J., Hudkins, K. L., Alpers, C. E., York, D., DeMartini, J. C. & Miller, A. D. (2006) Lung cancer induced in mice by the envelope protein of jaagsiekte sheep retrovirus (JSRV) closely resembles lung cancer in sheep infected with JSRV. *Retrovirology*, 3, 94.

Wu, H. & Mo, Y. Y. (2009) Targeting miR-205 in breast cancer. *Expert Opinion on Therapeutic Targets*, 13(12), 1439-1448.

Xi, S., Yang, M., Tao, Y., Xu, H., Shan, J., Inchauste, S., Zhang, M., Mercedes, L., Hong, J. A., Rao, M. & Schrump, D. S. (2010) Cigarette smoke induces C/EBP-beta-mediated activation of miR-31 in normal human respiratory epithelia and lung cancer cells. *PLoS One*, 5(10), e13764.

Xi, Y., Nakajima, G., Gavin, E., Morris, C. G., Kudo, K., Hayashi, K. & Ju, J. (2007) Systematic analysis of microRNA expression of RNA extracted from fresh frozen and formalin-fixed paraffin-embedded samples. *Rna*, 13(10), 1668-74.

Xiang, M., Zeng, Y., Yang, R., Xu, H., Chen, Z., Zhong, J., Xie, H., Xu, Y. & Zeng, X. (2014) U6 is not a suitable endogenous control for the quantification of circulating microRNAs. *Biochem Biophys Res Commun*, 454(1), 210-4.

Xiao, Z., Cheng, G., Jiao, Y., Pan, C., Li, R., Jia, D., Zhu, J., Wu, C., Zheng, M. & Jia, J. (2018) Holo-Seq: Single-cell sequencing of holo-transcriptome. *Genome Biology*, 19(1).

Xu, P., Vernooy, S. Y., Guo, M. & Hay, B. A. (2003) The Drosophila microRNA Mir-14 suppresses cell death and is required for normal fat metabolism. *Current Biology*, 13(9), 790-795.

Xu, Q., Sun, Q., Zhang, J., Yu, J., Chen, W. & Zhang, Z. (2013) Downregulation of miR-153 contributes to epithelial-mesenchymal transition and tumor metastasis in human epithelial cancer. *Carcinogenesis*, 34(3), 539-49.

Yanaihara, N., Caplen, N., Bowman, E., Seike, M., Kumamoto, K., Yi, M., Stephens, R. M., Okamoto, A., Yokota, J., Tanaka, T., Calin, G. A., Liu, C. G., Croce, C. M. & Harris, C. C. (2006) Unique microRNA molecular profiles in lung cancer diagnosis and prognosis. *Cancer Cell*, 9(3), 189-98.

Yang, J.-S., Maurin, T., Robine, N., Rasmussen, K. D., Jeffrey, K. L., Chandwani, R., Papapetrou, E. P., Sadelain, M., O'Carroll, D. & Lai, E. C. (2010a) Conserved vertebrate mir-451 provides a platform for Dicer-independent, Ago2-mediated microRNA biogenesis. *Proceedings of the National Academy of Sciences*, 107(34), 15163-15168.

Yang, J.-Y., Chang, C.-J., Xia, W., Wang, Y., Wong, K.-K., Engelman, J. A., Du, Y., Andreeff, M., Hortobagyi, G. N. & Hung, M.-C. (2010b) Activation of FOXO3a Is Sufficient to Reverse Mitogen-Activated Protein/Extracellular Signal-Regulated Kinase Kinase Inhibitor Chemoresistance in Human Cancer. *Cancer Research*, 70(11), 4709-4718.

Yang, W.-B., Chen, P.-H., Hsu, T.-I., Fu, T.-F., Su, W.-C., Liaw, H., Chang, W.-C. & Hung, J.-J. (2014) Sp1-mediated microRNA-182 expression regulates lung cancer progression. *Oncotarget*, 5(3), 740.

Yao, L., Zhou, Q., Wang, L. & Hou, G. (2017) MicroRNA-182-5p protects H9c2 cardiomyocytes from hypoxia-induced apoptosis by down-regulation of PTEN. *International Journal of Clinical and Experimental Pathology*, 10(5), 5220-5226.

Yao, Y., Shen, H., Zhou, Y., Yang, Z. & Hu, T. (2018) MicroRNA-215 suppresses the proliferation, migration and invasion of non-small cell lung carcinoma cells through the downregulation of matrix metalloproteinase-16 expression. *Exp Ther Med*, 15(4), 3239-3246.

Yap, M. W., Colbeck, E., Ellis, S. A. & Stoye, J. P. (2014) Evolution of the retroviral restriction gene Fv1: inhibition of non-MLV retroviruses. *PLoS Pathog*, 10(3), e1003968.

Yekta, S., Shih, I. H. & Bartel, D. P. (2004) MicroRNA-directed cleavage of HOXB8 mRNA. *Science*, 304(5670), 594-6.

Yeung, M. L., Yasunaga, J., Bennasser, Y., Dusetti, N., Harris, D., Ahmad, N., Matsuoka, M. & Jeang, K. T. (2008) Roles for microRNAs, miR-93 and miR-130b, and tumor protein 53-induced nuclear protein 1 tumor suppressor in cell growth dysregulation by human T-cell lymphotrophic virus 1. *Cancer Res*, 68(21), 8976-85.

Yin, P., Peng, R., Peng, H., Yao, L., Sun, Y., Wen, L., Wu, T., Zhou, J. & Zhang, Z. (2015) MiR-451 suppresses cell proliferation and metastasis in A549 lung cancer cells. *Molecular biotechnology*, 57(1), 1-11.

Yoda, M., Cifuentes, D., Izumi, N., Sakaguchi, Y., Suzuki, T., Giraldez, A. J. & Tomari, Y. (2013) Poly(A)-specific ribonuclease mediates 3'-end trimming of argonaute2-cleaved precursor microrna. *Cell Reports*, 5(3), 715-726.

York, D., Vigne, R., Verwoerd, D. & Querat, G. (1992) Nucleotide sequence of the jaagsiekte retrovirus, an exogenous and endogenous type D and B retrovirus of sheep and goats. *Journal of virology*, 66(8), 4930-4939.

York, D. F. & Querat, G. (2003) A history of ovine pulmonary adenocarcinoma (jaagsiekte) and experiments leading to the deduction of the JSRV nucleotide sequence, in Fan, H.

(ed), *Jaagsiekte Sheep Retrovirus and Lung Cancer*, 2003/02/25 editionSpringer-Verlag, 1-23.

You, J., Li, Y., Fang, N., Liu, B., Zu, L., Chang, R., Li, X. & Zhou, Q. (2014) MiR-132 suppresses the migration and invasion of lung cancer cells via targeting the EMT regulator ZEB2. *PLoS One*, 9(3), e91827.

You, X., Zhang, Z., Fan, J., Cui, Z. & Zhang, X.-E. (2012) Functionally Orthologous Viral and Cellular MicroRNAs Studied by a Novel Dual-Fluorescent Reporter System. *PLOS ONE*, 7(4), e36157.

Yousem, S. A., Finkelstein, S. D., Swalsky, P. A., Bakker, A. & Ohori, N. P. (2001) Absence of jaagsiekte sheep retrovirus DNA and RNA in bronchioloalveolar and conventional human pulmonary adenocarcinoma by PCR and RT-PCR analysis. *Hum Pathol*, 32(10), 1039-42.

Youssef, G., Wallace, W. A., Dagleish, M. P., Cousens, C. & Griffiths, D. J. (2015) Ovine pulmonary adenocarcinoma: a large animal model for human lung cancer. *ILAR J*, 56(1), 99-115.

Yu, L., Todd, N. W., Xing, L., Xie, Y., Zhang, H., Liu, Z., Fang, H., Zhang, J., Katz, R. L. & Jiang, F. (2010a) Early detection of lung adenocarcinoma in sputum by a panel of microRNA markers. *International Journal of Cancer*, 127(12), 2870-2878.

Yu, N., Zhang, Q., Liu, Q., Yang, J. & Zhang, S. (2017) A meta-analysis: microRNAs' prognostic function in patients with nonsmall cell lung cancer. *Cancer Medicine*, 6(9), 2098-2105.

Yu, S., Lu, Z., Liu, C., Meng, Y., Ma, Y., Zhao, W., Liu, J., Yu, J. & Chen, J. (2010b) miRNA-96 suppresses KRAS and functions as a tumor suppressor gene in pancreatic cancer. *Cancer Res*, 70(14), 6015-25.

Yuan, Y., Du, W., Wang, Y., Xu, C., Wang, J., Zhang, Y., Wang, H., Ju, J., Zhao, L., Wang, Z., Lu, Y., Cai, B. & Pan, Z. (2015) Suppression of AKT expression by miR-153 produced anti-tumor activity in lung cancer. *Int J Cancer*, 136(6), 1333-40.

Zhang, G. L., Li, Y. X., Zheng, S. Q., Liu, M., Li, X. & Tang, H. (2010a) Suppression of hepatitis B virus replication by microRNA-199a-3p and microRNA-210. *Antiviral Res*, 88(2), 169-75.

Zhang, J. G., Wang, J. J., Zhao, F., Liu, Q., Jiang, K. & Yang, G. H. (2010b) MicroRNA-21 (miR-21) represses tumor suppressor PTEN and promotes growth and invasion in non-small cell lung cancer (NSCLC). *Clinica Chimica Acta*, 411(11-12), 846-852.

Zhang, L., Lin, J., Ye, Y., Oba, T., Gentile, E., Lian, J., Wang, J., Zhao, Y., Gu, J., Wistuba, II, Roth, J. A., Ji, L. & Wu, X. (2018) Serum MicroRNA-150 Predicts Prognosis for Early-Stage Non-Small Cell Lung Cancer and Promotes Tumor Cell Proliferation by Targeting Tumor Suppressor Gene SRCIN1. *Clin Pharmacol Ther*, 103(6), 1061-1073.

Zhang, N., Wei, X. & Xu, L. (2013a) miR-150 promotes the proliferation of lung cancer cells by targeting P53. *FEBS Lett*, 587(15), 2346-51.

Zhang, Q. H., Sun, H. M., Zheng, R. Z., Li, Y. C., Zhang, Q., Cheng, P., Tang, Z. H. & Huang, F. (2013b) Meta-analysis of microRNA-183 family expression in human cancer studies comparing cancer tissues with noncancerous tissues. *Gene*, 527(1), 26-32.

Zhang, W. C., Chin, T. M., Yang, H., Nga, M. E., Lunny, D. P., Lim, E. K., Sun, L. L., Pang, Y. H., Leow, Y. N., Malusay, S. R., Lim, P. X., Lee, J. Z., Tan, B. J., Shyh-Chang, N., Lim, E. H., Lim, W. T., Tan, D. S., Tan, E. H., Tai, B. C., Soo, R. A., Tam, W. L. & Lim, B. (2016)

Tumour-initiating cell-specific miR-1246 and miR-1290 expression converge to promote non-small cell lung cancer progression. *Nat Commun*, 7, 11702.

Zhang, X., Li, T., Liu, F., Chen, Y., Yao, J., Li, Z., Huang, Y. & Wang, J. (2019) Comparative analysis of droplet-based ultra-high-throughput single-cell RNA-seq systems. *Molecular cell*, 73(1), 130-142. e5.

Zhao, Y., Xu, H., Yao, Y., Smith, L. P., Kgosana, L., Green, J., Petherbridge, L., Baigent, S. J. & Nair, V. (2011) Critical Role of the Virus-Encoded MicroRNA-155 Ortholog in the Induction of Marek's Disease Lymphomas. *PLOS Pathogens*, 7(2), e1001305.

Zheng, W., Zhao, J., Tao, Y., Guo, M., Ya, Z., Chen, C., Qin, N., Zheng, J., Luo, J. & Xu, L. (2018) MicroRNA-21: A promising biomarker for the prognosis and diagnosis of non-small cell lung cancer. *Oncology Letters*, 16(3), 2777-2782.

Zheng, Y., Chen, K.-l., Zheng, X.-m., Li, H.-x. & Wang, G.-l. (2014) Identification and bioinformatics analysis of microRNAs associated with stress and immune response in serum of heat-stressed and normal Holstein cows. *Cell Stress and Chaperones*, 19(6), 973-981.

Zhou, G., Wang, X., Yuan, C., Kang, D., Xu, X., Zhou, J., Geng, R., Yang, Y., Yang, Z. & Chen, Y. (2017) Integrating miRNA and mRNA Expression Profiling Uncovers miRNAs Underlying Fat Deposition in Sheep. *Biomed Res Int*, 2017, 1857580.

Zhou, L., Qiu, T., Xu, J., Wang, T., Wang, J., Zhou, X., Huang, Z., Zhu, W., Shu, Y. & Liu, P. (2013) miR-135a/b modulate cisplatin resistance of human lung cancer cell line by targeting MCL1. *Pathol Oncol Res*, 19(4), 677-83.

Zhou, X., Zhang, X., Yang, Y., Li, Z., Du, L., Dong, Z., Qu, A., Jiang, X., Li, P. & Wang, C. (2014) Urinary cell-free microRNA-106b as a novel biomarker for detection of bladder cancer. *Med Oncol*, 31(10), 197.

Zhu, W., Liu, X., He, J., Chen, D., Hunag, Y. & Zhang, Y. K. (2011) Overexpression of members of the microRNA-183 family is a risk factor for lung cancer: a case control study. *BMC cancer*, 11(1), 393.

Zhu, W., Zhou, K., Zha, Y., Chen, D., He, J., Ma, H., Liu, X., Le, H. & Zhang, Y. (2016) Diagnostic Value of Serum miR-182, miR-183, miR-210, and miR-126 Levels in Patients with Early-Stage Non-Small Cell Lung Cancer. *PLoS One*, 11(4), e0153046.

Zyrianova, I. M. & Koval'chuk, S. N. (2018) Bovine leukemia virus pre-miRNA genes' polymorphism. *RNA Biol*, 15(12), 1440-1447.

Appendix

Table 0.1. Summary of miRNA sequences found in sheep and sequences targeted by qPCR assays.

	Sequence found in small RNA sequencing (from 5′ to 3′)	Sheep miRNA sequence from miRBase (from 5′ to 3′)	miRNA assay name and sequence detected (from 5′ to 3′)	Dog miRNA sequence from miRBase (from 5′ to 3′)
miR-135b	UAUGGCUUUUCAUUCCUAUGUGA UAUGGCUUUUCAUUCCUAUGUG UAUGGCUUUUCAUUCCUAUGU UAUGGCUUUUCAUUCCUAUGUGU UAUGGCUUUUCAUUCCUAUGUGG UAUGGCUUUUCAUUCCUAUG UAUGGCUUUUCAUUCCUAUGUA UAUGGCUUUGCAUUCCUAUGUG UAUGGCUUUUCAUUCUUAUGU UAUGGCUUUUCACUCCUAUGUGA UAUGGCUUUUCCUUCCUAUGUG UAUGGCUUUUCAGUCCUAUGUGA UAUGGCUUUGCAUUCCUAUGUGA UAUGGCUUUUCAUUCUUAUGUGA UAUGGCUUUUCGUUCCUAUGUGA	Not in miRBase	hsa-miR-135b-5p: UAUGGCUUUUCAUUCCUAUGUGA	cfa-miR-135b: UAUGGCUUUUCAUUCCUAUGUGA

Table 0.1. Summary of miRNA sequences found in sheep and sequences targeted by qPCR assays.

	Sequence found in small RNA sequencing (from 5′ to 3′)	Sheep miRNA sequence from miRBase (from 5′ to 3′)	miRNA assay name and sequence detected (from 5′ to 3′)	Dog miRNA sequence from miRBase (from 5′ to 3′)
miR-182	UUUGGCAAUGGUAGAACUCACACU UUUGGCAAUGGUAGAACUCACAC UUUGGCAAUGGUAGAACUCACA UUUGGCAAUGGUAGAACUCAC UUUGGCAAUGGUAGAACUCCCACU UUUGGCAAUGGUAGAACUCCCAC UUUGGCAAUGGUAGAACUCACAA UUUGGCAAUGGUAGAACUCA UUUGGCAAUGGUAGAACUCACACA UUUGGCAAUGGUAGAACUCACU UUUGGCAAUGGUAGAACUCACACG UUUGGCAAUGGUAGAACUCUCACU UUUGGCAAUGGUAGAACUC UUUGGCAAUUGUAGAACUCACACU UUUGGCAAUGGUAGAACU	Not in miRBase	hsa-miR-182-5p: UUUGGCAAUGGUAGAACUCACACU	cfa-miR-182: UUUGGCAAUGGUAGAACUCACACU
miR-183	UAUGGCACUGGUAGAAUUCACU UAUGGCACUGGUAGAAUUCACUG AUGGCACUGGUAGAAUUCACUG AUGGCACUGGUAGAAUUCACU UAUGGCACUGGUAGAAUUCAC UAUGGCACUGGUAGAAUUCCCUG AUGGCACUGGUAGAAUUCAC UAUGGCACUGGUAGAAUUCACUA UAUGGCACUGGUAGAAUUCACA UAUGGCACUGGUAGAAUUCACUU AUGGCACUGGUAGAAUUCACUA UAUGGCACUGGUAGAAUU UAUGGCACUUGUAGAAUUCACU	Not in miRBase	hsa-miR-183-5p: UAUGGCACUGGUAGAAUUCACU	cfa-miR-183: UAUGGCACUGGUAGAAUUCACU

Table 0.1. Summary of miRNA sequences found in sheep and sequences targeted by qPCR assays.

	Sequence found in small RNA sequencing (from 5′ to 3′)	Sheep miRNA sequence from miRBase (from 5′ to 3′)	miRNA assay name and sequence detected (from 5′ to 3′)	Dog miRNA sequence from miRBase (from 5′ to 3′)
miR-200b	CAUCUUACUGGGCAGCAUUGGA CAUCUUACUGGGCAGCAUUGG CAUCUUACUGGGCAGCAU CAUCUUACUGGGCAGCAUUG CAUCUUACUGGGCAGCAUUGGU CAUCUUACUGGGCAGCAUUGA UAUCUUACUGGGCAGCAUUGGA CAUCUUACUGGGCAGCAUUGU CAUCUUACUAGGCAGCAUUGGA AUCUUACUGGGCAGCAUUGGA CAUCUUACUGGGCAGCAUU CAUCUUACUUGGCAGCAUUGGA CAUCUUACUGGGCAGCAUA UAUCUUACUGGGCAGCAUUGG AAUCUUACUGGGCAGCAUUGGA	Not in miRBase	hsa-miR-200b-5p: CAUCUUACUGGGCAGCAUUGGA	cfa-miR-200b: CAUCUUACUGGGCAGCAUUGGA

Table 0.1. Summary of miRNA sequences found in sheep and sequences targeted by qPCR assays.

	Sequence found in small RNA sequencing (from 5′ to 3′)	**Sheep miRNA sequence from miRBase (from 5′ to 3′)**	**miRNA assay name and sequence detected (from 5′ to 3′)**	**Dog miRNA sequence from miRBase (from 5′ to 3′)**
miR-205	UCCUUCAUUCCACCGGAGUCUG UCCUUCAUUCCACCGGAGUCU UCCUUCAUUCCACCGGAGUC UCCUUCAUUCCACCGGAGU UCCUUCAUUGCACCGGAGUCUG UCCUUCAUUACACCGGAGUCUG UCCUUCAUUCCAUCGGAGUCUG UCCUACAUUCCACCGGAGUCUG UCCUUCAUUCCACCGGAGUCUU ACCUUCAUUCCACCGGAGUCUG UCCUUCAUUCCAGCGGAGUCUG UCCUUCAUUUCACCGGAGUCUG UCCUUCAUUCCAUCGGAGUCU UCCUUCAUUCCUCCGGAGUCUG UCCUUCAUUCCAACGGAGUCUG	Not in miRBase	hsa-miR-205-5p: UCCUUCAUUCCACCGGAGUCUG	cfa-miR-205: UCCUUCAUUCCACCGGAGUCUG

Table 0.1. Summary of miRNA sequences found in sheep and sequences targeted by qPCR assays.

	Sequence found in small RNA sequencing (from 5′ to 3′)	Sheep miRNA sequence from miRBase (from 5′ to 3′)	miRNA assay name and sequence detected (from 5′ to 3′)	Dog miRNA sequence from miRBase (from 5′ to 3′)
miR-21	UAGCUUAUCAGACUGAUGUUGACU UAGCUUAUCAGACUGAUGUUGACA UAGCUUAUCAGACUGAUGUUGACC UAGCUUAUCAGACUGAUGUUGACG UAGCUUAUCAGACUGAUGUUGA UAGCUUAUCAGACUGAUGUUGAC UAGCUUAUCAGACUGAUGUUG UAGCUUAUCAGACUGAUGUUGAA UAGCUUAUCAGACUGAUGUU UAGCUUAUCAGACUGAUGU UAGCUUAUCCGACUGAUGUUGA UAGCUUAUCAGACUGAUGUUGG UAGCUUAUCAGACUGAUGUUGAU UAGCUUAUCAGACUGAUGUUGU UAGCUUAUCGGACUGAUGUUGA	oar-miR-21: UAGCUUAUCAGACUGAUGUUGAC	rno-miR-21-5p: UAGCUUAUCAGACUGAUGUUGA	cfa-miR-21: UAGCUUAUCAGACUGAUGUUGA
miR-31	AGGCAAGAUGCUGGCAUAGCU AGGCAAGAUGCUGGCAUAGC AGGCAAGAUGCUGGCAUAG AGGCAAGAUGCUGGCAUAGCA AGGCAAGAUGCUGGCAUAGCG AGGCAAGAUGCUGGCAUAGA UGGCAAGAUGCUGGCAUAGCU AGGCAAGAUUCUGGCAUAGCU AGGCAAGAUGCUGGCAUAGU	Not in miRBase	hsa-miR-31-5p: AGGCAAGAUGCUGGCAUAGCU	cfa-miR-31: AGGCAAGAUGCUGGCAUAGCUGU
miR-503	UAGCAGCGGGAACAGUACUGCAG	Not in miRBase	mmu-miR-503-5p: UAGCAGCGGGAACAGUACUGCAG	cfa-miR-503: UAGCAGCGGGAACAGUACUG

Table 0.1. Summary of miRNA sequences found in sheep and sequences targeted by qPCR assays.

	Sequence found in small RNA sequencing (from 5′ to 3′)	Sheep miRNA sequence from miRBase (from 5′ to 3′)	miRNA assay name and sequence detected (from 5′ to 3′)	Dog miRNA sequence from miRBase (from 5′ to 3′)
miR-96	UUUGGCACUAGCACAUUUUUGCU UUUGGCACUAGCACAUUUUUGC UUUGGCACUAGCACAUUUUUG UUUGGCACUAGCACAUUUUUUGA UUUGGCACUAGCACAUUUUUUGCA UUUGGCACUCGCACAUUUUUUGCU UUUGGCACUAGCGCAUUUUUUGCU UUUGGCACUGGCACAUUUUUUGCU UUUGGCACUAGCUCAUUUUUUGCU	Not in miRBase	hsa-miR-96-5p: UUUGGCACUAGCACAUUUUUGCU	cfa-miR-96: UUUGGCACUAGCACAUUUUUGCU
miR-191	CAACGGAAUCCCAAAAGCAGCUG AACGGAAUCCCAAAAGCAGCUG UAACGGAAUCCCAAAAGCAGCUG CAACGGAAUCCCAAAAGCAGCUU CAACGGAAUGCCAAAAGCAGCUG AAACGGAAUCCCAAAAGCAGCUG CAACGGAAUACCAAAAGCAGCUG CAACAGAAUCCCAAAAGCAGCUG CAACGGAAUCCCGAAAGCAGCUG CAACGGAAUCCCAAAAGCAGCU CAACGGAAUCCCAAAAGCAG CAACGGAAUCCCAAAAGCAGC	oar-miR-191: CAACGGAAUCCCAAAAGCAGCU	hsa-miR-191-5p: CAACGGAAUCCCAAAAGCAGCUG	cfa-miR-191: CAACGGAAUCCCAAAAGCAGCU

Table 0.2. Summary of Ct values from the qPCR results reported in Chapter 5.

miRNA	Sample	Ct value
Fig. 5.15		
miR-135b	1E5	28.06
miR-182	1E5	29.83
miR-183	1E5	30.18
miR-200b	1E5	40.00
miR-205	1E5	32.78
miR-21	1E5	20.20
miR-31	1E5	26.96
miR-503	1E5	33.99
miR-96	1E5	28.97
miR-191	1E5	27.50
miR-135b	2E3	26.83
miR-182	2E3	27.88
miR-183	2E3	28.35
miR-200b	2E3	40.00
miR-205	2E3	32.46
miR-21	2E3	18.79
miR-31	2E3	25.09
miR-503	2E3	31.32
miR-96	2E3	27.54
miR-191	2E3	25.96
miR-135b	3C9	26.15
miR-182	3C9	27.94
miR-183	3C9	28.99
miR-200b	3C9	40.00
miR-205	3C9	33.32
miR-21	3C9	17.97
miR-31	3C9	24.55
miR-503	3C9	31.13
miR-96	3C9	26.88
miR-191	3C9	25.53
miR-135b	Control MDCKs	26.96
miR-182	Control MDCKs	26.98
miR-183	Control MDCKs	27.84
miR-200b	Control MDCKs	33.01
miR-205	Control MDCKs	33.99
miR-21	Control MDCKs	19.16

Table 0.2. Summary of Ct values from the qPCR results reported in Chapter 5.

miRNA	Sample	Ct value
miR-31	Control MDCKs	25.48
miR-503	Control MDCKs	29.62
miR-96	Control MDCKs	26.83
miR-191	Control MDCKs	25.73
Fig. 5.21. A		
miR-135b	Lung slices mock-infected- day 8	31.27
miR-182	Lung slices mock-infected- day 8	29.32
miR-183	Lung slices mock-infected- day 8	25.71
miR-200b	Lung slices mock-infected- day 8	30.49
miR-205	Lung slices mock-infected- day 8	22.93
miR-21	Lung slices mock-infected- day 8	18.73
miR-31	Lung slices mock-infected- day 8	24.34
miR-503	Lung slices mock-infected- day 8	31.51
miR-96	Lung slices mock-infected- day 8	27.79
miR-191	Lung slices mock-infected- day 8	24.48
miR-135b	Lung slices CSC-GFP- day 8	33.16
miR-182	Lung slices CSC-GFP- day 8	29.59
miR-183	Lung slices CSC-GFP- day 8	27.12
miR-200b	Lung slices CSC-GFP- day 8	31.72
miR-205	Lung slices CSC-GFP- day 8	24.01
miR-21	Lung slices CSC-GFP- day 8	18.79
miR-31	Lung slices CSC-GFP- day 8	25.29
miR-503	Lung slices CSC-GFP- day 8	31.76
miR-96	Lung slices CSC-GFP- day 8	28.33
miR-191	Lung slices CSC-GFP- day 8	24.48
miR-135b	Lung slices CSC-GFP2AEnv- day 8	34.20
miR-182	Lung slices CSC-GFP2AEnv- day 8	30.88
miR-183	Lung slices CSC-GFP2AEnv- day 8	27.98
miR-200b	Lung slices CSC-GFP2AEnv- day 8	31.83
miR-205	Lung slices CSC-GFP2AEnv- day 8	24.39
miR-21	Lung slices CSC-GFP2AEnv- day 8	20.58
miR-31	Lung slices CSC-GFP2AEnv- day 8	25.66
miR-503	Lung slices CSC-GFP2AEnv- day 8	32.95
miR-96	Lung slices CSC-GFP2AEnv- day 8	29.92
miR-191	Lung slices CSC-GFP2AEnv- day 8	25.21
Fig. 5.21. B		
miR-135b	Lung slices mock-infected- day 8	31.27

Table 0.2. Summary of Ct values from the qPCR results reported in Chapter 5.

miRNA	Sample	Ct value
miR-182	Lung slices mock-infected- day 8	29.32
miR-183	Lung slices mock-infected- day 8	25.71
miR-200b	Lung slices mock-infected- day 8	30.49
miR-205	Lung slices mock-infected- day 8	22.93
miR-21	Lung slices mock-infected- day 8	18.73
miR-31	Lung slices mock-infected- day 8	24.34
miR-503	Lung slices mock-infected- day 8	31.51
miR-96	Lung slices mock-infected- day 8	27.79
miR-191	Lung slices mock-infected- day 8	24.48
miR-135b	Lung slices CSC-GFP- day 8	31.35
miR-182	Lung slices CSC-GFP- day 8	28.87
miR-183	Lung slices CSC-GFP- day 8	25.99
miR-200b	Lung slices CSC-GFP- day 8	31.44
miR-205	Lung slices CSC-GFP- day 8	23.26
miR-21	Lung slices CSC-GFP- day 8	18.59
miR-31	Lung slices CSC-GFP- day 8	24.43
miR-503	Lung slices CSC-GFP- day 8	33.01
miR-96	Lung slices CSC-GFP- day 8	27.24
miR-191	Lung slices CSC-GFP- day 8	24.61
miR-135b	Lung slices CSC-GFP2AEnv- day 8	33.62
miR-182	Lung slices CSC-GFP2AEnv- day 8	28.13
miR-183	Lung slices CSC-GFP2AEnv- day 8	25.50
miR-200b	Lung slices CSC-GFP2AEnv- day 8	30.65
miR-205	Lung slices CSC-GFP2AEnv- day 8	22.56
miR-21	Lung slices CSC-GFP2AEnv- day 8	17.98
miR-31	Lung slices CSC-GFP2AEnv- day 8	23.94
miR-503	Lung slices CSC-GFP2AEnv- day 8	32.87
miR-96	Lung slices CSC-GFP2AEnv- day 8	26.75
miR-191	Lung slices CSC-GFP2AEnv- day 8	24.08
Fig. 5.22. A		
miR-135b	Lung slices mock-infected- day 18	34.14
miR-182	Lung slices mock-infected- day 18	27.39
miR-183	Lung slices mock-infected- day 18	24.40
miR-200b	Lung slices mock-infected- day 18	30.80
miR-205	Lung slices mock-infected- day 18	22.51
miR-21	Lung slices mock-infected- day 18	17.92
miR-31	Lung slices mock-infected- day 18	23.81

Table 0.2. Summary of Ct values from the qPCR results reported in Chapter 5.

miRNA	Sample	Ct value
miR-503	Lung slices mock-infected- day 18	32.27
miR-96	Lung slices mock-infected- day 18	25.99
miR-191	Lung slices mock-infected- day 18	24.49
miR-135b	Lung slices CSC-GFP- day 18	31.85
miR-182	Lung slices CSC-GFP- day 18	26.88
miR-183	Lung slices CSC-GFP- day 18	24.06
miR-200b	Lung slices CSC-GFP- day 18	30.94
miR-205	Lung slices CSC-GFP- day 18	21.77
miR-21	Lung slices CSC-GFP- day 18	17.41
miR-31	Lung slices CSC-GFP- day 18	23.07
miR-503	Lung slices CSC-GFP- day 18	33.74
miR-96	Lung slices CSC-GFP- day 18	25.30
miR-191	Lung slices CSC-GFP- day 18	23.94
miR-135b	Lung slices CSC-GFP2AEnv- day 18	32.51
miR-182	Lung slices CSC-GFP2AEnv- day 18	27.48
miR-183	Lung slices CSC-GFP2AEnv- day 18	24.47
miR-200b	Lung slices CSC-GFP2AEnv- day 18	29.95
miR-205	Lung slices CSC-GFP2AEnv- day 18	21.46
miR-21	Lung slices CSC-GFP2AEnv- day 18	18.72
miR-31	Lung slices CSC-GFP2AEnv- day 18	23.31
miR-503	Lung slices CSC-GFP2AEnv- day 18	33.38
miR-96	Lung slices CSC-GFP2AEnv- day 18	26.33
miR-191	Lung slices CSC-GFP2AEnv- day 18	23.96
Fig. 5.22. B		
miR-135b	Lung slices mock-infected- day 18	34.14
miR-182	Lung slices mock-infected- day 18	27.39
miR-183	Lung slices mock-infected- day 18	24.40
miR-200b	Lung slices mock-infected- day 18	30.80
miR-205	Lung slices mock-infected- day 18	22.51
miR-21	Lung slices mock-infected- day 18	17.92
miR-31	Lung slices mock-infected- day 18	23.81
miR-503	Lung slices mock-infected- day 18	32.27
miR-96	Lung slices mock-infected- day 18	25.99
miR-191	Lung slices mock-infected- day 18	24.49
miR-135b	Lung slices CSC-GFP- day 18	32.32
miR-182	Lung slices CSC-GFP- day 18	27.07
miR-183	Lung slices CSC-GFP- day 18	24.47

Table 0.2. Summary of Ct values from the qPCR results reported in Chapter 5.

miRNA	Sample	Ct value
miR-200b	Lung slices CSC-GFP- day 18	30.27
miR-205	Lung slices CSC-GFP- day 18	22.44
miR-21	Lung slices CSC-GFP- day 18	17.68
miR-31	Lung slices CSC-GFP- day 18	23.55
miR-503	Lung slices CSC-GFP- day 18	32.05
miR-96	Lung slices CSC-GFP- day 18	25.48
miR-191	Lung slices CSC-GFP- day 18	24.24
miR-135b	Lung slices CSC-GFP2AEnv- day 18	35.22
miR-182	Lung slices CSC-GFP2AEnv- day 18	27.63
miR-183	Lung slices CSC-GFP2AEnv- day 18	24.80
miR-200b	Lung slices CSC-GFP2AEnv- day 18	31.77
miR-205	Lung slices CSC-GFP2AEnv- day 18	22.80
miR-21	Lung slices CSC-GFP2AEnv- day 18	18.42
miR-31	Lung slices CSC-GFP2AEnv- day 18	23.99
miR-503	Lung slices CSC-GFP2AEnv- day 18	32.46
miR-96	Lung slices CSC-GFP2AEnv- day 18	25.96
miR-191	Lung slices CSC-GFP2AEnv- day 18	24.69
Fig. 5.24		
miR-135b	lung slices not-infected 1- day 0	30.49
miR-182	lung slices not-infected 1- day 0	29.86
miR-183	lung slices not-infected 1- day 0	40.00
miR-200b	lung slices not-infected 1- day 0	34.18
miR-205	lung slices not-infected 1- day 0	26.93
miR-21	lung slices not-infected 1- day 0	21.61
miR-31	lung slices not-infected 1- day 0	27.57
miR-503	lung slices not-infected 1- day 0	37.09
miR-96	lung slices not-infected 1- day 0	30.61
miR-191	lung slices not-infected 1- day 0	24.26
miR-135b	lung slices not-infected 2- day 0	34.45
miR-182	lung slices not-infected 2- day 0	31.06
miR-183	lung slices not-infected 2- day 0	40.00
miR-200b	lung slices not-infected 2- day 0	34.83
miR-205	lung slices not-infected 2- day 0	27.97
miR-21	lung slices not-infected 2- day 0	21.42
miR-31	lung slices not-infected 2- day 0	27.76
miR-503	lung slices not-infected 2- day 0	40.00
miR-96	lung slices not-infected 2- day 0	40.00

Table 0.2. Summary of Ct values from the qPCR results reported in Chapter 5.

miRNA	Sample	Ct value
miR-191	lung slices not-infected 2- day 0	23.80
miR-135b	lung slices JSRV-infected 1- day 10	32.24
miR-182	lung slices JSRV-infected 1- day 10	23.44
miR-183	lung slices JSRV-infected 1- day 10	27.61
miR-200b	lung slices JSRV-infected 1- day 10	29.50
miR-205	lung slices JSRV-infected 1- day 10	23.06
miR-21	lung slices JSRV-infected 1- day 10	19.35
miR-31	lung slices JSRV-infected 1- day 10	24.42
miR-503	lung slices JSRV-infected 1- day 10	29.55
miR-96	lung slices JSRV-infected 1- day 10	24.74
miR-191	lung slices JSRV-infected 1- day 10	24.53
miR-135b	lung slices JSRV-infected 2- day 10	40.00
miR-182	lung slices JSRV-infected 2- day 10	22.44
miR-183	lung slices JSRV-infected 2- day 10	26.53
miR-200b	lung slices JSRV-infected 2- day 10	28.93
miR-205	lung slices JSRV-infected 2- day 10	21.98
miR-21	lung slices JSRV-infected 2- day 10	18.96
miR-31	lung slices JSRV-infected 2- day 10	23.84
miR-503	lung slices JSRV-infected 2- day 10	30.83
miR-96	lung slices JSRV-infected 2- day 10	23.55
miR-191	lung slices JSRV-infected 2- day 10	24.00
miR-135b	lung slices Mock-infected 1- day 10	34.61
miR-182	lung slices Mock-infected 1- day 10	23.81
miR-183	lung slices Mock-infected 1- day 10	28.17
miR-200b	lung slices Mock-infected 1- day 10	29.47
miR-205	lung slices Mock-infected 1- day 10	23.16
miR-21	lung slices Mock-infected 1- day 10	19.81
miR-31	lung slices Mock-infected 1- day 10	24.66
miR-503	lung slices Mock-infected 1- day 10	29.97
miR-96	lung slices Mock-infected 1- day 10	24.91
miR-191	lung slices Mock-infected 1- day 10	25.00
miR-135b	lung slices Mock-infected 2- day 10	40.00
miR-182	lung slices Mock-infected 2- day 10	23.33
miR-183	lung slices Mock-infected 2- day 10	26.91
miR-200b	lung slices Mock-infected 2- day 10	29.54
miR-205	lung slices Mock-infected 2- day 10	22.90
miR-21	lung slices Mock-infected 2- day 10	19.84

Table 0.2. Summary of Ct values from the qPCR results reported in Chapter 5.

miRNA	Sample	Ct value
miR-31	lung slices Mock-infected 2- day 10	24.59
miR-503	lung slices Mock-infected 2- day 10	31.01
miR-96	lung slices Mock-infected 2- day 10	24.41
miR-191	lung slices Mock-infected 2- day 10	24.83